Lecture Notes in Operations Research

Robin Qiu · Kelly Lyons · Weiwei Chen *Editors*

AI and Analytics for Smart Cities and Service Systems

Proceedings of the 2021 INFORMS International Conference on Service Science

MOREMEDIA

Springer

Lecture Notes in Operations Research

Lecture Notes in Operations Research is an interdisciplinary book series which provides a platform for the cutting-edge research and developments in both operations research and operations management field. The purview of this series is global, encompassing all nations and areas of the world.

It comprises for instance, mathematical optimization, mathematical modeling, statistical analysis, queueing theory and other stochastic-process models, Markov decision processes, econometric methods, data envelopment analysis, decision analysis, supply chain management, transportation logistics, process design, operations strategy, facilities planning, production planning and inventory control.

LNOR publishes edited conference proceedings, contributed volumes that present firsthand information on the latest research results and pioneering innovations as well as new perspectives on classical fields. The target audience of LNOR consists of students, researchers as well as industry professionals.

More information about this series at http://www.springer.com/series/16741

Robin Qiu · Kelly Lyons ·
Weiwei Chen
Editors

AI and Analytics for Smart Cities and Service Systems

Proceedings of the 2021 INFORMS International Conference on Service Science

Springer

Editors
Robin Qiu
Division of Engineering
and Information Science
Pennsylvania State University
Malvern, PA, USA

Weiwei Chen
Department of Supply Chain Management
Rutgers, The State University of New Jersey
Piscataway, NJ, USA

Kelly Lyons
Faculty of Information (Cross-appointed to
Computer Science), Faculty Affiliate,
Schwartz Reisman Institute
University of Toronto
Toronto, ON, Canada

ISSN 2731-040X ISSN 2731-0418 (electronic)
Lecture Notes in Operations Research
ISBN 978-3-030-90274-2 ISBN 978-3-030-90275-9 (eBook)
https://doi.org/10.1007/978-3-030-90275-9

This Springer imprint is published by the registered company Springer Nature Switzerland AG
The registered company address is: Gewerbestrasse 11, 6330 Cham, Switzerland

Contents

Deep Learning and Prediction of Survival Period for Breast Cancer Patients

Shreyesh Doppalapudi[1], Hui Yang[2], Jerome Jourquin[3], and Robin G. Qiu[1(✉)]

[1] Big Data Lab, Division of Engineering and Information Science, The Pennsylvania State University, Malvern, PA 19355, USA
{dshreyesh,robinqiu}@psu.edu

[2] Dept of Industrial Engineering, The Pennsylvania State University, University Park, PA 16802, USA
huy25@psu.edu

[3] Susan G. Komen, PO Box 801889, Dallas, TX 75380, USA
jjourquin@komen.org

Abstract. With the rise of deep learning, cancer-specific survival prediction is a research topic of high interest. There are many benefits to both patients and caregivers if a patient's survival period and key factors to their survival can be acquired early in their cancer journey. In this study, we develop survival period prediction models and conduct factor analysis on data from breast cancer patients (Surveillance, Epidemiology, and End Results (SEER)). Three deep learning architectures - Artificial Neural Networks (ANN), Convolutional Neural Networks (CNN), and Recurrent Neural Networks (RNN) are selected for modeling and their performances are compared. Across both the classification and regression approaches, deep learning models significantly outperformed traditional machine learning models. For the classification approach, we obtained an 87.5% accuracy and for the regression approach, Root Mean Squared Error of 13.62% and R^2 value of 0.76. Furthermore, we provide an interpretation of our deep learning models by investigating feature importance and identifying features with high importance. This approach is promising and can be used to build a baseline model utilizing early diagnosis information. Over time, the predictions can be continuously enhanced through inclusion of temporal data throughout the patient's treatment and care.

Keywords: Deep learning · Breast cancer · Survival period prediction · SEER cancer registry · Factor analysis · Feature importance

1 Introduction

Cancer is the second leading cause of death in the United States. According to the latest statistics from the U.S. National Cancer Institute, about 1.8 million new cancer cases are expected in 2020, with about 600,000 expected new deaths [1]. Breast Cancer is the most common cancer in the United States, with 276,480 estimated new cases and 40,170 estimated deaths in 2020 [2]. Though cancer is prevalent throughout the United States, the relative five-year survival rate for breast cancer patients varies by breast

R. Qiu et al. (Eds.): ICSS 2021, LNOR, pp. 1–22, 2021.
https://doi.org/10.1007/978-3-030-90275-9_1

cancer stage. Note that the average risk of a woman in the United States developing breast cancer sometime in her life is about 13% [3].

Estimated national expenditures for cancer care in the United States in 2017 were $147.3 billion [4]. The costs are expected to increase in the coming years with an aging population and newer, more advanced treatment options. An increase in the number of patients requiring care also drives up health care costs for treating the disease. Research on disease prognosis from early information and clinical data is still needed to better manage resources and time, for both the patient and the healthcare professionals. For patients, better prognosis early can help plan time spent in care and costs, while for healthcare professionals it can help plan medical resources, treatment and care strategy for each patient. These reasons make cancer survivability a topic of great importance to both researchers from the medical domain, computer intelligence, and medical professionals.

This study is aimed at predicting the survival period of a breast cancer patient, using the data obtained from Survey Epidemiology, and End Results (SEER) cancer registry [20]. The research problem is formulated through both classification and regression techniques. We investigate three different deep learning models and their performance at providing high dimensionality and highly non-linear decision boundaries and identifying features that drive survival prediction. This study contributes to identifying an appropriate approach to estimating and understanding survivability that could be widely and practically appropriate for medical use.

2 Related Works

Chronic diseases that may threaten the lives of patients and require continuous care and surveillance are the focus of a majority of previous research. These studies aim at projecting a timeline of survival to help both patients and healthcare professionals plan care, time, and resources.

Some researchers have focused on using the results from various laboratory tests and medical images such as Computerized Tomography (CT) or Magnetic Resonance Imaging (MRI) scans to predict disease survival for patients. Macyszyn *et al.* [5] have used a combination of Linear SVM for predictions and Kaplan-Meyer survival curves to plot the survival period and map the prognosis from the MRI images of patients with glioblastoma. Qian *et al.* [6] proposed Temporal Reflected Logistic Regression (TRLR), a model to predict survival probabilistic score on a set of patients diagnosed with heart failure at Mayo Clinic, Rochester. They showed that the new model outperformed the existing Seattle Heart Failure Model (SFHM). Marshall *et al.* [7] proposed a custom Bayesian model, Continuous Dynamic Bayesian Model, that differs in data availability at different points during the treatment of the patient, making effective use of the temporal data sequence. Zhang *et al.* [8] used LASSO as the regularization and feature selection method in a multilayer perceptron model to predict the 5-year survival of patients suffering from chronic kidney disease. Bellot *et al.* [9] developed Hierarchical Bayesian models for cardiovascular disease, which utilized a mixture of localized and individual patient data to build average survival paths for patients and specific survival paths for individual patients. They developed a personalized interpreter for the model to highlight the factors affecting the survival prediction for each patient.

Cancer has been the focus of a large body of research targeting multiple aspects: diagnosis, prognosis, best treatment estimation and survival period estimation. Gray *et al.* [10] tested the performance of the Predict algorithm (version 2), built for 5-year and 10-year prognostic indicators for breast cancer, using the Scottish Cancer Registry (SCR). They found that the algorithm overestimates some 5-year prognostic cases while the overestimation is lower for 10-year prognosis. Song *et al.* [11] built nomographs to predict overall and cancer-specific survival of patients with chondrosarcoma and identified the prognostic factors for 3-year and 5-year survival. Lynch *et al.* [12] compared multiple supervised machine learning methods to predict survival time of lung cancer patients. Tested algorithms include Linear Regression, Gradient Boosting Machine, Random Forest, Support Vector Machine and a custom stacking ensemble combining all the other machine learning algorithm models. The custom ensemble performed the best with an RMSE (Root Mean Squared Error) value of 15.30%. Sadi *et al.* [13] proposed the use of clustering cancer registry data before feature selection for classification model on survival period prediction. They used the Egyptian National Cancer Institute (NCI) cancer registry data to perform clustering and then build classification models inside each cluster to get a better sense of hyperparameter tuning and achieve better performance.

The SEER dataset provides comprehensive information on the early diagnosis of patients for multiple types of cancer along with the survival time for patients. It has been a part of a multitude of research around prediction of survival period. Bartholomai and Frieboes [14] compared multiple traditional machine learning models in an attempt to predict the exact survival period for a lung cancer patient by modeling the problem using both classification and regression techniques. They used Principal Component Analysis (PCA) to identify the features that have the biggest impact on the survival of lung cancer patients. Hegselmann *et al.* [15] developed models with a focus on producing reproducible models for further research use, to predict 1-year and 5-year survival for patients with lung cancer using logistic regression and multilayer perceptron models. Naghizadeh and Habibi [16] compared various ensemble machine learning models to predict survival in cancer comorbidity cases for various cancers. Dai *et al.* [17] built 1-year and 3-year nomographs to predict survival for triple negative breast cancer patients with a histology of infiltrating duct carcinoma. Imani *et al.* [18] used random forests as a modeling approach to predict survival in patients with breast cancer recurrences and identified the important variables in defining survivability for those patients. Kleinlein and Riano [19] built joint and stage-specific machine learning models to predict 5-year survival for breast cancer patients. They also tested the performance of these models over time from training to demonstrate the feature importance in selection for models. Shukla *et al.* [20] performed clustering using Self-Organizing Maps (SOM) and DBSCAN to cluster the patients into related cohorts and build multilayer perceptron to predict 3-year, 5-year and 7-year survival of breast cancer patients.

Most of previous research into survival prediction in breast cancer has focused on the binary classification model of whether a patient survives a preset period of time or not. To the best of our knowledge, little research has focused on the predicting the exact survial periods for breast cancer patients. This study aims to bridge this gap by utilizing deep learning models to predict survival periods in breast cancer cases, and further

provide interpretability to these models through feature importance analysis, revealing the features with the largest impact on the survival predictions.

3 Dataset

In this research study, the data was collected from Surveillance, Epidemiology, and End Results (SEER) program cancer registry. The SEER program is supported by the Surveillance Research Program (SRP) in NCI's Division of Cancer Control and Population Sciences (DCCPS) and was established to provide consistent statistics around cancer incidence in the United States. SEER collects its information from several population-based registries spread geographically across the United States and estimated to cover about 34.6% of the United States population. The SEER dataset is one of the biggest and most comprehensive databases on the early diagnosis information for cancer patients in the United States [21]. The SEER cancer registry includes information on primary tumor, tumor histology, morphology, the first course of treatment and follow-up with patients to record the vital status. All the records are de-identified, with very little demographic information and all the entries are encrypted to provide another layer of security for the patients' identity. It includes statistics on incidence of multiple types of cancer such as breast cancer, lung cancer, intestinal cancer, leukemia, lymphoma, prostate cancer and others.

3.1 Data Collection and Cleaning

The incidence files in the SEER cancer dataset are available as a set of ASCII text files with each row in a text representing a record in the registry and the information encrypted in codes. The whole database was segmented by sets of registries and the cancer type. We selected the November 2018 submission (which was made publicly available in April 2019) for our research.

This submission contained information for the diagnosis years of 1975–2016. For this research, we only selected the files for breast cancer and built Python codes to read ASCII text files and return comma separated values (.csv) files, which would be easier to ingest for data engineering purposes. The Python codes ignored all records with diagnosis year before 2004 to minimize the impact of now-defunct data fields on our modeling process. (The registry went through a major data overhaul in 2004 and new fields were added to replace the older fields.)

Further, the codes representing missing values in the registry were replaced by null values to standardize the data loss at both individual registry level and the national registry level. Also, the records of patients with cancer comorbidities were eliminated. Only patients with breast cancer and no comorbidities were considered to reduce the effect of other cancers on the survival analysis. Records with missing diagnosis year and survival time information were eliminated as these values could not be imputed, because any imputation for these fields affects the survival analysis directly. This cleaning resulted in a dataset with 197,038 records for analysis and modeling.

3.2 Data Preprocessing

The features were divided into categorical and quantitative variables. Also, features that are built on the target variable, such as variables defining cause of death classifications, were identified through domain knowledge gained by a better understanding of the dataset. These variables were not included in the modeling analysis to avoid model bias.

Different pre-processing techniques were used for categorical and quantitative variables. Variables with more than 20% missing values were eliminated from modelling, because they were either data collected during different time periods (before 2004 diagnosis year) or were not relevant measurements for breast cancer. For the remaining variables, the median and mode were used to impute missing values for quantitative and categorical variables, respectively. After the imputation, categorical variables were binarized using one-hot encoding.

Figure 1 shows the distribution of patients across different survival periods. For the classification approach of predicting survival period, the survival time in months was segmented into three bins '< =5 years', '5–10 years', and '>10 years' used as the target class for multiclass classification modeling. These classes were decided through knowledge gained from previous research approaches to this problem, where 5-year and 10-year survival models are the most common. Yet, imbalance exists in the data coming from '>10 years' class as shown in Fig. 2. To adjust for this imbalance, we upsampled other classes to create a balanced dataset for model tuning and evaluation. For the regression approach, we selected the survival time in months as the target variable.

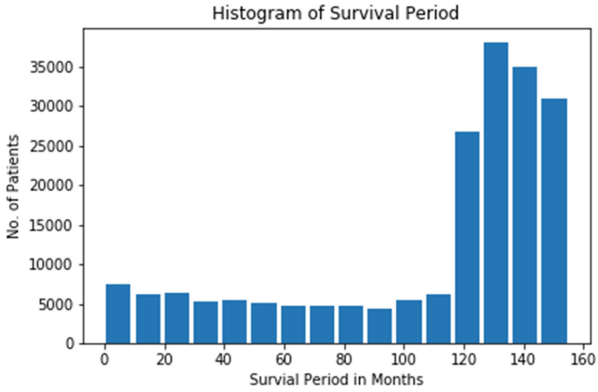

Fig. 1. A histogram to understand the distribution of breast cancer patients across various survival period.

The features have different scales, which could lead to a longer time for the model to converge and reach the global minima while also increasing the probability for the model to get stuck in local minima. Hence, the predictors were all normalized for the classification approach, while for the regression approach, the target variable was also scaled for easier comparison between errors across model iterations and between different models. The entire dataset was partitioned in the ratio of 80:20 into training and test

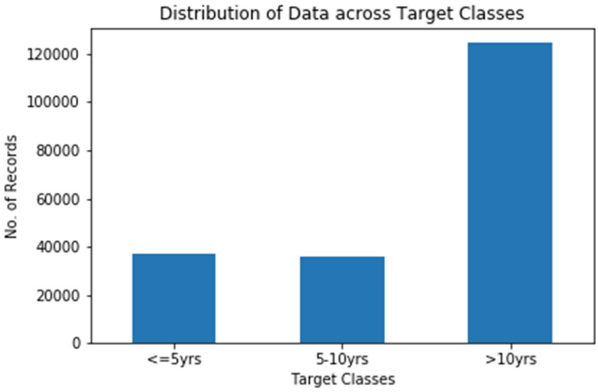

Fig. 2. Distribution of Records across the selected three target classes.

sets. The models were trained on the training set and the performance was observed on the test set.

4 Research Methodology

The data preprocessing methods remain similar for the two different approaches to the problem (i.e., classification and regression), except for the target variable in the dataset preparation. However, the model building methodologies differ for both approaches with the different tuning approaches and evaluation metrics for both approaches. Artificial Neural Networks (ANN), Recurrent Neural Networks (RNN), and Convolutional Neural Networks (CNN) are the three selected deep learning architectures to model the problem.

4.1 Deep Learning Architectures

This research study focuses on the performance of deep learning models in the space of cancer survival period prediction. For this purpose, we have selected three of the most popular deep learning architectures in practice today- ANN, RNN and CNN.

Neural networks are sub-field of the rapidly growing deep learning space, which is in itself a sub-field of machine learning. The rapidly growing popularity of deep learning can be attributed to its performance to model unstructured data such as text and images and to infer meaning at par with or better than human accuracy.

A basic building block of a neural network is a perceptron. A perceptron provides each input with a weight and creates a function to represent the input space. This representation is then passed through an activation function to produce a probability of the input sequence representing the output or not. The simplest perceptron model can mimic a logistic regression model through the use of just one perceptron. A neural network is formed by arranging groups of perceptrons in multiple layers to represent the output with activation functions defined for each layer. A perceptron is known as a neuron inside a neural network, with the name representing the tendency of neural network to mimic the performance of neurons inside the human brain. Neural networks have three major

units - input layer, hidden layers and an output layer. The size of the input and output layers are always defined by the problem, and the architecture of the hidden layers is always defined by a machine learning practitioner which helps to model the problem more efficiently. As the number of hidden layers increases, the defined representation becomes more complex and highly non-linear.

The earliest defined neural network is ANN [22], which consists of neurons arranged in multiple layers, with each neuron in one layer fully connected to each neuron in the next layer. The simplest ANN architecture consists of an input layer, a hidden layer, and an output layer. As the number of hidden layers increase, the number of parameters to train in the network increases and the representation becomes more complex.

A neural network where the output of a neuron is fed back as input after certain time units is known as RNN [23]. This ability makes it easy for them to model temporal sequences of data such as text and time-series data. But, with the output of neurons being fed back to the input neuron creates a gradient vanishing problem when the network is very large and the input sequence is too long. To overcome this problem, Long Short Term Memory Networks (LSTM) [24] were proposed as a variant of the simple RNN architecture. LSTM introduced the concept of a forget gate that limits the sequence size that is under consideration at any particular time, thereby overcoming the vanishing gradient problem. We use LSTM networks for our research and hereby in this paper, RNN refers to LSTM architecture.

A neural network model where the weights are shared across a few neurons in a layer is known as CNN [25]. The shared weights concept makes CNN both space and shape invariant and makes them the ideal network to model data from images and videos. This helps in bringing down the number of training parameters that would be required if the fully connected layers were used to model images. In this study, we are working with 1-dimensional data and hence, use the 1-D convnet architecture. In this paper, CNN refers to the 1-D convnet architecture.

4.2 Model Architecture and Parameters

4.2.1 Classification Model

The architecture and parameters of the classification model under study are given in Table 1. With '< =5 years', '5 – 10 years', and '>10 years' as the target classes, this model attempts to address a multiclass classification problem. Each model has a unique model architecture with a varying distribution of neurons in each layer, number of layers, and number of iterations (epochs) over which the model is trained. In addition, to prevent overfitting of the data, regularization was performed through the addition of Dropout layers between the hidden layers. A few hyper-parameters remain similar across all models, such as ReLU (Rectified Linear Unit) as the activation function in the hidden layers, Softmax as the activation function in the output layer, Adam (Adaptive Moments Estimation) as the optimizer with a 0.001 learning rate and Categorical Cross Entropy as the loss function.

ANN Model: The ANN model has 5 hidden layers with 600, 300, 100, 50 and 20 neurons in each layer, respectively. The model was run over 100 epochs with 10% Dropout layer after the first two hidden layers.

Table 1. Parameters for classification models

Parameters	ANN	RNN	CNN
Target classes	[<=5 Years, 5 – 10 Years, >10 Years]		
No. of hidden layers	5	4	5
No. of neuron in each hidden layer	[600, 300, 100, 50, 20]	[256, 128, 64, 32]	[512, 256, 128, 64, 32]
Activation functions in each layer	ReLU in hidden layers and Softmax on output layer		
Loss function	Categorical cross entropy		
Optimizer	Adam (Adaptive Moments Estimation) with 0.001 learning rate		
No. of epochs	150	100	100
Dropout layers for regularization	10% dropout layer after first two hidden layers	10% dropout layer after first two hidden layers	10% dropout layer after first and third hidden layers

RNN Model: The RNN model has 4 hidden layers with 256, 128, 64 and 32 neurons in each layer, respectively. The model was run over 100 epochs with 10% Dropout layer after the first two hidden layers.

CNN Model: The CNN model has 5 hidden layers with 512, 256, 128, 64 and 32 neurons in each layer, respectively. The model was run over 100 epochs with 10% Dropout layer after the first and third hidden layers.

4.2.2 Regression Model

The architecture and the parameters of the regression model under study are given in Table 2. With the normalized survival period as the target, this model attempts to address a regression problem. Mean squared error was selected as the loss function since it is a regression problem with each model having a varying distribution of neurons in each layer, number of layers, and number of iterations (epochs) over which the model is trained. Again, to prevent overfitting, Dropout layers were added to the models between the hidden layers to perform regularization of the network. A few hyper-parameters still remain similar across models such as ReLU (Rectified Linear Unit) as the activation function in the hidden layers, no activation function in the output layer, and Adam (Adaptive Moments Estimation) as the optimizer with a 0.001 learning rate.

ANN Model: The ANN model has 3 hidden layers with 100, 60, 20 neurons in each layer, respectively. The model was run over 20 epochs with no Dropout layer.

RNN Model: The RNN model has 2 hidden layers with 50, 20 neurons in each layer, respectively. The model was run over 25 epochs with 20% Dropout layer after the first and last hidden layers.

CNN Model: The CNN model has 2 hidden layers with 40, 20 neurons in each layer, respectively. The model was run over 50 epochs with no Dropout layer.

Table 2. Parameters for Regression models

Parameters	ANN	RNN	CNN
No. of hidden layers	3	2	2
No. of neuron in each hidden layer	[100, 60, 20]	[50, 20]	[20, 40]
Activation functions in each layer	ReLU in hidden layers		
Loss function	Mean squared error		
Optimizer	Adam (Adaptive Moments Estimation) with 0.001 learning rate		
No. of epochs	20	25	50
Dropout layers for regularization	None	20% dropout layer after every hidden layer	None

4.3 Model Tuning

The models were initially tuned over a large number of epochs to observe the performance of the models on both the training and test sets.

4.3.1 Classification Model

The plots of the training and test loss and accuracy vs. the number of epochs are shown in Fig. 3. The optimal numbers of epochs for the ANN, RNN, and CNN models are determined to be approximately 150, 100, and 100, respectively. The training loss and test loss can be seen to diverge with the test loss stabilizing due to regularization and the training loss decreasing at a rapid pace for all the models near the optimal number of epochs.

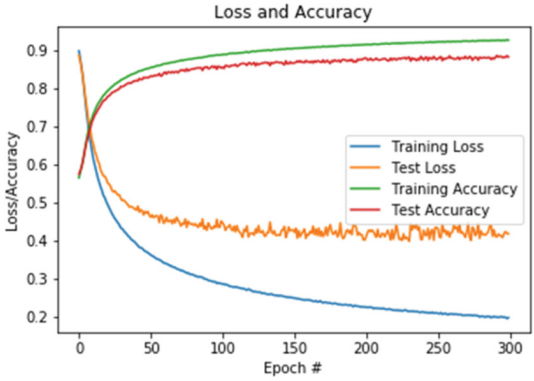

(a) ANN Model

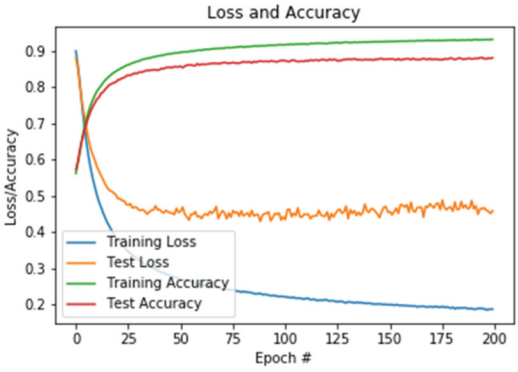

(b) RNN Model

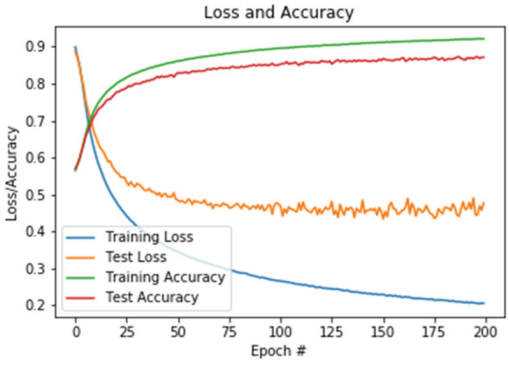

(c) CNN Model

Fig. 3. Epoch Plots for Classification models. Epoch plots are required to find the optimal number of Epochs to train the models by observing training loss and test loss and finding the point where over-fitting starts.

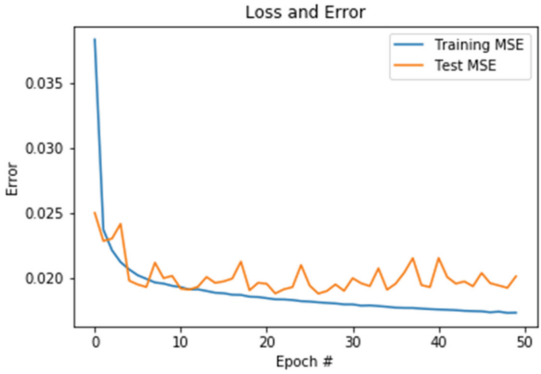

(a) ANN Model

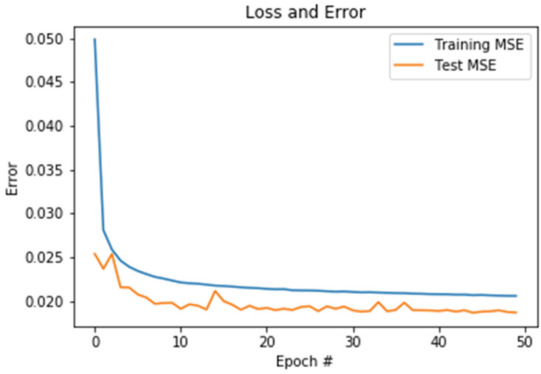

(b) RNN Model

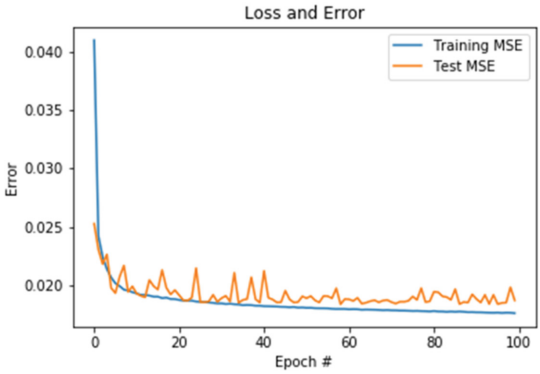

(c) CNN Model

Fig. 4. Epoch Plots for Regression models. Epoch plots are required to find the optimal number of Epochs to train the models by observing training loss and test loss and finding the point where over-fitting starts.

4.3.2 Regression Model

The plots of the training and test loss and accuracy vs. the number of epochs are shown in Fig. 4. The optimal numbers of epochs for the ANN, RNN, and CNN models are determined to be approximately 20, 25, and 50, respectively. The training loss and test loss can be seen to diverge near the optimal number of epochs with the test loss increasing and the training loss decreasing at a rapid pace for ANN model, while test loss stabilized and training loss decreased at a rapid pace for both the RNN and CNN model.

4.4 Models for Comparison with Previous Research

To put our results in perspective, we compared our results with the results from traditional machine learning models approaches. Feature selection for classification models was done using one-way ANOVA tests for continuous variables and χ^2 test for categorical variables. Similarly, for regression models, one-way ANOVA tests were used for categorical variables and univariate linear regression for continuous variables. These tests give variables that are most relevant to the breast cancer classification and regression models.

4.4.1 Classification Model

For the classification model, we have implemented the following models:

- *Random Forest Classifier* with 500 tree count, depth of 3 variables and minimum node size of 50.
- *Support Vector Machines* with a linear kernel, primal optimization and a regularization parameter of 1.7e07.
- *Naïve Bayes Classifier* with a Complement Multinomial distribution assumed for the features and Laplace smoothing parameter of 2.37.

The hyper-parameters for these models were selected through a random search for the optimal hyper-parameters.

4.4.2 Regression Model

For the regression model, three models were implemented:

- *Random Forest Regressor* with 500 tree count, depth of 3 variables and minimum node size of 50.
- *Gradient Boosting Machine* with 1000 tree count, interaction depth of 1, 0.21 learning rate and minimum node size of 100.
- *Line Regression Model* with default parameters.

The hyper-parameters for these models were selected through a random search for the optimal hyper-parameters.

4.5 Feature Importance

There has been a growing demand to increase the interpretability of machine learning models. This is especially true for the models that operate in heavily regulated industries such as healthcare, mortgages, government and military. Understanding feature importance in models is a step towards being able to interpret the learning patterns that the machine learning model interpreted from the data and would help in making the models more interpretable, bias-free and easier to audit. These reasons contribute to understanding feature importance being an important step in building machine learning models in the healthcare sector.

To understand important features towards predicting survival period, we employed two different types of model-agnostic machine learning model interpretation techniques - one to explain the predictions locally at each prediction level and another to explain predictions on a global level. At a local level, we aim to understand for each prediction which feature plays an important role in outputting that particular prediction. At a global level, we try to understand the impact each feature has on the final prediction. In other words, we look at the final output as a function of each predictor individually.

For local level interpretability, we used Shapley Addictive exPlanations (SHAP) [26] values to understand the features driving a set of sample predictions. SHAP is a framework for machine learning interpretation that combines many algorithms such as LIME [27], DeepLIFT [28], Shapley Sampling Values [29], Shapley Regression Values [30], Quantitative Input Influence [31] and layer-wise relevance propagation [32]. SHAP works as a model agnostic interpretation and has no performance issues even on blackbox models such as deep neural networks, random forests or gradient boosting machines. SHAP provides a feature ranking for each prediction based on the amount of influence each predictor had on the final prediction. SHAP value for a particular predictor is provided as a percentage importance considering the most important predictor to have a base value of 100%.

For global level interpretability, we have built Partial Dependence Plots (PDP) [33] to understand the effect that each feature in the dataset has on the final prediction across the complete training set. A partial dependence plot helps to visualize how the value of final prediction changes with the changes in the feature value. Also, the distribution of each feature was plotted to understand if the effect of each prediction is significant or not. Partial dependence plots work on the assumption of binary classification. Hence, to adapt it to the multiclass classification problem, we have employed One-vs-All approach to describe the feature importance for each class.

For this study we investigated the interpretability of the results from our deep learning models with the feature importance, which helps identify the most important features at the local level and global level of interpretability.

4.6 Experimental Setting

The processes of data extraction, cleaning, visualization, transformation and model building were done in Python. For those purposes, various open-source technological stacks such as Numpy [34], pandas [35], Scikit-learn [36], TensorFlow [37], Keras [38] and Matplotlib [39] were used. For providing the model interpretability and feature importance using SHAP and Partial Dependence Plots, InterpretML [40] was used.

5 Results and Discussion

We have used different evaluation metrics to evaluate the performance of the models for the classification and regression approaches due to the inherent differences in these approaches.

5.1 Evaluation Metrics

Precision, Recall, F-1 Score, Accuracy, and Cohen's κ were selected as the evaluation metrics for the classification models built in this study. These evaluation metrics are defined by the following equations [1–5]:

$$\text{Accuracy} = \frac{\text{TP} + \text{TN}}{\text{TP} + \text{FP} + \text{TN} + \text{FN}} \tag{1}$$

$$\text{Precision} = \frac{\text{TP}}{\text{TP} + \text{FP}} \tag{2}$$

$$\text{Recall} = \frac{\text{TP}}{\text{TP} + \text{FN}} \tag{3}$$

$$\text{F1Score} = 2 * \frac{\text{Precision} * \text{Recall}}{\text{Precision} + \text{Recall}} \tag{4}$$

$$\kappa = \frac{P_O - P_e}{1 - P_e} \tag{5}$$

where TP is True Positives, FP is False Positives, TN is True Negatives, FN is False Negatives, P_O is the probability of observed agreement, and P_e is the probability of random agreement between raters.

For the regression modeling, Root Mean Squared Error (RMSE), Mean Squared Error (MSE), and Coefficient of Determination (R^2) value were used as the evaluation metrics for the regression model. These evaluation metrics are defined by the following equations [6–8]:

$$MSE = \frac{1}{n}\sum_{i=1}^{n}\left(y_i - \hat{y}_i\right)^2 \tag{6}$$

$$RMSE = \sqrt{\frac{1}{n}\sum_{i=1}^{n}\left(y_i - \hat{y}_i\right)^2} \tag{7}$$

$$R^2 = 1 - \frac{\sum_{i=1}^{n}\left(y_i - \hat{y}_i\right)^2}{\sum_{i=1}^{n}\left(y_i - \bar{y}\right)^2} \tag{8}$$

where, y_i is the i^{th} observed value, $\hat{y}_i$ is the i^{th} predicted value, $\bar{y}$ is the mean of observed values, and n is the total number of values in the dataset.

5.2 Classification Model Results

Deep learning models significantly outperform other baseline models of Random Forest Classifier, SVM classifier and the Naïve Bayes Classifier (Table 3). ANN turns out to be the best performing model with achieving 87.50% accuracy, slightly higher than RNN and CNN.

As shown in Table 3, the performance of deep learning models decreases as the survival period of the class increases. ANN, RNN and CNN models have much lower performance on the '>10 years' class. In contrast, the traditional machine learning models have a much lower performance on the bounded class '5–10 years' in comparison with the unbounded '<=5 years' and '>10 years'. Note the exceptionally low performance of the random forest classifier on the middle class. Among the traditional machine learning models, the ensemble classifier Random Forest Classifier performs much better that SVM and Naïve Bayes Classifier. Naïve Bayes Classifier has the worst performance among all the classifiers at 48.82% accuracy.

The low recall for the '>10 years' and the low precision for the '5–10 years' for the deep learning models suggest that the models find it difficult to differentiate between medium length survival period prediction and long survival period prediction. This brings down the overall performance of the models over '5–10 years' and '>10 years' classes in comparison with the '<=5 years' class.

Table 3. Performance comparison of classification models

Model	Target class	Precision	Recall	F-1 score
ANN model	<=5 years	90.94%	94.29%	92.59%
	5–10 years	84.06%	91.67%	87.70%
	>10 years	87.73%	76.54%	81.75%
	Accuracy	87.50%		
	Cohen's κ	81.24%		
RNN model	<=5 years	89.05%	95.11%	91.98%
	5–10 years	85.48%	91.31%	88.30%
	>10 years	87.95%	75.97%	81.52%
	Accuracy	87.46%		
	Cohen's κ	81.18%		
CNN model	<=5 years	90.17%	93.85%	91.97%
	5–10 years	83.85%	89.60%	86.63%
	> 10 years	85.70%	76.32%	80.74%
	Accuracy	86.58%		
	Cohen's κ	79.87%		
Random forest classifier	<=5 years	63.84%	65.62%	64.72%

(*continued*)

Table 3. (*continued*)

Model	Target class	Precision	Recall	F-1 score
	5–10 years	52.16%	39.07%	44.68%
	>10 years	56.82%	69.56%	62.55%
	Accuracy	58.04%		
	Cohen's κ	37.07%		
SVM classifier	<=5 years	58.32%	62.98%	60.56%
	5–10 years	47.09%	29.89%	36.57%
	>10 years	53.65%	69.07%	60.39%
	Accuracy	53.93%		
	Cohen's κ	30.91%		
Naïve Bayes classifier	<=5 years	54.08%	56.69%	55.35%
	5–10 years	41.59%	30.35%	35.09%
	>10 years	48.67%	59.55%	53.56%
	Accuracy	48.82%		
	Cohen's κ	23.24%		

5.3 Regression Model Results

As shown in Table 4, deep learning models significantly outperform other baseline methods with a lower RMSE and higher R^2 value. CNN turns out to be the best performing model achieving 13.62% RMSE and 76.37% R^2 value. CNN's performance is just marginally better than that of ANN and RNN models.

We have plotted the RMSE vs. Survival Period in months along with support count in Fig. 5 for all the models to better understand the error progression over survival period. Figure 5 shows that the error in prediction for survival period is high for both breast cancer patients with long survival periods and for those with very short survival period. The error is lowest for the mid-level survival patients. This indicates that the models

Table 4. Performance comparison of regression models

Model	MSE	RMSE	R^2 value
ANN	0.020	13.98%	75.09%
RNN	0.020	13.99%	75.04%
CNN	0.019	13.62%	76.37%
Linear regression	0.022	15.01%	71.27%
Gradient boosting Machine	0.021	14.58%	72.68%
Random forest regression	0.021	14.16%	74.01%

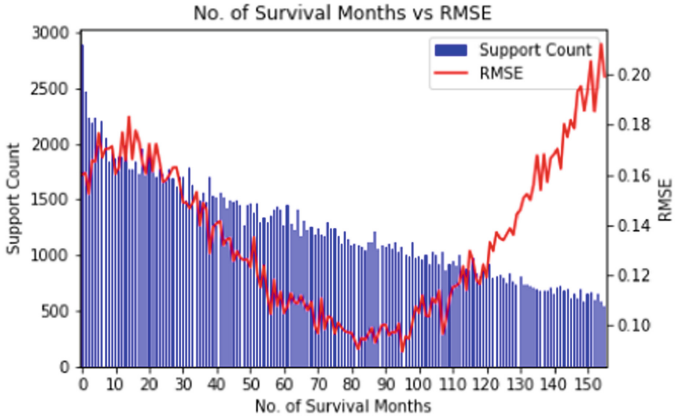

(a) ANN Model

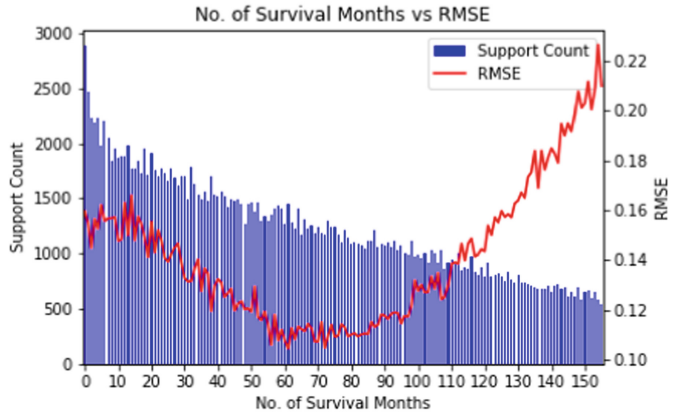

(b) RNN Model

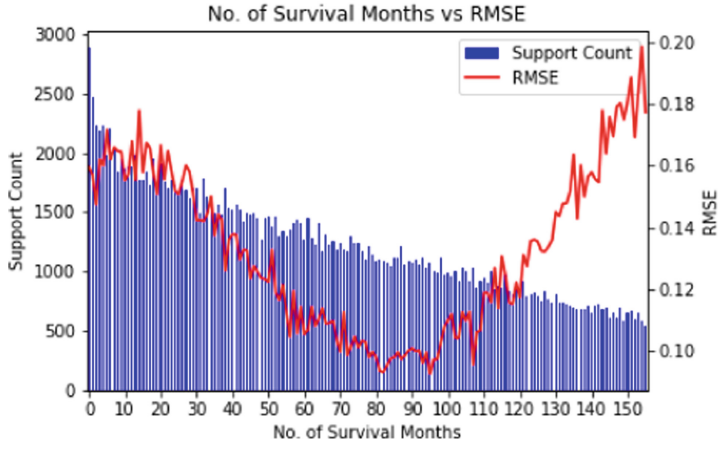

(c) CNN Model

Fig. 5. RMSE vs. No. of Survival Months plot for the deep learning models. The error in prediction is the lowest for mid-level survival period patients.

find it difficult to accurately estimate the survival period for low survival period patients since breast cancer patients have a high mean survival period. The confidence in the prediction is the highest for mid-level survival and again decreases for long survival period patients as the number of cases decreases for high number of survival months. This indicates that the regression approach cannot be useful in an unbounded approach to modeling the patient survival period. The regression approach works best when the survival period is bounded on the lower and higher side, away from which the error increases to an unacceptable level while the support for the survival period goes below an acceptable threshold value. For example, in the case of breast cancer, the survival period could be bounded between 60 and 120 months (5 and 10 years, respectively), as the RMSE is above 12% (which is assumed to be an acceptable threshold of error) for survival period less than 60 months or greater than 120 months. The other survival period needs more accurate substitution to help in predicting the exact survival period.

Also, notice the almost identical error progression occurs for all the deep learning models in the figure. This leads us to believe that various deep learning models can model a similar non-linear function from the predictors provided with the data to represent the survival period.

5.4 Discussion

As shown above, deep learning methods significantly outperform the baseline models which include traditional machine learning methods such as linear regression, random forests, gradient boosting machine, support vector machine and naïve Bayes across both classification and regression approaches. This again represents the ability to learn highly non-linear decision boundaries from high dimensional data, an aspect where neural networks tend to do better than other traditional machine learning approaches.

The performance of both RNN and CNN is not better than the performance of ANN across both classification and regression approaches. The absence of temporal or sequential data in the dataset could be responsible for this differential. RNN and CNN can shine with multi-dimensional data such as text or images where they optimize much faster. Their performance is comparable to ANN without temporal data and represent a loss of time in the project due to the longer training time that they take on a similar network size as an ANN. This reinforces that selection of model architecture depends more closely on the data than any other external factors.

This also opens another avenue to improve the performance of survival models - through the use of temporal data. The built models will be enhanced through the availability of temporal data, which can help in providing more accurate predictions. The build models can be further enhanced through the patient treatment period, resulting in the increase of prediction accuracy for cases with long survival period.

Prediction of survival period should still be bounded within an acceptable threshold for the regression approach as many other factors currently not represented in the data could drive the survival period for longer survival cases. The acceptable bounds for prediction should be defined based on a specific cancer type as the behavior and survival period distribution differs for each type of cancer. As a result, cancer-specific survival models help model the intricacies of each cancer with respect to the survival period.

Also, specifically for breast cancer, the error in regression for low survival period is high, which could be augmented by combining with a classification approach. The classification approach provided high performance on the low survival period class while the regression approach lagged in performance on low survival periods. A combination of both approaches could help provide a sufficient threshold for regression prediction which performs best for mid-range survival period. This hybrid approach helps in defining a tier-structure for predictions that can prove to be a more refined approach for healthcare professionals and patients to better plan medical resources, treatment and care strategy at an individual level. Also, the combined approach helps to define a threshold for high survival periods, where the performance of both models is lower. This threshold should define the maximum period for which the predictions can be made accurately either through a classification or regression approach.

5.5 Feature Importance

Feature importance was estimated at both the local and global prediction levels. The feature importance varied across multiple classes. Age at the time of diagnosis (*AGE_DX*) was an important driving factor in prediction, with higher value resulting in a low survival period prediction and lower age driving higher survival period. Also, the number of malignant comorbidity tumors (*MALIGCOUNT*) was another driving factor, especially for low survival period predictions with higher count leading to more confidence in the prediction of low survival period. Similarly, the number of benign tumors (*BENBORDCOUNT*) drives low survival period prediction, with a lower number of benign tumors leading to low survival period prediction. The tumor size (*CSTUMSIZ*) and extension (*CSEXTEN*), were important features for prediction of higher survival period, with lower tumor and lesser extension leading to higher survival period prediction. The number of radiation rounds (*RADIATNR*) represented another feature contributing highly to high survival period prediction, with an increasing number of rounds of radiations showing higher prediction contribution to higher survival period prediction.

Another important factor contributing to low survival period prediction is the grade of the cancer (*GRADE*), with a higher grade driving lower survival period prediction. Laterality of tumor (*LATERAL*) is an important factor for high survival period prediction, with higher laterality pushing for a higher survival period prediction. Derived AJCC T value (*DAJCCT*) and N value (*DJACCN*) provide another facet of higher survival period prediction with higher T & N values contributing to higher survival period prediction. A lower number of lymph nodes involved ((*CSLYMPHN*)) leads to higher survival period prediction.

Also, some features such as progesterone status (*PRSTATUS*), primary site for surgery (*SURGSITF*), first primary cancer (*FIRSTPRIM*), marital status (*MAR_STAT*) and race (*RACEIV*) are driving predictions at the local level, but the dependence is not seen at the global level. This indicates that these features are important to the model, but they drive the prediction through interaction with other variables, which cannot be observed through Partial Dependence Plots. Hence, these features need more scrutiny to understand their interactions with other variables and the effect of these interactions on the final prediction.

Finally, there are a few variables that are considered important by the models, but they represent information that is already convened through other variables. Hence, even if they are considered important to the predictions, they still represent information already conveyed through other variables. These variables include year of birth (*YR_BRTH*), age recode (*Age_1_REC*), adjusted AJCC stage variable (*ADJAJCCSTG*), administration of chemotherapy (*CHEMO_RX_REC*) and primary site (*PRIMSITE*).

6 Conclusions

This paper aims at providing new ways to predict breast cancer survival period by applying deep learning methods. We were able to model the survival period for breast cancer patients using ANN, RNN, and CNN and compare those models with baseline models consisting of linear regression, random forests, gradient boosting machine, support vector machine, and naïve Bayes model. We achieved 87.50% accuracy for the classification approach with the best-performing ANN model and 13.62% Root Mean Squared Error (RMSE) and 76.37% R^2 value for the regression approach with the best-performing CNN model. The deep learning models significantly outperformed the traditional machine learning baseline models for both the classification and regression approaches.

The performance of classification model was shown to be decreasing as the survival period in the class increases. This leads to the best performance on '<=5 years' class and lowest performance on '>10 years' class. In the regression approach, it was shown that the prediction error was the lowest for mid-range survival period and high for both low survival period and high survival period cases. Hence, a threshold of acceptable error specific to a cancer needs to be defined to estimate the maximum threshold of prediction to receive acceptable values and combine predictions with the classification models to improve the usability of prediction on low survival period cases.

Note that the performance of deep learning models does not differ much between models, reinforcing the selection of model architecture based on intrinsic characteristics of data. Adoption of hybrid architecture with different architectures in different layers could improve the models' performance, leading to an increased ability to model more complex decision boundaries, but with decreasing interpretability.

Finally, we analyzed feature importance at both the individual prediction level and the model as a whole. Important features were identified that drive both the low survival period prediction and high survival period prediction, along with the features that represent information through interactions with other features.

This study constitutes a proof-of-concept that our methodology can serve as a basis for developing models that will support healthcare professionals and patients plan medical resources, treatment and care strategy with just information collected early in the patient's cancer journey.

Acknowledgement. The authors of this work would like to acknowledge the NSF I/UCRC Center for Healthcare Organization Transformation (CHOT), NSF I/UCRC award #1624727 and in part by Susan G. Komen Foundation for funding this research. Any opinions, findings, or conclusions found in this paper are those of the authors and do not necessarily reflect the views of the sponsors.

Data Availability. The SEER cancer registry is made available through the NCI and the process to access the data along with the documentation is provided at https://seer.cancer.gov/data/.

References

1. National Cancer Institute (NCI): 'Cancer Stat Facts: Cancer of Any Site' (2019). https://seer.cancer.gov/statfacts/html/all.html
2. National Cancer Institute (NCI): 'SEER Cancer Stat Facts: Breast Cancer' (2019). https://seer.cancer.gov/statfacts/html/breast.html
3. Susan G. Komen: 'Breast Cancer Statistics' (2020). https://www.komen.org/breast-cancer/facts-statistics/breast-cancer-statistics/
4. National Cancer Institute (NCI), National Institutes of Health (NIH): 'Cancer Statistics' (2019), Available: https://www.cancer.gov/about-cancer/understanding/statistics
5. Luke, M., et al.: Imaging patterns predict patient survival and molecular subtype in glioblastoma via machine learning techniques. Neuro-Oncol. 18(3), 417–425 (2015)
6. Mingjie, Q., Pathak, J., Pereira, N.L., Zhai, C.: Temporal reflected logistic regression for probabilistic heart failure survival score prediction. In: 2017 IEEE International Conference on Bioinformatics and Biomedicine (BIBM), pp. 410–416. IEEE (2017)
7. Marshall, A.H., Hill, L.A., Kee, F.: Continuous dynamic bayesian networks for predicting survival of ischaemic heart disease patients. In: 2010 IEEE 23rd International Symposium on Computer-Based Medical Systems (CBMS), pp. 178–183. IEEE (2010)
8. Zhang, H., Hung, C.-L., Chu, W.C.-C., Chiu, P.-F., Tang, C.Y.; Chronic kidney disease survival prediction with artificial neural networks. In: 2018 IEEE International Conference on Bioinformatics and Biomedicine (BIBM), pp. 1351–1356. IEEE (2018)
9. Bellot, A., Van der Schaar, M.: A hierarchical bayesian model for personalized survival predictions. IEEE J. Biomed. Health Inform. 23(1), 72–80 (2018)
10. Gray, E., Marti, J., Brewster, D.H., Wyatt, J.C., Hall, P.S.: Independent validation of the PREDICT breast cancer prognosis prediction tool in 45,789 patients using Scottish cancer registry data. Br. J. Cancer **119**(7), 808–814 (2018)
11. Song, K., et al.: Can a nomogram help to predict the overall and cancer-specific survival of patients with chondrosarcoma? Clin. Orthop. Relat. Res. **476**(5), 987 (2018)
12. Lynch Chip, M., et al.: Prediction of lung cancer patient survival via supervised machine learning classification techniques. Int. J. Med. Inform. 108, 1–8 (2017)
13. Said, A.A., Abd-Elmegid, L.A., Kholeif, S., Abdelsamie Gaber, A.: Classification based on clustering model for predicting main outcomes of breast cancer using hyper-parameters optimization. Int. J. Adv. Comput. Sci. Appl. 9(12), 268–273 (2018)
14. Bartholomai, J.A., Frieboes, H.B.; Lung cancer survival prediction via machine learning regression, classification, and statistical techniques. In: 2018 IEEE International Symposium on Signal Processing and Information Technology (ISSPIT), pp. 632–637. IEEE (2018)
15. Hegselmann, S., Gruelich, L., Varghese, J., Dugas, M.: Reproducible survival prediction with SEER cancer data. In: Machine Learning for Healthcare Conference, pp. 49–66 (2018)
16. Naghizadeh, M., Habibi, N.: A model to predict the survivability of cancer comorbidity through ensemble learning approach. Expert Syst. **36**(3), e12392 (2019). Agrawal, Ankit, Sanchit Misra, Ramanathan Narayanan, Lalith Polepeddi, and Alok Choudhary. "A lung cancer outcome calculator using ensemble data mining on SEER data." In Proceedings of the tenth international workshop on data mining in bioinformatics, pp. 1–9. 2011
17. Dai, D., Jin, H., Wang, X.: Nomogram for predicting survival in triple-negative breast cancer patients with histology of infiltrating duct carcinoma: a population-based study. Am. J. Cancer Res. **8**(8), 1576 (2018)

18. Imani, F., Chen, R., Tucker, C., Yang, H.: Random forest modeling for survival analysis of cancer recurrences. In: 2019 IEEE 15th International Conference on Automation Science and Engineering (CASE), pp. 399–404. IEEE (2019)
19. Kleinlein, R., Riano, D.: Persistence of data-driven knowledge to predict breast cancer survival. Int. J. Med. Inform. **129**, 303–311 (2019)
20. Shukla, N., Hagenbuchner, M., Win, K.T., Yang, J.: Breast cancer data analysis for survivability studies and prediction. Comput. Methods Program. Biomed. 155, 199–208 (2018)
21. SEER Program, National Cancer Institute (NCI): 'SEER Incidence Data, 1975–2017' (2019), Available: https://seer.cancer.gov/data/
22. McCulloch, W.S., Pitts, W.: A logical calculus of the ideas immanent in nervous activity. Bull. Math. Biophys. **5**(4), 115–133 (1943)
23. Rumelhart, D.E., Hinton, G.E., Williams, R.J.: Learning internal representations by error propagation. No. ICS-8506. California Univ San Diego La Jolla Inst for Cognitive Science (1985)
24. Hochreiter, S., Schmidhuber, J.: Long short-term memory. Neural Comput. **9**(8), 1735–1780 (1997)
25. Fukushima, K.: Neocognitron: a self-organizing neural network model for a mechanism of pattern recognition unaffected by shift in position. Biol. Cybern. **36**(4), 193–202 (1980)
26. Lundberg, S.M., Lee, S.-L.: A unified approach to interpreting model predictions. In: Advances in Neural Information Processing Systems, pp. 4765–4774 (2017)
27. Ribeiro, M.T., Singh, S., Guestrin, C.: Why should i trust you? Explaining the predictions of any classifier. In: Proceedings of the 22nd ACM SIGKDD International Conference on Knowledge Discovery and Data Mining, pp. 1135–1144 (2016)
28. Shrikumar, A., Greenside, P., Kundaje, A.: Learning important features through propagating activation differences. In: Proceedings of the 34th International Conference on Machine Learning, vol. 70, pp. 3145–3153 (2017)
29. Štrumbelj, E., Kononenko, I.: Explaining prediction models and individual predictions with feature contributions. Knowl. Inf. Syst. **41**(3), 647–665 (2013)
30. Lipovetsky, S., Conklin, M.: Analysis of regression in game theory approach. Appl. Stoch. Model. Bus. Ind. **17**(4), 319–330 (2001)
31. Datta, A., Sen, S., Zick, Y.: Algorithmic transparency via quantitative input influence: theory and experiments with learning systems. In: 2016 IEEE Symposium on Security and Privacy (SP), pp. 598–617. IEEE (2016)
32. Bach, S., Binder, A., Montavon, G., Klauschen, F., Müller, K.-R., Samek, W.: On pixel-wise explanations for non-linear classifier decisions by layer-wise relevance propagation. PloS ONE **10**(7), e0130140 (2015)
33. Friedman, J.H.:Greedy function approximation: a gradient boosting machine. Ann. Stat. **29**, 1189–1232 (2001)
34. Travis, E.O.: A guide to NumPy. Trelgol Publ (2006)
35. McKinney, W.: Data structures for statistical computing in python. In: Proceedings of the 9th Python in Science Conference, vol. 445, pp. 51–56 (2010)
36. Pedregosa, F., et al.: Scikit-learn: machine learning in Python. J. Mach. Learn. Res. 12, 2825–2830 (2011)
37. Abadi, M., et al.: Tensorflow: a system for large-scale machine learning. In: 12th USENIX Symposium on Operating Systems Design and Implementation (OSDI 16), pp. 265–283 (2016)
38. Chollet, F., et al.: Keras (2015). https://github.com/fchollet/keras
39. Hunter, J.D.: Matplotlib: a 2D graphics environment. Comput. Sci. Eng. **9**(3), 90–95 (2007)
40. Harsha, N., Jenkins, S., Koch, P., Caruana, R.: Interpretml: a unified framework for machine learning interpretability. arXiv preprint arXiv:1909.09223 (2019)

Should Managers Care About Intra-household Heterogeneity?

Parneet Pahwa(✉), Nanda Kumar, and B. P. S. Murthi

Naveen Jindal School of Management, The University of Texas at Dallas,
800 W. Campbell Road, Richardson, TX 75080, USA
parneet.pahwa@utdallas.edu

Abstract. In this study we seek to study the implications of ignoring intra-household heterogeneity in choice models estimated using scanner data. Using a unique data set that identifies choices made by individual customers within a household, we estimate multinomial choice models at the household level with and without incorporating intra-household heterogeneity using the Markov Chain Monte Carlo (MCMC) procedures. We find that the estimates obtained at the customer level are significantly different from those obtained at the household level. We use the estimates obtained at the household and customer level to conduct a policy simulation to target households with a promotion. We find that using customer level estimates to target households with a promotion results in significantly higher profits relative to targeting based on household level estimates which ignores intra-household heterogeneity.

Keywords: Discrete choice · Markov Chain Monte Carlo · Intra-household heterogeneity · Data driven decision making

1 Introduction

Much of the extant empirical work on understanding consumers' brand choice has used household level scanner panel data to estimate models. Since the seminal work of [9], numerous studies have developed great insights into household purchasing behavior regarding their response to marketing mix variables, variety seeking, use of reference prices, and more recently, policy simulations. A well-known limitation of these models is that households may have multiple decision makers, each of whom may exhibit brand preferences and marketing mix sensitivities that are distinct from other decision maker(s) within the household. This is commonly referred to as intra-household heterogeneity or within household heterogeneity. While advances have been made with respect to modeling inter-household unobserved heterogeneity, little is known about the effects of intra-household heterogeneity.

The research issue that we seek to address here is whether models estimated at the individual customer level would yield significantly different insights from those estimated at the household level. Further, if these insights are different, what is the magnitude of the difference and what impact does it have on managerial actions. For

R. Qiu et al. (Eds.): ICSS 2021, LNOR, pp. 23–30, 2021.
https://doi.org/10.1007/978-3-030-90275-9_2

example, if one individual within a household has higher price sensitivity relative to another member in the household, how would a manager target the household with promotional offers? Purchase decisions are typically made at an individual customer level, but scanner data usually records only household level purchases. This limitation has prevented researchers from properly understanding the above issues.

In this study, we seek to investigate the above important issues using a unique proprietary dataset that identifies which individual customer within a household made the purchase on a given occasion, based on their use of a store reward card. The rich data allows us to estimate brand choice models both at the individual level and at the household level and compare the estimates. To achieve this objective, we estimate random coefficient multinomial logit models using Markov Chain Monte Carlo (MCMC) methods popularized in the literature by [1, 18] and many others. We obtain parameters of interest for each individual customer as well as for each household that comprises of two individual decision makers. We estimate the models for the frozen meals product category.

Using the parameters, we address the issues pertaining to the effects of using household level estimates instead of individual level estimates. Specifically, we ask: which households would a manager target for offering promotional deals; would the same households be targeted if individual estimates were available instead of household estimates and most importantly what implications do these have on profits?

We find that brand preferences and price sensitivities are significantly different between household- and individual- level models. Note that random coefficient models are capable of capturing a fair amount of inter-household variation in parameters due to unobserved variables in the model. In spite of including these controls, the differences in parameters are significant. We find that targeting based on individual level estimates can significantly increase profits relative to targeting based on household level estimates. In the frozen meals category, depending on the brand, the increase in profits ranges from 11%-61%. We also find that targeting the frequent shopper in the household with a promotion does not always result in higher profits relative to targeting households with a promotion based on household level estimates. We believe that these results have important managerial implications.

2 Literature Review

The availability of grocery scanner data at the household level led to a number of developments in brand choice models. The revolution was started by [9] who used multinomial logit models to predict brand choice and understand the effect of marketing mix variables such as price changes and promotions. Subsequent research focused on the importance of accounting for unobserved heterogeneity using random coefficients models [4, 8], latent class models [10], semiparametric approaches [4], and mixture models [3, 12]. The use of multinomial probit models was popularized by [15] that allowed for random coefficients and provided greater flexibility in modeling correlation in error terms of different brands.

Subsequent research focused on understanding variety seeking and inertial behavior of households using scanner data ([5–7, 16, 17]). These models typically incorporated

a state dependence parameter that captured the effect of past purchase of a brand on the current utility of the brand. The above papers find evidence of inertial behavior (or positive state dependence) in a number of frequently purchased packaged goods.

Consistent with the above literature, we estimate a random coefficient multinomial logit brand choice model using MCMC techniques. In the consumer's utility function, we allow for state dependence, in addition to brand preferences and price. This specification will permit us to test whether the response to price promotion is different in models that use household data relative to models that use individual data. With the exception of [2] who examine the effects of intra-household heterogeneity on brand choice in frequently purchased product categories, we are unaware of any other study that examines this issue. However, our study differs from [2] in that in their model in the absence of enough observations on an individual consumer in the household the preference parameters of that individual converge to that of the household level parameters. We envision a model in which consumers in a household are either frequent or infrequent shoppers, whose preference parameters are drawn from different hyper priors rather than a prior common to the household. So, in the absence of enough observations on an individual in the household the convergence of the individual preference parameters occurs to that of the hyper parameters of the frequent or infrequent shopper rather than to that of the individual household. Consequently, our study contributes to the limited literature on intra-household heterogeneity by adding another level of observed heterogeneity depending on whether the member in the household is a frequent (infrequent) shopper.

3 Data

We use transaction data from a large retail chain, which records each purchase transaction made by an individual customer in each shopping trip over a three-year period from 2009–2012, across many of its stores. In each trip made by a customer, we have information on the *size* of each UPC (in ounces) purchased, the *spending* on that UPC in that trip, the *date/time* of purchase and the *store* that it was purchased from. Each customer in the data set has a unique customer_id which in turn belongs to a unique household_id. Given our objective, we analyze households that have two customers with non-zero spending in the product category. We have complete product description (the brand information) for each UPC only in the frozen meals product category. We use these product descriptions to identify the *brand* and the *size* (in ounces) of the UPC that was purchased by the customer. Using the spending on the UPC and the size of each unit purchased we compute the price per ounce for the chosen brand. In addition to price, we create a variable to control for the effect of customer/households' past brand choice on the current choice. This variable takes a value 1, if the alternative was purchased in the previous choice occasion and is 0 otherwise. This variable serves to capture state dependence in brand choice. Past studies have found evidence of inertial behavior in a number of categories and we wish to test if the result holds for individual level estimates as well.

We restrict our attention in this category to the top six brands which account for 81% of the market share. In the frozen meals category, we have 524 households (1048 customers) making a total of 19,459 choices over the three year period. In Table 1, we

present descriptive statistics for the product category (frozen meals). For proprietary reason we had to mask the identity of the brands.

Table 1. Descriptive statistics

Brand	Banquet	Bird's eye	Healthy choice	Marie	Stouffer's	Weight watchers
Market share	10%	4%	6%	5%	60%	15%
Avg. price/oz ($)	0.13	0.18	0.3	0.24	0.27	0.32

4 Model

To account for intra-household heterogeneity and contrast it with a model which does not, we develop two models. We first consider a model which treats the household as a single decision-making unit and then develop a model which incorporates intra-household heterogeneity by treating consumers within a household as different decision-making units i.e. we allow for the brand preferences, sensitivity to price and past purchases to be different for consumers within a household.

The utility specification of the first model that a household, h, treated as a single decision-making unit, derives from choosing alternative j on choice occasion t is:

$$\begin{aligned} &U_{hjt} = X_{hjt}\beta_h + \varepsilon_{hjt}, \\ &h = \{1, 2, \ldots, H\}, j = \{1, 2, \ldots, J\}, t = \{1, 2, \ldots, T_h\} \end{aligned} \tag{1}$$

X_{hjt} contains (J-1) brand dummies, price/oz of the alternative and a dummy variable (to capture state dependence), which takes a value 1 if the alternative was chosen by the household in the previous choice occasion or zero otherwise. We assume that the error, ε_{hjt} has an extreme value distribution.

In our second model, to recognize that individual customers within a household may make trips on different occasions and that their preferences may be distinct from the other decision maker in the household we modify the utility function in Eq. (1) as follows:

$$\begin{aligned} &U_{hjt} = \left(X_{h1jt}\beta_{h1}\right)f_{h1t} + \left(X_{h2jt}\beta_{h2}\right)(1 - f_{h1t}) + \varepsilon_{hjt}, \\ &h = \{1, 2, \ldots, H\}, j = \{1, 2, \ldots, J\}, t = \{1, 2, \ldots, T_h\} \\ &f_{h1t} = 1, \text{ if frequent shopper in household } h \text{ buys at } t \\ &= 0, \text{ otherwise} \end{aligned} \tag{2}$$

An important distinction of this model from our base model in Eq. (1) is that in this model we recognize who in the household makes the shopping trip and we allow for the preferences to be heterogeneous across the customers in a given household. The dummy variable, f_{h1t} in Eq. (2) takes into account which customer in the household makes the shopping trip. So, for instance if the frequent shopper in household h makes the brand

choice decision in choice occasion t, then f_{h1t} takes a value 1 and takes a value zero if the infrequent shopper in household h makes the brand choice decision. Note that the brand preferences, sensitivities to price and the brand bought on the previous occasion, β_{h1} and β_{h2} are specific to the decision maker (customer) on that choice occasion. We estimate this model to obtain $\beta_h = \begin{bmatrix} \beta_{h1} \\ \beta_{h2} \end{bmatrix}$ which yields the preferences and sensitivities to marketing mix variables of both customers in each household. We obtain the household level parameters and obtain individual parameters for each household using Bayesian estimation procedures suggested by [1]. We describe this estimation procedure below.[1]

5 Results

In Tables 2a and 2b, we report the estimated posterior means of the preference parameters and the diagonal elements of the covariance matrix ($\hat{A}$ and $\hat{D}$) obtained from the models in Eqs. (1) and (2) respectively. As mentioned earlier, in frozen meals we have five brand dummies, the price coefficient and the state dependence parameter. Not surprisingly the model that incorporates intra-household heterogeneity has better fit. More importantly, from Table 2a, we can see that relative to the base brand Bird's Eye, on average Stouffer's is the most preferred and Banquet is the least preferred.

Table 2a. Estimates for Frozen Meals without intra-household heterogeneity

	A		Heterogeneity	
	Estimate	SE	Estimate	SE
Stouffer	3.16	0.14	2.85	0.49
Weight	0.70	0.21	7.60	1.14
Healthy	0.07	0.23	4.57	0.80
Marie	−0.16	0.21	5.05	0.77
Banquet	−0.67	0.20	7.66	0.98
Price	−5.37	0.72	56.38	10.99
Loyalty	1.56	0.04	0.36	0.05
Simulated likelihood			−12895	
AIC			25804	
BIC			25871.6	

The estimates of the variance suggest that there is substantial heterogeneity across households in brand preferences. The estimate of the price coefficient is −5.37 and the standard deviation is $\sqrt{56.38} = 7.50$, implying that there is a lot of heterogeneity across

[1] We use the standard MCMC estimation procedure to obtain the individual household level and customer level estimates.

Table 2b. Estimates for Frozen Meals with intra-household heterogeneity

	Frequent shopper				Infrequent shopper			
	A		Heterogeneity		A		Heterogeneity	
	Estimate	SE	Estimate	SE	Estimate	SE	Estimate	SE
Stouffer	3.46	0.17	3.98	0.58	3.15	0.18	3.78	0.82
Weight	0.85	0.24	9.39	1.20	0.19	0.26	7.08	1.09
Healthy	0.24	0.21	5.38	0.81	−0.11	0.26	5.69	1.16
Marie	0.08	0.21	5.75	0.99	−1.74	0.47	12.55	3.70
Banquet	−0.63	0.23	8.40	1.45	−0.82	0.25	9.90	1.65
Price	−6.37	0.66	53.96	13.73	−3.45	0.61	27.04	8.56
Loyalty	1.54	0.05	0.46	0.06	1.52	0.09	0.60	0.10
simulated likelihood			−12800					
AIC			25628					
BIC			25763.3					

households in their price sensitivity. Consistent with prior research, we find evidence of positive state dependence (or inertia) in purchase decisions over time at the household level. We observe that there is a smaller variance across households associated with the state dependence parameter. In Table 2b we report the estimates, $\hat{A}$ and $\hat{D}$ for the frequent and infrequent shoppers in the household. First, note that on average the brand preferences and sensitivity to price frequent and infrequent shopper in the household are quite different. For instance, frequent shopper is more price sensitive on average and has a stronger preference for brand Stouffer and while the infrequent shopper has a stronger dislike for Marie relative to the frequent shopper. The state dependence parameter estimate is almost the same for the two customers in the household and is close to the value in the model that does not incorporate intra-household heterogeneity. This suggests that customers within a household also exhibit inertia in their purchase decisions over time.

Comparison of the estimates in Tables 2a and 2b reveals that on average the brand preferences and sensitivity to price of the customers within a household are significantly different from the estimates obtained in the household level model. The price sensitivity of the frequent shopper in the household is almost −6.37 while the household level estimate is −5.37, which is approximately 19% higher while that of the infrequent shopper in the household is −3.45 which, is almost 36% lower than the household level estimate.

6 Managerial Implications

In this section we illustrate the difference in targeting implications based on household and customer level estimates. For the purpose of this illustration, we assume that a manager wants to run a promotion and target households with a discount. Given the

differences in household and customer level estimates, we expect that there will be a difference in profit between the two methods of targeting. However, our interest is in assessing the magnitude of difference in profit.

Table 3. Profitability of Targeting Households with and without recognizing intra-household heterogeneity

Brand	Profits based on HH level estimates	Number of HH targeted with a Promo using HH estimates	Profits based on Individual level estimates	Number of HH targeted with a Promo using Individual level estimates	Profit Difference
Stouffers	51.59	55	72.6	50	41%
Weight Watchers	40.49	165	56.39	69	39%
Healthy Choice	58.9	344	75.68	293	28%
Marie	52.36	277	84.4	308	61%
Banquet	1109.93	36	1226.77	20	11%
Bird's Eye	150.59	345	189.46	295	26%

To demonstrate the magnitude of the differences we segment and target households based on the estimates of the parameters obtained by the two models. We conduct this targeting exercise for each of the six brands and in so doing a household is targeted with a 10% price discount off the average price of the brand (while holding the price of all other brands at their average prices) if the profits from the discounted price exceeds that from the undiscounted price. Since, the parameter estimates obtained from the two models are different, the number of households targeted based on household estimates are different from those targeted using the customer level estimates.[2] Table 3 illustrates the difference in profits from targeting households based on estimates from recognizing intra-household heterogeneity with that from estimates that do not.

We would like to note that profits of all six brands are higher when individual level estimates are used to target households with a promotional discount. The difference in profits is substantially higher ranging from 11–61%. More interestingly, with the exception of one brand the increase in profits results from targeting fewer households with a promotion suggesting that promotions based on household level estimates may overestimate the efficacy of promotions relative to customer level estimates. We also explore the drivers of these differences in detail and whether targeting frequent shoppers in a household with a promotion leads to higher profits.[3]

7 Conclusion

In this paper, we study the importance of estimating brand choice models at the individual level, since the purchase decisions are made by individual shoppers. Prior research has

[2] Variable costs of the brands are assumed to be 80% of the average price.

[3] We are unable to provide these details in this version of the paper.

been unable to assess this issue since they relied on household level grocery scanner panel data. We find that the estimates obtained at the individual customer level are significantly different from those obtained at the household level. More importantly, our findings imply that targeting promotions based on customer level estimates result in smarter promotional decisions and higher profits relative to those based on household model estimates. Furthermore, the magnitude of these differences cannot be ignored in an industry that operates on razor thin margins.

References

1. Allenby, G.M., Rossi, P.E.: Marketing models of consumer heterogeneity. J. Econom. **89**, 57–78 (1999)
2. Bruno, HA., Cebollada, J., Chintagunta, P.K.: Targeting Mr. or Mrs. Smith: modeling and leveraging intrahousehold heterogeneity in brand choice behavior, **37**(4), 507–684
3. Bucklin, R.E., Lattin, J.M.: A two state model of purchase incidence and brand choice. Marketing Sci. Winter **10**(1), 24–39 (1991)
4. Chintagunta, P.K., Jain, D.C., Vilcassim, N.J.: Investigating heterogeneity in brand preferences in logit models for panel data. J. Mark. Res. **28**(November), 417–428 (1991)
5. Dube, J.P., Hitsch, G.J., Rossi, P.E.: State dependence and alternative explanations for consumer inertia. RAND J. Econ. **41**(3), 417–445 (2010)
6. Erdem, T.: A dynamic analysis of market structure based on panel data. Mark. Sci. **15**(4), 359–378 (1996)
7. Givon, M.: Variety seeking through brand switching. Mark. Sci. **3**(1), 1–22 (1984)
8. Gonul, F., Srinivasan, K.: Modeling unobserved heterogeneity in multinomial logit models: methodological and managerial implications. Mark. Sci. **12**, 213–229 (1993)
9. Guadagni, P.M., Little, J.D.C.: A logit model of brand choice. Mark. Sci. **2**(Summer), 203–238 (1983)
10. Kamakura, W., Russell, G.: A probabilistic choice model for market segmentation and elasticity structure. J. Mark. Res. **26**(November), 379–390 (1989)
11. McCulloch, R.E., Rossi, P.E.: An exact likelihood analysis of the multinomial probit model. Journal of Econometrics **64**, 207–240 (1994)
12. Murthi, B.P.S., Srinivasan, K.: Consumers' extent of evaluation in brand choice. J. Bus. **72**(2), 229–256 (1999)
13. Rossi, P., Allenby, G.: A Bayesian approach to estimating household parameters. J. Mark. Res. **30**(2), 171–182 (1993)
14. Rossi, P.E., McCulloch, R.E., Allenby, G.M.: The value of purchase history data in target marketing. Mark. Sci. **15**(4), 321–340 (1996)
15. Rossi, P., Allenby, G.: Bayesian statistics and marketing. Mark. Sci. **22**(3), 304–328 (2003)
16. Seetharaman, P.B., Ainslie, A.K., Chintagunta, P.K.: Investigating household state dependence effects across categories. J. Mark. Res. **36**(4), 488–500 (1999)
17. Seetharaman, P.B., Chintagunta, P.K.: A model of inertia and variety-seeking with marketing variables. Int. J. Res. Mark. **15**, 1–17 (1998)
18. Train, K.: "Discrete Choice Methods with Simulation, 2nd edn. Cambridge University Press (2009)

Penalizing Neural Network and Autoencoder for the Analysis of Marketing Measurement Scales in Service Marketing Applications

Toshikuni Sato(✉)

Department of Business Administration, Ishinomaki Senshu University, Ishinomaki, Miyagi 986-8580, Japan
tsato@isenshu-u.ac.jp

Abstract. This paper discusses penalized neural networks to establish a stable neural network model for survey data measured by traditional marketing scales. Interpreting estimated hidden units and weights in a neural network is often challenging because of its non-identifiability. Factor models in social science are a traditional non-identifiable model for analyzing questionnaire measurements. Hence, many studies have proposed identification conditions. Accordingly, we propose penalty functions that represent the equivalent identification conditions in standard factor models to reduce the non-identifiability and instability of neural networks. We apply these penalty functions in the empirical analysis of autoencoders with e-service quality scale data. The proposed method provides an explainable result that is theoretically reasonable in that e-service quality scale. While comparing the penalized autoencoder with traditional factor models, we discuss potential applications and tasks of the proposed method in service marketing research for further exploration.

Keywords: Stable neural network · Identifiability · Interpretability · Latent variable model · Construct measurements

1 Introduction

Artificial intelligence technology and machine learning (ML) topics have been discussed on various contexts in service industry and marketing areas, e.g., data analytics, customer engagement, job replacement issues, B2B service work, and customization [1–5]. Actual ML models, such as neural network and deep learning, are often referred to as a black box model because they provide humans difficult interpretations. Thus, many interpretation methods have been developed to achieve explainable models and results [6]. ML has become one of the commonly used methods for analyzing large-scale and unstructured data in various service domains. For example, the deep learning method, namely, natural language processing with word embeddings, is applied in user behavior modeling and sentiment analysis with textual data [7, 8]. However, the instability of neural network models is an additional issue related to the interpretability of ML [9–13].

R. Qiu et al. (Eds.): ICSS 2021, LNOR, pp. 31–42, 2021.
https://doi.org/10.1007/978-3-030-90275-9_3

In general, estimated weight parameters and hidden units (features) will be changed when learning a standard neural network even with the same data and network structure. Although such learning can achieve similar prediction accuracy, the model interpretation may be unexpectedly changed in each learning time. The instability issue is a natural property because the neural network is a non-identifiable model, which may not be a serious problem in forecasting tasks. Model identification in social sciences is very important to interpret the model and parameters. As a result, non-identifiable models, such as factor models, have been frequently discussed in related research areas [14–16]. Weight decay or regularization [17, 18] is also a known method for reducing the instability of neural networks, whereas we consider the extension of traditional factor model framework for establishing a stable neural network.

This paper presents a simple method for reducing the instability of neural networks by applying the typical identification conditions of the factor model. We focus only on the autoencoder because the factor model is an unsupervised model. Nevertheless, the discussions in this paper can be extended to various types of neural network and deep learning. The remainder of this paper is organized as follows. Section 2 presents a review of the necessary foundations of autoencoders and factor models. Section 3 explains our proposed method. The empirical application partially follows [19]'s e-service quality scale as one of the traditional service marketing scales. Then, Sect. 4 provides a comparison between the proposed models and traditional factor models. Lastly, Sects. 5 and 6 discuss the empirical analysis results and summarize the limitations and potential applications for future research, respectively.

2 Background

We briefly review a standard autoencoder [20, 21] and standard factor model [14, 15]. Their relationship is also presented according to [22] to understand the interpretation of autoencoders in line with the aspect of the traditional latent variable models.

2.1 Autoencoder

Suppose that $\boldsymbol{x}$ is a $(p \times 1)$ vector of inputs and that θ is a set of all parameters in the model. A standard autoencoder defines a mapping $\boldsymbol{x} = f(\boldsymbol{x}; \theta)$. Thus, the model aims to approximate its outputs. For instance, Fig. 1 shows the path diagram of the autoencoder with one hidden layer. Hence, the model is defined as follows:

$$\begin{aligned} \boldsymbol{x} &= \underset{(p\times q)}{\mathrm{W}}{}^{(2)}\boldsymbol{z}^{(1)} + \underset{(p\times 1)}{\boldsymbol{b}}{}^{(2)}, \\ \boldsymbol{z}^{(1)} &= f^{(1)}\left(\boldsymbol{u}^{(1)}\right), \\ \boldsymbol{u}^{(1)} &= \underset{(q\times p)}{\mathrm{W}}{}^{(1)}\boldsymbol{x}^{(0)} + \underset{(q\times 1)}{\boldsymbol{b}}{}^{(1)}, \end{aligned} \tag{1}$$

where the superscripts indicate the place of the layer or hidden layer, $\boldsymbol{W}$ is a matrix of weight parameter, $\boldsymbol{b}$ is a vector of bias (or constant or intercept) parameter, f is an activation function, $\boldsymbol{z}$ is a $(q \times 1)$ vector of a hidden unit, and a $(q \times 1)$ vector $\boldsymbol{u}$ is a

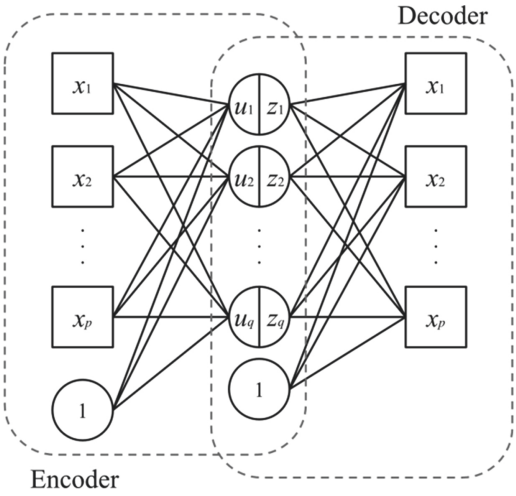

Fig. 1. Path diagram of autoencoder

latent variable before transformed by the activation function. Figure 1 and Eq. (1) show that the input and output stages corresponding to the third and first equations are called encoder and decoder, respectively.

We refer to $\boldsymbol{u}$ as hidden unit scores, whose restriction is one of the important points in this study. Because the hidden unit score is a latent variable, its variance can take an arbitrary positive value. Additionally, the magnitudes of the weight parameter depend on the magnitudes of variance for hidden unit score. These are known as indeterminacy of the solutions in the factor model [14, 22]. As discussed in Sect. 3, the variance of latent variable (factor score) is generally assumed to the unit variance in factor model. This implies that the estimates of weight parameter become standardized solutions by fixing the variance of factor score to 1. Hence, the magnitude of variance for the hidden unit score should be taken into account when comparing among the magnitudes of the weight parameter.

2.2 Relationship Between Factor Model and Autoencoder

One purpose of the autoencoder is dimensionality reduction of multivariate data to obtain lower dimensional latent variables (features), as with principal component analysis (PCA) and factor analysis. Here, we introduce the factor model as a traditional latent variable model; it covers PCA and factor analysis. Although both analyses have slightly different error term assumption [23], they are closely similar and related to autoencoder. The factor model is defined as follows:

$$\boldsymbol{x} = \boldsymbol{W}\boldsymbol{u} + \boldsymbol{b} + \boldsymbol{e}, \tag{2}$$

where $\boldsymbol{W}$ is a $(p \times q)$ matrix of factor loading, $\boldsymbol{u}$ is a vector of factor scores, and $\boldsymbol{b}$ is a vector of intercepts. In the autoencoder (Eq. 1), these correspond to the weight parameter, hidden unit scores, and bias parameter, respectively. Here, we emphasize that the hidden unit score corresponds to the factor score. Additionally, $\boldsymbol{e}$ is a $(p \times 1)$ vector of an error

term assumed as $E[\boldsymbol{e}] = \mathbf{0}$ and $E\left[\boldsymbol{ee'}\right] = \text{diag}\left\{\psi_1, \psi_2, \ldots, \psi_p\right\}$ in the standard factor analysis. Although probabilistic PCA assumes $E\left[\boldsymbol{ee'}\right] = \psi \boldsymbol{I}_p$[23], the standard PCA factor model assumes that $E\left[\boldsymbol{ee'}\right]$ is not a diagonal matrix [15]. In contrast to these specifications, PCA defines the weighted sum of observed variables $\boldsymbol{U} = \boldsymbol{XW}$ [22], where $\mathbf{U} = \{\boldsymbol{u}_1, \boldsymbol{u}_2, ..., \boldsymbol{u}_N\}$ is a $(N \times q)$ matrix of factor scores (or principle component scores), $\boldsymbol{X} = \{\boldsymbol{x}_1, \boldsymbol{x}_2, ..., \boldsymbol{x}_N\}$ is a $(N \times p)$ matrix of centered dataset with $\mathbf{1}'_N \mathbf{X} = \mathbf{0}_p$, $\mathbf{W}$ is a $(p \times q)$ matrix of factor loading (or weight parameter), and N is the sample size. Then, the PCA optimization as the weighted sum is given as follows:

$$\underset{\mathbf{W'W}=\boldsymbol{I}}{\arg\max} \|\boldsymbol{U}\|_2^2 = \underset{\boldsymbol{W'W}=\boldsymbol{I}}{\arg\max} \|\boldsymbol{XW}\|_2^2 = \underset{\boldsymbol{W'W}=\boldsymbol{I}}{\arg\max} \text{tr}\left\{\boldsymbol{W'X'XW}\right\}. \tag{3}$$

This equation provides the equivalent estimates for $\boldsymbol{W}$ in Eq. (2) with PCA assumption, so that PCA can be expressed as the weighted sum and factor models [22]. Although these two models differ in path diagram as shown in Fig. 2, they equally express the standard PCA.

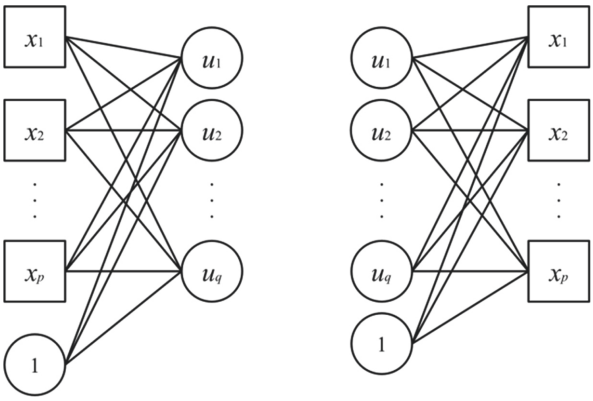

Fig. 2. Path diagrams of principal component analysis for weighted sum (left) and factor (right) models[1]

The PCA and autoencoder have a close relationship [25–27]. The autoencoder with one hidden layer and the linear activation function define the equivalent PCA optimization. To simplify, suppose $\boldsymbol{X} = \{\boldsymbol{x}_1, \boldsymbol{x}_2, ..., \boldsymbol{x}_N\}$ is a $(N \times p)$ matrix of centered dataset, set all bias parameters in $\boldsymbol{b}$ to zero, and substitute $\mathbf{Z} = \mathbf{U} = \mathbf{X}\boldsymbol{W'}^{(1)}$ to the decoder stage in Eq. (1). Then, we can rewrite the autoencoder model as follows:

$$\underset{(p\times q)}{\boldsymbol{X}} = \underset{(p\times q)}{\mathbf{X}}\ \underset{(q\times p)}{\boldsymbol{W'}^{(1)}}\ \boldsymbol{W'}^{(2)}. \tag{4}$$

To estimate the weight parameter in the autoencoder model, the following equation is optimized:

$$\underset{\boldsymbol{W}^{(2)}\boldsymbol{W'}^{(1)}=\boldsymbol{I}}{\arg\min} \left\|\boldsymbol{X} - \mathbf{X}\boldsymbol{W'}^{(1)}\boldsymbol{W'}^{(2)}\right\|_2^2 \tag{5}$$

[1] Note: Figure 2 displays only the relationship between observed variables and factor scores.Additionally, the intercept is assumed to be equal to zero in the usual case.

Additionally, if we assume $\boldsymbol{W'}^{(1)} = \boldsymbol{W}^{(2)} = \boldsymbol{W}$, i.e., weight-sharing (weight-tying) [26], then Eq. (5) is rewritten as follows:

$$\begin{aligned} \underset{\boldsymbol{W'W}=\boldsymbol{I}}{\arg\min} \left\| \boldsymbol{X} - \mathbf{X}\boldsymbol{W}\boldsymbol{W'} \right\|_2^2 &= \underset{\mathbf{W'W}=\boldsymbol{I}}{\arg\min} \left\{ \mathrm{tr}\left(\boldsymbol{X'X}\right) - \mathrm{tr}\left(\mathbf{W'}\boldsymbol{X'}\boldsymbol{X}\mathbf{W}\right) \right\} \\ &\cong \underset{\mathbf{W'W}=\boldsymbol{I}}{\arg\max} \, \mathrm{tr}\left\{ \mathbf{W'}\boldsymbol{X'}\boldsymbol{X}\mathbf{W} \right\}. \end{aligned} \tag{6}$$

This is one of the expressions for the PCA optimization so that Eq. (3) can be obtained by calculating the first equation as shown in Eq. (6) [22]. These results imply that the autoencoder contains the weighed sum and factor models for PCA. The encoder stage expresses the weighted sum model, whereas the decoder stage reflects the factor model. Comparing Figs. 1 and 2 also provides visual understanding of this insight. Therefore, the above discussions interpret the autoencoder as either the weighted sum or factor models. Section 3 below introduces our proposed method considering these traditional aspects.

3 Proposed Method

The factor model and other latent variable models, such as the latent Dirichlet allocation, are usually non-identifiable, so that the identification is often a common problem in latent variable models [24]. To reduce the non-identifiability in the factor model in Eq. (2), the following identification conditions are assumed [14, 15]:

$$\frac{1}{N}\boldsymbol{U'U} = \boldsymbol{I}_q, \tag{7}$$

$$\underset{(q\times p)}{\mathbf{W}'} \underset{(p\times q)}{\mathbf{W}} - \mathrm{diag}\{ \underset{(q\times p)}{\mathbf{W}'} \underset{(p\times q)}{\mathbf{W}} \} = 0 \ (\mathbf{W'W} \text{ is a diagonal matrix}). \tag{8}$$

These constraints provide stable estimates for the factor model, except the sign flips instability. For unrestricted factor score, the identification condition is given as follows [15]:

$$\underset{(p\times q)}{\boldsymbol{W}} = \left(\boldsymbol{I}_q, \boldsymbol{W}_2'\right)', \tag{9}$$

where $\boldsymbol{W}_2$ is a $((p-q)\times q)$ sub-matrix of $\boldsymbol{W}$. We adopt these constraints into the autoencoder estimation and extend a penalized neural network.

In ML, the penalization typically indicates a regularization, such as L1 (LASSO) or L2 (Ridge) norms for the weight parameters and output hidden units [20]. Similar to these methods, we add the penalties for the weight parameter and hidden unit score based on the above conditions. Suppose that N^* is an input sample size or batch size and that M^* is a set of the numbers of penalized layers. Then, we define the penalty functions for Eqs. (7) and (8) as follows:

$$Loss_{U:identity}(\boldsymbol{U}) = \frac{1}{2} \sum_{k\in M^*} \left\| \frac{1}{N^*}\boldsymbol{U'}^{(k)}\boldsymbol{U}^{(k)} - \boldsymbol{I}_{q(k)} \right\|_2^2. \tag{10}$$

$$Loss_{W:diag}(\boldsymbol{W}) = \frac{1}{2}\sum_{k\in M^*}\left\|\boldsymbol{W'}^{(k)}\boldsymbol{W}^{(k)} - \boldsymbol{W'}^{(k)}\boldsymbol{W}^{(k)}I_{q(k)}\right\|_2^2, \tag{11}$$

where the dimension of $\boldsymbol{W}^{(k)}$ is the number of inputs multiplied by the number of outputs in the k th layer. Additionally, the penalty function for Eq. (9) is given as follows:

$$Loss_{W:upper\ identity}(\boldsymbol{W}) = \frac{1}{2}\sum_{k\in M^*}\left\|\boldsymbol{W}^{(k)} - \left(I_{q(k)}, \boldsymbol{W'}_2^{(k)}\right)'\right\|_2^2 \tag{12}$$

Finally, the total loss functions for the proposed models are added to the above penalty functions. For instance, the total loss function of the autoencoder with Eqs. (10) and (11) is defined as follows:

$$E(\theta) = \frac{1}{N^*}\sum_{i=1}^{N^*} Loss\left(\boldsymbol{x}_i, \hat{\boldsymbol{x}}_i\right) + \lambda_1 Loss_{U:identity}(\boldsymbol{U}) + \lambda_2 Loss_{W:diag}(\boldsymbol{W}), \tag{13}$$

where λ_1 and λ_2 are hyperparameters. For neural network, we change $Loss\left(\boldsymbol{x}, \hat{\boldsymbol{x}}\right)$ to $Loss\left(y, \hat{y}\right)$ in Eq. (13), where y is a target variable. The standard backpropagation algorithm can be adapted with SGD, Adam, etc. Here, we introduce an additional penalty function for a candidate model as follows:

$$Loss_{U:corr}(\boldsymbol{U}) = \frac{1}{2}\sum_{k\in M^*}\left\|\mathrm{diag}\left\{\frac{1}{N^*}\boldsymbol{U'}^{(k)}\boldsymbol{U}^{(k)}\right\} - I_{q(k)}\right\|_2^2. \tag{14}$$

Equation 14 is used to approximate the correlation matrix between the hidden unit scores. Hence, we use this penalty function rather than Eq. (10) for a comparison with the correlated factor model.

4 Empirical Analysis

4.1 Data Collection

Data were collected on March 12–16, 2021, through a Japanese marketing research company that helps conduct an online survey for membership users in Japan. Following [19]'s procedure, participants were screened to ensure that they have at least one purchase from an online retailer in the past 6 months and provide truthful answers about their latest online shopping experience. We prepared 12 items of four latent constructs (website design, fulfillment, customer service, and security/privacy) that represent the main attributes of the e-service quality of online retailers [19]. Table 1 presents the details of these items. All 12 items for the latent constructs use a seven-point Likert scale ("1 = strongly disagree" to "7 = strongly agree"). The sample consists of 334 Japanese customers who purchased goods in the food and drink category[2].

[2] Note: Although the data were gathered from three categories (food and drink, fashion, and daily necessities), we used only one category data (food and drink) due to limitations of space.

Table 1. Measurement of latent constructs

Website design	
WD1	Overall, my experience at the online retailer's website is excellent
WD2	Overall, the quality of the online retailer's website is excellent
WD3	I am generally very satisfied with the website
Fulfillment	
FUL1	Overall, the online retailer's order fulfillment is excellent
FUL2	Overall, the quality of the online retailer's order fulfillment is excellent
FUL3	I am generally very satisfied with the order reliability
Customer service	
CS1	Overall, the online retailer's customer service is excellent
CS2	Overall, the quality of the online retailer's return handling is excellent
CS3	I am generally very satisfied with the customer service
Security/privacy	
SEP1	Overall, the online retailer's handling of data security is excellent
SEP2	Overall, the quality of the online retailer's security is excellent
SEP3	I am generally very satisfied with handling of private information

4.2 Comparative Models and Estimations

We estimate three candidate autoencoder models to compare the PCA, correlated factor analysis, and standard autoencoder with *tanh* (hyperbolic) activation function. The factor analysis adapts promax rotation to contrast the candidate model that assumes correlated hidden unit score. Table 2 presents the details of the candidate models and penalizations.

Model 1 assumes uncorrelated standardized hidden unit scores with linear activation function, whereas Model 2 assumes correlated standardized hidden unit scores. Although the penalties for Model 2 are not enough to identify the autoencoder [16], the weight parameter in Model 2 can be relatively compared by restricting the diagonal elements of the covariance matrix to 1s. Model 3 employs the *tanh* activation function with Eq. (14) and assumes that the weight matrix combined with the row weight vectors corresponding to the first items of each construct equals the identity matrix. This assumption follows the theoretical and empirical relationship of the marketing scale shown by [19]. The standard backpropagation algorithm with Adam (learning rate $= 0.01$) is used to optimize these autoencoder models. In addition, we use weight-sharing between the encoder and decoder weights to easily compare the PCA and factor analysis models. Grid search is conducted for hyperparameter tuning in each penalty function such that each assumption of the penalty functions is satisfied. We set only one hidden layer and four hidden units due to the measurement scale assumptions in Table 1. PCA and factor analysis also estimate four latent variables.

Table 2. Candidate autoencoder models and penalizations

	Equation (10)	Equation (11)	Equation (12)	Equation (14)	Activation
Model 1	Yes	Yes	No	No	Linear
Model 2	No	Yes	No	Yes	Linear
Model 3	No	No	Yes	No	Tanh

4.3 Result

Table 3 shows the result of the hyperparameter tuning of the penalty functions in each model. The sample covariance of the estimated factor scores (hidden unit scores) is reported on the upper side in each block of Table 4. Additionally, we calculate $\boldsymbol{W'W}$ with estimated factor loadings (or weights) and show them on the lower side in each block of Table 4. Table 5 presents the estimated factor loadings and weights. The bold font indicates that the values have an absolute value of more than 0.3.

Table 3. Hyperparameter settings

	Equation (10)	Equation (11)	Equation (12)	Equation (14)
Model 1	100	100	*Null*	*Null*
Model 2	*Null*	100	*Null*	100
Model 3	*Null*	*Null*	100	*Null*

5 Discussion

First, we discuss the validity of our proposed penalty functions. In Table 4, "Tanh AE" provides an uneven covariance and $\boldsymbol{W'W}$ because they are unrestricted. The results may change with the initial learning values. In contrast to "Tanh AE," Model 1 approximately estimates the unit variance matrix and diagonal $\boldsymbol{W'W}$ matrix. Model 2 also satisfies the constraints of Eqs. (11) and (14). Thus, the correlation matrix is approximated rather than the covariance matrix. In addition, Model 3 accurately satisfies the identification condition (Eq. 12) as shown in Table 5. Each row vector of the identity matrix in the weight is placed in the row of the corresponding first items of each construct. Therefore, we find that each penalty function performs well with sufficiently large hyperparameter value (see also Table 3). Here, we note that the exact unit covariance or correlation matrix is not estimated but calculated with the estimated hidden unit scores. Similarly, the covariance matrix provided by factor analysis does not indicate the exact correlation matrix. Additionally, PCA provides a diagonal covariance matrix and $\boldsymbol{W'W} = I$ as the constraints of the standard PCA. In contrast, the correlated factor analysis provides $\boldsymbol{W'W} \neq I$ due to the promax rotation for the factor loading.

Table 4. Penalty validation

	PCA				FA (promax rotation)				Tahn AE			
	F1	F2	F3	F4	F1	F2	F3	F4	F1	F2	F3	F4
Cov.												
F1	8.43	0.00	0.00	0.00	0.96	0.64	0.78	0.77	7.16	7.54	– 5.61	2.92
F2	0.00	1.03	0.00	0.00	0.64	0.96	0.69	0.72	7.54	10.79	– 6.94	3.16
F3	0.00	0.00	0.56	0.00	0.78	0.69	0.88	0.78	5.61	– 6.94	6.20	– 2.67
F4	0.00	0.00	0.00	0.49	0.77	0.72	0.78	0.89	2.92	3.16	– 2.67	3.33
W'W												
F1	1.00	0.00	0.00	0.00	2.75	0.17	0.41	0.37	2.23	0.28	– 0.05	0.08
F2	0.00	1.00	0.00	0.00	0.17	2.46	0.13	0.12	0.28	2.77	– 0.21	– 0.10
F3	0.00	0.00	1.00	0.00	0.41	0.13	1.21	0.20	– 0.05	– 0.21	2.17	– 0.06
F4	0.00	0.00	0.00	1.00	0.37	0.12	0.20	1.11	0.08	– 0.10	– 0.06	1.94
	Model 1				Model 2				Model 3			
	F1	F2	F3	F4	F1	F2	F3	F4	F1	F2	F3	F4
Cov.												
F1	0.81	0.03	– 0.01	– 0.01	1.03	0.89	– 0.80	0.83	5.72	5.81	5.25	4.05
F2	0.03	0.89	– 0.02	0.02	0.89	1.03	– 0.87	0.88	5.81	8.46	6.51	4.65
F3	– 0.01	– 0.02	0.88	0.03	– 0.80	– 0.87	1.04	– 0.68	5.25	6.51	6.90	4.66
F4	– 0.01	0.02	0.03	0.84	0.83	0.88	– 0.68	1.01	4.05	4.65	4.66	5.71
W'W												
F1	1.58	0.00	0.00	0.01	0.37	0.02	– 0.02	0.02	2.16	0.17	0.06	0.17
F2	0.00	0.58	0.00	0.00	0.02	0.38	– 0.01	0.01	0.17	2.68	0.15	– 0.04
F3	0.00	0.00	1.29	0.00	– 0.02	– 0.01	0.47	– 0.01	0.06	0.15	2.33	0.07
F4	0.01	0.00	0.00	2.19	0.02	0.01	– 0.01	0.48	0.17	– 0.04	0.07	2.17

Note: "FA (promax rotation)" and "Tanh AE" indicate the correlated factor analysis with promax rotation and the standard autoencoder with tanh activation function and weight-sharing, respectively.

PCA and Models 1 and 2 provide unclear results for the interpretations of the factor loadings and weights in Table 5. However, we obtain clear factor loading (weight) patterns in the correlated factor analysis and standard autoencoder. Factors 1–5 in the correlated factor analysis indicate fulfillment, security/privacy, website design, and customer service, whereas those in the standard autoencoder indicate website design, fulfillment, customer service, and security/privacy. Moreover, Model 3 categorizes the questionnaire items almost perfectly based on the theoretical relationships. Hence, this finding implies that our proposed penalty functions can be applied to autoencoders while considering the identifiability and theoretical relationship in the analysis of the traditional marketing scale measurements.

Table 5. Factor loadings (weights) estimates

	PCA				FA (promax rotation)				Tanh AE			
	F1	F2	F3	F4	F1	F2	F3	F4	F1	F2	F3	F4
WD1	0.27	0.26	0.06	**– 0.47**	**0.35**	– 0.07	**0.56**	– 0.01	**– 0.83**	**– 0.38**	– 0.25	0.25
WD2	0.27	0.01	0.29	**– 0.59**	0.04	0.11	**0.68**	0.04	**– 0.93**	– 0.13	– 0.29	– 0.06
WD3	**0.30**	0.10	0.13	– 0.26	0.17	0.04	**0.62**	0.13	**– 0.64**	**– 0.31**	– 0.03	0.02
FUL1	0.30	0.28	– 0.26	0.12	**0.86**	0.02	0.07	– 0.01	0.06	**– 0.80**	0.28	0.19
FUL2	**0.30**	0.27	– 0.29	0.10	**0.95**	0.06	0.05	– 0.11	0.10	**– 0.86**	0.23	0.13
FUL3	**0.30**	0.27	– 0.25	0.20	**0.82**	0.01	– 0.03	0.14	0.08	**– 0.72**	**0.36**	0.17
CS1	**0.31**	0.11	0.01	0.22	**0.40**	0.07	0.04	**0.47**	– 0.14	– 0.29	**0.56**	0.05
CS2	0.25	– 0.06	**0.77**	**0.39**	– 0.07	0.07	0.20	**0.59**	**– 0.43**	**0.64**	**1.01**	0.00
CS3	**0.30**	0.10	0.11	**0.30**	**0.31**	0.01	– 0.04	**0.69**	– 0.12	– 0.17	**0.64**	0.02
SEP1	0.28	**– 0.48**	– 0.16	– 0.01	0.01	**0.94**	0.01	0.00	– 0.13	– 0.14	0.10	**– 0.76**
SEP2	0.29	**– 0.46**	– 0.21	– 0.03	0.09	**0.95**	0.01	– 0.07	– 0.07	– 0.23	0.05	**– 0.77**
SEP3	0.28	**– 0.47**	– 0.10	0.01	– 0.03	**0.81**	0.03	0.12	– 0.08	– 0.14	0.11	**– 0.78**

	Model 1				Model 2				Model 3			
	F1	F2	F3	F4	F1	F2	F3	F4	F1	F2	F3	F4
WD1	– 0.08	**0.40**	0.21	**0.50**	**– 0.35**	– 0.07	0.09	0.05	**1.00**	0.00	0.00	0.00
WD2	**– 0.32**	0.23	0.15	**0.81**	– 0.23	0.07	0.22	0.22	**0.86**	0.09	– 0.21	0.16
WD3	0.04	– 0.07	0.22	**0.37**	– 0.15	– 0.16	0.11	0.13	**0.62**	0.23	0.09	0.02
FUL1	0.30	0.13	**0.33**	**– 0.54**	0.04	– 0.10	0.30	– 0.14	0.00	**1.00**	0.00	0.00
FUL2	0.29	0.11	0.25	**– 0.47**	0.15	0.00	**0.30**	– 0.27	0.03	**0.91**	0.09	– 0.10
FUL3	– 0.06	**– 0.30**	**0.42**	0.10	0.04	– 0.18	0.29	0.07	0.01	**0.77**	0.28	– 0.13
CS1	– 0.13	0.04	0.09	**– 0.49**	– 0.11	– 0.16	0.16	– 0.18	0.00	0.00	**1.00**	0.00
CS2	**– 0.93**	0.10	**– 0.39**	**– 0.49**	– 0.26	0.20	– 0.13	– 0.26	0.20	**– 0.36**	**0.85**	0.03
CS3	– 0.15	– 0.17	– 0.26	0.17	– 0.14	**– 0.33**	– 0.08	0.04	0.02	0.21	**0.67**	0.00
SEP1	0.05	**0.43**	0.09	– 0.27	– 0.14	0.10	0.12	**– 0.36**	0.00	0.00	0.00	**1.00**
SEP2	**0.31**	0.12	**– 0.35**	0.03	– 0.13	– 0.18	– 0.15	– 0.24	0.01	0.13	0.07	**0.74**
SEP3	**0.54**	0.07	**– 0.68**	0.18	0.08	– 0.30	– 0.22	– 0.16	0.01	0.06	0.11	**0.75**

Note: "FA (promax rotation)" and "Tanh AE" indicate the correlated factor analy sis with promax rotation and the standard autoencoder with tanh activation function and weight-sharing, respectively.

6 Concluding Remarks

In this paper, we introduced the penalizations for stable and explainable autoencoder based on several identification conditions of the factor model. Our proposed penalty functions constrained the estimates in the autoencoders so that the identification conditions are satisfied. Thus, we conclude that our method can help estimate a robust autoencoder for analyzing marketing scale measurements of theoretical constructs. We aim that the autoencoder and neural network may be available to both theory- and data-driven models in social science research. However, our proposed method has three limitations that need future study. First, the criterion-related validity of the proposed models should be investigated. For example, our future research can use a target variable, such as overall e-service quality or overall satisfaction, to compare the prediction performances between the proposed models. Second, interpreting and comparing the magnitudes of the weight parameter may be challenging when using a nonlinear activation function. Although Model 3 shows the best performance in the empirical analysis, this model does not constrain the covariance matrix of hidden unit scores. We note that the weight parameter does not represent a partial derivative relevant to the hidden unit score due to the nonlinear function. Therefore, approximations with the delta method

or partial dependence estimation may be potential solutions to evaluate the marginal effects of hidden unit score with nonlinear activation function [28, 29]. Additionally, we must examine the effectiveness of constraining the covariance matrix of hidden unit scores. Models 1 and 2 are convenient in comparing the magnitude of weight parameter because these models assume the unit variance of hidden unit score. However, it was difficult to explain the results produced by Models 1 and 2. Third, we implicitly supposed the undercomplete autoencoder model [20] whose hidden unit score dimension is less than the input (observed variable) dimension. Although our empirical analysis uses a small-scale data, the parameter regularization can be adapted to overcomplete and deep autoencoder model with large-scale data [20].

For future research, we plan to investigate the identifiability of neural networks in various situations. Although this paper contains several issues, our proposed method potentially extends the methodology of traditional marketing research. In the service industry area, many companies manage the big data platform and large amount of costumer information. For example, hotel companies can easily access customers' visiting histories and review text data. Our method may be available to analyze these unstructured data combined with traditional marketing measurements and achieve "knowledge fusion" [30] for obtaining a novel insight. These additional tasks will be addressed in our future research.

Acknowledgments. The author gratefully acknowledges the partial support of JSPS KAKENHI Grant Number 20K22125. The author would also like to thank Enago (www.enago.jp) for the English language review. Additionally, the two reviewers involved provided helpful and insightful comments that improved the overall quality of the manuscript, for which the author is thankful.

References

1. de Véricourt, F., Perakis, G.: Frontiers in service science: the management of data analytics services and future directions: New Challenges Serv. Sci. **12**(4), 121–129 (2020)
2. Hollebeek, L.D., Sprott, D.E., Brady, M.K.: Rise of the machines? customer engagement in automated service interactions. J. Serv. Res. **24**(1), 3–8 (2021)
3. Huang, M.H., Rust, R.T.: Artificial intelligence in service. J. Serv. Res. **21**(2), 155–172 (2018)
4. Pemer, F.: Enacting professional service work in times of digitalization and potential disruption. J. Serv. Res. 1094670520916801 (2020)
5. Yoganarasimhan, H.: Search personalization using machine learning. Manag. Sci. **66**(3), 1045–1070 (2020)
6. Fan, F., Xiong, J., Wang, G.: On Interpretability of Artificial Neural Networks: A survey. Preprint at https://arxiv. org/abs/2001.02522 (2020)
7. Boratto, L., Carta, S., Fenu, G., Saia, R.: Using neural word embeddings to model user behavior and detect user segments. Knowl.-Based Syst. **108**, 5–14 (2016)
8. Giatsoglou, M., Vozalis, M.G., Diamantaras, K., Vakali, A., Sarigiannidis, G., Chatzisavvas, K.C.: Sentiment analysis leveraging emotions and word embeddings. Expert Syst. Appl. **69**, 214–224 (2017)
9. Antun, V., Renna, F., Poon, C., Adcock, B., Hansen, A.C.: On instabilities of deep learning in image reconstruction and the potential costs of AI. Proc. Natl. Acad. Sci. **117**(48), 30088–30095 (2020)

10. Chugh, M., Whigham, P.A., Dick, G.: Stability of word embeddings using word2vec. In: Mitrovic, T., Xue, B., Li, X. (eds.) AI 2018: Advances in Artificial Intelligence. AI 2018. Lecture Notes in Computer Science, vol. 11320. Springer, Cham (2018). https://doi.org/10.1007/978-3-030-03991-2_73
11. Korkobi, T., Djemel, M., Chtourou, M.: Stability analysis of neural networks-based system identification. Model. Simul. Eng. (2008)
12. Rudin, C., Carlson, D.: The secrets of machine learning: ten things you wish you had known earlier to be more effective at data analysis. In: Operations Research & Management Science in the Age of Analytics, pp. 44–72, Informs (2019)
13. Wendlandt, L., Kummerfeld, J.K., Mihalcea, R.: Factors Influencing the Surprising Instability of Word Embeddings, arXiv preprint arXiv:1804.09692 (2018)
14. Anderson, T.W., Rubin, H.: Statistical inference in factor analysis. In: Proceedings of the Third Berkeley Symposium on Mathematical Statistics and Probability, vol. 5, pp.111–150 (1956)
15. Bai, J., Ng, S.: Principal components estimation and identification of static factors. J. Econ. **176**(1), 18–29 (2013)
16. Peeters, C.F.: Rotational uniqueness conditions under oblique factor correlation metric. Psychometrika **77**, 288–292 (2012)
17. Loshchilov, I., Hutter, F.: Decoupled Weight Decay Regularization. arXiv preprint arXiv:1711.05101 (2017)
18. Moody, J., Hanson, S., Krogh, A., Hertz, J.A.: A simple weight decay can improve generalization. Adv. Neural. Inf. Process. Syst. **4**, 950–957 (1995)
19. Blut, M.: E-Service quality: development of a hierarchical model. J. Retail. **92**(4), 500–517 (2016)
20. Goodfellow, Y., Bengio, A.: Courville and Y. Deep Learning, Cambridge MIT press, Bengio (2016)
21. Hinton, G.E., Salakhutdinov, R.R.: Reducing the dimensionality of data with neural networks. Science **313**(5786), 504–507 (2006)
22. Adachi, K.: Matrix-based Introduction to Multivariate Data Analysis, Singapore, Springer Singapore (2016)
23. Tipping, M.E., Bishop, C.M.: Probabilistic principal component analysis. J. R. Stat. Soc. Ser. (Stat. Meth.) **61**(3), 611–622 (1999)
24. Sato, T.: Bayesian estimation for identifiable topic models with latent dirichlet allocation, SSRN Electron. J. https://dx.doi.org/https://doi.org/10.2139/ssrn.3721769 (2020). (unpublished)
25. Baldi, P., Hornik, K.: Neural networks and principal component analysis: learning from examples without local minima. Neural Netw. **2**(1), 53–58 (1989)
26. Bishop, C.M. (ed.): Pattern Recognition and Machine Learning. ISS, Springer, New York (2006). https://doi.org/10.1007/978-0-387-45528-0
27. Bourlard, H., Kamp, Y.: Auto-association by multilayer perceptrons and singular value decomposition. Biol. Cybern. **59**(4), 291–294 (1988)
28. Sato, T.: Construct validation for a nonlinear measurement model in marketing and consumer behavior research. Data Sci. Serv. Res. Discuss. Pap. **101** (2019) (unpublished)
29. Sato, T.: Investigating the impacts of customer experience and attribute performances on overall ratings using online review data: nonlinear estimation and visualization with a neural network. Data Sci. Serv. Res. Discuss. Pap. **27**(105), 27-62 (2019)
30. Xu, Z., Frankwick, G.L., Ramirez, E.: Effects of big data analytics and traditional marketing analytics on new product success: a knowledge fusion perspective. J. Bus. Res. **69**(5), 1562–1566 (2016)

Prediction of Gasoline Octane Loss Based on t-SNE and Random Forest

Chen Zheng[1(✉)], Shan Li[1], Chengcheng Song[2], and Siyu Yang[3]

[1] College of Economics and Management, Nanjing University of Aeronautics and Astronautics, Nanjing 210016, China
zhengchen@nuaa.edu.cn

[2] College of Civil Aviation, Nanjing University of Aeronautics and Astronautics, Nanjing 210016, China

[3] College of Science, Nanjing University of Aeronautics and Astronautics, Nanjing 210016, China

Abstract. Octane loss is an important index to measure economic benefit in the process of gasoline refining. Therefore, it is of great significance to construct the prediction model of octane loss in industrial production. In view of the characteristics of numerous variables and complex relationship of variables in gasoline refining data, t-SNE and K-Means algorithms are used in this paper to do data reduction and clustering analysis, and then collinear matrix method is used to gradually select the input variables for model construction, and finally random forest regression algorithm is introduced to build the prediction model of octane loss. The experimental results show that compared with the traditional prediction model, the prediction accuracy of the random forest is significantly improved, and the weight value of each variable of the model can be obtained by means of information gain, which provides a reference for the control variable level in the workshop production process.

Keywords: Octane loss · t-SNE · K-Means · Random forest

1 Introduction

Octane number is an important variable reflecting the combustion performance of gasoline, and it is also the commercial label of gasoline. In the process of refining FCC gasoline from raw materials into products, industrial technologies such as desulfurization and olefins reduction were used, which greatly reduced the sulfur content of gasoline and improved the cleanness of gasoline, but also reduced the octane number of gasoline. Octane number loss is the difference between the octane number of raw gasoline and product gasoline, which is an important index to measure the economic benefit of petrochemical enterprises in the process of gasoline refining, so it is of great significance to establish a prediction model of octane number loss for petrochemical enterprises. In chemical modeling, methods such as data association or mechanism modeling are often used to select variables and construct models. However, the gasoline refining process is

R. Qiu et al. (Eds.): ICSS 2021, LNOR, pp. 43–54, 2021.
https://doi.org/10.1007/978-3-030-90275-9_4

extremely complex, the refining equipment is diverse, and the control variables have a highly nonlinear relationship, so the prediction effect of the traditional data association model is not very ideal. In recent years, machine learning methods have been widely used in the field of chemical modeling. Zheng [1] used the LSTM model to predict the combustion timing estimation of HCCI engine using mixed fuel under complex working conditions. Song [2] integrated the least square method with support vector machine to establish the inverse model of the air-fuel ratio system, and made dynamic feedforward compensation for the air intake in the transient air-fuel ratio model. Li [3] integrated genetic algorithm and particle swarm optimization to optimize BP neural network, and applied it to the prediction modeling of octane number, and achieved a good prediction effect. Xiao [4] established a prediction model for sulfur content of heavy gasoline distillate hydrogenation products by using RBF algorithm, which provided guidance for the production of the unit. Based on the RBF algorithm, Xu [5] used rough set and other methods to optimize it, and established the identification model of dynamic parameters of gasoline oil film, which improved the prediction accuracy of the model. As can be seen from the above, more and more scholars begin to pay attention to the application of machine learning methods in the field of chemical industry. When processing industrial data with many variables and complex relationship between variables, machine learning method can give play to the advantages of computational science to obtain key information in the chemical process, so as to improve the efficiency of the chemical process, raw material conversion rate or product yield and other variables.

Based on the above problems, this paper uses machine learning algorithm to build the octane number loss prediction model of gasoline. The model greatly improves the forecasting accuracy of octane loss and provides a more scientific forecasting guidance for the oil refining industry. In the future, refineries can control the variables that affect octane number loss according to this model, so as to reduce the loss and the economic cost.

In this paper, nonlinear reduction and clustering algorithms such as t-SNE are used to excavate the main variables affecting octane number loss from the high-dimensional data of gasoline refining, and random forest is used to build the corresponding prediction model.

2 Research Method

The research framework of this paper is mainly divided into three parts: data preprocessing, variable screening and model construction. Data preprocessing includes the completion of missing values of the original data and the elimination of outliers, and then the variable screening step is entered. Firstly, the data was processed by nonlinear dimensionality reduction. t-SNE algorithm was used to reduce and visually present the high-dimensional features of the original data, and K-means algorithm was used for clustering analysis. Secondly, the collinear matrix method is used to do linear dimensionality reduction, and the in-and-out modulus variables are gradually screened. Finally, random forest is introduced to construct the octane loss prediction model, and the prediction results are evaluated and analyzed.

3 Experiment

The data used in this study came from the historical data collected from the FCC gasoline refining desulfurization unit of a petrochemical enterprise in 4 years, with a total of 32 pieces. The sample data included 7 raw material properties, 2 raw adsorbent properties, 2 regenerated adsorbent properties, 2 product properties and 354 operational variables, a total of 367 variables. According to previous research experience, there is a high strength nonlinear correlation between these variables. After preprocessing the data for missing values and outliers, 303 variables were left for further screening.

3.1 Nonlinear Dimensionaliy Reduction

1) *Selection of dimension reduction method*

In view of the high-strength nonlinear relationship between the refining data, the T-SNE algorithm is used to reduce the dimension of the pre-processed samples and present them visually in the two-dimensional space, as shown in Fig. 1. The horizontal axis and the vertical axis are the values of the two fusion variables after dimensionality reduction, and each point in the figure represents a sample data. In order to verify the effectiveness of T-SNE for dimensionality reduction of nonlinear data, traditional Principal Component Analysis (PCA) and Kernel Principal Component Analysis (KPCA) were selected to perform the same operation on the data. The visual comparison obtained after dimensionality reduction by the three methods is shown in Fig. 1.

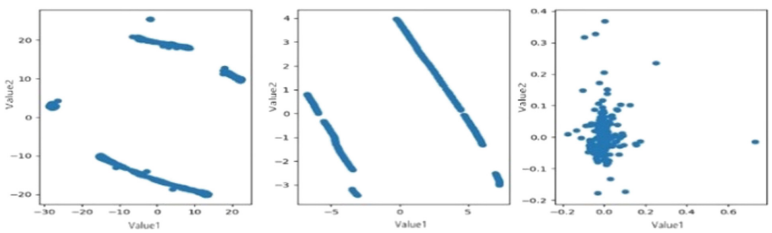

t-SNE PCA KPCA

Fig. 1. Dimensionality reduction visual contrast diagram

As can be seen from Fig. 1, after PCA clustering, there is an obvious linear relationship among the samples of each cluster, while the nonlinear relationship among the samples is ignored. The sample distribution of KPCA is relatively dispersed, and the samples with high similarity can not be separated well according to the density. While T-SNE roughly divides the samples into 4 categories, and the sample distribution of each category reflects the comprehensive characteristics of linear and nonlinear relations. As can be seen from the above, the clustering effect after T-SNE dimension reduction and visualization is significant, with good representativeness.

2) *Visual presentation and clustering*

Input the data after dimensionality reduction by t-SNE into K-means algorithm. In order to determine the appropriate cluster number K, the change curves of K value - and variance SSE were drawn, as shown in Fig. 2. The elbow method is used to determine the value of K: when K is 4, the change of SSE tends to converge, and the increase of K value will no longer cause a big change to SSE. Therefore, $K = 4$ is set as the number of clustering clusters of k-means. The clustering results are shown in Fig. 3. It can be seen that there is a strong linear relationship among some samples, while the clusters in the lower left corner are clustered, indicating a high degree of nonlinear correlation among the samples in the clusters. The four clusters generated by K-means clustering were named as cluster 1, cluster 2, cluster 3 and cluster 4, and the number of samples in each cluster was 78,137,82 and 28, respectively, with a total of 325 samples. After the t-SNE nonlinear dimensionality reduction step, the nonlinear relationship between the clusters has been basically eliminated.

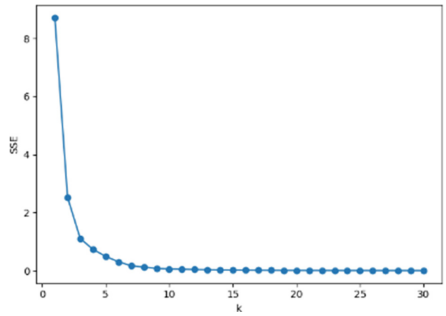

Fig. 2. Changing curve between K and SSE

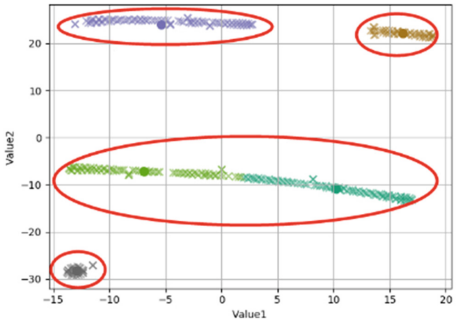

Fig. 3. Results of clustering

3.2 Linear Dimension Reduction

Linear dimensionality reduction is performed on the above output clustering results. The regression model of random forest is introduced into each cluster.

Under the condition of optimal model fitting, the weight value of each variable in the cluster is calculated, and the output results are based on the weight level. Some variables are shown in Table 1.

Random Forests adopts the idea of combination method, namely to multiple random sampling on the sample data structure N training samples classification tree (called a base classifier), every time in the process of building a base classifier, the outside of the training sample data as test data, known as the bag outside data, and through the error rate to evaluate the base classifier performance. Finally, the base classifiers are combined into a random forest classifier according to the voting criteria. In the process of constructing the classifier, Random Forest evaluates the importance of variables by sorting the importance of variables.

The basic principle of variable importance score (*VIM_ER*) based on the error rate replacement method is to randomly replace the values of each variable at the same time and measure the importance of the variable by calculating the difference between *OOB* error rates before and after the replacement. Specifically, in order to obtain the importance score of variable *Xi*, the random forest was constructed based on the training samples first, and the error rate of all *OOB* samples was estimated. Then, the values of variable *Xi* in all *OOB* samples were scrambled to obtain new out-of-bag data (OOB'), and the *ER* of the OOB' samples was estimated. Finally, the *ER* change values of out-of-bag data were calculated twice. Finally, the mean of *ER* change of all *OOB* samples is taken as the *Vim* of *Xi,* and the *Vim* of *Xi* is defined as follows:

$$VIM_i^{ER} = \frac{1}{Ntree} \sum_{t=1}^{Ntree} \left(ER_{it} - ER_{it}^{'} \right) \tag{1}$$

Where, *Ntree* is the number of trees in RF, ER_{it} is the error rate corresponding to the t tree before the substitution of variable *Xi*, and ER'_{it} is the error rate corresponding to the t tree after the substitution of variable *Xi*.

According to the calculation formula of *Vim*, if the variable *Xi* has no correlation with the label (category), the error rate of the corresponding data outside the bag will not change after random replacement of the variable. Theoretically, $VIM_i^{ER} = 0$; Conversely, if $VIM_i^{ER} > 0$, then the variable *Xi* is associated with the classification.

As can be seen from the table, on the one hand, the variables at the top of the weight ranking of each cluster almost have no intersection, indicating that there is a large difference between clusters and the clustering effect is significant. On the other hand, from the physical properties of the variables in the table, it can be concluded that the properties of the variables affecting the octane number loss can be roughly divided into three categories, namely, pressure variables, temperature variables and flow variables. In addition, Airspeed of reactor mass, Ratio of hydrogen to oil and Coke of raw adsorbent to be used also have a certain influence on the octane number loss.

Table 1. Weight table in every cluster

Ranking	Cluster_1	Weight (%)	Ranking	Cluster_2	Weight (%)
1	D-101 Pressure of raw material buffer tank	9.847	1	E-203 Temperature of shell side outlet tube	5.553
2	Temperature of refined gasoline outlet unit temperature	5.621	2	Pressure of lower loose air purifying air inlet device	3.431
3	Flow rate of steam intake device	4.024	3	1.0MPa Temperature of steam inlet device	2.834
4	R-101 Pressure drop in upper bed	2.589	4	D-107 flow lower loose wind	2.813
5	R-101 Pressure difference between upper and lower bed bottom grille	2.436	5	Flow rate of the purification air inlet device	2.749
6	Airspeed of reactor mass	2.207	6	Coke of raw adsorbent, wt %	1.992
Ranking	Cluster_3	Weight (%)	Ranking	Cluster_4	Weight (%)
1	D-109 Asorbent matrial level	9.335	1	S_ZORB AT-0004	7.239
2	8.0MPa Outlet of hydrogen backblowing compressor	7.911	2	Coke of raw adsorbent, wt%	3.4
3	ME-101 Pressure of backblow manifold	5.881	3	S_ZORB AT-0009	3.196
4	Ratio of Hydrogen to oil	3.809	4	S_ZORB AT-0013	2.692
5	Block the outlet air flow of hopper H2 filter	3.208	5	Pressure of preheater air outlet	2.141
6	D-204 liquid level	1.73	6	D-110 or the differential	2.026

The top 6 weights of each cluster, a total of 24 variables, were selected as the variables to be selected, and the collinearity analysis was carried out. Taking the Pearson correlation coefficient equal to 0.5 as the screening threshold, the collinear matrix among the variables was obtained. After screening, the highly linear correlation variables were shown in Fig. 4. As shown in Fig. 4, there is a highly linear relationship between the two groups of variables: the first group is Airspeed of reactor mass and 8.0MPa outlet of

hydrogen backblowing compressor; the second group is D-101 Pressure of raw material buffer tank, S_Zorb AT-0004, S_Zorb AT-0009, ME-101 Pressure of backblow manifold and R-101 Pressure drop in upper bed.

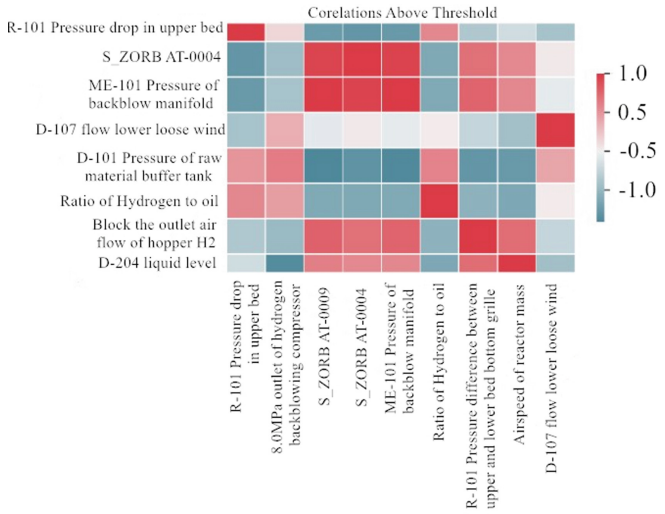

Fig. 4. Collinear matrix, R is equal to 0.5

In order to determine the excluded and inserted variables in the two groups, the Pearson correlation coefficient between each variable and octane number loss was calculated, as shown in Fig. 5. Finally, Airspeed of reactor mass with large correlation coefficient and D-101 Pressure of raw material buffer tank were selected as the input variables of the two groups.

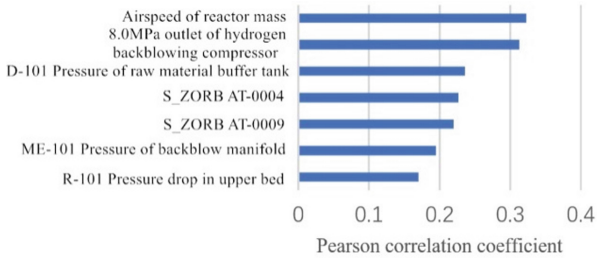

Fig. 5. Pearson correlation coefficient

Through the above variable screening steps, the final 19 variables into the module are obtained, as shown in Table 2.

Table 2. Final input variables

Types of variables	Names of variables
Flow rate	Flow rate of steam intake device
	D-107 flow of lower loose wind
	Flow rate of the purification air inlet device
	Air flow of blocking the outlet hopper H2 filter
Pressure	D-101 Pressure of raw material buffer tank
	R-101 Pressure drop in upper bed
	Pressure of lower loose air purifying air inlet device
	Pressure of preheater air outlet
	D-110 or the differential
Temperature	Temperature of refined gasoline outlet unit temperature
	E-203 Temperature of shell side outlet tube
	1.0MPa Temperature of steam inlet device
Others	Ratio of hydrogen to oil
	Airspeed of reactor mass
	Coke of raw adsorbent, wt %
	S_ZORB AT-0013
	D-109 Asorbent matrial level
	D-204 Liquid level

3.3 Prediction Model of Cotane Loss Based on Random Forfest

After the selection of variables, prediction model of octane loss was constructed using the regression algorithm of random forest. The data set after feature screening was divided into training set and test set according to the ratio of 8:2. Among them, 262 training sets were used for training model.63 test sets are used to test model accuracy. For the octane loss prediction model, the Error between the predicted value and the true value can directly reflect the prediction accuracy of the model, so this paper adopts Mean Absolute Error (MAE) as the evaluation variable of the model. The formula is as follows, where n is the number of samples.

$$MAE\left(y, y'\right) = \frac{1}{n}\sum_{i=0}^{n-1}\left\|y_i - y_i^{'}\right\|^2 \tag{2}$$

When the number of iterations is set to 200 and the model fitting effect is optimal, the prediction results in the training set and test set are shown in Table 3. The comparison between the predicted value and the actual value of the test set is shown in Fig. 6, where the abscissa represents the sample number of the test set.

Table 3. Prediction results of model

Data set	MAE
Training set	0.08
Testing set	0.11

In order to verify the superiority of the random forest model compared with other prediction models, linear regression, Support Vector Machine (SVM), k-nearest Neighbor (KNN) and decision tree algorithm are used to establish the prediction model of octane loss on the same data set. The comparison results are shown in Table 4. Through the prediction comparison of the above 5 models, it can be concluded that the prediction accuracy of random forest model is the highest, and the average absolute error MAE is 0.11. Decision tree model comes next, while linear regression and SVM model perform poorly.

In order to ensure the accuracy of the experiment and avoid the sample deviation caused by random sampling, the 10-fold cross-validation method was used to verify prediction models, and the 10-fold results were averaged. It can be seen from Table 4 that under the same data set, the 10-fold cross-validation result of the random forest model is still better than that of other models.

Table 4. Comparison of prediction results of different models

Regression model	MAE (Data set)	MAE (10-fold cross-validation)
Linear regression	0.19	0.19
SVM	0.17	0.16
KNN	0.17	0.16
Decision tree	0.16	0.15
Random forest	0.11	0.13

The above experiments show that random forest has a strong advantage in the algorithm selection of octane loss prediction model. The random forest integrates several weak learners, and the prediction accuracy is improved by learning improvement among each learner. Compared with the popular decision tree model and SVM model, the average absolute error MAE of the random forest model decreases by 0.05 and 0.06 respectively, and the prediction accuracy of the model is significantly improved.

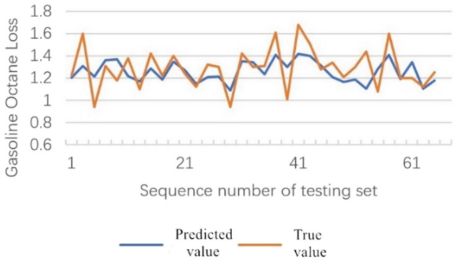

Fig. 6. Comparison of predicted value and real value

3.4 Analysis of Model Results

In order to analyze the main influencing variables of octane number loss, the eigen importance function of random forest was used to calculate the weight value of each variable when the model fitting effect reached the optimum. The results are shown in Table 5. As can be seen from the table, D-101 Pressure of raw material buffer tank has the highest weight value of the pressure of the raw material buffer tank, up to 20.547%; the second is Airspeed of reactor mass and Temperature of refined gasoline outlet unit temperature which are 9.478% and 8.297%, respectively. The sum of the weight of the top 5 variables is 51.527%, and the sum of the top 10 variables is 74.808%.

Table 5. Weight table of variables

Ranking	Names of variables	Weight (%)	Cumulative weight (%)
1	D-101 Pressure of raw material buffer tank	20.547	20.547
2	Airspeed of reactor mass	9.478	30.025
3	Temperature of refined gasoline outlet unit temperature	8.297	38.322
4	E-203 Temperature of shell side outlet tube	6.714	45.036
5	D-204 Liquid level	6.491	51.527
6	Flow rate of steam intake device	5.353	56.88
7	Ratio of hydrogen to oil	5.107	61.987
8	Pressure of preheater air outlet	4.536	66.523
9	Air flow of blocking the outlet hopper H2 filter	4.325	70.848
10	1.0MPa Temperature of steam inlet device	3.96	74.808

The top 10 variables are classified according to their physical properties. The pressure variables include D-101 Pressure of raw material buffer tank and Pressure of preheater air outlet; temperature variables include Temperature of refined gasoline outlet unit temperature, E-203 Temperature of shell side outlet tube and 1.0MPa Temperature of steam inlet device; The flow variables are the flow rate of the steam inlet device and the flow rate of the outlet gas of the locking hopper H2 filter. Other variables are Airspeed of reactor mass, D-204 Liquid level, and Ratio of hydrogen to oil.

According to the above analysis results, the enterprise can adjust the variables in the table according to the different physical properties, so as to reduce the octane number loss in the gasoline refining process, and bring intuitive economic benefits to the industrial production.

4 Conclusion

Gasoline refining process involves many variables, and the relationship between the variables is complex. In this paper, T-SNE and other methods are used to carry out nonlinear and linear dimensioning reduction for the high-dimensional variables in the original data, and the variables which have a greater impact on the octane number loss are gradually screened out. The prediction model is constructed with random forest algorithm, and a good prediction effect is achieved.

The successful application of this paper can provide relevant guidance for the variable control level of petrochemical enterprises in the gasoline refining process, so as to reduce the production cost and improve the production efficiency. The next research will continue to train the model, improve the prediction accuracy, and excavate the variation rules of variable control and octane loss, so as to further provide a specific debugging method to reduce the octane loss.

References

1. Zheng, X., He, J., Zhang, B.: Combustion timing estimation of hybrid HCCI engine under complex working conditions based on LSTM neural network. Chinese Journal of Scientific Instrument (2020)
2. Song, D., Li, L., Xie, Q.: Research on Transient Air-fuel Ratio Composite Control of Gasoline Engine Based on LS-SVM Inverse System, 2ed edn, vol. 39, pp. 9–13. Internal Combustion Engine Engineering (2018)
3. Li, W., Wang, M., Jiang, N.: Prediction of Octane Number of Hydrogenated Gasoline Components in Finishing Gasoline Blending Based on SHPSO-GA-BP, 7th edn, vol. 71, pp. 3191–3200 (2020)
4. Xiao, Q., Li, Y.: Application of RBF neural network in catalytic cracking gasoline hydrogenation unit, 1st edn, vol. 47, pp. 37–42. Petrochemical Engineering (2018)
5. Xu, H., Xu, Y., Xu, Y.: Study on Dynamic Parameter Identification of Gasoline Oil Film Based on CHAOS-RS-RBF Algorithm, 6th edn, vol. 5, pp. 29–36. Journal of Dali University (2020)
6. Zhou, H., Qi, S., Li, X.: Analysis of factors affecting octane number loss of gasoline in S Zorb unit, 9th edn, vol. 46, pp. 12–15. Chemical Industry in Yunnan (2019)

7. Zhao, Q.: Analysis of factors affecting octane number loss in catalytic gasoline hydrodesulfurization unit and improvement measures, 5th edn, vol. 49, pp. 8–14. Petroleum and Natural Gas Chemical Industry (2020)
8. Liu, C., Li, J.: Analysis of Factors Affecting Octane Number Loss of Gasoline in S Zorb Plant, 4th edn, vol. 36, pp. 12–15. Petrochemical Design (2019)
9. He, B., Ma, J., Gao, Y.: Urban daily water supply prediction based on multi-granularity characteristics and XG-Boost model, 5th edn, vol. 37, pp. 43–49, Journal of Changjiang River Scientific Research Institute (2019)
10. Wu, C.: Cause analysis and optimization measures of gasoline octane number loss in S Zorb unit, 14th edn, vol. 33, pp. 28–29. Chinese Petroleum and Chemical Standards and Quality (2013)
11. Wang, Y.: Research on automatic streaming data analysis method based on T-SNE and optimized SVM. School of Instrumentation Science and Optoelectronic Engineering, Beijing. Beijing Information Science and Technology University (2019)
12. Lu, H.: Water resource carrying capacity evaluation model based on random forest algorithm and its application in Hubei Province, 13th edn, vol. 59, pp. 72–76. Hubei Agricultural Sciences (2020)
13. Han, H.: Discussion on optimization measures to reduce octane loss of gasoline in S Zorb unit, 6th edn, vol. 37, pp. 87–89. Chinese Petroleum and Chemical Standards and Quality (2017)
14. Wang, L., Lu, H.: Defect Detection of Power User Label Feature Classification Software Based on K-means Algorithm, 18th edn, vol. 28, pp. 122–126. Electronic Design Engineering (2020)
15. Chen, T., Li, X.: Line loss anomaly discrimination method of low voltage station area based on K-means clustering algorithm, 2nd edn, vol. 5, pp. 2–6. Southern Power Grid Technology (2019)
16. Li, B., Jiang, P.: Identification of new and old characteristics of Korean pine seeds by T-SNE near infrared spectroscopy, 9th edn, vol. 40, pp. 2918–2924. Spectroscopy and Spectral Analysis

Introducing AI General Practitioners to Improve Healthcare Services

Haoyu Liu[1](✉) and Ying-Ju Chen[2]

[1] Faculty of Business, City University of Macau, Taipa, Macau
hyliu@cityu.mo
[2] School of Business and Management, Hong Kong University of Science and Technology, Kowloon, Hong Kong

Abstract. Artificial intelligence (AI) is being prevalently adopted in healthcare. Its contributions are witnessed in a range of services, including prognosis, diagnosis, and treatment, as well as in expanding the availability of clinical expertise. This paper studies the impact of an AI general practitioner on healthcare service systems, particularly physicians' workloads and patients' waiting times. We compare the service system with the AI general practitioner to the traditional two-tier service system, where the first level serves as a gatekeeper for the second level. The results provide valuable insights and implications for public policy on adopting AI in hospitals from an operational perspective.

Keywords: Artificial intelligence · Gatekeeper · Healthcare · Service systems

1 Introduction

Artificial intelligence (AI) is developing at a fast pace, with its global market size predicted to reach $328 billion in 2021 and break $500 billion by 2024 [1]. Among the diverse AI applications, healthcare is one of the most attention-grabbing and attractive areas, and AI healthcare is projected to expand at a compound annual growth rate (CAGR) of over 40% in the next five years. To respond to this growth sector, public policy regarding AI healthcare has been put forward by governments around the world. In October 2016, the United States released the report "Preparing for the Future of Artificial Intelligence", identifying problems related to AI healthcare and making recommendations for further actions. At the Artificial Intelligence Technology Strategy Council meeting in March 2017, the Japanese government prioritized AI for healthcare. In China, a white paper on AI healthcare was jointly published by the Artificial Intelligence Institute and the School of Medicine of Shanghai Jiao Tong University.

This paper is motivated by the trend and toward AI in healthcare. We focus on applying AI as a general practitioner, which comes within auxiliary diagnosis, one of the highlighted categories in the Chinese white paper on AI healthcare. In the form of a chatbot or mobile app, the AI general practitioner provides instructions to patients based on either pictures they take or texts in which they describe their symptoms. This gives patients access to professional advice anywhere the Internet is available and allows them

R. Qiu et al. (Eds.): ICSS 2021, LNOR, pp. 55–64, 2021.
https://doi.org/10.1007/978-3-030-90275-9_5

to obtain immediate help without waiting in a long queue at a hospital. At the same time, the AI general practitioner has limitations: It may lead to incorrect treatments, which can result for several reasons. First, because of limited medical knowledge, patients may fail to describe symptoms accurately or misunderstand the instructions provided by AI. Second, AI itself may make mistakes as a consequence of lacking high-quality data or learning from inappropriate past practices.

In this paper, we study the impact of the AI general practitioner on aspects of healthcare such as physicians' workloads and patients' waiting times. We compare the service system with the AI general practitioner to the typical two-tier service system, where the first level serves as a gatekeeper for the second level. Further, we explore how this emerging technology can be effectively and efficiently incorporated into healthcare service systems. The paper proceeds as follows. In the next section, we review the relevant literature. We describe the model in Sect. 3, and present analytical and numerical results in Sects. 4 and 5, respectively. Section 6 concludes the paper.

2 Literature Review

For a long time, healthcare has been a hot topic in operations management, which can help healthcare service systems reduce cost, enhance quality, and improve efficiency. Reference [2] discusses the general role of operational analysis in improving healthcare, and many papers have been published in this area since [2] first appeared. For example, reference [3] studies when to assign a nonprimary bed to a primary patient who has waited a long time for a primary bed to become available (i.e., overflow), in real time and under uncertainty. Their proposed approximate dynamic programming algorithm is remarkably effective in finding good overflow policies. Reference [4] investigates a stochastic appointment scheduling problem in an outpatient clinic with a single doctor by formulating the problem as a convex conic optimization problem with tractable semidefinite relaxation. Also looking at how to offer appointment slots to patients, reference [5] develops two models, nonsequential offering and sequential offering, to capture different types of interactions between patients and the scheduling system and maximize the total number of slots booked. Meanwhile, reference [6] studies the effects of rescheduling on no-show behavior in an outpatient appointment system for both new and follow-up patients. Finally, reference [7] surveys current research in healthcare operations management, and it is noteworthy that few of the previous papers consider the implications for healthcare when emerging technologies are involved.

Our paper examines a service system where AI serves as a general practitioner and explores how each party in the healthcare context is affected. The service system we look at is very close to that in the gatekeeper literature. This stream of research originates from [8], which describes a model of gatekeepers and experts and derives the optimal referral rate with a deterministic service rate and arrival rate. Reference [9] considers a similar model and provides financial and operational implications for outsourcing the gatekeepers and experts. There are also many related empirical works. Reference [10] considers a nested structure of the different levels of care, which bears significant similarities to the gatekeeper structure. It focuses on estimating costs and benefits associated with serving different customer types by different service levels in

a sophisticated healthcare setting. Reference [11] investigates how workload affects decisions in a gatekeeper service system using an operational and clinical data set from a maternity hospital. It finds that gatekeepers ration resource-intensive discretionary services for customers with noncomplex service needs and increase specialist referral rates for customers with complex needs. Moreover, reference [12] provides empirical evidence for the reorganization of general hospitals into separate divisions for routine and non-routine services, to overcome operational misalignments between the two types of services. In our paper, we use a gatekeeper service system as the benchmark and compare the performance of our AI general practitioner service system with it.

The rapid advances in AI have also attracted the attention of and aroused broad concern among academics in medicine [13, 14]. Reference [15] considers how radiologists and pathologists can make use of AI. Reference [16] explains the role of AI in medicine in general, and reference [17] discusses various ways that AI can help with healthcare. Our paper will tackle a specific problem in medicine and contribute managerial insights that complement this medicine-focused research by providing an operational perspective.

3 The Model

We consider a service system of medical specialists that introduces AI as a general practitioner (See Fig. 1). The system we examine is distinguished from a two-tier system, where the first level serves as a gatekeeper for the second level, in the following aspects. First, a patient can choose to receive treatment from either the AI general practitioner or direct from a medical specialist. Second, there is a chance that the general practitioner misdiagnoses the patient, which will lead to an extra delay in treatment. The arrival of patients follows a Poisson process with rate λ. Each patient is endowed with a condition of health $x \sim$ uniform [0,1]. A larger x reflects a more serious condition. A patient cannot observe his or her true condition, but perceives it either optimistically with probability p or pessimistically with probability 1-p. An optimist will utilize an AI general practitioner for treatment, while a pessimist will go straight to a medical specialist.

The AI general practitioner is assumed to have infinite capacity; i.e., it is always able to begin treating patients immediately. This is because a chatbot or mobile app can serve a massive number of patients at the same time, as long as the server does not break down. The treatment time for a patient under AI is relatively stable regardless of how severe his or her condition is, and therefore is assumed to be exogenously given as τ. The AI general practitioner has a chance of providing incorrect treatment with probability q. The reasons for such an incorrect treatment are not limited to mistakes made by AI, but may also result from errors on the part of the patients, such as failing to report accurate information or understand the instructions. If the patient receives the desired treatment, he or she will leave the system.

If an incorrect treatment is given, however, the patient will realize it after a while and will then visit a medical specialist. Since it usually takes time to see whether a treatment is effective or not, the incorrect treatment is associated with an additional stay in the system d. Also, the condition of the patient may deteriorate in the interval, which requires an additional time δ for the medical specialist to give treatment. In this paper, we focus on the case that both the additional stay and the extra treatment time are exogenously given constants.

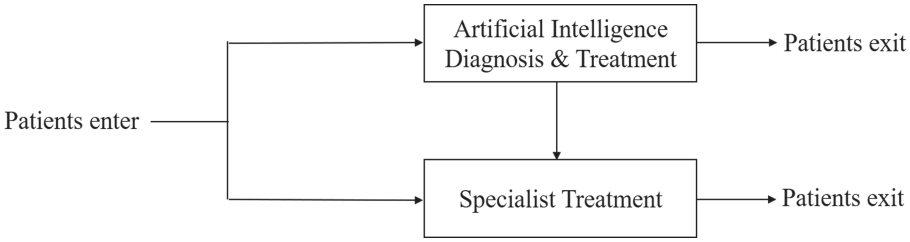

Fig. 1. The service system with an AI general practitioner

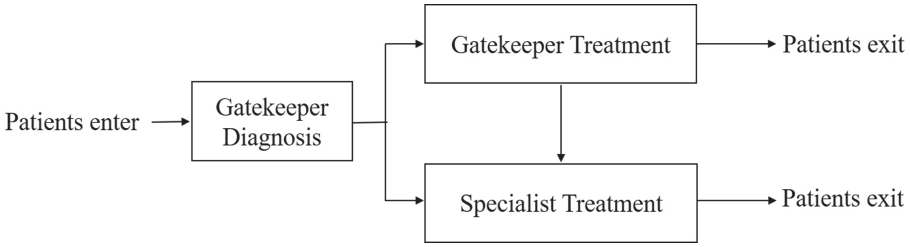

Fig. 2. The service system with a gatekeeper

Suppose there are n medical specialists in the system. Then the system is formulated as an n-server queue. There are two sources of arrivals, the patients who visit a medical specialist directly, and the patients who are misdiagnosed and visit a medical specialist after that. The treatment time for a patient with a condition x is αS, where α is a constant scaling and $S \sim \exp(1/x)$. The monotonicity suggests that the more severe the patient's condition is, the more time it takes to treat. Meanwhile, the convexity suggests that it is increasingly time-consuming to give treatment as the severity increases. We assume that a patient visiting a medical specialist will always be treated successfully and will then leave the system.

We compare the performance of the service system with an AI general practitioner to the two-tier service system with a gatekeeper [8, 9]. In the latter service system, the first level serves as a gatekeeper to the second level. A patient must first arrive at a gatekeeper, who may either treat the patient or refer the patient to a medical specialist (See Fig. 2). For ease of exposition, we denote the system with an AI general practitioner and that with a gatekeeper by AI and GK, respectively. Table 1 summarizes the notations used in this study.

4 Analytical Results

Here we consider a simplified model with one medical specialist and no incorrect treatment. We will present results for our full model in the next section. Denote by θ the threshold of the severity level at which the gatekeeper will refer a patient to the medical specialist. Then the severity levels of patients who arrive at the medical specialist under GK are uniformly distributed over $[\theta,1]$. It can be shown easily that the arrivals

to the medical specialist follow a Poisson distribution under both AI and GK, while the service time of the medical specialist follows a compound probability distribution of an exponential and a uniform distribution. Therefore, the queue for the medical specialist can be considered as M/G/1. Without loss of generality, we normalize α as 1.

Following [18], the expected queue length and expected waiting time follow the form

$$L_q = \frac{\Lambda^2 E[S^2]}{2(1-\rho)}$$

and

$$W_q = \frac{\Lambda E[S^2]}{2(1-\rho)}$$

respectively, where Λ is the arrival rate of direct-entry patients to the medical specialist, $\rho = \lambda E[S]$, and S denotes a random service time with a general distribution. To ensure a fair comparison, we first focus on the case where the flows of direct-entry patients to the medical specialists are the same under AI and GK, i.e., $\theta = p$. Then we have $\Lambda = (1 - \theta)\lambda = (1 - p)\lambda$. Under AI, E[S] and $E[S^2]$ are calculated as 1/2 and 1/3, respectively. Under GK, E[S] and $E[S^2]$ are calculated as $(1 + \theta)/2$ and $[(1 - \theta)^2 + 3(1 + \theta)^2]/12$, respectively. Both E[S] and $E[S^2]$ are greater under GK than under AI. Note that L_q and W_q are increasing in E[S] and $E[S^2]$.

Proposition 1. *Given the identical arrival rate of direct-entry patients to the medical specialists, AI performs better than GK.*

We conclude in Proposition 1 that AI achieves superior performance to GK in terms of queue length and waiting time. Patients with severe health conditions will visit medical specialists under GK, which causes medical specialists to be occupied with patients who need longer treatment time, which leads to longer queue length and waiting time. Though the performance of AI overwhelmingly dominates that of GK in the above model, we argue that the current results do not hold for our full model. If a patient is incorrectly treated by an AI and transferred to a specialist, his/her status will deteriorate due to the delayed treatment. As a consequence, a medical specialist needs to spend more time on him/her because the treatment time increases in the severity level. Therefore, the queue length and waiting time at the medical specialist under AI may be longer than that under GK. Moreover, if we consider a more realistic case where the probability of misdiagnoses is increasing in the patient's health condition, and the additional stay in the system after an incorrect treatment is related to the condition of a patient, the situation may become increasingly complicated. In such a case, a more detailed analysis should be conducted.

Proposition 2. *There exists a threshold p_0 on p, such that when $p < p_0$ AI performs worse than GK.*

In Proposition 2, we look at the case with nonidentical arrival rates. Since L_q and W_q are increasing in $\Lambda = (1 - p)\lambda$ and hence decreasing in p, we have the proposition. The superior performance of AI depends highly on the behavior of patients, especially

their trust in the treatment performed by a nonhuman. If patients are skeptical about emerging technologies, then the power of AI cannot be sufficiently exhibited. In such a case, patients will go to the medical specialist regardless of their health condition, which leads to inefficient use of hospital resources.

Table 1. Summary of notations

λ arrival rate of patients	x current severity level of patients
Λ arrival rate at the specialists	x_0 initial severity level of patients
S treatment time for human doctors	d delay until realizing incorrect treatment
τ treatment time for AI	δ extra treatment time due to delay
α constant scaling for service time	n number of specialists
p probability of patients being optimistic	θ threshold for gatekeeper referral
q probability of incorrect treatment	t time in the service system
W_q expected waiting time	L_q expected queue length

5 Numerical Results

We perform simulation to show how our analytical results change subject to multiple server queues with incorrect treatment. The simulation is conducted via Arena, specialized software for dynamic service systems. We simulate the service systems using identical random process generations to facilitate fair comparisons and variance reduction for 90 days. Specifically, we consider a system with two medical specialists, who work from 8:00 to 18:00 every day with a two-hour break from 12:00 to 14:00. The number of both the AI general practitioners and the gatekeepers is 1. The parameters are set as follows. The patient arrival follows a Poisson process, at a rate of $\lambda = 6$ per hour, where direct-entry patients seeing medical specialists can constitute 0.8, 0.85, 0.9, or 0.95 of the flow. (In the AI case, the proportion is the probability of pessimistic patients, while in the GK case, the proportion is the probability of severity level being higher than the threshold.) The flows of direct-entry patients seeing the medical specialists are required to be the same under AI and GK to ensure a fair comparison. We note that the optimistic and pessimistic patients' sizes cannot be controlled in reality to be the same as the proportion visiting the medical specialists. Therefore, we provide one more row with equal-sized optimistic and pessimistic patients, i.e., $p = 0.5$ under AI, for further reference. The treatment time under a medical specialist and a gatekeeper are exponentially distributed, scaled by constants $\alpha = 10$ and $\alpha = 5$, respectively, while the treatment time under an AI general practitioner is $\tau = 5$ min. The chance of being incorrectly treated by the AI general practitioner or the gatekeeper varies among 20%, 10%, and 0. When incorrect treatment happens, the patient will visit a medical specialist after $d = 1$ day, and there will be an additional treatment time $\delta = 3$ min.

We can see from Table 2 that the waiting time at the medical specialists under AI is shorter than that under GK, given the direct-entry patient flow. Because under GK, patients with the most severe health conditions will be sent straight to medical specialists, which leads to longer treatment time on average at the medical specialists: Patients waiting ahead of a particular patient are all severe cases and require lengthier treatment times. This influence is so strong that the AI service system with a lower cure probability sometimes performs better than the GK service system. Besides, patients may overstate their health conditions when talking to doctors, which may increase the treatment time and cause a longer waiting time for others. For example, when the direct-entry patients seeing the medical specialists compose 0.9 of the flow, and the cure probability is 80%, the average waiting time of AI is 273.41 min, which is smaller than that of GK (275.80 min). Table 2 also shows that the waiting time at the medical specialists decreases in both cure probability of the AI general practitioner and the gatekeeper. The reason behind this is that when the cure probability is high, the number of patients being referred to the medical specialists will be low, which decreases the waiting time at the medical specialists. Meanwhile, it is noteworthy that the relationship between the waiting time at the medical specialists and the proportion visiting the medical specialists is not monotone. On the one hand, increasing the proportion gives medical specialists greater pressure, which increases the waiting time. On the other hand, such an increment means more patients receive correct treatment the first time, and therefore, they need less time to be cured by the medical specialists. The two conflicting forces together drive the non-monotone relationship between the waiting time and the entry proportion.

Table 2. Waiting time at the medical specialists

		Cure probability		
		80%	90%	100%
Entry to the medical specialists (AI)	**0.5**	292.4	289.18	285.63
	0.8	284.4	267.62	251.81
	0.85	276.77	261.72	258.75
	0.9	273.41	261.27	245.81
	0.95	272.74	263.19	262.98
Entry to the medical specialists (GK)	**0.8**	285.95	276.53	280.49
	0.85	290.23	276.31	270.05
	0.9	275.8	269.74	259.22
	0.95	283.11	281.51	265.29

Note. Upper Panel: The Service System with an AI General Practitioner; Lower Panel: The Service System with a Gatekeeper. Rows present results for different proportions of patient arrivals as direct entry to medical specialists (0.8, 0.85, 0.9, 0.95), while columns present results for different cure probabilities (80%, 90%, 100%).

Table 3 suggests that the AI generates lower utilization of the medical specialists than GK for reasons similar to those described in the previous analysis. For example, when the direct-entry patients seeing the medical specialists constitute 0.95 of the flow, and the cure probability is 90%, the utilization of GK is 0.3587, which is larger than that of AI (0.1476). Table 3 also points out that the utilization of the medical specialists decreases in both cure probability of the AI general practitioner and the gatekeeper because, when the cure probability of the AI general practitioner or the gatekeeper is high, the number of patients being transferred to medical specialists will decrease, which then decreases the utilization of medical specialists. A final note is that we omit the comparison with the other benchmark where all patients go to the medical specialists directly because the queue length will be infinity and the server will be fully utilized under such a case.

Table 3. The scheduled utilization of the medical specialists

		Cure probability		
		80%	90%	100%
Entry to the medical specialists (AI)	**0.5**	0.5041	0.4267	0.3794
	0.8	0.3478	0.2333	0.1483
	0.85	0.3218	0.2229	0.1072
	0.9	0.2914	0.1801	0.0738
	0.95	0.2664	0.1476	0.034
Entry to the medical specialists (GK)	**0.8**	0.4345	0.3464	0.2718
	0.85	0.431	0.3538	0.2725
	0.9	0.3361	0.2488	0.1451
	0.95	0.4457	0.3587	0.2639

Note. Upper Panel: The Service System with an AI General Practitioner; Lower Panel: The Service System with a Gatekeeper. Rows present results for different proportions of patient arrivals as direct entry to medical specialists (0.8, 0.85, 0.9, 0.95), while columns present results for different cure probabilities (80%, 90%, 100%).

6 Discussion

The application of AI is becoming increasingly prevalent in healthcare. AI enhances performance of the healthcare service system from various aspects. However, a vast vacuum remains in the literature on how AI influences healthcare operations management. Classic studies focus on capacity planning, resource allocation, and redesign of processes, but none have considered the impact of emerging technologies such as AI. The introduction of AI to healthcare brings drastic changes in prognosis, diagnosis, treatment, and the availability of clinical expertise, among others. In this paper, we base our analysis on this trend in practice, and aim to fill in the research gap and motivate more research in this area.

Specifically, we examine the role of AI as a general practitioner in the form of a chatbot or mobile app. The AI first receives and analyzes pictures patients take or descriptions patients write about their symptoms. Then it makes diagnoses and offers treatment instructions accordingly. Note that the model fits not only the case of a service system with an AI general practitioner but also vast cases in agriculture. For crops, there are apps diagnosing plant diseases, pest damages, and nutrient deficiencies. These apps are able to offer corresponding treatment measures in the absence of experts. In animal husbandry, AI can also analyze conditions affecting cows and help farmers make decisions. Introducing AI to developing economies and the agricultural sector benefits the farmer by improving productivity and product quality.

We conclude the paper by pointing out future research directions to enrich the current content of our model. First, patients' conditions can be time-dependent. Denote by $x(x_0,t)$ the condition of a patient when the correct treatment is performed, where x_0 is the initial state of the patient upon arrival and t is the time the patient spends until the correct treatment is performed. The function $x(x_0,t)$ is increasing in both x_0 and t. Here, the consequence of delayed treatment is reflected in not only the waiting cost from a psychological perspective but also a deterioration of the condition from a physical perspective. Meanwhile, it is also possible that a patient is self-cured or spontaneously cured after a period, especially when the severity is low, which complicates the analysis. Second, rational patients may be considered. Upon arrival, a patient rationally decides on which doctor to visit, by comparing costs under the two treatment options. In particular, a patient faces a tradeoff between a long waiting time under a medical specialist's treatment and a possibility of misdiagnosis (and hence an even longer delay in treatment) under an AI general practitioner's treatment. In such a case, one needs to solve for the equilibrium and characterize the optimal strategy of patients in equilibrium.

The generalization of existing results to the case of misdiagnoses by the AI requires further study. For example, the probability of misdiagnoses q(x) may be an increasing function of the patient's condition, i.e., the more serious the patient's condition is, the more challenging for both the AI and the patient to perform the correct treatment and hence the more likely that misdiagnoses will happen. Moreover, the additional stay in the system d(x) after an incorrect treatment may also be correlated to the patient's condition x. On the one hand, a patient with more serious symptoms may deteriorate more quickly than a less severe one and hence visit the medical specialist very soon. On the other hand, patients with a more complicated situation usually expect to follow the instructions by AI for a longer time before they heal. Therefore, there may be a prolonged period before a follow-up consultation. To support the functional form for d(x), empirical evidence on follow-up consultation should be collected.

References

1. IDC Forecasts Improved Growth for Global AI Market in 2021. International Data Corporation (IDC), February 2021
2. Green, L.: Om forum - the vital role of operations analysis in improving healthcare delivery. Manuf. Serv. Oper. Manag. **14**(4), 488–494 (2012)
3. Dai, J., Shi, P.: Inpatient overflow: an approximate dynamic programming approach. Manuf. Serv. Oper. Manag. **21**(4), 894–911 (2019)

4. Kong, Q., Lee, C.-Y., Teo, C.-P., Zheng, Z.: Scheduling arrivals to a stochastic service delivery system using copositive cones. Oper. Res. **61**(3), 711–726 (2013)
5. Liu, N., Ven, P., Zhang, B.: Managing appointment booking under customer choices. Manag. Sci. **65**(9), 4280–4298 (2019)
6. Liu, J., Xie, J., Yang, K.-K., Zheng, Z.: Effects of rescheduling on patient noshow behavior in outpatient clinics. Manuf. Serv. Oper. Manag. **21**(4), 780–797 (2019)
7. Dai, T., Tayur, S.: Healthcare operations management: a snapshot of emerging research. Manuf. Serv. Oper. Manag. **22**(5), 869–887 (2019)
8. Shumsky, R., Pinker, E.: Gatekeepers and referrals in services. Manag. Sci. **49**(7), 839–856 (2003)
9. Lee, H.-H., Pinker, E., Shumsky, R.: Outsourcing a two-level service process. Manag. Sci. **58**(8), 1569–1584 (2012)
10. Chan, C., Green, L., Lekwijit, S., Lu, L., Escobar, G.: Assessing the impact of service level when customer needs are uncertain: an empirical investigation of hospital step-down units. Manag. Sci. **65**(2), 751–775 (2019)
11. Freeman, M., Savva, N., Scholtes, S.: Gatekeepers at work: An empirical analysis of a maternity unit. Manag. Sci. **63**(10), 3147–3167 (2017)
12. Kuntz, L., Scholtes, S., Sulz, S.: Separate and concentrate: Accounting for patient complexity in general hospitals. Manag. Sci. **65**(6), 2482–2501 (2019)
13. A digital revolution in health care is speeding up. The Economist, March 2017
14. A.I. versus M.D. The New Yorker, March 2017
15. Jha, S., Topol, E.: Adapting to artificial intelligence. J. Am. Med. Assoc. **316**(22), 2353–2354 (2016)
16. Rajkomar, A., Dean, J., Kohane, I.: Machine learning in medicine. N. Engl. J. Med. **380**, 1347–1358 (2019)
17. Topol, E.: Deep Medicine: How Artificial Intelligence Can Make Healthcare Human Again. Basic Books (2019)
18. Shortle, J., Thompson, J., Gross, D., Harris, C.: Fundamentals of Queueing Theory. Wiley (2018)

A U-net Architecture Based Model for Precise Air Pollution Concentration Monitoring

Feihong Wang, Gang Zhou(✉), Yaning Wang, Huiling Duan, Qing Xu, Guoxing Wang, and Wenjun Yin

Insights Value Technology, Beijing 100071, China

Abstract. Convolutional Neural Network (CNN) is one of the main deep learning algorithms that has gained increasing popularity in a variety of domains across the globe. In this paper, we use U-net, one of the CNN architectures, to predict spatial $PM_{2.5}$ concentrations for each 500 m × 500 m grid in Beijing. Different aspects of data including satellite data, meteorological data, high density $PM_{2.5}$ monitoring data and topography data were taken into consideration. The temporal and spatial distribution patterns of $PM_{2.5}$ concentrations can be learned from the result. Then, a customized threshold was added for each predicted grid $PM_{2.5}$ concentration to define high-value areas to find precise location of potential $PM_{2.5}$ discharge events.

Keywords: Convolutional Neural Network (CNN) · U-net · Deep learning · $PM_{2.5}$ concentration

1 Introduction

Beijing is a megacity with intensive energy consumption and relatively concentrated air pollutants emissions. Many factors contribute to the high concentration of $PM_{2.5}$ in Beijing, and one of them is its unique geographical location. It connects to Taihang Mountain on the west and Yanshan Mountain on the north, and the ridges form an arc- shaped barrier with an average elevation of 1000 m (3280 feet), which makes air pollutants difficult to diffuse. In addition, the air quality is also affected by its surrounding regions especially from the South where the air pollution level is higher.

With the implementation of $PM_{2.5}$ regulations in Beijing over the past few years, the concentration of $PM_{2.5}$ has decreased from 89 $\mu g/m^3$ to 38 $\mu g/m^3$ from 2013 to 2020, with a decreasing rate of 57.3%. However, it was still higher than the second level concentration limit of National Ambient Air Quality Standard (35 $\mu g/m^3$). Since 2019, the annual average concentrations of SO2, NO2, CO and PM10 have reached the second level concentration limit of National Ambient Air Quality Standard for two consecutive years, only $PM_{2.5}$ and O3 were still higher than the standard. And $PM_{2.5}$ composed the majority part in heavy pollution days. In 2020, $PM_{2.5}$ was still the major pollutant in heavy pollution days, accounting for 70.0%. Thus, $PM_{2.5}$ is still one of the major pollutants affecting air quality in Beijing. With its unique geographical location and complex air pollution situations, to continuously improve air quality in Beijing,

R. Qiu et al. (Eds.): ICSS 2021, LNOR, pp. 65–75, 2021.
https://doi.org/10.1007/978-3-030-90275-9_6

it is necessary to develop a method to better understand the pollutant concentration distribution and locate high discharge areas.

The current $PM_{2.5}$ monitoring system is a combination of traditional air quality monitoring systems (i.e. city monitors, state monitors, etc) and high-density IoT monitoring network based on low cost sensors. However, due to the limited number and the limitation of spatial distribution of monitors, it is difficult to obtain the pollution concentration of certain areas. The common way to obtain the concentration where a monitor does not exist is to use interpolation methods such as inverse distance weighting interpolation (IDW) and Kriging interpolation, etc. But the downside of interpolation methods is that it normally has a large error and is not quite reliable [1, 2].

Another method to calculate the concentration of $PM_{2.5}$ is using Satellite remote sensing technique. Compared with the traditional ground monitoring stations, satellite remote sensing technology can measure large spatial and temporal pollutant concentration. Satellite remote sensing technique has become one of the most important $PM_{2.5}$ concentration monitoring methods [3, 4]. Previous research has found that there is a correlation between Aerosol Optical Depth (AOD) and concentration of near-ground particles [5–8]. The $PM_{2.5}$ concentrations can be calculated by using multipleregression [9], Chemical Transport Model (CMT) [10] and Mixed Effect Model [11], etc. These models can measure pollutant concentration on a large spatial and temporal scale, but cannot capture partial changes.

Based on previous research, deep learning methods can also be used to compute the concentration of $PM_{2.5}$. This paper uses Convolutional Neural Network (CNN), a deep learning algorithm which takes surface meteorological data, topographical conditions, high-density $PM_{2.5}$ monitoring data, Satellite remote sensing data and grids data as input and outputs the grid $PM_{2.5}$ concentrations.

2 Method

Convolutional Neural Network (CNN) is a deep learning neural network which is composed of multiple layers of artificial neurons to process structured data such as images [12, 13]. The artificial neurons are mathematical functions which are designed to calculate the weighted sum of different inputs and yield an activation value. A typical CNN includes three layers: convolution layer, pooling layer and fully connected layer. The convolutional layers are to extract features from the input image, the pooling layers are to reduce the dimension of the input image and the fully connected layer is to map the extracted features into final output [14] (see Fig. 1).

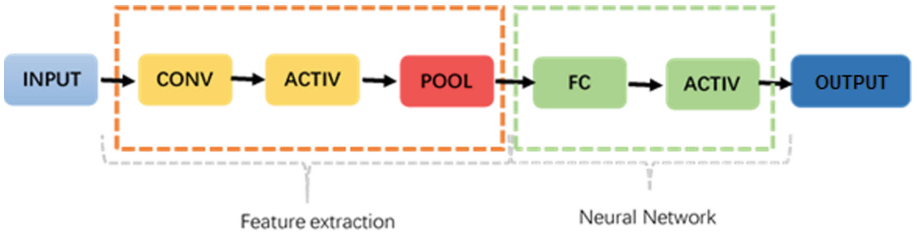

Fig. 1. Typical convolutional neural network process

2.1 Convolution and Activation

A convolution is a type of linear operation used to extract features from input images. It learns the image features by using a small square of data (known as a kernel or a filter and the data is called weights or parameters) multiplied with an array of the input data [14]. The kernel starts from the top left corner of the input image and slides to the right of the image by a predefined step size. For each sliding step, the dot product of the kernel and the pixel values gives a single activation value. After sliding all over the cells, an array of numbers was produced, known as an activation map or a feature map (see Fig. 2).

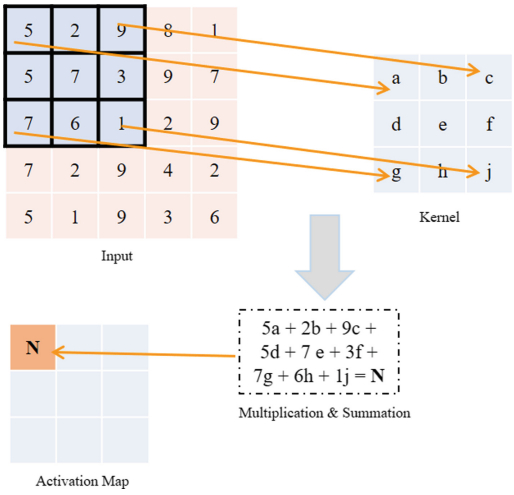

Fig. 2. Feature extraction process

The convolution process represents a linear relationship between the inputs and outputs, which results in one of the drawbacks that nonlinear functions could not well fit in such a process. Therefore, we combined it with nonlinear functions to increase the flexibility for more complex scenarios. The new component we added in the CNN architecture is an activation function. Among commonly used activation functions, such as Sigmoid, Tanh and ReLU, we chose ReLU in our case for its reliability.

If the input image has a size of W × W × D and the kernel with a spatial size of F and stride S and amount of padding P, then, the size of the output volume can be determined by the following formula:

$$W_{out} = \frac{W - F + 2P}{S} + 1$$

The size of output volume will be: Wout × Wout × D

2.2 Pooling Layer

Pooling layer is designed to reduce the spatial size of the featured maps as well as the needed amount of computations and weights in the way of replacing a pixel neighborhood of the output with a summary static such as Max Pooling, Min Pooling and Average Pooling. In this paper we will use Max pooling (see Fig. 3).

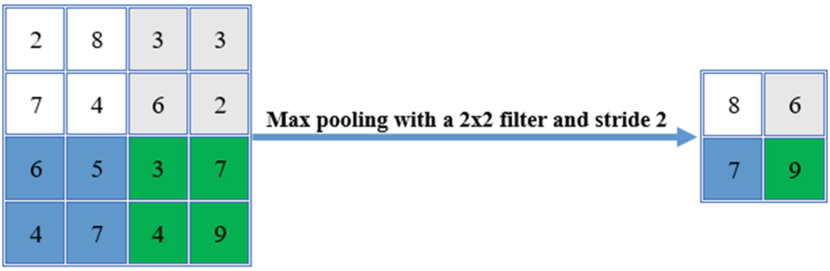

Fig. 3. Pooling process

If we have an activation map of size W × W × D, and a pooling kernel with a spatial size F and stride S and amount of padding P, then size of the output volume can be determined by formula:

$$W_{out} = \frac{W - F}{S + 1}$$

The size of output volume will be: Wout × Wout × D

2.3 Fully Connected Layer

A fully connected layer bridges all the neurons in the preceding steps by inputting and outputting vectors normally via the connection of a classification function, such as Sigmoid and Softmax [14]. In this paper, however, we will apply a regression function on the output since we are expecting to get the concentration of $PM_{2.5}$.

Generally used CNN architectures include VGG, Le Net-5 and U-Net. We will use U-Net in our case for modification of parameters in the process of data training. U-Net consists of two functions: contraction, following the convolution and pooling; and symmetric expanding, turning transposed convolutions into enabled precise localization [15]. In the contraction path, it uses 3 × 3 unpadded convolutions with ReLU as the activation function, followed by a 2 × 2 max pooling with a stride of 2 for spatial reduction. For the expansive path, it uses 2 × 2 transposed convolution with stride 2, then followed by two 3 × 3 convolutional layers to concatenate with a cropped version of the previous feature map (see Fig. 4).

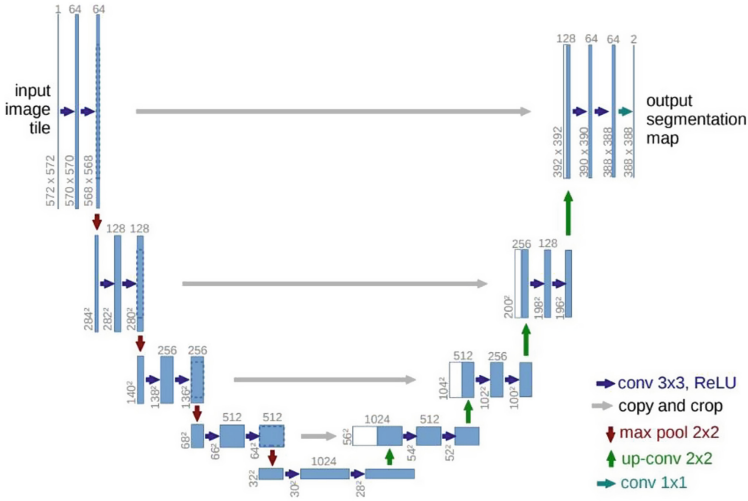

Fig. 4. U-net architecture

3 Data

3.1 Satellite Data

We chose to use the MODISL2G1km data from Satellite Terra and Aqua, obtained from NASA's website. The time period is set from 01/01/2020 to 12/31/2020. The data is pre-processed into 500 m * 500 m using bilinear interpolation method.

3.2 Meteorological Data

The Meteorological data, that includes temperature, atmospheric pressure, humidity, precipitation, evaporation, wind direction, and wind speed, is obtained from the National Meteorological Data Center based on the 18 monitoring spots in Beijing. Similarly, the data was pre-processed into 500 m * 500 m using Kriging interpolation approach for better result [16]. Time period is set from January 2020 to December 2020.

3.3 High Density $PM_{2.5}$ Monitoring Data

In 2016, more than a thousand sensors were set up for $PM_{2.5}$ monitoring. The spatial distribution of sensors is 3 km * 3 km in flat areas and 8 km $\times$ 8 km in mountain areas. And the data from January 2020 to December 2020 was used.

3.4 Topography Data

The topography data was obtained from the Shuttle Radar Topography Mission (SRTM) Digital Elevation Model (DEM) with a spatial resolution of 90 m * 90 m.

The data used in the model is shown in Table 1.

Table 1. Information of data items

Data	Parameter	Description	Unit	Data	Parameter	Description	Unit
$PM_{2.5}$	$PM_{2.5}$	Particle ≤ size 2.5 μm^3	$\mu g/m^3$	Meteorological Data	Pressure	Surface pressure	Pa
Satellite Data	AOD	MAIAC AOD	-		Temperature	2 m air temperature	°C
Land Utilization	VI	Vegetational Coverage	-		Humidity	Relative humidity	%
	LUC	Land Coverage	-		Precipitation	Total precipitation	mm
Topography	DEM	Digital Elevation Model	M		Evaporation	Evaporation	mm
	Relief	Surface relief	m		Wind Speed	10 m wind speed	m/s
	Aspect	Surface aspect	degree		Wind Direction	10 m wind direction	16 directions
	Slope	Surface slope	degree		Sunshine Duration	sunshine duration	Hour
					0 cm ground temperature	0 cm ground temperature	°C

4 Result

To train the data, we deployed pre-processed satellite data, $PM_{2.5}$ monitoring data, meteorological and topography data into one feature vector and then took the feature vector as the input of U-net architecture for feature extraction and pattern learning. For each feature vector, it contains 12 values for $PM_{2.5}$ monitoring data per month, 3 * 12 pre-processed AOD values, 9 * 18 * 12 meteorological values, one topography information value, 3 LUC and 6 VI values, which generate 2110 feature values. Then we used the corresponding values to define labels, such as the value of $PM_{2.5}$ higher than a certain threshold, we label it as 1. Finally we took the encoded data as a training dataset and deployed supervised learning based on U-net architecture. After the CNN model is trained, we then apply the network for $PM_{2.5}$ concentration predictions. The whole process is shown in Fig. 5.

For the accuracy of the model, we use Root Mean Squared Error (RMSE) to evaluate the predictions. The formula of the error function is defined as:

$$RMSE = \sqrt{\frac{1}{N}\sum_{t=1}^{N}\left(y_t - \hat{y}_t\right)^2}$$

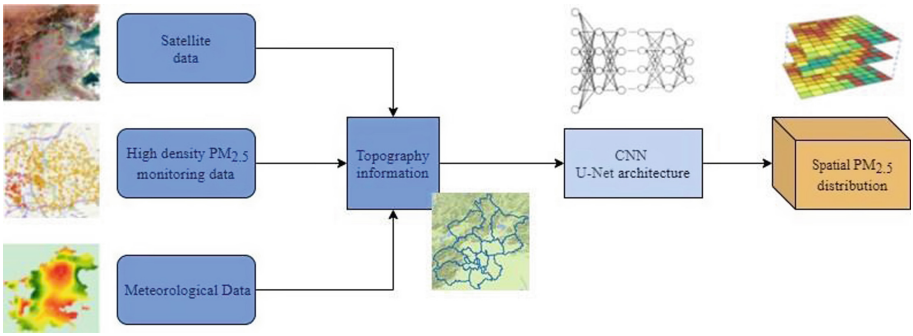

Fig. 5. Framework of grid $PM_{2.5}$ concentration prediction

Where N is the number of monitoring sensors, $\hat{y}_t$ is the predicted concentration for girds where a monitoring device exists and y_t is the actual monitored $PM_{2.5}$ concentration. The RMSE for annual average $PM_{2.5}$ concentrations is 2.24 and the monthly average is 4.76. We then calculated the correlation for each predicted concentration with actual monitored concentration. The result shows a positive relation correlation with a R^2 of 0.88 for annual average and 0.91 for monthly average. Figure 6 shows the scatter plot of the correlation between estimated $PM_{2.5}$ concentration and observed concentration.

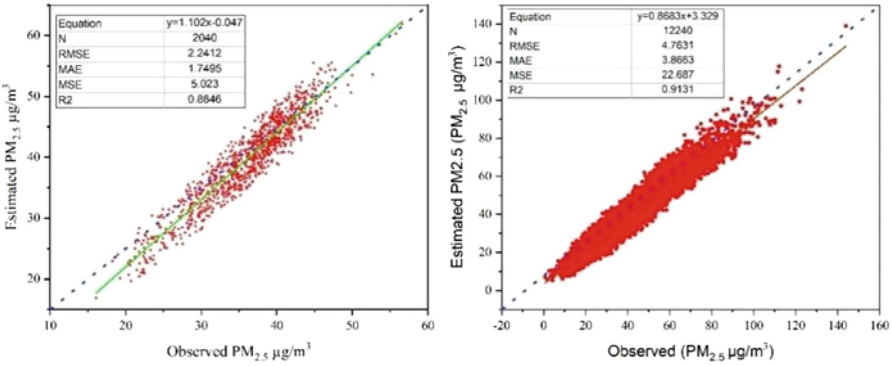

(a) Annual Average (b) Monthly Average

Fig. 6. Estimated $PM_{2.5}$ concentration and observed $PM_{2.5}$ concentration

To further examine the performance of the U-Net based model we deployed in our study, two other commonly used deep learning models were adopted and compared, and the results were listed in Table 2. We used the monthly averaged dataset for the comparison. The RMSE for Gated Recurrent Unit (GRU) and VGG16 were 8.52 and 6.54 respectively, which were much higher than the RMSE we got for the U-Net based model. Also, the R^2 for GRU and VGG 16 were 0.77 and 0.84, lower than that of the U-Net. In conclusion, the U-Net model we developed has done a relatively better job in terms of extracting, classifying, processing and predicting data.

Table 2. Comparison of the performance of models based on monthly predictions

Model	RMSE	R2
GRU	8.52	0.77
VGG 16	6.54	0.84
U-Net	4.76	0.91

5 Application

5.1 Beijing Spatial $PM_{2.5}$ Concentration Distribution

Beijing has been divided into 500 m * 500 m grids and with the output of the algorithm, we can obtain $PM_{2.5}$ concentration data for each grid. With the data, we can use data visualization techniques to display $PM_{2.5}$ concentration distributions of Beijing, which enable us to learn the patterns of distribution to get a clear idea of distribution characteristics in different time periods. Figure 7a shows $PM_{2.5}$ concentration spatial distributions of 2020. From the figure, it is obvious to see that the concentration of $PM_{2.5}$ gradually decreases from South to the North, showing a gradient distribution.

Besides annual distribution, we can also visualize monthly distributions to get more details of the patterns. Figure 7b shows the concentration distribution in January 2020. In January, the Southern part has the worst air quality especially in Fangshan, Daxing and Tongzhou districts, while the Northern part has the best air quality. And a small part of the northwest has a slightly higher pollution level than the North. The distribution has the same pattern as the annual $PM_{2.5}$ concentration distribution, which shows a gradient distribution from North to the South.

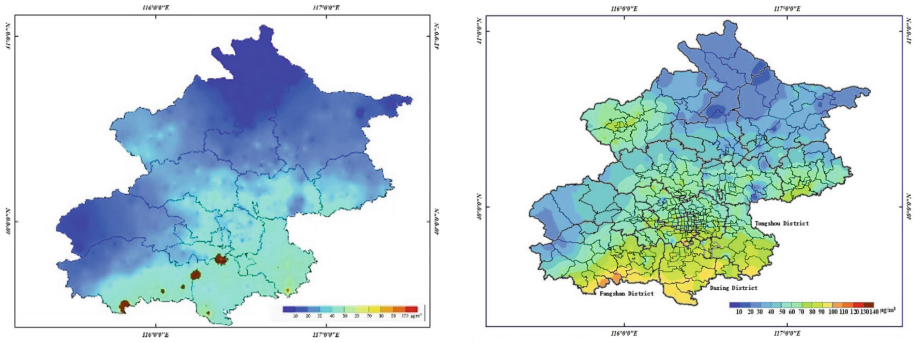

(a) Beijing $PM_{2.5}$ Distribution in 2020 (b) Beijing $PM_{2.5}$ Distribution in January 2020

Fig. 7. $PM_{2.5}$ Distribution in Beijing

5.2 High Value Areas

By creating the spatial distribution map, it delivers a general idea of the characteristics of $PM_{2.5}$ distributions of different time periods and concentration levels in each township. We then further processed the grid concentration data to add a customized threshold (i.e. 35 ug/m^3) by giving varied weights to different parts of the mega city, for example a higher weight is assigned to the grids inside the built-up area while those in the suburb have a lower weight. Then, the weighted concentration scores are calculated and ranked, the top 15% on the list will be automatically recognized as significant high-value area (marked with purple), the 16%–30% will be recognized as moderate high-value area (marked with red), and the 31%–45% will be recognized as normal high-value area (marked with orange). All high-value areas will be highlighted on the map. Each area where high value is densely distributed, is corresponding to higher pollution level in the spatial distribution. Take January 2020 as an example, from the spatial distribution (January in Fig. 7b), it is obvious that the pollution level is more severe in the South than the North, especially in Fangshan, Daxing and Tongzhou districts. The distribution of High Value areas in January (Fig. 8(A)) shows the same pattern as the spatial distribution. For each highlighted area, it means there is an occurrence of high pollution discharge in the specific area. Since the high discharge areas have been narrowed down to 500 m * 500 m grids and with geological information, it is possible to locate the discharge events. One of the ways to locate these areas are to enlarge the map and find the location information about a specific grid. Take a random high value area in Fangshan District in January 2020 as an example, when we enlarge the map, we can clearly see the location of the grid (Fig. 8(B)) is next to Beijing Tixiang Golf club and right by the toll gate of G4 highway. Thus it is possible to help local authorities find the source of discharge events and implement management strategies accordingly.

(a) High value area distribution

(b) Location of a high value area in Fengtai district

Fig. 8. $PM_{2.5}$ distributions in January 2020

6 Summary

This paper uses U-net architecture and combines Satellite sensing data, meteorological data, high-density $PM_{2.5}$ monitoring network data and topography data together as an

input for the deep learning model to calculate the spatial concentration of $PM_{2.5}$ for each 500 m * 500 m grid in Beijing. By visualizing the result, we obtained $PM_{2.5}$ concentration distribution patterns on a temporal and spatial scale. To further narrow down high concentration distribution areas, we added a customized threshold for each grid to locate high value areas. Spatial distribution shows overall distribution of Beijing, while high-value areas help identify specific high discharge events to enable authorities to find potential sources of pollutants. With the combination of spatial distribution of $PM_{2.5}$ and high-value areas, it is possible to help the city continuously improve its air quality. For next steps, we are planning to add more features such as pollution source data and high altitude meteorological data to further improve the accuracy of the result.

References

1. Lv, B., Hu, Y.: Improving the accuracy of daily PM2. 5 distributions derived from the fusion of ground-level measurements with aerosol optical depth observations, a case study in north China. Environ. Sci. Technol. **50**(9), 4752–4759 (2016)
2. Jiao, L., Xu, G.: LUR-based Simulation of the Spatial Distribution of $PM_{2.5}$ of Wuhan. Geomatics and Information Science of Wuhan University, vol. 40, no. 8, pp. 1088–1093 (2015). (in Chinese)
3. Beckerman, B.S., Jerrett, M.: A hybrid approach to estimating national scale spatiotemporal variability of $PM_{2.5}$ in the contiguous United States. Environ. Sci. Technol. **47**(13), 7233–7241 (2013)
4. Huang, X.H.H., Bian, Q.: Characterization of $PM_{2.5}$ major components and source investigation in suburban Hong Kong: a one year monitoring study. Aerosol Air Quality Res. **14**, 237–250 (2014)
5. Wang, J., Christopher, S.A.: Intercomparison between satellite -derived aerosol optical thickness and $PM_{2.5}$ mass: implications for air quality studies. Geophys. Res. Lett. **30**(21), 2095–2099 (2003)
6. Liu, Y., Sarnat, J.A.: Estimating ground-level $PM_{2.5}$ in the Eastern United States using satellite remote sensing. Environ. Sci. Technol. **39**(9), 3269–3278 (2005)
7. Schaap, M., Apituley, A.: Exploring the relation between aerosol optical depth and $PM_{2.5}$ at Cabauw, the Netherlands. Atmos. Chem. Phys. **9**(3), 909–925 (2009)
8. van Donkelaar, A., Martin, R.V.: Estimating ground-level $PM_{2.5}$ using aerosol optical depth determined from satellite remote sensing. J. Geophys. Res. Atmos. **111**, D21201 (2006)
9. Pu, L., Zhu, H.: Application of satellite remote sensing to ground-level $PM_{2.5}$ concentration estimation in Shanghai. Shanghai Municipal Center for Disease Control and Prevention, vol. 34, no. 2, pp. 99–105 (2017). (in Chinese)
10. Boys, B.L., Martin, R.V.: Fifteen-year global time series of satellite-derived fine particulate matter. Environ. Sci. Technol. **48**(19), 11109–11118 (2014)
11. Liu, Y., Paciorek, C.J.: Estimating regional spatial and temporal variability of $PM_{2.5}$ concentrations using satellite data, meteorology, and land use information. Environ. Health Perspect. **117**(6), 886–892 (2009)
12. Véstias, M.P.: A survey of convolutional neural networks on edge with reconfigurable computing. Algorithms **12**(8), 154–177 (2019)
13. Sharma, N., Jain, V.: An analysis of convolutional neural networks for image classification. Procedia Comput. Sci. **132**, 377–384 (2018)
14. Yamashita, R., Nishio, M., Do, R.K.G., Togashi, K.: Convolutional neural networks: an overview and application in radiology. Insights Imaging **9**(4), 611–629 (2018). https://doi.org/10.1007/s13244-018-0639-9

15. Ronneberger, O., Fischer, P., Brox, T.: U-Net: convolutional networks for biomedical image segmentation. In: Navab, N., Hornegger, J., Wells, W.M., Frangi, A.F. (eds.) MICCAI 2015. LNCS, vol. 9351, pp. 234–241. Springer, Cham (2015). https://doi.org/10.1007/978-3-319-24574-4_28
16. Li, J., Zhang, J.: Comparison of spatial interpolation methods of meteorological elements. Pratacultural Sci. **23**(8), 6–11 (2006). (in Chinese)

An Interpretable Ensemble Model of Acute Kidney Disease Risk Prediction for Patients in Coronary Care Units

Kaidi Gong and Xiaolei Xie(✉)

Departmentof Industrial Engineering, Tsinghua University, Beijing 100084, China
xxie@tsinghua.edu.cn

Abstract. Acute kidney injury (AKI), which refers to the abrupt decrease in renal function, is a common clinical condition in cardiovascular patients. The interaction between heart and kidney complicates the patient's condition, increasing the difficulty of treatment. Therefore, AKI is one of the focuses in the management of cardiovascular patients. Timely reversal of AKI is beneficial to the treatment of patients. In this study, we build a voting-based ensemble prediction model of acute kidney disease (AKD, referring to acute or subacute kidney damage for 7–90 days) risk for patients in coronary care units (CCU) based on clinical data within the first 6 h since CCU admission, in order to identify the patients whose AKI is hard to reverse. Then we interpret our prediction model using Shapley additive explanation values to help pinpoint important predictors and influence of clinical characteristics such as fluid status on AKD risk. The results show that our method has the potential to support clinical decision making.

Keywords: Acute kidney injury · Machine learning · Model interpretation · Clinical decision support

1 Introduction

Acute kidney injury (AKI) refers to the abrupt decrease in renal function, resulting in the retention of urea and other nitrogenous waste products and dysregulation of extracellular volume and electrolytes [1]. AKI can range from mild kidney impairment to severe kidney failure requiring dialysis. Previous studies have found that even mild kidney injury is related to poor prognoses and high resource consumption [2]. AKI is common in hospitalized patients: according to a meta-analysis conducted by the acute kidney injury advisory group of the, the overall pooled incidence rate and mortality rate of AKI reach 22.8% and 22.4% respectively [3]. The etiology of AKI can be classified into three categories: prerenal disease (caused by insufficient renal perfusion, often because of volume depletion), intrinsic renal disease (caused by intrinsic damages of renal tissues), and postrenal causes (caused by urinary tract obstruction). Approximately 65%–75% of cases of AKI in the hospital are due to either prerenal disease or acute tubular necrosis (ATN) [4]. If not reversed or treated timely, prerenal AKI can cause tissue death in the kidneys and lead to intrinsic AKI.

R. Qiu et al. (Eds.): ICSS 2021, LNOR, pp. 76–90, 2021.
https://doi.org/10.1007/978-3-030-90275-9_7

Nowadays, the prevalence of AKI and cardiorenal syndrome (CRS) is growing in hospitalized patients with cardiovascular diseases (CVD), attracting expanding focuses. AKI occurs in approximately 1/4 inpatients with CVD [5]. In the cardiac intensive care unit, AKI prevalence is reported to be 25%–50%, up to 1/3 of which is severe AKI [6]. On the one hand, heart diseases and kidney diseases share several common diseases such as diabetes, hypertension, and high cholesterol. On the other hand, dysfunctional heart and kidneys can impact each other through hemodynamic derangements, inflammatory signaling pathways, and neurohormonal activation, leading to mutual end-organ disease progression [7]. The majority of AKI in patients with CVD is caused by decreased renal perfusion due to low cardiac output and is usually reversible. Through supportive treatment and volume management, physicians can correct the reduced renal perfusion and reverse the hemodynamic damage earlier, thus facilitating the control of the disease and improving patient outcomes.

AKI occurrence, severity, and duration are all related to the short- and long-term outcomes of patients with CVD. For patients with acute heart failure, previous studies obtain different conclusions on the impact of transient AKI on prognosis, but all of them validate that persistent AKI significantly increases the mortality risk [8, 9]. For myocardial infarction patients, except for patients with transient mild AKI, the outcomes of all patients with persistent AKI or moderate/severe AKI are significantly worse than those without AKI [10, 11]. To improve the outcomes of patients with CVD, both AKI prevention and AKI recovery should be paid attention to.

Abundant research has worked on AKI prediction and prevention, but relatively less attention has been given to recovery from AKI. Through the study on approximately 17,000 critically ill patients with moderate or severe AKI, Kellum and his team observe five patterns of AKI recovery: early sustained reversal, relapse recovery, relapse no recovery, late reversal, and never reversed [12]. Early reversal is defined as the absence of AKI for at least 24 h within 7 days of the first onset of AKI in their study and is reported to be associated with significant improvement in outcome compared to late reversal and non-reversal. The counterpart of early reversal is acute kidney disease (AKD), which describes acute or subacute kidney damage for 7–90 days.

Early identification of persistent AKI is important in patient management [13], helping clinicians conduct extended evaluation and intervention to avoid further kidney damage and reciprocal deterioration between heart and kidneys. However, there are still limited prediction tools for persistent AKI and delayed recovery. Risk factors have not been investigated enough either. Though machine learning and artificial intelligence have been widely used in AKI management, most focus on AKI prediction [14], mortality prediction [15], and risk factors contributing to AKI [16]. Few have paid attention to the effect of treatment measures and other factors on the development or recovery of AKI. Previous studies [17, 18] mainly use resistive index, Cystain C, NGAL, and other biomarkers to differentiate rapid reversal of AKI from persistent AKI. Brown et al. [19] use step-wise multivariable negative binomial regression analysis to predict the AKI duration after cardiac surgery. They find that independent predictors involve baseline patient and disease characteristics, operative and post-operative factors. Peerapornratana and his colleagues [20] study sepsis-associated acute kidney disease and predict whether patients would develop AKD using logistic regression based on clinical variables and

biomarkers. While existing AKI biomarkers have limited predictability, the combination of biomarkers and clinical variables can achieve an area under the receiver operating characteristic curve (AUC) score of 0.74. They find that male sex, African American race, and high acute physiology score III significantly increase the odds of developing AKD, while high urine output and the use of mechanical ventilation significantly favor AKI early reversal. The interpretability of machine learning prediction models is also an important problem. While more and more complex models are applied to improve predictive performance, more challenges are encountered in practical application due to the lack of interpretability.

In view of these limitations in existing studies, this study uses machine learning methods to predict and analyze AKI recovery in CCU patients and focuses on the interpretability of the model to better support the management of AKI. Specifically, we investigate several base prediction models and their stacking and voting ensembles to predict the risk of developing AKD using the data within the first 6 h in CCU. Then based on the voting ensemble with the best prediction performance, we apply Shapley additive explanation (SHAP) values to interpret the model, identify important predictors, and analyze the impacts of fluid and blood pressure management on AKI recovery, so as to support clinical decision making.

2 Data Set

2.1 Data Source

The data used in this study is extracted from Medical Information Mark for Intensive Care (MIMIC-III) database. MIMIC-III database is a freely accessible critical care database [21], which is in accordance with the Health Insurance Portability and Accountability Act (HIPAA) Privacy Rule. The database includes 58,976 hospitalizations and 61,532 associated ICU stays from 46,520 patients admitted to the critical care units in Beth Israel Deaconess Medical Center between 2001 and 2012. Specifically, for adult patients, the data involves medical intensive care unit (MICU), surgical intensive care unit (SICU), coronary care unit (CCU), cardiac surgery recovery unit (CSRU), and trauma surgical intensive care unit (TSICU).

We extract adult CCU patient data with a primary diagnosis of CVD (ICD9 code: 390.−429.) and having AKI within the first 24 h in CCU. AKI is diagnosed and staged according to KDIGO (Kidney Disease: Improving Global Outcomes) criteria [22]. Patients older than 89 years old, with CCU length of stay less than 24 h, with baseline serum creatinine (SCr) higher than 4 mg/dL, receiving renal replacement therapy (RRT) before CCU admission or expired within 7 days after CCU admission are excluded. The final dataset includes 1,240 patients, among which 1,121 patients occur early reversal and 119 patients develop AKD (Fig. 1).

Through literature review and consultation with clinicians, we extract demographics, basic health conditions, vital signs, laboratory measures, fluids, and other interventions within the first 6 h in CCU to predict the risk of developing AKD. Table 1 lists the detailed clinical variables. The baseline SCr is estimated by the minimum serum creatinine level. Body mass index (BMI) is calculated from admission weight and height.

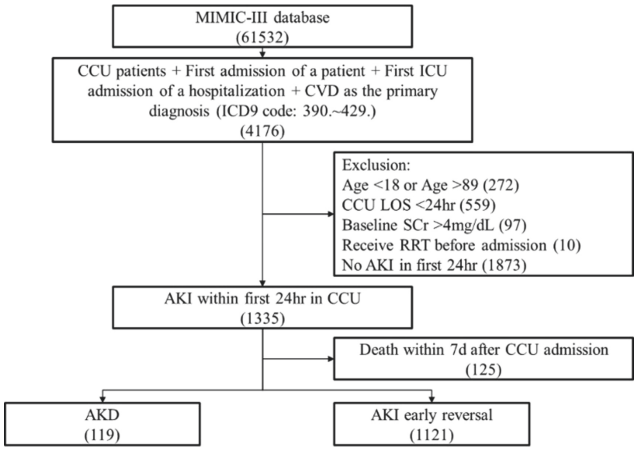

Fig. 1. Data inclusion and exclusion

Table 1. Clinical variables in the dataset

Class	Variable	Data type	Missing (%)	Class	Variable	Data type	Missing (%)
Demographics	Age	Numeric	0.0	Basic health conditions	Primary diagnosis	String	0.0
	Gender	Binary	0.0		Baseline creatinine	Numeric	0.0
	Ethnicity	Nominal	0.0		Diabetes mellitus	Binary	0.0
Vital signs	BMI	Numeric	12.1		Hypertension	Binary	0.0
	Body temperature	Numeric	3.9		CKD	Binary	0.0
	Systolic BP	Numeric	1.6		CHF	Binary	0.0
	Diastolic BP	Numeric	1.6		AKI stage	Ordinal	0.0
	Mean Arterial BP	Numeric	1.6	Fluids	Crystalloids	Numeric	0.0
	CVP	Numeric	82.7		Colloids	Numeric	0.0
	SpO2	Numeric	1.7		Normal saline	Numeric	0.0
	Heart rate	Numeric	1.3		Lactated ringers	Numeric	0.0
	Respiration rate	Numeric	1.3		Urine output	Numeric	0.0
Lab measurements	Albumin	Numeric	68.8		Net fluid balance	Numeric	0.0
	Bicarbonate	Numeric	10.7	Other interventions	Mechanic ventilation	Binary	0.0

(*continued*)

Table 1. (*continued*)

Class	Variable	Data type	Missing (%)	Class	Variable	Data type	Missing (%)
	BNP	Numeric	98.9		RRT	Binary	0.0
	BUN	Numeric	9.2		Diuretics	Binary	0.0
	Chloride	Binary	9.4		Epinephrine	Binary	0.0
	Creatinine	Numeric	9.2		Norepinephrine	Binary	0.0
	Hematocrit	String	6.4		Phenylephrine	Binary	0.0
	Hemoglobin	Ordinal	8.3		Vasopressin	Binary	0.0
	Lactate	Numeric	66.2		Dopamine	Binary	0.0
	Platelet	Numeric	9.8		Dobutamine	Binary	0.0
	Sodium	Nominal	7.7				
	White blood cell	Numeric	12.7				

Abbreviations: BP: Blood pressure; CVP: Central venous pressure; BUN: Blood urea nitrogen; BNP: Brain natriuretic peptide; CKD: Chronic kidney disease; CHF: Congestive heart failure

2.2 Data Pre-processing

To deal with the missing values, we first delete variables with more than 60% missing values including CVP, albumin, BNP, and lactate. Regarding other indicators containing missing values, median values are used to impute. For time-dependent variables including vital signs (except BMI) and laboratory measurements, we extract the maximum and minimum values within the first 6 h in CCU.

The primary diagnosis of each patient is recorded as the International Classification of Diseases (ICD-9) code in the MIMIC-III database. The first 3 digits are extracted and analyzed for each ICD-9 code. Top 6 frequent primary diagnoses (acute myocardial infarction, cardiac dysrhythmias, heart failure, other forms of chronic ischemic heart disease, other diseases of endocardium, and other diseases of pericardium) cover more than 90% of cases. We convert the primary diagnosis from a string to a one-hot vector based on these 6 primary diagnoses, with the elements referring to ICD-9 codes (410., 427, 428., 414., 424., 423.). 70% of the data is used for training and 30% for held-out tests.

3 Methods

3.1 Framework

Our prediction and interpretation framework is shown in Fig. 2. After data extraction and pre-processing, we first propose six base predictive models to handle the class imbalance problem. Then stacking ensemble and voting ensemble are applied to convert the weak learners to stronger ones. The stacking model trains a second-layer learning algorithm using the predictions of base-learners as input, which can typically enhance prediction accuracy and robustness than individual models. Soft-voting is an easy but useful

ensemble method in which the prediction probabilities of individual models are weighted averaging to obtain the final prediction. It can combine the advantages of different models and achieve better performance. Finally, the ensemble model is interpreted using SHAP values, which is model-agnostic and thus supports a wide range of prediction models. Through the model interpretation, not only do we identify important predictors, but also pinpoint the detailed impacts of predictors on AKD risk.

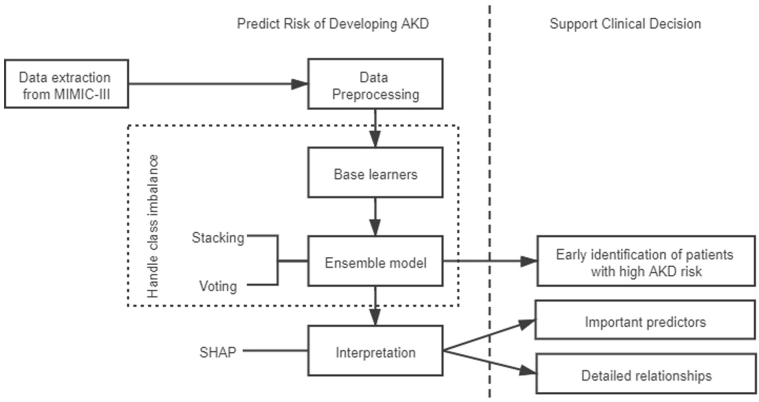

Fig. 2. Framework of AKD risk prediction and interpretation

3.2 Prediction

Logistic regression is popular in clinical prediction [14] for its solid theoretical foundation and nice interpretation, thus widely used as a baseline. Compared to linear models, tree models support non-linearity better. We explore three ensemble models of decision trees: random forest, XGBoost, and LGBM. Random forest obtains accuracy and robustness through bagging strategy [23]. XGBoost [24] and LGBM [25] achieve peak performance and efficiency with gradient boosting and parallel computing. To deal with the class imbalance problem, two strategies are considered: weight adjustment and over-sampling. The weight adjustment strategy increases the punishment of misclassifying minority examples, while over-sampling increases the number of minorities. ADASYN [26] is an efficient over-sampling method that can generate more synthetic data for "harder-to-learn" examples, i.e., minority examples with more majority examples in their neighborhood. Specifically, we investigate six base-learners, for which hyper-parameters are determined using 5-fold cross-validation on the training set and displayed in Table 2.

(1) Logistic regression with balanced class weight (LR): weight in the logistic regression model is adjusted to be inversely proportional to class frequency in the input data as $N/(N_c * N_i)$ for class i, where N, N_c, N_i refer to the number of total samples, number of classes, and number of samples in class i respectively. The penalization of the misclassification of minority class (i.e., class of AKD) is N_0/N_1 times as

much as that of majority class (i.e., class of early reversal), where N_0 and N_1 refer to the number of majority and minority class respectively.

(2) Random forest with balanced class weight (RF): similar to LR, class weights in the random forest model are adjusted to be inversely proportional to class frequencies in the input data.

(3) Extreme gradient boosting machine (XGBoost) with balanced class weight (XGB1): the weight of samples in the AKD class in XGBoost model is multiplied by N_0/N_1.

(4) XGBoost with half balanced class weight (XGB2): the weight of samples in the AKD class in XGBoost model is multiplied by $N_0/2N_1$. Reducing the weight weakens the penalization of misclassification of minority class and favors prediction specificity more.

(5) Combination of adaptive synthetic sampling (ADASYN) and XGBoost (XGB3): ADASYN, which generates more synthetic data for minority class based on a weighted distribution for different minority class samples according to their learning difficulty, is used for oversampling. It is an extension of synthetic minority oversampling technique (SMOTE), creating more examples in the vicinity of the boundary between the two classes than in the interior of the minority class. Then an XGBoost model is trained on the oversampling training set.

(6) Light gradient boosting machine with balanced class weight (LGBM): the weight of samples in the AKD class in LightGBM model is multiplied by N_0/N_1.

Table 2. Hyper-parameters for base-learners

Base-learner	Hyper-parameters
LR	penalty ='l2'; C = 0.001
RF	max_depth = 7; n_estimators = 100; min_samples_split = 150
XGB1	learning_rate = 0.1; n_estimators = 30; max_depth = 5; min_child_weight = 50; gamma = 0.1; subsample = 0.7; colsample_bytree = 0.9
XGB2	learning_rate = 0.1; n_estimators = 30; max_depth = 5; min_child_weight = 30; gamma = 0.1; subsample = 0.7; colsample_bytree = 0.8
XGB3	ADASYN: sampling_strategy = 1; n_neighbors = 5 XGBoost: learning_rate = 0.1; n_estimators = 30; max_depth = 5; min_child_weight = 50; gamma = 0.1; subsample = 0.7; colsample_bytree = 0.9;
LGBM	learning_rate = 0.1; n_estimators = 50; max_depth = 5; num_leaves = 30; min_child_weight = 50; subsample = 0.8; colsample_bytree = 0.8; reg_lambda = 0.1; reg_alpha = 0.1

Stacking and voting methods are applied to combine the weak base-learners to achieve better performance. In the stacking ensemble, logistic regression with balance classed weight is used as the meta-learner to train based on the predictions of base-learners. In the voting ensemble, weights are assigned as the F1 score of each base model.

We compare different combinations of base-learners to select the best base-learner group for both ensemble methods.

3.3 Interpretation

To obtain reliable model interpretation results, it is important to guarantee the consistency of feature attribution, which means that for model f and f', if

$$f'_x(S) - f'_x(S\backslash i) \geq f_x(S) - f_x(S\backslash i), \forall S \in F \tag{1}$$

then $\phi_i(f', x) \geq \phi_i(f, x)$, where F is the set of predictors and ϕ represents the feature attribution or feature importance. In other words, when the model changes, if the contribution of feature i to the model output does not decrease, then the importance of feature i should not decrease, either.

Traditional feature importance calculated by the weight or gain in tree-based models or by odds ratio in logistic regression cannot guarantee consistency. Therefore, for better interpretation, we employ the SHAP method [27] which originates from game theory and has a solid theoretical foundation. It calculates the marginal effect of each feature for each instance based on the game theoretically optimal Shapley values ϕ:

$$\phi_j(val) = \sum\nolimits_{S\subseteq\{x_1,\ldots,x_p\}\backslash\{x_j\}} \frac{|S|!(p-|S|-1)!}{p!} \cdot \left[val\left(S \cup \{x_j\}\right) - val(S)\right] \tag{2}$$

where, $\{x_1, \ldots, x_p\}$ are the p features in the model, x_j is the feature of interest, and

$$val(S) = \int \hat{f}(x_1, \ldots, x_p) dP_{x\notin S} - E_X \int \hat{f}(X) \tag{3}$$

presents the prediction of model f for feature values in subset S that are marginalized over features excluded in subset S.

The SHAP method estimates Shapley values in a kernel-based approach inspired by local surrogate models. It is model-agnostic, and can provide information both globally (for total dataset) and locally (for each instance).

4 Results

4.1 Comparison of Different Methodologies with All Patient Features

Table 3 lists the performance of different predictive models with all patient features. The results are reported as mean values with 95% confidence interval obtained from $n = 200$ bootstrap samples on the test set. The best performance for each metric among six base learners is underlined and the best among all models is in bold.

Table 3. Comparison of different methodologies with all patient features

	F1 score	AUC score	Accuracy	Sensitivity(Recall)	Specificity	Precision
LR	0.28[0.22,0.34]	0.66[0.58,0.75]	0.68[0.62,0.71]	0.64[0.50,0.78]	0.68[0.63,0.72]	0.18[0.14,0.22]
RF	0.31[0.21,0.41]	0.65[0.57,0.74]	0.80[0.76,0.84]	0.47[0.33,0.64]	0.83[0.79,0.88]	0.23[0.17,0.31]
XGB1	0.31[0.24,0.38]	0.69[0.61,0.76]	0.72[0.69,0.77]	0.64[0.50,0.78]	0.73[0.69,0.78]	0.20[0.16,0.26]
XGB2	0.28[0.15,0.43]	0.60[0.53,0.67]	**0.88[0.85,0.90]**	0.25[0.14,0.39]	**0.94[0.91,0.96]**	**0.32[0.18,0.48]**
XGB3	0.23[0.13,0.34]	0.58[0.51,0.67]	0.80[0.76,0.84]	0.31[0.17,0.47]	0.86[0.82,0.89]	0.19[0.11,0.27]
LGBM	0.29[0.23,0.35]	0.68[0.60,0.76]	0.67[0.62,0.71]	0.70[0.55,0.83]	0.66[0.61,0.72]	0.18[0.15,0.22]
Stack1	0.29[0.24,0.34]	**0.71[0.63,0.77]**	0.62[0.58,0.67]	0.81[0.67,0.94]	0.60[0.55,0.65]	0.18[0.15,0.21]
Stack2(-XGB2)	0.29[0.24,0.33]	0.70[0.63,0.77]	0.61[0.57,0.66]	0.81[0.67,0.92]	0.59[0.54,0.64]	0.18[0.14,0.20]
Stack2(-XGB3)	0.29[0.23,0.33]	0.70[0.62,0.77]	0.61[0.56,0.66]	0.80[0.67,0.92]	0.60[0.54,0.64]	0.17[0.14,0.20]
Stack3(-XGB2, -XGB3)	0.29[0.24,0.33]	**0.71[0.63,0.77]**	0.61[0.55,0.66]	**0.84[0.69,0.94]**	0.58[0.53,0.64]	0.18[0.15,0.20]
Vote1	0.31[0.18,0.43]	0.63[0.55,0.71]	0.84[0.81,0.88]	0.36[0.19,0.53]	0.90[0.86,0.93]	0.27[0.17,0.38]
Vote2(-XGB2)	0.31[0.19,0.43]	0.64[0.55,0.72]	0.83[0.80,0.87]	0.40[0.22,0.56]	0.88[0.85,0.92]	0.26[0.17,0.36]
Vote3(-XGB3)	**0.33[0.25,0.41]**	0.69[0.60,0.77]	0.77[0.72,0.81]	0.58[0.42,0.75]	0.79[0.75,0.83]	0.23[0.17,0.29]
Vote4(-XGB2, -XGB3)	**0.33[0.25,0.40]**	0.70[0.62,0.77]	0.73[0.69,0.78]	0.66[0.53,0.81]	0.74[0.70,0.79]	0.22[0.17,0.28]

Comparing the base predictive models, balanced weight inversely proportional to the number of samples for LR, XGB1, and LGBM largely increase the sensitivity of identifying high-risk AKD patient at the sacrifice of specificity. RF achieves better specificity but performs worse on sensitivity than LR, XGB1, and LGBM. When we adjust the weight of the minority class in XGB1 to half, though we can obtain higher specificity, XGB2 performs quite poorly on sensitivity and AUC score. Both F1 score and AUC score of XGB3 are the lowest. It achieves a bit higher sensitivity but lower specificity than XGB2. XGB1 outperforms the other five base-learners in both F1 score and AUC score.

Due to the relatively poorer AUC scores of XGB2 and XGB3, we test the performance of including and excluding these two base learners in the two ensembles. Results show that voting ensembles are more sensitive to the base models than stacking ensembles. In the stacking ensembles, since the meta-learner automatically learns the results obtained from the base learners, base-learners with better performance are favored more and the impacts of poorer base-learners are weakened. But in the voting ensembles, the impacts of poorer base-learners are greater than in stacking ensembles. The stacking ensembles achieve higher sensitivity while the voting ensembles achieve higher specificity because base-learner RF and XGB2 weight more in the voting ensembles. We select Vote4 (voting ensemble based on LR, RF, XGB1, and LGBM) as the final prediction model with the best F1 score of 0.33 and the second best AUC score of 0.70.

4.2 Comparison of Different Feature Groups

The performance of different feature groups is investigated based on the selected Vote4 model. Firstly, we compare the six different types of features, among which the group of laboratory measurements achieves the best performance than other groups. The reason is likely to be that ICU-level data can reflect the patient's clinical condition such as renal function and blood flows in this ICU stay more precisely and thus has higher predictability. Other interventions and basic conditions also achieve moderate performance, but favor specificity and sensitivity respectively. The group of demographic features performs the worst because it contains too limited information to evaluate the patient's condition. The relatively poor performance of vital signs and fluids might indicate that it is not enough to consider blood pressure and fluid status separately.

Secondly, considering that two of the most important things in AKI management are to maintain normal blood pressure and to optimize the patient's fluid status, we discuss the predictability of the feature combinations of fluids and other related variables. The results demonstrate that prediction based on fluids and blood pressure achieves much better performance than using fluids only, which demonstrates the necessity of considering both aspects in patient management. The inclusion of other interventions further improves the performance, achieving the best F1 score, AUC score, and accuracy among all the feature groups (Table 4).

Table 4. Comparison of different feature groups based on voting ensemble

	N	F1 score	AUC score	Accuracy	Sensitivity(Recall)	Specificity	Precision
Demographics	4	0.20[0.14,0.26]	0.56[0.47,0.64]	0.59[0.54,0.63]	0.52[0.36,0.68]	0.59[0.54,0.64]	0.12[0.09,0.16]
Basic conditions	11	0.24[0.18,0.31]	0.62[0.54,0.70]	0.65[0.60,0.70]	0.59[0.44,0.72]	0.65[0.60,0.71]	0.15[0.11,0.20]
Vital signs	15	0.22[0.16,0.30]	0.59[0.50,0.69]	0.66[0.61,0.71]	0.50[0.33,0.69]	0.68[0.63,0.73]	0.14[0.10,0.19]
Lab measurements	20	0.27[0.19,0.34]	0.64[0.55,0.72]	0.71[0.66,0.75]	0.54[0.37,0.69]	0.73[0.68,0.77]	0.18[0.12,0.22]
Other interventions	9	0.26[0.18,0.35]	0.61[0.54,0.69]	0.77[0.73,0.81]	0.42[0.28,0.58]	0.81[0.76,0.85]	0.19[0.13,0.26]
Fluids	6	0.22[0.16,0.30]	0.59[0.51,0.68]	0.68[0.63,0.72]	0.47[0.32,0.64]	0.70[0.65,0.75]	0.14[0.10,0.20]
Fluids + Other interventions	12	0.20[0.13,0.28]	0.56[0.48,0.65]	0.69[0.64,0.73]	0.41[0.25,0.56]	0.72[0.67,0.77]	0.14[0.08,0.19]
Fluids + Blood pressure	15	0.26[0.18,0.35]	0.62[0.54,0.70]	0.75[0.71,0.79]	0.45[0.31,0.61]	0.79[0.74,0.83]	0.18[0.13,0.25]
Fluids + Blood pressure + Other interventions	18	0.28[0.19,0.38]	0.64[0.55,0.72]	0.77[0.73,0.81]	0.47[0.31,0.64]	0.80[0.76,0.85]	0.20[0.13,0.27]

4.3 Important Predictors

Figure 3 presents the top 20 features obtained by SHAP methods. The horizontal axis corresponds to the SHAP value. The color reflects the feature value, where dark grey and light grey represent low values and high values respectively. For each feature, each dot in the bee-swarm plot corresponds to an individual instance. Higher SHAP values are associated with a higher risk of developing AKD. Besides variables related to blood pressure and fluids, the important predictors include mechanical ventilation, age, variables reflecting the renal function (e.g., blood urea nitrogen (BUN) and reference creatinine), variables related to blood cells (e.g., platelets and hemoglobin), and several vital signs (e.g., heart rate and respiration rate). Also, patients with acute myocardial infarction (ICD-9 code: 410.) should be paid attention to especially.

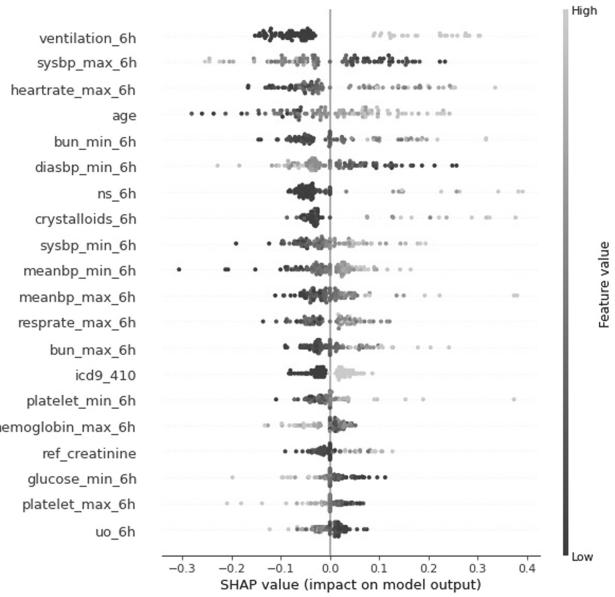

Fig. 3. Top 20 important predictors

4.4 Fluid Status and Blood Pressure Management for CCU Patients with AKI

To better support clinical decisions, more specifically, decisions on the fluid status and blood pressure management, we investigate the detailed relationship between several variables related to fluids and blood pressure using partial dependence plots. The results are shown in Fig. 4 and 5. Similar to Fig. 3, each dot corresponds to an individual instance. The horizontal and vertical axes represent the feature value and the SHAP value respectively.

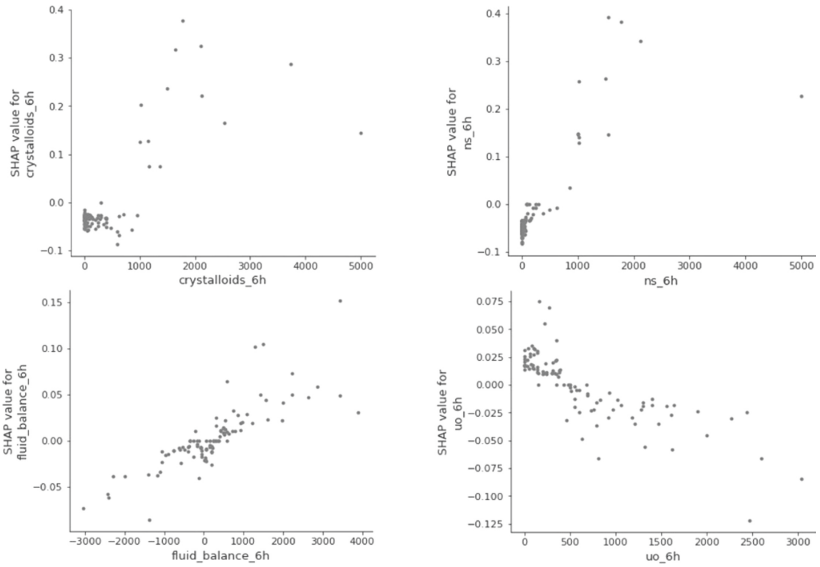

Fig. 4. Partial dependence plots of fluid variables

According to Fig. 4, excessive intravenous fluids (more than 1000 mL crystalloids within the first 6 h), high net fluid balance (more than 500 mL within the first 6 h), and low urine output (less than approximately 400 mL within the first 6 h) are associated with a higher risk of developing AKD.

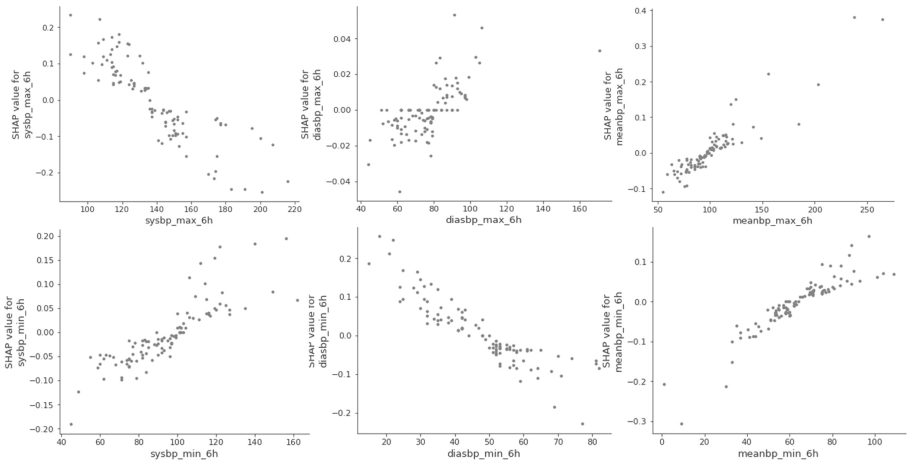

Fig. 5. Partial dependence plots of blood pressure variables

Figure 5 illustrates the relationships between AKD risk and systolic blood pressure (SBP), diastolic blood pressure (DBP), and mean arterial blood pressure (MAP). The

results suggest that 100 mmHg $\leq$ SBP $\leq$ 140 mmHg, DBP $>$ 50 mmHg, and MAP $<$ 100mmHg are associated with lower AKD risk.

5 Summary

AKI and CRS management have attracted more attention in the treatment for patients with cardiovascular diseases due to the increasing prevalence and the expanding studies on the interactions between heart and kidneys. Our study focuses the AKI development in CCU and proposes a voting-based ensemble model to predict the probability of AKI early reversal, or equivalently the risk of developing AKD, for patients with AKI based on the first 6 h data since CCU admission. The model can achieve a moderate performance with an AUC score of 0.70. The prediction model can help identify the CCU patients who are at high risk of AKD earlier and thus enable earlier interventions on these patients to improve their prognoses. To better support patient management, we also interpret our model using SHAP values. Not only do we identify important predictors but also pinpoint the relationships between the predictors and AKD risk. Specifically, we provide references on two of the most important approaches in decreasing the risk of persistent AKI including fluid management and blood pressure maintenance.

Our study still has some limitations. Most importantly, it is a mono-centric and retrospective study. Further external validation of the model is required to evaluate the generalization ability and stability. Secondly, we have not considered whether AKI would relapse for those patients with early reversal. Early reversal with relapse and early sustained reversal can be distinguished in future work.

Acknowledgements. The project is sponsored by Tsinghua-Toyota Joint Research Institute Interdisciplinary Program.

References

1. Chawla, L.S., et al.: Acute kidney disease and renal recovery: consensus report of the acute disease quality initiative (ADQI) 16 Workgroup. Nat. Rev. Nephrol. **13**(4), 241–257 (2017)
2. Uchino, S., Bellomo, R., Goldsmith, D., Bates, S., Ronco, C.: An assessment of the RIFLE criteria for acute renal failure in hospitalized patients. Crit. Care Med. **34**(7), 1913–1917 (2006)
3. Susantitaphong, P., et al.: World incidence of AKI: a meta-analysis. Clin. J. Am. Soc. Nephrol. **8**(9), 1482–1493 (2013)
4. Liano, F., Pascual, J.: Madrid Acute Renal Failure Study Group. Epidemiology of acute renal failure: a prospective, multicenter, community-based study. Kidney Int. **50**(3), 811–818 (1996)
5. Vandenberghe, W., et al.: Acute kidney injury in cardiorenal syndrome type 1 patients: a systematic review and meta-analysis. Cardiorenal Med. **6**(2), 116–128 (2015). https://doi.org/10.1159/000442300
6. Jentzer, J.C., et al.: Changes in comorbidities, diagnoses, therapies and outcomes in a contemporary cardiac intensive care unit population. Am. Heart J. **215**, 12–19 (2019)
7. Deferrari, G., Cipriani, A., La Porta, E.: Renal dysfunction in cardiovascular diseases and its consequences. J. Nephrol. **34**(1), 137–153 (2020)

8. Aronson, D., Burger, A.J.: The relationship between transient and persistent worsening renal function and mortality in patients with acute decompensated heart failure. J. Card. Fail. **16**(7), 541–547 (2010)
9. Krishnamoorthy, A., et al.: Transient and persistent worsening renal function during hospitalization for acute heart failure. Am. Heart J. **168**(6), 891–900 (2014)
10. Goldberg, A., Kogan, E., Hammerman, H., Markiewicz, W., Aronson, D.: The impact of transient and persistent acute kidney injury on long-term outcomes after acute myocardial infarction. Kidney Int. **76**(8), 900–906 (2009)
11. Choi, J.S., et al.: Relation between transient or persistent acute kidney injury and long-term mortality in patients with myocardial infarction. Am. J. Cardiol. **112**(1), 41–45 (2013)
12. Kellum, J.A., Sileanu, F.E., Bihorac, A., Hoste, E.A.J., Chawla, L.S.: Recovery after acute kidney injury. Am. J. Respir. Crit. Care Med. **195**(6), 784–791 (2017)
13. Ronco, C., Ferrari, F., Ricci, Z.: Recovery after acute kidney injury: a new prognostic dimension of the syndrome. Am. J. Resp. Crit. Care Med. **195**(6), 711–714 (2017)
14. Gameiro, J., Branco, T., Lopes, J.A.: Artificial intelligence in acute kidney injury risk prediction. J. Clin. Med. **9**(3), 678 (2020)
15. Lin, K., Hu, Y., Kong, G.: Predicting in-hospital mortality of patients with acute kidney injury in the ICU using random forest model. Int. J. Med. Inform. **125**, 55–61 (2019)
16. Chen, W., et al.: Causal risk factor discovery for severe acute kidney injury using electronic health records. BMC Med. Inform. Decis. Mak. **18**(1), 13 (2018)
17. Ninet, S., Schnell, D., Dewitte, A., Zeni, F., Meziani, F., Darmon, M.: Doppler-based renal resistive index for prediction of renal dysfunction reversibility: a systematic review and meta-analysis. J. Crit. Care **30**(3), 629–635 (2015)
18. Darmon, M., et al.: Diagnostic accuracy of Doppler renal resistive index for reversibility of acute kidney injury in critically ill patients. Intensive Care Med. **37**(1), 68–76 (2011)
19. Brown, J.R., Kramer, R.S., MacKenzie, T.A., Coca, S.G., Sint, K., Parikh, C.R.: Determinants of acute kidney injury duration after cardiac surgery: an externally validated tool. Ann. Thorac. Surg. **93**(2), 570–576 (2012)
20. Peerapornratana, S., Priyanka, P., Wang, S., et al.: Sepsis-associated acute kidney disease. Kidney Int. Rep. **5**(6), 839–850 (2020)
21. Johnson, A.E.W., et al.: MIMIC-III, a freely accessible critical care database. Sci. data **3**(1), 1–9 (2016)
22. Kellum, J.A., et al.: Kidney disease: improving global outcomes (KDIGO) acute kidney injury work group. KDIGO clinical practice guideline for acute kidney injury. Kidney Int. Suppl. **2**(1), 1–138 (2012)
23. Breiman, L.: Random Forests. Mach. Learn. 2001 451, **45** (1), 5–32 (2001)
24. Chen, T., Guestrin, C.: XGBoost: A Scalable Tree Boosting System, In: Proceedings of the 22nd ACM SIGKDD International Conference on Knowledge Discovery and Data Mining (2016)
25. Ke, G., et al.: LightGBM: a highly efficient gradient boosting decision tree. In: Advances in Neural Information Processing Systems, vol. 30 (2017). https://github.com/Microsoft/LightGBM. Accessed 12 Jul 2021
26. He, H., Bai, Y., Garcia, E.A., S. Li.: ADASYN: Adaptive synthetic sampling approach for imbalanced learning. In: Proceedings of International Joint Conference on Neural Networks, pp. 1322–1328 (2008)
27. Lundberg, S., Lee, S.-I.: A Unified Approach to Interpreting Model Predictions. In: Advances in Neural Information Processing Systems, vol. 2017-Decem, pp. 4766–4775 (2017). http://arxiv.org/abs/1705.07874. Accessed 6 Sep 2020

Algorithm for Predicting Bitterness of Children's Medication

Tiantian Wu(✉), Shan Li, and Chen Zheng

Department Nanjing University of Aeronautics and Astronautics, Nanjing 211106, China
wtt@nuaa.edu.cn

Abstract. The taste of drugs has always been a key factor affecting children's compliance. The children's preference for bitterness will cause them to fail to take the medicine on time and affect the treatment effect. To understand the taste of drugs is the premise of the study of drug correction and masking. The previous research methods usually use the oral taste method or the electronic tongue method to judge the taste of drugs, which has some inconveniences. In this paper, the smiles of the compound were used to derive the physicochemical descriptors and the MACCS fingerprint, and the prediction model of the bitter taste of children's drugs was constructed based on the random forest algorithm and XgBoost algorithm. The hospital data were used for verification and analysis to provide help for the development of correction and masking of children's medicines.

In this study, we first collected the bitter and non-bitter data by referring to the literature, using smiles of compounds to calculate the physicochemical descriptors and MACCS fingerprints as features, and using Pearson coefficients and SVM-REF for feature dimensionality reduction. Then, based on the random forest algorithm and XgBoost algorithm, the bitterness prediction model for children was constructed, and the 10-fold cross validation was used to optimize the model. Finally, the model is applied to some datasets to predict the content of bitter compounds. The results show that MACCS fingerprint is the most suitable for the prediction of bitter compounds. The classification effect of XgBoost is better than that of random forest. Model of xgboost-maccs has the best classification effect with 88% accuracy, and model of rf-descriptors has the classification effect with 83% accuracy.

Keywords: Bitter compounds · Molecular descriptor · Random forest · XgBoost · Classification model

1 Introduction

The taste of drugs is a key factor affecting the compliance of patients, especially children. Bitter taste is the most unacceptable taste of drugs. Bitter drugs mainly contain alkaloids and glycosides and enter the liver meridian. They often have the effects of clearing away heat and detoxifying, reducing tumor and cardiovascular diseases. They are widely used in clinical practice and account for a high proportion. A survey in the United States

R. Qiu et al. (Eds.): ICSS 2021, LNOR, pp. 91–102, 2021.
https://doi.org/10.1007/978-3-030-90275-9_8

showed that 90.8% of acute paediatric patients and 83.9% of chronic paediatric patients' main obstacles to taking medications are the unpleasant taste of the drugs.

Research has shown that the perception of bitterness is caused by the combination of bitter substances and bitter receptors, triggering a cascade of amplifying reactions that stimulate nerve cells to transmit nerve impulses to the cerebral cortex, ultimately leading to the formation of bitterness. Bitter receptor is a seven-times transmembrane G-protein coupled receptor (GPCRs), called T2Rs or Tas2Rs, which can mediate the bitter taste perception process of taste bud cells on the tongue. The specificity of the structure of each subtype of TAS2R enables it to identify a large number of bitter compounds with different structures [1].

Before correcting or masking a medicine, we need to know whether the medicine is a bitter taste medicine. It is known that the medicine is composed of a variety of compounds, and the main compound is the main reason for affecting its taste. Therefore, it can be predicted whether the compound is bitter thus predicting whether the drug is bitter. There are many methods for predicting the bitterness of compounds, such as oral taste method, electronic tongue method, calcium imaging method, etc. [2, 3]. These methods mainly have the following two problems: First, the direct use of the oral taste method will have safety, fatigue and individual differences, and the electronic tongue method have fewer bitter taste receptors, and the accuracy and precision are poor. Second, calcium imaging and electrophysiology are more complex, have more influencing factors, and have more limitations, which is not suitable for screening a large number of compounds.

In recent years, as the machine learning technology has become more maturer, the application field has become wider and wider, and scholars have begun to apply it to the prediction of bitterness. Rogers et al. [4, 5] used a dataset consisting of 649 bitter molecules and 1353 randomly selected molecules (expected to be non-bitter), to develop a Naïve Bayes classifier utilizing circular fingerprints as molecular descriptors. Huang et al. [6] used SVM to establish a BitterX tool based on the physicochemical descriptors, which can be used to predict bitterness of compounds. BitterPredict (developed by Dagan-Wiener et al.) [7] enhances the training data of BitterX and establishes a strict external verification set. It is a general predictor applicable to different chemical families. BitterPredict points out that about 40% of random molecules, some clinical and Experimental drugs and natural products are bitter. Some scholars also applied machine learning method to bitter-sweet taste prediction. Based on random forest algorithm, Banerjee and Preissner [8] used bitter, sweet compounds from BitterDB [9] and SuperSweet [10] to achieve bitter and sweet dichotomies prediction. Subsequently, Tuwani et al. [11] compared the performance of different molecular descriptors to further identify important features and feature blocks, and used random forest and Adaboost classifier to train the model for sweet and bitter binary classification prediction.

In this study, the data in the bitter database BitterDB [9] is collected as a positive set, and the non-bitter molecules (sweet and unflavored) that have been experimentally verified as a negative set, using fingerprints and chemical descriptors as signatures, using random forests and XgBoost classifier performs model training, and then selects the most suitable model for the prediction of bitter drugs by evaluating the performance of the model.

2 Materials and Methods

2.1 Data Preparation

The training data used in this study is divided into positive set and negative set.

Positive set: The positive set is mainly composed of BitterDB [9] and research articles. BitterDB serves as a central resource for information on bitter-tasting molecules and their receptors and its information is frequently used for choosing suitable ligands for experimental studies, for developing bitterness predictors, for analysis of receptors promiscuity and more. BitterDB currently contains 1041 compounds, including 50 short peptides, which were cited in the literature as bitter for human and/or were shown to activate at least one bitter taste receptor (in one of the four organisms—human, chicken, mouse or cat).

Negativate set: The negative set consists of sweet, unflavored and non-bitter data that has been experimentally verified. The negative set in this study is collected based on research articles [12, 13]. Some scholars upload research data when writing papers, so they can be downloaded directly.

Due to the large number of data sources, duplication of data is highly likely. In this paper, we use the drop_duplicates function in Pandas to remove the duplicate entries identical to smiles as the recognition criterion. After excluding duplicate data, there are 2435 data in total, including 914 bitter data and 1521 non-bitter data.

2.2 Molecular Representation

In this study, the physicochemical descriptors and MACCS keys of the compounds are used as characteristic attributes, and they are all calculated based on the smiles of compounds [14–16].

(1) Physicochemical descriptors

The physicochemical descriptors can reflect the physical and chemical properties of the compound. The physical properties include the atomic mass, the number of charges, and the electronegativity of the compound. The chemical properties include the number of compound bonds, structural information, and the number of rings. There are many softwares for calculating physicochemical descriptors, such as Dragon2D, Dragon2D/3D, ChemoPy and Canvas. In this study, ChemoPy [17] was used as a tool for calculating physical and chemical descriptors of compounds, and 10 groups were selected to describe the physicochemical properties and structure of the molecule from different angles. These 10 sets of feature descriptors are Constitutional descriptors(30), connectivity descriptors(44), Bcut descriptors(64), Moran descriptors(32), Geary descriptors(32), Molproperty descriptors(6), Charge descriptors(25), Basak descriptors(21), Estate descriptors(245) and MOE-type descriptors(60),totally 560 molecular descriptors (Table 1).

Table 1. Introduction to physical chemistry descriptors

Feature descriptors	Description	Number of descriptors
Constitutional descriptors	The structural information of the molecule, including the mass of the molecule, the number of various bonds in the molecule, the number of rings, etc.	30
Basak descriptors	Molecular polarity and polarizability	21
MOE-type descriptors	Related to the van der Waals surface area of the molecule	60
Moran descriptors	Measure spatial autocorrelation, that is, the potential interdependence between observation data of some variables in the same distribution area	32
Geary descriptors	Measure spatial autocorrelation, more sensitive to local spatial autocorrelation	32
Charge descriptors	Describe the charge properties of molecules	25
Estate descriptors	Describe the charge state of molecules	245

(2) Maccs

MACCS keys are molecular fingerprints, which can abstractly represent the specific structural characteristics of the molecule, mainly represented by segmenting the molecular structure and representing the molecular structure by obtaining segmented fragments. MACCS keys are fingerprints derived from the chemical structure database developed by MDL, known as cheminformatics, as a quick method for screening substructures in molecular databases. The public version of MACCS keys contains 166 keys, indicating that a total of 166 molecular structures have been examined, and each key corresponds to a specific molecular feature.

2.3 Dimensionality Reduction

In this paper, based on ChemoPy, a third-party library of Python, 10 sets of feature descriptors are calculated, totaling 560 molecular descriptors. Due to the duplication and redundancy of the information represented by some feature descriptors, it is necessary to perform feature selection operations on molecular descriptors before constructing the model. Feature selection can not only reduce over-fitting, reduce the number of features (dimension reduction), and improve the generalization ability of the model, but also can make the model better interpretability, enhance the understanding between features and feature values, and accelerate the training speed of the model, So as to obtain better model performance. In this paper, the feature selection of molecular descriptors is carried out through the point two-column correlation coefficient, Pearson correlation coefficient and the feature selection method based on SVM-RFE.

2.3.1 Point Biserial Correlation and Pearson

Point biserial correlation is suitable for calculating the correlation between categorical and continuous variables. In this study, it is used to calculate the correlation between the features and the results. In order to make the correlation between the features and the results as high as possible, this study retains the features with a coefficient value greater than 0.05.

Pearson can be used to measure the linear correlation between two continuous variables. In order to ensure the performance of the model, the correlation between each feature attribute should be as low as possible. Therefore, according to the calculated Pearson coefficient, if the coefficient between the two is large, greater than 0.9, it indicates that the two are strongly correlated, and the features with low correlation with the result are deleted.

2.3.2 SVM-REF

SVM-RFE is a sequence backward selection algorithm based on the principle of maximum separation of SVM. It first incorporates all features of the model to obtain the

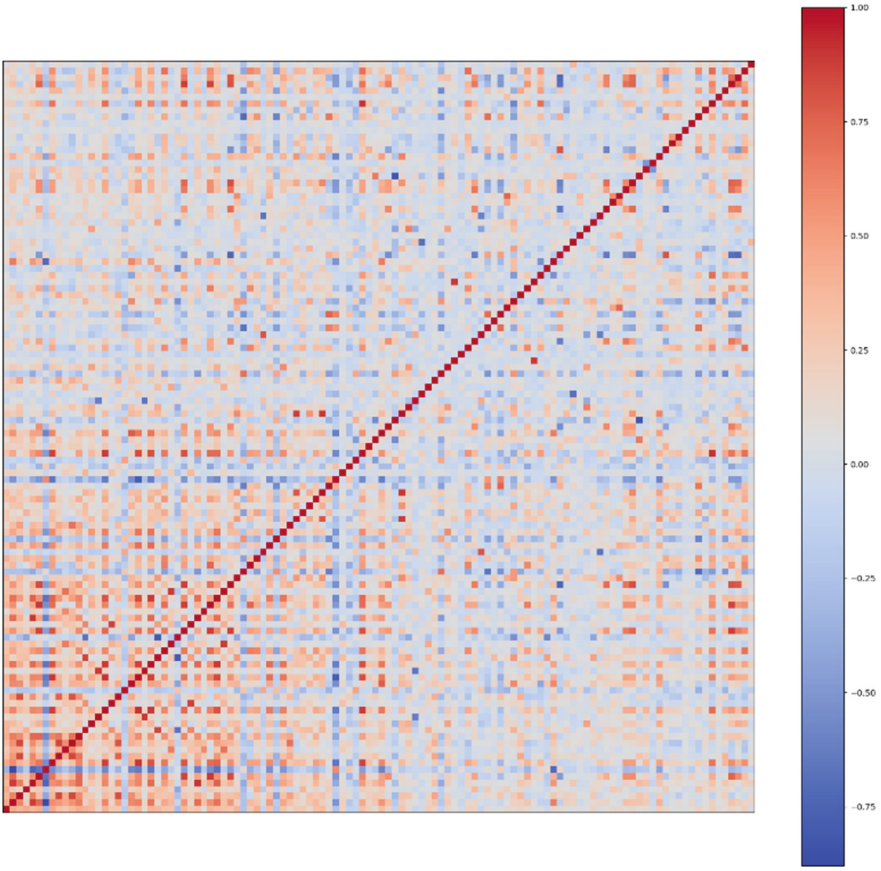

Fig. 1. The heatmap of Pearson correlation coefficients

weight of the feature, then removes the square of the coefficient with the smallest value and the corresponding feature of the model, and finally continue training in the model with the remaining features, and then select features until there are no features. The number of chemical descriptors has been reduced from 147 to 114. The heatmap of Pearson correlation coefficients within any two descriptors shows that the descriptors were weakly correlated with the each other (Fig. 1).

Scikit-learn was used for feature selection in this paper. First, specifies the support vector machine of the linear kernel function as the classifier by "estimator = svm.SVC(C = 0.8,kernel = 'linear',gamma = 20,decision_function_shape = 'ovr')", and then set ten-fold cross-validation through "selector = RFECV(estimator, step = 1, cv = 10, n_jobs = -1)", step = 1 means deleting a feature in the process of building the model for each iteration, and finally using "selector = selector.fit(X, y.astype('int'))" to train the model. "selector.ranking_" can reflect the ranking of feature scores, the smaller the value, the higher the ranking, "selector.support_" can reflect the selection of features, TRUE means selected, FALSE means eliminated.

2.4 Algorithms and Evaluation Metrics

XgBoost [18, 19] is an improvement to Boosting algorithm. Boosting algorithm can be used to reduce the deviation in supervised machine learning. It is a method of integrating several classifiers into a classifier. XgBoost improves on the basis of boosting, and adds a penalty term when building the model. Random forest [20] is an integrated learning method for classification, regression, and other tasks. It is a typical bagging algorithm that can prevent the occurrence of overfitting. Random forest uses the CART tree [21] as weak classifier. When generating each tree, the features selected by each tree are a small number of randomly selected features, while CART tree will select all the features for modeling. Therefore, random forest guarantees the randomness of the features.

Accuracy (ACC), accuracy (PPV), sensitivity (TPR), specificity (TNR), and F1-score were used to evaluate model performance. The accuracy reflects the proportion of all the judgment results of the classification model to the total observation value, and the precision reflects the proportion of the model prediction pair in all the results of the model prediction being Positive, and the sensitivity reflects on all the results of the true value of Positive. The specificity of the model prediction pair reflects the specificity of the model prediction pair in all results whose true value is Negative, and f1-score is an average result of the accuracy rate and the recall rate.

$$\mathrm{ACC} = \frac{TP + TN}{TP + TN + FP + FN} \tag{1}$$

$$\mathrm{PPV} = \frac{TP}{TP + FP} \tag{2}$$

$$\mathrm{TPR} = \frac{\mathrm{TP}}{\mathrm{TP} + \mathrm{FN}} \tag{3}$$

$$\mathrm{TNR} = \frac{\mathrm{TN}}{\mathrm{TN} + FP} \tag{4}$$

$$f1 = 2 * \frac{PPV * TPR}{PPV + TPR} \tag{5}$$

2.5 Model Construction

When machine learning method is used for classification, the training data is required to be balanced, that is, the number of bitter data and non-bitter data is the same. At present, among the training data using physical and chemical descriptors as feature descriptors, there are 888 bitter data and 1488 non-bitter data; among the training data using MACCS fingerprint as feature descriptor, there are 821 bitter data and 1215 non-bitter data. In this study, Pandas was used to downsampling non-bitter molecules to construct an equilibrium dataset for modeling. Taking the number of bitter molecules as the benchmark, non-bitter molecules were randomly sampled according to the ratio of the number of bitter molecules to the number of non-bitter molecules: 1:1, and a balanced data set was finally obtained.

In this study, physicochemical descriptors and MACCS keys are used as feature attributes, and random forest and XgBoost are used as classifiers to construct four models respectively. These four models are: RF + descriptors, RF + MACCS, XgBoost + descriptors and XgBoost + MACCS. The balanced data set is divided into a training set and a test set according to the ratio of 4:1. GridSearchCV is used to automatically find the optimal parameters of each model, thereby constructing the optimal model.

3 Results

In this study, we constructed four prediction models to predict whether the compound is bitter. Figure 2 shows the performance of these four models on the test set. It can be seen that the classification effects of the four models are relatively good. Among them, the classification effect of the model based on MACCS keys is better than the model based on physicochemical descriptors. At the same time, the effect of XgBoost as a classifier is better than that of random forest. Use XgBoost + MACCS has the best model effect and the accuracy reaches 0.88. Except for the combination of Random Forest and physicochemical descriptors, the sensitivity is slightly lower than the specificity. In other cases, the sensitivity is higher than or equal to the specificity, indicating that the model has a better prediction effect on the bitter set, that is, the model can more accurately identify bitter compounds.

Models will show different performance on different data sets, that is to say, the performance of the model cannot be judged by only one test. Because the amount of data in this study is not large, multiple tests cannot be conducted, so this article uses a 10-fold cross Validated method to test model performance. 10-fold cross validation is to train ten models at the same time to take the average, which is equivalent to different tests on a data set with the same model, but each training data set is not the same, just like expanding the data set. If the average performance of these ten models is good, it can prove to a certain extent that the model has a certain generalization ability.

After calculation, the average accuracy of the four models are as follows: "Xgb + MACCS": 0.87, "RF + MACCS": 0.86, "Xgb + descriptors": 0.85, "RF + descriptors":

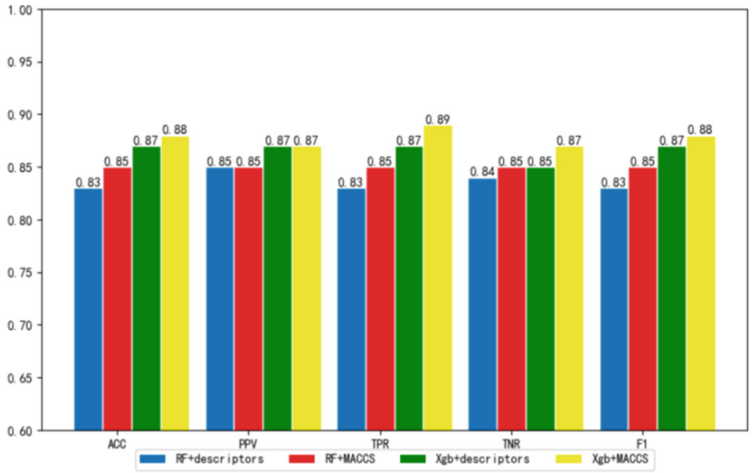

Fig. 2. Evaluation of model prediction results

0.84. Figure 3 shows the changes in the accuracy of different models tested on the test set after each training. It can be seen that the performance of "XGB + MACS" model is stable and the average accuracy is the highest. The combination of randomForest and physicochemical descriptor not only has unstable performance, but also has the lowest average accuracy.

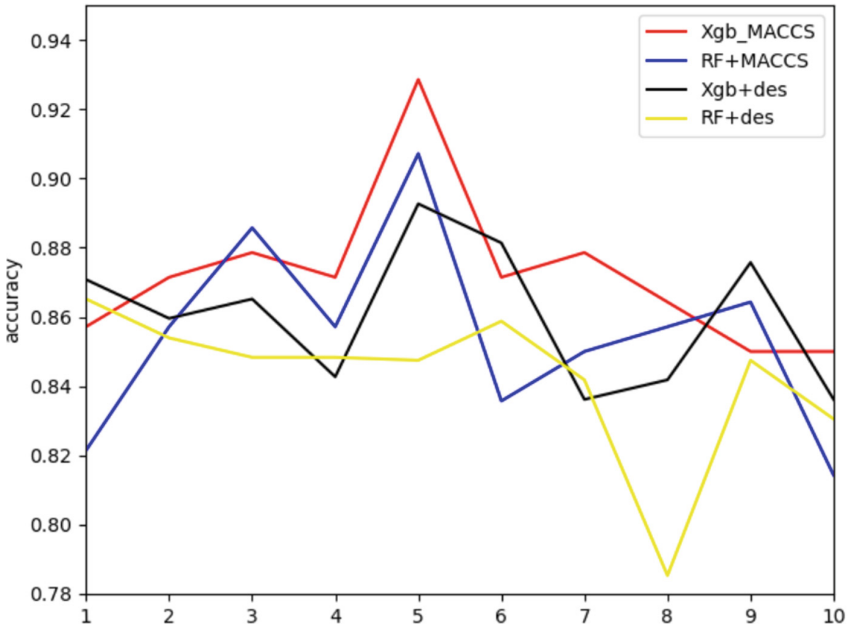

Fig. 3. Changes in accuracy of the four models

3.1 Chemical Features of Compounds

Whether the compound is bitter is closely related to the structure of the compound. One of the main objectives of this study is to analyze the important and frequent characteristics of bitter compounds. In order to understand which features, contribute most to the change in the expected class in the classifier, we computed the relative frequency distribution of all 166 features in both classes (Fig. 4). It is observed that the indexes containing the frequent features in bitter and non-bitter compounds are different signifying that the some chemical features are class specific.

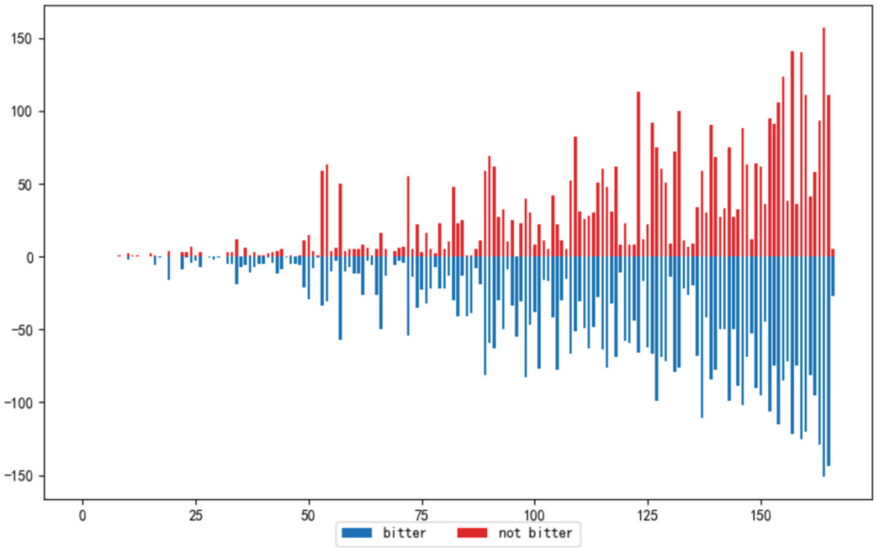

Fig. 4. MACCS keys frequency of bitter and non-bitter compounds

This study also calculates the correlation between the physicochemical descriptors and the taste of the compounds (Table 2). It can be seen that the influence of descriptors on the taste is very different.

3.2 Application of the Model

Among the four models, XgBoost and MACCS keys perform best when combined. In this study, the model was applied to several datasets. Specifically, we used FooDB (http://foodb.ca/), a dataset of food constituents, DrugBank [22] approved set46, and ChEBI [23] as a representative set of random molecules. These predictions can provide an estimate of the percentage of bitter molecules in the chemical datasets.

FooDB is the world's largest and most comprehensive resource on food constituents, chemistry and biology. The prediction results indicate that about 62% of the compounds may be bitter, which is a shocking proportion. This shows that many of the compounds that make up food are bitter, although the food itself is not bitter.

Table 2. Correlation coefficients between features and results

Physicochemical descriptors	Correlation coefficients	Physicochemical descriptors	Correlation coefficients
PEOEVSA7	0.389	bcute12	0.235
bcute1	0.379	Smax28	0.234
UI	0.331	Smax11	0.233
Smax29	0.320	GATSm2	0.230
bcute9	0.319	IC2	0.230
nring	0.285	bcutm8	0.229
mChi1	0.282	MATSv4	0.225
bcute15	0.281	bcutv3	0.224
slogPVSA5	0.278	nnitro	0.223
slogPVSA7	0.278	PEOEVSA6	0.216
naro	0.275	Smax17	0.214
Chi6ch	0.265	QNmin	0.212
MRVSA2	0.264	QNmax	0.209
EstateVSA1	0.247	ncarb	0.206
MATSm4	0.241	…	…

The DrugBank database is a unique bioinformatics and cheminformatics resource that combines detailed drug data with comprehensive drug target information. A total of 1371 compounds are predicted this time, and about 84% of the compounds are bitter, so most drugs are bitter.

The prediction on ChEBI represents the estimation of abundance of bitter compounds among random molecules. The results show that about 70% of the random molecules may have some bitter taste, which means that in many cases the random molecules are bitter.

4 Discussion and Conclusions

With the rapid development of machine learning, its application in the medical field is becoming more and more extensive, which also provides a new idea for the prediction of drug taste. In this study, based on the random forest and XgBoost algorithm, using the compound's features (physicochemical descriptors and MACCS keys) to construct four models, classify the taste of the compound, and use the test set to compare the prediction effects of the models.

The experimental results prove that the four models constructed in this research have good classification effects on the classification of bitter drugs. The research shows that: (1) For the two features in this study, MACCS keys is a better choice for building a classification model. (2) For the random forest algorithm and the XgBoost algorithm,

the prediction effect of the bitter compound classification model based on the XgBoost algorithm is better. (3) The combination of XgBoost and MACCS keys performs best; (4) The four models constructed in this paper can be used in practice, and the prediction effect on bitter compounds is better.

This study also used the optimal model for the bitterness prediction of some datasets, which are FooDB, DrugBank and CHEBI. The results show that about 62% of the compounds in FooDB are bitter, which is very different from our perception. Most of the compounds in Drug Bank are bitter, accounting for about 84%. About 70% of random molecules in CHEBI are bitter. This result is opposed to earlier assumption that random molecules are probably not bitter [24].

There are still improvements in this study: (1) Only physicochemical descriptors and MACCS keys are used as features for experiments, and other features can be selected for comparative analysis in the future. (2) The prediction model can only predict whether the compound is bitter, and cannot express the degree of bitterness. In the future, bitter compounds can be further subdivided.

Acknowledgements. This work was supported by National Natural Science Foundation of China (Grant No. 81603027), National Major Science and Technology Projects of China, China (grant no. 2018ZX09721003).

References

1. Wang, T., Chen, Q.: Research progress of physiological functions of g protein-coupled bitter taste receptors. World Latest Med. Inf. **18**(59), 28–29 (2018)
2. Zhou, Y., Dong, D., Zhang, S., Zhao, H.: Positive selection drives the evolution of bat bitter taste receptor genes. Biochem. Genet. **47**(3–4), 207–215 (2009)
3. Ntie-Kang, F.: Mechanistic role of plant-based bitter principles and bitterness prediction for natural product studies I: database and methods. Phys. Sci. Rev. **4**(7) (2019)
4. Bender, A., Mussa, H.Y., Glen, R.C., Reiling, S.: Molecular similarity searching using atom environments, information-based feature selection, and a Naïve Bayesian classifier. J. Chem. Inf. Comput. Sci. **44**, 170–178 (2004)
5. Rodgers, S., Glen, R.C., Bender, A.: Characterizing bitterness: identification of key structural features and development of a classification model. Chem. Inf. Model. **46**, 569–576 (2006)
6. Huang, W., et al.: BitterX: a tool for understanding bitter taste in humans. Sci. Rep. **6**, 1–8 (2016)
7. Dagan-Wiener, A., et al.: Bitter or not? BitterPredict, a tool for predicting taste from chemical structure. Sci. Rep. **7**, 12074 (2017)
8. Banerjee, P., Preissner, R.: BitterSweetForest: a random forest based binary classifier to predict bitterness and sweetness of chemical compounds. Front. Chem. **6**, 93 (2018)
9. Wiener, A., Shudler, M., Levit, A., Niv, M.Y.: BitterDB: a database of bitter compounds. Nucleic Acids Res. **40**, D413–D419 (2012)
10. Ahmed, J., et al.: SuperSweet–a resource on natural and artificial sweetening agents. Nucleic Acids Res. **39**, D377–D382 (2011)
11. Tuwani, R., Wadhwa, S., Bagler, G.: BitterSweet: building machine learning models for predicting the bitter and sweet taste of small molecules. Sci. Rep. **9**(1), 1–13 (2019)
12. In Hazardous Substances Data Bank: National Library of Medicine (US); Bethesda (MD) (2011). http://toxnet.nlm.nih.gov/cgi-bin/sis/htmlgen?HSDB

13. Kim, S., et al.: PubChem substance and compound databases. Nucleic Acids Res. **44**, D1202–D1213 (2016). https://doi.org/10.1093/nar/gkv951
14. Shi, J., Zhao, G., Wei, Y.: Computational QSAR model combined molecular descriptors and fingerprints to predict HDAC1 inhibitors. Médecine/Sci. **34**, 52–58 (2018)
15. Burden, F., Winkler, D.: Optimal sparse descriptor selection for QSAR using Bayesian methods. QSAR Comb. Sci. **28**(6–7), 645–653 (2009)
16. Zhao, L., Xiang, Y., Song, J., et al.: A novel two-step QSAR modeling work flow to predict selectivity and activity of HDAC inhibitors. Bioorganic Med. Chem. Lett. **23**(4), 929–933 (2013)
17. Cao Dongsheng, X., Qianna, Q.H., et al.: ChemoPy: freely available python package for computational biology and chemoinformatics. Bioinformatics **29**(8), 1092–1094 (2013)
18. Huang, J.-C., et al.: Predictive modeling of blood pressure during hemodialysis: a comparison of linear model, random forest, support vector regression, XGBoost, LASSO regression and ensemble method. Comput. Methods Programs Biomed. **195**, 105536 (2020)
19. Dong, W., Huang, Y., Lehane, B., Ma, G.: XGBoost algorithm-based prediction of concrete electrical resistivity for structural health monitoring. Autom. Constr. **114**, 103155 (2020)
20. Yao, H., Li, X., Pang, H., Sheng, L., Wang, W.: Application of random forest algorithm in hail forecasting over Shandong Peninsula. Atmos. Res. **244**, 105093 (2020)
21. Arifuzzaman, M., Gazder, U., Alam, M.S., Sirin, O., Mamun, A.A.: Modelling of asphalt's adhesive behaviour using classification and regression tree (CART) analysis. Comput. Intell. Neurosci. **2019** (2019)
22. Wishart, D.S., et al.: DrugBank: a comprehensive resource for in silico drug discovery and exploration. Nucleic Acids Res. **34**, D668–D672 (2006). https://doi.org/10.1093/nar/gkj067
23. Hastings, J., et al.: The ChEBI reference database and ontology for biologically relevant chemistry: enhancements for 2013. Nucleic Acids Res. **41**, D456–D463 (2012). https://doi.org/10.1093/nar/gks1146
24. Rodgers, S., Glen, R.C., Bender, A.: Characterizing bitterness: identification of key structural features and development of a classification model. J. Chem. Inf. Model. **46**, 569–576 (2006). https://doi.org/10.1021/ci0504418

Intelligent Identification of High Emission Road Segment Based on Large-Scale Traffic Datasets

Baoxian Liu[1,3], Gang Zhou[2], Yanyan Yang[1], Zilong Huang[2(✉)], Qiongqiong Gong[2], Kexu Zou[2], and Wenjun Yin[2]

[1] School of Environment, State Key Joint Laboratory of Environment Simulation and Pollution Control, Tsinghua University, Beijing 100084, China
[2] Insights Value Technology, Beijing 100071, China
huangzl@pku.edu.cn
[3] Beijing Key Laboratory of Airborne Particulate Matter Monitoring Technology, Beijing Environmental Monitoring Center, Beijing 100048, China

Abstract. The primary data, such as traffic flow, vehicle type composition, and road network speed in Beijing, is acquired through model simulation and investigation statistics. A dynamic calculation method of high-resolution vehicle emission inventory was constructed with ArcGIS as the platform based on the road network traffic information and vehicle emission factors. Meanwhile, the intelligent supervision and identification of high-emission road sections were carried out based on the spatiotemporal emission distribution characteristics of the road network. The results show that the spatial distribution of pollutant emission intensity decreases from the main urban area to the suburbs. The emission on ring roads and expressways presents a linear and radiant distribution pattern because of the large traffic flow. Besides, the emission intensity of pollutants shows a noticeable diurnal trend as high during the day and low at night, and mainly concentrates in the morning and evening peak hours. The dynamic road network emission can intelligently identify the high emission road segments in real-time, track the high-emission road segments, and provide critical technical means for traffic environment management.

Keywords: Emission inventory · High emission road segments · Road network · Traffic flow

1 Introduction

Motor vehicles are the primary source of key precursors of atmospheric pollution such as nitrogen dioxide and VOCs, contributing significantly to urban and regional secondary air pollution such as $PM_{2.5}$ and ozone [1]. The current regulation methods for motor vehicle emission contain drawbacks and uncertainties. For instance, the irregular road emission inspection method requires many workforces but can only inspect a narrow range of roads leading to a low efficiency for inspection. In addition, according to the previous law enforcement experience, the road congested segments or segments with

R. Qiu et al. (Eds.): ICSS 2021, LNOR, pp. 103–113, 2021.
https://doi.org/10.1007/978-3-030-90275-9_9

many large vehicles are selected for vehicle detection. However, since there is no necessary connection between vehicle emissions and road congestion, uncertainty remains in law enforcement objects. Moreover, the remote sensing monitoring technology for vehicle exhaust screens vehicles that release high-intensity emission [2–7]. This method can only filter out the vehicles that pass through the specified road segment but do not work for the other roads.

Influenced by the actual traffic flow of the road network and motor vehicle activity level, the spatial and temporal distribution of vehicle emission changes dynamically. Therefore, quickly and accurately identifying the high emission road segments became difficult in vehicle emission supervision. The high emission road segment indicates the road segment where there is a suspected concentration of high-emission vehicles or a high-incidence concentration. The high emission road segment narrows the range of the road segment to enforce the law efficiently based on the road high emission clue. The accuracy of high emission section identification depends on the refinement level of the road network emission inventories. Current emission inventories mainly consist of regional-scale emissions [8–10]. The spatiotemporal resolution of road network emissions is insufficient to accurately and dynamically identify and track high emission segments. There are significant uncertainties in the emissions generated by spatial allocation methods based on vehicle ownership [11, 12], leading to errors or omissions in judgments on high emission road segments. This study proposes an intelligent identification method of high emission road segments based on traffic flow big data. By establishing a dynamic road network emission inventory with a high spatial and temporal resolution, the intelligent and accurate identification of high emission and high occurrence road segments provides technical means for traffic environment management.

2 Methods and Materials

2.1 Technical Route

The scope of this study is the entire region of Beijing. Beijing encompasses 16,400 km^2, including 16 administrative districts that radiate outward from the main urban area according to the ring road. This study comprises two parts: the construction of high-resolution road network emission inventory and the identification of suspected high emission and high incidence road sections.

Firstly, based on the road network traffic flow data combined with vehicle emission factors, a calculation method for the emission inventory of major pollutants with a high spatial and temporal resolution was established (temporal resolution was hours, spatial resolution was road segments). Figure 1 shows the technical route schematic diagram for constructing vehicle emission inventory with high spatial and temporal resolution. The first step is to retrieve the hourly average speed of the road network from the open-source road network congestion map according to the real-time vehicle GPS positioning information. The second step is to construct a speed-flow density model based on the traffic observation point data, where road speed is used to retrieve real-time traffic flow. The real-time dynamic traffic information of the whole road network includes the computing time, road type, road length, traffic volume, vehicle composition, and average speed. Simultaneously, the emission factor model is used to simulate and

obtain the localized emission factors of each vehicle type. The hourly emission of a single road segment is calculated by the emission formula of a single road segment. Then, the hourly emission of each road segment can be obtained. Consequently, the whole road network's emission inventory is obtained by adding up the emission of each road segment. The hourly emission calculation formula of a single road segment [13] is as follows:

$$E_{i,j,h} = \sum EF_{j,k}(v) * Q_{i,k,h} * l_i \tag{1}$$

where $E_{i,j,h}$ is the total emission of pollutant j on the road segment i at hour h, in units of grams per hour (g/h); $EF_{j,k}(v)$ is the average emission factor of pollutant j for vehicle category k at speed v, in units of grams per kilometer (g/km); $Q_{i,k,h}$ is the traffic volume of vehicle category k on the road segment i at hour h, in units of vehicles per hour (veh/h); l_i is the length of road segment i, in units of kilometer (km).

In addition, according to the spatial and temporal distribution characteristics of the entire road network emission inventory, a certain proportion of roads with the highest emission are automatically selected, such as the top 10% of road network emissions. Then, these pre-selected suspected high-emission road segments are ranked in a descending order of emission severity to identify the typical high-emission road. According to the statistics of the occurrence frequency of high-emission road segments within a period, the road with high emission and a high incidence is further identified and locked to provide high emission clues for the motor vehicle regulation.

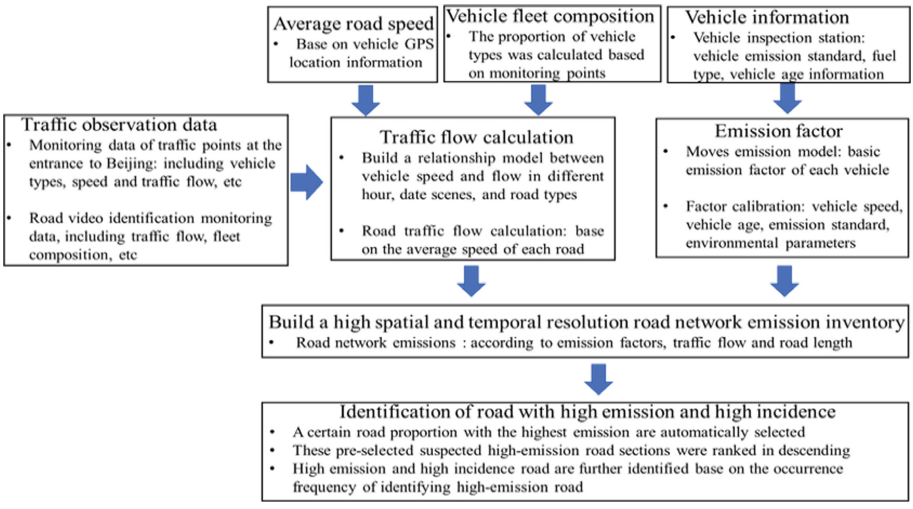

Fig. 1. High emission and high incidence road identification technology route diagram based on the high spatial and temporal resolution of the entire road network emission inventory.

2.2 Calculation of Emission Factors

The vehicle emission factor is an essential parameter in calculating vehicle emissions. It is widely known that vehicle emission rates are mainly related to vehicle characteristics, operating conditions, and environmental conditions. The vehicle characteristics include vehicle classification and utilization parameters. The vehicle classification comprises vehicle category, fuel type, and vehicle emission control level; the utilization parameters involve vehicle age and accumulated mileage; the operating conditions include cold or hot starts and average vehicle speed; the environmental conditions include ambient temperature, humidity, as well as altitudes.

In this study, the fundamental emission factors for each vehicle type, with different emission standards under various average speed bins, were calculated by the MOVES model. MOVES is a model developed in the USA, which introduces Vehicle Specific Power (VSP) to define tens of bins which denote the engine operating in different states, and has been widely studied and applied. MOVES calculated the basic emission factors based on the required data, such as the vehicle operating modes, motor vehicle activity, vehicle age distribution, road information, and meteorological parameters. According to the National Technical Guidelines of the Air Pollutant Emissions Inventory for Road Motor Vehicles and the actual composition of motor vehicles in Beijing, motor vehicles were divided into seven categories: light passenger cars (LPCs); medium passenger cars (MPCs); heavy passenger cars (HPCs); light-duty trucks (LDTs); medium-duty trucks (MDTs); heavy-duty trucks (HDTs) and buses. Since the traffic observation stations did not contain taxi and motorcycle information, this study did not consider taxi and motorcycle emissions. Each vehicle type was subdivided into subtypes according to fuel type and emission standards. The model estimated basic emission factors of the subtypes of each vehicle type at different average speeds. Finally, the comprehensive vehicle emission factors by vehicle type and various speeds were calculated using the following equation:

$$EF_{j,k}(v) = \frac{\sum_{f,m} P_{k,f,m} * EF_{j,k,f,m}(v)}{\sum_{f,m} P_{k,f,m}} \tag{2}$$

where $EF_{j,k}(v)$ represents the comprehensive emission factors of pollutant j, for vehicle category k, at speed v, in units of g/veh/km; $EF_{j,k,\mathrm{f},m}(v)$ represents the basic emission factors of pollutant j, for vehicle category k of fuel type f, with m emission standards, at speed v, in units of g/veh/km; $P_{k,f,m}$ represents the vehicle population proportion for vehicle category k of fuel type f, with m emission standards, in units of ratio.

2.3 Traffic Flow Simulation

2.3.1 Calculation of Road Speed

Accurate vehicle speed is a critical parameter when calculating vehicle emission factors. Speed is also crucial in road traffic flow calculation. To better understand the difference in emission intensities at different road types, this study selected five types of road to calculate the average speed, consisting of motorway, primary roads, secondary roads, tertiary roads, trunk roads. The hourly average speed covering all five road types was

obtained based on vehicle GPS data. Compared with the speed calculation method based on the congestion map, the hourly average speed in this study more comprehensively reflected the hourly traffic characteristics, which was closer to the actual traffic conditions. The vehicle's real-time longitude and latitude information was collected to match the vehicle trajectory with the road network. For example, as shown in Fig. 2, there were five roads and two adjacent vehicles' track points, point 1 and point 2. Four roads fell within a circle with a certain radius centred on track point 2, while road E was outside the circle, calculating the angle between the road segments A, B, C, and D and the line segment respectively, determining the minimum angle of road C. Calculating the distance of point 2 to segment C, which was less than the minimum distance threshold. The vehicle trajectory point matching with road C was completed. The speed of all vehicles on each road section during each calculation period was averaged to obtain the dynamic road hourly average speed, which is used for traffic flow calculation by using the road speed-traffic flow model.

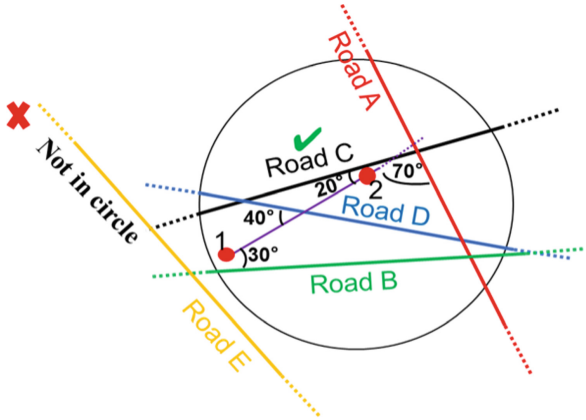

Fig. 2. Schematic diagram of fast matching method between vehicle driving track points and road network

2.3.2 Calculation of Traffic Flow

Traffic flow is a crucial parameter of motor vehicle activity levels. In current studies, hourly traffic flow data was either calculated by traffic density model or investigated by video collection and detection methods to express the relationship between the total volume and speed. In this study, the daily variation of vehicle flow and the quantitative relationship between vehicle speed and traffic flow were used to calculate the traffic flow. Traffic monitoring points have been installed. These traffic monitoring points covered all types of roads and represented the road traffic conditions in Beijing. Each monitoring point can collect the primary data such as hourly traffic flow and speed of the motor vehicle which is used for the construction of the speed-traffic flow quantitative relationship model, and further, obtain the proportion of each vehicle type in the total road traffic. Vehicle flow varied greatly in different periods, different days (such as workdays, weekends and holidays), and different road types. Therefore, this study built a quantitative

relationship model between vehicle speed and vehicle flow based on different situations such as periods, days, and road types. According to the statistical fitting analysis of speed and vehicle flow on each road type, as shown in Fig. 4, the quantitative relationship model between the speed and vehicle flow was obtained through the fitting analysis of the speed and vehicle flow at each monitoring point. The model was used to adjust the vehicle flow within the upper and lower ranges of the daily variation of vehicle flow according to the actual average road speed. Figure 3 shows the daily variation law of road traffic flow. The overall daily variation distribution of the traffic flow at each monitoring point was roughly described by analysing the daily variation of the road traffic flow at the monitoring point. With the statistical fitting analysis and the daily variation law of vehicle flow, the quantitative relationship model between speed and vehicle flow can be established at each monitoring point. By comparing these relationship models, under the same road type, select the corresponding model for each road in the entire road network according to the spatial proximity principle, and calculate the road traffic flow based on the average speed of each road calculated in Sect. 2.3.1.

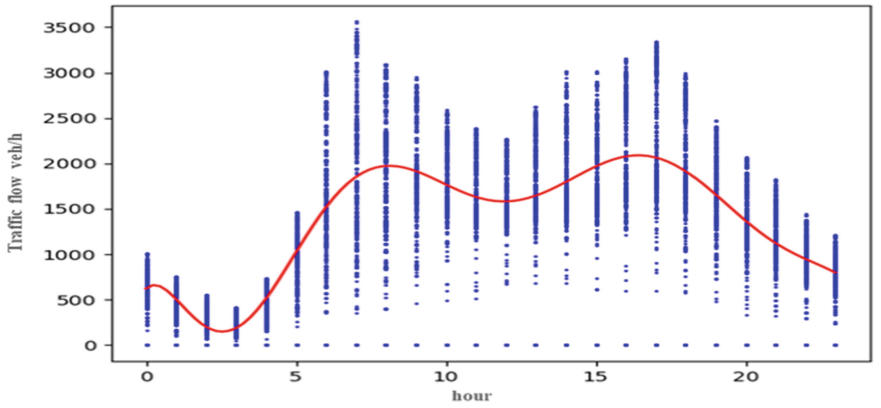

Fig. 3. Daily distribution map of road traffic flow

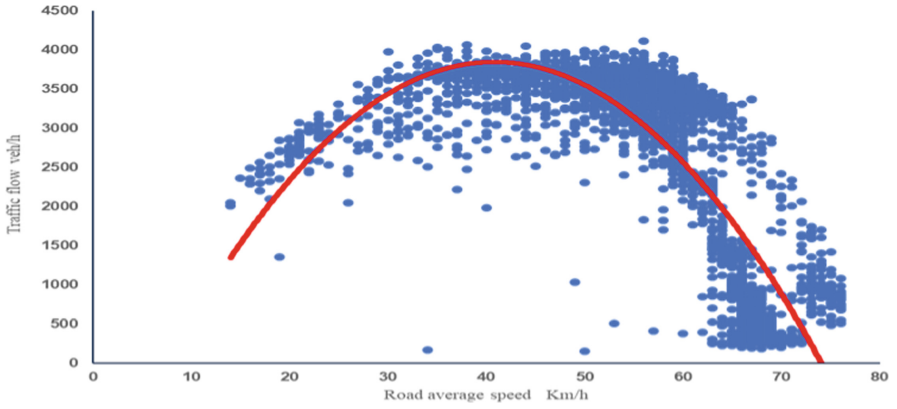

Fig. 4. Correlation between road average speed and traffic flow

2.3.3 Vehicle Fleet Composition

The emission varies significantly in different vehicle types or emission standards of a certain vehicle type, and thus more attention should be paid to emission control technologies. In addition, the calculation of emission inventory requires the traffic flow of each vehicle type, so the composition parameters of the fleet are crucial to the emissions calculation. The composition of vehicles on the road varies with hour and road type. Therefore, this study analyzed the composition ratio of each monitoring point according to different hours and road types. According to the spatial proximity principle of the same road type, the nearest monitoring point to each road is matched respectively to obtain the composition of each road in the road network. For example, as shown in Fig. 5, the Road is a main road, whereas monitoring point C is on the secondary road which is not consistent with the type of the Road, so monitoring point C is excluded; monitoring B on the primary road is the closest to the Road and they have the same road type, so B is selected. For the proportion of emission standards for each vehicle model, refer to the statistical data.

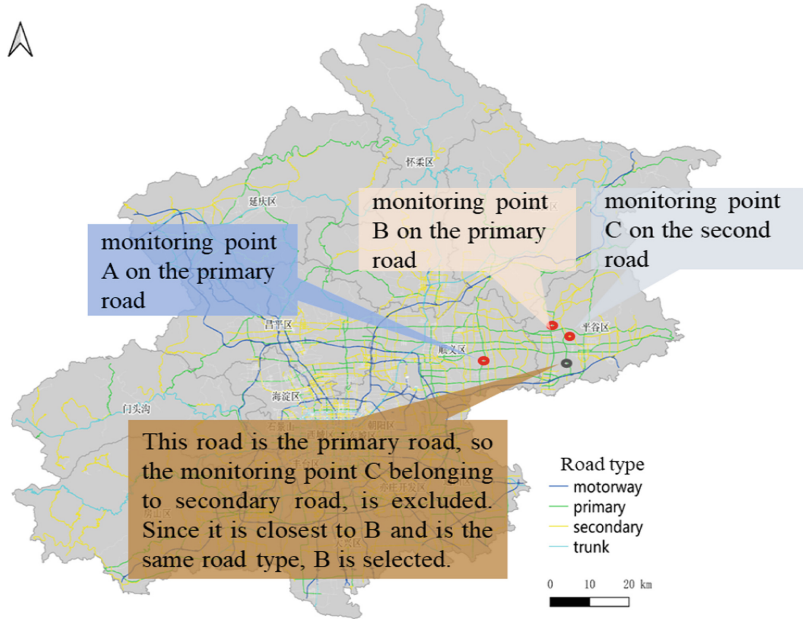

Fig. 5. Method for determining the composition of road fleet in the road network

2.4 Identification of High-Emission Road Segments

According to spatial and temporal distribution characteristics of the entire road network emission inventory (as shown in Fig. 6), a certain proportion of roads with the highest emission are automatically selected, such as the top 10% of road network emissions. These pre-selected suspected high-emission road sections were ranked in a descending

order according to the emission level. The typical high road segments will be confirmed based on the statistics of the occurrence frequency of high road segments within a period (see Fig. 7). The road with high emission and the high incidence is further identified and locked. It is considered the primary regulatory object to provide high-emission clues for motor vehicle regulation.

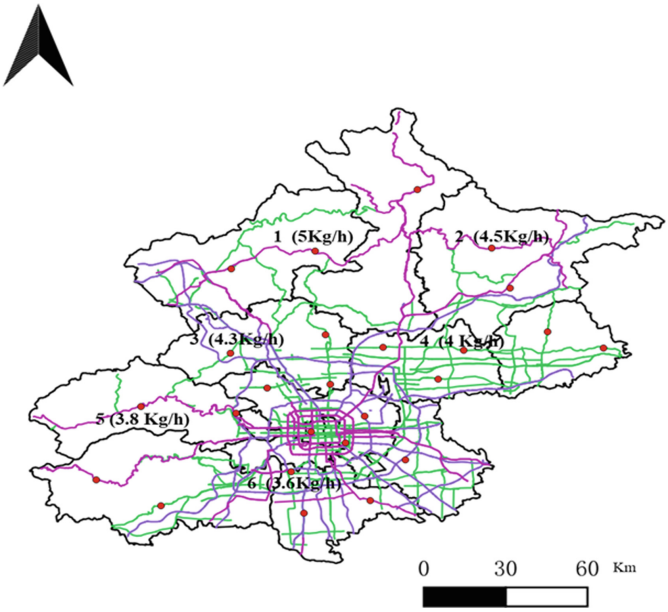

Fig. 6. Diagram of emission distribution and descending ranking of the road network

Number	roadID	emission	high emission incidence
1	A	5	10
2	B	4.5	2
3	C	4.3	5
4	D	4	7
5	E	3.8	1
...	...	...	...

descending

High emission threshold=3.8, five roads are selected as high emission road segment; A road has the highest high emission incidence

Fig. 7. Identification method of road segment with high emission and high incidence in the road network

3 Application

3.1 Road Network Emission Distribution

The spatial distribution of NOx emissions during morning peak hours shows an evident inhomogeneity in emission intensity, as illustrated in Fig. 8. Vehicle emission intensity decreases gradually and radially from the centre to the city outward. The high traffic volume and low vehicle speed lead to high emissions in the city centre. The large and concentrated traffic flow in the central region can easily cause traffic congestion. In the surrounding areas of Beijing, the emission is generally high in the areas where the urban freeways are.

As illustrated in Fig. 8, during the morning peak hours, the emission intensities on the ring roads are generally high. The reason causes that pattern is that more business activities and human activities occurred in the morning peak hours, leading to more intense traffic activities. Vehicles emit more pollutants when operating at low speed with frequent accelerations, decelerations, and idle mode.

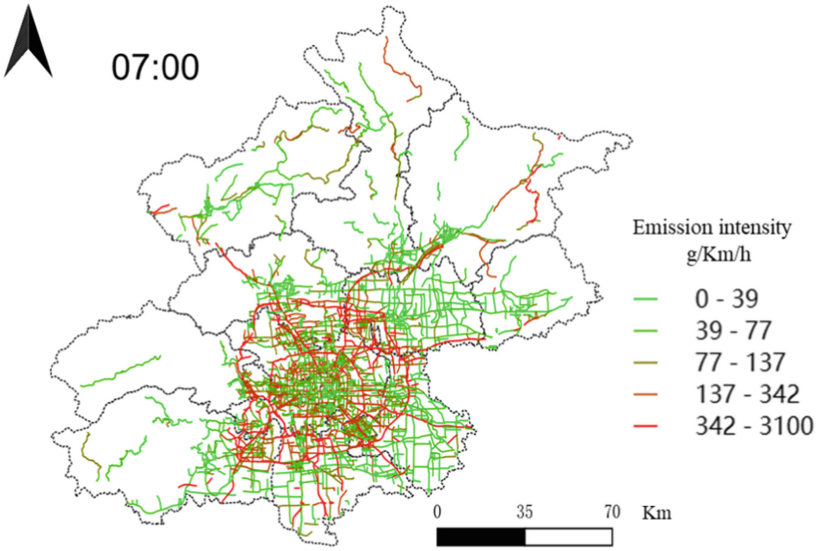

Fig. 8. The road network spatial distributions of NOx emissions during morning peak hours

3.2 Road Network Emission Daily Variation

The emission daily variation of different road types is shown in Fig. 9. Among different types of roads, the motorway has the highest NOx emission, followed by trunk, primary road, and the tertiary road has the lowest emission. It showed that NO_x mainly comes from the motorway and trunk. In terms of daily variation, the NO_x emission showed a bimodal distribution in the morning and evening. The morning peak hours were 7 to 8 o'clock, and the evening peak hours were 17 to 18 o'clock.

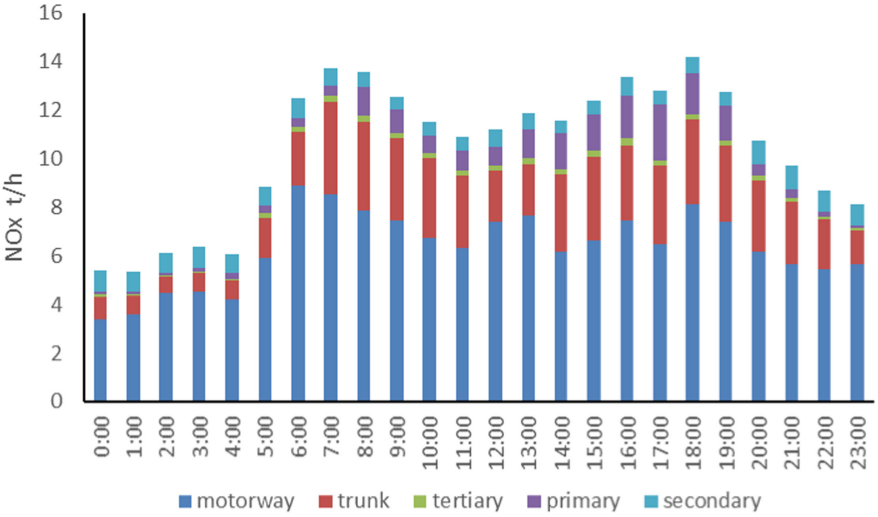

Fig. 9. Diurnal variation of NOx emission by road types

3.3 Identification Result of Road Segment with High Emission

Figure 10 shows the emission distribution of local regions in the morning peak on a working day. Apparently, emissions from the North Fourth Ring Road, the North Fifth Ring Road and the Beijing-Chengde Expressway are significantly higher. According to the identification method of the high emission sections of the road network, the high emission sections of the North Fifth Ring Road and the Beijing-Chengde Expressway can be identified accurately.

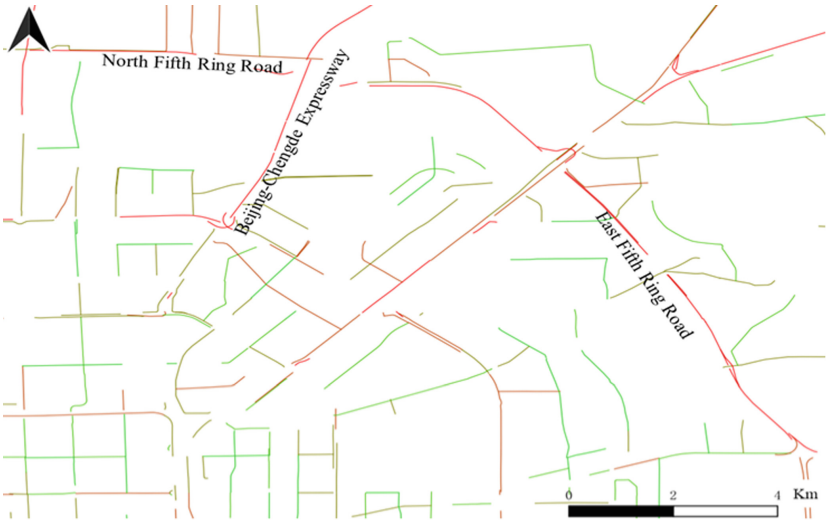

Fig. 10. Identification result of road segment distribution with high emission at morning peak hours

4 Summary

This study establishes a road network emission inventory with a high spatial and temporal resolution based on traffic flow and vehicle emission factors. There are spatial and temporal differences in the emission distribution of motor vehicle networks. The emission distribution laws of the dynamic network can achieve high emission road recognition and promote proper law enforcement for motor vehicles.

Acknowledgements. This work was supported by the Project of Beijing Science and Technology Commission (Z181100005418003, Z191100009119014).

References

1. Richter, A., Burrows, J., et al.: Increase in tropospheric nitrogen dioxide over China observed from space. Nature **437**(7055), 129–132 (2005)
2. Shao, Y.: Application of remote sensing monitoring in detection of CO and HC of vehicle exhaust gas. Guangzhou Chem. Ind. (2017)
3. Long, Z., Ge, Y., Jia, L., et al.: A research on the application of remote sensing to vehicle emission measurement. Autom. Eng. (2015)
4. Gao, X.L., Hu, T.J., Wang, K.: Research on motor vehicle exhaust pollution monitoring technology. Appl. Mech. Mater. **620**, 244–247 (2014)
5. Bishop, G.A., Stedman, D.H.: On-road remote sensing of automobile emissions in the Tulsa area: fall 2013. Carbon Dioxide (2014)
6. Tu, X., Dong, F., Qi, F., et al.: On-road remote sensing of CO and CO_2 of motor vehicle exhaust emissions in Beijing using a TDLAS system. In: Conference on Optical Technologies for Atmospheric, Ocean, and Environmental Studies, Beijing, China, p.1, 20041018–22 (2005)
7. Guo, H., Zhang, Q., Yao, S., et al.: On-road remote sensing measurements and fuel-based motor vehicle emission inventory in Hangzhou. China Atmos. Environ. **41**(14), 3095–3107 (2007)
8. Fu, L., Hao, J., He, D., et al.: Assessment of vehicular pollution in China. J. Air Waste Manag. **51**(5), 658–668 (2011)
9. Cai, H., Xie, S.: Estimation of vehicular emission inventories in China from 1980 to 2005. Atmos. Environ. **41**(39), 8963–8979 (2007)
10. Hao, J., He, D., Wu, Y., et al.: A study of the emission and concentration distribution of vehicular pollutants in the urban area of Beijing. Atmos. Environ. **34**(3), 453–465 (2000)
11. Zheng, B., Huo, H., Zhang, Q., et al.: High-resolution mapping of vehicle emissions in China in 2008. Atmos. Chem. Phys. **14**(18), 9787–9805 (2014)
12. Zheng, J., Che, W., Wang, X., et al.: Road-network-based spatial allocation of on-road mobile source emissions in the pearl river delta region, China, and comparisons with population-based approach. J. Air Waste Manag. **59**, 1405–1416 (2009)
13. Yang, D., Zhang, S., Niu, T., et al.: High-resolution mapping of vehicle emissions of atmospheric pollutants based on large-scale, real-world traffic datasets. Atmos. Chem. Phys. **19**, 1–22 (2019)

Construction Cost Prediction for Residential Projects Based on Support Vector Regression

Wenhui Guo(✉) and Qian Li

School of Management and Engineering, Nanjing University, Nanjing 210093, Jiangsu, China
MG1915019@smail.nju.edu.cn

Abstract. Accurate prediction of construction cost with the use of limited information in the initial phase of a construction project is critical to the success of the project. However, traditional cost estimation methods have poor accuracy and efficiency. It is important to utilize the knowledge gained from past projects and historical cost data to predict a new project's cost. Therefore, this research tries to develop a new methodology based on Support Vector Regression (SVR) for improving the accuracy and efficiency of prediction on a residential project's total construction cost and its main component costs including engineering project cost, installation project cost and decoration project cost. In this research, we constructed 15 attributes that correspond with the project characteristics and market price fluctuations, and developed 4 SVR models to predict the residential project's costs. To verify the prediction performance of the proposed model, a case study was performed on 84 residential projects in Chongqing, China. BP Neural Network (BPNN) and Random Forest (RF) were also used to compare the accuracy and stability of prediction results. The results show that the suggested SVR models achieve higher accuracy with 98.32% of the overall cost estimation compared with other models. This research shows that the developed model is effective in early decision making and cost management since the construction cost and its component cost can be predicted accurately before the completion of a project's design stage.

Keywords: Construction cost prediction · Residential projects · Support vector regression · Machine learning

1 Introduction

In the initial phase of the project, cost prediction is a critical process where crucial decisions about the project depend on it and limited information about the project is available. Accurate prediction of construction cost is the foundation of the cost control, and has great influence on the scientificity of investment decisions and the effectiveness of target cost control. It also influences the quality of the design scheme and the construction drawing budget of the next stage [1]. However, the importance of early cost prediction is in sharp contrast with the amount of information available in the early stage. Traditional cost estimation methods such as rough calculation method and index estimation method

R. Qiu et al. (Eds.): ICSS 2021, LNOR, pp. 114–124, 2021.
https://doi.org/10.1007/978-3-030-90275-9_10

cannot meet the needs of estimation accuracy and technological progress, which often affects the accuracy and rationality of investment objectives [2].

The long-term practice in the field of construction cost has accumulated a large amount of historical data. In the experience-oriented industries such as construction, the utilization of previous project knowledge is very important for managing recurring problems, especially in the early decision-making stage with limited information [3]. In recent years, with the variety of mathematical models and the rapid development of computer science, many researchers have applied artificial intelligence (AI) techniques and machine learning (ML) models such as ANNs, regression model, case-based reasoning (CBR), hybrid models such as neural-fuzzy models, and evolutionary computing (EC) such as genetic algorithm (GA) and genetic fuzzy models to accurately predict the construction cost in the initial phase of the project [4]. Wang et al. used ANNs and supportive vector machine (SVM) to predict cost at the conceptual stage based on 92 building projects and has a prediction accuracy of 92% [5]. Ahn et al. concluded that CBR can obtain reliable accuracy in cost prediction of construction projects in the early stage with limited information [6]. Stoy et al. used five independent variables to predict the early construction cost of German housing by simple linear regression model, and the mean absolute error was 0.096 [7]; Kwon et al. studied the maintenance cost prediction of old houses, and found that Monte Carlo Simulation has higher overall prediction accuracy than KNN for similar cases [8]. Another commonly used method is Building Information Modelling (BIM). It can automate cost estimation process and improve inaccuracies where New Rules of Measurement (NRM) for cost estimation can be extracted for automatic cost estimate based on a 4D BIM modelling software [9].

The research above enriches the method models of construction cost prediction and improves the prediction accuracy. But the prediction is mainly about the total construction cost, which helps decision-making, project application and fund preparation. It is also necessary to predict its main component cost accurately including engineering project cost, installation project cost and decoration project cost for compiling a feasible research report. Therefore, this research aims to develop 4 SVR models to predict costs suitable for the initial phase of the residential projects, which can get the construction cost of the proposed project accurately and quickly, and help the construction unit to make scientific investment decisions and target cost control. BP Neural Network (BPNN) and Random Forest (RF) were also used to compare the prediction results. We also point out that it is important to establish and improve the project cost database. It is an inevitable requirement for the development of construction industry to collect and analyse the information and data of past engineering projects and reveal their inherent laws for guiding future engineering practice.

2 Determination of Construction Cost Prediction Indicators for Residential Projects

2.1 Identification of Construction Cost Prediction Indicators

Due to the different engineering characteristics of different project types, the prediction indicators may also differ. Considering the reliability of cost data in multiple project

cases, this research selects residential projects for construction cost prediction. The construction cost studied in this research refers to the construction and installation project cost, which accounts for the largest proportion of the total investment in the project, including direct cost, indirect cost, profit and tax. Direct cost includes direct engineering cost and measure cost, and indirect cost includes stipulated fees and enterprise management fee. The construction and installation project cost are the construction price paid by the construction unit to the construction project.

The complexity and long-term of construction projects determine the complexity and variety of prediction indicators affecting the construction cost of residential projects, and the rationality of indicator selection determines the accuracy of construction cost prediction. The purpose of variables selection is to improve the prediction accuracy and provide a better understanding of collected data. Different scholars choose different indicators for cost prediction. For example, Ji et al. use 11 indicators to predict multi-family residential construction cost, including total number of households, total floor area, number of households per unit floor, number of elevators, number of floors, number of households supplied per unit elevator per floor, floor height, pit depth, roof type, corridor type and structure type [10]. In this research, by reading a large amount of literature and considering the engineering information that may be delivered during the initial phase, the key predictors that affect the construction cost of residential projects are divided into two categories: engineering attributes and market attributes, as shown in Table 1. Although external environmental factors, owners, contractors and other management levels also have impacts on construction cost, they are not used as a basis for prediction, considering the importance and parsimony of the indicators.

Table 1. Residential project construction cost prediction indicators

Indicator category	Sub-indicators
Engineering attributes	**Estimated cost indicators for engineering project:** gross floor area (m^2), overground floor area (m^2), underground floor area (m^2), number of overground floors, number of underground floors, number of households, total height (m), average floor height underground (m), type of foundation, type of earthquake resistance, number of elevators
	Estimated cost indicators for installation project: installation completeness of electrical engineering, HVAC, water supply and drainage works, fire engineering
	Estimated cost indicators for decoration project: type of entrance doors, type of exterior windows, total exterior wall area (m^2), type of exterior facade decoration, type of flooring, interior decoration level
Market attributes	Construction cost index

2.2 Quantification of Prediction Indicators

The indicator system identified above is divided into two categories: quantitative and qualitative indicators. Quantitative indicators have an impact on construction cost through numerical magnitude, while qualitative indicators are determined by design schemes, construction processes, and other means. Considering the design scheme and construction process commonly used in residential projects, the qualitative indicators are quantified and numbered 1, 2 and 3 respectively from small to large according to their characteristics on the unit cost with a scale of 1, as shown in Table 2.

Table 2. Quantification of qualitative indicators

Sub-indicators	Indicator quantification
Type of foundation	Independent foundation (1), strip foundation (2), raft slab foundation (3), pile foundation (4)
Type of earthquake resistance	Level 4 (1), Level 3 (2), Level 2 (3), Level 1 (4)
Installation completeness of electrical engineering	Simple (1), more complete (2), very complete (3)
Installation completeness of HVAC	Simple (1), more complete (2), very complete (3)
Installation completeness of water supply and drainage works	Simple (1), more complete (2), very complete (3)
Installation completeness of fire engineering	Simple (1), more complete (2), very complete (3)
Type of entrance doors	None (1), wood doors (2), steel doors (3), security doors (4)
Type of exterior windows	None (1), aluminium windows (2), steel windows (3), louvered windows (4)
Type of exterior facade decoration	None (1), paint (2), tile (3), dry hanging stone (4), curtain wall (5)
Type of flooring	Cement mortar (1), floor tile (2)
Interior decoration level	Simple (1), more complete (2), very complete (3)

The project attributes above are considered as static indicators, but the prices of labor and main materials fluctuate with market prices, so it is necessary to introduce construction cost index to adapt the prediction model to the impact of time changes on costs. Construction cost index is a rate reflecting the change of construction cost in a certain period relative to that in a base period, which can be used as a basis for adjusting the price difference of construction cost in different periods [11]. This research directly uses the construction cost index published by local governments, and the base period is uniformly January, 2017.

2.3 Reduction of Prediction Indicators

The purpose of indicator selection is to better collect data and improve prediction accuracy. Too many indicators can affect the performance of cost prediction methods, and

inappropriate indicators can reduce model accuracy [12]. In order to get suitable indicators to build the model, this research uses Pearson correlation coefficient to conduct correlation analysis on unit engineering project cost, unit installation project cost, unit decoration project cost as dependent variables and corresponding cost prediction indicators as independent variables. We delete indicators with correlation coefficient less than 0.3, and check the multiple covariance among indicators, because indicators with large degree of covariance will affect the cost estimation reliability of the results. After repeated adjustment and verification, 15 simplified prediction indicators were finally determined: overground floor area, underground floor area, number of overground floors, number of underground floors, number of households, type of earthquake resistance, number of elevators, installation completeness of electrical engineering, HVAC, water supply and drainage works, fire engineering, type of entrance doors, type of exterior windows, type of exterior facade decoration and interior decoration level.

3 Establishment of Construction Cost Prediction Model Based on Support Vector Regression

There are various methods to develop predictive models. The regression-based models are among of those popular and efficient ones. The earliest form of regression was the method of the least squares, but such kind of models can become deficient in complicated conditions. In this regard, artificial intelligence methods are greatly developed. There are many statistical and machine learning approaches. Support Vector Machine (SVM) is a novel ML technique to solve classification and regression problems, which maximizes prediction accuracy while avoiding overfitting [13]. Support Vector Regression (SVR), as a general method for solving high-dimensional function estimation problems, is based on Vapnik-Chervonenkis (VC) theory and seeks to identify a hyperplane that is located as close as possible to all data points by setting up a threshold [14].

SVR refers to fitting the sample number (x_i, y_i), $i = 1, 2, \ldots, n, x_i \in R^d, y_i \in R$ with a linear function $g(x) = wx + b$, assuming that all the sample data can be considered error-free in terms of the following linear function, controlling for the fitting accuracy ε.

$$\begin{cases} y_i - wx_i - b \leq \varepsilon \\ wx_i + b - y_i \leq \varepsilon \end{cases} \quad (i = 1, 2, \cdots n) \tag{1}$$

In order to control the complexity of the regression function used to fit, $0.5\|w\|^2$ needs to be minimized by introducing the relaxation factor $\varepsilon_i \geq 0$ and $\varepsilon_i^* \geq 0$ under the condition that the error is allowed to exist in the fitting process, so that the above condition is as follows.

$$\begin{cases} \mathrm{y_i} - \mathrm{wx_i} - \mathrm{b} \leq \varepsilon + \varepsilon_\mathrm{i} \\ \mathrm{wx_i} + \mathrm{b} - \mathrm{y_i} \leq \varepsilon + \varepsilon_\mathrm{i}^* \end{cases} \quad (\mathrm{i} = 1, 2, \cdots \mathrm{n}) \tag{2}$$

At this point, the optimization condition becomes to minimize $0.5\|w\|^2 + C\sum_{i=1}^{n}\left(\varepsilon + \varepsilon_i^*\right)$. The constant $C > 0$ is likewise a control for the degree of penalty beyond the ε sample, so that the problem can be transformed into the following.

$$\begin{aligned} maxQ(\alpha, \alpha^*) = &-\varepsilon\sum_{i=1}^{n}\left(\alpha_i^* + \alpha\right) + \sum_{i=1}^{n} y_i\left(\alpha_i^* - \alpha\right) \\ &-\tfrac{1}{2}\sum_{i,j=1}^{n}\left(\alpha_i^* - \alpha_i\right)\left(\alpha_j^* - \alpha_j\right)\left(x_i x_j\right) \end{aligned} \tag{3}$$

$$\begin{aligned} &s.t.\ \sum_{i=1}^{n}\left(\alpha_i - \alpha_i^*\right) = 0 \\ &0 \le \alpha_i, \alpha_i^* \le C, (i = 1, 2, \cdots n) \end{aligned} \tag{4}$$

Where α_i, α_i^* are **Lagrange** factors, and the final regression function is obtained as follows.

$$f(x) = (wx) + b = \sum_{i=1}^{n}\left(\alpha_i^* - \alpha_i\right)(x_i x) + b^* \tag{5}$$

The above is the mathematical procedure for fitting a function regression with SVR. It has provided accurate prediction performance in various areas (e.g., stock price, weather forecasting, cancer diagnosis) including cost prediction, and it has shown its advantages over the popular multilayer neural network approach in the global optimum solution, robustness to outliers, and accurate and rapid prediction results in small sets of data [15].

4 Case Application

4.1 Case Description

In order to ensure the accuracy of model prediction, the samples were selected with residential projects in Chongqing, considering the different prices of labour and main materials in different regions, and the differences in construction process and technical solutions. Moreover, since the structure type is an important factor affecting the construction cost, it is used as the control condition [7]. The dataset used in this research is not large, but in theory, large datasets allow for better machine learning. However, due to the private nature of construction costs, it is difficult to obtain cost data [16]. In this research, 137 groups of residential cost settlement data from 2017 to 2021 were collected through various channels such as Chongqing Engineering Cost Information Network and other relevant cost information websites and journals, and 84 groups were obtained for the case study after deleting the samples with serious data deficiencies, and the collected sample engineering structure types were all frame shear structures. By this sample selection method, the regional uniformity and category consistency of the samples were ensured. Some descriptive statistical information of the sample data is shown in Table 3.

4.2 Data Preprocessing

After the quantification of qualitative indicators, due to the different magnitudes of different engineering indicators and the large difference of the absolute values of the sample data, it is necessary to standardize the input vector and output vector of the

Table 3. Description of the residential project data

Attribute	Min.	Max.	AVG	SD
Overground floor area	2522.2	45555.28	15872.68	9595.917
Number of households	16	574	158.94	102.986
Number of overground floors	10	43	23.56	9.608
Number of elevators	0	7	2.76	1.168
Installation completeness of electrical engineering	1	3	1.49	0.649
Interior decoration level	1	3	2.08	0.564
Engineering project cost	704.494	1030.909	805.9567	73.78508
Installation project cost	69.207	352.401	141.8084	52.35981
Decoration project cost	120.301	566.191	312.6114	118.4331
Construction cost	1278.08	2199.17	1707.64	206.1755

sample data separately in advance to avoid poor training of the model. In this research, z-score normalization is used to transform the data with the following formula.

$$\overline{x}_i = \frac{x_i - \overline{x}}{\sigma} \tag{6}$$

$\overline{x}_i$ is the normalized data by **z-score**. x_i is the current data; $\overline{x}$ and σ are the mean and standard deviation of the data under index i, respectively.

4.3 Construction Cost Prediction

Accurate prediction of construction cost in the initial phase of a construction project is critical to the success of the project. It is the most basic basis for cost control in the whole project process. Underestimating cost is prone to cost overrun and overestimating cost easily affects investment decisions and capital preparation. But it is also necessary to predict the construction cost's main component cost for compiling the feasible research report. The construction cost to be predicted in this research refers to the construction and installation project cost, which accounts for the largest proportion of the total investment in the project, and mainly includes engineering project cost (EC), installation project cost (IC) and decoration project cost (DC) to be predicted. After the approximate reduction of the prediction indicators, the engineering project cost (EC) is predicted by using 7 independent variables including overground floor area, underground floor area, number of overground floors, number of underground floors, number of households, type of earthquake resistance and number of elevators. The installation project cost (IC) is predicted by using 4 independent variables including installation completeness of electrical engineering, HVAC, water supply and drainage works and fire engineering. The decoration project cost (DC) is predicted by using 4 independent variables including type of entrance doors, type of exterior windows, type of exterior facade decoration and interior decoration level. Finally, the construction cost (CC) is predicted by using 3 independent variables including EC, IC and DC.

Different kernel function types have a direct impact on the performance of the model. In this research, model optimization refers to selecting the kernel function and the corresponding kernel parameters that are most suitable for the sample data structure from three kernel functions: Linear Kernel, Polynomial Kernel and Radial Basis Function. Through many experiments, rbf kernel function with better prediction effect is adopted. 90% of the data is used for training models and 10% for testing models. In the training process, grid search is used to find the optimal parameters C and g of SVR models. Finally, the predicted results and true values of engineering project cost (EC), installation project cost (IC), decoration project cost (DC) and construction cost (CC) are shown in Fig. 1. The goodness of fit R^2 for predicting engineering project cost (EC), installation project cost (IC) and decoration project cost (DC) are 0.9687, 0.9478 and 0.9546 respectively. The goodness of fit R^2 used to predict the construction cost (CC) is as high as 0.9832. From the prediction results, the installation cost prediction model performed poorly on sample 34, but the overall prediction results are acceptable.

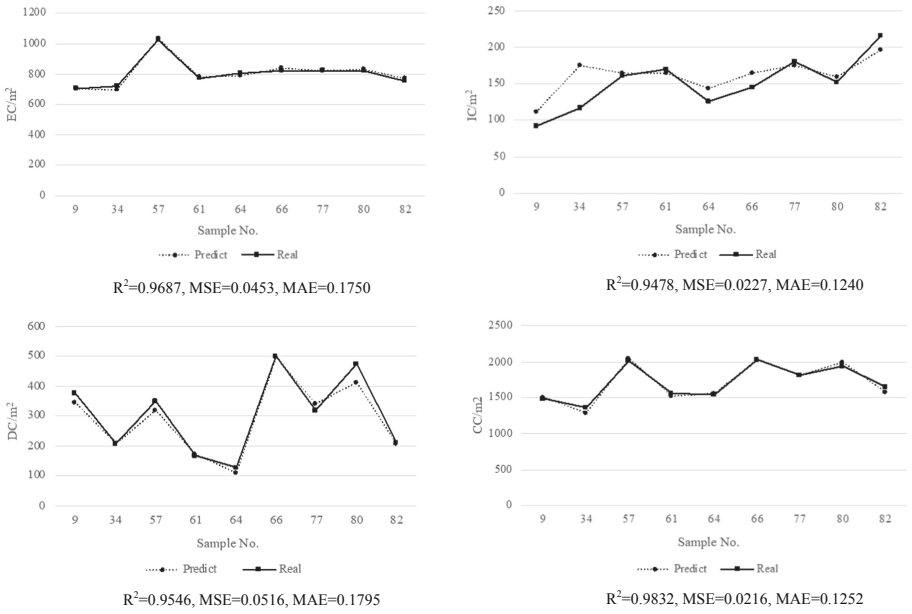

Fig. 1. Prediction results of EC, IC DC and CC used SVR

In order to effectively verify the prediction performance of SVR models, this research adopts BP Neural Network (BPNN) and Random Forest (RF) as control models. BPNN uses error back propagation to learn, which is composed of a large number of nodes and connections between nodes. RF introduces bagging and randomly selects split attributes, and its core idea is to generate multiple decision trees in parallel to form a forest to prevent over-fitting and achieve optimal classification or regression by increasing the breadth. The prediction results of the three models are shown in Table 4. R^2 is used to describe the accuracy of model fitting. The larger the value, the better. MSE and MAE are used to

describe the generalization ability of the model. The smaller the value, the better. On the whole, SVR models have the best overall prediction effect on four kinds of costs, and the prediction model developed in this research can effectively predict the construction cost of proposed residential projects.

Table 4. Comparison of prediction performance of SVR, BPNN and RF

Cost prediction	Model type	R^2	MSE	MAE
Engineering project cost (EC)	SVR	0.9687	0.0453	0.1750
	BPNN	0.9297	0.1016	0.2535
	RF	0.9432	0.0825	0.2427
Installation project cost (IC)	SVR	0.9478	0.0227	0.1240
	BPNN	0.9430	0.0321	0.1324
	RF	0.9325	0.0611	0.1865
Decoration project cost (DC)	SVR	0.9546	0.0516	0.1795
	BPNN	0.9444	0.0524	0.1974
	RF	0.9480	0.0590	0.2050
Construction cost (CC)	SVR	0.9832	0.0216	0.1252
	BPNN	0.9817	0.0239	0.1082
	RF	0.9747	0.0224	0.1120

5 Summary

A large number of historical data have been accumulated in the long-term practice of engineering cost field. How to make full use of these data combined with artificial intelligence to accurately calculate the reasonable cost of the proposed project is a research topic worthy of attention. In this study, SVR is proposed based on 84 completed residential projects in Chongqing, China. We not only predict the construction cost of residential projects, but also predict the main component costs, including engineering project cost (EC), installation project cost (IC) and decoration project cost (DC), with the prediction accuracy of 98.32%, 96.87%, 94.78% and 95.46%, respectively. All the prediction effects are good, which are higher than the prediction accuracy of BPNN and RF.

In this research, after eliminating the indicators whose correlation is greater than 0.9 and less than 0.3 by factor analysis, we use seven prediction indicators to predict EC, four prediction indicators to predict IC, and four prediction indicators to predict DC. When the data are normalized, we find that the data prediction result by z-score normalization is better than Min-max normalization, which may be related to Min-max normalization changing the relative distance of the data. Ahn et al. studied the performance evaluation of 5 different normalization methods including interval standardization, Gaussian

distribution-based normalization, z-score normalization, logistic function-based normalization, and ratio standardization [6]. It indicates that the data processing method has a certain influence on the accuracy of the model. To predict the construction cost, this research uses EC, IC and DC to make the SVR model instead of all the 15 prediction indicators, because the accuracy of the latter is only 93.02% and is not as high as 98.32% of the form. There are relatively large correlation indicators among all the 15 prediction indicators, while the correlation of EC, IC and DC is less than 0.3. It also indicates that the collinearity of prediction indicators will also affect the prediction accuracy, which is similar to the effect of the covariance between indicators studied by Ahn et al. on the case retrieval similarity based on CBR model in the prediction of construction cost [17].

Compared with traditional estimation methods such as index estimation, this cost prediction model developed by machine learning can save time and energy and avoid artificial estimation errors, playing an important role in determining a reasonable investment for the construction unit, compiling project proposals and feasibility study reports, and improving the investment benefit and enterprise management level. With the increase of completed engineering projects, the accumulation of cost data will make the model prediction effect better. So we also suggest that it is the inevitable requirement of the development of construction industry to establish and improve the engineering cost database, collect and analyze the engineering project information and reveal its internal law, which is used to guide the engineering practice.

References

1. Doloi, H.: Cost overruns and failure in project management: Understanding the roles of key stakeholders in construction projects. J. Constr. Eng. Manag. **139**(3), 267–279 (2013)
2. Doloi, S.M., Oberlender, G.D.: Predicting accuracy of early cost estimates using factor analysis and multivariate regression. J. Constr. Eng. Manag. **129**(2), 189–204 (2003)
3. Koo, C.W., Hong, T.H., Hyun, C.T., et al.: A study on the development of a cost model based on the owner's decision making at the early stages of a construction project. Int. J. Strateg. Prop. Manag. **14**(2), 121–137 (2010)
4. Jin, R., Cho, K., Hyun, C., Son, M.: MRA-based revised CBR model for cost prediction in the early stage of construction projects. Expert Syst. Appl. **39**(5), 5214–5222 (2012)
5. Wang, Y.R., Yu, C.Y., Chan, H.H.: Predicting construction cost and schedule success using artificial neural networks ensemble and support vector machines classification models. Int. J. Proj. Manag. **30**(4), 470–478 (2012)
6. Ahn, J., Ji, S.H., Ahn, S.J., et al.: Performance evaluation of normalization-based CBR models for improving construction cost estimation. Autom. Constr. **119**, 103329 (2020). (in press)
7. Stoy, C., Pollalis, S., Schalcher, H.R.: Drivers for cost estimating in early design: case study of residential construction. J. Constr. Eng. Manag. **134**(1), 32–39 (2008)
8. Kwon, N., Song, K., Ahn, Y.: Maintenance cost prediction for aging residential buildings based on case-based reasoning and genetic algorithm. J. Build. Eng. **28**, 101006 (2020). (in press)
9. Kim, S., Chin, S., Kwon, S.: A discrepancy analysis of BIM-based quantity take-off for building interior components. J. Manag. Eng. **35**(3), 1–12 (2019)
10. Ji, S.H., Park, M., Lee, M.A.: Case adaptation method of case-based reasoning for construction cost estimation in Korea. J. Constr. Eng. Manag. **138**(1), 43–52 (2012)
11. Elfahham, Y.: Estimation and prediction of construction cost index using neural networks, time series, and regression. Alexandria Eng. J. **58**(2), 499–506 (2019)

12. Song, M.L., Peng, J., Wang, J.L., Dong, L.: Better resource management: an improved resource and environmental efficiency evaluation approach that considers undesirable outputs. Resour. Conserv. Recycl. **128**, 197–205 (2012)
13. Lloyd, B.G.R.: Support vector machines for classification and regression. Analyst **135**(2), 230–267 (2010)
14. Gerald, T., David, T., Todd, L.: Advances in neural information processing systems. Comput. Math. Appl. **31**(7), 144–146 (1996)
15. Ahn, S.A., Han, S.B., Al-Hussein, M.A.: Improvement of transportation cost estimating for prefabrication for prefabrication-based large-scale GPS data features extract and support vector regression. Adv. Eng. Inform. **43**, 101012 (2020). (in press)
16. Hong, J.K., Shen, G.Q.P., Li, Z.D., et al.: Barriers to promoting prefabricated construction in China: a cost-benefit analysis. J. Clean. Prod. **172**, 649–660 (2018)
17. Ahn, J., Park, M., Lee, H., et al.: Covariance effect analysis of similarity measurement methods for early construction cost estimation using case-based reasoning. Autom. Constr. **81**(9), 254–266 (2017)

Evolution of Intellectual Structure of Data Mining Research Based on Keywords

Yue Huang(✉), Runyu Tian, and Yonghe Yang

School of Information Science, Beijing Language and Culture University, Beijing 100083, China
huang.yuet@blcu.edu.cn

Abstract. Data mining has made rapid progress in the past decade and detecting intellectual structure of data mining research is of great help to researchers. The purpose of this study is to detect the evolutional intellectual structure of data mining from the aspect of keywords. This study takes the 5,380 papers, published between 2007 and 2016 retrieved from 11 leading data mining journals defined by Google Scholar Metrics as the dataset. After data pre-processing, keyword frequency analysis is caried out to detect the three different developing patterns of keywords, which indicates that the research focus of data mining has shifted from such topics as association rule mining to large-scale complex networks. Then this paper constructs co-word matrices of high-frequency keywords of different time periods, namely 2007 to 2016 for the whole picture during these years, 2007 to 2011 and 2012 to 2016 for two periods. Clustering results show that there are four main data mining topics, and the attention has been paid more to graph data mining and complex network analysis in the past five years.

Keywords: Data mining · Intellectual structure · Co-word analysis · Clustering · Evolution analysis

1 Introduction

Along with social development and technical breakthrough, there has been a constant improvement in the utilisation of information technology and the acquisition of data. The three pillars of data mining, namely, database, artificial intelligence and mathematical statistics, have made rapid development. Data mining is the process of extracting implicit and useful information from massive data using an array of algorithms and strategies. The past decade has witnessed a significant leap of the data mining technology, and numerous studies related to data mining have appeared in top-level journals.

Intellectual structure [1] is a term in information science, which is defined as the clusters and relationships obtained by bibliographic analysis of a certain field using bibliographic clustering matrix. Each cluster corresponds to one subfield of research.

Bibliometrics and mapping of science [2] are two useful quantitative tools based on mathematics and statistics, which are widely used for studying and evaluating the researches in a given field. The intellectual structure, research fronts and development

R. Qiu et al. (Eds.): ICSS 2021, LNOR, pp. 125–140, 2021.
https://doi.org/10.1007/978-3-030-90275-9_11

trend of a specific topic can be detected by bibliometric methods. Conventional bibliometrics calculate yearly amount of publications, authors, contents, sources and citation frequency for a given field without digging deeper into the research themes. While, co-word analysis [3] is a type of content analysis, and when two keywords related to the same research topic appear concurrently in one paper, these two words are considered interrelated in some way. The higher the frequency of co-occurrence of the two words is, the closer their relationship (or the smaller their distance) is. Using modern statistical tools (such as factorial analysis, clustering and multi-dimensional scale analysis), the keywords are classified based on such 'distance' in a discipline. Therefore, the research highlights, structure and paradigm for the discipline can be identified. Compared with conventional bibliometrics, co-word analysis allows for an in-depth study of the research structure and highlights as well as the prediction of the development trend in a given discipline.

Co-word analysis has found extensive applications in such fields as medical and health science, social science, philosophy, humanities and information technology. The top three fields for which co-word analysis is applied most commonly are information technology, social science, and medical and health science, among which library and information science [4] related to information technology is the most extensively studied.

Existing studies on data mining are generally focused on data mining methodology and its application. However, few studies have been devoted to the evolution of intellectual structure in data mining. We believe that an analysis on the evolution of the intellectual structure in data mining field is crucial for identifying the development trend in this field and can providing reference for relative researchers.

To sum up, the aim of this paper is to apply co-word analysis to papers published in reputed journals on data mining in the past decade, with a purpose to explore the current status of data mining research and to detect the evolution of intellectual structure over a five-year cycle from 2007 to 2016.

2 Data

2.1 Data Source

Since data mining is not a subcategory of an existing discipline, making it is impossible to use the categories given by Web of Science, thus we take Google Scholar Metrics as the standard. Google Scholar Metrics provide an academic evaluation standard which uses two important metrics, h5-index and h5-median, to help researchers to assess the visibility and influence of recent articles in scholarly publications [5]. For a publication, h5-index is the h-index for articles published in the last five complete years, i.e., it is the largest number h such that h articles published in the last five years have at least h citations each. While h5-median is the median number of citations for the articles that make up its h5-index. Google Scholar Metrics provide a list of top publications (including both conferences and journals) based on the citations within Google, ordered by their five-year h-index and h-median metrics. In the sub-category 'date mining and analysis' of category 'engineering and computer science', there are nine conferences and 11 journals [6]. It is well-known that articles from top professional journals are strictly

peer-reviewed by experts. Therefore, we take journals from the Google Scholar Ranking of Data Mining and Analysis as data selection criteria (Table 1).

Table 1. Brief statistics of top journals of data mining and analysis based on Google Scholar Metrics

No.	Publication title	Starting year	H5-index	H5-median
1	IEEE Transactions on Knowledge and Data Engineering	1989	66	111
2	Knowledge and Information Systems	1999	38	52
3	ACM Transactions on Intelligent Systems and Technology	2010	37	68
4	Data Mining and Knowledge Discovery	1997	33	57
5	Wiley Interdisciplinary Reviews: Data Mining and Knowledge Discovery	2011	30	56
6	Social Network Analysis and Mining	2011	26	37
7	ACM Transactions on Knowledge Discovery from Data	2007	23	39
8	Advances in Data Analysis and Classification	2007	18	25
9	BioData Mining	2008	17	25
10	Statistical Analysis and Data Mining	2008	17	30
11	Intelligent Data Analysis	1997	16	21

It can be seen that most leading data mining journals do not have a long history (Table 1). Among these journals, IEEE Transactions on Knowledge and Data Engineering, first published in 1989, has the longest time span, which is shorter than many other computer science journals. Besides, seven journals are first published not earlier than 2007 and the rest journals are first issued before the 21st century. Hence, we take literature published in these leading journals between 2007 and 2016 to reflect the overall research status of data mining.

2.2 Data Acquisition

Web of Science [7] and Scopus [8] are two famous and authoritative abstract and citation databases, among which Web of Science provides more detailed information about literature. Thus, when papers from above journals are included in both databases, we use Web of Science (WOS) as the data source.

In the SCI-Expanded database of Web of Science core collection, journal titles were used to locate a specific journal, publication year was limited to 2007–2016, and document types included article and review. By this searching strategy, 4,815 bibliographic data were obtained from Web of Science. While in Scopus, the unique international standard serial number (ISSN) was used to search papers of these leadings journals that

were not included in Web of Science during 2007–2016, and 565 publications were found from Scopus. Thus, a collection of 5,380 publications were obtained, which contains 5,222 articles (97%) and 158 reviews (3%).

2.3 Data Preprocessing

2.3.1 Standardization of the Source Format

The bibliographic format is different between Scopus and WOS, so the format was first standardised. Depending on our need, 16 required fields with the same meaning were selected and compared in Web of Science and Scopus. Then, bibliographic data from the two data sources were merged into one database according to these 16 fields. The fields which were used in this paper are depicted as AU, TI, SO, DT, DE, ID, AB, C1, RP, CR, TC, SN, PY, VL, IS, and DI in WOS, and the meaning of fields are given in Table 2. No. 17 was added manually to indicate the data source of each literature.

Table 2. Fields used in the Experiment

No.	Field	Meaning
1	TI	Title
2	AU	Authors
3	C1	Addresses of all authors
4	RP	Address of reprint author
5	SN	ISSN
6	DE	Author keywords
7	ID	Keywords plus given by data source
8	AB	Abstract
9	DT	Document type
10	CR	Cited references
11	TC	Times cited
12	SO	Source
13	PY	Publication year
14	VL	Volume
15	IS	Issue
16	DI	DOI (Digital Object Identifier)
17	Data source	Web of Science or Scopus

2.3.2 Check of Keywords

Co-word analysis is premised on word frequency analysis. The 'DE' (author keyword) column was analysed and 13,252 different keywords were identified, though some inconsistent or erroneous records were contained. Some records were pure numbers, such as "454"; others were mistakenly treated as different keywords because of the non-standard punctuation mark, for example, 'fuzzy and probabilistic reasoning' and 'fuzzy, and probabilistic reasoning'; the same keywords in singular or plural form were mistakenly treated as different, for example, access control and access controls. There were many keywords which had similar meaning but different forms. The computer will treat the two differently spelt words as two distinct works regardless of the similarity in meaning, which causes great confusion to statistical analysis. Therefore, the keywords under analysis should be properly managed and uniformly indexed. Only in this way can co-word analysis realistically reflect the research theme of the paper based on co-occurrence frequency. We built a correction sheet listing the types of non-standardisation and the results of correction. There were six major types of non-standardisation, which were ranked in a decreasing order of the number of corrections in each type: singular or plural form, similar vocabulary, connector, acronym, gerund and mistaken data. The number of corrections in each type was 349, 122, 88, 45, 39 and 10, respectively. A total of 653 corrections were made, in which one keyword was deleted, two keywords were combined, and 1748 similar keywords were unified into one. Thus, the number of distinct keywords decreased from 13,252 to 11,502.

3 Analysis on the Evolution of Keyword Frequency

An analysis on the evolution of keyword frequency benefits the understanding on the shift of research highlights in data mining field in the past decade. From 2007 to 2016, the number of keywords was 826, 992, 1145, 1157, 1446, 1747, 2189, 2151, 2442 and 2510, respectively. It can be seen that except the number of keywords decreased by 38 from 2013 to 2014, while it increased on a yearly basis for the remaining years. From 2007 to 2016, the number of keywords increased from 826 to 2,510. In addition, the top 1% of the keywords within a year was considered high-frequency keywords in this paper, so there were 8, 14, 13, 15, 19, 18, 23, 25, 25 and 24, respectively. The high-frequency keywords vary from year to year and they are shown in Table 3. Fifty-one distinct keywords were detected in the high-frequency keywords list. The evolution characteristics of keywords in the data mining field can be summarised as follows.

Table 3. High-frequency keywords during 2007 and 2016

Year	High-frequency keywords (frequency)
2007	data mining (34), clustering (19), classification (15), machine learning (11), association rules (9), time series analysis (8), data streams (8), query processing (7)
2008	data mining (45), clustering (23), classification (17), association rules (11), machine learning (11), query processing (9), support vector machines (8), time series analysis (7), text mining (7), graph mining (6), feature selection (6), cost-sensitive learning (6), genetic algorithm (6), relational database (6)
2009	data mining (42), clustering (21), classification (17), feature selection (9), association rules (8), query processing (8), data streams (7), privacy (7), machine learning (7), spatial databases (6), algorithms (5), logistic regression (5), e-learning (5)
2010	data mining (29), clustering (28), classification (17), algorithms (13), machine learning (13), query processing (12), support vector machines (11), data streams (10), association rules (9), graph mining (8), privacy (8), feature selection (7), text mining (7), ontology (7), social network analysis (7)
2011	clustering (36), algorithms (36), data mining (35), classification (24), social network analysis (19), experimentation (19), machine learning (14), query processing (10), time series analysis (9), association rules (7), collaborative filtering (7), anomaly detection (7), design (7), human factors (7), economics (7), graph mining (7), dimensionality reduction (7), semi-supervised learning (7), information retrieval (7)
2012	algorithms (59), experimentation (42), data mining (37), clustering (30), social network analysis (27), classification (26), performance (22), design (20), feature selection (18), human factors (15), machine learning (14), query processing (11), topic model (9), text mining (9), measurement (9), anomaly detection (8), sentiment analysis (8), decision trees (8)
2013	algorithms (80), social network analysis (64), experimentation (58), data mining (46), clustering (35), design (32), performance (31), classification (23), machine learning (21), human factors (19), recommender systems (14), privacy (14), data streams (14), semi-supervised learning (11), collaborative filtering (10), theory (10), time series analysis (10), Twitter (10), measurement (9), query processing (9), trust (9), link prediction (9), ontology (9)
2014	social network analysis (56), clustering (51), data mining (45), classification (29), algorithms (23), privacy (13), experimentation (13), design (11), recommender systems (11), machine learning (10), data streams (10), collaborative filtering (9), feature selection (9), query processing (9), transfer learning (9), topic model (9), social media (9), text mining (9), big data (8), complex networks (8), measurement (8), graph mining (8), Twitter (8), pattern mining (8), performance (8)
2015	algorithms (88), experimentation (57), social network analysis (47), performance (46), data Mining (42), design (36), classification (33), clustering (27), machine learning (18), measurement (15), feature selection (15), theory (14), human factors (14), privacy (14), recommender systems (14), query processing (14), collaborative filtering (13), anomaly detection (11), Twitter (11), time series analysis (10), topic model (10), support vector machines (10), community detection (9), spatial databases (9), social media (9)
2016	social network analysis (51), algorithms (48), data mining (36), clustering (33), classification (30), performance (24), experimentation (22), recommender systems (21), machine learning (19), crowdsourcing (17), design (17), time series analysis (15), feature selection (15), collaborative filtering (14), big data (14), Twitter (12), query processing (12), prediction (11), data streams (11), anomaly detection (10), online learning (10), support vector machines (10), ensemble learning (10), topic model (10)

3.1 Some Keywords Appear Often the High-Frequency Keywords Over the 10 Years

Keywords 'data mining', 'clustering', 'classification', 'machine learning', and 'query processing' are always in the high-frequency list over the ten years. For example, 'data mining' is always among the top 1% keywords, or even among the top five keywords. This is because we included papers in the data mining field, which were published in the top journals in this field. 'Clustering' is always the top eight keywords, since clustering in one of the basic task of data mining. While keyword 'algorithms' appear eight times in the list over the ten years. These keywords not only represent the hot spots but also the highlights of research, among which clustering and classification are the two primary tasks in data mining.

3.2 Some Keywords Appeared in the Past, but not so in the Present

For example, 'association rule' appeared most frequently in the first five years, but not after 2012, which is in line with the fact that association rule was among the most extensively studied topic from 2007 to 2011. But as the progress is being made in the topic of association rule after 2012, association rule was no longer the high-frequency words after 2012.

3.3 Some Keywords Appeared only in the Recent Years, but not so in the Present

For instance, the keyword 'performance' did not appear in the first five years, but appeared between 2012 and 2016. 'Experimentation' did not appear in the first four years, but appeared every year in the next six years. 'Recommender systems' did not appear in the first six years, but appeared every year in the next 4 years. 'Social network analysis' did not appear in the first three years, but appeared every year in the next seven years. 'Design' did not appear in the first four years, but appeared every year in the next six years. 'Collaborative filtering' did not appear in the first four years, but appeared five times in the next six years, in 2011, 2013, 2014, 2015 and 2016. 'Twitter' did not appear in the first six years, but only appeared in the next four years. 'Topic model' did not appear in the first five years, but appeared in 2012, 2014, 2015 and 2016. "Measurement" did not appear in the first five years, but between 2012 and 2015.

Apparently, there has been a shift in research focus from 'association rule' in the first five years to 'performance', 'experimentation', 'social network analysis', 'design', 'Twitter', 'topic model' in the next five years. Obviously, along with the rapid development of network and other information technologies, the data scale and associations between the objects increase. This increases the availability of data, and more and more researchers attempt at data characterization in terms of network. Recent years have seen a growing number of studies on large-scale complex networks.

4 Matrix Construction for Co-word Analysis

4.1 Word Frequency Estimate

There are two ways to determine the high-frequency words. The first is empirical, in which the researchers make an objective choice of high-frequency words by weighing between the number and frequency of words selected. The second is to use the Zipf's law [9] for setting the threshold of high frequency. In the Zipf's law, $T = (-1+\sqrt{1+8\times I1})/2$, where T is the threshold of high frequency of keywords, and I1 is the number of keywords with a frequency of 1. This law depicts the relationship between the frequency of low-frequency words and the word count. However, if there are many technical terms with extremely high or low frequency, the Zipf's law is not an appropriate method to determine the threshold of word frequency. In our study, I1 = 9112, and final T = 134, and there were only eight keywords with frequency above 134, which was no sufficient to reflect the knowledge points for a given discipline. Further analysis revealed that there were too many low-frequency words, leading to an excessively high I1 but a very low T. The threshold of high-frequency words was too low. Therefore, the Zipf's law was not applicable to the choice of high-frequency words in our study. Here g-index was used to determine the threshold of high-frequency words. Experiment using real data has demonstrated that g-index is more accurate than the Zipf's law, as it can overcome the defect of the Zipf's law in defining the low-frequency words while reducing the objectivity in the choice of technical terms. The g-index is concerned with the contribution of high-frequency words without considering the low-frequency words. This feature makes it highly suitable for co-word analysis which focuses on high-frequency words. The g-index is calculated as follows: The source papers are ranked in a decreasing order of the number of citations, and the g-value is found so that the sum of the number of citations for the first g papers is equal to or above g^2 and the sum of the number of citations for the first g+1 papers is below $(g+1)^2$. The g-index is defined as follows: the score for the number of keywords related to a research theme is g. For a total number N of keywords for a given research theme, the cumulative frequency of g keywords is equal to or above g^2 and the cumulative frequency of g+1 keywords is equal to or above $(g+1)^2$. We calculated the g-index as 71 in this study, which corresponded to keywords with a frequency above 25. Thus 77 keywords were chosen as the high-frequency words. Further inspection of these keywords showed that they sufficiently represented the knowledge points of the discipline.

4.2 Construction of Co-word Matrix

The high frequency co-word matrix was constructed for the data mining field (Table 4).

Table 4. High-frequency co-word matrix (partial)

Keywords	Active learning	Algorithms	Anomaly detection	Association rule	Bayesian network	Big data
Active learning		7	1			
Algorithms	7		3	9	2	4
Anomaly detection	1	3		1		
Association rule		9	1		1	
Bayesian network		2		1		
Big data		4				

As indicated by the above matrix which is yet to be analyzed by relevant software, data mining is an interdisciplinary science, which is closely connected with mathematics, computer science, and networks.

5 Clustering Analysis of the Co-word Matrix

The intellectual structure of the data mining field was visualized using University of California at Irvine NETwork (UCINET). Clustering analysis was performed to the co-word matrix using the cohesive subgroup analysis tool of UCINET. Cohesive subgroup is a generalized concept of subgroup, and the purpose of cohesive subgroup analysis is to reveal the substructure in the cluster. Cohesive subgroup analysis is consistent with clustering analysis.

Before cohesive subgroup analysis using fractions toolkit of UCINET, keywords without reflecting the true research themes were removed. For example, 'data mining' was removed, and other keywords such as 'algorithm', 'design', 'experiment', 'knowledge discovery', 'performance' and 'theory' which caused great confusion to the clustering, were also removed. The clustering results became more reasonable after removing these keywords. To map the evolution of the intellectual structure in data mining, co-word analysis was first performed for the year 2007 to 2016 on the whole and then separately for different time periods, i.e., 2007–2011 and 2012–2016. Co-word matrices were built, with a size of 70, 35 and 52, respectively.

For these three matrices, two to ten clusters were experimented (Table 5). Based on the generated density tables, the number of errors and density were examined (density was considered qualified if the density of the diagonal matrix was higher than other matrix densities in the row, with the least errors).

Table 5. Statistics of clustering results

Time span / Number of clusters	2007-2011		2012-2016		2007-2016	
	Density qualified	Errors	Density qualified	Errors	Density qualified	Errors
2	√	424	√	960	√	1792
3	√	274	√	654	√	1216
4	**√**	**208**	**√**	**506**	**√**	**954**
5	×	—	×	—	×	—
6	×	—	×	—	×	—
7	×	—	×	—	×	—
8	×	—	×	—	×	—
9	×	—	×	—	×	—
10	×	—	×	—	×	—

It can be seen from Table 5 that under each condition, the optimal result was achiecved with four clusters, where the density satisfied the requirement and the number of errors was the smallest. The clustering result was analyzed for each condition.

5.1 Analysis on the Intellectual Structure in Data Mining from 2007 to 2016

Clustering analysis was performed for the co-word matrix from 2007 to 2016, and the resulting density tables are shown in Table 6. The density of the diagonal matrix is the largest in each row with four clusters. The difference is greater between some numbers of clusters (e.g., three clusters vs. four clusters), but smaller between other numbers of clusters (e.g., two clusters vs. four clusters). Due to space limitation, the clustering result of the first cluster is shown in Fig. 1, and the main research topic of each class is analysed as below.

Table 6. Density table of keyword clusters (2007–2016)

Density table	1	2	3	4
1	**0.93**	0.33	0.15	0.61
2	0.33	**1.00**	0.25	0.94
3	0.15	0.25	**0.78**	0.28
4	0.61	0.94	0.28	**1.50**

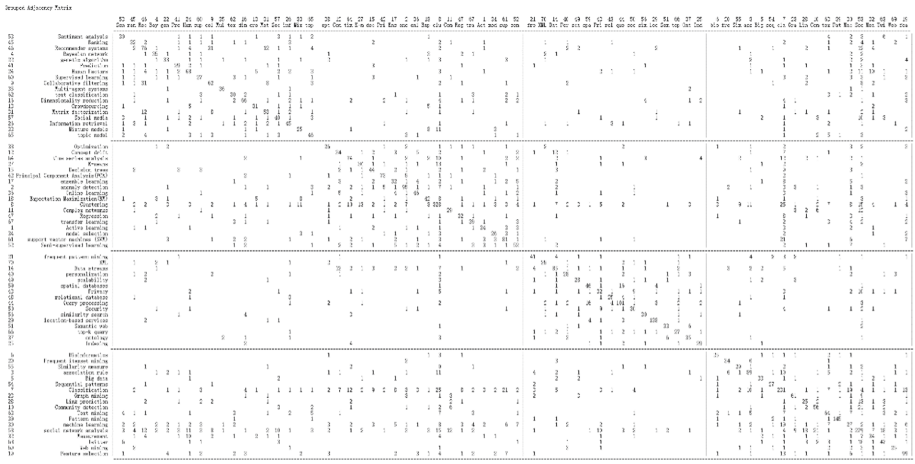

Fig. 1. Clustering result of keywords during 2007 and 2016

5.1.1 Text Classification and Recommender System

Keywords related to this research theme include Bayesian network, collaborative filtering, crowdsourcing, dimensionality reduction, genetic algorithm, human factors, information retrieval, matrix factorisation, mixture models, multi-agent systems, prediction, ranking, recommender systems, sentiment analysis, social media, supervised learning, text classification, and topic model. Among these keywords, collaborative filtering, prediction, ranking, recommender systems, and social media are associated with the recommendation algorithm for a large-scale network under a multi-media environment. While Bayesian network, crowdsourcing, supervised learning, text classification, sentiment analysis, and topic model are associated with text classification and classification is a supervised method.

5.1.2 Clustering and Approaches based on Machine Learning

Keywords related to this research theme include active learning, anomaly detection, clustering, complex networks, concept drift, decision trees, ensemble learning, expectation maximization (EM), K-means, model selection, online learning, optimisation, principal component analysis (PCA), regression, semi-supervised learning, support vector machines (SVM), time series analysis, transfer learning. K-means algorithm is a classical clustering algorithm. Active learning, concept drift, decision trees, ensemble learning, EM, model selection, online learning, optimisation, PCA, regression, SVM, and transfer learning are all data mining methods based on machine learning.

5.1.3 Database-Based Data Mining Techniques and Ontology Semantics

Database was developed earlier than the data mining technology, which did not emerge until the 1980's to 1990's. Keywords related to this research theme include frequent pattern mining, XML, data streams, personalisation, scalability, spatial databases, privacy, relational database, query processing, security, similarity search, location-based

services, semantic web, top-k query, ontology, and indexing, among which frequent pattern mining was first applied to the database for data mining, and data streams later emerged after the extension of frequent pattern mining to the data stream field. While spatial database and relational database are the two major types of database in data mining, query processing, similarity research, top-k query and indexing are important means to improve the efficiency of databases at an early stage in data mining development. In this class, XML, semantic web and ontology were associated with semantic study.

5.1.4 Bioinformatics Data Mining, Network Data Mining, Association Rule Mining, and Text Mining

Keywords related to this research theme include bioinformatics, frequent itemset mining, similarity measure, association rule, big data, sequential patterns, classification, graph mining, link prediction, community detection, text mining, pattern mining, machine learning, social network analysis, measurement, Twitter, web mining, feature selection. Bioinformatics, similarity measure and sequence pattern identification are used for bioinformatics data mining. Keywords such as big data, graph mining, link prediction, community detection, social network analysis, Twitter, and web mining represent a major research topic in graph mining, link prediction, community identification and social network analysis under big data. Frequent itemset mining and association rule are also the keywords which represent the highlights in data mining studies. Text mining is another keyword related to this research theme, which overlaps with the keyword in the second class. This agrees with the fact that the overlapping density of cluster 2 and 4 (0.94) are relatively large in the density matrix.

5.2 Analysis on the Intellectual Structure of Data Mining from 2007 to 2011

Clustering analysis was then applied to the co-word matrix from 2007 to 2011. The resulting density table is shown in Table 7. The density of diagonal matrix in each row is the largest with four clusters. The clustering result is shown in Fig. 2, and the main research topic of each class is analysed.

Table 7. Density table of keyword clusters (2007–2011)

Density table	1	2	3	4
1	**1.38**	0.59	0.20	0.44
2	0.59	**0.96**	0.18	0.27
3	0.20	0.18	**0.33**	0.10
4	0.44	0.27	0.10	**0.75**

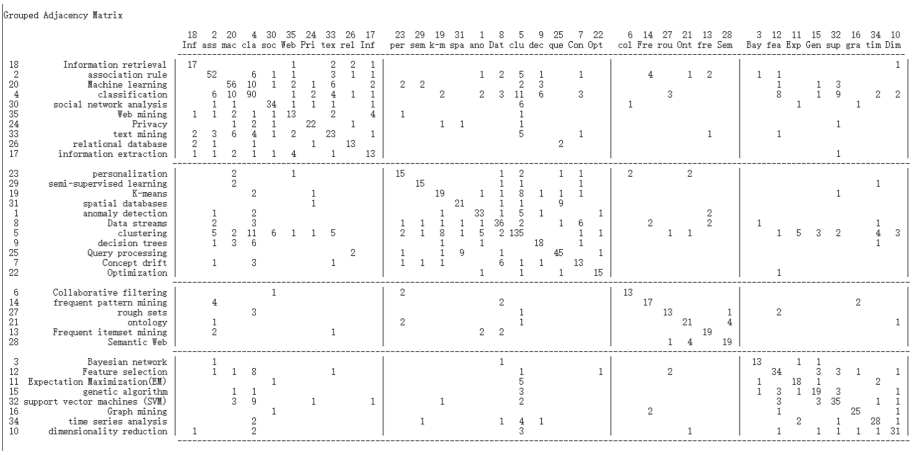

Fig. 2. Clustering result of keywords during 2007 and 2011

5.2.1 Text Data Mining

The keywords include information retrieval, association rule, machine learning, classification, social network analysis, web mining, privacy, text mining, relational database, and information extraction. Keywords such as information retrieval, classification, text mining and information extraction indicate they are related with text mining, as text mining often focuses on classification based on extracted words.

5.2.2 Clustering and Data Stream Mining

The keywords include personalisation, semi-supervised learning, k-means, spatial databases, anomaly detection, data streams, clustering, decision trees, query processing, concept drift, and optimisation. Among these keywords, k-means is a classical clustering algorithm. Besides, keywords such as anomaly detection, data streams, semi-supervised learning and concept drift indicate studies that detect anomaly in data stream using semi-supervised learning algorithm.

5.2.3 Frequent Pattern Mining, Semantics-Related Study and Collaborative Filtering

The keywords include collaborative filtering, frequent pattern mining, rough sets, ontology, frequent itemset mining, and semantic web. Generally speaking, the research subthemes in this class are less closely corelated, and the density is only 0.33 for this class.

5.2.4 Dimensionality Reduction and Machine Learning Studies

The keywords include Bayesian network, feature selection, EM, genetic algorithm, SVM, graph mining, time series analysis, and dimensionality reduction. Keywords such

as feature selection and dimensionality reduction usually appear in studies on dimensionality reduction for high-dimensional data. Other keywords generally appear in the conventional methods based on machine learning.

5.3 An Analysis on the Intellectual Structure of Data Mining from 2012 to 2016

Clustering analysis was then applied to the co-word matrix from 2012 to 2016. The resulting density table is shown in Table 8. The clustering result is shown in Fig. 3, and the main research topic of each class is analysed.

Table 8. Density table of keyword clusters (2012–2016)

Density table	1	2	3	4
1	**1.03**	0.27	0.79	0.65
2	0.27	**0.81**	0.51	0.31
3	0.79	0.51	**0.99**	0.49
4	0.65	0.31	0.49	**0.92**

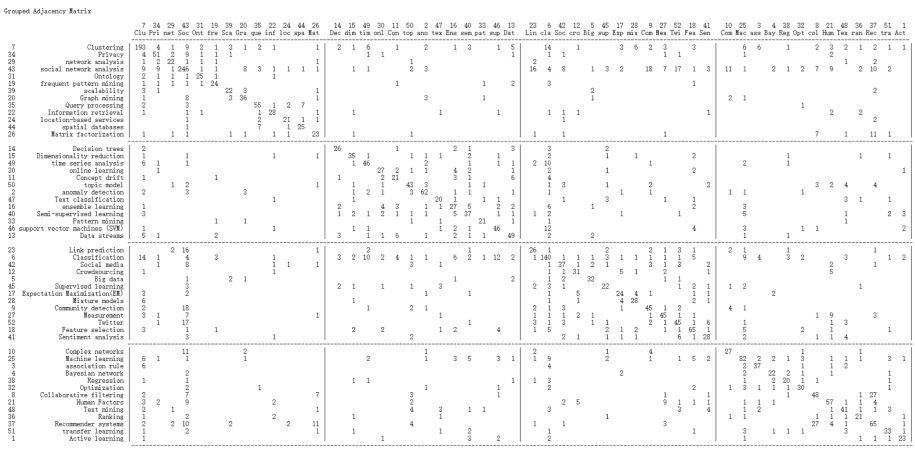

Fig. 3. Clustering result of keywords during 2012 and 2016

5.3.1 Graph Mining and Spatial Data Mining

The keywords include clustering, privacy, network analysis, social network analysis, ontology, frequent pattern analysis, scalability, graph mining, query processing, information retrieval, location-based services, spatial databases, and matrix factorization. Keywords network analysis, social network analysis and graph mining indicate that graph mining is done from the perspective of social network analysis or a more extensive

network. Keyword scalability, query processing, information retrieval, location-based services, spatial databases, matrix factorization usually appear in the research theme of spatial data mining and its application.

5.3.2 Data Stream Mining and Classification

The keywords include decision tree, dimensionality reduction, time series analysis, online learning, concept drift, topic model, anomaly detection, text classification, ensemble learning, semi-supervised learning, pattern mining, SVM, and data streams. Keywords time series analysis, concept drift, anomaly detection and data streams analysis usually appears in the studies on concept drift detection in data stream mining and time series mining. Keywords decision trees, topic model, text classification, ensemble learning, semi-supervised learning, pattern mining, SVM usually appears in classification.

5.3.3 Complex Network Analysis

Keywords include link prediction, classification, social media, crowdsourcing, big data, supervised learning, EM, mixture models, community detection, measurement, Twitter, feature selection, and sentiment analysis. The appearance of keywords link prediction, social media, big data, community detection, Twitter, feature selection and sentiment analysis indicates that in a big data era, the network scale has been expanding constantly and complex network analysis has become a research theme in data mining and this research theme is also closely related to graph mining.

5.3.4 Recommender System

The keywords include complex networks, machine learning, association rule, Bayesian network, regression, optimization, collaborative filtering, human factors, text mining, ranking, recommender systems, transfer learning, and active learning. Keywords complex networks, collaborative filtering, ranking and recommender systems usually appear in recommendation algorithms.

6 Conclusions

We retrieved data mining studies from Web of Science and Scopus databases from 2007 to 2016. Keywords were extracted from the retrieved papers and co-word analysis was carried out. Clustering was applied to the co-word matrices and the evolution of the intellectual structure of data mining field was mapped. Our research indicates that from 2007 to 2016, the research focus in data mining has shifted from basic tasks of data mining such as association rule mining to research based on large-scale complex networks. Clustering results of high frequency co-word matrix show that there are four main topics of data mining research during 2007 to 2016: text classification and recommender system, clustering and approaches based on machine learning, database-based data mining techniques and ontology semantics, and bioinformatics data mining, network data mining, association rule mining, and text mining. Furthermore, by comparison, the main focus of

data mining shifted from text mining, clustering and data stream mining, frequent pattern mining, semantics-related study and collaborative filtering, dimensionality reduction and machine learning studies during 2007 to 2011 to graph mining and spatial data mining, data stream mining and classification, complex network analysis, recommender system during 2012 to 2016. In future studies, we will derive algorithms to review the extracted keywords and consider analysis of the clustering results by combining expert knowledge.

Acknowledgments. This work is supported by Science Foundation of Beijing Language and Culture University (supported by 'the Fundamental Research Funds for the Central Universities') (21YJ040007).

References

1. Zhao, D., Strotmann, A.: Evolution of research activities and intellectual influences in information science 1996–2005: Introducing author bibliographic-coupling analysis. J. Am. Soc. Inform. Sci. Technol. **59**(13), 2070–2086 (2008)
2. Chen, C.: Science mapping: a systematic review of the literature. J. Data Inf. Sci. **2**(2), 1–40 (2017)
3. Callon, M., Courtial, J.P., Turner, W.A., Bauin, S.: From translations to problematic networks - an introduction to co-word analysis. Soc. Sci. Inf. Sur Les Sci. Soc. **22**(2), 191–235 (1983)
4. Milojević, S., Sugimoto, C.R., Yan, E., Ding, Y.: The cognitive structure of library and information science: analysis of article title words. J. Am. Soc Inf. Sci. Technol. **62**(10), 1933–1953 (2001)
5. "Google Scholar Metrics", Google Scholar (2017). https://scholar.google.com/scholar/metrics.html. Accessed 20 Mar 2017
6. "Top publications - Data Mining & Analysis – Google Scholar", Google Scholar (2017). https://scholar.google.com/citations?view_op=top_venues&hl=en&vq=eng_dataminingan alysis. Accessed 20 Mar 2017
7. "Web of Science", Thomson Reuters (2017). https://app.webofknowledge.com. Accessed 23 Mar 2017
8. "Scopus", Elsevier (2017). http://www.scopus.com. Accessed 23 Mar 2017
9. Zipf, G.K.: Human Behavior and the Principle of Least Effort, p. 1. Addison-Wesley, Cambridge, Massachusetts (1949)

Development of a Cost Optimization Algorithm for Food and Flora Waste to Fleet Fuel (F^4)

Kate Hyun[1], Melanie L. Sattler[1], Arpita H. Bhatt[1], Bahareh Nasirian[2], Ali Behseresht[1], Mithila Chakraborty[1], and Victoria C. P. Chen[2(✉)]

[1] Department of Civil Engineering, University of Texas at Arlington, Arlington, Texas 76019, USA
[2] Department Industrial, Manufacturing and Systems Engineering, University of Texas at Arlington, Arlington, Texas 76019, USA
vchen@uta.edu

Abstract. As cities strive for more sustainable transportation systems, many are considering renewable fuels for fleets. Biogas has several advantages as an alternative fuel. Composed primarily of methane, it can be cleaned for use in natural gas vehicles or burned in a turbine/engine to generate electricity for electric vehicles. Biogas can reduce air pollutant emissions from fleet vehicles; in addition, if wastes are used to produce the biogas in digesters, the problem of urban wastes is reduced. Many cities already have anaerobic digesters that convert sewage sludge at water resource recovery facilities (WRRFs) to biogas. Because of its abundance in landfilled waste (22%), food waste is of current critical concern to the US Environmental Protection Agency. Yard (flora) waste comprises an additional 7.8% of waste going to landfills. Both food and yard waste could be used to boost biogas production in WRRF digesters. One main question is: What WRRF locations with existing digesters are the best candidates to produce vehicle fuel from food/yard waste? In this paper, we present an optimization that balances trade-offs between food/yard waste transportation costs and capital/operating costs for expanding digesters. An example study is conducted for the City of Dallas, Texas.

Keywords: Food Recovery Hierarchy · Waste management · Anaerobic digestion · Facility location

1 Introduction

Nationwide, 22% of the waste that goes to landfills is food waste, and 7.8% is yard (flora) waste (US EPA [1]). In Dallas/Fort Worth, food waste constitutes 28% of what goes to landfills, and yard waste is 3.2% (NCTCOG [2]). According to EPA's Food Recovery Hierarchy, if food waste cannot be reduced outright or used to feed hungry people or animals, the next priority is using it to generate energy, rather than composting or sending it to the landfill (US EPA [3]). Both food and yard waste can be used to supplement biogas production in anaerobic digesters (AD). Many cities already have ADs that convert sewage sludge at water resource recovery facilities (WRRFs) to biogas. With 14,748

R. Qiu et al. (Eds.): ICSS 2021, LNOR, pp. 141–153, 2021.
https://doi.org/10.1007/978-3-030-90275-9_12

WRRFs across the US (Center for Sustainable Systems [4]), substantial potential exists for expanding the co-digestion of food and yard waste at WRRFs. Digesting the food waste generated by a single average American in one year, which is around 248 lb (US EPA [1]), could provide enough energy for an electric vehicle (EV) to travel about 41 miles or a compressed natural gas (CNG) vehicle to travel around 22 miles.[1]

Enhancing existing WRRF infrastructure to accommodate food and yard waste, to generate biogas for vehicle fuel, involves determining which WRRF with ADs are the best candidates for co-digestion. The best candidates would provide the most biogas for the least cost. Determining this is not straightforward, however, because of the large number of potential WRRFs, waste collection routes, and variables that impact the cost. The 16-county region served by the North Central Texas Council of Governments, for example, has 9 existing ADs at WRRF (NCTCOG [10]). Trade-offs must be balanced between food/yard waste transportation costs and capital costs for expanding ADs, cleaning gas/generating electricity, and installing refueling stations.

Until this F^4 project, there was not a model for determining the best use of existing AD infrastructure for food/yard waste to fuel conversion. Galli et al. [11] provided a qualitative (not quantitative) model of food waste generation and recovery for social purposes for Italy. Several studies have developed food supply network models [12, 13], but they do not apply to waste. Lee et al. [14] developed a system dynamics food waste model for Hong Kong, consisting of sub-models for food waste generation, waste treatment, landfilling, and government expenditure. A similar model, however, is not available for the US. Several general models are available to facilitate municipal solid waste management decisions in the US, including Solid Waste Optimization Lifecycle Framework (SWOLF, NCSU [15]) and Municipal Solid Waste Decision Support Tool (MSW-DST, RTI International [16]). However, these models are not specific to food/yard waste and do not address the issue of using existing AD infrastructure to convert food/yard waste to fleet fuel. EPA's Co-Digestion Economic Analysis Tool (Co-EAT, Rock and Ricketts [17]) is not specific to food/yard waste and requires 78 input values, which are not readily available.

In this paper, we focus on the F^4 Optimization that utilizes information acquired in the larger F^4 project to optimize the allocation of food/yard waste to WRRF locations. The next section describes the estimation of WRRF AD capital and operating costs, food and yard waste generation, and costs to transport waste from collection zones to WRRF locations. Section 3 presents the optimization formulation, and Sect. 4 discusses results for City of Dallas case study. Finally, concluding remarks are given in Sect. 5.

[1] Note: These calculations assume a mid-range biogas yield of 0.017 m^3/lb wet food waste [5], and biogas with mid-range methane content of 60%, with heating value of 600 Btu/ft^3 (Swedish Gas Technology Centre [6]). The EV calculation also assumes a mid-range steam turbine efficiency of 42.5% for electricity generation (range 40–45%) [7] and electricity consumption of a 2011 Nissan Leaf (3.7 mi/kWh). The CNG calculation assumes that the CNG vehicle gets about the same fuel economy as a conventional gasoline vehicle on a gasoline-gallon-equivalent basis (US DOE [8]). The fuel economy of a 2015 CNG Honda Civic (31 MPG) (Compare.com [9]) is used. Miles traveled for the EV exceeds the CNG vehicle because of the low efficiency (15–25%, Webber, 2007) of the CNG vehicle's internal combustion engine (ICE). Although the steam turbine used to generate the electricity has only a 40–45% efficiency, the efficiency of the electric motor in the EV is 60–75%, which gives an overall efficiency of around 29%, which is greater than the 15–25% range for the ICE.

2 Input Parameter Information

Alternative methods of estimating AD capital and operating costs were explored by reviewing the literature and talking to UTA construction and structures faculty members, and city personnel. Section 2.1 discuss AD capital costs, Sect. 2.2 describes AD operating costs, and Sect. 2.3 provides costs for waste pre-processing and biogas conversion costs.

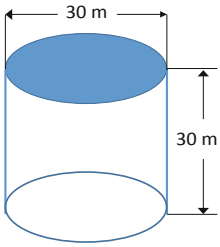

Fig. 1. 5 MG AD

2.1 AD Capital Costs

Table 1 below estimates capital costs for a 30 m diameter x 30 m tall cylindrical concrete AD (5 million gallon capacity), as shown in Fig. 1, which is a common shape and size for new ADs at wastewater treatment plants [18]. Concrete and steel rebar for the AD were estimated based on plans of existing ADs at the Village Creek Water Reclamation Facility in Fort Worth, Texas, with height adjusted to 30 m tall (the actual ADs are 30 m in diameter but only about 10 m tall). Although additional rebar was added to a height of 30 m in the wall, the rebar diameter was not increased to be able to carry excess load associated with a taller AD wall.

Table 1. Capital cost of a 30–m concrete anerobic digester [18–20]

Type of cost	Specific information	$ value
Concrete for walls and base (cub yd)	2355	$706,556
Steel rebar for walls and base (ft)	168,679	$131,642
Mixer (LM20-20-96 model, Ovivo)	20 hp motor and 96-inch Hydrodisk	$340,000
Cover (Steel Cover, floating, Westech)	For 30 m tank diameter	$400,000
Subtotal Cost 1 ($)		**$1,578,198**
Other Costs	Heating, Pumping, Electrical: 40% of Subtotal Cost 1	$631,279
Subtotal Cost 2 ($)		**$2,209,477**
Consultants Cost	6% of Subtotal Cost 2	$132,569
Contractors Cost	12.5% of Subtotal Cost 2	$276,185
Foundation cost (including contractor)		$500,000
Grand Total Cost ($)		**$3,118,230**

2.2 AD Operating Costs

Operating costs were estimated for new ADs only, not for the existing ADs, which are already treating sludge (additional operating costs for adding food and yard waste

to the existing ADs were not considered). Operating costs were estimated as the sum of mixing costs, pumping costs, and heating costs. Mixing and pumping costs were estimated assuming 20 hp and 15 hp motors, respectively; 3–4 h of operation per day [21]; waste feed rate of 15 tons/day [21]; motor efficiency of 80% [7]; and average cost of commercial power in the US for 2019 of $0.11/kWh (US EIA [22]). Heating costs were estimated based on the heat needed to raise the temperature of the waste to 95°F, a mid-range temperature for mesophilic ADs, as well as to compensate for losses. Our survey of WWRF facilities with ADs found mesophilic ADs to be most common. The waste heat capacity was assumed to be the same as that of water, since a digester operated in wet mode would contain 75–90% water content. Heat transfer coefficients for concrete walls, roof, and floor of the AD were taken from Metcalf & Eddy [23]. The efficiency of electric resistance heating was taken as100% (US DOE [8]).

2.3 Waste Pre-processing and Biogas Conversion Costs

Only one grinder for pre-processing food and yard waste and one biogas conversion system/refueling station could be added per WRRF site, assuming that there is no existing grinder or biogas conversion system/refueling station. Capital and operating costs are given in Table 2.

Table 2. Capital and operating costs for waste pre-processing and biogas conversion equipment

Equipment	Capital costs	Operating costs
Grinder for pre-processing food and yard waste	$900,000 (Mobark 6600 Grinder), with replacement every 5 years (per manufacturer)	$1/ton processed (CBI [24])
Turbine-generator set for conversion to electricity	$1015 * kW (Installed cost of gas compression/treatment, turbine/generator, site work and housing, US EPA [25]) $250,000 (installed interconnecting electrical equipment, US EPA [25])	$0.0144 * kWh (US EPA [25])
Reciprocating engine-generator set for conversion to electricity	$1300 * kW + $1,100,000 (Installed cost of gas compression/treatment, turbine/generator, site work and housing, US EPA [25]) $250,000 (installed interconnecting electrical equipment, US EPA [25])	
CNG conversion	$95,000 * ($ft^3$/min) 0.6 (cleaning, compression, and fueling station equipment, US EPA [25]) $250,000 (installed interconnecting electrical equipment, US EPA [25])	$1/(gallon gasoline equivalent) (US EPA [25]) 3.587 m^3 CNG = 1 gallon gasoline equivalent

2.4 Food and Yard Waste Generation Estimates

Table 3 shows 12 categories contributing to food waste and 4 categories contributing to yard waste. The US EPA's Excess Food Opportunities map provides institution-specific food waste values in tons/year for seven of the food waste categories: educational institutions (not universities), correctional facilities, food banks, food manufacturers/processors, food wholesale/retail, healthcare facilities, hospitality industry, restaurants & food services. For the remaining food waste categories, as well as the yard waste categories, the following basic equation was used:

Waste produced per category per block group (mass/year) = [Waste generation rate (mass/activity/year)]*[Activity level/block group].

The "Rate" column of Table 3 shows waste generation rate values obtained from literature. Each rate can then be multiplied by the city- or region-specific activity level to obtain waste estimates in tons/year, using the equations given in the "Calculation of waste per block group in tons/year" column in Table 3. Activity levels can be obtained from geographic information system (GIS) sources given in the "GIS Data Source" column. In the case of parks and commercial lawns, the GIS data sources provided are specific to the Dallas case study, so similar sources will need to be obtained for other regions.

Table 3. Waste categories, generation rate, and GIS information

Waste category		Amount of waste generated		GIS data source
Type	Specific	Rate	Calculation of waste per block group in tons/year	
Food waste	Single-family households	5 lb per household per week [26]	Rate * No. of single-family residences per block group * 52 weeks/year * 1 ton/2000 lbs	US Census Bureau - ACS 2019 https://www.census.gov/
	Multi-family households	1 lb per unit per week [26, 27]	Rate * No. of multi-family units per block group * 52 weeks/year * 1 ton/2000 lbs	US Census Bureau - ACS 2018 https://www.census.gov/
	Universities	0.39 lb per student per day [26]	Rate * No. of students per block group * 365 days/year * 1 ton/2000 lbs	US Department of Education https://nces.ed.gov/collegenavigator/?s=TX
	Educational institutions (not universities), correctional facilities, food banks, food manufacturers & processors, food wholesale/retail, healthcare facilities, hospitality industry, restaurants & food services	Institution-specific, tons per year (US EPA [28])	Already given in tons/year, waste for different facilities aggregated over the block group	US EPA Excess Food Opportunities Map https://geopub.epa.gov/ExcessFoodMap/

(*continued*)

Table 3. (*continued*)

Waste category		Amount of waste generated		GIS data source
Type	Specific	Rate	Calculation of waste per block group in tons/year	
	Special event centers and recreation facilities	150–4200 lb per employee per year (NRDC [29])	Rate * No. of employees per block group * 1 ton/2000 lbs	ArcGIS Business Analyst https://iuscappa.maps.arcgis.com/home/index.html
Yard waste	Single-family households	16 lb per household per week [26]	Rate * No. of single-family residences per block group * 52 weeks/year * 1 ton/2000 lbs	US Census Bureau - ACS 2019 https://www.census.gov/
	Golf courses	269 lb per acre per week (US EPA [30])	Rate * No. of acres per block group * 52 weeks/yr * 1 ton/2000 lbs	Google Maps, Google Earth, ArcGIS Online Maps https://www.google.com/maps?hl=en&tab=wl1
	Parks	538 lb per acre per week (US EPA [30])	Rate * No. of acres per census block group * 52 weeks/yr * 1 ton/2000 lbs	NCTCOG's Regional Data Center https://data-nctcoggis.opendata.arcgis.com/
	Commercial lawns	538 lb per acre per week (US EPA [30])	Rate * No. of acres per census block group * 52 weeks/yr * 1 ton/2000 lbs	NCTCOG's Regional Data Center, City of Dallas GIS Services https://gis.dallascityhall.com/shapefileDownload.aspx; https://data-nctcoggis.opendata.arcgis.com/

2.5 Transportation Cost Estimates

The transportation costs used by the F^4 Optimization include two components: (1) fuel cost to transport food/yard waste to WRRF locations with existing or potential ADs and (2) garbage truck personnel cost, consisting of one driver and one helper. The routing of a garbage truck through a waste collection zone follows the existing truck routes given by the local waste collection agency; therefore, this routing is not considered in the F^4 Optimization. Given the locations of the food/yard waste collection zones and the candidate WRRF locations, round-trip distances from the centroid of each waste collection zone to each WRRF location were determined using the shortest path algorithm for the transportation network in ArcGIS. The fuel cost estimate for the resulting vehicle miles traveled (VMT) was then calculated assuming a diesel garbage truck fuel economy of 1.7 miles per gallon and the unit cost of $2.92 per gallon of diesel fuel (AFLEET, Argonne National Lab [35]). Each garbage truck is assumed to transport up to 12 tons per trip, and an assumption of the F^4 Optimization is that all food/yard waste from a collection zone is transported to the same WRRF location. To estimate the corresponding personnel cost for the VMT, a vehicle speed of 30 miles per hour is assumed to convert to the number of hours of driving, and the hourly pay rates of $20/hour for the driver and $10.40/hour for the helper are used. In summary, the transportation cost from each waste collection zone to each candidate WRRF location was estimated as follows:

Number of trips = [Total tons food and yard waste for zone] / [12 tons per trip], rounded up to nearest integer.

Fuel cost = [VMT per round-trip]*[Number of trips]*[gallon diesel/1.7 miles]*[$2.92/gallon diesel].

Personnel cost = [VMT per round-trip]*[Number of trips]*[hour/30 miles]*[$20/hour + $10.40/hour].

Transportation cost = Fuel cost + Personnel cost.

3 F^4 Optimization

The F^4 Optimization was developed, with inputs and outputs shown in Fig. 2. The model determines the overall least-cost system of ADs for converting food/yard waste to fleet fuel. In particular, the F^4 Optimization is important when there are multiple candidate WRRF locations, including those with existing ADs and those where new ADs could be built. The optimization then determines the allocation of food/yard waste from each collection zone to a WRRF location, so as to minimize total cost. For existing ADs, the amount of sludge that is already being processed is needed to appropriately reduce that AD's available capacity to digest additional food/yard waste.

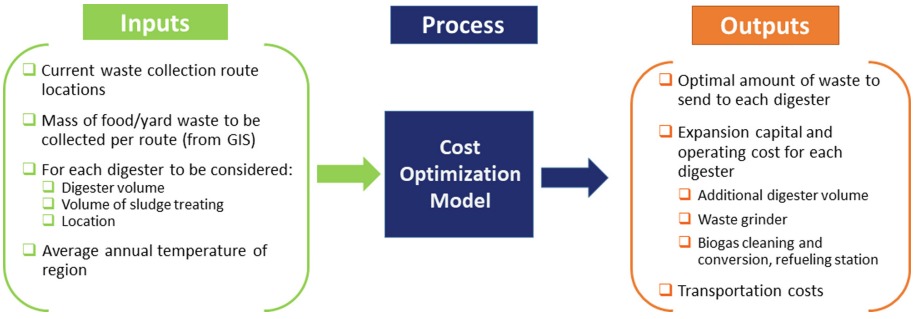

Fig. 2. F^4 Optimization inputs and outputs

The optimization balances trade-offs between food/yard waste transportation costs (Sect. 2.5) and capital and operating costs (Sects. 2.1 and 2.2) for ADs, waste grinders, biogas cleaning and conversion, and refueling stations. For example, as shown in Fig. 3, small capacity ADs in multiple locations may require lower transportation costs due to the shorter travel distances (lower VMT) between waste collection zones and nearest WRRF locations. However, higher capital costs would be necessary to add additional AD capacity and provide gas upgrading/conversion equipment and refueling stations at these multiple WRRF locations. A large AD at a central facility could minimize the capital expansion costs (cost per unit of waste digested); however, higher transportation costs are expected since all the waste must be transported to the single central facility.

Define the following notation for input parameters:

N_Z = # of waste collection zones for food/yard pick-up;

N_L = # of candidate WRRF locations with ADs;

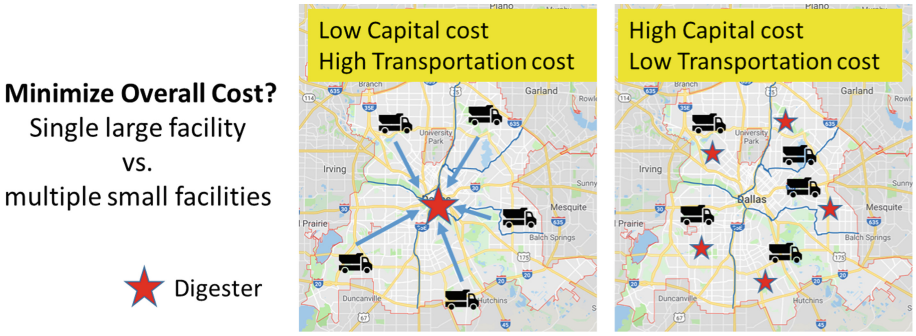

Fig. 3. Optimization balancing of transportation costs with AD facility capital costs

D_i = food/yard waste amount (demand) to be collected from collection zone $i = 1, \ldots, N_Z$;
S_l = total available AD capacity at WRRF location $l = 1, \ldots, N_L$;
C_l = AD cost (capital and operating) at WRRF location $l = 1, \ldots, N_L$;
T_{il} = transportation cost from waste collection zone i to WRRF location l.

As described in Sect. 2.5, the transportation costs did not consider the number of trucks needed to transport waste but did account for the number of garbage truck trips to transport the entire food/yard waste amount at a collection zone to the same WRRF location. Define the decision variables as:

$$x_{il} = \begin{cases} 1 \text{ if food/yard waste from collection zone } i \text{ is transported to WRRF location } l, \\ 0 \text{ otherwise;} \end{cases}$$

$$y_{il} = \begin{cases} 1 \text{ if at least one AD is used at WRRF location } l, \\ 0 \text{ otherwise.} \end{cases}$$

The optimization formulation can then be written as follows:

$$\text{Min} \sum_{i=1}^{N_Z} \sum_{l=1}^{N_L} T_{il} x_{il} + \sum_{l=1}^{N_L} C_l y_l$$

$$s.t. \sum_{l=1}^{N_Z} D_l x_{ll} \leq S_l y_l \ \forall l,$$

$$\sum_{l=1}^{N_L} x_{il} = 1 \forall i,$$

$$x_{il} \in \{0, 1\}, y_l \in \{0, 1\}.$$

The first constraint ensures that food/yard waste transported to each WRRF location l can be processed by the AD capacity available at that location. The second constraint specifies that the food/yard waste from each collection zone is assigned to exactly one WRRF location. Finally, the objective is to minimize costs (as defined in Sect. 2), where the first term comprises the transportation costs, and the second term adds the capital and operating costs due to the ADs.

4 Case Study for City of Dallas

Dallas has two WRRFs, Central and Southside. The only existing AD is located at Southside, so sludge at Central is currently pumped to Southside to be treated by the AD. The Dallas case study considered the following two scenarios:

(1) Consider the use of a new AD (5.6 MG) at Dallas Central in addition to the existing AD at Southside.
(2) Consider expanding AD capacity at Southside by adding a 5.6 MG AD.

For these scenarios, the process of developing the optimization input parameters was tested using GIS City of Dallas GIS Services [31], Google Maps [32]). The F^4 Optimization code was developed in Gurobi [33] and executed for Scenario (1) to determine the optimal decisions for transporting food/yard waste to ADs. In actuality, barriers exist to the addition of ADs at Dallas Central. The City of Dallas previously had ADs at Dallas Central, which were closed due to limited land availability and odor issues in the surrounding community. Consequently, Scenario (2) was calculated as a benchmark for comparison.

Waste collection route information was obtained from the City of Dallas, and food/yard waste were aggregated by block group and garbage route. It was assumed that 33% of Dallas food waste and 31% of yard waste is sent to an AD, while 67%, or 2/3 of food waste, is assumed to be fed to the hungry (Hoover [34]). The national average amount of yard waste currently landfilled is 31% (US EPA [1]). The F^4 Optimization executed for Scenario (1) and the optimal cost was compared to the cost for Scenario (2). The following assumptions were made in running the F^4 Optimization:

- Diesel garbage trucks are used to transport food and yard waste (not electric or CNG).
- AD operating costs are considered only for food & yard waste (not sludge).
- Biogas from AD digestion of food and yard waste only (not sludge) is used to generate electricity (for other garbage trucks).

		Scenario 1			Scenario 2
		Southside	Dallas Central	Total	Southside
Food/Yard Waste	# of routes	31	251	**282**	**282**
	Food waste (tons/year)	4,847	51,974	**56,821**	**56,039**
	Yard waste (tons/year)	125,153	1,724,064	**1,849,217**	**1,849,999**
	Total Mass (tons/year)	130,000	1,776,037	**1,906,037**	**1,906,038**
Facility Costs - Capital and Operation	Digester	$ 11,061,524	$ 155,619,571	**$166,681,095**	**$ 166,681,180**
	Grinder	$ 10,151,765	$ 61,876,173	**$72,027,938**	**$ 65,961,273**
	Biogas conversion	$ 9,778,009	$ 127,250,547	**$137,028,555**	**$ 136,528,314**
	Total (for 50 years)	$ 30,991,297	$ 344,746,291	**$375,737,589**	**$ 369,170,767**
Transportation cost	Total (for 50 years)	$ 2,651,882,303	$ 57,057,200,025	**$59,709,082,328**	**$ 101,675,109,264**
Total Cost (for 50 years)		$		**60,084,819,917**	**$ 102,044,280,031**

Fig. 4. City of Dallas feasibility study optimization results

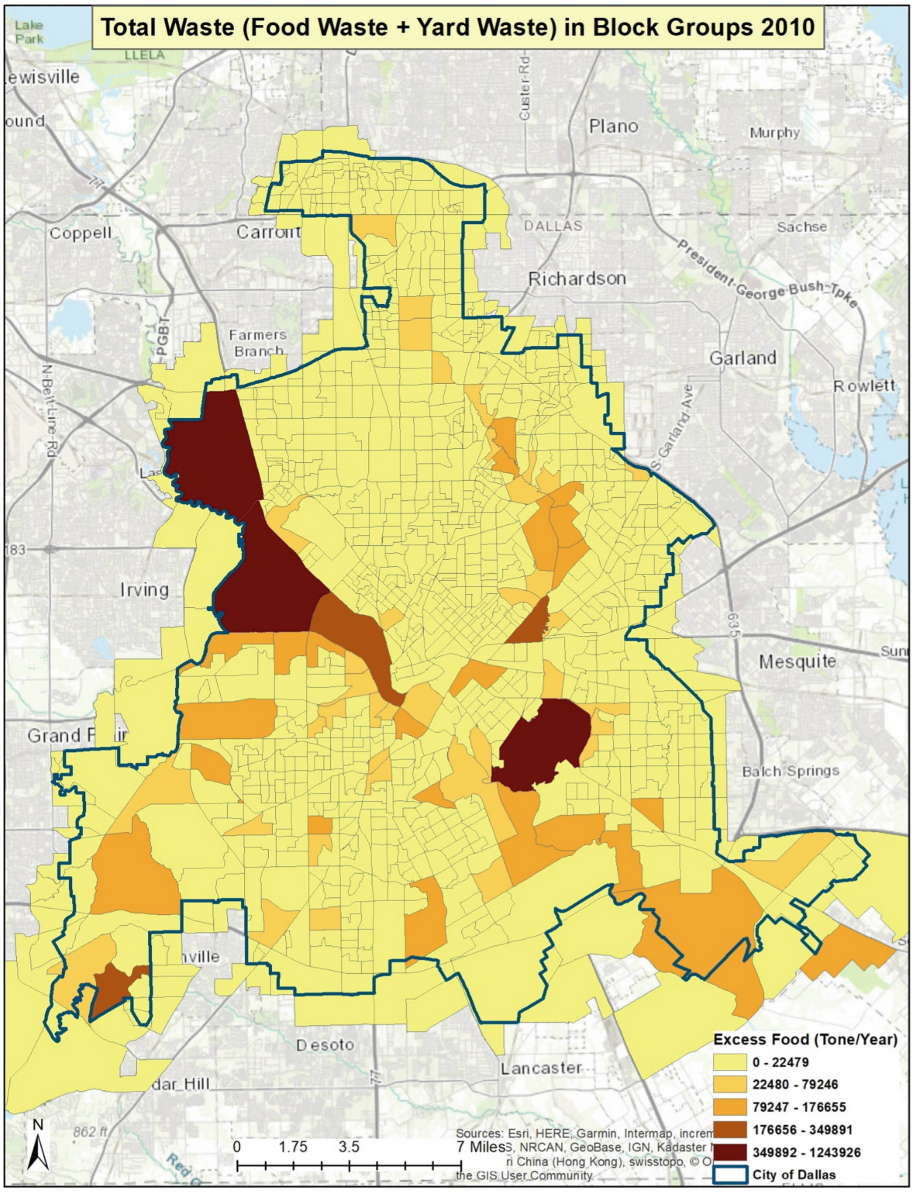

Fig. 5. Total food/yard waste for the City of Dallas aggregated by block group

Figure 4 shows the optimization results. Figure 5 shows the GIS output the food/yard waste at collection zones defined by block groups. In total, the Dallas case study has $N_Z = 285$ waste collection zones and $N_L = 2$ candidate WRRF locations. The amount of food/yard waste D_i ($i = 1, \ldots, 285$) is pulled from the GIS output. For Scenario (1), the AD capacity size S_l at each WRRF location ($l = 1, 2$) is 5.6 MG. At Southside, the

AD cost C_1 excludes AD capital and operating costs since the AD already exists and is operating, but at Central, the AD cost C_2 must include both the capital cost for the new AD and its operating cost.

The following can be observed in Fig. 4:

- For Scenario (2), the existing ADs at Southside are not large enough to accommodate the food and yard waste, so an additional AD must be added.
- Since a digester must be added for both scenarios, the AD capital and operating costs are approximately equal for both scenarios.
- Grinder costs are higher for Scenario (1) (Southside & Central), because a grinder must be provided at each location, vs. only one at Southside for Scenario (2).
- There is a small, fixed cost for biogas conversion that must be paid twice for Scenario (1), once for each AD.
- Overall WRRF costs are higher for Scenario (1) due primarily to the grinder.
- Transportation costs are higher for Scenario (2) with Southside alone.
- Overall, costs are higher for Scenario (2) with Southside alone, because the greater transportation costs for Scenario (2).

5 Conclusions and Future Work

The F^4 Optimization results for the Dallas case study demonstrate the ability to compare options to achieve the most cost-effective strategy that makes use of WRRF locations with existing ADs. While the optimization model is straightforward, significant effort was required to generate reasonable input parameters for the optimization. The results from the F^4 Optimization allow comparison between Scenario (1) involving multiple WRRF locations and Scenario (2) that is a simple AD expansion at a single WRRF location. Transportation costs are seen to have a significant impact on the optimal decision, which is an important practical finding. These results have been incorporated into the larger project to justify the benefit of sending food/yard waste to existing ADs at WRRFs and generating biogas for fleet fuel.

Future work will generalize the optimization to address other elements. The current F^4 Optimization is focused on the assignment of waste collection zones to WRRF locations with ADs. An extended optimization can additionally consider different types of AD locations, AD capacity decisions, and waste transportation decisions. In this paper, only WRRF locations were considered, but ADs can also exist at industrial and farm locations. In the current F^4 Optimization, ADs have a fixed capacity, so increasing capacity is achieved by building more ADs. However, the optimization in the future can consider new ADs to be constructed with varying capacities. Further, there are multiple types of trucks for transporting waste, including different fuel types. The amount of food/yard waste generated within a collection zone requires multiple truck trips and could be transported by different types of trucks to different AD locations. Consequently, the optimization can consider vehicle fleet size and mix in the future.

Acknowledgement. This work was supported by a grant from the Center for Transportation Equity, Decisions, and Dollars (CTEDD) funded by U.S. Department of Transportation Research

and Innovative Technology Administration (OST-R Grant Number: 69A3551747134) and housed at The University of Texas at Arlington.

References

1. https://www.epa.gov/sites/production/files/201807/documents/2015_smm_msw_factsheet_07242018_fnl_508_002.pdf
2. North Central Texas Council of Governments - NCTCOG Personal Communication (2019)
3. https://www.epa.gov/sustainable-management-food
4. http://css.umich.edu/sites/default/files/Wastewater%20Treatment_CSS04-14_e2020.pdf/
5. Deublein, D., Steinhauser, A.: Biogas from waste and renewable resources, Wiley (2008)
6. http://www.sgc.se/ckfinder/userfiles/files/BasicDataonBiogas2012.pdf/
7. Webber, M.: Introduction: energy uses, basics, and fundamentals, energy technology and policy, Center for Lifelong Engineering Education (2007)
8. https://afdc.energy.gov/fuels/natural_gas_basics.html/
9. https://www.compare.com/auto-insurance/guides/natural-gas-vehicles-guide
10. https://www.nctcog.org/nctcg/media/Environment-and-Development/Documents/Natural%20Resources/Water%20Quality/Final-2018-WQMP_1.pdf
11. Galli, F., Cavicchi, A., Brunori, G.: Food waste reduction and food poverty alleviation: a system dynamics conceptual model. Agric. Hum. Values **36**(2), 289–300 (2019). https://doi.org/10.1007/s10460-019-09919-0
12. Cheshmberah, M., et al.: A mathematical model for optimum single-commodity distribution in the network of chain stores: a case study of food industry. Manage. Sci. Lett. **1**(4), 575–582 (2011)
13. Mogale, D.G., et al.: Two Stage Indian Food Grain Supply Chain Network Transportation-Allocation Model. IFAC,**49**(12), 1767–1772 (2016)
14. Lee, C.K.M., Ng, K.K.H., Kwong, C.K., Tay, S.T.: A system dynamics model for evaluating food waste management in Hong Kong, China. J. Mater. Cycles Waste Manage. **21**(3), 433–456 (2018). https://doi.org/10.1007/s10163-018-0804-8
15. https://jwlevis.wixsite.com/swolf/about/.
16. https://mswdst.rti.org/
17. https://cfpub.epa.gov/si/si_public_record_report.cfm?Lab=NRMRL&dirEntryId=343653/
18. Ripley, L.: Senior Environmental Engineer, Freese and Nichols, Personal Communication (2020)
19. Shapoorian, B.: Academic staff, University of Texas at Arlington Department of Civil Engineering, Personal Communication (2019)
20. Hossain, S.: Professor, University of Texas at Arlington Department of Civil Engineering, Personal Communication (2020)
21. Michael Hyatt, P.E.: Eastern Bay Municipal Utility District - EB MUD (2019). Personal Communication with Associate Engineer, Resource Recovery (2019)

22. https://www.eia.gov/energyexplained/electricity/prices-and-factors-affecting-prices.php/
23. Metcalf, L., Eddy, H.P.: Wastewater Engineering: treatment and Reuse, 4th edn. revised by Tchobanoglous, G., et al., McGraw Hill (2004)
24. https://www.terex.com/cbi/en/equipment/horizontal-grinders/
25. U.S. Environmental Protection Agency - US EPA. LFGcost Web Model (Version 3.2), Landfill Methane Outreach Program by US EPA, Resources for Funding Landfill Gas Energy Projects (2017)
26. Solid Waste Association of North America (SWANA), Food Waste Diversion Programs and their Impacts on MSW Systems, SWANA Applied Research Foundation (2016)
27. Solid Waste Association of North America (SWANA), Source Separation and Collection of Food Waste from Multi-Family Dwellings, SWANA Applied Research Foundation (2006)
28. https://geopub.epa.gov/ExcessFoodMap/
29. https://www.nrdc.org/resources/wasted-how-america-losing-40-percent-its-food-farm-fork-landfill/
30. https://www.epa.gov/facts-and-figures-about-materials-waste-and-recycling/yard-trimmings-material-specific-data/
31. https://gis.dallascityhall.com/shapefileDownload.aspx/
32. https://www.google.com/maps?hl=en&tab=wl1
33. https://www.gurobi.com/
34. https://www.nrdc.org/sites/default/files/food-waste-city-level-report.pdf/
35. https://afleet-web.es.anl.gov/afleet/

A Comparative Study of Machine Learning Models in Predicting Energy Consumption

Ana Isabel Perez Cano and Hongrui Liu(✉)

Department of Industrial and System Engineering, San Jose State University, San Jose, CA 95192, USA
hongrui.liu@sjsu.edu

Abstract. Climate change and the integration of renewable energy resources into the electricity grid in recent years are making electricity consumption very vulnerable. Traditional time series forecasting methodologies make predictions based on historical trends and patterns and are inadequate to address the changing environmental parameters in real-time. Machine learning methods, on the other hand, are more flexible in taking into consideration of parameters such as temperature, wind power, and market price, which are likely to fluctuate in real-time and influence electricity consumption. In this research, we propose to develop an accurate prediction model for hourly electricity consumption using machine learning. We will use California consumption data from US Energy Information Administration and hourly local climatological data (LCD) from National Oceanic and Atmospheric Administration for the study. Six machine learning models that include Linear Regression, K-Nearest Neighbors (KNN) Regression, Gradient Boosting, Random Forest Regression, Long Short-Term Memory (LSTM) – a Recurrent Neural Network, and Support Vector Machine (SVM) will be used, and their prediction accuracy will be compared and analyzed.

Keywords: Energy consumption · Forecasting · Data analytics · Machine learning

1 Introduction

Accurate electricity consumption prediction plays a significant role in energy planning and market operation. The energy suppliers and independent system operators are making strategic decisions in dispatch schedules and pricing based on the prediction results to reduce cost. The integration of renewable energy resources to the electricity grid in recent years and climate change are making prediction more difficult. With the help of artificial intelligence, the prediction can be improved by utilizing multiple climate and market parameters to achieve a higher degree of accuracy.

Our work aims to study and compare different machine learning models in predicting energy consumption for a selected region in California. We will train six modern machine learning models: Linear Regression, k-NN Regression, Gradient Boosting, Random Forest, LSTM and a Support vector machine algorithm to predict the energy consumption and compare their prediction accuracy.

R. Qiu et al. (Eds.): ICSS 2021, LNOR, pp. 154–161, 2021.
https://doi.org/10.1007/978-3-030-90275-9_13

1.1 Related Work

The prediction of demand in the electricity sector is one of the areas where many models and techniques have been utilized. These methods can be categorized into three different groups [1–8]. The first group is based on statistical methods such as regression, time series and econometric. The predication is made either from historical time series data (univariate models) or from exogenous variables such as time or socioeconomic factors [9, 10]. The second group includes models that are based on artificial intelligence. This group has more development in the recent years, where the results are compared with traditional methods. For example, a SVR model is applied in forecasting load with seasonal/cyclic pattern in [11]. A comparison study of six univariate methods for short-term electricity demand forecasting is presented in [12]. The third group consists of empirical models that rely on human judgment and intuition. For example, a hybrid empirical mode decomposition and state space model is developed in [13], where the empirical mode decomposition is applied to decompose the total time series (noise filtering), and the state space model is employed to forecast every sub-series (feature extraction), with the state space model parameters being optimized using maximum likelihood via a Kalman filter. A summary of some representative research on load forecast using machine learning is shown in Table 1.

Table 1. Representative studies about demand forecasting

Paper	Serie	Country	Model	Data
[14] Vellasco, Pacheco, Ribeiro and de Souza (2004)	Hourly (1996–1998)	Brasil	Neuro-fuzzy BSP model (Hierarchical Neuro-Fuzzy BSP (Binary Space Partitioning))	Temperature, comfort index and the profile of consumption
[15] Egelioglu, Mohamad and Guven (2001)	Yearly (1988–1997)	Cypress	Multiple Regression	Electricity price, and number of consumers and tourists
[16] Azadeh, Ghaderiy Sohrabkhani (2007)	Monthly	Iran	ANN integration (MLP - multilayer perceptron), time series and ANOVA	20 years of history
[17] Bianco, Manca and Nardini (2009)	Yearly (1970–2007)	Italy	Lineal Regression	GDP, population
[18] Ghiassi, Zimbray Saidane (2006)	Monthly (1982–1997)	Taiwan	Dynamic Artificial Neural Networks (DAN2)	Weather. It is predicted monthly, quarterly and yearly
[19] Senjyu, Mandal, Uezatoy Funabashi (2004)	Hourly	Japan	Recurrent neural network structure	Temperature

2 Data Resource

Two data sets were selected for the study. The first one is the electricity demand that can be obtained from The U.S. Energy Information Administration. The second one is the hourly local climatological data (LCD) downloaded from The National Oceanic and Atmospheric Administration. The data from Imperial Irrigation District (IID), which is an irrigation district that serves the Imperial Valley in Southern California was selected for the study to limit the project scope. It contains more than 38k electricity demand data records from 07/01/2015 to 10/11/2019. The electricity demand (in Megawatt hours) is given hourly in UTC time selected area IID. The electricity demand distribution in IID is shown in Fig. 1. The Balancing Authority Areas in California and Local Climatological Data Station location are shown in Fig. 2.

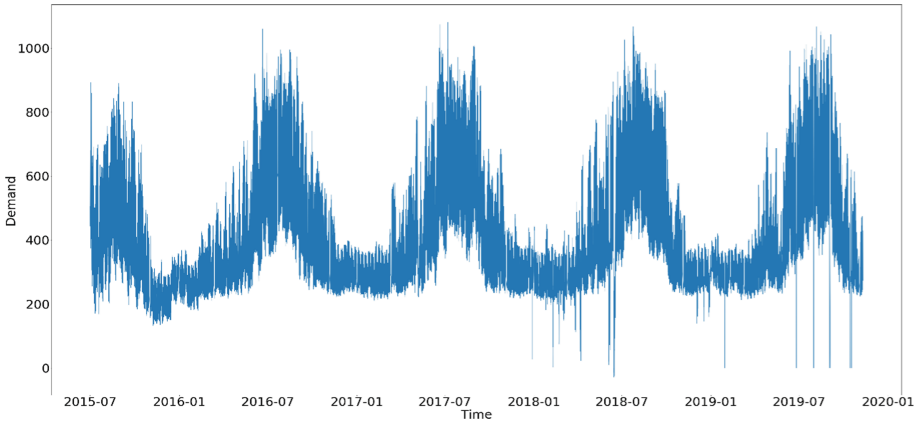

Fig. 1. Hourly electricity demand for Imperial Irrigation District (IID) between 07/01/2015 to 10/11/2019.

The documentation developed for the dataset related to the LCD provides a synopsis of climatic values for a single weather station over a specific month. The documentation summaries are a product of surface observations from both manual and automated (AWOS, ASOS) stations with source data taken from the National Centers for Environmental Information's Integrated Surface Data (ISD) dataset. The climatic values given in the LCD include hourly, daily, and monthly measurements of temperature, dew point, humidity, winds, sky condition, weather type, atmospheric pressure and more.

2.1 Data Preparation

The data in LCD is processed to remove redundancy and then transformed to be appropriate for the machine learning algorithms. For example, the data that has daily values are converted into hourly values. The columns with too many missing data are removed as they don't provide much value to the prediction result. The date time values are rounded up to the closest hour and duplicates are dropped to remove redundancies. Some columns

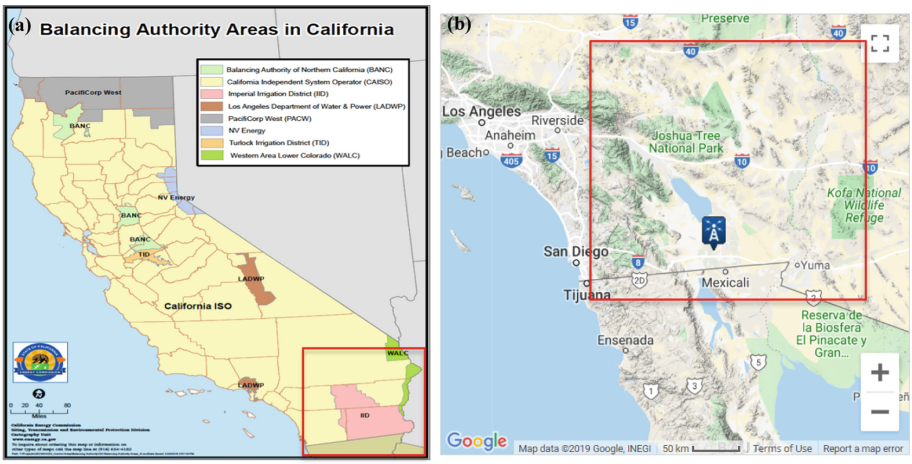

Fig. 2. **(a)** Balancing authority areas in California; **(b)** Local Climatological Data station location.

in the data set are categorical values, for example, "sky condition", that are not readily recognized by the machine learning algorithms and they are transformed into other codes. This is done by creating different columns for each sky type with a number "1" assigned in the column corresponding to the categorical value. We encode the time of the day by creating a new column with daytime value "0" (from 6am to 6 pm) and night-time value "1". Two new columns, namely, Hourly Cooling Degrees and Hourly Heating Degrees are created to represent the amount of heating/cooling necessary for different temperature ranges (number of degrees below/above 65 degrees Fahrenheit). These two new columns are more relevant information to energy consumption.

For the electricity demand dataset, the main preparation is to drop all possible NaN values and duplicated values, and align the hourly period with the one given in the LCD dataset. The two data sets are then merged for further processing.

2.2 Data Pre-processing

The pre-processing that we conduct is mainly a multiple ordinary least squares (OLS) regression (see Fig. 3), and the Pearson's Correlation Coefficients (see Fig. 4). We perform the OLS regression to check which features are important for predicting electricity demand and which ones are insignificant. The features with high p-value are removed from the dataset. The Pearson's coefficient shows us the relationship between the features and the energy demand. The features with low or similar correlations are dropped since they will not affect much to our prediction. After these steps, the last part is to create the train and test sets with a proportion of 70% and 30% respectively.

	coef	std err	t	P>|t|	[0.025	0.975]
const	2018.9806	162.119	12.454	0.000	1701.223	2336.738
DailyCoolingDegreeDays	1.9824	0.096	20.583	0.000	1.794	2.171
DailyHeatingDegreeDays	7.7641	0.177	43.780	0.000	7.416	8.112
HourlyAltimeterSetting	-34.4952	38.116	-0.905	0.365	-109.203	40.212
HourlyDewPointTemperature	1.1787	0.145	8.117	0.000	0.894	1.463
HourlyDryBulbTemperature	11.6450	0.136	85.773	0.000	11.379	11.911
HourlyPrecipitation	406.9173	112.243	3.625	0.000	186.918	626.917
HourlyRelativeHumidity	0.2165	0.079	2.741	0.006	0.062	0.371
HourlySeaLevelPressure	200.9969	18.733	10.729	0.000	164.279	237.715
HourlyStationPressure	-207.8445	31.468	-6.605	0.000	-269.523	-146.166
HourlyVisibility	-0.7146	0.706	-1.012	0.312	-2.099	0.669
HourlyWetBulbTemperature	-22.6038	0.763	-29.634	0.000	-24.099	-21.109
HourlyWindSpeed	0.9805	0.095	10.360	0.000	0.795	1.166
HourlyCoolingDegrees	23.7267	0.712	33.347	0.000	22.332	25.121
HourlyHeatingDegrees	-13.4864	0.649	-20.772	0.000	-14.759	-12.214
HourlySkyConditions_BKN	85.2605	6.226	13.693	0.000	73.057	97.464
HourlySkyConditions_CLR	21.0008	5.289	3.970	0.000	10.634	31.368
HourlySkyConditions_FEW	61.8896	6.024	10.274	0.000	50.083	73.697
HourlySkyConditions_OVC	63.9696	6.196	10.324	0.000	51.824	76.115
HourlySkyConditions_SCT	65.5595	6.713	9.766	0.000	52.402	78.717
HourlySkyConditions_VV	69.5109	19.659	3.536	0.000	30.978	108.044
TimeofDay	46.9723	1.220	38.505	0.000	44.581	49.363

Omnibus:	6354.504	Durbin-Watson:	0.177
Prob(Omnibus):	0.000	Jarque-Bera (JB):	114764.933
Skew:	-0.259	Prob(JB):	0.00
Kurtosis:	11.552	Cond. No.	4.20e+04

Fig. 3. OSL regression results

Demand correlations (Pearson)	
HourlyDryBulbTemperature	0.802241
DailyCoolingDegreeDays	0.724417
HourlyWetBulbTemperature	0.697698
HourlyCoolingDegrees	0.566626
HourlyDewPointTemperature	0.414165
HourlyWindSpeed	0.138901
HourlySkyConditions_FEW	0.131749
HourlySkyConditions_BKN	0.117281
HourlySkyConditions_SCT	0.069457
HourlySkyConditions_OVC	-0.005508
HourlyPrecipitation	-0.006292
HourlySkyConditions_VV	-0.017802
HourlySkyConditions_CLR	-0.146022
TimeofDay	-0.147483
DailyHeatingDegreeDays	-0.352719
HourlyRelativeHumidity	-0.408133
HourlySeaLevelPressure	-0.542874
HourlyStationPressure	-0.548463
HourlyHeatingDegrees	-0.636728

Fig. 4. Pearson's Correlation Coefficients.

3 Machine Learning Models

We used six machine learning algorithms for the comparison study as described below.

- Linear Regression (LR): LR performs the task to predict a dependent variable value (y) based on a given independent variable (x). So, this regression technique finds out a linear relationship between x (input) and y(output) using Ordinary least squares Linear Regression. The Ordinary Least Squares procedure seeks to minimize the sum of the squared residuals. This means that given a regression line through the data we calculate the distance from each data point to the regression line, square it, and sum all the squared errors together.
- KNN Regression: The principle behind nearest neighbor methods is to find a predefined number of training samples closest in distance to the new point and predict the label from these. The number of samples can be a user-defined constant (k-nearest neighbor learning) or vary based on the local density of points (radius-based neighbor learning). The distance can, in general, be any metric measure: standard Euclidean distance is the most common choice. Neighbors-based regression is used in cases where the data labels are continuous rather than discrete variables.
- Gradient Boosting: Gradient Tree Boosting or Gradient Boosted Regression Trees (GBRT) is a generalization of boosting to arbitrary differentiable loss functions. GBRT tries to create a strong learner from an ensemble of weak learners. The default loss function for regression is least squares.
- Random Forest: A random forest is a meta estimator that fits a number of classifying decision trees on various sub-samples of the dataset and uses averaging (mean prediction) of the individual trees to improve the predictive accuracy and control over-fitting. The sub-sample size is set to be always the same as the original input sample size.
- Long Short Time Memory (LSTM): LSTM algorithm is a type of Recurrent Neural Network (RNN) that allows the network to retain long-term dependencies at a given time from many timesteps before. RNNs were designed to that effect using a simple feedback approach for neurons where the output sequence of data serves as one of the inputs. However, long term dependencies can make the network untrainable due to the vanishing gradient problem. LSTM is designed precisely to solve that problem.
- Support Vector Machine (SVM): SVM performs classification by finding the hyperplane that maximizes the margin between classes. SVR is class of SVM capable of working with continuous values. In SVR, we try to fit the error within a certain threshold (epsilon).

4 Results and Conclusions

The training data set was used to train the six machine learning algorithms to obtain predictive models for electricity demand. The accuracy of the six predictive models was tested using the test data set. The results are summarized in Table 2. The R^2 values refer to the percentage of the response variable variation that can be explained by the model. The Root Mean Square Error (RMSE) indicates the absolute fit of the model to the data (how close the observed data points are to the model's predicted values). The LSTM

gives the best results with the highest $R^2 = 0.9848$ and lowest RMSE = 24.08 as shown in Table 2. The LSTM is capable of learning from its own errors through the training of a large data set (more 38k data records) in the case, and continuously adjusting the weights of the features, and thus provided the most preeminent result. The loss that is measured in mean-absolute error versus epoch for the LSTM is shown in Fig. 5. The loss from the testing data set stays higher than the training data set, which indicate the model is not overfitted.

Table 2. Model accuracy results

Model	R^2 Test	R^2 Train	RMSE
LSTM	0.9848	–	24.08
Random Forest	0.8319	0.9712	74.17
KNN Regression	0.8290	0.8931	74.80
SVM – SVR	0.8284	0.8353	74.93
Gradient Boosting	0.8250	0.8358	75.67
Linear Regression	0.7285	0.7290	94.26

It is observed that the LSTM takes much longer computation time in training a predicative model compared to the other methods. This could be not practical for even larger data size. The reason is that LSTM learns from its own errors through thousands of iterations. A thorough feature analysis to reduce insignificant features before training a LSTM model is thus worthy of investigation to improve computation efficiency. In addition, hyperparameters used in the machine algorithms, such as weight initialization, learning rate, activation function, and etc., may have significant impact to the result accuracy and execution time. We plan to explor these issues in our future studies.

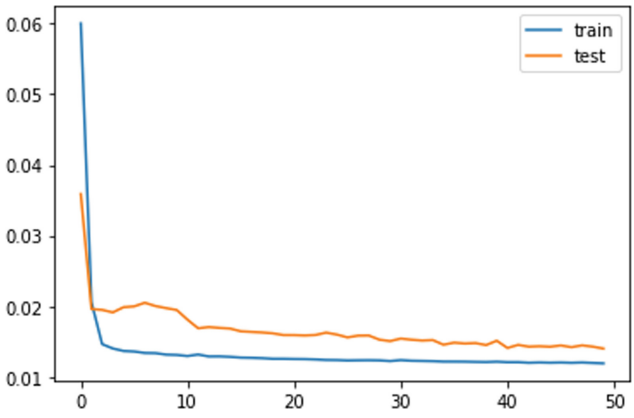

Fig. 5. Loss measured in mean-absolute error versus epoch for both training and testing of LSTM model.

References

1. Gramillano, R.: Predicting Electricity Demand in LA - Outperforming the Government (2019). https://towardsdatascience.com/predicting-electricity-demand-in-la-outperforming-the-government-a0921463fde8
2. Rueda, V.M., Velásquez Henao, J.D., Franco Cardona, C.J.: Recent advances in load forecasting using nonlinear models. Dyna (Medellin, Colombia) **78**(167), 36–43 (2011)
3. California Energy Commission. https://www.energy.ca.gov/
4. Climate Data Online: National Centers for Environmental Information, National Oceanic and Atmospheric Administration. https://www.ncdc.noaa.gov/
5. EIA Data Sets, U.S. Electric System Operating Data. U.S. Energy Information Administration. [Online]. Available: https://www.eia.gov/
6. Scikit-learn. https://scikit-learn.org/stable/index.html
7. Brownlee, J.: Linear regression for machine learning. https://machinelearningmastery.com/linear-regression-for-machine-learning/
8. Usha, T.M., Appavu Alias Balamurugan, S.: Seasonal based electricity demand forecasting using time series analysis. Circuits Syst. **7**, 3320–3328 (2016). https://doi.org/10.4236/cs.2016.710283
9. Abdel-Aal, R.E., Al-Garni, A.Z.: Forecasting monthly electric energy consumption in eastern Saudi Arabia using univariate time-series analysis. Energy **22**, 1059–1069 (1997)
10. Saab, S., Badr, E., Nasr, G.: Univariate modeling and forecasting of energy consumption: the case of electricity in Lebanon. Energy **26**, 1–14 (2001)
11. Hong, W.C., Dong, Y., Lai, C.Y., Chen, L.Y., Wei, S.Y.: SVR with hybrid chaotic immune algorithm for seasonal load demand forecasting. Energies **4**, 960–977 (2011)
12. Taylor, J., De Menezes, L., Mcsharry, P.: A comparison of univariate methods for forecasting electricity demands up to a day ahead. Int. J. Forecast. **22**(1), 1–16 (2006)
13. Hu, Z., Ma., J., Yand, L., Yao, L., Pang, M.: Monthly electricity demand forecasting using empirical mode decomposition-based state space model. Energy Environ. **30**(7), 1236–1254 (2019. https://doi.org/10.1177/0958305X19842061
14. Vellasco, M., Pacheco, M., Ribeiro, L., De Souza, F.: Electric Load forecasting: evaluating the Novel Hierarchical Neuro Fuzzy BSP Model. Int. J. Electr. Power Energy Syst. **26**(2), 131–142 (2004)
15. Egelioglu, F., Mohamad, A., Guven, H.: Economic Variables and Electricity Consumption in Northern Cyprus. Energy **26**(4), 355–362 (2001)
16. Azadeh, A., Ghaderi, S.F., Sohrabkhani, S.: Forecasting electrical consumption by integration of Neural Network, Time Series and ANOVA. Appl. Math. Comput. **186**(2), 15 1753–1761 (2007)
17. Bianco, V., Manca, O., Nardini, S.: Electricity consumption forecasting in italy using linear regression models. Energy **34**(9), 1413–1421 (2009)
18. Ghiassi, M., Zimbra, D.Y., Saidane, H.: Medium term system load forecasting with a dynamic artificial neural network model. Electr. Power Syst. Res. **76**(5), 302–316 (2006)
19. Senjyu, T., Mandal, P., Uezato, K.Y., Funabashi, T.: Next day load curve forecasting using recurrent neural network structure. IEE ProceGeneration, Transmission and Distribution **151**(3), 388–394 (2004)

Simulation Analysis on the Effect of Market-Oriented Rental Housing Construction Policy in Nanjing

Qi Qin, Mingbao Zhang, and Yang Shen(✉)

College of Economics and Management, Nanjing University of Aeronautics and Astronautics, Nanjing 210006, Jiangsu, China
Shen.y@nuaa.edu.cn

Abstract. In order to simulate the effect of market-oriented rental housing construction policy in Nanjing, in this article we use the multi-agent simulation modeling method to build a simulation model. The implementation effect of different policy measures is simulated by setting different parameters in the simulation model. Based on the parameters and variables formed from the questionnaire survey data in Nanjing, we run the simulation model 5 times on the Anylogic software. We conclude by formulating policy recommendations for the implementation and adjustment of the policy. The results show that the subjective factors of consumers and housing supply are crucial in the process of market-oriented rental housing construction policy. Not only the supply side and the demand side of the rental housing market should be comprehensively considered, but a variety of policies should be combined and implemented at the same time to achieve significant results.

Keywords: Market-oriented rental housing construction policy · Multi-agent simulation · Anylogic

1 Introduction

In China, the real estate market has developed rapidly in recent years. As urbanization continues to advance and the floating population continues to increase, low - and middle-income consumers are increasingly experiencing "housing difficulties", and the housing problem of residents needs to be solved urgently. In order to improve residents' living conditions, the concept of "rent and purchase simultaneously" was proposed in the report to the 19th CPC National Congress in 2017. The housing rental market in China plays an important role in the implementation of the policy of "rent and purchase simultaneously". As one of the pilot cities of rental housing construction in China, it is necessary for Nanjing to promote market-oriented rental housing construction policy.

Market-oriented rental housing refers to two major types of newly built or rebuilt houses that adopt market-oriented operation models, are invested by park platforms or enterprises and institutions, and are used for rental housing [1]. Newly-built housing refers to newly leased housing built on newly transferred business land, low-efficiency

R. Qiu et al. (Eds.): ICSS 2021, LNOR, pp. 162–172, 2021.
https://doi.org/10.1007/978-3-030-90275-9_14

land, owned land by enterprises and institutions, and collective construction land. Renovated houses refer to leased houses that have been renovated in accordance with regulations on qualified stock houses.

For the research on the market-oriented rental housing, scholars have relevant opinions. Rong Yan [2] proposed that rental housing market has a problem: it is difficult to balance the three elements of cost, safety and availability. Wenbo Cui [3] believes that the standardization problem in housing rental market is an important reason for the relatively low proportion of leasing. And it is also an important issue that needs to be solved in the market-oriented of rental housing. Ting Shao [4] put forward the problems and solutions in the domestic housing leasing market from the supply side, demand side, market and legislation. Yonghui Li et al. [5] explored the practical model of affordable housing from multiple perspectives such as land supply, financing, and security. Yan Wang et al. [6] analyzed the game behaviors among different types of consumers in China's real estate market and believed that the development costs of real estate developers should be reduced to further reduce the housing price. At the same time, we should pay attention to the game behavior among consumers and restrict the consumption behavior of investment consumers. Lin Wang et al. [7] put forward suggestions on the academic research direction of rental housing in the future by studying domestic literatures related to the development of rental housing.After analyzing the current situation of China's real estate market, Gongde Dong [8] proposed that it is necessary to encourage multiple social subjects to join the real estate market. Especially for the rental housing market, the provision of long-term rental housing is more important.

For the study of multi-agent simulation methods, domestic scholars Lin Huo et al. [9] built an interest rate policy simulation model based on a neural network multi-agent simulation system to analyze the applicable scenarios of interest rate policies. Jiahan Chen et al. [10] proposed the impact of the merger policy on housing prices and consumer decision-making, and finally summarize the relevant policy recommendations.

Based on the above review, this paper adopts the method of multi-agent modeling to simulate and deduct relevant policies of market-oriented rental housing construction in Nanjing, and studies the interactive relationship between various subjects in the real estate rental market and establishes a simulation model. The model is used to simulate the decision-making behavior of consumers affected by real estate policy. This paper analyzes the impact of market rental housing construction policies in Nanjing on consumers' rental decisions, and provides suggestions for the implementation and adjustment of the policy. At the same time, it provides a feasible method for the study of policy effect.

2 Policy Mechanism

In the real estate market, consumers as the provider of demand, and the government as the provider and implementer of policies play an important role in the policy simulation model. This article selects consumers and the government as the two main bodies, and analyzes the process of how consumers make decisions when the government releases relevant policies as shown in Fig. 1.

Set the following policy effect evaluation indicators: the absolute value of supply and demand in the real estate rental market; the balance between rental supply and demand;

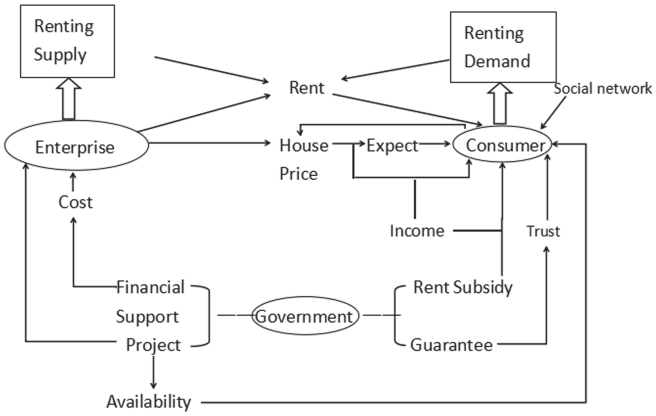

Fig. 1. Process of policy measures

the absolute value of the number of renters among consumers; the ratio of the number of buyers to the number of renters.

3 Model Building

3.1 Basic Assumptions

1) Consumers are all non-property holders. When entering the model, they need to rent a house to solve the housing problem.
2) Consumers' decision to rent a house to purchase a house is generally an irreversible process. In order to characterize the growth of the consumer population, after buyers of houses exit the model, the same number of new consumers enter the model.
3) The operation of the model follows the assumptions of economics.

3.2 Consumer Agent Building

3.2.1 House-Buying Capacity Constraints

For consumers, the first thing they face is the budget constraint when they face the decision of buying and renting a house.

$$S_f = F_j \times 30\% \times (1 + r) \tag{1}$$

Among them, S_f is the real estate down payment that consumers need to pay; F_j is the full price of the real estate, which can be set according to the actual situation; r is the transaction tax rate to be paid when buying the real estate, initially set at 3%.

Consumers will retain a portion of their monthly net income as the accumulation of funds for the down payment for the purchase of a house. In this model, a system dynamics method is adopted to describe the accumulation of funds of consumers. Regarding the part of the consumer's monthly income used to accumulate the purchase funds as a flow,

their property is accumulated as a stock. After a period of accumulation, the property accumulation of some consumers can reach the critical value of the down payment.

$$Z_c = In_c \times w \times t \tag{2}$$

Among them, Z_c is the consumer's property accumulation; In_c is the consumer's monthly net income; w is the consumer's income stability; t is the time in months.

Two indicators are used to determine whether consumers can afford down payment for real estate. First one is the value of the consumer's ability to purchase a house.

$$N_1 = Z_c \times J - S_f \tag{3}$$

Among them, N_l is the value of the consumer's ability to purchase a house; J_t is the subsidy provided by the consumer's family to pay for the down payment for the purchase of a house.

According to bank lending conditions, the consumer's monthly turnover needs to be more than twice the monthly payment.

$$In_c \geq 2Y_g \tag{4}$$

Among them, Y_g is the monthly payment required by consumers. This calculation is based on the equal principal and interest method, and assumes that the repayment period is 30 years.

$$Y_g = \left(F_j - S_f\right) \times i \times \frac{(1+i)^{360}}{(1+i)^{360} - 1} \tag{5}$$

Among them i is the loan interest rate.

In summary, the conditions for determining whether consumers can afford the down payment for housing are as follows:

$$\begin{cases} N_l \geq 0 \text{ and } In_c \geq 2Y_g & \text{BUY A HOUSE} \\ \text{other times} & \text{CAN'T BUY A HOUSE} \end{cases}$$

3.2.2 House-Buying Willingness Constraints

By referring to domestic and foreign scholars on the factors influencing house purchase decision, construct the expression of house purchase intention value.

$$G_f = k_1\left(H_d - Y_g'\right) + k_2[l_1 \frac{X_l + F_l + S_h}{3} + l_2 S_z] \tag{6}$$

Among them, G_f is the consumer's willingness to buy a house; k_1, k_2 is the influence coefficient; H_d is the maximum loan repayment limit acceptable to the consumer; $Y_g^{'}$ is the proportion of the monthly payment in the consumer's monthly net income; l_1, l_2 is the consumer's own psychological influence coefficient; X_l is the consumer's psychological affiliation needs; is the consumer's social welfare needs; S_h is the consumer's influence on the housing situation of other consumers in their social network; S_z is consumers' expectation of whether house prices will rise in the future.

3.2.3 House-Renting Willingness Constraints

According to the domestic scholars' theory of the "trilemma" problem of the rental market, the expression of the willingness to rent a house is constructed.

$$Z_f = \frac{Z_j + X_r + K_d}{3} \tag{7}$$

Among them, Z_f is the consumer's willingness to rent; Z_j is the influence of house rent on the consumer's rental decision; X_r is the degree of consumer trust in renting; K_d is the degree of availability of rental housing.

In summary, the conditions for consumers to make decisions about buying and renting houses are as follows:

$$\begin{cases} Z_f \geq G_f \text{ BUY A HOUSE} \\ Z_f \geq G_f \text{ RENT A HOUSE} \end{cases}$$

3.3 Government Agent Building

Government entities influence the behavior of different entities by implementing control measures in the real estate market. In this model, the specific measures of government departments are based on the construction measures of market-oriented rental housing in Nanjing mentioned above.

4 Simulation Analysis

4.1 Simulation Experiment Design

The experiment assumes that initially there are 3000 consumers who need to solve the housing problem, and their incomes are not equal. When consumers enter the model, they must first choose renting a house as the way to solve the housing problem. After the accumulation of time and personal wealth, the value of some consumers' ability to buy a house can increase to positive, and the income level can obtain bank loans to change the way of living, while the rest of consumers cannot change the way of living. The decision-making process of consumers to buy or rent a house will be affected by government policy regulation. In this experiment, the implementation of each policy of the government department will have an impact on different parameters or variables. The simulation experiment separately counts the purchasers and renters among consumers, as well as the total supply and demand in the market, and forms charts.

4.2 Data Processing and Parameter Acquisition

This paper uses questionnaires to obtain the variables and parameters of consumers. Among them, 550 questionnaires were distributed in Nanjing, 532 were recovered, 15 invalid questionnaires were removed, and 517 valid questionnaires were finally obtained. Through the processing of the questionnaire data, the values of the variables and parameters related to the consumer subject are obtained as shown in Table 1.

Table 1. Distribution of parameters

Symbol	Distribution	Symbol	Distribution
F_j	The initial value is 2 million yuan	l_1	U ~ (0,1)
r	The initial value is 3%	l_2	U ~ (0,1)
In_c	N ~ (0.5,0.25)	X_l	Triangular Distribution(0.2,1,0.4)
w	Triangular Distribution(0.2,1,0.4)	F_l	Triangular Distribution(0.2,1,0.4)
J_t	Triangular Distribution(10,100,40)	S_h	Triangular Distribution(0.2,1,0.6)
K_1	U ~ (0,1)	S_z	Triangular Distribution(0.2,1,0.4)
K_2	U ~ (0,1)	Z_j	Triangular Distribution(0.2,1,0.4)
H_d	Triangular Distribution(0.2,0.8,0.4)	X_r	Triangular Distribution(0.2,1,0.4)
i	The initial value is 0.68%	K_d	Triangular Distribution(0.2,1,0.4)

Through questionnaire data, Nanjing real estate data in the past five years, and Nanjing Housing Security and Real Estate Bureau documents, the values of the parameters of government entities are obtained. Table 2 shows the settings of the main policy tools of government departments in the model.

Table 2. Policy measures

Symbol	Meaning	Influence	Measure
x_j	Provide new renting housing construction projects	Increase the supply of rental housing and increase the availability	Increase housing supply by 500. The K_d parameter is increased by 0.21
g_j	Provide rebuilding renting housing construction projects	Increase the supply of rental housing and increase the availability	Increase housing supply by 300. The K_d parameter is increased by 0.16
z_j	Provide financial support for undertaking enterprises	Reduce costs and rents. Increase the impact of renting	The Z_j parameter is increased by 0.15
b_z	Provide protection for the renting process	Increase consumer trust	The X_r parameter is increased by 0.23
b_t	Provide renting subsidy	Increase consumer trust	The X_r parameter is increased by 0.13

4.3 Simulation Experiment Analysis

4.3.1 No Policy Measures

First, observe the operation of the real estate leasing market without the influence of government policies as shown in Fig. 2. The initial supply of the leasing market was

800. When the time runs to about 16 months, the number of buyers and renters in the real estate market is the same. When the time runs to about 40 months, the rental market can reach a balance between supply and demand, and the number of renters accounts for about 0.20. It is more in line with the reality.

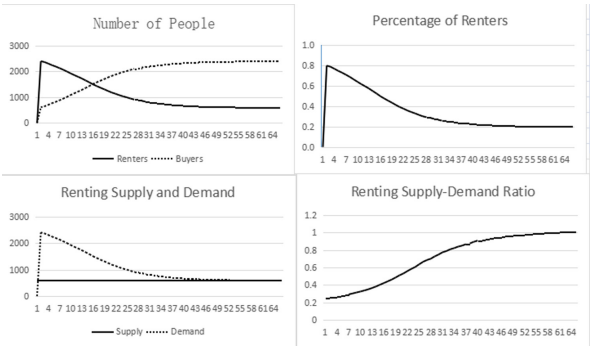

Fig. 2. No policy measures

4.3.2 Policy Measures

1) The government provides policies for new renting housing projects.

Adjust the parameters to the initial state, implement x_j, z_j, b_z and operation of the real estate leasing market is shown in Fig. 3. It can be seen that when new leased housing projects are implemented and financial support is provided to undertaking enterprises and institutions, the total supply in the lease market will increase. Due to the increase in supply and the decrease in the cost of enterprises, the level of rents will fall appropriately, and the decline in the number of renters will slow down. When the time runs to about 22 months, the number of buyers and renters in the rental market is flat. When the time runs to about 35 months, the rental market has reached the level of supply and demand. When the time runs to about 40 months, the rental market has stabilized, and the proportion of renters is about 0.39.

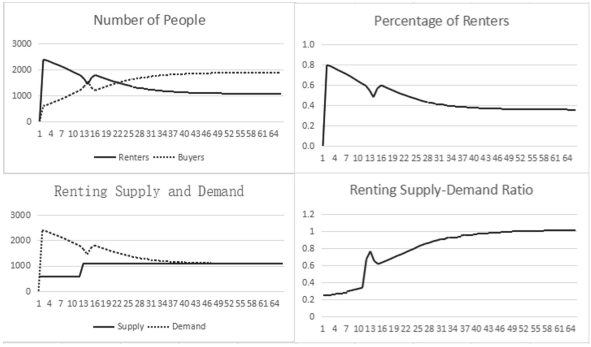

Fig. 3. New renting housing projects

2) The government provides policies for rebuilding renting housing projects.

Adjust the parameters to the initial state, implement g_j, z_j, b_z and operation of the real estate leasing market is shown in Fig. 4. It can be seen that the total supply in the leasing market will increase when the project is implemented to rebuild rental housing and provide financial support to the undertaking enterprises and institutions. Due to the increase in supply and the decrease in the cost of enterprises, the level of rent will drop appropriately, and the number of renters will rise. Due to insufficient supply, the number of renters is gradually decreasing. When the time runs to about 20 months, the number of buyers and renters in the rental market is flat. When the time runs to about 40 months, the rental market reaches the level of supply and demand. When the time runs to about 50 months, the rental market has stabilized, and the proportion of renters is about 0.37.

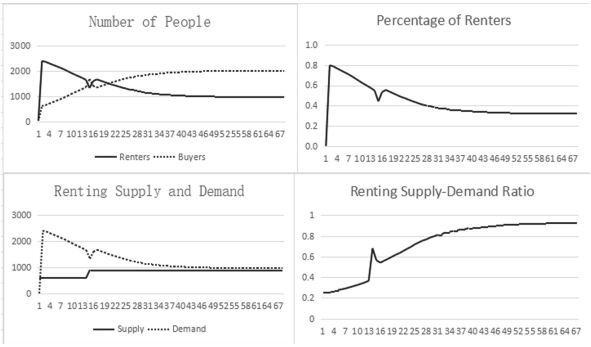

Fig. 4. Rebuilding renting housing projects

3) The government provides rental subsidies for specific groups of people.

Adjust the parameters to the initial state, implement b_t, and operation of the real estate leasing market is shown in Fig. 5. It can be seen that the total demand in the rental market will increase when the rental subsidy policy is issued for specific groups of people. Due to the insufficient increase in the total supply, the rent level will rise appropriately, and then the number of renters will drop. When the time runs to about 15 months, the number of buyers and renters in the rental market is the same. When the time runs to about 28 months, the rental market has reached the level of supply and demand. Subsequently, due to the decrease in demand in the leasing market, the level of rents further declines, and the number of renters in the leasing market will increase. When the time runs to about 62 months, the rental market has stabilized, and the proportion of renters is about 0.21.

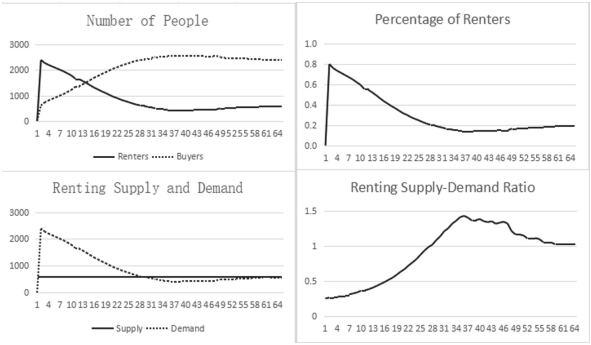

Fig. 5. Rental subsidies

4) The government provides a combination of new renting housing projects and issuance of rental subsidies.

Adjust the parameters to the initial state, implement x_j, z_j, b_z, b_t and operation of the real estate leasing market is shown in Fig. 6. When new housing projects are implemented and rental subsidies are issued, the total supply and total demand in the rental market will increase. However, because the supply is less than the demand, the number of renters is gradually decreasing. When the time runs to about 18 months, the number of buyers and renters in the rental market is flat, and then due to insufficient supply, the number of renters will drop appropriately. When the time runs to about 60 months, the rental market reaches the level of supply and demand. When the time runs to about 65 months, the rental market has stabilized, and the number of renters accounted for about 0.48.

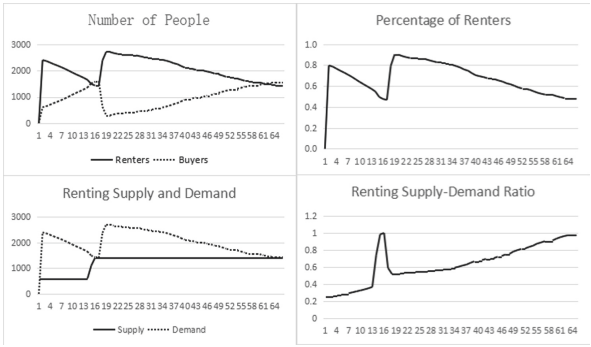

Fig. 6. Combination

4.3.3 Summary

In summary, Nanjing's market-oriented rental housing construction policy can expand the total supply and total demand of the rental market through different policies and combinations. Among them, the provision of new and renovated housing policies can

greatly increase the supply of rental housing. According to relevant economic theories, the rent level will fall and the number of renters will rise. Granting subsidies to specific groups of people can bring benefits to some renters. However, the lack of supply and high demand in the leasing market will lead to an increase in the level of rents. Due to the increase in costs, the number of renters will decrease, and the policy effect will be small. When a combination of new rental housing and subsidies for specific groups are implemented, the total supply in the rental market is increased on the one hand, and the total demand in the rental market is increased by reducing the cost of renting houses for consumers on the other hand. From the experimental results, the proportion of renters among consumers under the implementation of the combined policy has increased by more than 20% compared with the implementation of other policies. In general, the combination policy can simultaneously increase the supply and demand in the rental market, which is conducive to achieving a balance of supply and demand in the rental market and stabilizing the rent level.

5 Suggestions and Conclusions

5.1 Suggestions

1) Fully consider the subjective factors of consumers and promote the "same right for renting and buying." This simulation experiment confirms that consumer's subjective factors have a greater impact on the purchase and renting decisions, so we should focus on protecting the public service rights of the renting consumers, so as to increase the proportion of consumer renting.
2) Coordinate multiple parties to implement combined policies to control the balance of housing supply and demand. The purpose of the market-based rental housing policy is to effectively increase the supply and demand in the rental market through the role of the market, enhance the security of rental housing and stabilize the rent level. The balance of supply and demand in the rental market should be controlled by coordinating multiple policy entities to implement policies on the supply side and the demand side at the same time.
3) Grasp the operation and expectations of the real estate market, and adjust the content of the policy in a timely manner. This simulation model simulates the market-oriented rental housing construction policy, and this process can provide a reference for the actual policy implementation and adjustment. Simulation policy operation is helpful for comprehensive analysis of current leasing market operation and policy expectations in the next stage. In turn, the policy plan can be implemented and adjusted more accurately to ensure the timely control of the policy on the operation of the house purchase and leasing market.

5.2 Conclusions

This paper uses Anylogic software to conduct multi-agent simulation experiments to simulate consumer decision-making behaviors during the operation of the market-oriented rental housing construction policy in Nanjing, and analyze the effects of different measures in the policy on the real estate rental market. In the process, the objective and

subjective factors that affect consumers' decisions on renting and buying houses were fully considered. The relevant data of Nanjing consumers were obtained through questionnaire surveys, and the values of variables and parameters were obtained from them to ensure the validity of the experimental results of the model. During the implementation of the market-based rental housing policy, attention should be paid to guaranteeing the legitimate rights and interests of rental consumers, controlling the balance of supply and demand in the rental market, strengthening the security during the rental process, and maintaining the healthy and stable development of the rental market.

Acknowledgements. Foundation item: National Social Science Foundation item: "Research on Simulation and Effect Evaluation of the Policy of 'Purchase and Leasing' in the Real Estate Market from the Perspective of Big Data". (18BGL193).

References

1. Administrative Measures for the Construction of Market-oriented Rental Housing in Nanjing
2. Yan, R.: The housing rental system: value elements and the 'triadic dilemma'. J. East China Normal Univ. (Philosophy and Social Sciences Edition), **52**(03), 160–168+184 (2020)
3. Cui, W., Liu, X.: Analysis of my country's housing rental market standardization under the policy of 'renting and purchasing simultaneously.' Dev. Res. **05**, 47–52 (2020)
4. Shao, T.: Development dilemma and policy breakthrough of china's housing rental market. Int. Urban Plan. 1–10 (2020)
5. Li, Y., Liu, N.: Practical research on multi-agent supply from the perspective of new housing security. J. Hunan Univ. Fin. Econ. **36**(03), 22–29 (2020)
6. Yan, W., Kun, W., Mingyan, Z.: Discussion on the game between different consumer groups in real estate industry. Shanghai Real Estate **4**(02), 27–29 (2020)
7. Lin, W., Deng, L.: A review on the development of rental and purchase and housing rental. China Real Estate **4**(12), 32–37 (2020)
8. Dong, D.: Research on the housing system of multi-agent supply and multi-channel guarantee for rent and purchase. North. Econ. Trade **4**(12), 7–8 (2018)
9. Huo, L., Wei, S., Xu, S.: Regulations and contingent interest rate policy selection under the new economic normal based on multi-agent simulation. Syst. Eng. Theory Pract. **37**(09), 2289–2296 (2017)
10. Chen, J., Luo, Z., Shen, Y., et al.: Simulation research on real estate rental and purchase decision under housing policy. J. Eng. Manage. **34**(03), 142–147 (2020)

Accidents Analysis and Severity Prediction Using Machine Learning Algorithms

Rahul Ramachandra Shetty and Hongrui Liu(✉)

Department of Industrial and System Engineering, San Jose State University, San Jose, CA 95192, USA
hongrui.liu@sjsu.edu

Abstract. Traffic congestion and road accidents have been important public challenges that impose a big burden on society. It is important to understand the factors that contribute to traffic congestions and road accidents so that effective strategies can be implemented to improve the road condition. The analysis on traffic congestion and road accidents is very complex as they not only affect each other but are also affected by many other factors. In this research, we use the US Accidents data from Kaggle that consists of 4.2 million accident records from February 2016 to December 2020 with 49 variables for the study. We propose to use statistical techniques and machine learning algorithms that include Logistic Regression, Tree-based techniques such as Decision Tree Classifier and Random Forest Classifier (RF), and Extreme Gradient boosting (XG-boost) to process and train a large amount of data to obtain predictive models for traffic congestion and road accidents. The proposed predictive models are expected to be more accurate by incorporating the impact of multiple environmental parameters. The proposed models will assist people in making smart real-time transportation decisions to improve mobility and reduce accidents.

Keywords: Traffic congestion · Road accidents · Predictive model · Machine learning

1 Introduction

Traffic congestion and road accidents have been major public challenges and are affecting the people' daily lives in different ways. The situation is getting worse in the recent years due to the population growth and the boom in ecommerce in many urban areas [1]. According to the annual study from INRIX in 2019, the average time Americans lost to traffic increased by two hours from 2017 to 2019 [2]. Road accidents may have an even more significant impact on persons' lives depending on the severity of the event. In the US, over 38,000 people die in road crashes each year, and 2.35 million are injured or disabled according to the statistics report from the Association for Safe International Road Travel (ASIRT) in 2020 [3]. It is important to understand the root cause of traffic congestion and road accidents and their association so that effective policies or transportation decision tools can be implemented to improve roadway safety

R. Qiu et al. (Eds.): ICSS 2021, LNOR, pp. 173–183, 2021.
https://doi.org/10.1007/978-3-030-90275-9_15

and relieve traffic congestion. The analysis on traffic congestion and road accidents is very complex as they are affected by many factors, such as road demographics, time of the day/week, weather conditions, and events that may change in real-time [4, 5]. The development of advanced technologies such as GPS (Global Positioning System) and IoT (Internet of Things) offers great visibility and transparency of roadway conditions nowadays. The information, if utilized appropriately, can help people understand the impact factors on traffic congestion and make timely transportation decisions to improve mobility of people and goods. Since the year of 2015, the Department of Transportation (DOT) launched a series of Smart City Challenge [6], asking for ideas to create an integrated, first-of-its-kind smart transportation system that would use data, applications, and technology to revolutionize the transportation systems to help improve people's lives.

In response to the aforementioned needs, some research has been conducted in the field of road accident and traffic congestion analysis using data analytics models. A data mining technique with k-means algorithm to identify locations with high number of accidents and the affecting factors was conducted in [7]. A detection system that uses Artificial Neural Network (ANN), Support Vector Machine (SVM), and RF machine learning algorithms to understand vehicle behaviours and detect accidents on freeways was developed in [8]. Machine learning algorithms Adaboost, RF, and naïve Bayes were used to predict the severity of injuries due to accident in [9]. The K-means clustering algorithm together with association rule mining was used to find various patterns in the road accident in [10]. Artificial neural network models utilizing Feedforward Multilayer Perceptron (FFMLP) was used to predict road accidents for time series forecasting in [11]. A LSTM-GBRT (long short-term memory, gradient boosted regression trees) model was used to predict the safety level of traffic accidents in [12].

We propose to use statistical techniques and machine learning algorithms to process and train the large amount of data offered by advanced information technologies to obtain robust predictive models for traffic congestion and road accidents. Machine learning algorithms used in the study include logistics regression, decision tree classifier, random forest classifier, and XG-Boost. The predicted target is the severity of the accidents, which is a measure of the impact of road accidents on traffic congestion. The study also includes analysis to identify the factors that have a significant impact on road accidents. Data from Kaggle for US accidents with information on weather, location, period, and POI attributes are used for the analysis. The objective is to build a robust model using machine learning algorithms for predicting the severity of road accidents. This information can be used to make important decisions to minimize time spent on the road. This study contributes the existing literature by analyzing a large amount of data (4.2 million records) and high dimensional features (49 features), and comparing five machine learning algorithms to obtain an accurate predictive model. In addition, we studied the trade-off between the computation effort and model accuracy to provide an insight on implementing a practical model in real life.

This paper is organized as follows. In Sect. 2, we present the data source and perform data exploratory analysis and pre-processing. We introduce the machine learning methodologies used to train the predictive models in Sect. 3. The numerical results of the case study, conclusions and future work are discussed in Sect. 4.

2 Data Source

Collected from Kaggle under the title US Accidents, our dataset consists of 4.2 million records of car accidents from February 2016 to December 2020 across 49 states of the United States. The data set has 49 variables with 17 categorical variables, 13 Boolean variables, 16 numerical variables, 2 Date Time stamps, and 1 string. Out of the 49 variables, 12 of them are traffic attributes, 9 of them are location attributes, 11 of them are weather attributes, and 13 of them are point of interest (POI) attributes.

2.1 Exploratory Data Analysis

The data entries on Kaggle are from three sources, MapQuest, Bing and other. We select the data from Bing for our analysis as the target variable "severity" is better classified with less conflicts. The accident severity from Bing was given four levels, where 1 indicates the least impact on traffic (i.e., short delay as a result of the accident) and 4 indicates a significant impact on traffic (i.e., long delay) [13]. The average impacted area on the road is 0.01 miles by severity 1 accident, 0.27 miles by severity 2 accident, 0.55 miles by severity 3 accident, and 0.96 miles by severity 4 accident. To limit the scope of the study, the data set was brought down to a state level and California was identified to be the state that has the highest number of accidents for further study. The number and severity of the accidents in California are shown in Fig. 1(a). There are 5534 accidents with severity 1, 414,069 accidents with severity 2, 20,592 accidents with severity 3, and 8316 accidents with severity 4. It is observed that the data is imbalanced with the highest number of severity level 2 accident. In Fig. 1(b), it shows how the accidents spread across the state of California.

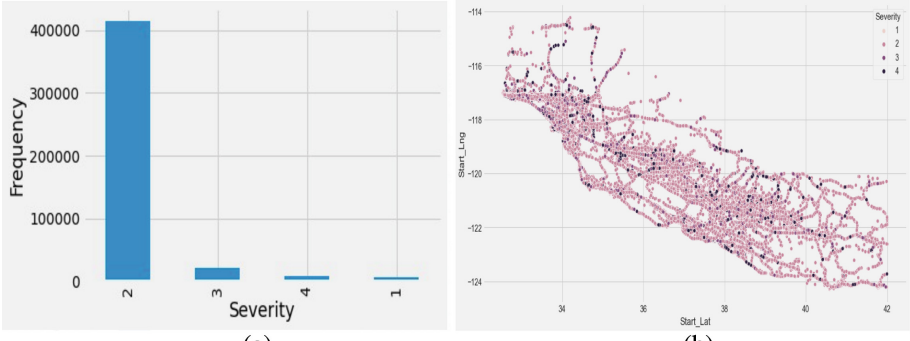

(a) (b)

Fig. 1. (a) Entries with respect of severity (b) Severity of accidents across CA

The correlation between different attributes and the target variable, severity, was then studied to have an initial understanding of the impact of the attributes to the target variable. It shows that a higher number of accidents occurred when the weather condition is fair (Fig. 2(a)), with 0 precipitation (Fig. 2(b)), the wind is calm (Fig. 3(a)), less wind speed, and higher visibility (Fig. 3(b)). Other weather features such as pressure, humidity,

and windchill did not show any significant impact to the target variable (Fig. 4(a) and Fig. 4(b)).

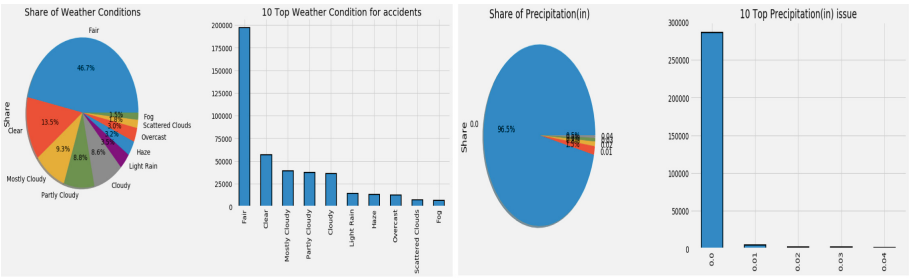

(a) (b)

Fig. 2. Number of accident due to (a) Weather condition, (b) Precipitation

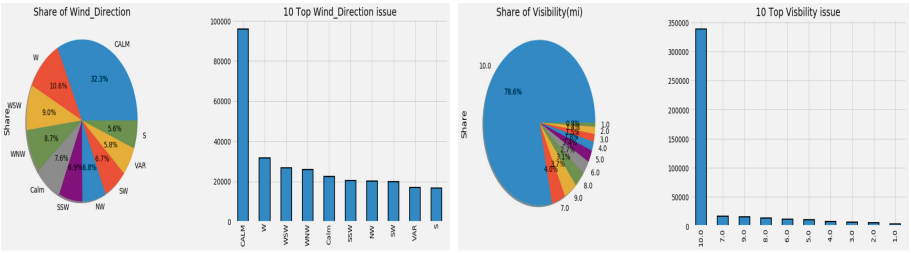

(a) (b)

Fig. 3. Number of accident due to (a) Wind direction, (b) Visibility

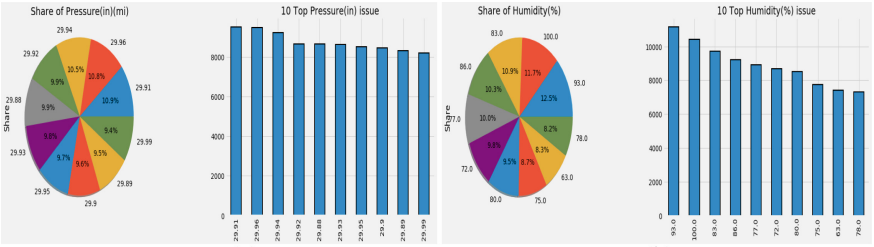

(a) (b)

Fig. 4. Number of accident due to (a) Pressure, (b) Humidity

Feature extraction is then used to extract hour, week, month, and year information from the period of day attribute. The result shows that a large number of accidents took place on weekdays other than on weekends (Fig. 5(a)). Over a year, October, November, and December had more accidents compared to the other months, as shown in Fig. 5(b), The time between 4 to 6 pm had a higher number of accidents during a day as shown in Fig. 5(c).

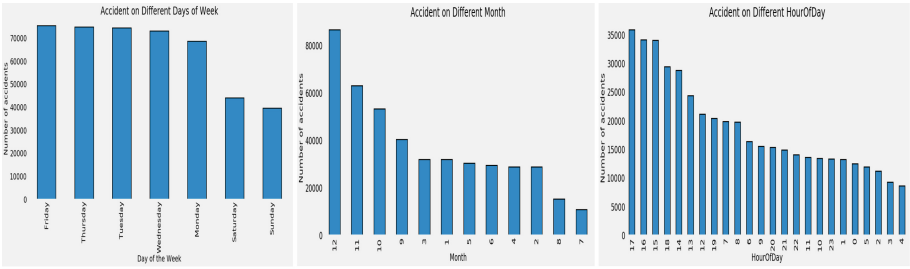

(a) (b) (c)

Fig. 5. Number of the accident in (a) Day of the week, (b) Month in a year (c) Time of the day

A multivariate analysis was conducted on the POI attributes by grouping stop, station, and railway. There were a significant number of accidents when all the three signs are missing, or there is a missing sign in giving way, crossing, and bump, as shown in Fig. 6.

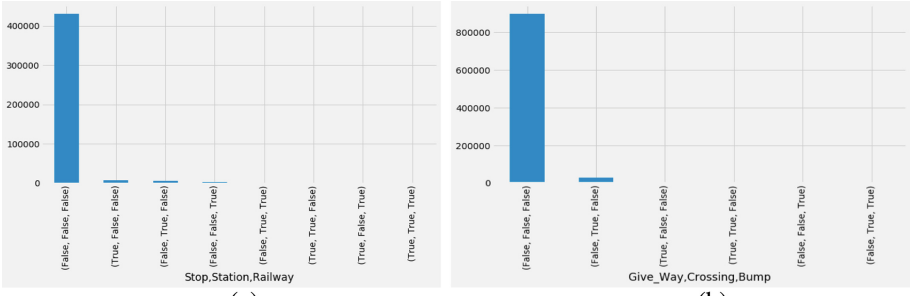

(a) (b)

Fig. 6. Number of accidents with POI attributes

The analysis on the location attributes shows that LA (Los Angeles) is the city that has the highest number of accidents in California with 44.5% of overall accidents as shown in Fig. 7.

The duration of traffic that was affected by an accident was calculated from the start time and end time of the traffic. Together with the distance (in miles) that was affected by the accident, number of accidents and severity, we could study the relationship between congestion and road accident. It was observed the more severe accidents (severity 2, 3 and 4) decrease with increasing congestion as shown in Table 1.

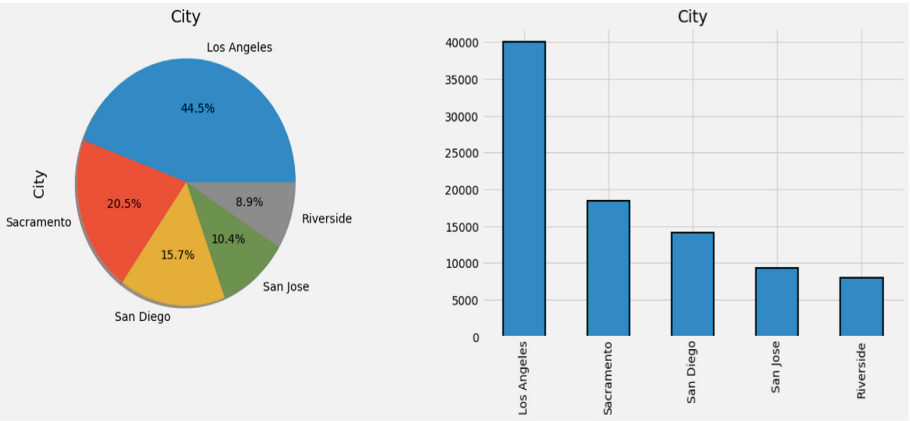

Fig. 7. Number of accidents in cities

Table 1. Relationship between accident and congestion

Severity of the accident	Number of accident	Average distance impacted in miles	Average duration impacted in mins
1	5137	0.0104	21.96
2	386,915	0.273	159.29
3	20,371	0.555	195.05
4	8086	0.9623	494.25

2.2 Data Preprocessing

The data is cleaned and prepared for the different machine learning algorithms to train the predictive models in this step. Feature engineering techniques are used to extract time features and to analyze any trends or patterns over time. Feature selection techniques are used to handle the high dimensionality by identifying features of high importance. Features such as Precipitation that contains too many null values are dropped. Features such as country, state, turning loop, and source, which have a single unique value each, and those such as 'ID', and 'description' who have no impact to the prediction target are removed from the data set. The chi-square test is used to evaluate categorical variables, Pearson correlation is used to remove highly correlated features, and single or constant value features are dropped using variance threshold. There are 25 features reaming in our data set after the cleaning. The data is them split into X (the independent features) and y (prediction target, severity). We use 70% of the data as the training set and 30% for testing model accuracy. Feature encoding is performed on train and test set separately to avoid data leakage and overfitting. The prediction target, the severity levels are converted into categorical values and all the other features are converted to numerical values using pandas categorical (). code. Data Imputation is used to fill the missing values with a

median. SMOTE is used to balance the data set by duplicating the minority data from the minority data population.

3 Methodology

We used four machine learning algorithms to train the predicative models as described below.

- Multivariable logistic regression: A classification algorithm that takes less effort and time to train the model. It converts the loss function to cross-entropy, and probability prediction to multinomial probability distribution using maximum likelihood estimation to predict different severity classes. The target variable has 4 classes and hence Multinomial logistic regression is used over logistic regression.
- Decision tree: This is a supervised technique that uses different algorithms to split a node into multiple sub-nodes on all variables and selects the best split that provides the best result. The tree splits at the topmost node where the outcome is represented by the branches and the leaf consists of class. The tree is stopped once it reaches the defined stopping criteria. The terminal node represents the mode which is the predictor for that region. The decision tree requires minimal data cleaning which is helpful in our data set as there are 49 multidimensional features and over 448 k entries. A decision tree is also easy to interpret.
- Random Forest (RF): RF algorithm eliminates high variance by adding randomness to the model. It works by creating multiple decision trees using a bootstrapping method by random sampling with replacement. A bagging technique is used for output from each decision tree. The final output is the mode of the output of all the individual decision trees. To eliminate overfitting and to overcome bias RF is used.
- Extreme Gradient boosting (XG-Boost): The algorithm boosts the model and builds a base model that provides an output that is used to find the residual. The residual is the dependent variable for the subsequent tree and the features are used in decision and terminal nodes. Gain is calculated using the similarity score at each node and the highest gain achieved is used for splitting the tree. Similarly, multiple trees are drawn sequentially. Finally, the output from the base model and the subsequent trees are used to predict the output. use the patterns in residual to its advantage by strengthening the model with weak predictions and therefore predicts gives low errors. Ensemble machine learning techniques are used as the prediction is obtained by a combination of trees that reduces variance by bagging, bias by boosting and improve model accuracy by stacking.

Python packages including Pandas, NumPy, matplotlib, seaborn, and date-time from python are used for data analysis and data visualization. Synthetic Minority Oversampling Technique (SMOTE) is used for randomly oversampling the data that utilizes the k-nearest neighbor algorithm to create synthetic data by increasing the number of records without adding any new information or variation to the model. The upscaled data is then fitted to the different machine learning algorithm to train models to predict the accident severity.

4 Results and Future Work

The training data set that includes 25 features was used to train the four machine learning algorithms to obtain predictive models for accident severity. The test data set is then used to test the accuracy of the four predictive models. The four prediction models were first trained using the original imbalance data set, and then the balanced data set by applying SMOTE technique. The accuracy score, Precision, Recall and F1 score of the four predictive models are summarized in Tables 2, 3 and 4. The four models trained from the original imbalanced data have similar accuracy. The accuracy of the linear regression model dropped significantly after applying SMOTE technique, when the data set is expanded to have 268,139 more entries to balance the data set. The algorithms Decision Tree, RF and XG-boost exhibited better robustness with both imbalanced and balanced data and they did better with balanced data in predicting the non-dominant severity 3 and 4 events as shown in Tables 3 and 4. Study has been conducted to further reduce the features from 25 to 14 using balanced data to understand the trade-off between computation expense and model accuracy. Again, Decision Tree, RF and XG-Boost are demonstrated to have a better robustness in terms of the accuracy score as shown in Table 5.

The RF model handles noise, multi-class variables, and high variance well, while the boosting technique learns from the past errors to improve prediction accuracy. It was observed that the tuning of hyperparameters plays a significant role in the prediction results for the two models. Further studies will be conducted to explore the optimal settings for the parameters. In the study of the trade-off between the computation effort and model accuracy, we simply removed 10 out of the 25 features based on the data analysis earlier. The accuracy score didn't change significantly for all the models. Further studies will be conducted to investigate the impact of the features in details so we can establish a removing sequence depending on the required model accuracy. With the availability of the large data set, we will also explore the use of deep learning algorithms for the analysis in the future.

The obtained predictive model together with the real time visibility of the environmental conditions offered by advanced information technologies can help build a smart transportation system to guide people make instant decisions to minimize their time spent on the road.

Table 2. Summary of accuracy score with imbalanced data

	Multivariable linear regression	Decision tree	Random forest	XG- Boost
Original imbalanced data	95.30	95.03	96.50	96.38
Balanced data -SMOTE	52.24	93.86	95.22	93.89

Table 3. Result summary with original imbalanced data

Multivariable logistic regression	Precision	Recall	F1 Score	Support
Severity 1	0.60	0.27	0.38	1546
Severity 2	0.96	1	0.98	85,184
Severity 3	0.23	0.01	0.01	1914
Severity 4	0.35	0.01	0.01	984
Decision Tree	Precision	Recall	F1 Score	Support
Severity 1	0.69	0.71	0.70	1546
Severity 2	0.98	0.98	0.98	85,184
Severity 3	0.29	0.30	0.29	1914
Severity 4	0.30	0.36	0.33	984
Random Forest	Precision	Recall	F1 Score	Support
Severity 1	0.73	0.74	0.73	1546
Severity 2	0.97	0.99	0.98	85,184
Severity 3	0.47	0.16	0.24	1914
Severity 4	0.60	0.23	0.34	984
XG-Boost	Precision	Recall	F1 Score	Support
Severity 1	0.71	0.79	0.75	1546
Severity 2	0.91	0.99	0.98	85,184
Severity 3	0.47	0.10	0.17	1914
Severity 4	0.64	0.22	0.32	984

Table 4. Result summary with balanced data (SMOTE)

Multivariable logistic regression	Precision	Recall	F1 Score	Support
Severity 1	0.16	0.92	0.27	1546
Severity 2	0.98	0.52	0.68	85,184
Severity 3	0.04	0.47	0.08	1914
Severity 4	0.02	0.30	0.04	984
Decision Tree	Precision	Recall	F1 Score	Support
Severity 1	0.64	0.71	0.68	1546
Severity 2	0.98	0.96	0.97	85,184
Severity 3	0.24	0.37	0.29	1914
Severity 4	0.22	0.36	0.27	984
Random Forest	Precision	Recall	F1 Score	Support
Severity 1	0.66	0.80	0.72	1546
Severity 2	0.98	0.98	0.98	85,184
Severity 3	0.30	0.37	0.33	1914
Severity 4	0.43	0.34	0.38	984
XG-Boost	Precision	Recall	F1 Score	Support
Severity 1	0.72	0.80	0.76	1546
Severity 2	0.97	0.99	0.98	85,184
Severity 3	0.49	0.10	0.17	1914
Severity 4	0.61	0.23	0.33	984

Table 5. Summary of accuracy score with 14 features

Model	Multivariable linear regression	Decision tree	Random forest	XG- Boost
Accuracy Score	52.73	93.81	95.19	94.66

Acknowledgements. The work is sponsored in part by Mineta Transportation Institute (MTI Grant # 21-1100-5726).

References

1. Sardjono1, W., Selviyanti, E., Perdana, W.G.: Modeling the relationship between public transportation and traffic conditions in urban areas: a system dynamics approach. In: Journal of Physics: Conference Series, vol. 1465, p. 012023 (2019)
2. https://inrix.com/press-releases/2020-traffic-scorecard-us/
3. https://www.asirt.org/safe-travel/road-safety-facts/

4. Yuan, Z., Zhou, X., Yang, T.: Hetero-ConvLSTM: a deep learning approach to traffic accident prediction on heterogeneous spatio-temporal data. In: Proceedings of the 24th ACM SIGKDD International Conference on Knowledge Discovery & Data Mining, pp. 984—992. ACM, New York (2018)
5. Lu, W., Luo, D., Yan, M.: A model of traffic accident prediction based on convolutional neural network. In: 2017 2nd IEEE International Conference on Intelligent Transportation Engineering (ICITE), pp. 198–202 (2017)
6. https://www.transportation.gov/smartcity
7. Kumar, S., Toshniwal, D.: A data mining approach to characterize road accident locations. J. Mod. Transp. **24**(1), 62–72 (2016). https://doi.org/10.1007/s40534-016-0095-5
8. Dogru, N., Subasi, A.: Traffic accident detection using random forest classifier. In: 2018 15th Learning and Technology Conference (L&T), pp. 40–45 (2018). https://doi.org/10.1109/LT.2018.8368509
9. AlMamlook, R.E., Kwayu, K.M., Alkasisbeh, M.R., Frefer, A.A.: Comparison of machine learning algorithms for predicting traffic accident severity. In: 2019 IEEE Jordan International Joint Conference on Electrical Engineering and Information Technology (JEEIT), pp. 272–276 (2019). https://doi.org/10.1109/JEEIT.2019.8717393
10. Nandurge, P.A., Dharwadkar, N.V.: Analyzing road accident data using machine learning paradigms. In: 2017 International Conference on I-SMAC (IoT in Social, Mobile, Analytics and Cloud) (I-SMAC), pp. 604–610 (2017). https://doi.org/10.1109/I-SMAC.2017.8058251
11. Kouziokas, G.N.: Neural network-based road accident forecasting in transportation and public management. In: Nathanail, E.G., Karakikes, I.D. (eds.) CSUM 2018. AISC, vol. 879, pp. 98–103. Springer, Cham (2019). https://doi.org/10.1007/978-3-030-02305-8_12
12. Zhang, Z., Yang, W., Wushour, S.: Traffic accident prediction based on LSTM-GBRT model. J. Control Sci. Eng. **2020**, 1–10 (2020). https://doi.org/10.1155/2020/4206919
13. Moosavi, S., Samavatian, M.H., Parthasarathy, S., Teodorescu, R., Ramnath, R.: Accident risk prediction based on heterogeneous sparse data. In: Proceedings of the 27th ACM SIGSPATIAL International Conference on Advances in Geographic Information Systems (2019). https://doi.org/10.1145/3347146.3359078

Estimating Discrete Choice Models with Random Forests

Ningyuan Chen[1], Guillermo Gallego[2], and Zhuodong Tang[2(✉)]

[1] Department of Management, University of Toronto Mississauga, Toronto, Canada
[2] Department of Industrial Engineering & Decision Analytics, Hong Kong University of Science and Technology, Hong Kong, China
ztangai@connect.ust.hk

Abstract. We show the equivalence of discrete choice models and a forest of binary decision trees. This suggests that standard machine learning techniques based on random forests can serve to estimate discrete choice models with an interpretable output: the underlying trees can be viewed as the internal choice process of customers. Our data-driven theoretical results show that random forests can predict the choice probability of any discrete choice model consistently. Our numerical results show that using random forests to estimate customer choices can outperform the best parametric models in two real datasets in a shorter running time.

Keywords: Discrete choice model · Random forest · Machine learning · Online retailing

1 Introduction

Discrete choice models (DCM) have become central to revenue management and e-commerce as they enable firms to predict consumer's choice behavior when confronted with a given assortment of products. Firms that can get inside the mind of their consumers enjoy unique advantages that allow them to implement effective strategies to improve profits or market shares. Firms can then further invest in technologies that sharpen their predictive power. This virtuous cycle has created a number of market juggernauts while those incapable of playing in this field are disappearing from the landscape.

To understand and predict consumers' choice behavior, academics and practitioners have proposed several frameworks, some of which are widely adopted in the industry. One ubiquitous framework is **model-then-estimate**. In this framework, a parametric DCM is proposed to explain how a consumer chooses a product when offered an assortment. The parameters are then estimated using historical data.

In the model-then-estimate framework, there is a trade-off between flexibility and accuracy. A flexible DCM incorporates a wide range of patterns of consumers' behavior, but it may be difficult to estimate and may overfit the training data. A parsimonious model may fail to capture complex choice patterns in the

R. Qiu et al. (Eds.): ICSS 2021, LNOR, pp. 184–196, 2021.
https://doi.org/10.1007/978-3-030-90275-9_16

data. Even estimated correctly, it would be misspecified and not perform well in prediction. The key to a successful model is to reach a delicate balance between flexibility and predictability. Not surprisingly, it is not straightforward to find the "sweet spot" when selecting among the large class of parametric DCMs.

Another framework favored by data scientists is to **estimate without models**. Advanced machine learning algorithms are applied to historical sales data, and used to predict future choice behavior. The framework skips "modeling" entirely and does not attempt to understand the rationality (or irrationality) hidden behind the patterns observed in the training data. With engineering tweaks, the algorithms can be implemented efficiently and capture a wide range of choice behavior. For example, neural networks are known to be able to approximate any continuous functions.

This approach may sound appealing: if an algorithm achieves impressive accuracy when predicting the choice behavior of consumers, why do we care about the actual rationale in consumers' minds when they make choices? There are two counterarguments. First, the firm may be interested in not only making accurate predictions but also in other goals such as finding an optimal assortment that maximizes the expected revenue, which may not have appeared in the data. Without a proper model, it is unclear if the goal can be formulated as an optimization problem. Second, when the market environment is subject to secular changes, having a reasonable model often provides a certain degree of generalizability while black-box algorithms may fail to capture an obvious pattern just because the pattern has not appeared frequently in the past.

In this paper, we introduce a data-driven framework which we call **estimate-and-model** that combines machine learning with interpretable models, and thus retains the strengths of both frameworks mentioned previously. The model we propose, binary choice forests, is a mixture of binary choice trees, each of which reflects the internal decision-making process of a potential customer. We show that the binary choice forest can be used to approximate *any* DCM, and is thus sufficiently flexible. Moreover, it can be efficiently estimated using random forests [6], a popular machine learning technique that has stood the test of time. Random forests are easy to implement using R or Python [14,17] and have been shown to have extraordinary predictive power in other applications.

Our interpretable framework has unique advantages compared with existing DCMs in literature. For theoretical analysis, we show the random forest can accurately approximate *any* DCMs with sufficient data while existing parametric models have misspecification errors and overfitting problems. In comprehensive numerical studies on real datasets, we show random forests (1) have more accurate and robust performance than best parametric model; (2) benefit tremendously from increasing sample size compared to other DCMs; (3) run much more efficiently than the estimation method based on the expectation-maximization (EM) algorithm for large datasets.

1.1 Literature Review

We first review DCMs proposed in the literature following the model-then-estimate framework, in the order of increasing flexibility but more difficult estimation. The MNL model [15] has very few parameters (one per product), which are easy to estimate [21]. The nested logit model, the Markov chain DCM, the mixed logit model and the rank-based DCM (see, e.g., Williams [22], Train [21], Farias et al. [9], Blanchet et al. [4]) are able to capture more complex choice behavior than the MNL model. However, the computational feasibility and susceptibility to overfitting remain a challenge in practice. In addition, the class of RUM belongs to the class of regular models with the property that the probability of choosing an alternative cannot increase if the offered set is enlarged. Experimental studies show strong evidence that regularity may be violated in practice [19]. Several models are proposed to capture more general behavior than RUM [1,10,11,16], but it is not yet clear if the estimation for such models can be done efficiently.

The specifications of random forests used in this paper are introduced by Breiman [6], although many of the ideas were discovered even earlier. The readers may refer to Hastie et al. [12] for a general introduction. Although random forests have been very successful in practice, little is known about their theoretical properties. To date, most studies are focused on isolated setups or simplified versions of the procedure. In a recent study, Scornet et al. [18] establish the consistency of random forests in regression problems, under less restrictive assumptions. Scornet [3] provide an excellent survey of the recent theoretical and methodological developments in the field.

A recent paper by [8] proposes a similar tree-based DCM. Our studies differ substantially in the estimation step: we focus on random forests, while [8] follow an optimization approach based on column generation.

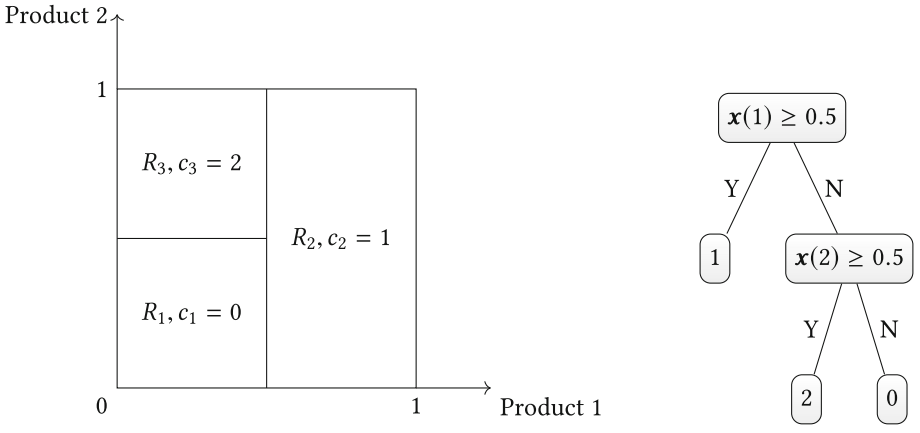

Fig. 1. A binary choice tree representation of the partition.

2 Discrete Choice Models and Binary Choice Forests

Consider a set $[N] \triangleq \{1, \ldots, N\}$ of N products and define $[N]_+ \triangleq [N] \cup \{0\}$ where 0 represents the no-purchase option. Let $\boldsymbol{x} \in \{0,1\}^N$ be a binary vector representing an assortment of products, where $\boldsymbol{x}(i) = 1$ indicates the inclusion of product i in the assortment and $\boldsymbol{x}(i) = 0$ otherwise. A **discrete choice model** (DCM) is a non-negative mapping $p(i, \boldsymbol{x}) : [N]_+ \times \{0,1\}^N \to [0,1]$ such that

$$\sum_{i \in [N]_+} p(i, \boldsymbol{x}) = 1, \quad p(i, \boldsymbol{x}) = 0 \quad \text{if} \quad \boldsymbol{x}(i) = 0. \tag{1}$$

Here $p(i, \boldsymbol{x}) \in [0,1]$ represents the probability that a customer selects product i from assortment $\boldsymbol{x}$. We refer to a subset S of $[N]$ as an assortment associated with $\boldsymbol{x} \in \{0,1\}^N$, i.e., $i \in S$ if and only if $\boldsymbol{x}(i) = 1$. In the remaining paper, we use $p(i, S)$ and $p(i, \boldsymbol{x})$ interchangeably.

A **binary choice tree** $t(\boldsymbol{x})$ maps $\boldsymbol{x} \in \{0,1\}^N$ into $[N]_+$ by sequentially splitting $[0,1]^N$ along N products, as illustrated by the right panel of Fig. 1. Moreover, to be consistent with DCMs, we require that $t(\boldsymbol{x}) = i$ only if $\boldsymbol{x}(i) = 1$. Equivalently, a binary choice tree partitions $\{0,1\}^N$ into a number of regions, denoted as $\{R_i\}$. Each R_i corresponding to a leaf node of the tree. The tree assigns a label c_i for all $\boldsymbol{x} \in R_i$. Therefore, one can write $t(\boldsymbol{x}) = \sum_{R_i} c_i \cdot \mathbb{I}_{\{\boldsymbol{x} \in R_i\}}$. A binary choice tree representation of a partition when $N = 2$ is demonstrated in Fig. 1.

A **binary choice forest** (BCF) is a convex combination or a mixture of multiple binary choice trees. More precisely, a binary choice forest can be written as

$$f(i, \boldsymbol{x}) = \sum_{b=1}^{B} w_b \mathbb{I}_{\{t_b(\boldsymbol{x}) = i\}}$$

where the $t_b(\boldsymbol{x})$ and w_b are, respectively, binary choice trees and non-negative weights summing up to one. A BCF can be interpreted as decisions made by B consumer types or segments, with consumers of type b having weight w_b and making decisions based on binary choice tree $t_b(\boldsymbol{x})$.

Notice that $f(i, \boldsymbol{x})$ maps $[N]_+ \times \{0,1\}^N \mapsto [0,1]$ just like DCMs do, so a BCF is always a DCM according to the definition (1). The converse is also true by the next theorem.

Theorem 1. *Every BCF is a DCM. Every DCM can be represented as a BCF with at most* $N \cdot 2^{N-1} + 1$ *binary choice trees.*

A recent paper by Chen and Mišić [8] has independently shown, by construction, that any choice model can be represented by a decision forest where each of the trees has depth $N + 1$. Our result provides a smaller number of binary choice trees needed for the representation.

3 Data and Estimation

The main goal of this paper is to provide a practical method to estimate BCFs using random forests, which have been shown to be able to approximate all DCMs. The numerical recipe for random forests is widely available and implementable.

We assume that arriving consumers make selections independently based on an unknown DCM $p(i, \boldsymbol{x})$, and that a firm collects data of the form $(i_t, \boldsymbol{x}_t)$ (or equivalently (i_t, S_t)) where $\boldsymbol{x}_t$ is the assortment offered to the tth consumer and $i_t \in S_t \cup \{0\}$ is the choice made by consumer $t = 1, \ldots, T$. Our goal is to use the data to construct a family of binary choice trees as a means to estimate the underlying DCM $p(i, \boldsymbol{x})$ represented by a BCF. We view the problem as a classification problem: given the input $\boldsymbol{x}$, we would like to provide a classifier that maps the input to a class label $i \in [N]_+$, or the class probabilities.

To this end we use a random forest as a classifier. The output of a random forest consists of B individual binary decision trees (CART), $\{t_b(\boldsymbol{x})\}_{b=1}^B$, where B is a tunable parameter. Although a single tree only outputs a class label in each region, the aggregation of the trees, i.e., the forest, is naturally equipped with the class probabilities. Then the choice probability of item i in the assortment $\boldsymbol{x}$ is estimated as

$$\sum_{b=1}^{B} \frac{1}{B} \mathbb{I}_{\{t_b(\boldsymbol{x})=i\}}, \tag{2}$$

which is a BCF measuring the proportion of trees that assign label $i \in [N]_+$ to input $\boldsymbol{x}$.

We now review the basic mechanism of CART and describe how it can be used to estimate random forests. The CART mechanism performs recursive binary splitting of the input space $[0,1]^N$, which is extended from $\{0,1\}^N$. In each iteration, it selects a product $i \in [N]$ and a split point to split the input space. More precisely, the split (i, s_i) divides the observations to $\{(i_t, \boldsymbol{x}_t) : \boldsymbol{x}_t(i) \le s_i\}$ and $\{(i_t, \boldsymbol{x}_t) : \boldsymbol{x}_t(i) > s_i\}$. In our problem, because $\boldsymbol{x}_t \in \{0,1\}^N$ is at the corner of the hypercube, all split points between 0 and 1 create the same partition of the observations and thus we simply set $s_i \equiv 0.5$. To select a product for splitting, an empirical criterion is optimized to favor splits that create "purer" regions. That is, the resulting region should contain data points that mostly belong to the same class. We use a common measure called *Gini index*: $\sum_{R_j} \frac{t_j}{T} \sum_{k=0}^{N} \hat{p}_{jk}(1 - \hat{p}_{jk})$ where t_j is the number of observations in region R_j of the partition and $\hat{p}_{jk}$ is the empirical frequency of class k in R_j. It is not hard to see that the Gini index takes smaller values when the regions contain predominantly observations from a single class. In this case, a product is selected that minimizes the measures and the partition is further refined by a binary split. This splitting operation is conducted recursively for the regions in the resulting partition until a stopping rule is met.

The main drawback of CART is its tendency to overfitting the training data. If a deep decision tree is built (having a large number of splits), then it may fit the training data well but introduce large variances when applied to test data. If the tree is pruned and only has a few leaves (or regions in the input space), then it loses the predictive accuracy. Random forests, by creating a number of decision trees and then aggregating them, significantly improve the power of single trees and moves the bias-variance trade-off toward the favorable direction. The basic idea behind random forests is to "shake" the original training data in various ways in order to create decision trees that are as uncorrelated as possible. Because the decision trees are deliberately "decorrelated", they can afford to be deep, as the large variances are remedied by aggregating the "almost independent" trees. Interested readers may refer to [12] for a formal discussion.

Next, we explain the details of random forests. To create B randomized trees, for each $b = 1, \ldots, B$, we randomly choose z samples with replacement from the T observations (a bootstrap sample). Only the sub-sample of z observations is used to train the bth decision tree. Splits are performed only on a random subset of $[N]$ of size m to minimize the resulting Gini index. The random sub-sample of training data and random products to split are two key ingredients in creating less correlated decision trees in the random forest. The depth of the tree is controlled by the minimal number of observations, say l, in a leaf node for the tree to keep splitting.

These ideas are formalized in Algorithm 1. The use of random forests as a generic classifier has a few benefits: (1) Many machine learning algorithms such as neural networks have numerous hyper-parameters to tune and the performance crucially depends on a suitable choice of hyper-parameters. Random forests, on the other hand, have only a few hyper-parameters. In the numerical studies in this paper, we simply choose a set of hyper-parameters that are commonly used for classification problems, without cross-validation or tuning, in order to demonstrate the robustness of the algorithm. In particularly, we mostly use $B = 1000$, $z = T$, $m = \sqrt{N}$ and $l = 50$. (2) The numerical recipe for the algorithm is implemented in many programming languages such as R and Python and ready to use.

More specifically, because of the structure of the application, there are three observations. (1) Because the entries of $\boldsymbol{x}$ are binary $\{0, 1\}$, the split position of decision trees is always 0.5. Therefore, along a branch of a decision tree, there can be at most one split on a particular product, and the depth of a decision tree is at most N. (2) The output random forest is not necessarily a BCF. In particular, the probability of class i, or the choice probability of product i given assortment $\boldsymbol{x}$, may be positive even when $\boldsymbol{x}(i) = 0$, i.e., product i is not included in the assortment. To fix the issue, we adjust the probability of class i by conditioning on the trees that output reasonable class labels:

$$\sum_{b=1}^{B} \frac{1}{\sum_{j:\boldsymbol{x}(j)=1} \sum_{b=1}^{B} \mathbb{I}_{\{t_b(\boldsymbol{x})=j\}}} \mathbb{I}_{\{t_b(\boldsymbol{x})=i, \boldsymbol{x}(i)=1\}}.$$

Algorithm 1. Random forests for DCM estimation

1: Data: $\{(i_t, \boldsymbol{x}_t)\}_{t=1}^{T}$
2: Tunable hyper-parameters: number of trees B, sub-sample size $z \in \{1, \ldots, T\}$, number of products to split $m \in \{1, \ldots, N\}$, terminal leaf size $l \in \{1, \ldots, z\}$
3: **for** $b = 1$ to B **do**
4: Select z observations from the training data with replacement, denoted by Z
5: Initialize the tree $t_b(\boldsymbol{x}) \equiv 0$ with a single root node
6: **while** some leaf has greater than or equal to l observations belonging to Z and can be split **do**
7: Select m products without replacement among $\{1, \ldots, N\}$
8: Select the optimal one to split among the m products that minimizes the Gini index
9: Split the leaf node into two
10: **end while**
11: Denote the partition associated with the leaves of the tree by $\{R_1, \ldots, R_M\}$; let c_i be the class label of a randomly chosen observation in R_i from the training data
12: Define $t_b(\boldsymbol{x}) = \sum_{i=1}^{M} c_i \mathbb{I}_{\{\boldsymbol{x} \in R_i\}}$
13: **end for**
14: The trees $\{t_b(\cdot)\}_{b=1}^{B}$ are used to estimate the class probabilities as (2)

(3) When returning the class label of a leaf node in a decision tree, we use a randomly chosen tree instead of taking a majority vote (Step 11 in Algorithm 1). While not being a typical choice, it seems crucial in deriving our consistency result (Theorem 2), because a majority vote would favor the choice of product that most consumers make and ignore less attractive products.

4 Why Do Random Forests Work Well?

Many machine learning algorithms, including random forests, have strong performances in practice. However, with a few exceptions, they do not provide an explanation for the predictions. We now show that given enough data, random forests are consistent for *any* DCM. To obtain our theoretical results, we impose mild assumptions on how the data is generated.

Assumption 1. There is an underlying DCM from which all T consumers independently make choices from the offered assortments, generating data $(i_t, \boldsymbol{x}_t)$, $t = 1, \ldots T$.

Notice that the assumption only requires consumers to make choices independently. We do not assume that the offered assortments $\boldsymbol{x}_t$s are IID, and allow the sequence of assortments offered $\boldsymbol{x}_t$ to be arbitrary as the assortments are chosen by the firm and are typically not randomly generated. Such a design reflects how firms select assortments to maximize expected revenues or to explore customer preferences.

For a given assortment $\boldsymbol{x}$, let $k_T(\boldsymbol{x}) \triangleq \sum_{t=1}^{T} \mathbb{I}_{\{\boldsymbol{x}_t=\boldsymbol{x}\}}$ be the number of consumers who see assortment $\boldsymbol{x}$. We are now ready to establish the consistency of random forests.

Theorem 2. *Suppose Assumption 1 holds, then for any* $\boldsymbol{x}$ *and* i*, if* $\liminf_{T\to\infty} k_t(x)/T > 0$*,* l_T *is fixed,* $z_T \to \infty$*,* $B_T \to \infty$*, then the random forest is consistent:*

$$\lim_{T\to\infty} \mathsf{P}\left(\left|\sum_{b=1}^{B_T} \frac{1}{B_T} \mathbb{I}_{\{t_b(\boldsymbol{x})=i\}} - p(i,\boldsymbol{x})\right| > \epsilon\right) = 0$$

for all $\epsilon > 0$*.*

According to Theorem 2, the random forest can accurately predict the choice probability of any DCM, given that the firm offers the assortment for many times. Theorem 2 guarantees good performance of the random forest when the seller has collected a large dataset. This is a typical case in online retailing, especially in the era of "big data". Random forests thus provide a novel *data-driven* approach to model customer choices. In particular, the model is first trained from data, and then used to interpret the inherent thought process of consumers when they make purchases. By Theorem 2, when the historical data has a large sample size, the model can accurately predict how consumers make decisions in reality.

5 Numerical Experiments

In this section, we conduct a comprehensive numerical study based on two real datasets. The historical data is of the form $(i_t, S_t)_{t=1}^{T}$. Under parametric model like MNL and Markov chain model, we postulate a DCM and then maximize the log-likelihood function

$$\mathcal{LL} = \sum_{t=1}^{T} \log(p(i_t, S_t|\boldsymbol{\theta})), \tag{3}$$

where $\boldsymbol{\theta}$ is the parameters of DCM. MNL proposed by [15] has closed-form choice probability $p(i,S) = \exp(v_i)/(1+\sum_{j\in S}\exp(v_j))$, where $v_j, j \in S$ is the utility of product j. The log-likelihood function is concave and we can optimize it via the Python package "SciPy" [21]. Markov chain (MC) model proposed by [4] assumes that a customer likes alternative j most with probability λ_j. If alternative j is not available, with probability ρ_{ji} the customer transits to alternative i. The customer will keep transiting until he selects a product in S or outside option 0. Since there are $O(N^2)$ parameters in the Markov chain model, it is not easy to directly optimize the log-likelihood function. [20] develop an EM algorithm to estimate parameters. In contrast, our random forest can be easily estimated using Algorithm 1 with the Python package "scikit-learn".

[2] conduct systematic and exhaustive numerical experiments on synthetic, semi-synthetic and real data, and show Markov chain model has an outstanding empirical performance compared to MNL, the nested logit, the mixed logit,

and rank-based DCM. We choose the MNL and the Markov Chain models as benchmarks because the MNL model is one of the most widely used DCM and the Markov chain model has been shown as the best parametric model [2].

5.1 Real Data: IRI Academic Dataset

In this section, we compare different models on the IRI Academic Dataset [7]. The IRI Academic Dataset collects weekly transaction data from 47 U.S. markets from 2001 to 2012, covering more than 30 product categories. Each transaction includes the week and the store of purchase, the universal product code (UPC) of the purchased item, number of units purchased and total paid dollars.

The preprocessing follows the same steps as in Jagabathula and Rusmevichientong [13] and Chen and Mišić [8]. In particular, we regard the products sharing the same vendor code as the same product. Each assortment is defined as the unique combination of stores and weeks. Such an assortment includes all the products that are available in the store during that week. We conduct the analysis for 31 categories separately using the data for the first two weeks in 2007. We only focus on the top nine purchased products from all stores during the two weeks in each category and treat all other products as the no-purchase alternative.

Unfortunately, sales data for most categories are too large for the EM algorithm to estimate the Markov chain model. For example, carbonated beverages, milk, soup and yogurt have more than 10 million transactions. For computational efficiency, we uniformly sample 1/200 of the original data size without replacement. This does not significantly increase the sampling variability as most transactions in the original data are repeated entries.

To compare different estimation procedures, we use five-fold cross validation to examine the out-of-sample performance. We follow [2] and evaluate the empirical root mean squared error (RMSE) in the validation set. That is, for estimated choice probabilities $\hat{\mathsf{P}}$ and validation set $\mathcal{T}$, we define

$$RMSE\left(\hat{\mathsf{P}}, \mathcal{T}\right) = \sqrt{\frac{\sum_{(i,S)\in\mathcal{T}} \sum_{j\in S\cup\{0\}} \left(\mathbb{I}_{\{j=i\}} - \hat{\mathsf{P}}(j,S)\right)^2}{\sum_{(i,S)\in\mathcal{T}} (|S|+1)}}. \tag{4}$$

The result is shown in Table 1 comparing random forests to MNL and the Markov chain model. Random forests outperform the other two in 24 of 31 categories, especially for large data sizes. According to Berbeglia et al. [2], the Markov chain choice model has already been shown to have a strong performance in synthetic and real-world studies. Table 1 fully demonstrates the potential of random forests as a framework to model and estimate consumer behavior in practice.

For robustness, we also test the result when considering the top five/fifteen products instead of nine. The results are shown in Fig. 2. We compare the difference between benchmark (MNL, Markov) and random forest in RMSE divided by the standard deviation of random forest. Random forest performs the best

among the three models in 25 and 27 out of 31 categories, respectively. When the data size is large, random forests can outperform MNL and Markov chain more significantly.

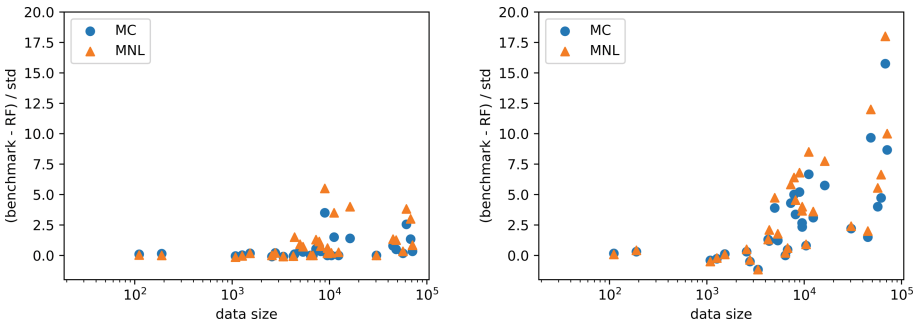

Fig. 2. Compare the RMSE of random forest with MNL and Markov when focusing on the top five (left) and top fifteen (right) purchased products.

We run our algorithm on a server with 2.50 GHz dual-core Inter Xeon CPU E5-2680 and 256 GB memory. In terms of computation time, the random forest is the most efficient, while the EM algorithm used to estimate the Markov chain model takes much longer. For the product category "milk" with 56,849 data points, the random forest only takes 10.7 s, while the Markov chain takes 7115 s. Overall, our algorithm outperforms the best parametric models in terms of accuracy and efficiency.

5.2 Real Data: Hotel

In this section, we apply the random forest algorithm to a public dataset [5]. The dataset includes transient customers (mostly business travelers) who stayed in one of five continental U.S. hotels between March 12, 2007, and April 15, 2007. The minimum booking horizon for each check-in date is four weeks. Rate and room type availability and reservation information are collected via the hotel and/or customer relationship officers (CROs), the hotel's websites, and offline travel agencies. Since there is no direct competition among these five hotels, we process the data separately. A product is uniquely defined by the room type (e.g., suite). For each transaction, the purchased room type and the assortment offered are recorded.

When processing the dataset, we remove the products that have less than 10 transactions. We also remove the transactions whose offered assortments are not available due to technical reasons. For the transactions that none of the products in the available sets are purchased by the customer, we assume customers choose the no-purchase alternative.

Table 1. The summary statistics (the data size, the number of unique assortments in the data, and the average number of products in an assortment) of the IRI dataset after preprocessing and the average and standard deviation of the out-of-sample RMSE (4) for each category when considering the top 9 products.

Product category	# Data	# Unique assort	# Avg prod	RF	MNL	MC
Beer	10,440	29	5.66	**0.2717** (0.0006)	0.2722 (0.0009)	0.2721 (0.0008)
Blades	1,085	36	4.83	0.3106 (0.0041)	**0.3092** (0.0039)	0.3096 (0.0040)
Carbonated beverages	71,114	24	5.42	**0.3279** (0.0004)	0.3299 (0.0005)	0.3295 (0.0005)
Cigarettes	6,760	48	5.73	**0.2620** (0.0031)	0.2626 (0.0034)	0.2626 (0.0034)
Coffee	8,135	46	6.26	**0.2904** (0.0011)	0.2934 (0.0010)	0.2925 (0.0011)
Cold cereal	30,369	15	6.80	**0.2785** (0.0004)	0.2788 (0.0003)	0.2787 (0.0003)
Deodorant	2,775	20	6.75	0.2827 (0.0005)	0.2826 (0.0006)	**0.2826** (0.0006)
Diapers	1,528	13	3.85	**0.3581** (0.0027)	0.3583 (0.0023)	0.3583 (0.0025)
Facial tissue	8,956	22	4.09	**0.3334** (0.0007)	0.3379 (0.0011)	0.3375 (0.0008)
Frozen Dinners/Entrees	48,349	35	6.46	**0.2733** (0.0004)	0.2757 (0.0003)	0.2750 (0.0003)
Frozen pizza	16,263	50	5.32	**0.3183** (0.0002)	0.3226 (0.0001)	0.3210 (0.0001)
Household cleaners	6,403	18	6.67	0.2799 (0.0011)	0.2798 (0.0010)	**0.2798** (0.0010)
Hotdogs	7,281	66	5.06	**0.3122** (0.0012)	0.3183 (0.0006)	0.3170 (0.0008)
Laundry detergent	7,854	51	6.14	**0.2738** (0.0018)	0.2875 (0.0019)	0.2853 (0.0018)
Margarine/Butter	9,534	15	6.60	**0.2985** (0.0005)	0.2995 (0.0004)	0.2990 (0.0004)
Mayonnaise	4,380	38	5.08	**0.3212** (0.0027)	0.3242 (0.0011)	0.3230 (0.0007)
Milk	56,849	32	4.72	**0.2467** (0.0007)	0.2501 (0.0005)	0.2538 (0.0013)
Mustard	5,354	42	6.21	**0.2844** (0.0009)	0.2856 (0.0006)	0.2852 (0.0006)
Paper towels	9,520	34	5.71	**0.2939** (0.0011)	0.2964 (0.0009)	0.2959 (0.0009)
Peanut butter	4,985	31	4.97	**0.3113** (0.0019)	0.3160 (0.0006)	0.3146 (0.0011)
Photography supplies	189	30	3.63	0.3456 (0.0090)	**0.3399** (0.0090)	0.3456 (0.0098)
Razors	111	10	2.60	**0.3269** (0.0334)	0.3294 (0.0251)	0.3323 (0.0218)
Salt snacks	44,975	28	5.50	**0.2830** (0.0006)	0.2844 (0.0007)	0.2840 (0.0007)
Shampoo	3,354	25	6.68	0.2859 (0.0007)	**0.2855** (0.0008)	0.2856 (0.0008)
Soup	68,049	23	6.96	**0.2709** (0.0006)	0.2738 (0.0007)	0.2729 (0.0007)
Spaghetti/Italian Sauce	12,377	32	5.88	**0.2901** (0.0004)	0.2919 (0.0007)	0.2914 (0.0006)
Sugar substitutes	1,269	40	5.35	0.3092 (0.0047)	**0.3085** (0.0047)	0.3085 (0.0047)
Toilet tissue	11,154	23	5.65	**0.3084** (0.0006)	0.3126 (0.0004)	0.3132 (0.0016)
Toothbrushes	2,562	45	6.04	0.2860 (0.0010)	0.2859 (0.0004)	**0.2858** (0.0006)
Toothpaste	4,258	33	6.00	**0.2704** (0.0009)	0.2708 (0.0012)	0.2708 (0.0012)
Yogurt	61,671	42	5.19	**0.2924** (0.0013)	0.2976 (0.0009)	0.2960 (0.0009)

We use five-fold cross-validation and RMSE defined in (4) to examine the out-of-sample performance. In Table 2 we show the summary statistics of the five datasets after preprocessing. We also show the out-of-sample RMSE for each hotel (average and standard deviation). In addition, we show the performance of the independent demand model (ID), which does not incorporate the substitution effect and is expected to perform poorly, in order to provide a lower bound of the performance.

We find that the random forest algorithm outperforms the parametric methods for large datasets (Hotel 1, 2 and 3). For smaller data sizes (Hotel 4 and 5), the random forest is on par with the best parametric estimation procedure (Markov chain) according to Berbeglia et al. [2].

Table 2. The summary statistics (the total number of products, the data size for in-sample and out-of-sample tests, the number of unique assortments in the data, and the average number of products in an assortment) of the five hotel datasets and the average and standard deviation of the out-of-sample RMSE across five folds.

	# Prod	# In-sample	# Out-sample	# Unique assort	# Avg prod
Hotel 1	10	1271	318	50	5.94
Hotel 2	6	347	87	26	3.27
Hotel 3	7	1073	268	25	4.32
Hotel 4	4	240	60	12	2.33
Hotel 5	6	215	54	21	3.52
	RF	MNL	MC	ID	
Hotel 1	**0.3040** (0.0046)	0.3098 (0.0031)	0.3047 (0.0039)	0.3224 (0.00430)	
Hotel 2	**0.3034** (0.0120)	0.3120 (0.0148)	0.3101 (0.0124)	0.3135 (0.0178)	
Hotel 3	**0.2842** (0.0051)	0.2854 (0.0065)	0.2842 (0.0064)	0.2971 (0.0035)	
Hotel 4	0.3484 (0.0129)	**0.3458** (0.0134)	0.3471 (0.0125)	0.3584 (0.0047)	
Hotel 5	0.3219 (0.0041)	0.3222 (0.0069)	**0.3203** (0.0046)	0.3259 (0.0058)	

References

1. Berbeglia, G.: The generalized stochastic preference choice model. Working Paper (2019)
2. Berbeglia, G., Garassino, A., Vulcano, G.: A comparative empirical study of discrete choice models in retail operations. Working paper (2018)
3. Biau, G., Scornet, E.: A random forest guided tour. TEST **25**(2), 197–227 (2016). https://doi.org/10.1007/s11749-016-0481-7
4. Blanchet, J., Gallego, G., Goyal, V.: A markov chain approximation to choice modeling. Oper. Res. **64**(4), 886–905 (2016)
5. Bodea, T., Ferguson, M., Garrow, L.: Data set-choice-based revenue management: data from a major hotel chain. Manuf. Serv. Oper. Manage. **11**(2), 356–361 (2009)
6. Breiman, L.: Random forests. Mach. Learn. **45**(1), 5–32 (2001)
7. Bronnenberg, B.J., Kruger, M.W., Mela, C.F.: Database paper-the IRI marketing data set. Mark. Sci. **27**(4), 745–748 (2008)
8. Chen, Y.C., Mišić, V.V.: Decision forest: a nonparametric approach to modeling irrational choice. Working paper (2019)
9. Farias, V.F., Jagabathula, S., Shah, D.: A nonparametric approach to modeling choice with limited data. Manage. Sci. **59**(2), 305–322 (2013)
10. Feng, G., Li, X., Wang, Z.: On the relation between several discrete choice models. Oper. Res. **65**(6), 1516–1525 (2017)
11. Flores, A., Berbeglia, G., Van Hentenryck, P.: Assortment and price optimization under the two-stage LUCE model. Working paper (2017)
12. Hastie, T., Tibshirani, R., Friedman, J.: The Elements of Statistical Learning. SSS, Springer, New York (2009). https://doi.org/10.1007/978-0-387-84858-7
13. Jagabathula, S., Rusmevichientong, P.: The limit of rationality in choice modeling: formulation, computation, and implications. Manage. Sci. **65**(5), 2196–2215 (2018)
14. Liaw, A., Wiener, M.: Classification and regression by randomforest. R News **2**(3), 18–22 (2002)

15. McFadden, D.: Conditional logit analysis of qualitative choice behaviour. In: Zarembka, P. (ed.) Front. Econ., pp. 105–142. Academic Press, New York, New York, NY, USA (1973)
16. Natarajan, K., Song, M., Teo, C.P.: Persistency model and its applications in choice modeling. Manage. Sci. **55**(3), 453–469 (2009)
17. Pedregosa, F., et al.: Scikit-learn: machine learning in python. J. Mach. Learn. Res. **12**, 2825–2830 (2011)
18. Scornet, E., Biau, G., Vert, J.-P., et al.: Consistency of random forests. Ann. Stat. **43**(4), 1716–1741 (2015)
19. Simonson, I., Tversky, A.: Choice in context: tradeoff contrast and extremeness aversion. J. Mark. Res. **29**(3), 281–295 (1992)
20. Şimşek, A.S., Topaloglu, H.: An expectation-maximization algorithm to estimate the parameters of the markov chain choice model. Oper. Res. **66**(3), 748–760 (2018)
21. Train, K.E.: Discrete Choice Methods with Simulation. Cambridge University Press, Cambridge (2009)
22. Williams, H.C.: On the formation of travel demand models and economic evaluation measures of user benefit. Environ. Plan. A **9**(3), 285–344 (1977)

Prediction and Analysis of Chinese Water Resource: A System Dynamics Approach

Qi Zhou(✉), Tianyue Yang, Yangqi Jiao, and Kanglin Liu

School of Traffic and Transportation, Beijing Jiaotong University, Beijing 100044, China
18251134@bjtu.edu.cn

Abstract. The data show that the shortage and deterioration of water resources have brought serious impact on China, and these problems need to be solved. In this paper, the four causal chains of China's water resources system are constructed by comprehensively considering the factors of population, society and economic development, and the system dynamics method for forecasting China's water resources demand from 2013 to 2025 is established. Based on the analysis of the proposed water system dynamics model, the total water demand, water conservancy investment and water recycling in China under different water resources strategies are predicted. Under the water resources strategy of high investment in water conservancy facilities, low wastewater discharge rate and high wastewater purification rate, the total water demand in China in 2025 will be about 722 billion M^3, the investment in water conservancy facilities will exceed 6815 billion yuan and the recycled water will exceed 43 billion M^3. In addition to population and economic factors, we also pay attention to environmental factors. In addition, we introduce water shortage coefficient and environmental pollution coefficient to evaluate the environmental benefits of different policies. From the perspective of our sustainability model and integrated numerical results, several interesting management insights were observed. For example, by reducing the discharge of domestic and production sewage, improving the sewage purification rate and investment in water infrastructure, the water shortage coefficient will be reduced by about 8.96%, and the environmental pollution coefficient will be reduced by about 14.8%, which is conducive to promoting the future development of China's water resources, as well as the environment and economy.

Keywords: System dynamics · Prediction · Water demand · Water resources development strategy

1 Introduction

Water is an indispensable substance in creature body. The basic necessities of human life are inseparable from water. According to authoritative data, China's share of water resources has reached 6% of the world's total water resources. However, 9.6 million square kilometers of land support 1.4 billion people, which makes China's per capita share of water resources being only 2710 m^2, less than 25% of the world's per capita water resources, ranking 88th in the world. The shortage of water resources cannot meet

R. Qiu et al. (Eds.): ICSS 2021, LNOR, pp. 197–211, 2021.
https://doi.org/10.1007/978-3-030-90275-9_17

the needs of the population. The reasons for water shortage include water pollution、the low recycling utilization rate of water resources and the publicity and management of water resources are not in place. Water shortage has brought many impacts on China: flood disaster, drought disaster and soil erosion.

Specifically, first flood disaster, the accumulated direct economic loss exceeds 1.1 trillion yuan, which is about 1/5 of the fiscal revenue in the same period. Then drought disaster, due to the lack of water supply, the annual output value of industry is directly affected by 230 billion yuan. In normal and dry years, grain production is reduced by 10–25 billion kg, but in severe drought years, grain output is nearly 50 billion kg. The third one is water environment; one is soil erosion. The average annual area of soil and water loss increased by development and construction activities in China reaches 10000 km^2, and the earthwork waste accumulated every year is about 3 billion tons, 20% of which flows into rivers, which directly affects flood protection. The another one is that the water pollution is serious. Because of the rapid increase of industrial wastewater discharge, it is discharged into the river without treatment, which leads to the deterioration of water environment represented by Huaihe River and Taihu Lake pollution.

One of the national policies adopted by China is to rationally control the total amount of development. Then, optimize the allocation of water resources.

The main contributions of this research include:

1. Research Object: We forecast chinese water demand, wastewater and recycled water from 2013 to 2025, analyze implications of implementing different water strategies and identify feasible measures to conserve water.
2. Model formulation: We consider population and economic development factors, construct four significant relations of chain effect in Chinese water resources system. Based on the relations of four chains, we establish a system dynamics (SD) approach to predict water demand, recycled water and wastewater of China from 2013 to 2025. Then we introduce two indicators: water shortage coefficient and environmental pollution coefficient to evaluate the environmental benefits. After that, we adjust relevant parameters according to authoritative documents and analyze the implications of different strategies.
3. Managerial implications: The final results of predicted water demand show that the total amount of water resources development in the national management policy is in urgent need of effective control. From the perspective of system dynamics model, we suggest that the optimal water resources development strategy suitable for China is to reduce the domestic sewage and production sewage discharge, increase the sewage purification rate, and improve the investment of Chinese water conservancy facilities, so that the environmental benefits and economic benefits can be maximized.

2 Literature Review

In the aspect of water resources prediction, there are various methods of water resources prediction, such as multi-objective analysis method, multi-objective decision TOPSIS method, least squares support vector machine method, water resources supply and demand balance method, etc. In the simulation and prediction of water supply and

demand matching in water deficient cities such as Lanzhou [1], only linear and nonlinear equations were used to simulate and predict the water demand of agriculture, industry, ecology and urban and rural life in Lanzhou, then the spatiotemporal matching water shortage of Lanzhou including its districts and counties in the future period was obtained under different water supply schemes; Wang et al. [2] combined with grey correlation analysis and multiple linear regression model, quantitatively predicted the supply and demand of water resources in different planning years; Meng et al. [3] established a fractional order cumulative grey prediction model to predict the per capita water consumption of China's provinces and cities from 2019 to 2024, and found that there are great differences in the per capita water consumption of different regions; Shuang et al. [4] determined the explanatory variables related to economy, community, water use and resource availability, established 11 statistical and machine learning models, conducted interpolation and extrapolation scenarios, and predicted the water consumption in Beijing Tianjin Hebei region.

To put forward appropriate water resources policies, the multi-objective optimization model is established in the allocation of water resources, which takes the unified allocation of water quantity and water quality into account. The theory of water demand hierarchy is put forward, which can forecast the domestic water demand in the future and fine tune the urban water resource management. Zheng Zang and Xinqing Zou [5] used panel model to study the intensity evolution trend of domestic water, agricultural water, industrial water and ecological water among provinces in China. It was found that the proportion of tertiary industry, the rate of industrial wastewater standard, annual precipitation and per capita GDP had significant influence on water demand. Gao et al. [6] comprehensively considered various factors affecting the water demand in China and established the water supply and demand forecasting model by regression prediction method. The analysis shows that the most important factor affecting Chinese water demand is the GDP, and the adjustment of industrial structure has a certain influence on water demand, especially, the influence of industrial development on water consumption is higher than that of agriculture. Because of the strong control of water price by government and low price of water, water price has little influence on demand [6].

At present, the application of SD model in water resources prediction is still in its infancy. In modern circumstance, most of the water resources prediction of SD model is based on the demand and supply of industrial, agricultural and ecological water. We not only forecast the water demand from 2013 to 2025, but also predicts the future recycled water according to the established water system. In addition to the population and economic factors, we also employ the environmental factors, introduces the water shortage coefficient and environmental pollution coefficient to evaluate the environmental benefits of different policies, and puts forward some policy suggestions suitable for the sustainable development of water resources in China.

3 Problem Statement and Solution Approach

3.1 Theory and Method of System Dynamics

System dynamics can be used to analyse information feedback system, system structure and function, which has the characteristics of systematization, integrity and dynamic.

The system dynamics model can be used in time dynamic analysis considering the best goal of the whole system and it has been successfully applied to strategic analysis and management decisions of social, economic and ecological complex systems universally. Moreover, SD model has been used to deal with the problems about water resources carrying capacity, water demand prediction and water supply and demand balance analysis in some researches.

We apply the System Dynamics method to construct the social-water resources system model. By changing the relevant parameters, the model can reflect the economic, social and ecological benefits obtained under different strategies. After that this paper can make scheme comparison and selection, so as to propose the optimal water resources strategy.

3.2 System Analysis Water Resources in China

The proposed SD model starts with the interaction and mutual constraints of resources, population, economy and environment, and form a feedback system structure. The following are the main chains in the system model (Fig. 1):

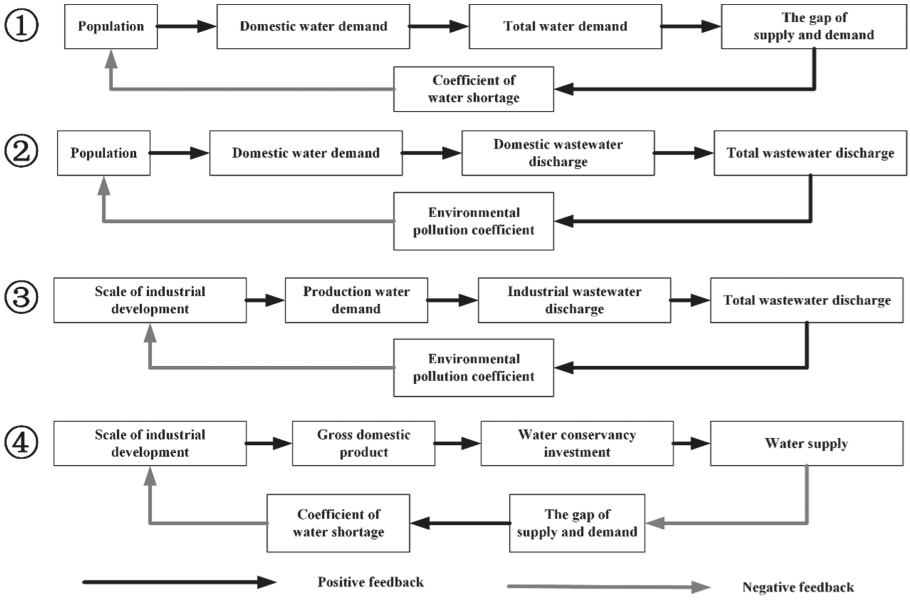

Fig. 1. Main chains in the system model

Chain ① reveals that population growth requires the consumption of water resources. With population growth, the more water resources are consumed, and when the water supply does not reach the consumption rate of water resources, it will restrict population growth and industrial development.

Chains ② and ③ indicate that water pollution restricts social and economic development. The more the population and industrial output value, the more wastewater

discharge; the more serious the pollution of the water environment, the less the total population; the more economic losses will be caused, and further affect the expansion of the industrial scale.

Chain ④ indicates the positive feedback growth of economic development and water supply, the industrial development promotes the increase of regional GDP. With the increase of water conservancy investment, the water supply will increase and the industrial scale will expand.

In addition to building the main chain, this paper also adds the dynamic variables like population growth, and build casual graph of this system (Fig. 2):

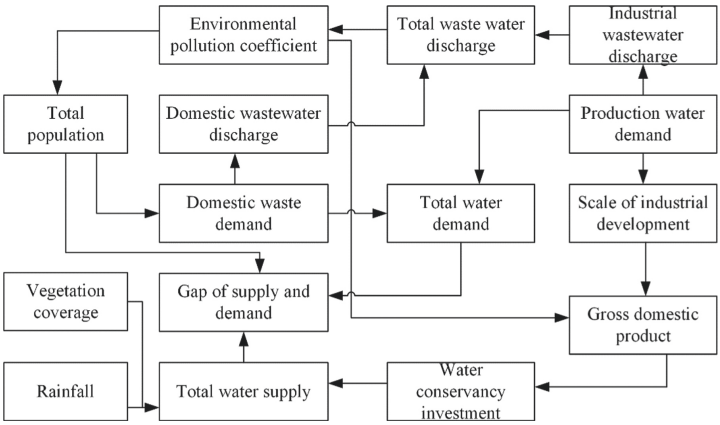

Fig. 2. Causality diagram of water SD model in China

3.3 Constructing System Dynamics Model

Based on the data of water resources supply and demand and social and economic development from 2003 to 2012, we establish a social-water resources system model by using ANYLOGIC simulation software.

Model Assumptions

1 Population growth rate is affected by water scarcity and environmental pollution;
2 The residents' water consumption per capita is a constant and it will not be affected by the change of time;
3 Through searching the literature, we suggest that the unit consumption cost of water resources has little effect on the limitation of water resources [4]. Therefore, when adjusting the parameters, the water price is fixed, so it is assumed that the cost required for the supply or production of water per cubic meter remains unchanged.
4 As the ecological water consumption only accounts for 2% of the total water consumption, the water demand is divided into domestic water and production water.

Notations

To construct a SD model, it is necessary to consider four factors: constant, stock, dynamic variable and flow equation.

In reference to the formulation of sewage discharge coefficient and recycled water coefficient in reference [5], we utilize water shortage coefficient and environmental pollution coefficient as the index of ecological benefit.

For the system, the physical quantities and meanings are as follow (Tables 1, 2, 3 and 4):

Table 1. Constant

Symbol	Definition
i	Population growth rate
P	Water consumption per capita
M	Cost of supply water per cubic metre
W_m	Water conservancy investment rate
W_r	Wastewater purification rate
Q	Domestic wastewater discharge rate
W_i	Industrial wastewater discharge rate

Table 2. Stock

Symbol	Definition
D_w	Domestic water demand
P_w	Production water demand
W_d	Domestic wastewater amount
W_p	Production wastewater amount
S	Water supply
W_t	Total wastewater discharge
D	Total water demand
R_w	Purified wastewater amount
W_c	Water conservancy investment

Table 3. Dynamic variables

Symbol	Definition
y	The year of y
N_y	Population in the year of y
G_{1y}	GDP of primary industries in the year of y
i_{1y}	GDP growth in primary industries in the year of y
G_{2y}	Secondary GDP in the year of y
i_{2y}	Growth GDP secondary industry in the year of y
G_{3y}	Tertiary GDP in the year of y
i_{3y}	Growth GDP tertiary industry in the year of y
G_y	Total GDP in the year of y
C_l	Coefficient of water shortage
C_p	Environmental pollution coefficient

Table 4. Equation

Definition	Equation
Coefficient of water shortage	$Cl = (D-S)/D$
Environmental pollution coefficient	$Cp = Wt \times (1-Rw)/S$
Domestic wastewater amount	$Wt = Wd + Wp$
Purified wastewater amount	$Rw = Wt \times Wr$
Domestic wastewater amount	$Wd = N \times Q$
Production wastewater amount	$Wp = Pw \times Wi$
The population in the year of y	$Ny = Ny_{-1} \times (1 + i \times (1-C_l) \times (1-Cp))$
The GDP in the year of y	$G_y = G_{1(y-1)} \times (1 + i_{1(y-1)} \times (1-C_l) \times (1-C_p)) + G_{2(y-1)} \times (1 + i_{2(y-1)} \times (1-C_l) \times (1-C_p)) + G_{3(y-1)} \times (1 + i_{3(y-1)} \times (1-C_l) \times (1-C_p))$

3.4 Simulation Schemes

We collect relevant data from 2003 to 2012 and take 2012 as the current year to simulate the water resources system. The end of simulation time is 2025. The initial values of the main variables are fitted with historical data and initialized.

Main initial values in the proposed SD model (Table 5):

Table 5. Initial values of the system dynamics model

Parameter	Symbol	Value
Population growth rate	i	169‰
Water consumption per capita	P	453.9 m^3
Cost of supply water per cubic metre	M	4.78 CNY
Water conservancy investment rate	W_m	5.67%
Wastewater purification rate	W_r	77%
Domestic wastewater discharge rate	Q	7.60%
Industrial waste water discharge rate	W_i	8.10%

We use ANYLOGIC to establish and simulate the proposed SD model (Fig. 3).

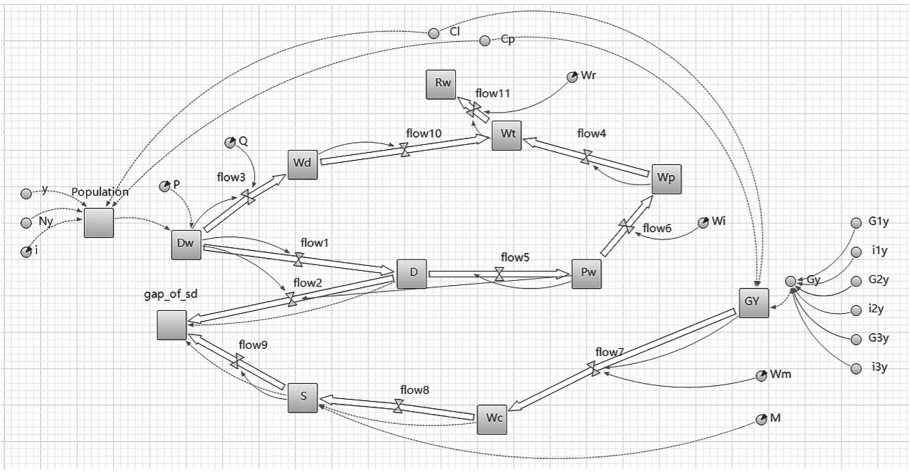

Fig. 3. System dynamics model

By adjusting the relevant parameters of the proposed SD model, we address four strategies:

First, the traditional development strategy, namely **low water investment rate, high wastewater discharge rate and low wastewater purification rate,** assumes that the model runs according to the existing initial value to analyse the supply and demand trend of water resources.

The second development strategy is **low water investment rate, low wastewater discharge rate and high wastewater purification rate.** The measures of reducing

wastewater discharge rate in production process and improving wastewater utilization rate are adopted to modify the wastewater recycled rate, industrial wastewater discharge rate and domestic wastewater discharge rate in the model, so as to analyse the change trend of water resources.

The third development strategy is high water conservancy investment rate, which is **high wastewater discharge rate and low wastewater purification rate**. By increasing the investment in water conservancy facilities, the water supply can be increased, in order to reduce the supply and demand gap of water resources in the system, and then affect the social and economic development. This paper has modified the "investment rate of water conservancy facilities" in the model to analyse the supply and demand trend of water resources.

The fourth strategy is to combine strategy 2 and strategy 3, which is **high water conservancy investment rate, low wastewater discharge rate and high wastewater purification rate**, and modify the three initial values of the model, namely, wastewater recycled rate, industrial wastewater discharge rate and water conservancy facilities investment rate, to observe the trend of water resources supply and demand in the model.

Contents of the modification and basis for the modification:

The main targets this paper modified are investment rate of water conservancy facilities, wastewater discharge rate and wastewater recovery and utilization rate.

The investment rate of water conservancy facilities is based on *the in-depth Investigation and Investment Strategy Feasibility Report of China Water Conservancy Industry Market Development in 2020–2026* published by China gold enterprise information international consulting and statistics of Ministry of water resources show that: from 2010 to 2019, the total investment in water conservancy construction in China shows a fluctuating growth trend. According to this trend, the annual growth rate of water conservancy investment in China will maintain a high level, the investment and construction of water conservancy industry will continue to increase, so this paper set the value to 80%.

The wastewater discharge rate is based on the situation of reducing untreated wastewater discharge to the environment mentioned in *The National Comprehensive Water Resources Planning (2010–2030)*. The average wastewater discharge rate from 2003 to 2012 is 7.6%. According to the contents of the comprehensive plan, this paper sets the wastewater discharge rate of 7% in 2025.

The wastewater recovery and utilization rate are based on the national wastewater discharge and reclaimed water volume target set in *The National Comprehensive Water Resources Planning (2010–2030)*, and the recycling coefficient of the reclaimed water in 2030 is estimated to be about 17%, so the recovery utilization rate in 2025 will be set at 15% (Table 6).

Table 6. Modifying table of control parameters of different strategies

Parameter	Unit	Strategy 1	Strategy 2	Strategy 3	Strategy 4
Population growth rate	‰	169	169	169	169
Water consumption per capita	m^3	453.9	453.9	453.9	453.9
Cost of supply water per cubic meter	%	5.67	5.67	5.67	5.67
Water conservancy investment rate	%	77	77	80	80
Domestic wastewater discharge rate	%	7.6	7	7.6	7
Wastewater purification rate	%	8.1	15	8.1	15

3.5 Output Results

After we input all initial data, ANYLOGIC simulate the operation of this system and output relevant index changes. The main index changes in the model simulation are shown in the Figs. 4, 5, 6, 7, 8 and 9 and the simulation results are shown in the Table 7.

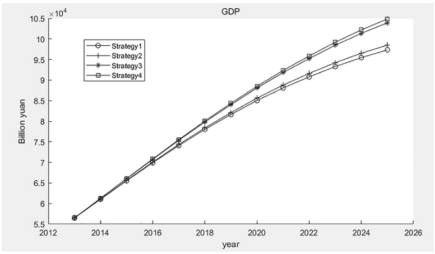

Fig. 4. GDP value from 2013 to 2025

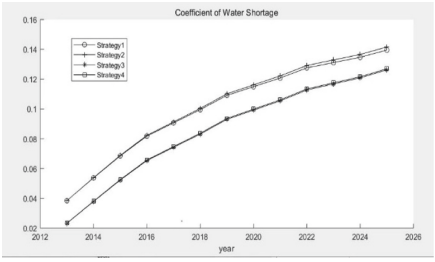

Fig. 5. Coefficient of water shortage from 2013 to 2025

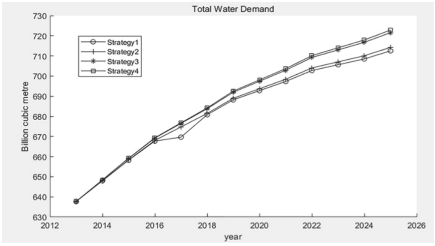

Fig. 6. Total water demand from 2013 to 2025

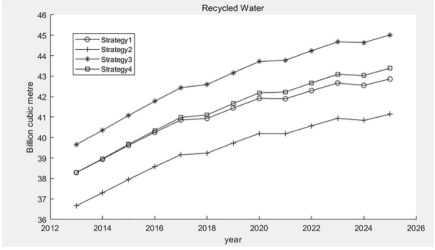

Fig. 7. The amount of recycled water from 2013 to 2025

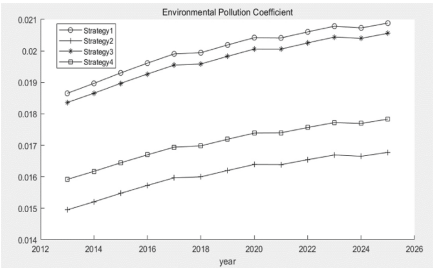

Fig. 8. Environmental pollution coefficient from 2013 to 2025

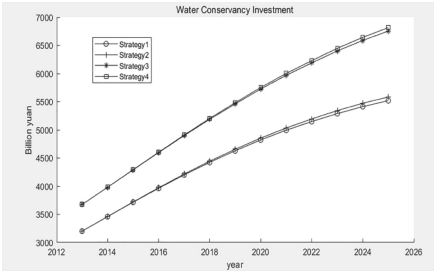

Fig. 9. Water conservancy investment from 2013 to 2025

Table 7. Comparison of China Water Resources Systems dynamics results 2025

Comparison of China Water Resources Systems dynamics results 2025				
Parameter (Unit)	Strategy1	Strategy2	Strategy3	Strategy4
The value of GDP (10^8¥)	973417.55	984978.36	1039143.00	1048594.50
Total water demand (10^8m^3)	7125.14	7142.20	7215.49	7228.59
Water conservancy investment (10^8¥)	55192.78	55848.27	67544.29	68158.64
The amount of purified wastewater (10^8m^3)	428.66	411.47	450.14	433.95
Coefficient of water shortage	0.1395	0.1416	0.1262	0.1270
Environmental pollution coefficient	0.0209	0.0168	0.0206	0.0178

3.6 Comparative Analysis

According to the research results of Cao et al. [9], the average relative error between the simulated value and the actual value of the main index can be less than 10%, so the simulation result can be considered to be effective. According to our SD model, after substituting the values, the relevant values of strategy 1 are compared with the total water demand values collected from 2013 to 2019 in China Water Resources Bulletin. We find that the prediction error of total water demand from 2013 to 2016 is less than 10%, and the result is effective. However, since 2017, the deviation of the predicted results has exceeded 10%. We think that this is related to the relevant water-saving policies implemented in China. Strategy 1 in our model is an original state, that is, the calculated value is the predicted value not regulated by policies. For strategy 2, 3 and 4, we only use the strategy to be executed in the future to adjust the parameters, but the actual situation is more complex. The actual value will be affected by many water-saving measures implemented by the Chinese government (Table 8).

For example, in 2016, in terms of domestic water saving, some areas implemented step-by-step water prices for households and raised water prices for non residents; In

Table 8. Comparison of actual water consumption and predicted total demand

Comparison of actual water consumption and predicted total demand					
Year	Actual water consumption	Total water demand of strategy 1 ($10^8 m^3$)	Relative error	Total water demand of strategy 4 ($10^8 m^3$)	Relative error
2013	6183.4	6376.383132	0.03120987	6378.120622	0.031490866
2014	6095	6479.235214	0.06304105	6484.468453	0.063899664
2015	6103.2	6581.843096	0.07842494	6592.234551	0.080127564
2016	6040.2	6677.180372	0.10545683	6694.190304	0.108272955
2017	6043.4	6742.851601	0.11573809	6768.276004	0.119945065
2018	6015.5	6808.522829	0.13182991	6842.361705	0.137455192
2019	6021.2	6881.944505	0.14295232	6925.366375	0.150163817

2017, the three departments issued the Water Saving Society Construction of "the 13th five year" Plan, vigorously promote water-saving policy; In 2018, China's national development and Reform Commission and the Ministry of water resources jointly issued the National Water Saving Action Plan, focusing on "double control of total amount and intensity", "agricultural water saving and efficiency", "industrial water saving and emission reduction", "urban water saving and loss reduction", "water saving and open source in key areas" and "scientific and technological innovation leading". After the implementation of these policies, the total amount of water use in China has been effectively controlled, the overall water use structure has been gradually adjusted, and the overall water use efficiency has reached the world average level. According to the statistics of China economic network, in 2019, the national water consumption of 10000 yuan GDP and 10000 yuan industrial added value decreased by 24% and 28% respectively compared with 2015, and the effective utilization coefficient of farmland irrigation water reached 0.559.

Among all the water-saving policies, advanced wastewater treatment process; speeding up the construction of water conservancy in grasslands and pastoral areas, and developing water-saving irrigation agriculture; continuing to promote water-saving water supply major water conservancy project construction and other important suggestions and measures are coincide with our management suggestions from SD model, which shows that our model, to a certain extent, can put forward management suggestions for the actual situation, which has reference value.

4 Numerical Results

Compared with strategy 1, the wastewater discharge rate of strategy 2 decreased from 7.6% to 7%, and the wastewater purification rate increased from 8.1% to 15%. As a result, the environmental pollution coefficient decreased by 19.6%, indicating that

limiting the wastewater discharge rate and increasing the purification rate can reduce the environmental pollution coefficient and alleviate water pollution.

Compared with strategy 1, strategy 3 increased the investment rate of water conservancy facilities to 80%, increased the water supply, and reduced the water shortage coefficient by 9.5%, which can alleviate the shortage of water resources, but the environmental pollution coefficient is only reduced by 1.4%, which is still greater than 0.02, and the serious problem of environmental pollution still exists.

Strategy 4 combines the advantages of strategy 2 and strategy 3. Compared with strategy 1, under strategy 4, the water shortage coefficient decreased from 0.1395 to 0.1270, a decrease of 8.96%, and the environmental pollution coefficient decreased from 0.0209 to 0.0178, a decrease of 14.8%. It can not only alleviate the shortage of water resources, but also reduce environmental pollution, while maintaining the trend of economic growth. In addition, our results are similar to those predicted by Gao Jun et al.

From the results of the SD model, we conclude that adjusting the sewage discharge rate and sewage utilization rate can help solve the problem of environmental pollution. Raising the investment amount of water conservancy facilities can alleviate the shortage of water resources.

Moreover, we evaluate different strategies according to three aspects: economic benefit, ecological benefit and water utilization efficiency. From the perspective of economic benefit, strategy 4 can create the highest GDP, followed by strategy 3; from the perspective of ecological benefit, strategy 3 has the highest sewage treatment capacity, followed by strategy 4; in terms of water utilization efficiency, although the total water demand of strategy 3 and strategy 4 is higher than that of strategy 1 and strategy 2, the water shortage coefficient of strategy 3 and strategy 4 is lower than that of strategy 1 and strategy 2. This illustrates that strategy 3 and strategy 4 can alleviate the situation of water shortage.

After analysing the results of different strategies with this proposed SD model, we propose that: to maximize the environmental benefits, water utilization benefits and economic benefits, the suitable measures for Chinese government to take are reducing the discharge of domestic sewage and production sewage, improving the sewage purification rate and increasing the investment rate of Chinese water conservancy facilities.

5 Conclusion

Taking China as the research object, this paper constructs a sustainable development model of water resources based on China's population, economy and environment. We collected relevant data from 2003 to 2012, and changed the parameters of the proposed sustainable development model according to relevant policies, so as to predict China's total water demand, water conservancy investment and water recycling under different water resources strategies. Among them, under the water resources strategy of high investment in water conservancy facilities, low waste water discharge rate and high waste water purification rate, the total water demand of China in 2025 is about 722 billion M^3, the investment in water conservancy facilities will exceed 6815 billion yuan and the recycled water will exceed 43 billion M^3. From the perspective of maximizing

social and environmental benefits, we put forward measures to ensure the sustainable development of water resources: although the contradiction between supply and demand of water resources will still exist in the next 13 years, the water shortage coefficient can be reduced to 0.1270 and the environmental pollution coefficient can be reduced to 0.0178 by increasing the investment rate of water conservancy, improving the recovery rate of wastewater and reducing the direct discharge rate of wastewater, so that the contradiction of water resources can be alleviated.

The interaction and restriction of each subject in the system can be taken into account in terms of the proposed SD model. By utilizing the model with ANYLOGIC, we dynamically analyse the complex social water resources system and intuitively compare various managerial implications.

However, the proposed SD model has some shortcomings. It does not take the impact of major accidents on the population growth rate into account, such as epidemics. Additionally, in terms of water demand, we simply divide it into domestic water and production water, without considering public and ecological water.

Although SD model has a certain degree of reference value, it is still only a simplified analysis of the complex system of water resources in China. In the future, more important factors need to be considered, such as overseas allocation of water resources, water demand of ecological environment, consumption of surface water and groundwater. Besides single factor analysis, it also needs to consider the comprehensive effects of various factors, and then, further explore the complex system of water resources in China. In the future, we will try to combine GIS technology with the proposed sustainable development model, and extend it to other geographical scales, such as urban agglomerations and basins with different levels of water resources development.

Acknowledgements. This research is partly supported by the fellowship of China Postdoctoral Science Foundation (grant number 2021M690009) and the Fundamental Research Funds for the Central Universities (grant numbers 2021RC202).

References

1. Wang, M., Yin, S., Lu, L.: Simulation and prediction of water resources supply and demand matching in water deficient cities: a case study of Lanzhou city in Gansu province. Econ. Geogr. **40**(02), 92–99 (2020)
2. Wang, G., Xiao, C., Qi, Z., Liang, X., Meng, F., Sun, Y.: Water resource carrying capacity based on water demand prediction in Chang-Ji economic circle. Water **13**, 16 (2021)
3. Meng, X., Wu, L.: Prediction of per capita water consumption for 31 regions in China. Environ. Sci. Pollut. Res. **28**(23), 29253–29264 (2021). https://doi.org/10.1007/s11356-021-12368-0
4. Shuang, Q., Zhao, R.T.: Water demand prediction using machine learning methods: a case study of the Beijing–Tianjin–Hebei region in China. Water **13**, 310 (2021)
5. Zheng, Z., Xinqing, Z.: Test of convergence characteristics of Chinese mainland water resources intensity: an empirical study based on interprovincial panel data. J. Nat. Resour. **31**(06), 920–935 (2016)
6. Jun, G., Na, Z., Qisheng, G.: Water supply and demand model and forecast in China. Stat. Decis. **18**, 85–87 (2014)

7. Wang, W., Zhang, L., Wang, Z.: Analysis of secondary supply and demand balance of regional water resources based on system dynamics. S. N. Water Diversion Water Conservancy Sci. Technol. **12**(01), 47–49 + 81 (2014)
8. Honggang, Q., Yang Ning, C., Huimin, L., et al.: Analysis of water resources based on SD model in Yanqi county, Xinjiang. Quatern. Res. **30**(1), 209–215 (2010)
9. Qiwen, C., Bao Chao, G., Chaolin, G.W.: SD model and Simulation of urbanization in China based on water resource constraint. Geogr. Res. **38**(01), 167–180 (2019)
10. Zhou, S.L., McMahon, T.A., Walton, A., Lewis, J.: Forecasting daily urban water demand: a case study of Melbourne. J. Hydrol. **236**(3–4), 153–164 (2000). https://doi.org/10.1016/S0022-1694(00)00287-0
11. Liu, C., Liao, H., Xiong, X., Huang, D.: A review of U.S. water resources management research and its enlightenment to China. Future Dev. **34**(06), 45–49 (2011)
12. Gao Qisheng, L.: Analysis on long-term demand forecast and regional difference of water resources in China. Resour. Environ. AridAreas **30**(01), 90–94 (2016)
13. Taizheng, C., Jingwei, H., Jun, C.: Advances in quantitative re-search on optimal allocation of water resources in China resource. Science **35**(01), 132–139 (2013)
14. Li, J.: A study on the optimal utilization of water resources in the process of urbanization in Dongting lake area (2013)
15. Wang, L.: Mathematical model for comprehensive evaluation of sustainable development and utilization of water resources (2004)
16. Qian, Z.: Comprehensive report on China's sustainable development of water resources strategy. In: Proceedings of the 2001 Annual Meeting of the Chinese Society of Water Resources (2001)

Pricing and Strategies in Queuing Perspective Based on Prospect Theory

Yanyan Liu[1], Jian Liu[1(✉)], and Chuanmin Mi[2]

[1] School of Economics and Management, Nanjing University of Science and Technology, Nanjing 210094, Jiangsu, China
jianlau@njust.edu.cn

[2] School of Economics and Management, Nanjing University of Aeronautics and Astronautics, Nanjing 211106, Jiangsu, China

Abstract. Due to customers' heterogeneity, enterprises/service providers usually adopt a service classification for different customers. However, service classification will result in a redistribution of waiting time, reducing wait time for priority customers by increasing wait time for regular customers. In this way, customers will form a psychological utility by comparing the expected waiting time between different queues. In this paper, we study a traditional non-preemptive M/M/1 queuing system in which incorporate customer preferences (loss aversion and gain seeking) will generate a psychological utility, which leads to the switch of customers and further impacts the revenue. In our paper, we analyze the monopoly queuing system in which customers can't go away freely, and study it from three perspectives: revenue, social welfare, and customer utility. Firstly, we find that from the perspective of revenue maximization, enterprises should choose visual queue for queue classification. Next, enterprises should adopt unobservable queues for service classifications from social welfare maximization. Then, from customer utility maximization, enterprises should cancel service classification and keep regular customers only. Our results not only reaffirm existing research on the benefits of offering differentiated service and pricing by the service providers but also challenge some commonly accepted practices.

Keywords: Queuing · Service classification · Prospect theory · Objective optimization · Strategy and pricing

1 Introduction

The researches on queuing are very significant in improving the quality of service. Queuing involves Internet networks, healthcare, amusement parks, bank queuing service, vehicle routing arrangement, tourism management, etc. When the service system's capacity is limited, and customers' demands are high, enterprises should enhance capacity. Otherwise, if the capacity cannot be increased, queuing is inevitable. Service providers should effectively distinguish customer heterogeneity and adopt service classification to reduce waiting costs and improve queuing efficiency and customer satisfaction due to customer heterogeneity.

R. Qiu et al. (Eds.): ICSS 2021, LNOR, pp. 212–226, 2021.
https://doi.org/10.1007/978-3-030-90275-9_18

These literatures [1–4] focus on the $c\mu$ rule and $Gc\mu$ rule and point out that from the perspective of minimizing waiting costs, enterprises should prioritize customers with high waiting costs and set different levels of priorities for customers corresponding to their waiting costs. However, these researches have not considered the customer behaviour caused by their psychological changes in the queuing process, resulting in customers' switch and further influencing the revenue.

Customers who seek service assess three attributes of the service system: the service reward, the payment, and the expected waiting time. Although numerous factors affect customer queuing behaviour, in this paper, we focus on the expected waiting time and assume that customers will form a reference point for waiting time before entering the service system. We also assume that people make their decisions about whether to upgrade beforehand. For instance, customers need to decide which ticket (e.g., VIP or regular) to purchase before entering an amusement park or a museum. Therefore, they will decide based on historical information regarding the service system's expected waiting time.

Besides, one particular example that drove the research is the Express Pass of Universal Studios, which permits holders to bypass the regular lines (which could be hours long during peak time) but could cost twice as much as a regular entrance fee. This seems reasonable to use the park's limited resources better because the park can generate extra revenue from customers who prefer to spend more and want to wait less in line. Even though regular customers choose not to pay the priority fee, they may still experience resentment and boredom due to perceived unfairness and time loss (as reflected in some of the negative online reviews of Universal's Express Pass). Such concerns and complaints about the priority service are expected because they inherently result in a redistribution of waiting time from higher-priority customers to lower-priority customers. Customer segmentation will cause differences in waiting times between different queues, and customers may have behavioral preferences that may impact the queuing design [5].

In our paper, we study customer preference [6, 7] based on prospect theory, loss aversion and gain seeking. It was found [8] that a long wait time would cause harm to customers in the regular queue, while a short wait would have a positive impact on customers in the priority queue. Based on this research, we assume that customers will form a reference point of waiting time before entering the service system. If the customer waiting time is shorter than the reference waiting time, they will be pleased due to their gain-seeking preference, and the service utility will thus be enhanced (utility of positive psychology). In contrast, if customers' waiting time is longer than the preference waiting time, they will be impatient due to their loss-aversion preference, and their service utility will decrease (utility of negative psychology).

The existing literature on customer behaviors in queuing problems mainly focuses on customers' psychological impatience with high waiting costs [9, 10] and offers priority service. However, they have not considered customers' psychological behaviors after they get priority service. Meanwhile, there is not enough attention to the psychological of regular customers who seem to be in "vulnerable groups" in the queuing process.

This paper proposes the optimal service strategy (a queuing mechanism) and the corresponding optimal service pricing (priority fee) based on different optimization objectives incorporating customers' loss aversion and gain-seeking in an M/M/1 queuing system.

This paper will focus on addressing the following two questions: (1) How do the preferences work in queuing? (2) What are the implications of the preferences for queue design, pricing, revenue, social welfare, and customers' utility? To that end, the paper studies the monopoly service system in which customers cannot abandon the system (e.g., VISA application, etc.); thus, customers just have two options: regular or priority, and displays psychological changes by setting customer preference parameters. In some situations, enterprises set the VIP service windows and the regular service windows at the positions where they can see each other in our daily life (e.g., boarding gate, Banks, etc.). Comparatively, sometimes enterprises set the VIP service windows and the regular service windows at positions where they cannot see each other (e.g., Internet call center, etc.). The visualization and comparison in the service process for different types of customers will further stimulate customer's psychological changes (Norman, 2009). In this paper, the setting of service windows under different circumstances is analyzed; we find the setting of distance between service windows for different types of customers will also affect enterprise revenue and social welfare changes.

This paper's innovation: By introducing customers' gain-seeking and loss-aversion preference parameters, we want to establish the utility models for priority and regular customers. Then, we build the corresponding models of the priority service pricing, enterprise revenue, social welfare, overall customer utility and then optimize these objectives. The study suggests that enterprises should adopt visual queues to classify services from the perspective of revenue. Obviously, with the increase of preference parameters, more customers will choose to prioritize by paying a higher priority service fee if they feel unhappy in the regular queue or want to obtain gain-seeking preference in the priority queue. From the perspective of social welfare, enterprises should adopt unobservable queues for service classifications due to the social welfare decreasing with the loss aversion parameter in the system. Lastly, from the perspective of utility, enterprises should eliminate queue classification and adopt the strategy of retaining only regular customers.

This paper's central architecture: first, we describe the utility model of customers in the scenario where customers have two kinds of preferences. On this basis, we build the function of the priority service pricing and the function of enterprise revenue. Next, we optimize the functions of enterprise revenue, social welfare, and overall customer utility. We analyze these optimal solutions for the above three objectives and extract the corresponding service strategies and insights. We then compare the optimal solutions of these above three optimized objectives with the optimal solutions under the condition where customers' preferences are not considered. Finally, we summarize the main contributions of this study and point out further research.

2 The Literature Review

Two kinds of directions are involved with this research on the service system: Customer classification and Customer Preferences. Next, we will carry out the relevant literature review from the above two aspects, respectively.

Smit first suggested optimizing the $c\mu$ rule (the highest index $\mu_k(t)c_k(t)$ first) to minimize waiting cost in a deterministic and static environment [11]. Cox and Smith proved that the $c\mu$ rule was also optimal in a stochastic and dynamic environment with an arbitrary time horizon [12]. Mandelbaum and Stolyar developed the generalized $c\mu$ ($Gc\mu$) rule minimizing both instantaneous and cumulative queuing costs [13]. Che further showed that the $c\mu$ rule was not necessary for revenue maximization [14]. Huang et al. considered two types of patients (right after triage and in-progress) with congestion costs; at the same time, in-progress patients served by the $Gc\mu$ rule and μ were modified to explain feedback for in-progress patients [15]. Bassamboo and Randhawa believed that customers became differentiated as time progressed and made efforts to investigate the optimal scheduling policies that differentiate between customers to minimize the performance metrics [9].

Optimal Priority strategies in unobservable queues with convex delay costs were considered [16]. Adiri and Yechiali proposed an optimal priority-purchasing strategy, which is of control limit type [17]. Alperstein made an effort to determine the optimal number of priority classes and prices to create higher revenue and show all priorities' control limits [18]. Wang and Baron analyzed the M/M/c queue with two priority classes with preemptive rule and focused on low-priority performance [10]. Yang et al. studied the optimal time trading strategies of priority auction, which is good for the social planner by improving system efficiency and the service provider by enhancing revenue [19].

Customers' Preferences on Waiting Time: Zohar and Shimkin characterized a model that customers' patience depends on the anticipated mean waiting time [20]. This literature investigated how informed anticipated delays affect customers' choice (balk or renege) [21]. Yang et al. first researched customers' service pricing, considering customers' loss aversion behavior but failed to consider the corresponding changes of waiting time caused by the customer flow, which was influenced by customers' preference behavior [22]. The literature [23, 24] studied customers who are sensitive to time, and their preferences on price and lead-time influence optimal strategies for different aims. Hedayati et al. point if flows have equal weight, the device's allocation is fair if equal bandwidth is allocated to each (backlogged) flow in every time interval [25].

Impatience of Customers: Movaghar studied the general customer impatience and mainly concerned customers' impatience measured by the deadline until the beginning of service [26]. Garnet et al. analyzed the simplest abandonment model, with customers' patience being exponentially distributed more practically for call centers [27]. Armony et al. studied the unobservable queue where customers cannot realize the total numbers of customers in the system; their impatience would determine their balking or reneging [28]. Moyal considered customers' impatience by a stochastic recursive sequence and derived their patient times while waiting [29]. Batt and Terwiesch provided evidence for queue length, and observable queue flow would influence customer abandonment [30]. Finally, Ibrahim et al. studied how the uncertainty of delay announcement (e.g., the LES announcement policy) influences customers' patience in call centers [31].

Different from previous studies, this paper considers loss-aversion and gain-seeking in a service system by comparing customer waiting time and reference waiting time. This is motivated by the observations and studies in [8, 32].

3 The Model Setup

In practice, Nazerzadeh and Randhawa proposed that segmenting customers with heterogeneous waiting costs into two types or infinite types would bring identical revenue [33]. Therefore, in this paper, we study customer segmentation only based on two types of customers (priority and regular), which are also most commonly studied in the literature [34] and observed in practice.

We model the service provider as a single-server queue. Customers can self-select based on the priority fee structure, allowing the service provider to make extra revenue from priority fees. This section assumes that customers enter the service system with the arrival rate λ and the service rate is μ. Enterprises charge each customer who enters the system a fixed fee c. If the customer chose to pay an extra priority service fee K, he (she) would join the "special group," which is given a priority. It means customers who pay the overall fee $K + c$ earn a priority relative to customers who only offer the fixed fee c (This paper assumes the service progress cannot be interrupted (non-preemptive)). The priority setting for a service system reduces the priority customers' waiting time W_1 by increasing the regular customers' waiting time W_2. ($W_2 \geq W_1$).

Norman proposes that customers have negative feelings due to having to wait longer than expected [32]. Customer segmentation involves a reset of the waiting time by increasing regular customers' waiting time to reduce the priority customers' waiting time. Clearly, the high priority service will bring negative emotions among regular customers since their waiting time becomes longer than before when the service providers did not introduce the customer segmentation and kept only one queue in the system. In our paper, we adopt the expected waiting time W in a FCFS (First come, First served) queuing system as the reference waiting time of customers, which is also the waiting time when the service providers cancel the customer classification and keep only one queue in queuing. Obviously, when service providers introduce customer segmentation, the regular customers' waiting time (low-priority) denoted as W_2 exceeds the expected waiting time W (i.e., $W_2 \geq W$) in a FCFS queuing system. As a result, the negative psychological utility will generate for regular customers due to the loss-aversion preference [22]. However, the priority customers' expected waiting time is less than the reference waiting time (i.e., $W \geq W_1$), their utility increases because of gain-seeking psychology [8].

This paper denotes the loss aversion and gain-seeking psychology by parameters α and β, respectively. It is obvious $\alpha \geq 0$, $\beta \geq 0$. Based on the above principle and the contrasts of customers' waiting time in the queuing with the expectation of waiting time, and the preferences for loss aversion and gain-seeking, this paper uses the gap between the regular customers' expected waiting time and the reference waiting time $W_2 - W$, and loss-aversion parameter α to express the negative utility $\alpha(W_2 - W)$ caused by the loss aversion psychology of regular customers. Relatively, we use the gap between the priority customers' expected waiting time and the reference waiting time $W - W_1$, and gain-seeking parameter β to express the positive utility $\beta(W - W_1)$ caused by the gain-seeking psychology of priority customers.

Therefore, customers have identical loss aversion parameter α, the larger the gap of $W_2 - W$, the larger the negative utility. When the gap is unchangeable, the negative utility

will be more extensive if the loss aversion is larger. If customers exist identical gain-seeking parameter β, the larger the gap of $W - W_1$, the larger the positive utility. When the gap of $W - W_1$ is unchangeable, the positive utility will be larger if the gain-seeking is larger.

3.1 The Utility Model

We assume that each customer who enters the service system can obtain a service utility R'. Each customer pays a fee of c or $K + c$ when they enter the service system, and their corresponding waiting time is W_2 or W_1 respectively. We assume customers' unit waiting costs is H. Due to the high complexity of the analysis on customer waiting costs, this paper did not focus on research on the distribution function of unit waiting costs for customers and further suppose that unit waiting costs H obeys the uniform distribution [35] in the interval $G([\underline{h}, \overline{h}])$(assume $\underline{h} = 0$ and normalize $\overline{h} = 1$). Thus, the utility function of priority customers and regular customers are as below,

$$\{U_1 = R' - K - H \cdot W_1 + \beta(W - W_1) - c;\ U_2 = R' - H \cdot W_2 - \alpha(W_2 - W) - c(\alpha \geq 0; \beta \geq 0) \tag{1}$$

Here, the differences between existing literature and this paper are that regular customers' utility $U_2 \neq R' - H \cdot W_2 - c$ and the utility of priority customers $U_1 \neq R' - K - H \cdot W_1 - c$ [34]. This is because the paper considers the negative utility caused by regular customers' loss aversion and the positive utility of priority customers' gain-seeking.

For a monopoly queue system [36], priority customers' expected waiting time W_1, and regular customers' waiting time W_2 can be expressed as follows,

$$\{W_1 = \rho/\mu(1 - \rho\theta);\ W_2 = \rho/\mu(1 - \rho)(1 - \rho\theta) \tag{2}$$

Canceling the customer segmentation and keeping an FCFS queue in the system will obtain the expected waiting time W in the monopoly queue system (i.e., equilibrium reference waiting time) as follows [36]:

$$W = \theta W_1 + \xi W_2 = \rho/\mu(1 - \rho) \tag{3}$$

Among them, θ is the ratio of customers who join the priority queue, where $\rho = \lambda/\mu$ is the offered load of service system. In this paper, we only study the condition of $0 < \rho < 1$.

If enterprises adopt the FCFS policy and cancel the customer segmentation, there has $W_2 = W_1 = W$, then the customers' references do not work, and the psychological utility will disappear in queuing (i.e., $\alpha(W_2 - W) = \beta(W - W_1) = 0$).

In our model, we only have information about the expected wait time. Because we suppose that customers decide which queue to join before entering the system. For example, when deciding whether to enter the system, customers can browse the website (https://touringplans.com/), access to the BBS and ask a friend to explore queuing time history information. Recall that customers at Universal Studios had to pay for express passes before entering the park. Although the customer's personal experience of psychological negative utility or positive utility problem was stronger, the perceptions of

waiting time occurred after he had decided whether to purchase the Express Pass. In our paper, we don't model customers as having a priori belief of dynamic renewal after each service encounter. On this basis, we will construct the corresponding new utility model in the next section, involving the psychological utility of customers.

3.2 The Priority Service Fee and Revenue Management

Customers enter a monopoly queue system (i.e., customers cannot abandon system freely), whether choosing to join the regular queue or the priority queue depends on the overall expected utility for these two service types.

When customers enter the monopoly system, they just have two options: priority or regular. The utility for these two kinds of customers should satisfy $U_1 \geq U_2$ if customers choose priority queue.

The priority service fee $K(\theta)_{(\alpha,\beta)}$ for customers entering the priority queue and the ratio of priority customers θ, loss aversion preference parameter α and gain-seeking preference parameter β is shown in Eq. (4)

$$K(\theta)_{(\alpha,\beta)} = \left(\rho^2 \Big/ \mu(1-\rho)(1-\theta\rho)\right)((1+\beta)(1-\theta)+\alpha\theta)\,(0 \leq \theta \leq 1) \quad (4)$$

We assume that $R(\theta)_{(\alpha,\beta)}$ denotes the enterprise revenue, the function relation between enterprise revenue $R(\theta)_{(\alpha,\beta)}$ and the ratio of priority customers θ, loss aversion preference parameter α and gain-seeking preference parameter β is shown in Eq. (5)

$$R(\theta)_{(\alpha,\beta)} = \left(\rho^3\theta \Big/ (1-\rho)(1-\theta\rho)\right)((1+\beta)(1-\theta)+\alpha\theta)+\lambda c\,(0 \leq \theta \leq 1) \quad (5)$$

4 Objective Optimization and Insights Analysis

4.1 Revenue Maximization

We optimize the function of revenue $R(\theta)_{(\alpha,\beta)}$, subject to $0 \leq \theta \leq 1$, the corresponding optimal solutions are shown below.

Lemma 1: If $0 < \alpha < (1-\rho)(1+\beta)\big/(2-\rho)$, the optimal ratio of priority customers in the queueing system, the corresponding optimal priority fee, and the optimal revenue of service provider are as follows

$$\begin{cases} \theta^*_{(\alpha,\beta)(R)} = \left(1-\sqrt{1-(1+\beta)\rho\big/(1+\beta-\alpha)}\right)\Big/\rho \\ K(\theta^*)_{(\alpha,\beta)(R)} = \left(\rho\big/\mu(1-\rho)\right)\left((1+\beta-\alpha)-\sqrt{(1+\beta-\alpha)^2-\rho(1+\beta)(1+\beta-\alpha)}\right) \\ R(\theta^*)_{(\alpha,\beta)} = \left(\rho((1+\beta-\alpha)-\sqrt{(1+\beta-\alpha)^2-(1+\beta-\alpha)(1+\beta)\rho})^2\big/(1-\rho)(1+\beta-\alpha)\right)+\lambda c \end{cases} \quad (6)$$

When there are two kinds of queues (e.g., regular queue and priority queue) in the system, the optimal ratio of priority customer $\theta^*_{(\alpha,\beta)}$ decreases with β, however, increases with α. The optimal priority service fee for the classification of service $K(\theta^*)_{(\alpha,\beta)}$ increases with α and β respectively. Meanwhile, the maximum revenue $R(\theta^*)_{(\alpha,\beta)}$ also increases with the parameters α and β, respectively.

Therefore, the enterprise should stimulate the priority customers' gain-seeking parameter and the regular customers' loss aversion parameter to get more revenue. Obviously, with the increase of loss aversion for regular customers, more customers will prefer to enter the priority queue for service (increase the ratio of priority customers and enhance the priority service pricing for service classification to improve the revenue). With the increase of gain-seeking for priority customers, enterprises should reduce the ratio of priority customers and enhance the priority fee to improve enterprise revenue.

Lemma 2: If $\alpha \geq (1-\rho)(1+\beta)\big/(2-\rho)$, the optimal solutions are as follows:

$$\left\{\theta^*_{(\alpha,\beta)(R)} = 1; K(1)_{(\alpha,\beta)} = \alpha\left(\rho^2\Big/\mu(1-\rho)^2\right); R(1)_{(\alpha,\beta)} = \alpha\rho^3\Big/(1-\rho)^2 + \lambda c\right. \tag{7}$$

Obviously, with the increase of loss aversion parameter, all customers in the system will join the priority queue. When there is only one queue (all customers join the priority queue), the gain-seeking parameter β of priority customers does not affect the queuing (because the priority customers' expected waiting time is identical to the reference waiting time, i.e., $W_1 = W$). In this way, the revenue is only related to the loss aversion parameter α. Both the optimal priority service fee for the classification of service $K(\theta^*)_{(\alpha,\beta)}$ and the maximum value of enterprise revenue increase with the increase of α. Similarly, the enterprises should further increase regular customers' loss aversion preference parameter α and priority customers' gain-seeking preference parameter β to get more revenue.

Lemma 3: If the enterprises cancel the classification of service (i.e., $\theta = 0$) and only retain regular customers in the system. In this way, there is just one type of customer, and then the queue system transfers into FCFS (i.e., $W_2 = W = W_1$). Then, we will get $\alpha(W_2 - W) = \beta(W - W_1) = 0$, which means that the psychological parameters do not work in the queuing.

Thus, the maximum value of enterprise revenue is $R(0)_{(\alpha,\beta)} = \lambda c$ under this condition.

Combined with the above three Lemmas and further derive the following conclusion and management insight.

Management Insight 1: From the perspective of revenue maximization, enterprises should adopt the classification of service. Because the revenue increases with the loss aversion and gain-seeking, enterprises should set the service windows of the priority queue and regular queue at the positions where they can see and perceive each other (Observable queues). Stimulate and increase customers' loss aversion parameter and gain-seeking parameter by the direct perception and contrast, and further enhance the priority service fee to obtain more revenue.

The main work of this section can be attributed to Table 1.

Table 1. The optimal service strategy and pricing based on revenue maximization

Customers' preference	$0 < \alpha < (1-\rho)(1+\beta)/(2-\rho)$	$\alpha \geq (1-\rho)(1+\beta)/(2-\rho)$
Optimal strategy	Classification of service (Observable)	Classification of service (Observable)
System design	Two active queues	Priority queue only
Optimal priority fee	$K^* = \frac{\rho((1+\beta-\alpha)-\sqrt{(1+\beta-\alpha)^2-\rho(1+\beta)(1+\beta-\alpha)})}{\mu(1-\rho)} > 0$	$K^* = \frac{\rho^2}{\mu(1-\rho)^2}\alpha > 0$

4.2 Social Welfare Maximization

When the enterprises offer a service classification to customers, and the ratio of priority customers in the queue system is θ. Thus, customers whose waiting time costs satisfy $H \geq \overline{h}(1-\theta) = (1-\theta)$ will join the priority queue and customers whose waiting time costs satisfy $H \leq \overline{h}(1-\theta) = (1-\theta)$ will join the regular queue. The social welfare produced by the service system includes two aspects, revenue of service provider, and customers' utility.

Therefore, the function of social welfare is as follows,

$$SW(\theta)_{(\alpha,\beta)} = R(\theta)_{(\alpha,\beta)} + U(\theta)_{(\alpha,\beta)} = R(\theta)_{(\alpha,\beta)} + \lambda \int_0^{(1-\theta)} U_2(H)dH + \lambda \int_{(1-\theta)}^{1} U_1(H)dH \tag{8}$$

Thus, we can further derive the function of social welfare in Eq. (9),

$$SW(\theta)_{(\alpha,\beta)} = \lambda R' + \lambda W\left(\left(\theta^2(2\alpha-2\beta-1)\rho - 2\rho\theta(\alpha-\beta-1) - 1\right)\Big/2(1-\theta\rho)\right) \tag{9}$$

Maximize the social welfare function of $SW(\theta)_{(\alpha,\beta)}$, subject to $0 \leq \theta \leq 1$, and the corresponding optimal solutions are as follows.

Lemma 4: If $\alpha < 0.5 + \beta$, the optimal ratio of priority customers in the queueing system, the optimal priority fee, and the optimal social welfare of the queuing system are as below

$$\begin{cases} \theta^*_{(\alpha,\beta)(SW)} = (1-\sqrt{1-\rho})/\rho \\ K(\theta^*)_{(\alpha,\beta)} = \rho^2((1+\beta) - (1+\beta-\alpha)(1-\sqrt{1-\rho})/\rho)\Big/(\mu(1-\rho)\sqrt{1-\rho}) \\ SW(\theta^*)_{(\alpha,\beta)} = \lambda R' + \lambda([(2\beta+1-2\alpha)(1-\sqrt{1-\rho})/\rho)(1-\sqrt{1-\rho}) - \sqrt{1-\rho}]/2\sqrt{1-\rho})W \end{cases} \tag{10}$$

If the social welfare becomes maximized and there are two kinds of queues in the queue system, the optimal priority service fee for classification of service $K(\theta^*)_{(\alpha,\beta)}$ increases with the parameters α and β. The maximum social welfare $SW(\theta^*)_{(\alpha,\beta)}$ increases with parameter β, however, decreases with parameter α.

Thereby, enterprises should further enhance the priority customers' gain-seeking parameter and reduce the regular customers' loss aversion parameter (i.e., enterprises should enhance customers' service experience, reduce the dissatisfaction of regular customers, and improve satisfaction for priority customers) to seek for more massive social welfare.

Lemma 5: If $\alpha \geq \beta + 0.5$, the optimal ratio of priority customers, the optimal priority fee, and the optimal social welfare of the system are as below

$$\left\{\theta^*_{(\alpha,\beta)(SW)} = 1;\ K(1)_{(\alpha,\beta)(SW)} = \alpha\rho^2 \Big/ \mu(1-\rho)^2;\ SW(1)_{(\alpha,\beta)} = \lambda R' - \lambda W \Big/ 2 \right. \tag{11}$$

If the social welfare is maximized and all the customers select priority service, the optimal priority service fee $K(1)_{(\alpha,\beta)}$ increases with the loss aversion parameter (if all the customers enter the priority queue, $W = W_1$ and gain-seeking parameter β has no effect the service system). The social welfare is fixed value and unchangeable with the changes in customers' psychology.

Lemma 6: If the enterprises cancel the classification of service (i.e., $\theta = 0$) and only retain the regular customers. The maximum value of social welfare for the service system is $SW(0)_{(\alpha,\beta)} = \lambda R' - \lambda W \Big/ 2$.

Combined with the above three kinds of situations, when considering customer psychology preferences, there has $SW(\theta^*)_{(\alpha,\beta)} \geq SW(1)_{(\alpha,\beta)} = SW(0)_{(\alpha,\beta)}$. We can further obtain the following conclusions and management insights.

Management insights 2: From the perspective of social welfare maximization, enterprises should adopt service classification. However, with the increase of loss aversion, the corresponding social welfare decreases. On this basis, enterprises should set the service windows of priority customers and regular customers at positions where they cannot see each other (Unobservable queues). This aims to reduce the stimulus of regular customers' loss aversion parameter and increase social welfare.

This central work in this section can be summed up in Table 2.

Table 2. The optimal service strategy and pricing based on SW maximization

Customers' preference	$\alpha < 0.5 + \beta$	$\alpha \geq 0.5 + \beta$
Optimal strategy	Classification of service (Unobservable)	Classification of service (Unobservable)
System design	Two active queues	Priority queue only
Optimal priority fee	$K^* = \frac{\rho^2\left((1+\beta)-(1+\beta-\alpha)\frac{1}{\rho}(1-\sqrt{1-\rho})\right)}{\mu(1-\rho)\sqrt{1-\rho}} > 0$	$K^* = \frac{\rho^2}{\mu(1-\rho)^2}\alpha > 0$

4.3 Utility Maximization

According to the Eq. (8) for social welfare, we can derive the function of overall customers' utility $U(\theta)_{(\alpha,\beta)}$ as follows,

$$U(\theta)_{(\alpha,\beta)}=\lambda R' - \lambda\Big((2\alpha\theta\rho + 1 - \theta^2\rho)\Big/2(1-\theta\rho)\Big)W - \lambda c \tag{12}$$

Then optimize the function $U(\theta)_{(\alpha,\beta)}$, subject to $0 \le \theta \le 1$. The optimal ratio of priority customers, optimal priority fee, and the optimal customers' utility are as follows.

Lemma 7: $$\left\{\theta^*_{(0,0)(U)} = 0;\ K(0)_{(0,0)(U)} = 0;\ U(0)_{(0,0)}=\lambda R' - \lambda W\big/2 - \lambda c \right. \tag{13}$$

All customers select to enter the regular queue (i.e., no customer enters the priority queue), we can derive the corresponding conclusion and insight.

Management Insights 3: When the overall customer utility is maximized, the enterprise should cancel service segmentation and just keep regular queuing; under this condition, the queue system was transferred into FCFS discipline. This is because the expected waiting time of customers align with the reference waiting time ($W_2 = W = W_1$), and the customers' loss aversion parameter, gain-seeking parameter have no effect on the system (i.e., $\alpha(W_2 - W) = \beta(W - W_1) = 0$).

5 Comparison Analysis of the Optimal Solutions

This section compares the optimal solutions of the above three optimized objectives with the optimal solutions that ignored customers' psychology preference (i.e., the existing literature) to explain the differences in this paper and the traditional work.

(1) If we do not consider the customer preferences (i.e., $\alpha = \beta = 0$), when revenue is maximized, we also should adopt the service classification. The optimal ratio of priority customers in the queuing system, the optimal priority fee, and the optimal revenue of service provider are as below.

$$\left\{\theta^*_{(0,0)(R)} = \frac{1}{\rho}(1-\sqrt{1-\rho});\ K(\theta^*)_{(0,0)(R)} = \frac{\rho(1-\sqrt{1-\rho})}{\mu(1-\rho)};\ R(\theta^*)_{(0,0)} = \frac{\rho(1-\sqrt{1-\rho})^2}{(1-\rho)} + \lambda c \right. \tag{14}$$

The optimal service strategy adopted from the perspective of enterprise revenue maximization has the following relations:

$$\left\{\theta^*_{(\alpha,\beta)(R)} > \theta^*_{(0,0)(R)};\ K(\theta^*)_{(\alpha,\beta)(R)} > K(\theta^*)_{(0,0)(R)};\ R(\theta^*)_{(\alpha,\beta)} > R(\theta^*)_{(0,0)} \right.$$

Thus, if enterprises can charge a higher priority fee by utilizing customers' psychology, then stimulate more customers to require the priority service to generate more revenue.

(2) If we do not consider the customer preferences (i.e., $\alpha = \beta = 0$), when social welfare is maximized, we also need to adopt service classification. The optimal ratio of priority customers, the priority fee, and the optimal social welfare of the queueing system are as below.

$$\left\{\theta^*_{(0,0)(SW)} = \frac{1}{\rho}(1-\sqrt{1-\rho});\ K(\theta^*)_{(0,0)(SW)} = \frac{\rho(1-\sqrt{1-\rho})}{\mu(1-\rho)};\ SW(\theta^*)_{(0,0)} = \lambda R' - \lambda\frac{\sqrt{1-\rho}-(1-\rho)}{\rho}W\right. \tag{15}$$

Based on the perspective of social welfare maximization, the adopted optimal queue strategy has the following relations.

$$\left\{\theta^*_{(\alpha,\beta)} = \theta^*_{(0,0)};\ K(\theta^*)_{(\alpha,\beta)} > K(\theta^*)_{(0,0)};\ \left\{\begin{array}{l} SW(\theta^*)_{(\alpha,\beta)} > SW(\theta^*)_{(0,0)}\ if\ \beta > \alpha \\ SW(\theta^*)_{(\alpha,\beta)} = SW(\theta^*)_{(0,0)}\ if\ \beta = \alpha \\ SW(\theta^*)_{(\alpha,\beta)} < SW(\theta^*)_{(0,0)}\ if\ \beta < \alpha \end{array}\right.\right.$$

Thus, when enterprises focus on utilizing customers' psychology, they can charge a higher priority service fee for service classification. However, the optimal ratio of priority customers has not changed. If customers' loss aversion parameter and gain-seeking parameter satisfy $\alpha \leq \beta$, there has $SW(\theta^*)_{(\alpha,\beta)} \geq SW(\theta^*)_{(0,0)}$. If customers' loss aversion parameter and gain-seeking parameter satisfy $\alpha \geq \beta$, there has $SW(\theta^*)_{(\alpha,\beta)} \leq SW(\theta^*)_{(0,0)}$. According to the prospect theory, most customers' psychology should satisfy $\alpha \geq \beta$, thereby the maximum value of social welfare produced in the service system is less than the optimal solution for the existing literature.

(3) If we do not consider the customer preferences (i.e., $\alpha = \beta = 0$), when customers' utility is maximized, we should cancel the classification of service and retain regular queue only or adopt the classification of service, while don't charge any priority service fee, then make all customers join the priority queue. The optimal solutions under the two conditions are shown.

$$\left\{\begin{array}{l} \theta^*_{(0,0)(U)} = 0 \\ K(0)_{(0,0)(U)} = 0 \\ SW(0)_{(0,0)} = \lambda R' - \lambda W/2 \end{array}\right. \quad \text{and} \quad \left\{\begin{array}{l} \theta^*_{(0,0)(U)} = 1 \\ K(1)_{(0,0)(U)} = 0 \\ SW(1)_{(0,0)} = \lambda R' - \lambda W/2 \end{array}\right. \tag{16}$$

So, in order to maximize the utility of customers, enterprises should cancel the extra priority service fees and maintain regular queues.

6 Conclusions and Future Research

This paper incorporates the regular customers' loss aversion preference and priority customers' gain-seeking preference into the model of customers' queuing utility via a monopoly queue system (i.e., customers cannot abandon the system). This paper studies the relevant research and drives some valuable conclusions and insights for service providers considering customer preferences from three perspectives: revenue, social welfare, and overall utility.

First, from the perspective of revenue maximization, enterprises should adopt the classification of service and set the service windows of priority customers and regular customers at the positions where they can see each other to make a sharp contrast between the two kinds of customers—stimulating regular customers' loss aversion preference and priority customers' gain-seeking preference by the intuitive perception to get more revenue. Then, from the perspective of social welfare maximization, enterprises should also adopt the classification of service. However, the service providers should set the service windows of priority customers and regular customers where they cannot perceive each other. This aims to make regular customers cannot feel priority customers' existence and reduce the stimulation for regular customers' loss aversion preference and further to get more social welfare. Later, enterprises should cancel service classification and retain regular customers only from the perspective of utility maximization. Finally, compared with the optimal solutions of existing methods, the analysis suggests that enterprises will earn more revenue when considering customers' psychological preferences. If loss aversion is larger than gain-seeking, the service system's social welfare is less than the existing conclusion. However, if the loss aversion is lighter than gain-seeking, the system will produce higher social welfare. From the perspective of customer utility, enterprises adopt the same strategy and get the same utility, whether they consider customers' psychological preferences.

Our future research directions are as follows. Firstly, in order to analyze the processability, this paper used the uniform distribution of waiting costs. Although we expect the structural results of our paper to apply to other distribution types, confirming this expectation is a worthy goal. Secondly, understand that the exact waiting time can affect the extent to which customers are affected by psychological incentives. So, the construction of a utility model considering the actual waiting time of customers is another research problem worth paying attention to. In future work, we will also extend our research to non-monopoly queue system (that is, customers can abandon the system depend on the utility).

Acknowledgements. This research is supported by the National Natural Science Foundation of China (Grant nos. 71671092, and 72071112). We thank the ICSS 2021 organizing committee and anonymous reviewers for their helpful comments.

References

1. Afèche, P., Pavlin, J.M.: Optimal price/lead-time menus for queues with customer choice: segmentation, pooling, and strategic delay. Manage. Sci. **62**(8), 2412–2436 (2016)
2. Pinedo, M.: Stochastic scheduling with release dates and due dates. Oper. Res. **31**(3), 559–572 (1983)
3. Van Mieghem, J.A.: dynamic scheduling with convex delay costs: the generalized $c\mu$ rule. Ann. Appl. Probab. **5**(3), 809–833 (1995)
4. Ward, A.R., Armony, M.: Blind fair routing in large-scale service systems with heterogeneous customers and servers. Oper. Res. **61**(1), 228–243 (2013)
5. Shunko, M., Niederhoff, J., Rosokha, Y.: Humans are not machines: the behavioral impact of queueing design on service time. Manage. Sci. **64**(1), 453–473 (2018)

6. Barberis, N.C.: Thirty years of prospect theory in economics: a review and assessment. J. Econ. Persp. **27**(1), 173–196 (2013)
7. Kahneman, D., Tversky, A.: Prospect theory: an analysis of decision under risk. Econometrica **47**(2), 263–291 (1979)
8. Alexander, M., MacLaren, A., O'Gorman, K., White, C.: Priority queues: where social justice and equity collide. Tour. Manage. **33**(4), 875–884 (2012)
9. Bassamboo, A., Randhawa, R.S.: Scheduling homogeneous impatient customers. Manage. Sci. **62**(6), 2129–2147 (2016)
10. Wang, J.F., Baron, O., Scheller-Wolf, A.: M/M/c queue with two priority classes. Oper. Res. **63**(3), 733–749 (2015)
11. Smith, W.E.: Various optimizers for single-stage production. Naval Res. Logist. Q. **3**(1–2), 59–66 (1956)
12. Cox, D.R., Smith, W.L.: Queues. Wiley, New York (1961)
13. Mandelbaum, A., Stolyar, A.L.: Scheduling flexible servers with convex delay costs: heavy-traffic optimality of the generalized $c\mu$ Rule. Oper. Res. **52**(6), 836–855 (2004)
14. Che, P.: Incentive-compatible revenue management in queueing systems: optimal strategic delay. Manuf. Serv. Oper. Manage. **15**(3), 423–443 (2013)
15. Huang, J., Carmeli, B., Mandelbaum, A.: Control of patient flow in emergency departments, or multiclass queues with deadlines and feedback. Oper. Res. **63**(4), 892–908 (2015)
16. Haji, R., Newell, G.F.: Optimal strategies for priority queues with nonlinear costs of delays. J. Appl. Math. **20**(2), 224–240 (1971)
17. Adiri, I., Yechiali, U.: Optimal priority-purchasing and pricing decisions in nonmonopoly and monopoly queues. Oper. Res. **22**(5), 1051–1066 (2005)
18. Alperstein, H.: Note—optimal pricing policy for the service facility offering a set of priority prices. Manage. Sci. **34**(5), 666–671 (1998)
19. Yang, L.Y., Debo, L.G., Gupta, V.: Trading time in a congested environment. Manage. Sci. **63**(7), 2377–2395 (2017)
20. Zohar, E., Shimkin, N.: Adaptive behavior of impatient customers in tele-queues: theory and empirical support. Manage. Sci. **48**(4), 566–583 (2002)
21. Jouini, O., In, Z., Dallery, Y.: Call centers with delay information: models and insights. Manuf. Serv. Oper. Manag. **13**(4), 534–548 (2011)
22. Yang, L., Guo, P.F., Wang, Y.L.: Service pricing with loss averse customers. Oper. Res. **66**(3), 761–777 (2018)
23. Che, P., Baron, O., Kerner, Y.: Pricing time-sensitive services based on realized performance. Manuf. Serv. Oper. Manag. **15**(3), 492–506 (2013)
24. Hafızoğlu, A.B., Gel, E.S., Pınar, K.: Price and lead time quotation for contract and spot customers. Oper. Res. **64**(2), 406–415 (2016)
25. Hedayati, M., Shen, K., Scott, M.L., Marty, M.: Multi-queue fair queueing. In: 2019 USENIX Annual Technical Conference, pp. 301–314 (2019)
26. Movaghar, A.: On queueing with customer impatience until the beginning of service. Queueing Syst. **29**(2–4), 337–350 (1998)
27. Garnet, O., Mandelbaum, A., Reiman, M.: Designing a call center with impatient customers. Manuf. Serv. Oper. Manage. **4**(3), 208–227 (2002)
28. Armony, M., Plambeck, E., Seshadri, S.: Sensitivity of optimal capacity to customer impatience in an unobservable M/M/S queue (why you shouldn't shout at the DMV). Manuf. Serv. Oper. Manag. **11**(1), 19–32 (2009)
29. Moyal, P.: On queues with impatience: stability, and the optimality of Earliest Deadline First. Queueing Syst. **75**(2–4), 211–242 (2013). https://doi.org/10.1007/s11134-013-9342-1
30. Batt, R.J., Terwiesch, C.: Waiting patiently: an empirical study of queue abandonment in an emergency department. Manage. Sci. **61**(1), 39–59 (2015)

31. Ibrahim, R., Armony, M., Bassamboo, A.: Does the past predict the future? The case of delay announcements in service systems. Manage. Sci. **63**(6), 1762–1780 (2017)
32. Norman, D.A.: Designing waits that work. MIT Sloan Manage. Rev. **50**(4), 23–28 (2009)
33. Nazerzadeh, H., Randhawa, R.S.: Near-optimality of coarse service grades for customer differentiation in queueing systems. Prod. Oper. Manage. **27**(3), 578–595 (2018)
34. Gavirneni, S., Kulkarni, V.G.: Self-selecting priority queues with burr distributed waiting costs. Prod. Oper. Manag. **25**(6), 979–992 (2016)
35. Gavirneni, S., Kulkarni, V.G.: Concierge medicine: applying rational economics to health care queuing. Cornell Hosp. Q. **55**(3), 314–325 (2014)
36. Gross, D., Shortle, J.F., Thompson, J.M., Harris, C.M.: Fundamentals of Queueing Theory, 4th edn. Wiley, New York (2008)

Research on Hotel Customer Preferences and Satisfaction Based on Text Mining: Taking Ctrip Hotel Reviews as an Example

Jing Wang(✉) and Jianjun Zhu

College of Economics and Management, Nanjing University of Aeronautics and Astronautics, Nanjing 211106, Jiangsu, China
zhujianjun@nuaa.edu.cn

Abstract. In the hotel industry, online reservation has become one of the main ways to gain customers, which has brought huge profits. Online hotel review analysis can help hoteliers get customer feedback and improve service quality, so as to enhance their competitiveness. Hence, this study proposes a complete online hotel review analysis process based on text mining to reflect customer preferences and satisfaction, improving the accuracy of consumer preference factor extraction, using sentiment score to indicate customer satisfaction to supplement comprehensive evaluation method mentioned commonly in the existing processes. The value of the proposed process was demonstrated through an example using online Ctrip hotel reviews. It showed that customers prefer three factors: environment, service and location. The study also revealed customer satisfaction by sentiment score distribution graphs. The conclusions and future suggestions are described at the end.

Keywords: Online hotel reviews · Customer preferences · Customer satisfaction · Text mining · Sentiment analysis

1 Introduction

In recent years, with the rapid popularization and development of "Internet Plus" and E-commerce industry, online hotel reservation service has become the preferred way of business travel and holiday travel. Online reviews are a key source of customer feedback for businesses. The analysis of online hotel reviews is not only helpful for consumers to grasp hotel reputation in time to decide purchase intention, but also important for hoteliers to adjust their services promptly according to customer feedback results.

Text mining is an emerging technology that attempts to extract meaningful information from unstructured textual data [1], and various text mining techniques have been developed to quantify textual information [2]. As most information (over 80%) is stored as text, text mining is believed to have a high commercial potential value [3]. Most recently, many researchers have successfully analyzed large amounts of online review texts based on text mining in the hotel industry to obtain customer feedback. For instance, Xu and Li (2016) analyzed online customer reviews of hotels using latent

R. Qiu et al. (Eds.): ICSS 2021, LNOR, pp. 227–237, 2021.
https://doi.org/10.1007/978-3-030-90275-9_19

semantic analysis and found that the determinants that create either customer satisfaction or dissatisfaction toward hotels are different and are specific to particular types of hotels [4]. He et al. (2017) presented an approach of using natural language preprocessing, text mining and sentiment analysis techniques to analyze online hotel reviews [5]. This study found that both extremely satisfied and extremely dissatisfied hotel customers share a common interest in the five categories: food, location, rooms, service, and staff. Ahani et al. (2019) developed a new method for the use of Multi-Criteria Decision-Making (MCDM) and soft computing approaches to identify the important factors for hotel selection based on previous travelers' reviews on TripAdvisor. The results identified four customer segments, namely "Highly Satisfied Travelers", "Satisfied Travelers", and "Moderately Satisfied Travelers", showing that different travelers have various degrees of satisfaction with dissimilar preferences [6]. However, most previous research conducted on online hotel review texts only from the perspective of customer preferences analysis, such as studying the factors that hotel customers pay most attention to when choosing hotels, lacking a comprehensive analysis of both customer preferences and customer satisfaction.

Aiming at solving the problems mentioned above on online hotel review text mining, this study proposes a complete online hotel review analysis process based on a variety of text mining techniques to bring one-stop service to hoteliers. Firstly, Octopus data collector is used to crawl online review texts of Ctrip hotels, and it is necessary to preprocess these reviews. Secondly, the Jieba word segmentation tool of Python is used for word segmentation and keyword extraction, and word cloud is provided for visualize customer preferences. Thirdly, SnowNLP package, which is suitable for sentiment analysis of Chinese text, is selected to calculate sentiment value of these reviews. With sentiment score distribution graphs, customer satisfaction is indicated. The results are verified by accuracy rate, precision rate, recall rate and F1-Score. The process proposed in this study has solved the following problems well:

1) With the characteristics of online hotel reviews, constructing hotel dictionary and stop word list to optimize the effect of word segmentation.
2) Extracting keywords from online hotel reviews and visualizing them with word cloud images to obtain hotel customer preferences, so that hoteliers can make more targeted improvements.
3) Performing sentiment polarity analysis on online hotel reviews and visualizing using sentiment score distribution graphs to reflect customer satisfaction.

2 Online Hotel Review Analysis Process

Online hotel review analysis process based on text mining mainly includes three steps: data acquisition, data analysis and sentiment analysis, as shown in Fig. 1.

1) ***Data acquisition***. Octopus data collector is used to crawl online hotel reviews. The original reviews need to be preprocessed, including text deduplication and deleting blank lines.

2) ***Data analysis***. Firstly, building hotel review dictionary considering the characteristics of hotel reviews; Then, the review texts are segmented, keywords extracted by Python's Jieba word segmentation tool. At last, the results are visualized using word cloud.
3) ***Sentiment analysis***. SnowNLP package, which is suitable for Chinese text sentiment analysis, is used to calculate sentiment value of these review texts. The results are visualized by sentiment score distribution graphs and are verified by accuracy rate, precision rate, recall rate and F1-Score.

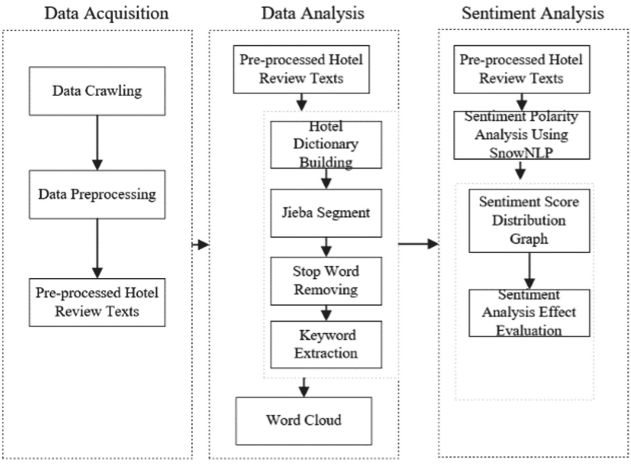

Fig. 1. Online hotel review analysis process based on text mining

3 Data Acquisition

3.1 Data Crawling

Ctrip is an online ticketing service company, founded in 1999 and headquartered in Shanghai, China. With more than 600,000 member hotels at home and abroad, Ctrip is the leading hotel reservation service center in China. Octopus data collector is a commonly used data crawling software, which is more convenient and easier, and can be used to simulate real user behavior for data collection. In this study, Octopus data collector was used to crawl relevant data of 50 three-star hotels on Ctrip in Qingdao. The data collected included hotel name, consumer name, consumer rating, consumer specific review text and review time. For the purpose of studying hotel customer preferences and satisfaction based on textual data, we choose review texts for analysis. The number of review texts selected for each hotel was close to 200, and the total number of review texts was close to 10,000.

3.2 Data Preprocessing

Data preprocessing is a significant part of data mining. Raw data collected is "dirty," and usually have many imperfections [7], such as redundancies, incompleteness, disorder, and so on. Without data preprocessing, word segmentation, keyword extraction and sentiment analysis of data will increase a lot of work, and even affect the accuracy of experimental results. Therefore, it often involves more time and effort to preprocess raw data to obtain clean, accurate and concise data. The original reviews crawled needs to be preprocessed, mainly including text deduplication and deleting blank lines.

In the reviews crawled, there are a lot of repeated data. The main two reasons for repeated texts in the reviews crawled are as follows:

1) Repeated reviews may be posted by the same customer because the same customer may book multiple rooms in a hotel at the same time (with different occupants). However, in order to save time, the customer may make same or similar reviews about these booked rooms. There is no shortage of valuable reviews, but even if there are valuable reviews, only the first one is meaningful.
2) Consumers copied the reviews that had already been published by other consumers who came earlier. As can be seen from the characteristics of the language, in most cases, valuable reviews published by different customers will not be completely repeated. If there are completely repeated reviews, they are generally meaningless and are most likely to be copied and pasted from someone else's review. It is obvious that only the earliest review is useful.

The existence of repeated data will increase the workload and restrict the efficiency of text mining. Additionally, the weight of repeated data in the whole sample is greater than that of other data, so it is easier to produce the bias of the results. Thus, no matter what kind of review text data is obtained, the primary processing should be text deduplication. Text deduplication refers to the removal of repeated hotel review texts. It is available to compare each review with the others to eliminate repeated reviews [8]. After text deduplication, all but one of the many identical reviews remained.

In addition to text deduplication, deleting blank lines is also necessary. Deleting blank lines refers to the removal of blank lines in hotel review texts. When customers edit hotel review texts, they often take the way of paragraphing and line feed. In order to facilitate word segmentation in the follow-up text, blank line removing is carried out on review texts. Finally, preprocessed reviews are obtained.

4 Data Analysis

Data analysis is composed of hotel dictionary building, Jieba segment, stop word removing, keyword extraction and word cloud generation.

1) ***Hotel dictionary building***. The existing word segmentation dictionary does not contain some specific words. In order to optimize word segmentation effect, we need to build hotel dictionary before the word segmentation of hotel review texts. Hotel

reviews, for instance, often appear "closer to a scenic spot", so these spot names need to supplement hotel segmentation dictionary.

2) ***Jieba segment***. Text segmentation is to cut a sequence of Chinese characters into single words according to the standard. Chinese word segmentation is much more difficult than English. In the process of feature selection, different segmentation effects directly affect the weight of words in the text, thus affecting the effect of data mining. Jieba, a simple and efficient Chinese word segmentation package, is used here. Based on the prefix dictionary, it can efficiently scan the word graph, generate a directed acyclic graph (DAG) which is composed of all possible word generation situations of Chinese characters in a sentence, and then use dynamic programming to find the maximum probability path to find the maximum segmentation combination based on word frequency. It supports a variety of segmentation modes and algorithms, including precision mode, full mode, search engine mode. Among them, precision model is suitable for text analysis.
3) ***Stop word removing***. Stop word removing is deleting unnecessary words and characters from segmentation result set. At present, there are many online stop word list, such as Harbin Institute of Technology (HIT) stop word list and Baidu stop word list. In this study, we use stop word list of HIT. After word segmentation, if a stop word is included in the results of word segmentation, it will be directly removed. Although there is a universal stop word list, if you want to improve the effectiveness of word segmentation, it is better to create your own stop word list. In view of the specific situation of hotel reviews, this study adds some common but meaningless words in hotel reviews to stop word list, such as "hotel", "Qingdao", "check in", "next time", "special", "super" and so on.
4) ***Keyword extraction***. Based on term frequency–inverse document frequency (TF-IDF) algorithm [9], Jieba is used to extract keywords from the results of word segmentation, and the top 20 keywords with TF-IDF values are obtained, which directly reflects the most concerned factors of hotel consumers on the service of the hotel. Keyword extraction results of a hotel is shown in Table 1.

Table 1. Review keyword list of a hotel

Rank	Keyword	TF-IDF value
1	Breakfast	0.3144
2	Clean	0.1970
3	Good	0.1891
4	Front Desk	0.1634
5	Comfortable	0.1479
6	Healthful	0.1329

(*continued*)

Table 1. (*continued*)

Rank	Keyword	TF-IDF value
7	Service	0.1253
8	Fangte	0.1109
9	Parking Lot	0.0953
10	Enthusiastic	0.0896
11	Environment	0.0876
12	Neat	0.0790
13	Quiet	0.0775
14	Service Attitude	0.0728
15	Recommend	0.0726
16	Decoration	0.0719
17	High Cost Performance	0.0705
18	High Tech Zone	0.0668
19	Location	0.0619
20	Business Trip	0.0619

As can be seen from the Table 1, the three most important keywords in customers' reviews of this hotel are breakfast, clean and good. Based on thematic clustering [10], the keywords in Table 1 can be classified into four categories: environment, service, location and overall evaluation, as shown in Table 2.

Table 2. Four categories of review keywords

Category	Number of keywords	Total TF-IDF Value
Environment	7	0.7938
Service	6	0.8608
Location	4	0.3015
Overall Evaluation	3	0.3322

The keywords contained in every category and their TF-IDF values are indicated in Fig. 2. It can be summarized that customers prefer two factors: environment and service, of which have more elements and higher total TF-IDF value.

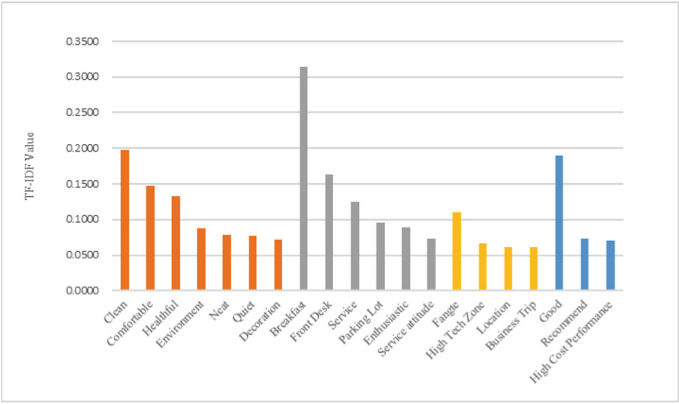

Fig. 2. Keywords contained in every category

5) ***Word cloud generation***. In order to enable hoteliers to obtain customer preference more intuitively, make better use of hotel review texts to adjust and improve service in time and enhance customer satisfaction, statistical analysis results are visualized in the form of word cloud. Word cloud, also known as label cloud, is the prominent visual presentation of the "keywords" with higher frequency in the text data. The rendering of keywords forms color pictures, so that you can appreciate the main expression meaning of the text data at a glance. Here, the WordCloud library, a word cloud generator in Python, is used to generate word clouds based on the keywords in Table 1 and their TF-IDF values, as shown in Fig. 3.

Fig. 3. Hotel review keyword word cloud

As can be seen intuitively from this word cloud, customers generally think that the hotel is in a good location, located in the high-tech zone, close to Fangte scenic spot,

suitable for business travelers to live; The environment of the hotel is clean, healthful, neat and quiet, and there is a parking lot. Service attitude is enthusiastic and breakfast is provided. In general, this hotel has a good reputation and high cost performance, and is recommendable.

5 Sentiment Analysis

5.1 Sentiment Polarity Analysis Using SnowNLP

Sentiment polarity analysis refers to the analysis and judgment of the positive and negative emotions of the texts. There are mainly two methods based on lexicon and machine learning [11]. The former needs to use the annotated sentiment dictionary. The latter requires a large number of manually annotated corpus as the training set, and achieves sentiment classification by extracting text features and constructing classifiers. In general, machine learning is more accurate than lexicon based and has greater flexibility due to the richness of semantic expressions.

In this study, SnowNLP based on Bayesian model is used to analyze sentiment polarity of hotel review texts. SnowNLP is a Python library for natural language processing in Chinese. It can easily conduct sentiment analysis on the content of Chinese text, and the sentiment score is between 0 and 1. The score is greater than 0.5, indicating positive emotion. When the score is less than 0.5, the emotion is more negative; The closer you get to zero, the more negative the emotion is.

After using SnowNLP to analyze sentiment polarity of 50 three-star hotel review texts, the sentiment scores of these texts were calculated. Some results of sentiment analysis are shown in Table 3. As can be seen from the Table 3, the first three reviews contain positive words such as “Good”, “Convenient”, and “Great”. Using SnowNLP to analysis, their sentiment scores are all above 0.9, showing strong positive emotions. With negative words like “poor”, “disappointing”, and “troublesome”, the sentiment scores of last three reviews are especially small, of which sentiment polarity are negative.

With 0 and 1 as a starting point and end point, 0.01 for the interval length, the quantity of these sentiment scores belonging to every subinterval was counted to construct sentiment score distribution graphs. And sentiment score distribution graphs of two of these hotels are shown in Fig. 4.

As can be intuitively seen from Fig. 4, reviews of hotel on the left were generally positive; While reviews of hotel on the right showed negative emotions on the whole. The total number of reviews with an emotional score of almost 0, that is, completely negative reviews, was close to 70.

Table 3. Sentiment scores of some hotel reviews

Rank	Reviews	Sentiment polarity	Sentiment score
1	Good, stayed for three days in a row, subway entrance and business district are downstairs	Positive	0.998
2	Just go out by the subway, located in a bustling area, very convenient for eating and shopping	Positive	0.955
3	Great location, rich breakfast, warm service, parking lot provided	Positive	0.947
4	The facilities are old, environment is messy and the sanitation is not good enough	Negative	3.933e–06
5	The sanitation of the hotel is poor, and air conditioner is just as useless as a furnishing. And service staff is also disappointing, it is recommended not to stay	Negative	0.020
6	The elevator needs to be transferred to the fourth floor and above. This is a bit troublesome, and you can't directly reach the floor you are going to. The service is ordinary, nothing special, and the overall feeling is not good!	Negative	0.055

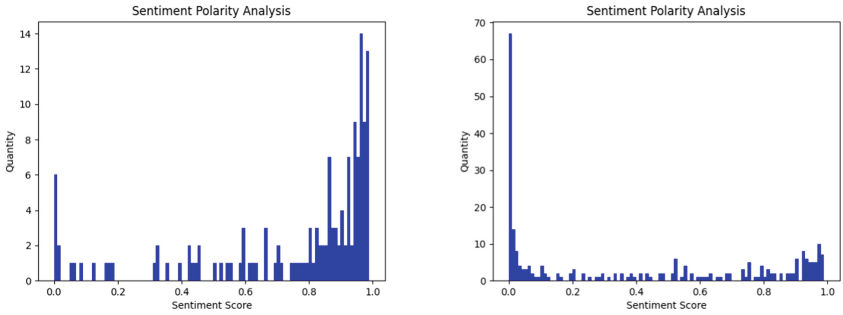

Fig. 4. Sentiment score distribution graphs of two hotels

5.2 Sentiment Analysis Effect Evaluation

In order to measure the effect of sentiment polarity analysis, this study uses four criteria, namely accuracy rate, precision rate, recall rate and F1-score, to evaluate. Accuracy rate reflects the proportion of correct reviews in all reviews in sentiment polarity analysis; Precision rate reflects the proportion of reviews with true positive (negative) emotional orientation among the reviews judged as positive (negative) emotional orientation; Recall rate reflects the proportion of correctly judged positive (negative) emotional orientation reviews to the total positive (negative) orientation reviews; F1-Score is a weighted average of accuracy and recall, which takes into account accuracy and recall. The definition

of F1-Score is presented in Eq. (1).

$$F1 - Score = \frac{2Precision \times Recall}{Precision + Recall} \tag{1}$$

where, Precision = precision rate and Recall = recall rate.

Based on sentiment analysis results of the 50 three-star hotels, the average values of the four criteria are shown in Table 4.

Table 4. Sentiment analysis effect Evaluation criteria

Accuracy	Category	Precision rate	Recall rate	F1-Score
0.87	Positive	0.79	0.91	0.85
	Negative	0.91	0.80	0.85

As can be seen from the Table 4, for positive category, the probability that reviews of which the actual emotion is positive can be judged by SnowNLP is higher, reaching 0.91. But precision rate is not high, for reviews judged by SnowNLP as emotionally positive, we are only 79% confident that the judgment is correct.

For negative category, for reviews judged by SnowNLP as emotional negative, we have a 91% certainty that the judgment is correct; However, recall rate is not high, and the probability that actual negative emotional reviews can be judged by SnowNLP is only 0.80.

The F1-Score of both types of reviews is 0.85, indicating that sentiment polarity analysis effect of SnowNLP is good.

6 Summary

In order to help hotels that support online reservation service to obtain customer feedback and improve services, this study proposes a complete online hotel review analysis process based on text mining to revealing customer preferences and satisfaction. Taking Ctrip hotel reviews as an example, it uses Python Jieba word segmentation tool to segment and extract keywords from online hotel review texts, and uses word cloud for visualization. The SnowNLP package is used to conduct sentiment analysis. And the research results were verified by accuracy rate, precision rate, recall rate and F1-Score. But there are still some shortcomings: First, the trained model in SnowNLP library is based on the data of E-commerce product reviews. In this study, SnowNLP library was directly used for sentiment analysis without retraining the model. Secondly, this research only uses SnowNLP library based on Bayesian model for sentiment analysis, and subsequent research can also use other natural language processing algorithms, such as support vector machines (SVM), for comparative analysis.

References

1. He, W., Zha, S., Li, L.: Social media competitive analysis and text mining: a case study in the pizza industry. Int. J. Inf. Manage. **33**(3), 464–472 (2013)
2. Cao, Q., Duan, W., Gan, Q.: Exploring determinants of voting for the "helpfulness" of online user reviews: a text mining approach. Decis. Support Syst. **50**(2), 511–521 (2011)
3. Gupta, V., Lehal, G.S.: A survey of text mining techniques and applications. J. Emerg. Technol. Web Intell. **1**(1), 60–76 (2009)
4. Xu, X., Li, Y.: The antecedents of customer satisfaction and dissatisfaction toward various types of hotels: a text mining approach. Int. J. Hosp. Manag. **55**, 57–69 (2016)
5. He, W., Tian, X., Tao, R., Zhang, W.: Application of social media analytics: a case of analyzing online hotel reviews. Online Inf. Rev. **41**(7), 921–935 (2017)
6. Ahani, A., et al.: Revealing customers' satisfaction and preferences through online review analysis: the case of Canary Islands hotels. J. Retail. Consum. Serv. **51**, 331–343 (2019)
7. Ramirez-Gallego, S., Krawczyk, B., Garcia, S., et al.: A survey on data preprocessing for data stream mining: current status and future directions. Neurocomputing **239**, 39–57 (2017)
8. Garcia, S., Luengo, J., Herrera, F.: Tutorial on practical tips of the most influential data preprocessing algorithms in data mining. Knowl.-Based Syst. **98**, 1–29 (2016)
9. Salton, G., Yu, C.T.: On the construction of effective vocabularies for information retrieval. ACM Sigplan Notices **10**(1), 48–60 (1975)
10. Waring, R.: The negative effects of learning words in semantic sets: a replication. System **25**(2), 261–274 (1997)
11. Khan, F.H., Qamar, U., Bashir, S.: eSAP: a decision support framework for enhanced sentiment analysis and polarity classification. Inf. Sci. **367–368**, 862–873 (2016)

Broadening the Scope of Analysis for Peer-to-Peer Local Energy Markets to Improve Design Evaluations: An Agent-Based Simulation Approach

Steven Beattie and Wai-Kin Victor Chan(✉)

Tsinghua-Berkeley Shenzhen Institute, Tsinghua University, Shenzhen 518000, Guangdong, People's Republic of China
chanw@sz.tsinghua.edu.cn

Abstract. Local energy markets (LEM's) have emerged as an important factor in the development of energy systems which coordinate distributed and privately-owned generation resources. LEM's may enable energy transactions between physically or virtually connected users (consumers and prosumers); local power system load balancing, increased energy system resilience, and local socioeconomic improvement may be supported. We present an agent-based LEM simulation, modeling a prominent real-world LEM using a double-sided auction-based design (CDA), and demonstrate a novel approach to LEM design analysis. A range of fixed local-level supply-demand ratios are evaluated independently to increase results' generalizeability, and individualized agent results are considered in the analysis. Previous results suggesting CDA may improve local outcomes compared to a baseline market are confirmed. However, potential design issues related to energy affordability for consumers and sale profitability for prosumers are also observed. Similarly, while local-level results show maximized market efficiency, agent-level results suggest considerable matching success disparities in the local marketplace, despite the use of homogeneous agents with well-tuned learning models. Further data analysis shows that agents' day-to-day outcomes may also vary considerably under CDA. Results may provide decision support to system engineers and policy-makers, and may support LEM design and analysis work.

Keywords: Local energy market · Mechanism design · Decision support · Agent-based simulation · Sociotechnical systems

1 Introduction

The introduction of renewable generation resources into the consumer market has led to the emergence of a new type of agent in energy systems. The prosumer is an entity which utilizes distributed energy generation resources (e.g. residential solar panels), and accordingly may act as either an energy producer or consumer, depending on its

R. Qiu et al. (Eds.): ICSS 2021, LNOR, pp. 238–253, 2021.
https://doi.org/10.1007/978-3-030-90275-9_20

current demand and generation. At the same time, local energy marketplaces (LEM's) – in which users may buy and sell energy within the local community – have emerged in smart grid research as a tool for encouraging prosumption, safely integrating prosumer energy into distribution grids, and helping to balance local supply and demand. There are three main LEM network topologies; agent-to-grid (current retail market in most places); "organized prosumer groups" or cooperative systems; and peer-to-peer (p2p), which support direct connections between user agents [1]. For the p2p system design, double sided auction-based designs are among the most popular [2].

LEM's are often proposed for use in microgrid-based energy systems. However, LEM use in a microgrid requires ensuring that market settlement is consistent with optimal dispatch scheduling and stability constraints in the physical distribution network. This additional complexity in system design can be avoided by the deployment of a virtual LEM platform which runs independently from the physical power grid. A number of recent energy projects have taken this approach to system design, such as the Brooklyn Microgid project in Brooklyn, New York, U.S. [3].

In the current testing phases of the Brooklyn Microgrid, a virtual LEM (owned and operated by LO3 Energy) connects energy consumers and prosumers for trading on a virtual, peer-to-peer double auction-based platform. At the physical level, the traditional, centralized distribution grid is the only trading partner for local users; energy is only delivered from the main grid, and excess prosumer energy is routed exclusively into the same main grid. But in the virtual LEM, peer-to-peer transactions may allow consumers to reduce their energy bills by trading directly with local prosumers. For prosumers, additional value may be realized from their renewable generation via LEM trading. This increase in generation incentive may indirectly lead to higher amounts of renewable generation being supplied to the main grid, which may present either an issue or opportunity for the main power grid. For example, system voltage issues may arise, or alternatively, local load balancing services may be produced, depending on energy distribution system design & management [1].

Agent-based simulation is often used to conduct LEM design analysis [4–10]. Current agent-based simulation analysis of LEM design has generally focused on system-level assessments of local market price and efficiency, and prosumer benefit. When energy affordability is considered, it is generally discussed in terms of relative increases in affordability compared to the baseline market. Consumer outcomes are generally considered in aggregate, and outcome analysis is usually limited to aggregated consumer benefit compared to the baseline retail market. An exception to this is [4], in which agents' outcome variance across all settlement times is considered; however, in this work, an auction-based market mechanism is not considered. Additionally, previous analyses generally consider a limited sampling of real-world generation and demand data, which may reduce the ability of researchers to generalize their results beyond the specific system implementation examined.

In the current work, we implement an agent-based simulation environment reflecting the virtual LEM platform used in the Brooklyn Microgrid, as presented by [3]. The LEM simulation is settled as a day-ahead market. Agent implementation utilizes the reinforcement learning method and value function modeling used by [11]. Environment and agent parameters are tuned according to real-world values; learning parameters are

tuned via simulation tests. We extend previous analyses of double-sided auction-based LEM's in two ways. First, the simulation design allows us to consider a wide range of supply-demand ratios possible in real-world systems; the results reflect expected outcomes from each considered market state. Second, we present an improved agent-level analysis; along with local-level outcome metrics, the results analysis additionally considers individual outcomes for simulated agents.

This paper first presents environment and agent design, before discussing experiment design and results analysis. Along with conclusions and recommendations based on study results, opportunities for follow-up work are discussed. The presented approach to simulation design and outcome analysis may support generalized assessment of the potential impact of LEM design on local communities, across system implementations. Results may provide decision support towards realizing the development and adoption of energy infrastructure projects which promote positive social impacts and support effective, justifiable public utility distribution via distributed energy systems.

2 Methodology

The presented agent-based simulation study of potential LEM design impact on system users in the surrounding community can be broken down into three distinct sections; simulation environment design, agent design, and experiment design. Environment design looks at system-level parameters and market implementation, and a simulation execution overview. Agent design focuses on agent variables, user value function modelling, and agent learning. Simulation scenarios and data analysis are presented in experiment design. NetLogo was used for simulation implementation and execution, while R was used for data analysis and results plotting.

2.1 Environment Design

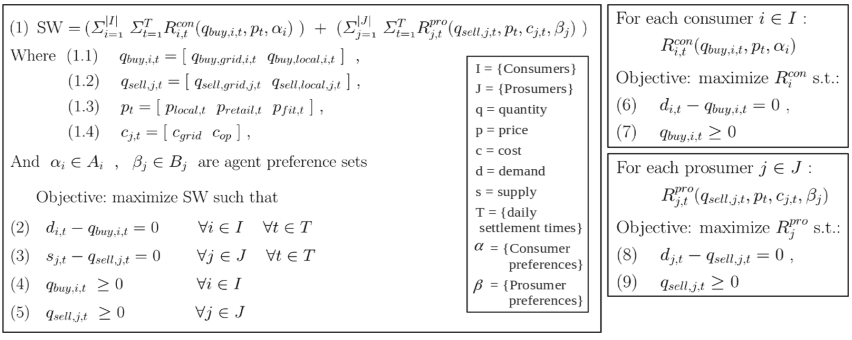

Fig. 1. System-level and agent-level local energy market modeling

The Brooklyn Microgrid (BMG) pilot project currently utilizes a prominent example of an auction-based virtual LEM. The local energy system and virtual LEM design are

discussed in detail in [3]. This LEM is well-represented by the grid-connected LEM model shown in Fig. 1. The LEM settlement platform utilizes a peer-to-peer network among agents, and implements a double-sided auction with merit-order bid matching, discrete settlement times, and a closed "order book" limiting information on other agents. A uniform market clearing price is produced at each settlement time, in which the price used for all transactions in a given settlement is given by the bidding price of the last consumer matched locally. In the following sections, this "closed double auction" is called "CDA".

Social welfare maximization is a common approach to modeling virtual LEM's [10, 18]; the objective is satisfied by market efficiency maxima. In the LEM modeled, though, market objective satisfaction is an emergent characteristic of agent-level behavior in the marketplace. Agents seek to maximize their own returns from the marketplace according to value function representations, as indicated on the right-hand side of Fig. 1.

In the simulation environment, a local retail energy grid market is implemented, representing the retail energy market in the Brooklyn, NY area. In the retail market, consumers pay a retail fee for energy used, and prosumers may export excess generation to the main grid at a "feed-in-tariff" compensation rate. In simulations, the grid market is automatically executed after the local market is settled -- ensuring all users' current outstanding demand is met and outstanding supply is allocated, and satisfying constraints (2), (3), (6), (8). System-level constraints (4), (5) are satisfied by agent implementations of (7), (9). Sufficient grid supply and stability are assumed in the modeling. Distribution system constraints are currently outside of study scope; in most current cases, including the BMG, the LEM is not directly linked to distribution or scheduling mechanisms. Connecting these two "sides" of the system is also outside of current scope. Preference sets α and β are not used here, but are included to support follow-up work (Table 1).

Table 1. Summary of global parameters used in simulation environment

Global Parameters		
Name	**Description**	**Initialization**
numDays	Days simulated	365 (fixed)
warmUp	Model training period length	90
numAgents	How many agents included	100
epsilon, lambda	Learning model parameters	0.01, 0.083
FiT	Prosumer to grid sale price	$0.058 usd/ kWh
retail-price	Grid to agent sale price	$0.179 usd/ kWh
conDailyDem	Consumer daily demand	19.64 kWh
proDailyGen	Prosumer daily generation (as % of demand)	[101%, 110%, ..., 190%, 200%, 210%,..., 290%, 300%]

Simulation execution begins with system-level and agent-level initialization of model parameters and state variables. Market settlement produces supply and demand matching, transaction quantities, and a uniform local price. Results from market settlement are then passed to agents for processing. For simplicity, variable retail market pricing (e.g. time-of-use) is not simulated; retail and feed-in-tariff prices are constant. A day-ahead settlement market is simulated. At the beginning of each simulation run, a training period ("warmUp") is executed, in which results metrics are not collected and agents' learning models are trained for the evaluation period ("numDays").

Feed-in-tariff (FiT) is estimated based on [15], and retail-price is fixed at the real-world 2019 average for Brooklyn, New York [16]. Fixed parameters are constant throughout all included experiments. Epsilon (ε) and lambda (λ) are agent learning model parameters which are also constant for all agents. The variable parameter, prosumers' daily generation (PDG), is fixed in each simulation but varies across simulation scenarios. It is represented as a percentage of agent demand, which is fixed to the 2019 average demand for Brooklyn, New York in 2019 [17]. Note that the supply and demand given to each agent, at each time step, is fixed and uniform (in a given scenario). Commonly in previous studies, variable parameters within each scenario also include heterogeneous and non-constant supply and demand values for agents. As opposed to being an over-simplification, this simulation design supports improved evaluation of emergent market design impacts, and production of a more generalized analysis with less influence of factors distinct from the design itself (e.g. spatial, temopral, or system-specific).

2.2 Agent Design

$$
\begin{array}{ll|ll}
(10) & pot\_local\_cost_{i,t} = c_{retail,t} \times q_{buy,grid,i,t} & (13) & local\_profit_{j,t} = c_{local,t} \times q_{sell,local,j,t} \\
(11) & act\_local\_cost_{i,t} = c_{local,t} \times q_{buy,local,i,t} & (14) & grid\_profit_{j,t} = c_{FiT,t} \times q_{sell,grid,j,t} \\
(12) & R^{con}_{i,t}(q_{buy,i,t}, c_t) = pot\_local\_cost_{i,t} - act\_local\_cost_{i,t} & (15) & R^{pro}_{j,t}(q_{sell,j,t}, c_t) = grid\_profit_{j,t} + local\_profit_{j,t}
\end{array}
$$

Fig. 2. Agent value function representation according to agent type (con: consumer, pro: prosumer)

Currently, we adopt the user agent value functions presented in [11], which are represented in Fig. 2. These value functions may be thought of as modeling users with full preference for own-economic benefit. Consumers' value derived from the local market is represented by the amount of savings realized by their local market settlement, as compared to if they had secured their energy supply from the retail grid market exclusively. For prosumers, local market value is represented as the amount of profit produced by energy sales. As in previous work, prosumers' operation costs are approximated to zero, reflecting the low operation cost for solar PV generation systems.

Table 2. Summary of agent-level variables

General Agent Variables			
Set?	**Var. Name**	**Basic Info**	**Initialization**
Y	isProsumer	Boolean classifier	Agent-set split 50/50
Y	cNum	Integer; id within group	Sequential init.
Y	strategies	Vector; range of prices considered	Initialized by model
N	bidProps	Vector; current propensity for each bid price	Set daily by model
N	bidProbs	Vector; current probability for each bid price	Set daily by model
N	bidStrategy	Double; current bid strategy (price) chosen	Set daily by model
Y	maxBid	Double; highest bid price considered	Initialized by model
N	demand	Double; current demand	Set daily by model
Y	income	Integer; annual income	Initialized by model
N	funds	Double; current funds	Updated daily
Y	pt1, pt2	Double; user preferences	Initialized by model

Prosumer-Specific Variables			
Set?	**Var. Name**	**Basic Info**	**Initialization**
Y	pNum	Integer; id within group	Sequential init.
N	generation	Double; current generation	Set daily by model
N	askProps	Vector; current propensity for each ask price	Set daily by model
N	askProbs	Vector; current probability for each ask price	Set daily by model
N	askStrategy	Double; current ask strategy chosen	Set daily by model
Y	minAsk	Double; lowest bid price accepted	Initialized to FiT

The two agent types simulated are consumer and prosumer, randomly chosen; a summary of important variables is shown in Table 2. Agent type determines the agent's access to generation resources; consumers are energy purchasers, and for simplicity we model prosumers strictly as energy suppliers. At each time step, agents submit their supply and demand quantities to the market, along with their chosen corresponding bidding or asking price *a*. Submitted prices are chosen independently according to each agent's learning model; specifically, according to current strategy selection probabilities *p*, which are calculated according to strategy propensities *d*. Once the market has been settled, each agent's results are then used to evaluate their benefit from the local market, R^{con} for consumers and R^{pro} for prosumers. Strategy propensities *d* are then updated using each agent's calculated *R* value.

For each $s \in$ S strategies:

$p_{n,s,t} = \frac{d_{n,m,t}}{\sum_s^S d_{n,s,t}}$

$P_{n,t} = \{p_{n,1,t}, p_{n,2,t}, ..., p_{n,S,t}\}$

$a_t \leftarrow Multi(P_{n,t})$

< Chosen strategy a_t submitted to market >

< Market execution results received by agent >

Then, for each $s \in$ S strategies:

$$d_{n,s,t+1} = (1-\lambda) \cdot d_{n,s,t} + \begin{cases} R_{n,t}(q_{n,t}, c_t, x_n) \cdot (1-\epsilon) & (if\ s = a_t) \\ d_{n,s,t} \cdot (\frac{\epsilon}{|S|-1}) & (otherwise) \end{cases}$$

(Where $n \in$ N agents, $t \in$ T settlements, $a_t =$ action @ t, $x = \{\alpha, \beta\}$)

Fig. 3. Overview of agent learning update at each simulation step

The Modified Roth-Erev (MRE) learning model (see Fig. 3) is used to simulate user agent adaptation with the goal of maximizing own-benefit. The model does not consider complex strategy formation (e.g. undercutting of competing sellers in the short term to increase market share in the long term), but was developed based on extensive data collected from marketplace behavior studies [12, 13]. The "improved" form is utilized in simulation-based LEM studies [11, 14]. Each agent has an independent MRE model. Strategies are chosen from a multinomial distribution in which the probability of each strategy choice is continually updated. The strategy set used in this work is {0.06, 0.07, …, 0.16, 0.17}, representing discretized bid/ask price strategies in USD/kWh between local feed-in-tariff and retail prices, as in previous work. With repeated model update, the probability of selecting unsuccessful strategies under the MRE model are comparatively reduced, and successful strategy probabilities become comparatively increased. Learning "memory" is represented by ε, while learning "rate" is represented by λ.

2.3 Experiment Design

Overall, the study is designed to eliminate as many extraneous variables as possible. Agents of each type are homogeneous to one another, all agents utilize identically-tuned learning models, and PDG is the sole variable parameter in our study. Accordingly, the system dynamics and outcomes explored in the results analysis can be clearly attributed to two sources: market design and agent behavior.

PGD is given as a percentage of agents' (constant) energy demand, and is varied in each simulation scenario. In this way, a clear and unique ratio of supply and demand are produced in each scenario, which we refer to in following sections as SDR for simplicity. For example, if PDG is 150% of agent demand, prosumers may satisfy 100%

of own demand, and may additionally supply 50% of their own demand quantity to the marketplace. The SDR here is 0.5, as supply and demand homogeneity means 50% of consumer demand can be satisfied locally. Twenty-one SDR's are considered in the current study, and are given by the set {0.01, 0.1, 0.2, …, 0.9, 1, 1.1, …, 1.8, 1.9, 2}.

Each of the 21 SDR's considered represents a unique simulation scenario produced. All simulations use 50 consumers and 50 prosumers, in order to avoid sampling-related issues in the results. Each simulation consists of 365 independent market settlements (after "warmUp") from which results metric data are collected. (Table 3) One-hundred repetitions are performed in each scenario, for a total of 3650 local market settlements considered per scenario. For analysis, each scenario's agent data is separated by agent type, consumer and prosumer.

Table 3. Summary of evaluation metrics used for simulation results

Evaluation Metrics		
Name	**Description**	**Data Points**
Local Market Price	What is the average market price produced in market settlement?	Uniform price, stored directly from market
Local Market Efficiency	Is all possible local supply and demand allocated efficiently, according to current supply-demand balance?	Computed from consumer grid cost, prosumer grid sales
Agent Market Returns	How much cost savings for consumers; how much profit for prosumers?	Stored directly from each agent
Agent Benefit Variation	Are an individual agent's average returns from the LEM consistent?	Computed from daily agent-specific results

For each simulation run in a given scenario, agent outcomes at each time step are averaged; scenario results for each metric are then calculated based on statistics of the set of averages collected from user agents. Specifically, results plots consider the minimum, mean, and maximum agent averages reported for all simulation runs in each scenario. The produced min, mean, and max results curves do not cross in any results plot; these values are represented on each plot by the top, middle, and lowest curves, respectively -- or left, middle, and right, respectively.

3 Results and Discussion

3.1 Learning Model Tuning

As one of the two included factors in results emergence is agent behavior, special attention is paid to agent learning model tuning. Previous work has used an exhaustive search for tuning [14]. Based on the parameter space analysis in [25], $\lambda = 0.083$, and ε in {0.001, 0.01, 0.02, …, 0.07, 0.08, 0.083} were tested in an environment with four agents; 2 consumers, and 2 prosumers. Means of 100 simulation runs for each parameter combination were used for data analysis. First, we look for maximized market efficiency and monotonically-decreasing price curve, followed by maximized bid-ask competitiveness. Specifically, agents should continually try to out-bid or undercut others using the smallest necessary increment to price. Average bids and asks should be near identical to one another, as same-type agents are homogeneous to one another. Due to analysis complexity, NetLogo's Behavior Search was not used.

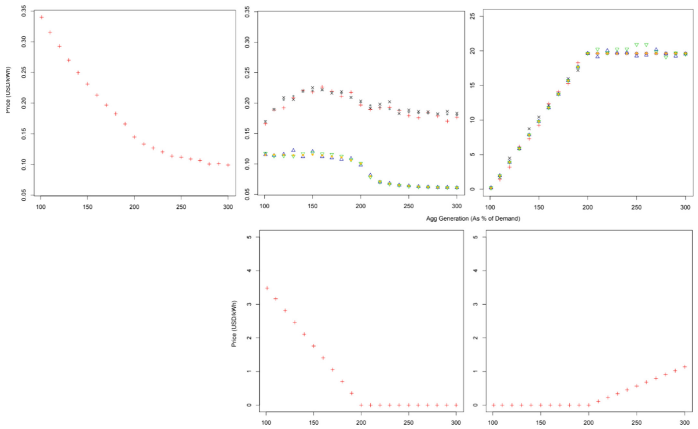

Fig. 4. Parameter tuning test results for $\lambda = 0.083$, $\varepsilon = 0.01$. Top row, left to right: average local market price, average bid/ask prices, average quantity matched locally. Bottom row, left to right: consumer cost from main grid market, prosumer profit from main grid market. In all cases, price scale does not affect shape of results. Section 2.3 explains x-axis labeling. In average bid/ask price and average matched quantity plots, crosses represent consumers, and triangles represent prosumers.

Parameter tuning test results (Fig. 4) showed learning convergence within the parameter space searched, with only small differences in outcomes from each test. Compared to other tested combinations, results for $\lambda = 0.083$ and $\varepsilon = 0.01$ best satisfied all three evaluation criteria. The current model tuning results are consistent with [14] and appear consistent with [11]. Further test results indicated that a 90-day "agent warm-up" period was sufficienty to produce learning convergence for all agents, using this parameter combination. As shown in Fig. 4, local market efficiency is maximized in all cases. When SDR $<= 1$, all local supply is allocated locally, and when SDR > 1, all local demand is satisfied locally. The price curve produced reflects expected supply-demand pricing and competitive price-setting. Further, consumers were competitive with one another throughout all simulations, in each SDR considered; the same result can be seen for prosumers as well (top-middle and top-right of Fig. 4).

A notable gap between consumer and prosumer strategies was present with all parameter combinations tested, which may have an effect on local market prices. If this gap was closed, we would expect to see local prices stay higher for longer when SDR $<$ 1, fall lower (and more quickly) towards feed-in-tariff when SDR > 1, or both. However, this suggests that prices derived from a model or model tuning which produces a more narrow gap would further confirm the following study results in Sect. 3.2, with the exception that an affordability threshold may be met in lower SDR's. In any case, consider that a consumer's bid price must meet or exceed a prosumer's asking price in a given settlement time, in order for LEM transaction matching to be possible between them. Accordingly, the gap between consumer and prosumer prices indicates that agent learning is not an inhibiting factor in local matching for individual agents. Thus, results

in the following sections related to matching success can clearly be attributed to market mechanism design dynamics, as opposed to being a product of learning algorithm dynamics.

This gap may be closed in alternative learning models, but the MRE model is empirically validated [12, 13] and provides consistency with previous works such as [11, 14]. A fundamental goal of this work is to produce a generalizable analysis of market dynamics and expected local outcomes under the considered CDA market design. Aside from being a technically-sound basic approach to reinforcement learning, the MRE model was developed based on behavioural data from multiple empirical studies on users' real-world market behaviour. Accordingly, results may be appropriate for system implementations which utilize either direct user input or autonomous user agents.

3.2 Local Market Prices

An often-expected benefit of LEM's is increased energy affordability for consumers. Consumers currently spend as much as 13% of their income on energy in New York's retail energy markets [19] while New York recognizes an affordability threshold at 6% of income [20]. Based on a retail price of $0.175 USD/kWh, we can thus consider a hypothetical price threshold of $0.083 USD/kWh which may produce energy affordability for all consumers (Fig. 5).

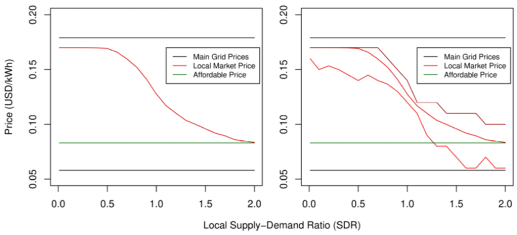

Fig. 5. Local market prices. Left shows mean average price, right shows min, mean, and max average price. Baseline retail and feed-in-tariff prices from the main grid are plotted for reference at 0.17 USD/kWh and 0.053 USD/kWh respectively. A hypothetical locally-affordable price for all consumers, derived in the proceeding paragraph, is plotted at 0.083 USD/kWh.

Consistent with previous works (e.g. [3, 7, 8, 21]), system-level results show that the auction-based market can be expected to improve relative affordability and profitability locally, in most SDR's, compared to the baseline market (Fig. 4). In general however, the affordability threshold is not met. On average, affordability threshold achievement requires SDR $>= 2$. Further, when SDR $<= 0.5$, the average local market price of $0.165 USD/kWh may not significantly increase economic value for system users, compared to baseline retail market value.

In current pilot testing phases, the virtual LEM operating in the Brooklyn Microgrid has reported potential increases in some prosumers' benefit preference satisfaction, and decreased energy costs for prosumers, but local market prices lower than baseline retail have not yet been reported. [22] If the market generally operates in low-SDR ranges, as

is strongly suggested by [22, 23], these results may help explain outcomes from current tests. This result may be important to consider, as LEM's are commonly expected to support the realization of a prominent role for distributed generation-based energy systems (e.g. microgrids) in public utility distribution networks. In public utility distribution generally, resource affordability is an important goal; these results suggest that this goal may not be met under the CDA market design, unless a high average-SDR operating range is achieved in real-world systems.

At the same time, profitability for prosumers may be undermined in high-SDR's, according to simulation results. When SDR $>$ 1.6, the minimum average price produced falls well below the affordability threshold, to the lowest allowed local market price of \$0.06 USD/kWh. In these cases, prosumer profit may be increased without breaking affordability for any local consumer. Holding other factors equal, we may consider the CDA market as providing sub-optimal benefit to prosumers in these cases, and therefore also sub-optimal generation incentive. This result may depend to some extent on the agent learning model used, but nevertheless suggests further investigation.

3.3 Local Market Efficiency

Results in Fig. 4 (left side) support the conclusion that an auction-based LEM settlement mechanism can achieve local market efficiency if temporal matching of supply and demand can be achieved (e.g. using energy storage resources) [10, 11]. In [10], it is noted that maximized market efficiency produces social welfare maxima. When SDR $<=$ 1, all local supply is allocated locally; similarly, when SDR $>$ 1, all local demand is satisfied by local\supply. Thus, local market efficiency maximized, and the market objective is satisfied by the current modeling.

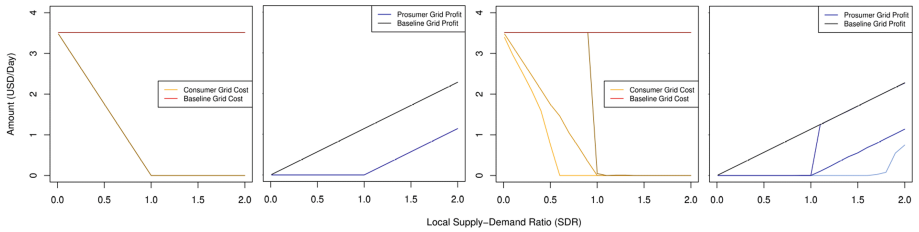

Fig. 6. Local-level and agent-level market efficiency. Left to right: consumer and prosumer grid cost, respectively, and then consumer grid cost and prosumer grid profit again, respectively, with agent-level outcome resolution. In all plots, values produced without the local market (i.e. only baseline main-grid market) are top-most for consumers, left-most for prosumers.

There are significant differences in efficiency, however, when results are separated according to agent-level outcomes (Fig. 6, right side). These can be considered agent matching success differences under merit-order matching in CDA. When an agent finds a match in the local market, they are able to either partially or completely avoid using the more-expensive/less-profitable retail marketplace. Thus, an agent's grid-derived cost decreases as their local matching success increases, and the converse is true for grid-derived profit. The LEM meets all demand of some consumers when SDR $>$ 0.5 while

others are not matched at all until SDR >= 1. Similarly, some prosumers are unable to match when SDR > 1, while others consistently find matches in SDR's in {0.01, 0.1, …, 1.8}.

In Sect. 3.1, agents were shown to remain competitive with other agents of the same type (prosumer or consumer) in all SDR's, under the current parameter tuning. Therefore, we conclude that these results emerge from market design itself. Specifically, these outcomes may be produced by the merit-order bid matching used in CDA.

While technical market access is realized for all agents in the local marketplace, we may consider "effective" market access as whether or not an agent can, in general practice, expect to secure matches for their supply or demand locally. These results imply significant differences in effective market access among LEM users under the CDA design, and support the p2p market design analysis provided by [24]. Effective access for system users under normal operation is another important goal of public utility distribution; these results suggest another obstacle for CDA market use in distributed energy infrastructure, beyond supplementary energy markets like the one currently demonstrated by LO3 Energy in the Brooklyn Microgrid. This issue may also suggest against CDA use in islanded microgrid systems; in these systems, energy cooperatives may provide a more suitable design [1].

3.4 Local Market Returns and Outcome Stability

Local market benefit results are shown in Fig. 7 (left-side plots). When SDR < 0.5, the mean and maximum local cost averages observed for consumers in each SDR differ by less than $0.5 USD/day. The largest gap is observed when SDR = 0.7, at around $1 USD/day. Consumer average cost results are more consistent when SDR >= 1, where the range between minimum and maximum is around $1 USD/day, and the mean is near the median between these. For low-income consumers, a cost difference of $1 USD/day may have a significant impact on household finances. Also, the minimum average local consumer cost observed is zero when SDR < 1, indicating that some consumers may see zero benefit from the LEM unless an average system operating state of SDR >= 1 is achieved. For prosumers, local market profits are consistent and low when SDR <= 1, with the largest min-max difference of about $0.5 USD/day at SDR = 1. When SDR < 0.6, no difference in prosumer profits are observed. However, in cases when SDR > 1, significant differences are produced. Mean observed profit average was around $2 USD/day, maximum was nearly $3.5 USD/day, and some prosumers saw $0 USD/day average profit from the local market.

Aside from indicating a potential issue with distributive fairness, a wide range of results for similar agents raises an important question: are day-to-day agent outcomes consistent? To answer this question, standard deviations of agents' individual results across all settlements in a simulation were calculated, and minimum, mean, and maximum reported standard deviations (σ) were plotted for each SDR. The results are shown in the right-side plots of Fig. 7. According to the current results, some consumers and prosumers may consistently experience no variation (i.e. $\sigma = 0$) in their benefit from the local market. However, for most agents in many SDR scenarios, this may not be the case. For both types of agents, average day-to-day outcomes from the LEM may vary by

over $1.5 USD; for consumers, the maximum variation observed was $1.7 USD, while for prosumers the maximum was $1.9 USD.

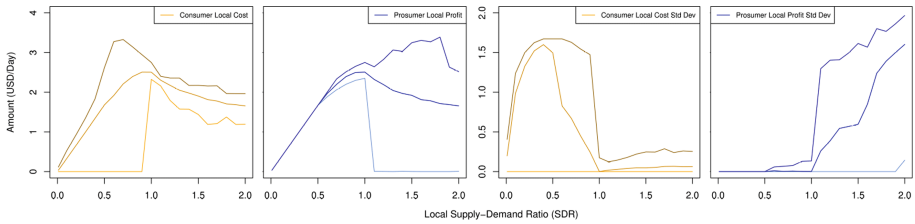

Fig. 7. Statistics of agent-level market benefit and variation in agents' daily results. From left to right: consumer local cost, prosumer local cost, standard deviation in consumer daily cost, standard deviation in prosumer daily profit.

A steep increase in mean and maximum observed variation is seen for consumers when SDR < 0.4. Most consumers will often find no matching with local suppliers in this SDR range, due to relative supply scarcity and the use of merit-order bid matching. Accordingly, many consumers' local costs are zero, initially. But as relative local supply increases, the number of consumers securing local matches increases consistently. Due to competitive bidding and merit-order bid matching, though, individual matching consistency remains low. More consumers are able to consistently secure bid matching in the local market when SDR $>= 0.4$; average and maximum observed outcome variation decrease as SDR $\rightarrow 1$, and average consumer outcome variation is near zero when SDR $>= 1$.

Maximum outcome variation greater than zero for consumers and prosumers when SDR > 1 and SDR $<= 1$, respectively, suggests some degree of sub-optimality in agent learning. But on average, prosumer outcome variation is approximately zero when SDR $<= 1$. When SDR > 1, maximum observed prosumer variation increases sharply, reaching $1.3 USD when SDR $= 1.1$. When SDR > 1, average variation increases in an overall linear trend, eventually reaching $1.6 USD. As SDR increases, each prosumer's supply increases, meaning that fewer prosumers are matched with local buyers. Considering prosumer competitiveness, and the CDA's merit-order bid matching use, fewer matches in each market settlement means greater inconsistency in individual prosumers' matching success.

As indicated in [14], multiple Nash equilibra can be shown for computational electricity markets - thus, such notable levels of day-to-day agent results variation may be surprising. However, the LEM represents an example of a non-stationary multi-agent strategic game; non-stationarity is known to be an issue in these games for equilibrium convergence guarantees under value-based multi-agent learning algorithms [26]. For systems using such learning, the concept of *cyclic equilibrium* has emerged, in which systems are shown to converge to cycling through states produced by a finite set of stationary learning policies. In these cases, we can consider that the length of a cycle may be directly related to the variation in agent outcomes produced by the range of cycle states. Consistent with previous observations of a variety of possible Nash equilibria points in

electricity markets, these results suggest that there exists a wide -- but not unbounded -- number of equilibria that a CDA-based LEM may converge to in a given SDR.

For consumers, the suggested potential variation in day-to-day outcomes would mean uncertainty in energy bills. While undesirable for all consumers, this would have a stronger impact on low-income users. Low-income Brooklyn Microgrid users, for example, may be vulnerable to this impact if they choose to participate in the LEM. For prosumers, outcome volatility implies increased investment risk. Over time, sustained volatility may produce less-favorable financing terms for potential new prosumers, which itself entails a number of negative impacts. Possible cyclic equilibria and day-to-day outcome variation under CDA design should therefore be considered in future work.

4 Conclusion and Future Work

In this study, expected system-level and agent-level outcomes from a simulated local energy marketplace (LEM) were evaluated. The local energy market was modeled after the virtual LEM operated by LO3 Energy in the Brooklyn Microgrid, which features a double-sided auction mechanism with closed order book and discrete settlement times (CDA). Simulations were separated into scenarios according to 21 possible supply-demand ratios (SDR's) for real-world settlement. Results were analyzed according to four metrics; from each metric, potential issues in expected outcomes were discovered, which may emerge from CDA market design dynamics.

While real-world supply generation and load demand will vary spatially and temporally in energy systems, including in LEM's, consider that a unique SDR is produced at each market settlement time. Thus, expected real-world LEM impacts may be evaluated as a weighted sum of SDR-specific analysis results. To reduce simulation complexity and more clearly isolate the impact of market design itself, the current work only considers average consumer demand; real-world deviation from average demand may be represented by independent scalings of each term in the weighted summation. This analysis approach may produce a more generalized view of expected market design outcomes, compared to previous approaches. Currently, data from real-world LEM settlement is generally not made public. However, results should be further validated as real-world LEM settlement data becomes available.

The current simulation analysis suggests that the CDA market may improve outcomes at the local level compared to the baseline retail market. However, in nearly all SDR scenarios considered, a local affordability threshold was not met on average -- while some SDR outcomes suggest a potential deficit in profitability for prosumers. Additionally, while results show that the CDA market may maximize local-level market efficiency, agent-level results may be far less optimal. Significant differences in market benefit and effective access are seen among the homogeneous agents simulated, and many SDR scenarios may produce volatility in agents' day-to-day market outcomes. Affordability is an important goal for energy systems, and LEM sale profitability is essential for systems where supply from distributed and privately-owned generation resources is expected to be available. Additionally, the simulated market produced significantly varied outcomes for similar user agents. Further results analysis suggests potential for considerable volatility in day-to-day outcomes for user agents in a CDA market, which may produce issues for

both consumers (low-income consumers especially) and prosumers, and may potentially inhibit user base growth. Further investigation of these mechanism design concerns is recommended.

The current results may support researchers working to identify and address LEM design issues, system engineers in designing successful energy projects, and community and public-policy decision-makers in making informed choices regarding local energy projects and related policies. We can consider LEM's as examples of complex sociotechnical systems; therefore, LEM design development and analysis may be significantly improved by considering factors such as local socioeconomic inequality, and by modeling heterogeneity in the energy sale or purchase preferences of system users. The current results suggest that notable disparities may be found in agent-level LEM outcomes under the CDA market design if these factors are integrated into agent modeling. Currently, all agents exclusively consider their own economic benefit, but other user preferences may include a desire to support the LEM, even at greater cost / lower profit, for social or environmental reasons. Further analysis of CDA and other LEM designs, and further design comparison work following [4] and [11], may support the development of effective and equitable next-generation energy infrastructure via distributed energy systems integrating renewable generation.

Acknowledgements. This research was funded by the Guangdong Pearl River Plan (2019QN01X890), National Natural Science Foundation of China (Grant No. 71971127), and the Hylink Digital Solutions Co., Ltd. (120500002). Funding sources had no role in the areas of study development, execution, data analysis, results interpretation, or manuscript production. Authors also declare that they hold no conflicts of interest in any of these areas. SB would like to thank Dr. Yao Hu for valuable support and feedback in manuscript drafting and submission.

References

1. Parag, Y., Sovacool, B.K.: Electricity market design for the prosumer era. March 2016. https://doi.org/10.1038/NENERGY.2016.32
2. Tushar, W., Saha, T.K., Yuen, C., Smith, D., Poor, H.V.: Peer-to-peer trading in electricity networks: an overview. IEEE Trans. Smart Grid **11**(4), 3185–3200 (2020). https://doi.org/10.1109/TSG.2020.2969657
3. Mengelkamp, E., Gärttner, J., Rock, K., Kessler, S., Orsini, L., Weinhardt, C.: Designing microgrid energy markets: a case study: the Brooklyn Microgrid. Appl. Energy **210**, 870–880 (2018). https://doi.org/10.1016/j.apenergy.2017.06.054
4. Zhou, Y., Wu, J., Long, C.: Evaluation of peer-to-peer energy sharing mechanisms based on a multiagent simulation framework. Appl. Energy **222**(9), 993–1022 (2018). https://doi.org/10.1016/j.apenergy.2018.02.089
5. Liang, Y., Member, S., Guo, C., Ding, Z., Hua, H.: Agent-based modeling in electricity market using deep deterministic policy gradient algorithm. IEEE Trans. Power Syst. **8950**(c), 1–13 (2020). https://doi.org/10.1109/TPWRS.2020.2999536
6. Tellidou, A.C., Bakirtzis, A.G., Member, S.: Agent-based analysis of capacity withholding and tacit collusion in electricity markets. IEEE Trans. Power Syst. **22**(4), 1735–1742 (2007)
7. Rosen, C., Madlener, R.: An auction design for local reserve energy markets. Decis. Support Syst. **56**, 168—179 (2013). https://doi.org/10.1016/j.dss.2013.05.022

8. Cintuglu, M.H., Martin, H., Mohammed, O.A.: Real-time implementation of multiagent-based game theory reverse auction model for microgrid market operation. IEEE Trans. Smart Grid **6**(2), 5090 (2016)
9. Wang, Z., Member, S., Paranjape, R.: Optimal residential demand response for multiple heterogeneous homes with real-time price prediction in a multiagent framework. IEEE Trans. Smart Grid **8**(3), 1–12 (2015)
10. Lamparter, S., Becher, S., Fischer, J.: An agent-based market platform for smart grids, pp. 1689–1696 (2010)
11. Mengelkamp, E., Staudt, P., Garttner, J., Weinhardt, C.: Trading on local energy markets: A comparison of market designs and bidding strategies. In: International Conference on the European Energy Market EEM (2017). https://doi.org/10.1109/EEM.2017.7981938
12. Roth, A.E., Erev, I.: Learning in extensive-form games: experimental data and simple dynamic models in the intermediate term. Games Econ. Behav. **8**(1), 164–212 (1995). https://doi.org/10.1016/S0899-8256(05)80020-X
13. Erev, I., Roth, A.E.: Roth erev reinforcement learning 1998.pdf. Am. Econ. Rev. **88**(4), 848–881 (1998)
14. Nicolaisen, J., Petrov, V., Tesfatsion, L.: Market power and efficiency in a computational electricity market with discriminatory double-auction pricing. IEEE Trans. Evol. Comput. **5**(5), 504–523 (2001)
15. Average Monthly Electricity Bills. Consolidated Edison, Inc. [Online]. http://www.coned.com/_external/cerates/documents/average_monthly_electricity_bills.pdf. Accessed 18 Jul 2021
16. Monthly Average Retail Price of Electricity - Residential - NYSERDA. https://www.nyserda.ny.gov/Researchers-and-Policymakers/Energy-Prices/Electricity/Monthly-Avg-Electricity-Residential. Accessed 07 Jul 2021
17. Electricity Rates and Usage for Brooklyn, NY, New York Energy Ratings. [Online]. https://www.nyenergyratings.com/electricity-rates/new-york/brooklyn. Accessed 18 Jul 2021
18. Khorasany, M., Mishra, Y., Ledwich, G.: Market framework for local energy trading: a review of potential designs and market clearing approaches (2018). https://doi.org/10.1049/iet-gtd.2018.5309
19. Kontokosta, C.E., Reina, V.J., Bonczak, B.: Energy cost burdens for low-income and minority households: evidence from energy benchmarking and audit data in five U.S. cities. J. Am. Plan. Assoc. **86**(1), 89–105 (2020). https://doi.org/10.1080/01944363.2019.1647446
20. Mayor, N.Y.C., August, E.O.: Understanding and Alleviating Energy Cost Burden in New York City NYC Mayor's Office of Sustainability and the Mayor's Office for Economic Opportunity, August 2019
21. Mengelkamp, E., Notheisen, B., Beer, C., Dauer, D., Weinhardt, C.: A blockchain-based smart grid: towards sustainable local energy markets. Comput. Sci. Res. Dev. **33**(1–2), 207–214 (2017). https://doi.org/10.1007/s00450-017-0360-9
22. Livingston, D., Sivaram, V., Freeman, M., Fiege, M.: Applying blockchain technology to decentralized, no. 4, pp. 2–3 (2018). [Online]. https://blogs.systweak.com/applying-blockchain-technology-to-waste-management/
23. Brooklyn Microgrid Gets Approval for Blockchain-based Energy Trading | Energy Central. https://energycentral.com/c/iu/brooklyn-microgrid-gets-approval-blockchain-based-energy-trading?utm_medium=PANTHEON_STRIPPED. Accessed 08 Jul 2021
24. Sousa, T., Soares, T., Pinson, P., Moret, F., Baroche, T., Sorin, E.: Peer-to-peer and community-based markets: a comprehensive review. Renew. Sustain. Energy Rev. **104**, 367–378 (2019). https://doi.org/10.1016/j.rser.2019.01.036

25. Beattie, S.: Supplementary Material on Parameter Space Reduction for Agent Learning Model Tuning Tests. [Online]. Available: https://tinyurl.com/5bvuwjea. Accessed 18 Jul 2021
26. Zhang, K., Yang, Z., Başar, T.: Multi-Agent Reinforcement Learning: A Selective Overview of Theories and Algorithms. Handbook of Reinforcement Learning and Control, pp. 321–384 (2021)

The Power of Analytics in Epidemiology for COVID 19

Mohammed Amine Bennouna[1], David Alexandre Nze Ndong[2], Georgia Perakis[2], Divya Singhvi[3], Omar Skali Lami[1(✉)], Ioannis Spantidakis[1], Leann Thayaparan[1], Asterios Tsiourvas[1], and Shane Weisberg[2]

[1] Operations Research Center, Massachusetts Institute of Technology, Cambridge, MA 02139, USA
oskali@mit.edu
[2] Sloan School of Management, Massachusetts Institute of Technology, Cambridge, MA 02139, USA
[3] NYU Stern School of Business, New York, NY 10012, USA

Abstract. Mitigating the COVID-19 pandemic poses a series of unprecedented challenges, including predicting new cases and deaths, understanding the true prevalence, and allocating the different vaccines across regions. In this paper, we describe our efforts to tackle these issues. We first discuss the methods we developed for predicting cases and deaths using a novel ML based method we call MIT-Cassandra. MIT-Cassandra is currently being used by the CDC and is consistently among the top 10 methods in accuracy, often ranking 1st amongst all submitted methods. We then use this prediction to model the true prevalence of COVID 19 and incorporate this prevalence into an optimization model for fair vaccine allocation. The latter part of the paper also gives insights on how prevalence and exposure of the disease in different parts of the population can affect the distribution of different vaccine doses in a fairway. Finally, and importantly, our work has specifically been used as part of a collaboration with MIT's Quest for Intelligence and as part of MIT's process to reopen the institute.

Keywords: COVID-19 · Prevalence · Machine learning · Epidemiology · Ensemble methods · Optimization of vaccine distribution

1 Introduction

COVID-19 is an infectious disease caused by the acute respiratory syndrome coronavirus-2, SARS-CoV-2. Starting in 2019, the virus quickly spread throughout the world. The proportionally high level of asymptomatic cases, limited testing resources, and the higher mortality rate compared to the seasonal flu has forced society to dramatically change how it operates both economically and socially.

All levels of government, institutions, and private organizations have rushed to respond to this pandemic. Nevertheless, the changing nature of the pandemic has made short- and long-term planning of activities difficult. A challenge that has impacted organizations' ability to respond to the pandemic is the high level of asymptomatic carriers

R. Qiu et al. (Eds.): ICSS 2021, LNOR, pp. 254–268, 2021.
https://doi.org/10.1007/978-3-030-90275-9_21

as asymptomatic individuals are considered responsible for over half of all COVID-19 spread. Ideally population-wide testing would lead to the identification and isolation of asymptomatic carriers, but this is not a feasible solution with current testing capabilities.

This leaves governments and institutions unable to assess the true risk they face when making decisions. Understanding true infection levels has become particularly important as the United States has begun the roll out of different vaccines (in the US there are three vaccines so far). Supply of these vaccines is currently limited. State-level governments need to decide how to allocate vaccines, including whether to prioritize first or second doses. In this paper, we tackle these issues by proposing a novel, end-to-end framework for case and death prediction. We then transform the detected cases into true cases to determine the true prevalence of the disease. Finally, we optimize over vaccine allocation based on the predicted prevalence under fairness and other operational constraints.

1.1 Contributions

- **We introduce an ensemble method that accounts for different aspects in the COVID-19 case and death evolution**: We first develop four individual predictive models, each of which captures different aspects of the disease progression. These four models are aggregated to create accurate deaths and cases predictions. We provide upper bounds on the prediction error for each individual model, we illustrate that the aggregate model's prediction is more robust to changes in the pandemic and we prove prediction accuracy and variability bounds for the aggregate model.
- **We demonstrate accurate short- and long-term predictions for both cases and deaths**: We compare our model to other models used by the Center for Disease Control (CDC) and we show that our models consistently perform among the best both in the short-term and long-term future and at several different stages of the pandemic.
- **We propose a prevalence method to estimate true disease spread**: We propose a method for determining the "true" cases of COVID-19 estimating the prevalence of the disease in different regions.
- **We propose an optimization framework for determining the distribution of different vaccines and discuss interesting insights**: The optimization model we propose incorporates population heterogeneity for different types of vaccines with varying efficacy. The optimization model accounts for varying prevalence of COVID-19 in each region, as well as different mortality rates for different age groups. Using this model, we are able to create recommendations for state-level governments and the corresponding counties and show insights into the structure of optimal vaccine allocation.
- **We discuss the impact of this work through our collaboration with MIT and the CDC**: The work in this paper has been the outcome of a collaboration on the MIT COVID-19 Response System (MCRS). The prediction and prevalence models in this paper were developed as part of the MCRS effort since accurate forecasts of local prevalence rates are crucial to understanding the appropriate degree of returning to MIT campus. Furthermore, the models in this paper are used on the CDC website (under the name of **MIT-Cassandra** to help the CDC and government entities understand and mitigate the spread of the pandemic.

1.2 Literature Review

In this paper we introduce different predictive models of COVID-19. The first model is a feature-based Markovian representation approach and is related to offline Reinforcement Learning (RL). Offline RL [1] tackles situations where experimentation is not feasible, and learning is performed only from a fixed batch of transition data. The second model is a Nearest Neighbor Approach on timeseries inspired by the KNN algorithm. To the best of our knowledge, despite some early work by [2], there have not been as many applications of KNN to time series prediction problems until recently. The third model is a Deep Learning approach based on the Bidirectional Long Short-Term Memory (LSTM) Networks [3]. The final prediction method we use is a generalized compartmental epidemiology model that can account for multiple waves of the pandemic, introduced in [4]. In addition to constructing four different models for COVID-19 case and death prediction, we also aggregate these outputs into final combined predictions for cases and deaths. Although we will not delve deeply into a literature review of this area due to space limitations, we refer the interested reader to [5] and [6] and the references therein for an in-depth discussion of ensemble methods for aggregation. This aggregated model is then used for extrapolations to true prevalence and optimal vaccine allocation.

2 Predicting COVID19 Detected Cases

When choosing a prediction model for the evolution of the disease, there are several trade-offs to consider. Some models, such as the epidemiological models impose a lot of structure on the problem, based on prior knowledge, while others, such a machine learning method learn general classes of functions from the data, with little to no problem-specific structure. It is unclear what model to choose based on these trade-offs. We identify four popular classes of such models: reinforcement learning, machine learning, deep learning, and epidemiological models. We combine all of these to bring together the best of all worlds. We focus on four novel individual models that we have developed or extended for this problem, one from each of these four classes.

i. **A feature-based Markovian representation approach** that constructs a Markov Decision Process (MDP) representation of the COVID-19 evolution. We refer to this method as MRL that is, Minimal Representation Learning. MRL assumes the observed COVID-19 data on the evolution of each region was generated from an unknown continuous state space Markovian dynamic system where the states correspond to the features of regions (e.g. growth rate, mobility, government retractions). MRL uses the observed data to learn a partition of the feature space into "states" of a finite reduced MDP representation of this dynamic system. This learnt MDP representation of COVID-19 evolution allows then to predict future evolution and counterfactuals given alternative restrictive measures. We further introduce a randomized version of MRL we name r-MRL. r-MRL uses *random batch-sampling* from the set of paths as well as *bootstrapping* from the set of features in order to learn multiple MDP representations and combines them for a more robust prediction.
ii. **A nearest-neighbor weighted time-series approach** that generalizes the k-nearest neighbors approach for time-series prediction. We refer to this method as KNN. The

KNN explores the *similarity* between the observed time-series and its relation to the time-series we want to predict. To model this relationship, we develop a new inverse weight distance metric to determine relevant time-series neighbors and demonstrate that the method performs exceptionally well on real data. In addition, we discuss how to incorporate other features like temperature and vaccination percentage to further increase the prediction accuracy. Finally, the nature of our model allows for interpretable results since it matches current behavior of the disease with previous observations in other regions.

iii. **A Deep Learning approach** that generalizes the recurrent neural network approach. The algorithm is based on a time-series clustering method that generates state-clusters upon which different Bidirectional Long Short-Term Memory (Bi-LSTM) Networks are trained. The Deep Learning approach allow us to leverage the significant COVID-19 data and features that are available to discover highly complex *functional forms* and understand the *recurrent* nature of the evolution prediction.

iv. **An epidemiological approach** that generalizes the SEIRD epidemiological model into a chained version that is able to capture the various waves of the pandemic. We refer to this epidemiological model by C-SEIRD (the abbreviation stands for Chained SEIRD). The C-SEIRD, contrary to the other models, is specifically designed for epidemiological modelling and imposes a structure with *physical interpretation* on the disease evolution. This model leverages the medical understanding of the disease evolution with differential equations and allows *multiple peaks* to better tailor to the COVID-19 structure.

2.1 An Aggregate Predictive Method: MIT-Cassandra

Let $N \in \mathbb{N}$ be the number of regions for which we want to make a prediction. Let $T \in \mathbb{N}$ the number of time periods used in the data to train the models. In this paper, time periods refer to number of days. We define $H \in \mathbb{N}$ as the time horizon for the predictions, i.e., we make predictions for time $t \in [T+1, T+H]$.

We apply these models to make predictions for each region $i \in [N]$, at each time period $t \in [T+1, T+H]$. In this section, we discuss how to aggregate these predictions in order to obtain one single "best" prediction. For its forecasts for COVID-19 cases and deaths, the CDC uses a simple average of select submitted models that have performed well historically. We will extend and go one step further by using Machine Learning (ML) on an appropriate validation set in order to create the final prediction through an ensemble of the four proposed methods in this paper.

2.1.1 Formulation

Let $\hat{y}_{i,t,m}$ denote the predicted outcome value (assume this represents the cumulative number of cases for simplicity) for region i at time t made by model $m \in \mathcal{M}$. $\mathcal{M}$ is the set of all individual models that we want to aggregate. $\hat{y}_{i,t}$ represents the actual outcome value for i at time t. We assume all models were trained up to a time $T_{val} < T$. We choose a class of ML functions $\mathcal{F}$. Our goal is to find for each region i, the best aggregator f_i within this class that takes predictions $\hat{y}_{i,t,m}$, $\forall m \in \mathcal{M}$ and outputs a single

prediction $\hat{y}_{i,t}$ i.e., $\hat{y}_{i,t} = \hat{y}_{i,t}^{agg} = f_i\big(\hat{y}_{i,t,m}\big), m \in \mathcal{M}$. We assume that for each individual model $m_o \in \mathcal{M}$, the function $f_i(\hat{y}_{i,t,m}), m \in \mathcal{M} = \hat{y}_{i,t,m_0}, \forall i, t$ belongs to the set $\mathcal{F}$. We formulate the training problem, for $i \in [N]$, in terms of cases as the problem of minimizing the sum of absolute errors. In the final model we built for MIT and posted on the CDC website, we set $\mathcal{F}$ to be within several ML function forms: Regularized Linear Models, Support Vector Machines (SVM), Classification and Regression Trees (CART), Random Forests (RF), and XGBoost.

2.1.2 Provable Guarantees

We show that the proposed aggregation yields more accurate and robust results than the individual models do separately. We begin by showing that the aggregate model under mild assumptions performs at least as well as the best individual model in-sample, and then we show that the model is also more robust and stable out-of-sample.

Theorem 1. Consider the aggregate model as discussed. Then the aggregate model has:

1. (*In-Sample Predictions*) lower in-sample mean absolute error than each of its individual models. i.e.

$$\sum_{t=T_{\text{vat}}}^{T} \left|y_{i,t} - f_i\big(\hat{y}_{i,t,m}, m \in \mathcal{M}\big)\right| \leq \min_{m \in \mathcal{M}} \sum_{t=T_{\text{vat}}}^{T} \left|y_{i,t} - \hat{y}_{i,t,m}\right|$$

$$\leq \sum_{t=T_{\text{vat}}}^{T} \left|y_{i,t} - \hat{y}_{i,t,m_0}\right|, \forall m_0 \in \mathcal{M}, \forall i \in [N]$$

2. (*Out-of-Sample Predictions*)

   a. (*Robustness*) a lower out-of-sample mean absolute percentage error than at least one of its individual models: that is,

$$E\big[\left|y_i - \hat{y}_i\right|\big] \leq \max_{m \in \mathcal{M}} E\big[\left|y_i - \hat{y}_{i,m}\right|\big]$$

   when $\mathcal{F}$ is the set of convex combinations.

   b. (*Variance*) a lower out-of-sample variance than at least one of its individual models: that is,

$$\text{var}\big(\hat{y}_i\big) \leq \max_{m \in \mathcal{M}} \text{var}\big(\hat{y}_{i,m}\big)$$

Theorem 1 guarantees that the aggregate model always has a better in-sample fit in terms of predictive error. Theorem 1.2.(a) and 1.2.(b) show that the aggregation method reduces variability and also adds robustness to the final prediction. These results compare the aggregate model to the worst performing model for out-of-sample predictions. As such, the worst-performing model is not known in advance and may be different for the worst expected value and the worst variability. The aggregate model ensures a minimum

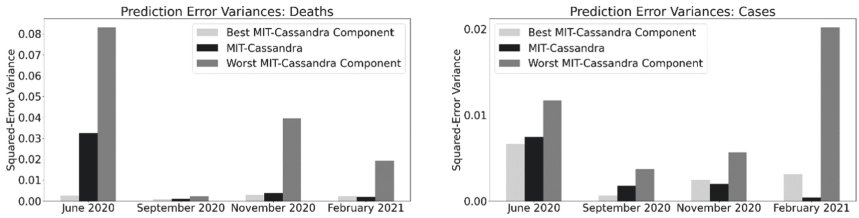

Fig. 1. Experiments with COVID-19 data show the variance of the errors of the aggregate model predictions (black) always are lower than at least one of the component models (gray), and close to that of its more stable component model (light gray)

level of performance across the board out-of-sample, while being the best in-sample. We can also observe experimentally in Fig. 1 that the variance of the error itself (wMAPE) for predictions of deaths (left) and cases (right) by the aggregate model is lower than at least one of its component models at various stages in the pandemic and is close to that of its most stable component model. This evidence is indicative of high-quality predictions, both in terms of bias and variance.

3 Results with Actual COVID-19 Data

3.1 Data Sources and Feature Spaces

Multiple data courses were utilized in order to construct the dataset used by the models. Cases and deaths are collected from the Center for Systems Science and Engineering of John Hopkins. State-level social distancing policies are retrieved from the COVID19StatePolicy Github repository, and global population mobility reports are collected from Google. We used historical weather data provided by the National Climatic Data Center (NCDC) of National Oceanic and Atmospheric Administration (NOAA) and Demographics data provided by the US Census Bureau.

The MRL feature space was constructed based on the historical growth rates, on both cases and deaths, including multiple lags to capture short-term and long-term effects. Ratios on differences between cases and deaths helped as well refining the MDP state space. Finally, we incorporated mobilityrelated data such as the average time spent in commutes per region in 2020 from Google that proved to be relevant. Experimental results for the Bi-LSTM and KNN models showed that in addition to deaths and cases, past mobility and temperature improved case predictions by more than 20% the accuracy of the models. Moreover, for deaths prediction past case growth rates also improved the predictive power of the models. Finally, in the latest predictions starting January 2021, we have also included vaccinations as a feature in all models, except the C-SEIRD, which is not feature based.

3.2 Model Predictions

The component and aggregate models predict the cumulative number of deaths and cases for each state or county in the US. To measure prediction accuracy, we use the mean

Table 1. Accuracy of the MIT-Cassandra model at various points during the pandemic in US regions. Alaska, Hawaii excluded

Month	Region	wMAPE-Deaths	wMAPE-Cases
June, 2020	Midwest	0.118	0.427
	Northeast	0.029	0.716
	South	0.062	0.462
	West	0.026	0.305
	USA	0.051	0.440
September, 2020	Midwest	0.015	0.210
	Northeast	0.004	0.087
	South	0.024	0.159
	West	0.009	0.367
	USA	0.013	0.205
November, 2020	Midwest	0.056	0.111
	Northeast	0.009	0.267
	South	0.038	0.387
	West	0.030	0.356
	USA	0.031	0.262
February, 2021	Midwest	0.022	0.499
	Northeast	0.020	0.525
	South	0.027	0.477
	West	0.016	0.219
	USA	0.022	0.438

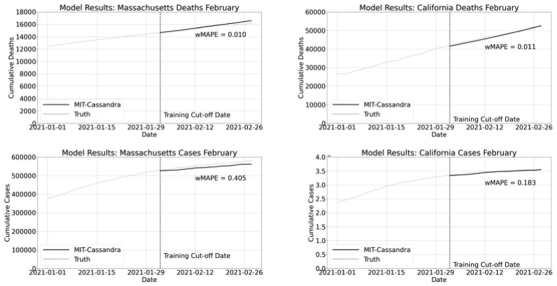

Fig. 2. Statewide predictions (black) from the aggregate model alongside true death and detected case counts (gray) for the month of February in Massachusetts (left) and California (right)

absolute percent error weighted by the true number of deaths or cases in each state (wMAPE, i.e., weighted Mean Absolute Percentage Error). Table 1 shows prediction accuracy for the aggregate model across different US regions as well as across the country as a whole.

We test the model on four months at different points during the pandemic. For each of these months, the models were trained and validated up to the last date of the previous month, and all predictions beyond that date were out-of-sample. Due to data issues, the states of Alaska and Hawaii (as well as the District of Columbia and other US territories) are excluded from the averages shown here.

For the purpose of estimating prevalence and optimally allocating vaccine doses, it is important to demonstrate that the aggregate model makes accurate predictions on the level of individual states as well. The plots in Fig. 2 show more precisely cumulative deaths and cases alongside our aggregate model predictions for Massachusetts and California for the month of February. The model is able to closely approximate the true evolutions of cases and deaths in these states at this time: average percentage errors for these predictions over this month are shown on the plots.

We extensively benchmark these results at different time periods, with different time horizons, for the predictions for both cases and deaths against the state-of-the-art models submitted to the CDC. We find that our model is particularly competitive in terms of out-of-sample wMAPE, being consistently in the top 10 methods (out of more than 50), and often ranking 1st at different stages of the pandemic. The results can be seen in Tables 2 and 3.

In the next section will discuss estimating the true prevalence of the disease, as opposed to the number of detected cases, which is essential for optimizing vaccine allocation.

Table 2. Model results comparing to CDC models for predicting deaths

Month	1 week ahead		2 weeks ahead		3 weeks ahead		4 weaks ahead	
	wMape	CDC Rank	wMape	CDC Rank	wMape	CDC Rank	wMape	CDC Rank
June	0.019	1	00.39	2	0.07	12	0.108	15
September	0.012	30	0.015	23	0.019	11	0.022	7
February	0.011	1	0.019	1	0.028	5	0.041	14

Table 3. Model results comparing to CDC models for predicting cases

Month	1Â week ahead		2Â weeks ahead		3Â weeks ahead		4 weaks ahead	
	wMape	CDC Rank	wMape	CDC Rank	wMape	CDC Rank	wMape	CDC Rank
September	0.168	14	0.189	7	0.211	7	0.224	7
November	0.260	6	0.254	1	0.254	1	0.278	2

4 From Detected Cases to True Prevalence

One major challenge of most COVID-19 predictive methods is that they are trained on confirmed cases, rather than the true number of cases. In this section, we propose a model that determines the true cases from the detected cases, also referred to as prevalence, using random testing serology data from the CDC.

The main intuition for our prevalence model is that testing is limited and is not done uniformly at random but is rather biased towards the population that is more likely to test positive. Rather than a constant ratio between positivity rates in tests and prevalence, we assume a linear relationship. For a random person in the population of interest, we denote $\mathcal{I}$ the random variable of being infected, $\mathcal{T}$ the random variable of being tested, $\mathcal{N}$ the random variable of not being tested ($\mathcal{N} = \overline{\mathcal{T}}$). In what follows we assume that test results for COVID-19 are 100% accurate. The linearity assumption can then be written as follows $\mathbb{P}(\mathcal{I}|\mathcal{N}) = \alpha\mathbb{P}(\mathcal{I}|\mathcal{T})$, where α is a constant capturing how likely it is for someone to be infected knowing that one is not tested versus one is tested. This gives rise to Eq. (1).

$$\mathbb{P}(\mathcal{I}) = \mathbb{P}(\mathcal{I}|\mathcal{T})\mathbb{P}(\mathcal{T}) + \mathbb{P}(\mathcal{I}|\mathcal{N})\mathbb{P}(\mathcal{N}) = \mathbb{P}(\mathcal{I}|\mathcal{T})(\alpha + (1-\alpha)\mathbb{P}(\mathcal{T})) \tag{1}$$

We notice that $\mathbb{P}(\mathcal{T})$ and $\mathbb{P}(\mathcal{I}|\mathcal{T})$ can be evaluated empirically by tests over population and detected cases over tests, respectively. Hence, we obtain Eq. (2), which we can compute from the data and the predictions as long as we know the value of constant α.

$$\#Infected = (\#Cases/\#Tests) \times Population \times \left[\alpha + (1-\alpha) \times (\#Tests/Population)\right] \tag{2}$$

In order to evaluate α for a given region, we use serology and random testing data from the CDC (https://www.cdc.gov/coronavirus/2019-ncov/cases-updates/geographic-seroprevalence-surveys.html). This data provides an estimate for $\mathbb{P}(\mathcal{I})$ in different regions and times, which we can use to solve for α. The advantage of this method is that while the different probabilities are time-dependent, α is not. This implies that we can use this α for back-testing and future predictions.

For the purpose of allocating vaccines optimally, we must estimate this true prevalence for each county so that we can allocate vaccines to areas where they will make the most difference. As an example, Fig. 3 shows detected cases (left) and estimated prevalent cases during this span (right) for each county in Massachusetts, as our case study focuses on county-level allocation for this state.

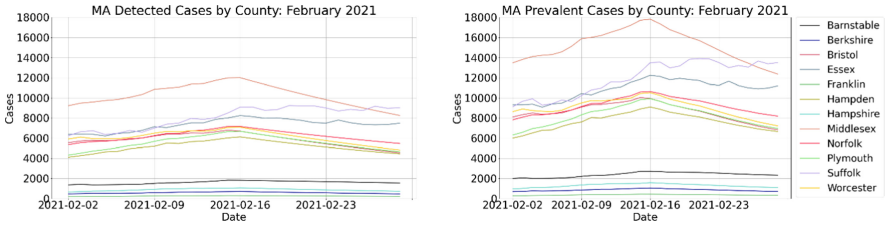

Fig. 3. Detected cases (left) and estmated total cases (right) in each Massachusetts county during the month of Feburary 2021. Total prevalence using $\alpha = 0.11$

5 Application to Vaccine Allocation

5.1 Model Formulation

In this section we use the prevalence estimation and case and death predictions determined in the previous sections, in particular Fig. 3 in order to optimize the different vaccine allocations across counties and for different population types, vaccine types, and across first and second doses. The goal is to minimize the expected number of deaths (alternatively expected number of cases) under capacity and fairness constraints.

We consider the problem of a centralized planner who has to allocate a finite number of 1-dose (K_1) and 2-dose (K_2) vaccines across J counties over T time periods. Each county is heterogeneous and is resided by I different population types. Population types differ from one another based on characteristics that drive the spread of the virus, and the efficacy of the vaccine. The objective of the centralized planner is to minimize the total expected number of deaths. To model this objective, we fist define other population level parameters.

For a vaccine $k \in [K_1 + K_2]$ let $p_{1,k}$ and $p_{2,k}$ denote the probability of being immune to the virus after receiving one and two doses respectively. Also for an individual, $i \in I$, let $\hat{p}_{t,i,j}$ denote the probability of being infected by the virus without any immunity at time t, at county j. This probability is given by our predicted prevalence. Once an individual from a population gets the virus, we let the mortality of the individual be

given by $m_{t,i,j}$. Finally, since we are solving a multi-period problem, we also need to model the evolution of the pandemic over the population. To accomplish this, we let $n^0_{t,i,j}$, $n^{1,k}_{t,i,j}$, $n^{2,k}_{t,i,j}$, and $c^0_{t,i,j}$, $c^{1,k}_{t,i,j}$, $c^{2,k}_{t,i,j}$ denote the number of susceptible people and the number of cases that received 0, 1 and 2 doses of vaccine k respectively, at time t, in county j, from population i. We let $v^{1,k}_{t,i,j}$ and $v^{2,k}_{t,i,j}$ denote the decision variable of the central planner which denotes the number of *allocated* vaccines for the first and the second dose to different counties, population types, and time.

There are a few considerations that must be accounted for, including population dynamics based on when people of particular subgroups get infected and vaccinated, fairness constraints to ensure the allocation across regions is equitable and capacity constraints. We model that the centralized planner wishes to minimize the total expected number of deaths, over time region and sub-population.

$$\min_{v} \sum_{t=1}^{T}\sum_{i=1}^{I}\sum_{j=1}^{j}\Bigg(n^0_{t,ij}\hat{p}_{t,j,j}m_{t,i,j} + \sum_{k=1}^{K}\Big(n^{1,k}_{t,i,j}\hat{p}_{\ell,i,j}m_{t,i,j}\big(1-p_{1,k}\big) + n^{2,k}_{t,ij}\hat{p}_{r,j,j}m_{t,i,j}\big(1-p_{2,k}\big)\Big)\Bigg),$$

$$\text{s.t.} \sum_{i=1}^{1}\sum_{j=1}^{J}\Big(v^{1,k}_{t,i,j} + v^{2,k}_{t,ij}\Big) \le V_{max,k,t} + \forall t \in [T], \forall k \in [K]$$

$$n^0_{t,i,j} = n^0_{t-1,i,j} - \sum_{k=1}^{K} v^{1,k}_{t,i,j} - c^0_{t-1,i,j}, \forall t \in [T], \forall i \in [I], \forall j \in [J],$$

$$n^{1,k}_{t,i,j} = n^{1,k}_{t-1,i,j} - v^{2,k}_{t,i,j} + v^{1,k}_{t,i,j} - c^{1,k}_{t-1,i,j}, \forall t \in [T], \forall i \in [I], \forall j \in [J], \forall k \in [K],$$

$$n^{2,k}_{t,i,j} = n^{2,k}_{t-1,i,j} + v^{2,k}_{t,i,j} - c^{2,k}_{t-1,i,j}, \forall t \in [T], i \in [I], \forall j \in [J], \forall k \in [K],$$

$$n^0_{t,i,j}, n^{1,k}_{t,i,j}, n^{2,k}_{t,i,j}, v^{1,k}_{t,i,j}, v^{2,k}_{t,i,j} \ge 0, \forall t \in [T], i \in [I], \forall j \in [J], \forall k \in [K].$$

$$n^{2,k}_{t,i,j} = v^{2,k}_{t,i,j} = 0, \forall t \in [T], i \in [I], \forall j \in [J], \forall k \in [K_1]. \tag{3}$$

To condense the formulation further and make it easier to solve, we use the following new notations: $\beta^{1,k}_{t,i,j} = \sum_{s=t}^{T} \hat{p}_{s,i,j}m_{t,i,j}p_{1,k}$ and $\beta^{2,k}_{t,i,j} = \sum_{s=t}^{T} \hat{p}_{s,i,j}m_{t,i,j}\big(p_{2,k}-p_{1,k}\big)$ and $V^1_{t,i,j,max} = n^0_{0,i,j} - \sum_{s=0}^{t-1} c^0_{s,i,j}$ and $V^2_{t,i,j,max} = n^{1,k}_{0,i,j} - \sum_{s=0}^{t-1} c^{1,k}_{s,i,j}$ (note that these quantities are known and can be pre-computed). The idea behind this re-formulation is transforming minimizing the expected number of deaths to maximizing the expected reduction in deaths through vaccination. We rewrite Formulation (3) into the equivalent Formulation (4). Formulation (4) is exactly our initial vaccine allocation problem, but notice that it does not include the evolution constraints, which are replaced by upper bounds on the number of people eligible for vaccination in each sub-population. This results in a linear integer program with a totally uni-modular matrix defining its feasible region. As a result, (4) can be solved fast and efficiently with a simple linear relaxation.

5.2 Intuition on the Vaccine Allocation Policy

We notice, however, that the vaccination priority (between the different populations and due to the fairness constraints) across counties, populations, time, vaccine type, and first vs. second-dose is determined depending on the values of the coefficients β (these are computed in advance, and depend on the prevalence, the mortality rate, and the vaccine dose efficacy). Given these observations, we obtain the following takeaways directly:

- Note that $\beta^{s,k}_{t,i,j} > \beta^{s,k}_{t+1,i,j} \forall t, j$ and $s \in [1, 2]$. This confirms mathematically that we should vaccinate any given population as soon as possible.
- Note that $\beta^{1,k}_{t,i,j} - \beta^{2,k}_{t,i,j} = \sum_{s=t}^{T} \hat{p}_{s,i,j} m_{s,i,j} \left(2p_{1,k} - p_{2,k}\right)$. For the same time t, population i, and county j, priority between vaccinating first and second doses (for 2-dose vaccines) is entirely determined by the sign of $2p_{1,k} - p_{2,k}$. If $2p_{1,k} > p_{2,k}$, then priority is given to vaccinating entirely the population with the first-dose of the vaccines, and only after that administering the second dose to the population. If $2p_{1,k} < p_{2,k}$, then second-dose administration is prioritized.

$$
\begin{aligned}
\max_v \quad & \sum_{t=1}^{T} \sum_{i=1}^{I} \sum_{j=1}^{J} \sum_{k=1}^{K} \left(\beta^{1,k}_{t,i,j} v^{1,k}_{t,i,j} + \beta^{2,k}_{t,i,j} v^{2,k}_{t,i,j} \right) \\
\text{s.t.} \quad & \sum_{i=1}^{I} \sum_{j=1}^{J} \left(v^{1,k}_{t,i,j} + v^{2,k}_{t,i,j} \right) \leq V_{max,k,t}, \forall t \in [T], \forall k \in [K], \\
& \sum_{i=1}^{I} \sum_{k=1}^{K} \left(v^{1,k}_{t,i,j} + v^{2,k}_{t,i,j} \right) \geq V_{min,t,j}, \forall t \in [T], \forall j \in [J], \\
& 0 \leq \sum_{k=1}^{K} \sum_{s=1}^{t} v^{1,k}_{s,i,j} \leq V^{1}_{t,i,j,max}, \forall t \in [T], \forall i \in [I], \forall j \in [J], \\
& 0 \leq \sum_{s=1}^{t} v^{2,k}_{t,i,j} \leq V^{2,k}_{t,i,j,max} + \sum_{s=1}^{t} v^{1,k}_{s,i,j}, \forall t \in [T], \forall i \in [I], \forall j \in [J], \forall k \in [K], \\
& v^{2,k}_{t,i,j} = 0, \forall t \in [T], i \in [I], \forall j \in [J], \forall k \in [K_1]. \qquad (4)
\end{aligned}
$$

- We also observe several trade-offs between population i, county j, and vaccine type k. The proposed formulation allows us to answer questions around prioritizing highly-effective vaccines in low-prevalence areas, or low-effectiveness vaccines in high-prevalence areas, or vaccinating the high-susceptible population in low prevalence areas or the low-susceptible population in high-prevalence areas.
- Note that (4) does not assume a lag between first and second dose vaccines. Nevertheless, it can be directly incorporated by replacing the second population limit constraint by $0 \leq \sum_{s=1}^{t} v^{2,k}_{s,i,j} \leq V^{2,k}_{t,i,j,max} + \sum_{p=1:\max(t-t_{lag},0)} v^{1,k}_{s,i,j} \forall t, i, j, k$, where t_{lag} denotes the lag which is typically equals 21–28 days, but we can also consider different lags for each vaccine.

5.3 Results with Actual COVID-19 Data

We test this approach on the different Massachusetts (MA) Counties, with three vaccines that we call vaccine MD, vaccine PF and vaccine AZ, with respectively immunity rates for 1 dose of $p_{1,1} = 40\%$, $p_{1,2} = 50\%$ and $p_{1,3} = 75\%$, and immunity rates for 2 doses of respectively $p_{2,1} = 90\%$, $p_{2,2} = 95\%$ and $p_{2,3} = 85\%$.

We utilize the prevalence in each of the 14 MA Counties on February 1st and predict the prevalence and the number of cases in the following 100 days regardless of vaccination. In particular, we split the population into nine age groups: 0–4, 5–17, 18–29, 30–39, 40–49, 50–64, 65–74, 75–84, and 85 +, similar to the process of the CDC[1]. In this experiment, we use as prevalence the output of the aggregate model, without using any age breakdown, i.e., we consider that for the same county, the prevalence across different age groups is the same. We also assume that the mortality is time and county-independent. Additionally, we set the fairness constraint to be equal to half of what the population-proportional allocation would have given (for illustrative purposes, but centralized planner can set this fairness constraint to any value). Finally, we impose a minimum of 28 days-lag between a first and second dose vaccination for the MD vaccine, 21 for the PF vaccine, and 30 days for the AZ vaccine. We show our results in Figs. 4 and 5.

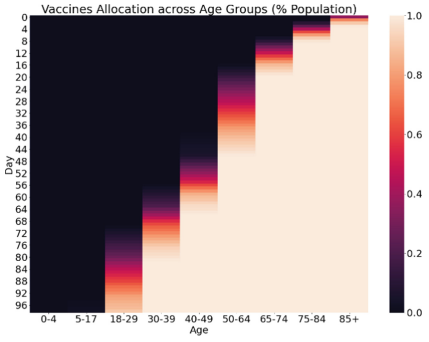

Fig. 4. Cumulative Optimal Vaccine Allocation by Age Group (Represented in % of Age Group Population). The graph is read top to bottom, and the bar for each age group becomes white when 100% of the population of this age group received at least one shot of any vaccine.

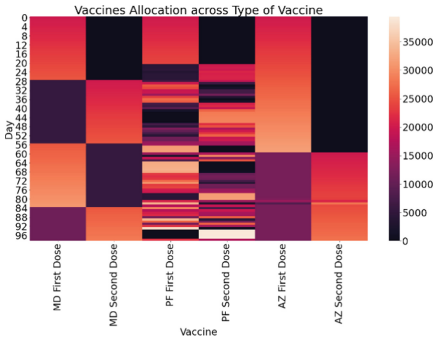

Fig. 5. Optimal Vaccine Allocation by Vaccine Type

Figure 4 shows that the most at-risk population should be vaccinated first, while some people that are less at risk but are in high-prevalence areas should also be vaccinated in parallel but sparingly. Figure 5 shows interesting insights on the vaccine distribution, both among vaccines, but also between first and second doses. For vaccine MD we see that the property $2p_{1,1} \leq p_{2,1}$, applies, which means second dose vaccines should be

[1] https://www.cdc.gov/coronavirus/2019-ncov/covid-data/investigations-discovery/hospitalization-death-by-age.html.

always prioritized (everything else being equal). The figure also shows clearly in the first two columns that as the population is vaccinated with a second dose as soon as they are eligible (28 days after first vaccination for MD, and 21 for PF), first doses are given only in an alternate fashion when the same population cannot receive a second dose yet. For the PF vaccine, $2p_{1,2} > p_{2,2}$, however these two values are very close, so although the prioritization should go to first doses, when a subgroup is entirely vaccinated with a first dose, it is sometimes more effective to start a second dose vaccination for this subgroup instead of moving to another subgroup. This is why the alternation between first and second dose vaccines is less dominant than what we see for vaccine MD. For AZ, where the second dose is mainly a booster, we have $2p_{1,3} \gg p_{2,3}$, we observe that the optimization model prioritizes almost always the first dose vaccination over the second dose vaccination. This translates to few or no second doses of AZ being administered until the end of the experiment.

In conclusion, our optimization approach allows us to understand optimal vaccine allocation in a data-driven way. The broad strokes of the allocation policy align with widely held expectations of how vaccines should be distributed. Namely, high risk age groups and high prevalence areas should be prioritized, but the optimization approach we propose captures more explicitly the tension between these two rules. For example, Fig. 4 seems to suggest that we need to begin to vaccinate lower risk groups if they are in high prevalence areas before finishing with the higher risk groups in low prevalence areas. The figure also shows how the two-dose allocation policy should play out for different vaccines given their respective first and second dose protection.

6 Impact and Conclusion

This work is an outcome of a collaboration on the MIT Covid-19 Response System (MCRS). MCRS is a joint effort between the MIT Quest for Intelligence and Lincoln Lab to model the effects of returning to campus. MCRS estimates these effects using de-identified data of campus mobility, with data access and usage overseen by MIT's Legal, Ethical, and Equity Committee and the IT Governance Committee. The prevalence predictions have been important for reopening the institute by providing MIT senior administration with the forecasts they need to consider as they make policy decisions on the degree of allowing access to the campus for different groups (students, faculty, staff and visitors among others). For more information, see the MCRS FAQ at https://covid-19.mit.edu/mit-covid-19-response-system-mcrs-faq.

In addition, MIT-Cassandra, the predictive method discussed in this paper is now part of the CDC models that are used to predict the cases and deaths in different parts of the US. It is consistently among the top 10 models (out of more than 50 models) at different stages of the pandemic, and is ranked 1st overall in several months for both detected cases and detected deaths as shown in the following sections. It is also important to note that the proposed optimization formulation for vaccination is general, and can easily be applied to different vaccination centers throughout the world.

6.1 CDC Benchmark

To evaluate the success of our models, we benchmark them against a collection of models selected by the CDC. In Fig. 6, we present results that compare our models with

the posted CDC models made publicly available on the COVID-19 Forecast Hub. For illustrative purposes we show predicted deaths for the month February 2021, as shown in Fig. 6. The exact results of our model can be found in Table 2. Predictions from these models are uploaded weekly and forecast weekly deaths and cases up to 5 weeks out. For the purpose of benchmarking congruently, our methods are trained and validated on data up until the day the CDC predictions are posted. Predictions beyond that date are purely out-of-sample.

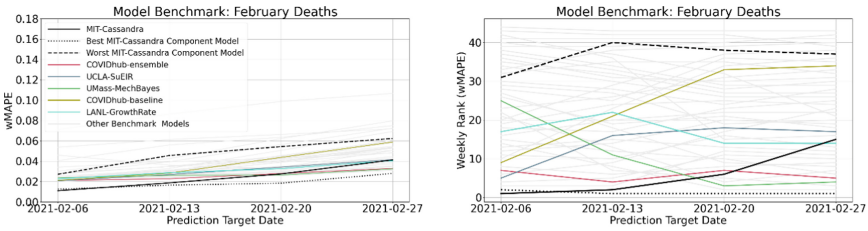

Fig. 6. Benchmarking the aggregate and best and worst components (black) v. top performing models at the CDC (top 5 models shown in color). Comparisons in terms of deaths (left) and rank (right). All results are out-of-sample and made on January 31, 2021

The success of this approach leads to our model consistently performing in line with the top tier CDC models (top 15 and often top 5), which themselves are selected from a much larger pool of candidate models (more than 50 models). When predicting deaths for February, the aggregate model outperforms all other models active at the time in the first week and never ranks outside the top 15 for longer term predictions. In general, it is clear that the ensemble method proposed in this paper adds significant value and enables results in-line with or better than top-performing models.

6.2 Conclusion

This end-to-end framework allows to generate state-of-the-art predictions by leveraging powerful and complementary individual models, and while having provable guarantees. It also includes a model to go from these predictions for detected cases to true prevalence. True prevalence is vital to decision-makers and is used in our framework to optimize vaccine allocation, resulting in actionable insights and recommendations. This entire framework is open-source and has been extensively used by MIT Quest and by the CDC to combat COVID-19 and mitigate its effects.

References

1. Levine, S., Kumar, A., Tucker, G., Fu, J.: Offline reinforcement learning: tutorial, review, and perspectives on open problems (2020)
2. Yakowitz, S.: Nearest-neighbour methods for time series analysis. J. Time Ser. Anal. **8**(2), 235–247 (1987)

3. Gers, F.A., Schmidhuber, J., Cummins, F.: Learning to forget: continual prediction with LSTM. In: 1999 Ninth International Conference on Artificial Neural Networks ICANN 99. (Conf. Publ. No. 470), vol. 2, pp. 850–855 (1999)
4. Perakis, G., Singhvi, D., Skali Lami, O., Thayaparan, L.: Fighting covid-19: aA multipeak sir-based model for learning waves and optimizing testing (2021)
5. Dietterich, T.G.: Ensemble methods in machine learning. In International workshop on multiple classifier systems, pp. 1–15. Springer (2000)
6. Sagi, O., Rokach, L.: Ensemble learning: a survey. Wiley Interdisciplinary Rev. Data Min. Knowl. Discovery **8**(4), e1249 (2018)

Electric Vehicle Battery Charging Scheduling Under the Battery Swapping Mode

Yuqing Zhang(✉)

School of Economics and Management, Beijing Jiaotong University, Beijing 100089, China

Abstract. Electric vehicle battery recharging on the swapping mode has grown up as an important option other than the plug-in charging mode in China, given that several auto giants have been dedicated in constructing their battery swapping systems. However, the lack of effective operational methods on battery recharging and transportation scheduling has aroused a big challenge on the practical application of the swapping mode, which enables the necessity of our work. This study proposes a joint optimization model of recharging and scheduling of electric vehicle batteries with a dynamic electricity price system, which is able to identify the optimal charging arrangement (the recharging time and the quantity of recharging batteries) as well as the optimal transportation arrangement (the transportation time and the quantity of transporting batteries). For the validation purpose, a numerical study is implemented based on dynamic electricity prices in Beijing.

Keywords: Electric vehicle · Battery charging · Battery swapping · Battery logistics

1 Introduction

Automobile exhaust has become an important cause of air pollution in recent decades. Electric vehicles (EVs) are clean, which can effectively reduce people's dependence on fossil fuels. The usage of EVs instead of fossil fuel-based internal combustion vehicles (ICVs) has unparalleled advantages in reducing vehicle emissions [1–3]. But the range anxiety of consumers has severely limited the popularity of EVs. Instead of the battery charging mode, the battery swapping mode can separate the charging process from the battery swapping operation. The whole operation time is less than 10 min, which is much faster than recharging. Under the battery swapping mode, the battery charging time and quantity can be scheduled reasonably so as to reduce the impacts on the safety and quality of power grid [4]. Furthermore, the depleted batteries of EVs can be charged during off-peak hours with a discounted electricity price, which can also reduce the charging cost.

Current studies on battery swapping mode rarely address the joint optimization of charging and battery transportation. To bridge this gap, we propose a mathematical model of centralized charging and scheduling of EVs batteries with the goal of minimizing total cost, which aims to answer the following questions: (a) how to determine the charging

R. Qiu et al. (Eds.): ICSS 2021, LNOR, pp. 269–278, 2021.
https://doi.org/10.1007/978-3-030-90275-9_22

time and quantity of the batteries; (b) how to optimize the transportation scheduling of batteries between the battery charging station (BCS) and the battery swapping station (BSS). The innovation of the present work is multi-fold. First, our model takes into account the dynamic electricity prices, which not only maintains the security of the grid but also reduces charging costs. Secondly, we combined the centralized charging process of batteries and the transportation scheduling of batteries to make joint optimization decisions. On the basis of meeting consumers' random demand and matching dynamic electricity prices, our model dispatches the transportation of batteries between BSS and BCS, so as to determine the optimal transportation time and quantity of batteries. Finally, we highlight the managerial implication of the joint decision model of EV battery centralized charging and transportation scheduling by carrying out sensitivity analysis.

The remainder of this paper is organized as follows. Section 2 reviews the latest studies on EV swapping mode. The optimization model is presented in Sect. 3. Section 4 presents the details for solving the problem. Section 5 provides some managerial implication. The potential future directions are outlined in Sect. 6.

2 Literature Review

There are a lot of studies on the charging strategies of EVs [5–8]. However, there are also many insurmountable challenges on the charging strategies such as long charging time, charging inconvenience and so on. In recent years, with the introduction of BSS, more and more scholars pay attention to the battery swapping mode [9].

Most of the research on the battery exchange strategy focuses on the optimization of charging time of EV under the swapping mode. For example, Ref. [10] proposed a novel centralized charging strategy of EVs under the battery swapping scenario based on spot electric price. Ref. [11] focused on EV battery swapping station coordinated charging dispatch method based on CS algorithm to achieve the optimization of daily charging plan of battery swapping station (BSS). Ref. [12] propose a dynamic operation model of BSS in electricity market based on the short-term battery management, and acquires additional revenue by responding actively to the price fluctuation in electricity market. Ref. [13] designed a typical connection mode of electric vehicle charging and battery exchange infrastructure, which can provide guidance for the planning of electric vehicle charging and battery exchange infrastructure interconnected with the grid. Ref. [14] proposed an optimized charging mode (OCM) to determine the impact of drivers' switching behavior on power grid and power generation cost. Ref. [15] proposed a comprehensive optimal allocation method for EV switching stations based on orderly charging strategy. Ref. [16] considered the demand of EV users and the load of power grid, and proposed a strategy model of EV switching station to optimize the benefits. Ref. [17] proposed the optimization framework of the battery switching station operation model.

Most of the existing studies focus on the charging process of the battery exchange system, while ignoring the transportation scheduling process between BCSs and BSSs. However, we propose a centralized charging strategy and transportation scheduling method of EV batteries under the battery swapping mode, which considers the battery transportation scheduling problem between BCS and BSS and the matching problem

between battery charging and the time-of-use electricity price of the State Grid. It is much closer to the operating conditions of the system in real life.

3 Centralized Battery Charging and Optimized Scheduling Model

3.1 Problem Description

We introduce a mathematical formulation of this problem. First, the model discretizes the continuous time according to a certain time granularity. According to the time-of-use electricity price mechanism and the uncertainty of demand, managers need to make decisions at the endpoints of each time grain. For BSS, the managers need to make decisions about when to transport how manAy batteries from BCS to meet the customer's demand for electricity conversion. For BCS, the decision is when to charge the depleted batteries, so as to meet the demand of BSS while minimizing the charging cost. Certain transportation costs will be incurred in the process of transportation. For the whole system, in order to minimize the total cost, on the basis of meeting the demand, when to transport and how many batteries to transport are also the contents to be decided.

3.2 Model

The scenario of the model is presented as follows:

(1) The battery belongs to BSS in BSCS;
(2) The model includes one BCS and one BSS;
(3) BSS cannot charge the depleted batteries (DBs);
(4) The battery type is the same. DBs all have the same SOC, so does the fully charged batteries (FCBs), so they are charged at the starting point of time granularity, and all batteries have the same charging time;
(5) The battery delivery time between BCS and BSS is not considered;
(6) The total operating period is divided into discrete time periods. Let g represent the time granularity;
(7) Electricity prices change over time and only at the end points of time granularity.
(8) To extend battery life, the battery does not stop charging until it is fully charged.

In our model, the cost of battery charging and dispatching in BSCS consists of two parts:

(1) The electricity cost P_i for battery charging under the time-of-use tariff mechanism;
(2) The transportation cost of batteries dispatched between BCS and BSSs;

The variables and parameters are shown in Table 1.
The model is formulated as:

$$\min \ \mathrm{S} = \sum_{t=1}^{T} \left(g \cdot PoC \cdot Q_t \cdot \sum_{i=t}^{t+M-1} p_i \right) + \mathrm{TP} \sum_{t=1}^{T} (T_t^{in} + T_t^{out}) \tag{1}$$

Table 1. Notations

Variable	Meaning
t	The index for time periods;
g	The length of time period t;
TP	Single vehicle single transport cost;
P_t	Electricity price at time period t;
W_t	The number of full batteries in the BSS at the beginning of the t period;
D_t	Power exchange demand at the beginning of t;
Q_t^*	BCS full battery number at the beginning of t;
Q_t^+	Number of batteries charged in t period;
Q_c	The maximum transport capacity of a single vehicle;
N_{occup}	The ratio of full batteries to the capacity of the swapping station at initial time;
N_c	The proportion of charging piles that are not occupied in the initial BCS;
M	Number of time particles required for a single battery to be fully charged;
C_{aps}	The maximum number of cells a BCS can hold;
C_{apc}	The maximum number of cells a BCS can hold;
PoC	Charging power;
T	The total time window length of this study;
Decision Variables	
Q_t	Number of batteries charged at the beginning of t;
TQ_t^{out}	Number of batteries shipped from BSS to BCS at the beginning of t;
TQ_t^{in}	Number of batteries shipped from BCS to BSS at the beginning of t;
T_t^{out}	Number of vehicles transporting batteries from BSS to BCS at the beginning of t;
T_t^{in}	Number of vehicles transporting batteries from BCS to BSS at the beginning of t;

Subject to

$$W_1 = C_{\text{aps}} \times N_{\text{occup}} \ (t = 1) \tag{2}$$

$$W_t = W_{t-1} - D_{t-1} + TQ_{t-1}^{in} \quad (t \geq 2) \tag{3}$$

$$W_t \geq D_t \tag{4}$$

$$Q_1^* = (1 - N_c) \times C_{apc} - TQ_1^{in} \ (t = 1) \tag{5}$$

$$Q_t^* = Q_{t-1}^* + Q_{t-1}^+ - TQ_t^{in} \ (t \geq 2) \tag{6}$$

$$TQ_t^{in} \leq Q_t^* \tag{7}$$

$$Q_t^+ \begin{cases} Q_{t-M+1}, t \geq M \\ 0, t < M \end{cases} \tag{8}$$

$$\sum_{i=1}^{t} Q_i \leq \sum_{i=1}^{t} TQ_i^{out} \tag{9}$$

$$\sum_{i=1}^{t} TQ_i^{out} \leq \sum_{i=1}^{t} D_i \tag{10}$$

$$\sum_{i=1}^{t} TQ_i^{in} - \sum_{i=1}^{t} TQ_i^{out} \leq C_{aps}\left(1 - N_{occup}\right) \tag{11}$$

$$\sum_{i=1}^{t} TQ_i^{out} - \sum_{i=1}^{t} TQ_i^{in} \leq N_c \cdot C_{apc} \tag{12}$$

$$\frac{TQ_t^{out}}{Q_c} \leq T_t^{out} \leq \frac{TQ_t^{out}}{Q_c} + 1 \tag{13}$$

$$\frac{TQ_t^{in}}{Q_c} \leq T_t^{in} \leq \frac{TQ_t^{in}}{Q_c} + 1 \tag{14}$$

$$t, P_t, W_t, Q_t^*, Q_t, Q_t^+, TQ_t^{in}, TQ_t^{out}, T_t^{in}, T_t^{out} \geq 0 \tag{15}$$

Objective function (1) is the minimum sum of battery charging cost and transportation cost.

Constraints can be divided into three categories, including:

(I) Constraints on the Number of Fully Charged Batteries in BSS

Constraint (2) indicates that the number of full batteries in the initial BSS is equal to the number of available batteries placed in the initial BSS.

Constraint (3) indicates that the number of full batteries in BSS in period t is equal to the sum of the number of full batteries in BSS in period $t-1$ and the number of batteries shipped into BSS, minus the number of batteries required in period $t-1$ Constraint (4) indicates that the electrical changing demands that can be met in each phase should not exceed the total amount of fully charged batteries available in the current phase of the electrical changing station.

Constraint (11) is the inventory capacity constraint in BSS, indicating that the difference between the number of batteries shipped in and out of BSS in period t should not exceed the inventory capacity in BSS in period $t-1$.

(II) Constraints on the Number of Fully Charged Batteries in BCS

Constraint (5) The number of fully charged cells in the initial BCS is equal to the number of available cells placed in the initial BCS minus the number of fully charged cells shipped out of the first BCS.

Constraint (6) indicates that the number of fully charged cells in BCS at period t is equal to the sum of the number of fully charged cells in BCS at the beginning of period

$t-1$ and the number of fully charged cells at the beginning of period $t-1$ minus the number of cells shipped out of BCS at the beginning of period t.

Constraint (7) indicates that the number of batteries shipped out of BCS in each period should not exceed the total amount of fully charged batteries available in the charging station in the current period.

Constraint (12) is the constraint of BCS internal free charging capacity, indicating that the difference between the number of batteries transported in and out of BCS in period t should not exceed the spare charging capacity in BCS in period $t-1$.

(III) Battery Charge Time Constraint

Constraint (8) indicates that when the charging time of the battery is greater than or equal to the time particle size of M, the battery is fully charged.

(IV) Battery Transport Constraints in Logistics System

Constraint (9) indicates that the number of batteries charged from the initial period to the current period should not exceed the total number of empty batteries in each BCS period.

Constraint (10) indicates that the number of batteries shipped out of BSS from the initial period to the current period should not exceed the demand for changing electricity.

Constraints (13) and (14) are vehicle constraints for transport.

Constraint (15) indicates that all variables are integers not less than 0.

4 Numerical Example Analysis

We solve the problem by using LINGO mixed integer programming solver.

4.1 Parameter Settings

(1) $g = 0.5$: The time particle size is 0.5, indicating that a decision should be made every 0.5 h in the charging station, including whether to start charging a new batch of empty batteries and whether to transport the fully charged batteries to the changing station;
(2) $M = 10$: Suppose it takes 5 h to fully charge a battery. That is 10 time granularities;
(3) $C_{aps} = C_{apc} = 400$: BSS and BCS can hold up to 400 batteries;
(4) $N_{occup} = 0.8$: Initially, 20% of the inventory capacity of BSS is idle, which means 80% of the existing inventory is occupied by full batteries;
(5) $N_c = 1$: There is no battery in the initial state of BCS;
(6) $Q_c = 50$: The maximum transport capacity of a single vehicle is 50 batteries;
(7) $TP = 200$: A transportation cost is 200 yuan;
(8) $PoC = 3$: The charging power is 3 kwh;
(9) $D \sim Passion\ (15)$: Referring to the average visit times of gas stations in real life, the demand is set to follow the Poisson distribution with an average of 15;
(10) P: According to the peak hours and corresponding electricity prices published by China Power Grid. The specific setting of electricity price is shown in Table 2:

Table 2. Electricity price distribution in different periods.

Electricity intensity	Period of time	Electricity price (yuan /kwh)
Peak	7:00–11:00	1.234
Normal	11:00–19:00	0.856
Peak	19:00–23:00	1.234
Trough	23:00–7:00 (Next day)	0.376

(11) T: The research time is set as the time for all the initial fully charged batteries in BSS to be swapped out plus an integer multiple of M, combined with the above parameters, a research cycle $= 21+3$*M, considering the continuity of the model for the study cycle and repeatability, will postpone back 10 research cycle time granularity, namely the total time of this study window set to $21 + 3$*M $+ 10$, the start time of study based on real life set to 7:00 in the morning.

4.2 Model Solving

This part assumes that the electrical changing demand D follows the Poisson distribution with an average value of 15, and a group of samples with a capacity of 61 are randomly sampled. According to the electrical changing demand represented by this group of samples, the optimal charging time and quantity distribution as well as the battery transportation time and quantity distribution between the electrical changing station and the charging station are solved.

Figure 1 shows the quantity distribution of electrical changing demands represented by this group of samples.

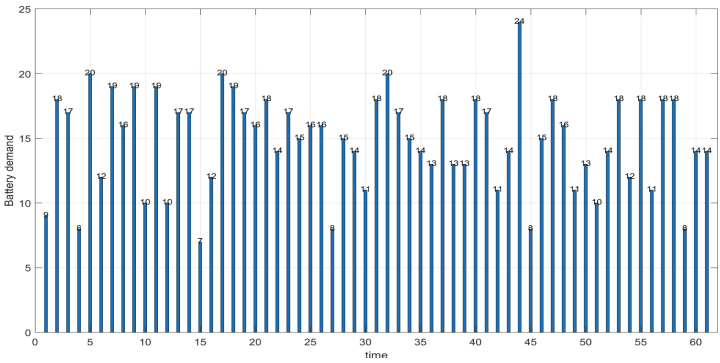

Fig. 1. Electrical changing requirements for each time granularity during the study period

According to the determination principle of total time window length, the study cycle is 61 time granularity. The optimal solution under this sample electrical changing demand is shown in Fig. 2. Obviously, most batteries avoid the peak electricity consumption period and choose to start charging when the electricity price is normal or low.

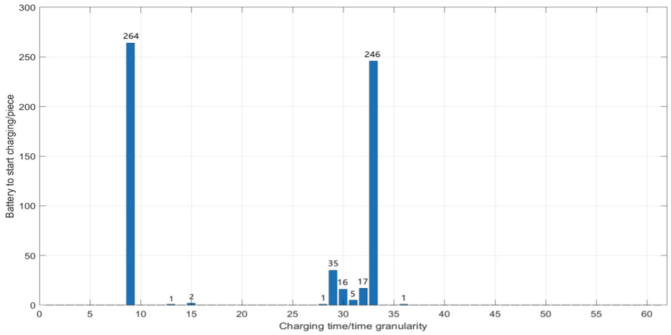

Fig. 2. Optimal charging time and quantity distribution of BCS.

Figure 3 shows the distribution of transportation time and quantity of batteries from BCS to BSS. We can found that the battery transportation time is relatively concentrated.

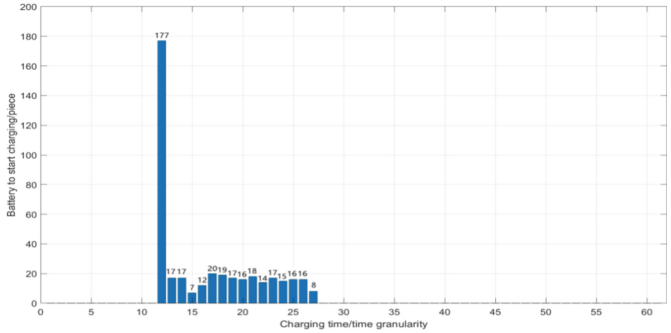

Fig. 3. Optimal time and quantity distribution of batteries from BSS to BCS.

The distribution of full charged battery transportation time and quantity from BCS to BSS is shown in Fig. 4.

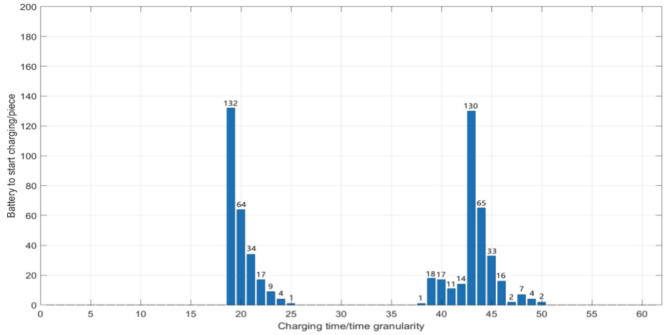

Fig. 4. Optimal time and quantity distribution of the battery from BCS to BSS.

5 Managerial Implication

From the above analysis, some managerial insights are drawn as follows:

(1) It is easy to adapt the method to other similar practical scenarios, given that different scenarios could be mapped to the corresponding sets of parameter values, like various electricity prices, transportation capacity, demand distribution, etc.
(2) Good timing of centralized charging of batteries is vital to save charging costs and reduce power grid losses. For example, according to Table 3, nearly 90% of the batteries are charged in the off-peak period, which lead to lower charging cost and mitigates the peak load of the power grid.
(3) The company needs to make a trade-off between transportation cost and response speed. Figure 4 shows only no more than 10 batteries are shipped in many time periods for rapid response, which implies the company could obtain the shipping economy of scale by slowing down its response speed and consequently reduce the transportation cost.

Acknowledgement. This work is supported by Beijing Social Science Foundation (No. KBHZ15040531).

References

1. Zhang, W.L., Wu, B., Li, W.F., et al.: Discussion on development direction and energy supply mode of pure electric vehicle in China. Grid Technol. **33**(4), 1–5 (2009)
2. Chen, J.W., Jun, Y., Min, Z., et al.: The two-echelon capacitated electric vehicle routing problem with battery swapping stations: formulation and efficient methodology. Eur. J. Oper. Res. S0377221718306076 (2018)
3. Su, W., Eichi, H.R., Zeng, W., et al.: A Survey on the electrification of transportation in a smart grid environment. IEEE Trans. Ind. Inf. **8**(1), 1–10 (2012)
4. Fernandez, L.P., Gomez, S.R.T., Cossent, R., et al.: Assessment of the impact of plug-in electric vehicles on distribution networks. IEEE Trans. Power Syst. **26**(1), 206–213 (2011)

5. Tao, Y., Huang, M., Chen, Y., et al.: Orderly charging strategy of battery electric vehicle driven by real-world driving data. Energy **193**, 116806 (2020)
6. Studli, S., Griggs, W., Crisostomi, E., et al.: On optimality criteria for reverse charging of electric vehicles. IEEE Trans. Intell. Transp. Syst. **15**(1), 451–456 (2014)
7. Deilami, S., Masoum, A.S., Moses, P.S., Masoum, M.A.S.: Real-time coordination of plug-in electric vehicle charging in smart grids to minimize power losses and improve voltage profile. IEEE Trans. Smart Grid **2**(3), 456–467 (2011). https://doi.org/10.1109/TSG.2011.2159816
8. Qiu, D., Yang, H.M., Lai, M.Y.: Optimal bidding strategy and EV charging management of intelligent regional aggregators based on CVaR method. Syst. Eng. Theory Pract. **38**(8), 1994–2005 (2018)
9. Zheng, Y., Dong, Z.Y., Xu, Y., et al.: Electric vehicle battery charging/swap stations in distribution systems: comparison study and optimal planning. IEEE Trans. Power Syst. **29**(1), 221–229 (2014)
10. Kang, Q., Wang, J.B., Zhou, M.C., et al.: Centralized charging strategy and scheduling algorithm for electric vehicles under a battery swapping scenario. IEEE Trans. Intell. Transp. Syst. **17**(3), 659–669 (2016)
11. Zheng, J., Xie, T., Liu, F., Wang, W., et al.: Electric vehicle battery swapping station coordinated charging dispatch method based on CS algorithm. In: Information Technology and Mechatronics Engineering Conference (ITOEC). IEEE (2017)
12. Yang, S., Yao, J., Kang, T., et al.: Dynamic operation model of the battery swapping station for EV (electric vehicle) in electricity market. Energy **65**(1), 544–549 (2014)
13. Song, Y., Li, J., Ji, G., et al.: Study on the typical mode of EV charging and battery swap infrastructure interconnecting to power grid. In: China International Conference on Electricity Distribution. IEEE (2016)
14. Rao, R., Zhang, X., Xie, J., et al.: Optimizing electric vehicle users' charging behavior in battery swapping mode. Appl. Energy **155**, 544–549 (2015)
15. Wang, T., Ling, Y., Liu, J., et al.: Integrated optimal configuration of electric vehicle charging and battery-swapping station based on ordered charging strategy. In: Power & Energy Society General Meeting. IEEE (2018)
16. Infante, W.F., Ma, J., Chi, Y.: Operational strategy and load profile sensitivity analysis for an electric vehicle battery swapping station. In: IEEE International Conference on Power System Technology. IEEE (2016)
17. Sarker, M.R., Pandzic, H., Ortega-Vazquez, M.A.: Optimal operation and services scheduling for an electric vehicle battery swapping station. IEEE Trans. Power Syst. **30**(2), 901–910 (2015)

Information Design for E-consult Between Vertically Competing Healthcare Providers

Zhenxiao Chen, Yonghui Chen, and Qiaochu He(✉)

College of Business, Southern University of Science and Technology, Shenzhen 518055, Guangdong, China
heqc@sustech.edu.cn

Abstract. The concern of patient referral service has raised much attention in recent years. A newly-developed e-consultation service offers a communication platform for primary care physicians (PCPs) and specialists. The goal of this work is to find out the impact of information design in such a referral system. The complete information situation is regarded as a basic case in this study. Interestingly, our finding shows that a complete information disclosure policy may negatively affect patients' collective welfare. Therefore, a more delicate information design can help to further reduce possible welfare loss.

Keywords: Referral medical care · Information design · Patient welfare

1 Introduction

Recently in hospital outpatient clinics, the matching of patients with an appropriate level of healthcare has raised much attention. Patients normally lack medical literacy and cannot choose the best care option. This inappropriate decision can lead to overcrowding and delay in the healthcare system [1]. To optimally utilize limited clinical resources and bridge care gaps, the most critical decision is identifying the capacity needs of clinical resources and establish relevant management methods [2]. For example, a newly emerging and flexible e-consultation service provides a communication platform for primary care physicians (PCPs) and specialists [3]. In such a referral system, the providers in the platform make a diagnosis of patients' severity and then give suggestions to the patients. PCPs and specialists can share information and expertise through this process, which could improve the diagnosis accuracy of PCPs and the referral efficiency of severe patients [4]. E -consults are intended to improve access to specialty expertise for patients and providers without the need for a face-to-face visit [5], and this innovative and flexible service is expected to improve the accuracy of diagnosis and the distribution of medical resources. Besides, with the help of a dedicated information provision policy, the platform can mitigate the excessive medical treatment in the current healthcare system and navigate the patients to more proper decisions.

R. Qiu et al. (Eds.): ICSS 2021, LNOR, pp. 279–285, 2021.
https://doi.org/10.1007/978-3-030-90275-9_23

Investigations on the gatekeeper system have been conducted for a long period [6]. However, the understanding and analysis of the information design in such a referral system are still limited. In terms of the factors that influence referrals, a mix of physicians, healthcare system structure, and patients are found to influence the referral process [7–9]. As for effective methods to improve the referral system, An et al. [10] show that relevant public health interventions could be beneficial in some conditions. The establishment of referral standards for primary healthcare is also to be important [11]. Shaw and Melton [12] indicate that the extra payment to GPs can reduce some unnecessary referrals but may lead to missed diagnoses and trust loss. Besides, the introduction of the e-consultation platform is also proved to be effective in reducing congestion and increasing overall patient welfare [3]. But only complete information is discussed previously, the method of information design has not been discussed yet.

Herein, we propose a game-theoretic model, where patients make their choices with the suggestions from an e-consultant system. First, we investigate the situation that patients are fully informed of information about their illness severity and make decisions. Next, an e-consultant platform aims to maximize the total patient welfare and reveals part of the information to the patients. For these two cases, we compare the patient distribution and the total welfare. Our findings can provide interesting insights into the application of e-consultation and the deployment of information design in the healthcare system.

2 Problem Description and Basic Model

As mentioned, patients normally lack medical literacy and cannot choose the best care option even they are informed of their illness severity. We develop a two-level healthcare system, which consists of PCPs and specialists. Figure 1 delineates the sequence of events in the e-consultation system. The process can be summarized as follows:

- A patient attends the preliminary screening through the e-consultation platform with no information about his illness severity.
- A provider in the platform is in charge of the patient's first diagnosis and comes up with an ambiguous result.
- The PCP communicates with a specialist through the e-consultant system, subsequently, they make an accurate diagnosis.
- The provider in the system receives the complete information about the patient's severity and then discloses this information to the patient according to the system instructions.
- The patient is informed of the severity and makes his visit decision (PCP or specialist or no visit).

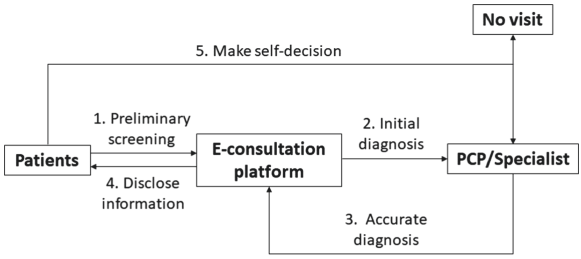

Fig. 1. Sequence of events in the e-consultation system

2.1 Complete Information

All patients are fully informed of their severity and each patient makes his/her own decision. The equilibrium of patient utility is achieved at the two thresholds (see Fig. 2), such that the following equations hold:

$$\theta_1 V_P - c\lambda_P - p_P = \theta_1 V_S - c\lambda_S - p_S \tag{1}$$

$$\theta_0 V_P - c\lambda_P - p_P = 0 \tag{2}$$

$$\lambda_N + \lambda_P + \lambda_S = 1 \tag{3}$$

Equations 1 and 2 represent the utility equilibrium at the two thresholds (θ_0, θ_1). For calculation simplification, we assume the utility of all patients of no visit is zero. These thresholds could be decision references for the platform to design further information provision policy. A single patient utility is influenced by the severity θ, treatment quality V, congestion cost $c\lambda$, and charged price p. λ_N is the number of patients with no visits. λ_P and λ_S represent the total visits to PCPs and specialists. The congestion cost only depends on the congestion level, since patients of different severities may incur the same congestion cost and they pay more attention to providers' service.

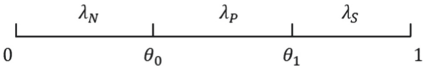

Fig. 2. Patient visit under complete information situation

2.2 First-Best Division

Unlike the complete information situation, the provider receives complete information about patients' illness from the e-consultation platform and reveals part of the information to the patients. At this moment, the main aim is to maximize the total utility of the whole patient. The maximization problem can be formulated as:

$$\max_{\theta_0,\theta_1} U_T = \int_{\theta_0}^{\theta_1} U_P(\theta) d\theta + \int_{\theta_1}^{1} U_S(\theta) d\theta \tag{4}$$

$$U_j(\theta) = \theta V_j - c\lambda_j - p_j, \quad \forall j \in \{P, S\} \tag{5}$$

3 Analysis and Results

Firstly, we examine the characteristics of patient numbers in the complete information situation.

Proposition 1. *Under complete information, the equilibrium outcomes are as below:*

- *The patient population of no visit,* $\boldsymbol{\lambda_N = \frac{(p_S+c)c+p_P(V_S-V_P+c)}{(V_P+c)(V_S-V_P+c)+cV_P}}$
- *The patient population of visiting PCPs,* $\boldsymbol{\lambda_P = \frac{(p_S+c)V_P-p_P(V_S+c)}{(V_P+c)(V_S-V_P+c)+cV_P}}$
- *The patient population of visiting specialists,* $\boldsymbol{\lambda_S = \frac{(V_P+c)(V_S-p_S)+V_p(p_P-V_P)}{(V_P+c)(V_S-V_P+c)+cV_P}}$

The patient distribution is influenced by the exogenous variables mentioned before. From the viewpoint of the healthcare system, we mainly discuss the impacts of treatment quality and price in the two-level system.

Lemma 1. *Given the expressions of the total visit to PCP (*$\boldsymbol{\lambda_P}$*), specialist (*$\boldsymbol{\lambda_S}$*), and no visit (*$\boldsymbol{\lambda_N}$*). Table 1shows the characteristics of these mentioned variables:*

Table 1. Effect of the exogenous variables on the patient distribution

	λ_N	λ_P	λ_S
p_P	↑	↓	↑
p_S	↑	↑	↓
V_P	–	↑	↓
V_S	↓	↓	↑

↑ (increasing); ↓ (decreasing); - (not monotonous)

The impacts of p_P, p_S, and V_S on patients' visits are intuitive, while the impact of V_P on the total healthcare visits is more profound. The impacts of healthcare costs exhibit the same characteristics, the increasing cost of PCP leads to the change of some patients from PCPs to specialists; similarly, the rise of specialist cost leads to more patients visiting the PCP. In addition, the increase of both these two costs will cause the increase of patient population who do not intend to visit a PCP or specialist.

The impact of the treatment quality provided by specialists V_S is different. With the improvement of this quality, some patients who previously visit PCPs are attracted by the specialist service and change their minds. However, it is noticed this improvement cause a more crowded situation in the system.

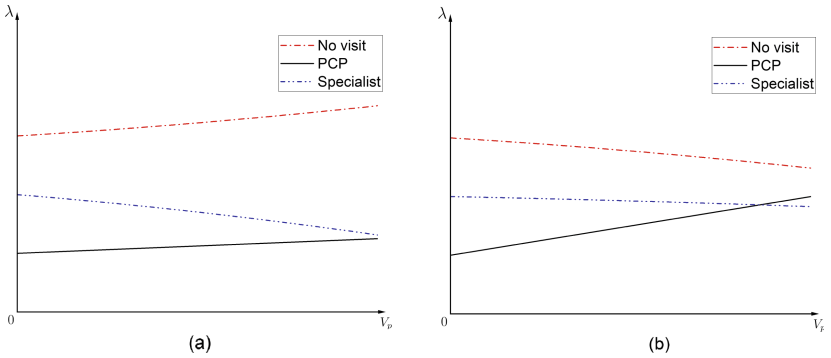

Fig. 3. Effect of V_P on patient distribution

Figure 3 shows the effect of V_P on patient distribution. The increase of V_P shows some similar characteristics as V_S. When PCP treatment quality improves, some patients change their visits from a specialist to a PCP. The change of total visit depends on the value of the treatment quality. Only if the specialist's treatment quality is sufficiently low and specialists charge a quite large price (shown in Fig. 3(b)), then the increase of V_P decreases the total healthcare requirement. In other conditions, it is indicated in Fig. 3(a) that the improvement of V_P aggravates crowding in the health system.

Next, the complete information case is compared with the first-best division. The first-best division represents the ideal information design method where the whole patient welfare is maximized. The distribution of patients is shown in Fig. 4.

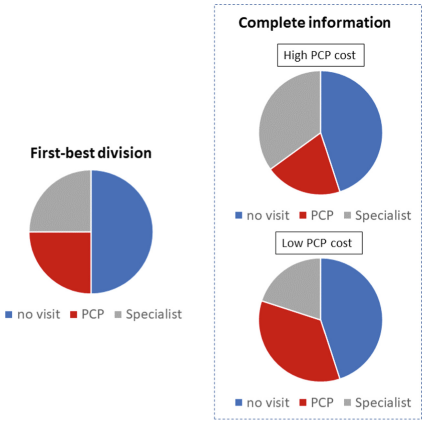

Fig. 4. Patient distribution under the first-best division and complete information situations

Proposition 2. *Complete information disclosure policy leads to crowded queue in the healthcare system and may negatively affects patients' collective welfare.*

In general, if all patients fully realize their severities, many patients are induced to visit a PCP or a specialist. When compared with the first-best division, a more crowded queue happens, and this leads to the loss of total patient welfare. Besides, the PCP treatment cost is found to be important. If the PCP cost is low enough, this crowded queue is caused by the increase in the patient population who plan to visit PCPs.

4 Conclusions

The e-consultant platform provides an innovative referral service. The application of this system can empower patient engagement and improve continuity of care, and enhance the delivery of high-value care, thereby improving the quality of life of patients and reducing the healthcare cost for society as a whole. Our findings show that: (1) charged price and treatment quality influence patient decisions, and the treatment quality of the lower provider is found to be more complicated and should be paid attention to in a two-level healthcare system; (2) Patients with complete information can lead to an overcrowded choice. Our results show that a dedicated information provision policy could be effective to relieve this crowded situation and benefit the patients' collective welfare. In addition, the outcomes obtained under the first-best division and complete information could be references for the platform to make information provision policies, like disclosing genuine information to the part of the patients according to the calculated thresholds.

References

1. Levin, A.: Consequences of late referral on patient outcomes. Nephrol. Dial. Transplant. **15**(SUPPL. 3), 8–13 (2000). https://doi.org/10.1093/oxfordjournals.ndt.a027977
2. van Bussel, E.M., van der Voort, M.B.V.R., Wessel, R.N., van Merode, G.G.: Demand, capacity, and access of the outpatient clinic: a framework for analysis and improvement. J. Eval. Clin. Pract. **24**(3), 561–569 (2018). https://doi.org/10.1111/jep.12926
3. Clark, C.R.: Modeling and analysis. ECCM **18** (2014)
4. Gleason, N., et al.: Adoption and impact of an eConsult system in a fee-for-service setting. Healthcare **5**(1–2), 40–45 (2017). https://doi.org/10.1016/j.hjdsi.2016.05.005
5. Vimalananda, V.G., et al.: Electronic consultations (e-consults) to improve access to specialty care: a systematic review and narrative synthesis. J. Telemed. Telecare **21**(6), 323–330 (2015). https://doi.org/10.1177/1357633X15582108
6. Shumsky, R.A., Pinker, E.J.: Gatekeepers and referrals in services. Manage. Sci. **49**(7), 839–856 (2003). https://doi.org/10.1287/mnsc.49.7.839.16387
7. Ludke, R.L.: An examination of the factors that influence patient referral decisions. Med. Care **20**(8), 782–796 (1982). https://doi.org/10.1097/00005650-198208000-00003
8. Forrest, C.B., Nutting, P.A., Von Schrader, S., Rohde, C., Starfield, B.: Primary care physician specialty referral decision making: patient, physician, and health care system determinants. Med. Decis. Mak. **26**(1), 76–85 (2006). https://doi.org/10.1177/0272989X05284110
9. Delikurt, T., Williamson, G.R., Anastasiadou, V., Skirton, H.: A systematic review of factors that act as barriers to patient referral to genetic services. Eur. J. Hum. Genet. **23**(6), 739–745 (2015). https://doi.org/10.1038/ejhg.2014.180
10. An, C., O'Malley, A.J., Rockmore, D.N., Stock, C.D.: Analysis of the U.S. patient referral network. Stat. Med. **37**(5), 847–866 (2018). https://doi.org/10.1002/sim.7565

11. Siddiqi, S., et al.: The effectiveness of patient referral in Pakistan. Health Policy Plan. **16**(2), 193–198 (2001). https://doi.org/10.1093/heapol/16.2.193
12. Shaw, D., Melton, P.: Should GPs be paid to reduce unnecessary referrals? David Shaw is concerned that such payments will lead to missed diagnoses and loss of trust, but Peter Melton says that with proper safeguards they will improve patient care. BMJ **351**(November), 10–11 (2015). https://doi.org/10.1136/bmj.h6148

Order Batching Problem in O2O Supermarkets

Kewei Zhou, Kexin Gao, and Shandong Mou(✉)

Department of Supply Chain and Operations Management, Central University of Finance and Economics, Haidian District, Beijing 100081, China
smou@cufe.edu.cn

Abstract. With the development of omni-channel retailing, the O2O retailing combining traditional offline with online channels brings both opportunities and challenges to conventional supermarkets. As an important factor for supermarkets' online service capabilities, order picking has become a critical point for the survival and development of O2O supermarkets. Thus, how to fulfil customer orders efficiently as well as accurately has become an urgent problem. In order to improve the order fulfilment performance of O2O supermarkets, we build an order batching mathematical model which aims at minimising the total Late Finish Time (LFT). A genetic algorithm is applied to solve this model. By analysing extensive numerical experiment outputs, we discuss the influences of SKU concentration of online customer orders, the mean and variance of Maximum Allowable Completion Time (MACT) on the performance of order batching and tardiness. Besides, the Degree of Congestion (DOC) which reflects the potential conflict between online order fulfilment and offline customer shopping is particularly discussed. We lastly provide managerial insights and some practical recommendations for O2O supermarkets.

Keywords: O2O supermarket · Order picking problem · In-store order fulfilment · Omni-channel retailing

1 Introduction

With the development of omni-channel retailing, the combination of online and offline channels, namely the O2O business model, has brought both opportunities and challenges to traditional supermarkets. In recent years, major retail supermarkets, such as Fresh Hema, Wumart and Yonghui superstores, have started their online business. By integrating the Internet with physical retail channels, the retailers aim to provide seamless shopping experiences for customers. In the meantime, a timely delivery from supermarkets to consumers has been transformed from value-added services to standard operations. Order picking efficiency, as an important criterion of online service, has become a crucial point for the survival and healthy development of O2O supermarkets. Therefore, how to complete the order picking process in an efficient and accurate approach has become an urgent problem to be resolved.

In recent years, a few studies focus on mathematical optimisation of the order picking process to solve the problem of online orders picking in O2O supermarket. From the

R. Qiu et al. (Eds.): ICSS 2021, LNOR, pp. 286–299, 2021.
https://doi.org/10.1007/978-3-030-90275-9_24

point of view of food picking constrains in fresh supermarkets, Zhang et al. (2020) considered the Joint Order Batching and Picker Routing Problem (JOBPRP) and conducted mathematical optimisation models with and without category constraints, respectively. An algorithm was proposed to resolve the model with the objective of minimising the total processing time [1]. Huang et al. (2020) established an optimisation model and solutions for group order picking in large online supermarkets based on the JIT streamline framework. Theoretical recommendations for improving order picking efficiency are then proposed [2]. Focusing on the performance of omni-channel fresh food supermarkets, Wang (2019) designed a joint optimisation scheme of order picking and distribution from aspects of total delay time, default rate and total cost. [3]. Huang (2018) designed a scheme of order picking optimisation scheme including mixed assembly flow and established a mathematical model to verify the feasibility of the scheme, which has certain guiding significance for supermarkets to improve the comprehensive ability of online business [4].

In the broader literature, the Order Batching Problem (OBP) is widely studied using operations research, heuristic, and greedy algorithm methods. Henn and Schmid (2013) took the composition of picking orders, their processing times, and the sequence according to which they are released into account and built an order batching model to minimise the total tardiness for a given set of customer orders [5]. Bozer and Kile (2007) introduced a mixed-integer programming model of order batching problems with the purpose of obtaining the best solution to the problem of offline order batching, but this method is recommended only for instances where the order quantity is small (up to 25) [6]. Based on the FCL picking system of "man-on-goods", Wang and Pei (2017) built an order batching model with the objective of reducing the picking path and applied heuristics to obtain better solutions. Simulation experiments were conducted using the order data of the logistics centre [7]. In the case of "goods-to-man" order picking systems, Yan et al. (2020) considered the capacity of picking equipment and the physical limitation of workers and established an order batching model aiming at minimising the picking time. A heuristics including clustering algorithm and a genetic algorithm was proposed to solve the model. A simulation experiment was conducted to prove the effectiveness and practical significance of the proposed model [8]. Sun et al. (2020) comprehensively considered the influence of the quantity and volume of commodities with a joint optimisation model of order batching and picking path that minimises the total picking time. A nested genetic algorithm based on a clustering algorithm was designed to solve the joint optimisation problem [9].

Literature analysis suggests that the following issues need further discussion: (1) there are a few mathematical studies focusing on O2O order fulfilment service. (2) although the existing research on order batching have been detailed studied, most of them are designed for traditional logistics warehouse. There are few order batching models specified for O2O supermarket. After analysing and summarising the existing research results, we focus on the online order batching within O2O supermarkets. Considering the similarities and differences between supermarket and warehouse as well as the difference between the online and offline business, we then design a scenario-oriented order batching model. By comprehensively considering the order picking time, the travel time of the picker between shelves and the batch processing time, we proposed

an order batching model with the objective of minimising the total tardiness. The tardiness is characterised by the difference between order completion time and due time. This paper converts the dynamic online order receiving and picking pattern of O2O supermarket into a static order picking problem by setting a fixed interval time window which is broadly accepted in practice. This transformation can not only simplify the algorithm but also improve the efficiency of batch selection. In addition to the general constraints, such as the total quantity and order capacity of batches, the proposed model also takes additional factors such as the picking path planning into account. Further, this study designed a genetic algorithm to solve the problem. In numerical experiments analysis, we calculated the LFT of eight different situations (that are characterised by Item-Oriented Concentration (IOC), mean and variance of Maximum Allowable Completion Time (MACT)) to verify the adaptability and validity of the genetic algorithm under the certain supermarket layout and online order arrival time distribution. By comparing numerical examples of eight scenarios, we draw the conclusions and put forward relevant management advice about online order processing management for every traditional enterprise that is undergoing the transformation to O2O business model with problems such as low order picking efficiency and high picking movement repetition. It has significant practical implications for O2O supermarkets to improve operational efficiency and enhance core competence. Besides, the Degree of Congestion (DOC) that indicates the operational conflict between online order fulfilment and offline customer shopping is particularly discussed.

In the rest of this research, Sect. 2 discusses the order fulfilment problem in O2O supermarkets and Sect. 3 establishes the order batching mathematical models and algorithm. Extensive numerical experiments are conducted in Sect. 4. Section 5 concluded this research with a summary of research contributions and future research.

2 Problem Description

The objective function of the online order batching model is to minimise total order tardiness, that is, to meet customers' timeliness requirements to the maximum extent. The realisation of minimising tardiness can ensure that the completion due time of each order within a specific time window can be satisfied, improving the operational efficiency of the O2O supermarket as well as customer satisfaction. Considering the specific time-window of O2O supermarket online order batching, we suppose that customer order information (including the time of arrival, estimated time of ordering and delivery completion time, and commodities information) is known in advance. The system automatically generates the picking sequence which satisfies both the goal of minimising total order tardiness and constraint conditions of order picking process.

Based on manual picking conditions, the online order batching problem of the O2O supermarket can be described as follows. It is known that the O2O supermarket has $\|S\|$ shelves, and each shelf has $\|H\|$ storage locations allowing to place an SKU. The O2O supermarket stores a total of $\|M\|$ types of commodities, and the storage location of each specific commodity is known. The layout of the O2O supermarket is shown in Fig. 1.

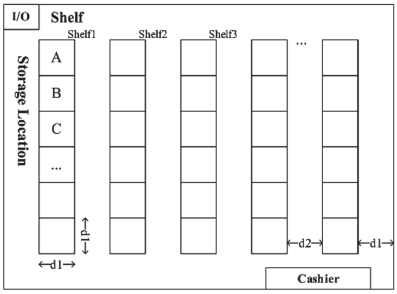

Fig. 1. O2O supermarket shelf layout

Suppose that there are $\|O\|$ orders with different completion times, which requires $\|P\|$ pickers to pick in a certain sequence. The item information contained on each order is known. The time of picking a particular item from the shelf and splitting and combining orders is known and constant. Assuming that the path of each picker is *S*-shaped, that is, the picking process starts from the starting point and follows the *S*-shaped path along the shelf until the last commodity (within a batch) is picked, then return to the starting point directly. The question is: how to group orders with different due time requirements into batches to reach the goal of minimising the total order tardiness. Based on the analyses above, we set up the following assumptions:

(1) There is no commodity shortage in each online order of the O2O supermarket.
(2) The shelf and storage location of each specific commodity is fixed.
(3) Each commodity is placed on the specific location of the specific shelf according to certain association rules.
(4) The same commodities in different batches of orders cannot be selected together.
(5) The time that a picker picks an item is not affected by his or her skill or proficiency.
(6) It takes the same unit picking time for pickers to select items located on different shelves and locations.
(7) The picker can only pick items from one side of the shelves.
(8) The picker cannot pick items located in different positions on the same shelf at the same time. That is, if the picker should pick items at more than one position on a certain shelf in the same batch, the total time he spent on the shelf equals the product of the number of places he will pick and the unit picking time.
(9) The picking time of the same commodity is proportional to the picking quantity of the commodity, that is, the picker picks items one by one, and the situation that pickers pick multiple items at the same time does not exist.
(10) The batch processing time (including the time that the system splits and merges orders into batches and the time that pickers restore batches into original orders and pack commodities into respective delivery packages) does not change according to the scale of orders but is only related to the quantity of batches.
(11) The picking process consists of the following processes: after receiving a certain picking order after batch processing, the picker starts to pick from the entrance of the supermarket in accordance with the principle of S-shaped path along the

shelf until the last commodity (within a batch) is picked, then directly returns to the starting point from the location of the last commodity.

(12) During the whole process, the picker should complete picking the whole quantity of the commodity within the batch at one time once he arrives at the location of the specific commodity location. At the same time, the picker cannot follow the repeated path (that is, he should strictly abide by the regulation that starting to pick from the entrance and returning to the entrance after completing the batch picking).

(13) Assuming that the distance between shelves in the supermarket is wide enough, multiple pickers can finish the picking work at the same time without causing congestion.

3 The O2O Order Batching Model and Algorithm

3.1 Variable Definition

To establish a mathematical model for online order batching problem of O2O supermarkets, we make the variable definition as follows.

Sets:

O	Sets of customer orders, $O = \{1, 2, ..., \|O\|\}$, indexed by i, and j
S	Sets of shelves, $S = \{1, 2, ..., \|S\|\}$, indexed by s, and t
H	Sets of locations, $H = \{1, 2, ..., \|H\|\}$, indexed by h
M	Sets of commodities, $M = \{1, 2, ..., \|M\|\}$, indexed by m
P	Sets of pickers, $P = \{1, 2, ..., \|P\|\}$, indexed by p
B	Sets of picking batches, $B = \{1, 2, ..., \|B\|\}$, indexed by k

Parameters:

Q	Maximum quantity of orders of each batch
q_{im}	The quantity of commodity m within order i
t_1	Time for the picker to search, pick and check per commodity
t_2	The batch processing time
T_{1i}	Total picking time of commodities within order i
T_{2i}	Total disposing time of order i
T_{3i}	Total shelf travel time of order i
a_{im}	$a_{im} = 1$ Order i contains commodity m, otherwise $a_{im} = 0$
b_{msh}	$b_{msh} = 1$ Commodity m is placed in location h of shelf s, otherwise $b_{msh} = 0$
v	Average walking speed of the picker during picking process
T_i	Due time for completion of order i
d_1	Width and depth of the square storage location

(*continued*)

(*continued*)

d_2	Distance between two adjacent shelves and the distance between the outermost shelf and the boundary of the O2O supermarket
$m_{s_u h_u}$	Commodity u is placed in storage location hu of shelf su, the matrix shows as follows: $\begin{pmatrix} m_{11} & \cdots & m_{p1} \\ \vdots & \ddots & \vdots \\ m_{1q} & \cdots & m_{pq} \end{pmatrix}$ m_{11} represents commodity 1, m_{1q} represents commodity q and m_{pq} represents commodity r

Decision variables:

X_{ki}	$X_{ki} = 1$ If order i is assigned to batch k. to pick, otherwise $X_{ki} = 0$
Y_{ks}	$Y_{ks} = 1$ If picking process of batch k should visit shelf s., otherwise $Y_{ks} = 0$
Z_{km}	$Z_{km} = 1$ If batch k. includes commodity m, otherwise $Z_{km} = 0$
V_{ksh}	$V_{ksh} = 1$ If picking process of batch k should visit storage location h of shelf s, otherwise $V_{ksh} = 0$
U_{kst}	$U_{kst} = 1$ If batch k contains shelf $arc(s, t)(s \neq ts, t \in S)$, otherwise $U_{kst} = 0$
D_k	Picking distance of batch k
$d_{m_{s_0 h_0}, m_{s_u h_u}}$	Distance between commodity $\left(m_{s_u h_u}\right)$ and starting point $\left(m_{s_0 h_0}\right)$
$d_{m_{s_u h_u}, m_{s_v h_v}}$	Distance between two commodities $\left(m_{s_u h_u}, m_{s_v h_v}\right)$
Td_i	LFT of order i
ct_i	Time of completing picking process of order i

3.2 Mathematical Model

The Order Picking Time (OPT) includes the time splitting and merging orders into batches, walking time for pickers to complete picking process, the time that picker retrieves commodities from the corresponding location of the corresponding shelf and the time that pickers restore batches into original orders and pack commodities into respective delivery packages. In terms of commodity retrieval time, this research assumes that the time for pickers to search, pick and check per commodity is same and constant. At the same time, the completion time of the batch is related to order quantity. Therefore, we set up the picking time equals the product of the time for pickers to search, pick and check each commodity and the total quantity of each category of the commodity within the same batch.

If the completion time does not exceed its due time, LFT is 0; otherwise, LFT equals the difference between batch completion time and due time. Consequently, the objective function that minimises the total order tardiness and constraints can be described as follows.

$$\min \sum\nolimits_{i\in O} Td_i \tag{1}$$

$$T_{1\mathrm{i}} = t_1 \sum\nolimits_{k\in B} \sum\nolimits_{m\in M} a_{im} \cdot x_{ki} \cdot q_{im} \forall i \in O \tag{2}$$

$$T_{2\mathrm{i}} = t_2 \tag{3}$$

$$T_{3\mathrm{i}} = \sum\nolimits_{k\in B} \frac{D_k}{v} \cdot x_{ki} \quad \forall i \in O \tag{4}$$

$$\mathrm{T}_{1\mathrm{i}} + \mathrm{T}_{2\mathrm{i}} + \mathrm{T}_{3\mathrm{i}} = ct_i \quad \forall \mathrm{i} \in O \tag{5}$$

$$\mathrm{Td_i} = \max\{0,\ ct_i - T_i\}\ \ \forall i \in O \tag{6}$$

$$D_k = d_{m_{s_0 h_0}, m_{s_u h_u}} + \sum d_{m_{s_u h_u}, m_{s_{u+1} h_{u+1}}} + d_{m_{s_v h_v}, m_{s_0 h_0}} \forall u \in S \tag{7}$$

$$d_{m_{s_u h_u}, m_{s_v h_v}} = \min \left\{ \frac{|S_u - S_v| \times (d_1 + d_2) + |H_u + H_v - 1| \times d_1}{|S_u - S_v| \times (d_1 + d_2) + |2H - H_u - H_v + 1| \times d_1} \forall u \in S \right. \tag{8}$$

$$d_{m_{s_0 h_0}, m_{s_u h_u}} = S_u \times d_1 + (H_u - 1) \times (d_1 + d_2) + 0.5 d_2 \tag{9}$$

$$\sum\nolimits_{t=0}^{\|S\|+1} U_{kst} = 2V_{ksh} \ \ \forall k \in B, \forall s \in S \tag{10}$$

$$U_{s(t+1)pk} - U_{stpk} = 0 \tag{11}$$

$$U_{0pk} = 1 \tag{12}$$

$$U_{s0k} = 1 \tag{13}$$

$$\sum\nolimits_{k\in B} X_{ki} = 1 \quad \forall i \in O \tag{14}$$

$$\sum\nolimits_{i\in O} X_{ki} \le Q \quad \forall k \in B \tag{15}$$

$$\sum\nolimits_{i\in O} a_{im} \cdot X_{ki} \le n \cdot Z_{km} \quad \forall k \in B, \forall m \in M \tag{16}$$

$$Z_{km} \le \sum\nolimits_{s\in \mathrm{S}} b_{msh} \cdot V_{shpk} \ \ \forall k \in B, \forall m \in M, \forall h \in H \tag{17}$$

$$X_{ki} \in \{0, 1\} \forall i \in O, \forall k \in B \tag{18}$$

$$Y_{ks} \in \{0, 1\} \forall s \in S, \forall k \in B \tag{19}$$

$$Z_{km} \in \{0, 1\} \forall m \in M, \forall k \in B \tag{20}$$

$$V_{ksh} \in \{0, 1\} \forall s \in S, \forall h \in H, \forall k \in K \tag{21}$$

$$U_{kst} \in \{0, 1\} \forall k \in K, \forall s, t \in S, s \neq t \tag{22}$$

$$Td_i \geq 0 \forall i \in O \tag{23}$$

$$ct_i \geq 0 \forall i \in O \tag{24}$$

Constraint (2) represents total picking time of commodities within the order. Constraint (3) indicates the total batch processing time of an order. Constraint (4) denotes the total shelf walking time of an order. Constraint (5) represents the completing time of an order. Constraint (6) represents the LFT of an order. Note that the average walking speed may vary due to the Degree of Congestion (DOC) which reflects potential conflict between online order fulfilment and offline customer shopping. Constraint (7) represents the total shelf walking distance of orders of each batch (where $m_{s_u h_u}$ and $m_{s_v h_v}$ respectively represent is the first and the last commodity to pick in the order). Constraint (8) represents the walking distance between two commodities $\left(m_{s_u h_u}, m_{s_v h_v}\right)$. Constraints (9) represents the distance between any commodity $\left(m_{s_u h_u}\right)$ and the starting point $\left(m_{s_0 h_0}\right)$. Constraint (10) is that a particular storage location corresponding each commodity of the batch can only be visited once. Constraints (11–13) represents that the picker cannot follow the repeated path during the picking process (that is, pickers should strictly follow the one-way path from the entrance to the exit). Constraint (14) represents that each order can only be assigned to one batch. Constraint (15) represents that the number of orders assigned to each batch does not exceed the specified maximum quantity. Constraint (16) represents that if any order in batch k picked by picker p contains commodity m, the batch ought to contain commodity m. Constraint (17) represents that if the batch k selected by picker p contains commodity m, picker p should visit to the corresponding location where commodity m during the picking process. Constraints (18–24) represents constraints of decision variables.

3.3 Genetic Algorithm

Due to page length, we here only report the crucial information related to the genetic algorithm. The key detailed information of genetic algorithm programmed by C++ is shown as follows. We first generated 1,000 chromosomes, each with 80 gene loci (representing 80 orders), each coded within the range of 1–15 (representing which batch index an online order was assigned to). The selection operator is that the first 25% of LFT (in

the descent order) in the population is reserved to the next generation. The total number of chromosomes is unchanged while the crossover, selection and mutation operators influence the rest of the population. The crossover rule is that two numbers between 1 and 80 are randomly generated, and all gene fragments between the two loci on two chromosomes are exchanged during pairing. The mutation rule of the algorithm is that there is a 15% chance of mutation at every gene locus on every chromosome during the replication process.

4 Numerical Test and Computational Result Analysis

4.1 Experimental Data Setups

The mathematical model and genetic algorithm are verified by the following experiments. Suppose that one O2O supermarket has 25 shelves (ranging from 1 to 25), each shelf with 4 layers (denoted by A, B, C, D). The O2O supermarket stores 100 SKUs. The distribution of item storage is shown in Table A1 of Appendix[1]. There are 15 workers available to do order picking work within the specific time window.

Suppose the supermarket receives 80 online orders within this time window. Considering the effect of item storage location on the picking efficiency, it is assumed that the supermarket, in order to improve the picking efficiency, placing high-frequency online-purchased items close to the supermarket's entrance. Table A2 in Appendix* shows the item information contained in each online order while the probability of each item being ordered follows a uniform distribution (i.e., there is no Item-Ordered Concentration (IOC)). Table A3 in Appendix* shows the item information contained in each order when the probability of each item appearing in each order is in a decreasing distribution (i.e., there exists IOC). The item information without IOC is generated randomly. The cumulative distribution probability of commodities of item information with IOC follows a quadratic function $y = -0.0103x^2 + 0.1693x + 0.2988$.

The rest of the relevant parameters are shown in Table 1. The output results of the genetic algorithm are shown in Table A6–A13 of Appendix*.

Table 1. Settings of experimental parameters

Parameter	Value	Parameters	Value
$\|\|M\|\|$	100	t_1	2 (s)
$\|\|S\|\|$	25	t_2	30 (s)
$\|\|H\|\|$	4	V	0.5 (m/s)
$\|\|O\|\|$	80	d_1	1.5 (m)
$\|\|Q\|\|$	10	d_2	1.5 (m)

[1] Appendix can be found from Google Drive shared files (https://drive.google.com/file/d/1qrzS9VRwyzkAPI0l-HlkzDHiVtHwDHav/view?usp=sharing).

4.2 Computational Result Analysis

We calculated the LFT of eight situations (characterized by IOC, mean and variance of MACT), and analyzed the output results from these three different perspectives. In the aspect of IOC, we considered two cases of IOC $= 1$ and IOC $= 0$. In regards to the mean value of MACT, we set $\mu = 30$ and $\mu = 45$. In regards to the variance of MACT, we set $\delta = 5$ and $\delta = 15$. Then, we used Excel Random Generator to generate 4 sets of normal distributions which obey N(30, 5), N(30, 15), N(45, 5) and N(45, 15), respectively in the range of 10 to 70. Some features of the output results are shown in the Table 2 below.

Table 2. Comparing results of different situations

	IOC	Mean	Std.dev.	Min.	Max.	Mean	Std. dev.
Situation 1	Yes	30	5	19825	20326	10082	225.27
Situation 2	Yes	30	15	19915	20409	20150	180.64
Situation 3	Yes	45	5	18564	19228	18866	250.30
Situation 4	Yes	45	15	18542	19196	18875	233.20
Situation 5	No	30	5	26955	27491	27247	218.50
Situation 6	No	30	15	26758	27367	27054	226.62
Situation 7	No	45	5	25802	26264	25948	181.10
Situation 8	No	45	15	25848	26422	26229	225.57

4.2.1 The Impact of IOC

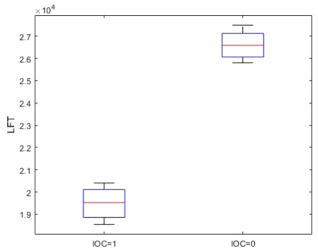

Fig. 2. Boxplot of batch results with different IOC

We considered the first questions. Q1: *Whether is there an LFT difference between situations with or without the IOC considerations?* To answer this question, we computed the paired-difference t-test between the output of these two situations, and the p-value was 8.581×10^{-31}. It suggests that there do exist a significant difference in LFT between the results of the two situations (Fig. 2).

The IOC of online customer orders has a remarkable impact on the total tardiness. The layout that matches online order picking may not be suitable for offline customers. For

this phenomenon, the O2O supermarket may take the similarity of commodity category and the occurrence frequency of the online order commodity as the basis to rearrange the in-store commodity layout. The rearrangement of commodity layout suitable for both offline customer and online order picking can not only enhance the efficiency of order picking but also provide consumers with a better in-store shopping experience. Therefore, O2O supermarkets may arrange their storage location based on the weighted proportion of their online and offline orders.

4.2.2 Mean and Variance of MACT

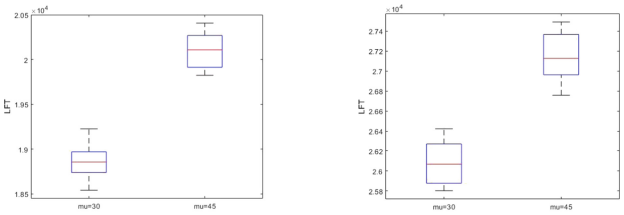

Fig. 3. Boxplot of batch results with different means of MACT

We then proceeded to investigate this phenomenon in a more precise way, answer Q2: *Whether does the mean value of MACT have a significant effect on batch results and total LFT?* To answer this question, we performed a one-way ANOVA of the output results. An independent-samples F-test revealed support for the hypothesis that the mean of MACT has a significant effect on batch results and the total LFT ($F = 171.6328$ for high IOC, $F = 99.3184$ for low IOC) (Fig. 3).

The mean of MACT has a significant difference to the total tardiness. To resolve this problem, the O2O supermarket can analyse the peak period of online orders and summarise the relevant laws, set up a flexible personnel arrangement and increase the number of spare staff. The new schedule can satisfy the order picking demand in the peak period so that the total LFT is reduced and the order performance rate is improved (Fig. 4).

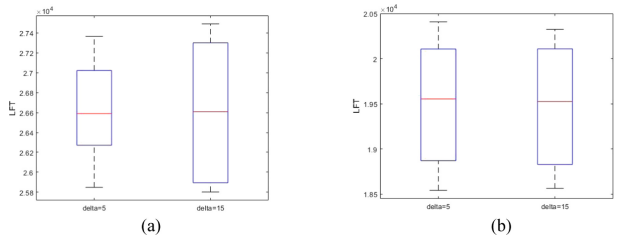

Fig. 4. Boxplot of batch results with different variances of MACT

Finally, we answer Q3: *Whether does the variance of MACT have a crucial effect on batch results and total picking time?* Similarly, we performed a one-way ANOVA of the output results. An independent-samples F-test revealed that the variance of MACT doesn't have a significant effect on batch results and the total LFT ($F = 0.0155$ for high IOC, $F = 0.0262$ for low IOC). We suppose the reason is that we have not yet taken (1) the differences of employee proficiency and (2) workload balance into account. In future research, we will take the employee's proficiency and work balance into account to carry on further consummates to the model.

4.2.3 The Degree of Congestion

The order picking efficiency in traditional warehouses in an e-commerce situation is mainly affected by the features of online orders. However, O2O supermarket has to deal with online orders as well as serve offline consumers simultaneously. The potential overlap of peak and nonpeak periods of online and offline channels would affect the efficiency of online order fulfilment.

Considering the differences of order batching processes in O2O supermarkets and traditional warehouses, we then conduct experiments to answer Q4: *Whether do the order batching processes of O2O supermarkets make a significant difference compared to that of traditional warehouses?* We use the average walking speed to characterise the peak and nonpeak periods of offline channel. Extensive computer experiments are conducted in the following three scenarios: (1) Online-Peak Offline-Peak, (2) Online-Peak Offline-Average, (3) Online-Peak Offline-Nonpeak. Scenarios (1) and (3) represent the various situations of O2O supermarkets, and Scenario (2), serving as benchmark, represents traditional warehouses.

We calculated the LFT of these three aforementioned scenarios (characterized by DOC), in which the Average Walking Time per Unit Distance (AWT) varies ±50%. In the experiments, the number of orders is set 100 to simulate the peak period of online channel, and other parameters are unchanged. For each scenario, we conducted 20 independent replications. Tables A4 and A5 in Appendix* shows detailed order information in these experiments. Some features of the output results are shown in Table 3.

Table 3. Comparing results of different scenarios

	AWT	Min.	Max.	Mean	Std. dev.
Scenario 1	4	31063	33956	32521.9	788.3943
Scenario 2	3	27762	29817	28710.8	645.5647
Scenario 3	2	23905	25828	24839.2	683.3751

We computed the paired-difference *t*-test between the output of Scenarios (1) and (2), and the *p*-value was 7.83×10^{-8}. We also computed the paired-difference t-test between the output of Scenarios (3) and (2), and the p-value was 7.81×10^{-10}. Both of the result suggest that there does exist a significant difference in LFT between the results of the

two situations. In other words, the potential conflicts between online and offline channels in O2O supermarkets have significant impacts on the performance of order batching. Compared with traditional warehouses, managers have to consider more factors when making order batch decisions compared with that in the traditional warehouses (Fig. 5).

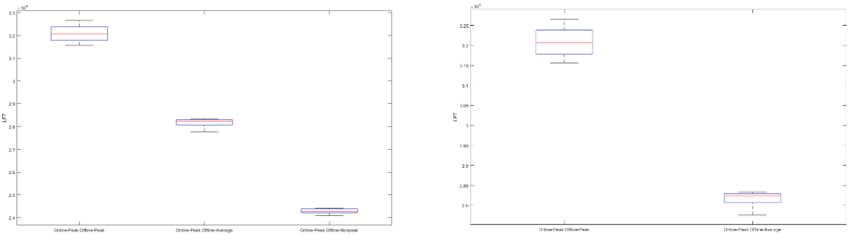

(a) (b)

Fig. 5. Boxplot of batch results with different DOC

5 Summary

Based on the O2O supermarkets, this paper constructs an order batching model with the target of minimising the total LFT, which is solved by a genetic algorithm. By designing the typical scenarios and conducting numerical analysis, the paper puts forward relevant management advice to O2O supermarkets to achieve the goal of enhancing operational efficiency and the service level.

The contributions of this paper are two-fold. First, the paper formulates the mathematical model built on the traditional order batching model, and concentrates on the difference between traditional warehouse and the O2O supermarket. Considering the degree of congestion between online and offline channels, we conclude that the O2O supermarket should be committed to provide comfortable shopping experience for online and offline customers by (1) rearranging commodity storage location based on the weighted proportion of their online and offline orders, (2) building robust and flexible personnel schedules, and (3) intentionally shrinking online channel traffic when it comes to offline-peak. Second, we set a fixed time window to transform the dynamic order arrival into a relatively static order picking problem. This paper designs a genetic algorithm based to solve the problem and carries on the analysis with the data of different supermarket layout and picking time, which not only shows the adaptability and validity of the model, but also provides management suggestions for O2O supermarket online order batching problem.

In the future, we aim to take more real-world operational characteristics of O2O supermarket into account. To improve the accuracy of the model, the relevant factors such as the proficiency of pickers and workload balance should be considered, and we will consider the picker's congestion problem of the O2O supermarket. Besides, in order to continually improve our research from several aspects and enhance the practical value of our research, we will continue to optimise and modify our existing algorithm as well as get more accurate order data by conducting market research.

References

1. Zhang, J., Zhang, Y., Zhang, X.: The study of joint order batching and picker routing problem with food and nonfood category constraint in online-to-offline grocery store. Int. Trans. Oper. Res. **28**(5), 2440–2463 (2020)
2. Hang, M.-f., Zhang, Y.-k.: JIT assembly line-based order picking process optimization method for online supermarkets. Chin. J. Manag. Sci. **28**(5), 159–166 (2020). (in Chinese)
3. Wang, X.: Integrated optimization of order picking and delivery in X fresh supermarket under new retail. Thesis for the master's degree, Beijing Jiao tong University (2019). (in Chinese)
4. Huang, X.: A mixed assembly line-based optimization method of order picking operations of online supermarkets. Thesis for the master's degree, North China Electric Power University (2018). (in Chinese)
5. Henn, S., Schmid, V.: Metaheuristics for order batching and sequencing in manual order picking systems. Comput. Ind. Eng. **66**(2), 338–351 (2013)
6. Bozer, Y.A., Kile, J.W.: Order batching in walk-and-pick order picking systems. Int. J. Prod. Res. **46**(7), 1887–1909 (2007)
7. Zhuan, W., Zeping, P.: Order batching algorithm based on heuristic picking route for saving mileage. Comput. Eng. Appl. **54**(23), 203–209 (2018)
8. Yan, J., Chang, L, Feng, L.: "Online order batching and picking path planning model and algorithm", [J/OL]. Computer Engineering and Applications, pp. 1–10 (2020)
9. Junyan, S., Zhirui, C., Yaru, N., Yuanyuan, Z., Fang, H.: Joint optimization of picking operation based on nested genetic algorithm. J. Comput. Appl. **40**(12), 3687–3694 (2020)
10. Ardjmand, E., Bajgiran, O.S., Youssef, E.: Using list-based simulated annealing and genetic algorithm for order batching and picker routing in put wall based picking systems. Appl. Soft Comput. J. **75**, 106–119 (2018)
11. Chen, T.-L., Cheng, C.-Y., Chen, Y.-Y., Chan, L.-K.: An efficient hybrid algorithm for integrated order batching, sequencing and routing problem. Int. J. Prod. Econ. **159**, 158–167 (2015)

Integrating Empirical Analysis into Analytical Framework: An Integrated Model Structure for On-Demand Transportation

Yuliu Su[1], Ying Xu[1(✉)], Costas Courcoubetis[1], and Shih-Fen Cheng[2]

[1] Engineering Systems and Design, Singapore University of Technology and Design, Singapore 486830, Singapore
xu_ying@sutd.edu.sg

[2] School of Computing and Information Systems, Singapore Management University, Singapore 178902, Singapore

Abstract. On-demand transportation services have been developing in an irresistible trend since their first launch in public. These services not only transform the urban mobility landscape, but also profoundly change individuals' travel behavior and demand for cars. In this paper, we propose an integrated model structure which integrates empirical analysis into a discrete choice based analytical framework to investigate a heterogenous population's choices on transportation mode and car ownership with the presence of ride-hailing. Distinguished from traditional discrete choice models where individuals' choices are only affected by exogenous variables and are independent of other individuals' choices, our model extends to capture the endogeneity of supply demand imbalance between ride-hailing service providers and users. Through equilibrium searching and counterfactual analysis, we further quantify the magnitude of impacts of platform operations and government policies on car demand, usage and traffic conditions. The structure of the model and managerial insights are explained in detail.

Keywords: Ride-hailing · Peer-to-peer sharing · On-demand platforms · Mobility as a service

1 Introduction

In the past decade, with the ubiquity of connectivity and proliferation of smart phones, we have witnessed the emergence of peer-to-peer ride-hailing platforms such as Uber, Grab and Go-Jek [1]. While this new form of peer-to-peer service has disruptively changed the on-demand mobility sector, discussions about its impacts on our society and environment have been inconclusive. On the one hand, this new form of peer-to-peer sharing has brought improvement on social welfare, in terms of creating more employment opportunities, enabling individuals to earn additional income [2, 3], encouraging shared rides,

Electronic supplementary material The online version of this chapter (https://doi.org/10.1007/978-3-030-90275-9_25) contains supplementary material, which is available to authorized users.

R. Qiu et al. (Eds.): ICSS 2021, LNOR, pp. 300–315, 2021.
https://doi.org/10.1007/978-3-030-90275-9_25

eliminating wasteful driving, and thus reducing traffic and vehicle emissions [4–6]. On the other hand, criticism has also arisen for these platforms' quest for profits and market shares by diverting non-driving trips to driving mode [7], which leads to unnecessary driving demand and excess supply. For example, a survey in US shows that in the absence of ride-hailing, about 49% to 61% of ride-hailing trips would not have taken place at all or would have been made by other modes such as walking and public transportation [8]. Moreover, we find that the impacts of peer-to-peer ride-hailing platforms on car ownership are also two-fold. On the one hand, ride-hailing may have a cannibalization effect on demand for cars [9], reducing individuals' incentive to own a car. On the other hand, ride-hailing may lead to a value enhancement effect on car ownership [9], adding more valuations with purchasing a car [10, 11]. For example, a study on new vehicle registrations in China shows that Uber entry is significantly associated with an 8% increase in car ownership [12].

A key feature leading to the above unresolved debates is that, different from traditional taxi service, in the peer-to-peer ride-hailing sector the drivers are flexible individuals. As a result, ride-hailing platform could not fully control the capacity of their service supply. Moreover, since individuals could switch between the supply side and demand side (i.e., being a driver or a rider) [13], the interaction adds more challenges for the platforms to balance supply and demand, not to mention to optimize the utilization of the capacity. Hence, to study the impacts of ride-hailing, it is critical to understand how individuals' decisions on being a driver or a rider for the platforms are affected, and these decisions are also coupled with other decisions on travel model as well as car ownership and usage. Although there are a few attempts in investigating the mechanism of peer-to-peer markets, most of them focus on product sharing (e.g., car renting) and adopt an analytical framework (e.g., [9, 14] and [15]). As these analytical studies are usually formatted as an equilibrium searching problem through analytical calculation or simulation, they may be challenged by its simplifications and lack of validation by empirical data in practice.

To the best of our knowledge, empirical studies focusing on peer-to-peer on-demand service platforms are relatively limited. To enrich this research stream, this paper introduces an integrated model structure which connects theoretical models with empirical analysis to investigate a heterogenous population's choices on car ownership, usage and transportation mode with the presence of ride-hailing. Specifically, we first develop a discrete choice framework which captures heterogenous individuals' choices among different strategies facing ride-hailing. They decide whether to purchase a personal car, how to use the car if s/he owns one (either serve for the platform or solely use for personal need), and whether to use the platform service or not when needed. These strategies are affected by various factors such as wages, working hours, price sensitivity, perception of traveling in a private car compared to public transportation, and benefits and costs of owning a personal car, etc., which are all included in our model. Moreover, noticing that in the two-sided on-demand platform context, each individual's choice depends on the dynamics between supply and demand, which is a collective result of the whole population's decision. We also incorporate such endogeneity of the supply and demand imbalance and connect the two sides through a matching function, which is also embedded into the choice functions. We then empirically calibrate our model using publicly

disclosed data in the Singapore ride-hailing marketplace. Based on our model, we further conduct counterfactual analysis to quantify the magnitude of impacts of platform operations and government policies on ownership and traffic, which yields empirical assessment of the peer-to-peer transportation service platform.

The principal contributions of our paper are summarized as follow.

a. We introduce an integrated model structure which integrates empirical analysis into a discrete choice-based equilibrium framework. As in the two-sided on-demand platform context, each individual's choice depends on the dynamics between supply and demand, which is a collective result of the whole population's decision, endogeneity of the supply and demand balancing rises as a challenge (for example, more platform drivers lead to higher chance and shorter waiting time for riders to grab a car, and thus higher the utility for riders). Commonly used choice models are limited to capture such endogeneity as they consider the variables affecting individuals' choices as exogenous and the population's choices are independent of each other's. Distinguished from the traditional choice models, our framework overcomes this chal1lenge by incorporating the endogeneity of supply and demand imbalance through a matching function and formalizing individuals' choices as a game equilibrium as a function of others' choices. Moreover, although our model is developed with a focus of peer-to-peer ride-hailing, it can easily be generalized to other peer-to-peer markets including both product sharing and on-demand service platform.
b. Our integrated model demonstrates flexibility with data scarcity. A common challenge for empirical studies is the lack of access to data. For example, to develop a discrete choice model, large volume of individual-level choice data are usually required, which are commonly collected through large scale interview or discrete choice experiment survey. The data collection could be costly and time-consuming, and may also incur privacy issues (as the survey involves questions about individuals' demographic information such as wage, traveling needs and mode preference). Conversely, our model demonstrates the flexibility of parameters being estimated with sparse aggregate-level data. We use publicly disclosed data on distribution of car ownership and usage in the Singapore ride-hailing marketplace to calibrate our model parameters. Our approach sheds lights on applying scarce data on empirical settings.
c. Our analyses inform the debate on how ride-hailing may affect ownership, usage and traffic with the sophisticated consideration of supply demand matching propensity. The main findings suggest that ride-hailing may demonstrate both cannibalization effect and value enhancement effect on car ownership depending on different conditions. The cannibalization effect of ride-hailing on own car ownership is mainly due to its lower price compared to conventional taxis. In terms of individuals' decision of whether and how to participate in the peer-to-peer ride-hailing service, their choices are affected not only by ride-hailing price or driving cost but also the dynamics between supply and demand imbalance. For example, we observe that although the increase of service price increases platform drivers' earnings, it in fact leads to fewer platform drivers due to a diminishing user base, which lowers demand and matching propensity. We further investigate the relationship between platform revenue and

ride-hailing payment. Our analysis suggests that due to the supply demand dynamics, the platform's revenue does not increase monotonically with service charges; there exits an optimal price level which allows the platform to maximize its revenue.

The remainder of this paper is organized as follows. Section 2 reviews related literature in peer-to-peer sharing. In Sect. 3 we introduce the framework of our integrated model in detail. Section 4 specifies the data we used for our empirical setting and the calibration process of our model parameters. In Sect. 5 we present the equilibrium analysis under various counterfactual scenarios. Section 6 concludes the work with a discussion of the findings and future research directions.

2 Literature Review

Peer-to-peer sharing has attracted growing research interest in recent years. Studies related with peer-to-peer sharing can be broadly classified into two categories with respect to their study focuses. The first category focuses on peer-to-peer resource/product sharing, which allows owners to rent out their products/assets to non-owners for a short term (e.g., Airbnb for accommodation sharing and Zipcar for car renting). Most of the papers in this group study the impacts of product sharing on individuals' decisions on product ownership from different perspectives such as product manufacturer (e.g., [9, 16] and [14]) or the platform owner (e.g., [15]). The second category focuses on peer-to-peer on-demand service, which connects users requiring a time-sensitive service with independent service providers (e.g., Uber for transportation service and Deliveroo for food delivery service). Most papers in this category investigate how the interactions between the supply and demand in the two-sided market are affected by different factors, such as [17] by the factor of dynamic pricing, [18] by customers' sensitivity to delay and service providers' independence, [19] by payout ratio (i.e., the ratio of wage paid to service providers over price charged from consumers) and [20] by service providers' self-scheduling. In addition, a few other studies investigate the effectiveness of different contract designs for stakeholders of the on-demand service platform such as [21] and [22]. Some other studies adopt a game theoretic framework to examine the organization of the on-demand service such as [23] and [24]. The early works in peer-to-peer sharing are dominated by theoretical arguments that construct analytical framework to explain and investigate the mechanism of and agents' interactions in the innovative marketplace.

Although previous analytical studies provide the first insights about individuals' choices with the presence of sharing economy, the majority of them has focused on system equilibrium and/or welfare of service providers and customers, which are obtained through analytical calculation or simulation and are not validated by empirical data in practice [25]. The empirical studies on on-demand platforms are relatively limited, mostly focusing on using statistical regression models to study the impact of sharing economy on ownership or traffic congestion. For example, [7, 12] and [3] use longitudinal data and difference-in-difference models to investigate the influence of the entry of Uber on traffic congestion, new vehicle ownership and rates of entrepreneurial activities respectively. [26] structure a before-and-after assessment and employ a fixed-effects panel data regression model to analyze the impact of ride-hailing on traffic congestion

in a major city. [25] use a probit regression estimated by a modified Heckman two-stage method to study the impact of financial incentive on platform drivers' decision of whether to work and corresponding number of work hours. However, a key shortcoming of regression methods such as difference-in-difference is that their statistical results do not always imply an unbiased estimate of the causal effect as mentioned in [27].

It is worth noting that despite the growing abundance of literature in sharing economy, many controversial questions still remain and need to be answered. Given the fact that analytical work would be challenged by the simplifications and that existing empirical studies fail to effectively explain the causation and have limited prediction power, there are calls for research integrating analytical methodologies with empirical methodologies. Such action could improve the validity as well as the explanatory power and prediction capability of the model, which could provide in-depth managerial insights. So far, we have noticed one paper [28] attempting this integrated methodology. The authors first introduce a dynamic model and then use empirical data to calibrate the model. However, their focus is the peer-to-peer durable goods sharing market; and they do not consider the matching rates as a dynamic result of supply and demand but exogenously specified. As far as we know, no studies have yet attempted to analyze on-demand service platforms, in particular the ride-hailing platform, by using such integrated methodology. Motivated by the lack of relevant research, in this paper we propose a model structure that integrates empirical analysis into analytical framework with the consideration of endogenous supply demand matching to study the peer-to-peer on-demand service platform.

3 The Model

3.1 Agents' Strategies and Payoffs

Our study objects (agents) are a working age population consisting of individuals who are eligible for driving, below retirement age, and most importantly, have a regular travel need. To satisfy their travel needs, individuals may choose to own a personal car to satisfy the travel need. Once with a private car, with the presence of ride-hailing, the individual also has an opportunity to choose to work for the platform as a driver (either full-time or part-time). In contrast, without a personal car, the individual could decide between using the ride-hailing service or other transportation service such as public transportation. Accordingly, we construct a set of five strategies $\Sigma = \{N, P, F, U, A\}$ for the individuals to choose from.

- [N] Non-platform driver: An individual who owns a personal car but only uses the car to satisfy her own travel needs.
- [P] Part-time platform driver: An individual who owns a personal car and has a regular full-time job. She drives for the platform during after-work time to earn extra income.
- [F] Full-time platform driver: An individual who owns a personal car and forgoes the regular job with wage w to work full-time on the platform.
- [U] User: An individual who does not own a personal car but prefers to satisfy her travel needs by using the ride-hailing service.

- [*A*] Abstinent: An individual who does not own a personal car and whenever she needs a ride, she chooses public transportation.

Each individual chooses its strategy based on its expected long term payoffs, which are characterized as the average utility associated with each strategy per period. The individuals' travel needs is denoted by M_i per period. Due to the comfort and convenience, traveling in private cars generates positive payoffs compared with taking public transportation. We normalize the utility of taking public transportation to zero, and use γ_i to indicate individual i's relative utility gain of traveling in private cars per kilometer. Correspondingly, strategies *N, P, F, U* enjoy a utility gain of $\gamma_i M_i$ compared with strategy *A*. For strategies *N, P, F*, a fixed car ownership cost[1] k and a variable cost c (such as petrol and toll) will incur. Considering the convenience to access the car, strategies *N, P, F* also enjoy a convenience benefit of b_N, b_P and b_F respectively. Furthermore, for simplicity, we assume that all part-time and full-time platform drivers work the same amount of time t_P and t_F respectively to provide the ride-hailing service. More, all individuals but the full-time platform drivers (strategy F) are assumed to own a regular full-time job with wage w_i per period. Each individual is further characterized by its price sensitivity $\theta_i \geq 0$.

Before introducing the payoff functions, some characteristics of the ride-hailing market are worth mentioning. In the two-sided ride-hailing market, the matching between the drivers and riders could not be perfect due to spatial and temporal constraints. As a result, a platform driver could only be matched with a rider with a proportion of $\alpha \in (0, 1)$ out of the driver's total working time, while a platform user's request could only be successfully fulfilled with probability $\beta \in (0, 1)$. With the chance of $1 - \beta$, the platform user must resort to public transportation, which is assumed to be always available.

Next we specify the payoff functions for each strategy of individual i. The subscript i in the equations indicates that the corresponding variables are individual specific, variables with strategy subscript (such as b_N) are assumed to be homogeneous for individuals in the same strategy group ("N"), and variables without subscript are common across the whole population.

- [*N*] A non-platform driver has a regular job with wage w per period. She possesses a personal car and uses it to satisfy her own travel needs M_i and thus gain a payoff of $\gamma_i M_i$ from traveling in a private car. She also pays for the fixed ownership cost k and variable cost c per kilometer. Price sensitivity θ_i converts monetary value to utility. She also earns a convenience benefit b_N from owning a car. In this case the payoff is

$$V_{N,i} = \theta_i w_i + \gamma_i M_i - \theta_i (c M_i + k) + b_N .$$

- [P] A part-time platform driver possesses a car and has a regular job as a non-platform driver. However, she uses the car not only to satisfy her own travel need M_i but also provide ride-hailing service on the platform after this regular job. The term

[1] In order to participate in ride-hailing, platform drivers are required to possess a private car. They could either purchase a personal car or rent a car from the platform. In our model formulation we do not distinguish between these two ways as essentially they both represent a fixed ownership cost k.

$\theta_i t_P s(\alpha\rho - c) - t_P l$ represents the additional benefit from the part-time ride-hailing service. t_P is the time she works as a part-time ride-hailing driver while s is the average driving speed. The product of t_P and s converts the working hours to total kilometers supplied on the platform. Due to market friction and supply-demand imbalance, out of the $t_P s$ kilometers she supplies for the platform, only α fraction is effectively used by serving a passenger, generating an earning of $t_P s\alpha\rho$, where ρ is the per kilometer earnings from providing the service. We assume that while providing the service, the driver is always driving around with or without a traveler in her car as she may be driving towards higher demand areas to search for new customers. Therefore, she always incurs a variable driving cost c during time period t_P. As a result, the net profit from part-time ride-hailing service is $t_P s(\alpha\rho - c)$. Again, θ_i converts monetary profit to utility. Also, as the part-time platform driver works overtime with consideration of her regular job, she incurs a loss of leisure time utility l per time unit during her working time t_P on the platform. The above modeling assumptions imply the following payoff:

$$V_{P,i} = \theta_i w_i + \gamma_i M_i - \theta_i(cM_i + k) + b_P + \theta_i t_P s(\alpha\rho - c) - t_P l.$$

- [F] A full-time platform driver gives up her regular job and takes providing ride-hailing service as her full-time job. Therefore, she forgoes the wage w from her previous regular job (hence $\theta_i w_i \times 0$). Similar to a part-time platform driver, the net income from being a full-time platform driver is expressed by $t_F s(\alpha\rho - c)$. The average working time of the full-time platform driver's previous regular job is denoted by λ. The full-time platform driver may choose to work overtime on the platform. The term $(t_F - \lambda)_+$ is an indicator of whether the full-time platform driver incurs a utility loss of leisure time. If total working time on the platform t_F is larger than λ, it suggests that the full-time driver works overtime and incurs a leisure loss l per unit time. Hence, the payoff of a full-time platform driver is given by

$$V_{F,i} = \theta_i w_i \times 0 + \gamma_i M_i - \theta_i(cM_i + k) + b_F + \theta_i t_F s(\alpha\rho - c) - (t_F - \lambda)_+ l.$$

- [U] A user is by definition an individual that uses ride-hailing service to satisfy her transportation needs. She pays r dollars per kilometer for hailing a car. However, due to market frictions, only β percentage of times a user can be successfully matched with a car. If she fails to find a private-hire car, then with probability $1 - \beta$the user opts for public transport. Thus, the corresponding payoff is given by

$$V_{U,i} = \theta_i w_i + \beta\big(\gamma_i M_i - \theta_i r M_i\big).$$

- [A] An abstinent individual chooses not to buy a car nor use ride-hailing service. Whenever she has a travel need, she opts for the outside option such as public transport or walking. We normalize the utility of the outside option to zero and the cost of the outside option is assumed to be negligible. Thus the payoff function of the abstinent only consists a term of her regular job wage. Therefore, the payoff of an abstinent is

$$V_{A,i} = \theta_i w_i.$$

3.2 Choice Model and Population Share

Among all the five agent types listed in Sect. 3.2, some individuals may be constrained by exogenous reasons to be of a certain type. For example, some may not have driving license or are not physically fit for driving. Therefore, we consider the population divided into two segments S_1, S_2. The first segment is eligible for driving and hence has access to all five strategies *N, P, F, U, A*. The other segment cannot act as a driver (at least in the short term where the decision model is defined) and hence has access to either the strategy of *U* or *A*, i.e., user or abstinent. We use discrete choice model to study the choices of the heterogeneous population.

Discrete choice models based on multinomial logit have been used extensively in the field of transportation research [29]. According to random utility theory (RUT) [30], in additional to the systematic part of the utility V_{ij} as specified in the payoff functions, there is a random part ε_{ij} which captures the unobservable factors. We assume ε_{ij} are independently and identically distributed type-I extreme random variables. Therefore, for the five strategies listed in Sect. 3.2, the probability P_{ij} of individual i choosing strategy $j \in \{N, P, F, U, A\}$ in the two population segments can be expressed as

$$\begin{aligned} S_1 : P_{ij} &= \frac{e^{V_{ij}}}{e^{V_{i,N}}+e^{V_{i,P}}+e^{V_{i,F}}+e^{V_{i,U}}+e^{V_{i,A}}}, j = N, P, F, U, A, \\ S_2 : P_{ik} &= \frac{e^{V_{ik}}}{e^{V_{i,U}}+e^{V_{i,A}}}, k = U, A. \end{aligned}$$

As the heterogeneity of the population is characterized by individual-specific variables $(\theta_i, \gamma_i, w_i, M_i)$, the integral of above equations over the joint distribution of $f(\theta, \gamma, w, M)$ produces the choice shares of the five strategies within each segment. Specifically,

$$\begin{aligned} S_1 : S_{j,S1} = \int \frac{e^{V_{ij}}}{e^{V_{i,N}} + e^{V_{i,P}} + e^{V_{i,F}} + e^{V_{i,U}} + e^{V_{i,A}}} f(\theta, \gamma, w, M) d\theta d\gamma dw dM, \\ j = N, P, F, U, A, \end{aligned}$$

$$S_2 : S_{k,S1} = \int \frac{e^{V_{ik}}}{e^{V_{i,U}} + e^{V_{i,A}}} f(\theta, \gamma, w, M) d\theta d\gamma dw dM, k = U, A.$$

Let us further assume that a fraction of the population belongs to S_1 and $1 - a$ fraction belongs to S_2, then the population shares of strategies *N, P, F* are

$$S_j = a \int \frac{e^{V_{ij}}}{e^{V_{i,N}} + e^{V_{i,P}} + e^{V_{i,F}} + e^{V_{i,U}} + e^{V_{i,A}}} f(\theta, \gamma, w, M) d\theta d\gamma dw dM, j = N, P, F, \tag{1}$$

and the population shares of strategies *U* and *A* are

$$\begin{aligned} S_k = a \int \frac{e^{V_{ij}}}{e^{V_{i,N}} + e^{V_{i,P}} + e^{V_{i,F}} + e^{V_{i,U}} + e^{V_{i,A}}} f(\theta, \gamma, w, M) d\theta d\gamma dw dM \\ + (1 - a) \int \frac{e^{V_{ik}}}{e^{V_{i,U}} + e^{V_{i,A}}} f(\theta, \gamma, w, M) d\theta d\gamma dw dM, k = U, A. \end{aligned} \tag{2}$$

It is worth noting that Eqs. (1) and (2) have no closed form solution. However, we can approximate the integral through simulation. Specifically, we first draw R samples $(\theta^r, \gamma^r, w^r, M^r)$ from the joint distribution $f(\theta, \gamma, w, M)$, then use this as an empirical distribution to compute the average of the probability P_{ij} over individuals of the population instead of the integral. This average is the simulated population share of the five strategies:

$$\begin{aligned}
\hat{S}_j &= a\left(\frac{1}{R}\sum_{r=1}^{R}\frac{e^{V_j^r}}{e^{V_N^r}+e^{V_P^r}+e^{V_F^r}+e^{V_U^r}+e^{V_A^r}}\right), j = N, P, F, \\
\hat{S}_k &= a\left(\frac{1}{R}\sum_{r=1}^{R}\frac{e^{V_k^r}}{e^{V_N^r}+e^{V_P^r}+e^{V_F^r}+e^{V_U^r}+e^{V_A^r}}\right) + (1-a)\left(\frac{1}{R}\sum_{r=1}^{R}\frac{e^{V_k^r}}{e^{V_U^r}+e^{V_A^r}}\right), j = U, A.
\end{aligned} \tag{3}$$

A challenge in estimating above population shares is the endogeneity of ride-hailing matching probabilities α and β, which are functions of the supply (population shares of platform drivers) and demand (population share of users). More precisely, controlling other factors, if α increases, a platform driver has higher chance to serve a customer and thus obtain higher income. Therefore, strategies P and F become more tempting and corresponding population shares S_P and S_F, i.e., the supply of service will increase. However, as the supply of the service increases, the matching rate α will conversely tend to decrease. User's matching probability β acts in a similar vein. This observation implies that there is a circular dependence between supply and demand and the matching rates α and β. To characterize this dependence, we incorporate below matching functions based on the work of [15] into our model:[2]

$$\alpha = t \cdot \frac{D}{D+S}, \beta = t \cdot \frac{S}{D+S}. \tag{4}$$

Under our model specification, the supply and demand can be further expressed as the mileage supplied and requested:

$$Supply = (S_P t_P + S_F t_F)S, Demand = S_U E(M). \tag{5}$$

In (4), the parameter $t \in (1, \min\{\frac{Demand+Supply}{Demand}, \frac{Demand+Supply}{Supply}\})$ characterizes the level of matching friction in the two-sided market: the higher t is, the lower the matching friction, hence the higher the matching propensity.

4 Data

Our empirical context will be the Singapore ride-hailing marketplace, which acts as an ideal research subject for the following reasons. Firstly, as an island country, the transportation system of Singapore is relatively closed with few foreign vehicles entering

[2] According to [15], Eq. (4) is derived based on deterministic fluid approximation of a multi-server loss queuing system with arrival rate D and total service rate S, in which, α corresponds to the system utilization and β corresponds to the probability at which a job request could find an idle server upon arrival.

from outside, which guarantees that supply of the peer-to-peer ride-hailing service is provided within the region. Given the fact that the Singapore government records the private hire/ride-hailing car population over time, this unique feature makes the number of platform drivers easily trackable, which is not the case in other cities. For example, in San Francisco, previous study finds that about 80% of the Uber drivers actually live outside of the city and bring their cars into the city every morning to provide for peer-to-peer service [5]. As the supply is from both internal and external, such an open system brings difficulty in modeling the dynamics between supply and demand. Secondly, due to the strict regulations of the Singapore government, the level of car ownership is being monitored over time. In order to own and use a vehicle (no matter for personal use or for ride-hailing service), car owners are required to obtain a quota licence called "Certificate of Entitlement (COE)" through bidding. Since the number of cars are strictly controlled by the government, the supply of private car is relatively stable over the years and the COE quotas made available for each year is limited. In view of the fact that the price of the car itself (determined by its open market value) is relatively stable, the bidding price of COE can be viewed as a proxy for demand of cars as the total number of cars allowed is relatively constant.

In the following sections, we elaborate on how we calibrate our model based on the Singapore ride-hailing marketplace. We focus on the population with age between 20 and 64 for those who are eligible to drive and below retirement age. Specifically, we use publicly disclosed data in year 2017 to calibrate our model and data in year 2016, 2018 and 2019 to conduct robustness check and validity test. Values of our model parameters are determined through two ways. First, some parameters such as travel demand and wage distribution do not depend on our model specification and can be *estimated* from available data directly. However, other parameters such as price sensitivity, perception of traveling in private cars, convenience benefit of car ownership and utility loss of working overtime cannot be obtained through the data directly. Therefore, we *calibrate* these parameters by searching for the values that make our model captures the reality i.e., generates the calibrated population shares as close as the actual ones.

4.1 Estimated Parameters

Table 1 summarizes the values of the parameters estimated directly from data for year 2017. The travel demand is estimated by fitting a lognormal distribution based on average monthly mileage of private cars and distribution of taxi trip distance (including both street hailing and requests from ride-hailing platforms). Wage distribution of the population is obtained by fitting a lognormal distribution to the household income data. As mentioned previously, the ownership cost of a private car consists of car retail price and the cost of COE. Therefore, we approximate the ownership cost as the sum of both car price and COE cost. Usually, ride-hailing platforms take a commission fee from drivers for each trip. They also provide various incentive schemes to attract more supply. Thus platform drivers' earning ρ is estimated as the sum of after-commission trip fare and incentive rewarded.[3] The value of matching friction level t is determined by setting the

[3] See example of a major ride-hailing company's incentive scheme on 2019: https://www.gojek.com/sg/blog/sg-driver-incentives-gojek-singapore/.

Table 1. Estimated parameter values for year 2017

Parameter	Symbol	Estimate
Travel demand	M	lognormal (3.75, 0.38^2) km/day
Regular job wage	w	lognormal (7.89, 0.86^2) \$/mth
Ownership cost of car	k	60 \$/day
Driving cost	c	0.13 \$/km
Average driving speed	s	40 km/hr
Regular working hours	λ	45 h/week
Part-time platform driver working hours	t_P	7 h/week
Full-time platform driver working hours	t_F	49 h/week
User payment for ride-hailing	r	0.99 \$/km
Driver earning from ride-hailing	ρ	1.00 \$/km
Market friction level	t	1.3

matching rates α and β reflecting the Singapore ride-haling market. As suggested by the taxi occupancy data (fraction of driving time a taxi is occupied with a passenger), the representative matching rate for platform drivers is around 0.5, hence we estimate t $= 1.3$ which leads to $\alpha = 0.505$ and $\beta = 0.895$. More details of the estimation refer to online Appendix.[4]

4.2 Calibrated Parameters

The remaining model parameters (sensitivity of money θ, convenience benefit of possessing a car b_N, b_P and b_F, utility difference between traveling in a private car and public transport γ, and loss of leisure utility l) cannot directly be estimated from the data. We assume that θ and γ independently follow a lognormal distribution with parameters $(\theta_\mu, \theta_\sigma^2)$ and $(\gamma_\mu, \gamma_\sigma^2)$ respectively. We calibrate $(\theta_\mu, \theta_\sigma^2, \gamma_\mu, \gamma_\sigma^2, b_N, b_P, b_F, l)$ by minimizing the sum of squared percentage differences between the calibrated and actual population shares by solving below optimization problem:

$$\begin{aligned} &min \sum_j \left(\frac{\hat{S}_j - S_j}{S_j} \right)^2, j = N, P, F, U, A, \\ &s.t.\, b_N, b_P, b_F, l \geq 0 \end{aligned} \tag{6}$$

where $\hat{\boldsymbol{S}}_{\boldsymbol{j}}$ are the calibrated population shares as in Eq. (3) and $\boldsymbol{S}_{\boldsymbol{j}}$ are the actual population shares. The objective function value of our calibration is 9.98×10^{-7}, which suggests that the model matches the actual population shares very well. The values of the calibrated parameters are listed on online Appendix.

[4] Online Appendix available at: https://drive.google.com/file/d/1DQkbJSBWFoFIMmAEMxkfeo7qjJrT2CRI/view?usp=sharing.

4.3 Model Validation

We validate our calibrated model by testing its prediction power. Recall that we use only the 2017 data to calibrate the values of parameters ($\boldsymbol{\theta_\mu}, \boldsymbol{\theta_\sigma^2}, \boldsymbol{\gamma_\mu}, \boldsymbol{\gamma_\sigma^2}, \boldsymbol{b_N}, \boldsymbol{b_P}, \boldsymbol{b_F}, \boldsymbol{l}$), thus we could apply the model to different years 2016, 2018 and 2019 to compare the predicted and actual population shares. Table 2 lists the prediction results. We can see that the predicted population shares are fairly close to the actual ones and capture the trend of its variation.

Table 2. Predicted vs. actual population shares

	Non-platform driver (S_N)				Platform drivers ($S_P + S_F$)			
	2016	2017	2018	2019	2016	2017	2018	2019
Predicted population share	18.80%	19.17%	20.70%	21.70%	2.91%	3.10%	2.97%	3.20%
Actual population share	19.32%	19.16%	19.37%	19.57%	2.81%	3.11%	2.90%	3.17%

5 Counterfactual Analysis

In this section, we use the calibrated model to conduct numerical experiments to examine how choice shares of the five strategies might change with new policies. In particular, we focus on the variations of driving cost and ride-hailing payment as they are the most commonly used means of market intervention and platform operations.

As mentioned in Sect. 4, due to the government's regulation, the population of private cars can be considered as a constant number. Explicitly, the number of non-platform drivers, part-time platform drivers and full-time platform drivers sums up to this constant number; and demand for cars (including both non-platform drivers and platform drivers) is captured by the bidding price of COE which is a component of car ownership cost k. Therefore, we have two equilibrium loops in our numerical experiments, one for car ownership constraint (total number of cars fixed) and the other for ride-hailing service supply-demand balancing (through dynamics between matching rates α and β). Below we present the main results of the counterfactual analyses.

5.1 Model Equilibria from Varying Driving Cost

Figure 1 illustrates the variation of population shares of platform drivers and users with respect to driving cost per kilometer at equilibria. As driving cost increases, the number of platform driver decreases whereas the population of users increases even with lower matching propensity. This may be because with rising driving cost, for those who prefer traveling in a private car, self-driving becomes too expensive and they would rather switch to ride-hailing services. The equilibrium results further show that the

increase of driving cost would lead to slight decrease in car demand and VKT, which suggests that actions affecting driving cost such as controlling road tax and fuel tax may help to mitigate traffic but with limited effectiveness. Therefore, other measures such as improving accessibility public transportation may worth considering (More results available on online Appendix).

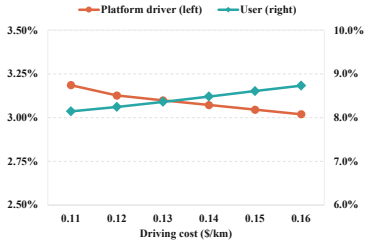

Fig. 1. Population share change w.r.t driving cost

5.2 Model Equilibria from Varying Ride-Hailing Payment

Figure 2 illustrates the variation of population shares of platform drivers and users w.r.t. ride-hailing payment. As expected, the proportion of ride-hailing users slashes with higher ride-hailing payment. Such a phenomenon brings a two-fold impact on platform drivers. On the one hand, the higher payment promises higher earnings for drivers as their income is proportionate of user charges. On the other hand, as there are fewer users, hence less demand, the matching rate for drivers decreases. In our analysis, the effect of the former is dominated by the latter. As ride-hailing payment increases, although the earnings from busy period increases for platform drivers, their total effective income instead decreases more significantly due to the lower matching propensity. Thus, we observe the diminishing population shares of both part-time and full-time platform drivers.

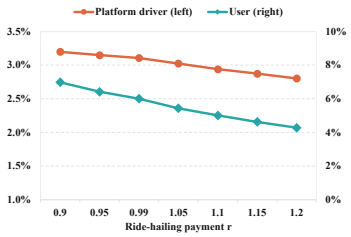

Fig. 2. Population share change w.r.t ride-hailing payment

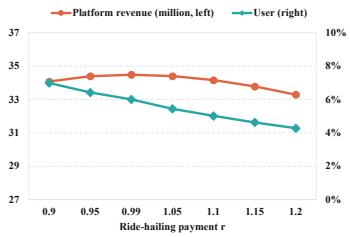

Fig. 3. Platform revenue w.r.t ride-hailing payment

The equilibrium results further show that, unexpectedly, the increment in riding price would lead to a slight increment in car demand. Since the total number of cars is a constant number, with the population of platform drivers dropping, non-platform

drivers increase. However, more non-platform drivers do not necessary lead to higher COE price. This observation suggests that as ride-hailing becomes more expensive, non-car owners who prefer to travel in a private car are more likely to buy a personal car rather than turning to public transportation. Moreover, as shown in Fig. 3, the platform's revenue does not increase monotonically with ride-hailing payment but peaks around 1.05 dollars per kilometer and then starts to diminish. This observation suggests that although higher charges bring higher commission fees for the platform, the enlarging loss of users counteracts such an incremental effect. Thus, increasing service charges to attain higher revenue is not sustainable and there exits an optimal payment level which allows the platform to maximize its revenue (More results available on online Appendix).

6 Conclusions

In this paper we introduce an integrated model structure that integrates empirical analysis into an analytical framework to assess the impact of on-demand platform on mobility choice, ownership and traffic congestion. By introducing matching functions, we further incorporate the endogeneity of supply demand imbalance of the two-sided on-demand service market into the model. Our analyses provide several managerial insights: to control traffic and curb VKT growth, measures through regulating driving cost such as increasing road tax and gasoline tax may have limited effectiveness. Other procedures such as improving accessibility public transportation may worth considering. For platform revenue management, our results suggest that there exits an optimal payment level which allows the platform to maximize its revenue. Although raising user charges within a certain range would increase the platform's profit, it is not sustainable as higher charges leads to enlarging loss of users, which brings a counteracting effect.

Acknowledgements. This research was partially funded by grant from the Singapore Ministry of Education (T2-1712).

References

1. Tafreshian, A., Masoud, N., Yin, Y.: Frontiers in service science: ride matching for peer-to-peer ride sharing: a review and future directions. Serv. Sci. **12**(2–3), 44–60 (2020)
2. Hall, J.V., Krueger, A.B.: An analysis of the labor market for Uber's driver-partners in the United States. ILR Rev. **71**(3), 705–732 (2018)
3. Burtch, G., Carnahan, S., Greenwood, B.N.: Can you gig it? An empirical examination of the gig economy and entrepreneurial activity. Manage. Sci. **64**(12), 5497–5520 (2018)
4. Fellows, N., Pitfield, D.: An economic and operational evaluation of urban car-sharing. Transp. Res. Part D: Transp. Environ. **5**(1), 1–10 (2000)
5. Anderson, D.N.: "Not just a taxi"? For-profit ridesharing, driver strategies, and VMT. Transportation **41**(5), 1099–1117 (2014)
6. Alexander, L., Jiang, S., Murga, M., Gonzalez, M.C.: Origin–destination trips by purpose and time of day inferred from mobile phone data. Transp. Res. Part C: Emerging Technol. **58**, 240–250 (2015)
7. Li, Z., Hong, Y., Zhang, Z.: An empirical analysis of on-demand ride sharing and traffic congestion. In: Proceedings of the International Conference on Information Systems (2016)

8. Clewlow, R.R., Mishra, G.S.: Disruptive transportation: the adoption, utilization, and impacts of ride-hailing in the United States. Institute of Transportation Studies, University of California, Davis (2017)
9. Jiang, B., Tian, L.: Collaborative consumption: strategic and economic implications of product sharing. Manage. Sci. **64**(3), 1171–1188 (2016)
10. Weber, T.A.: The question of ownership in a sharing economy. In: 2015 48th Hawaii International Conference on System Sciences, pp. 4874–4883. IEEE (2015)
11. Filippas, A., Horton, J.J., Zeckhauser, R.J.: Owning, using, and renting: some simple economics of the 'sharing economy.' Manage. Sci. **66**(9), 4152–4172 (2020)
12. Gong, J., Greenwood, B.N., Song, Y.: Uber might buy me a Mercedes Benz: an empirical investigation of the sharing economy and durable goods purchase. Available at SSRN 2971072 (2017)
13. Benjaafar, S., Hu, M.: Operations management in the age of the sharing economy: what is old and what is new? Manuf. Serv. Oper. Manag. **22**(1), 93–101 (2020)
14. Weber, T.A.: Product pricing in a peer-to-peer economy. J. Manage. Inf. Syst. **33**(2), 573–596 (2016)
15. Benjaafar, S., Kong, G., Li, X., Courcoubetis, C.: Peer-to-peer product sharing: implications for ownership, usage, and social welfare in the sharing economy. Manage. Sci. **65**(2), 477–493 (2018)
16. Abhishek, V., Guajardo, J., Zhang, Z.: Business models in the sharing economy: manufacturing durable goods in the presence of peer-to-peer rental markets. Available at SSRN 2891908 (2020)
17. Banerjee, S., Riquelme, C., Johari, R.: Pricing in ride-share platforms: a queueing-theoretic approach. Available at SSRN 2568258 (2015)
18. Taylor, T.A.: On-demand service platforms. Manuf. Serv. Oper. Manage. **20**(4), 704–720 (2018)
19. Bai, J., So, K.C., Tang, C.S., Chen, X., Wang, H.: Coordinating supply and demand on an on-demand service platform with impatient customers. Manuf. Serv. Oper. Manage. **21**(3), 556–570 (2019)
20. Gurvich, I., Lariviere, M., Moreno, A.: Operations in the on-demand economy: staffing services with self-scheduling capacity. In: Hu, M. (ed.) Sharing economy. SSSCM, vol. 6, pp. 249–278. Springer, Cham (2019). https://doi.org/10.1007/978-3-030-01863-4_12
21. Cachon, G.P., Daniels, K.M., Lobel, R.: The role of surge pricing on a service platform with self-scheduling capacity. Manuf. Serv. Oper. Manage. **19**(3), 368–384 (2017)
22. Hu, M., Zhou, Y.: Price, wage and fixed commission in on-demand matching. Available at SSRN2949513 (2019)
23. Benjaafar, S., Bernhard, H., Courcoubetis, C., Kanakakis, M., Papafragkos, S.: Drivers, riders, and service providers: the impact of the sharing economy on mobility. Manage. Sci. (2021)
24. Benjaafar, S., Ding, J.-Y., Kong, G., Taylor, T.: Labor welfare in on-demand service platforms. Available at SSRN (2020)
25. Sinchaisri, P., Allon, G., Cohen, M.: The impact of behavioral and economic drivers on Gig economy workers. In: Academy of Management Proceedings, vol. 2019, p. 10216. Academy of Management, Briarcliff Manor (2019)
26. Erhardt, G.D., Roy, S., Cooper, D., Sana, B., Chen, M., Castiglione, J.: Do transportation network companies decrease or increase congestion? Sci. Adv. **5**(5), eaau2670 (2019)
27. Fredriksson, A., de Oliveira, G.M.: Impact evaluation using Difference-in-Differences. RAUSP Manage. J. **54**, 519–532 (2019)
28. Fraiberger, S.P., Sundararajan, A., et al.: Peer-to-peer rental markets in the sharing economy. NYU Stern School of Business Research Paper, vol. 6 (2015)

29. Keyes, A.K., Crawford-Brown, D.: The changing influences on commuting mode choice in urban England under Peak Car: a discrete choice modelling approach. Transport. Res. F: Traffic Psychol. Behav. **58**, 167–176 (2018)
30. McFadden, D.: The measurement of urban travel demand. J. Public Econ. **3**(4), 303–328 (1974)

Additive Manufacturing Global Challenges in the Industry 4.0 Era

Yober J. Arteaga Irene and Wai Kin Victor Chan(✉)

Shenzhen International Graduate School, Tsinghua University, Shenzhen 518000, Guangdong, China
chanw@sz.tsinghua.edu.cn

Abstract. Additive Manufacturing (AM) technology could revolutionize the way industry makes products. However, there are still challenges that must be overcome since these are slowing down AM adoption by industry. Therefore, this research aims to uncover these limitations based on a systematic literature review. The findings of this study show that there are five global challenges that AM is currently dealing with, technical aspects, supporting technologies, management of operations, supply chain configuration, and legal innovation.

Keywords: Additive manufacturing · 3D printing · Operations management · Industry 4.0

1 Introduction

Industry 4.0 (I4.0) refers to the Fourth Industrial Revolution, and it is the main keyword used by researchers, policy makers and entrepreneurs when describing how worldwide industrial systems will evolve in the near future [1]. It is also defined as smart manufacturing because it is based on the advanced digitalization of factories [2]. I4.0 specifically is comprised of, but no limited to, different technologies such as Internet of Things, Cloud Computing, Blockchain, Augmented Reality, Artificial Intelligence, Big Data and Analytics, Simulation, Autonomous Robot and AM [3–5]. From this group of highly heterogeneous technologies, the latter would play a key role in the transformation processes of industry by substituting the conventional manufacturing (CM) methods.

AM is defined as a process of joining materials to make parts from a 3D model data, usually layer upon layer, as opposed to subtractive manufacturing and formative manufacturing methodologies [6]. Various industry sectors such as automotive, aerospace and medical devices are paying attention to AM due to its unique advantages compared to other CM methods [7]. AM essentially offers two benefits over CM, the freedom of geometry to efficiently manufacture complex components and products, and the chance to flexibly manufacture low quantities down to a single unit which is afforded by the absence of cost related to tooling and changeover [8], other benefits include low upfront capital investment [9], less material waste [10, 11], and highly personalized one-off products in the medical sector [12–14]. However, despite the aforementioned benefits,

R. Qiu et al. (Eds.): ICSS 2021, LNOR, pp. 316–336, 2021.
https://doi.org/10.1007/978-3-030-90275-9_26

AM technology has not yet been fully adopted by industry as a substitute for CM methods. AM might be considered as a technology that is still under development, so the reasons, that could explain the slow AM adoption, could be related to limiting factors (challenges) that are limiting its deployment in the I4.0 era. Therefore, the main aim of this paper is to identify, consolidate and synthesize the current AM challenges that must be overcome so that the industry adopts AM as the main production technology.

The paper begins by first presenting the literature review methodology in Sect. 2. This is followed by explaining the findings, in Sect. 3, which are classified into five categories, technical limitations, supporting technologies, management of operations, supply chain configuration, and legal innovation. Based on the essence of each category, conclusions are drawn in Sect. 4. Lastly, directions for future research are presented in Sect. 5.

2 Literature Review Methodology

The research method used in this study was based on a systematic literature review [15], consisting of an in-depth qualitative analysis of the state of the art published research materials in the field.

The central question that this research asks, then, is: What are the global challenges that are slowing down the adoption of AM technology by industry? To answer this question, the review was carried out in four stages as depicted in Fig. 1.

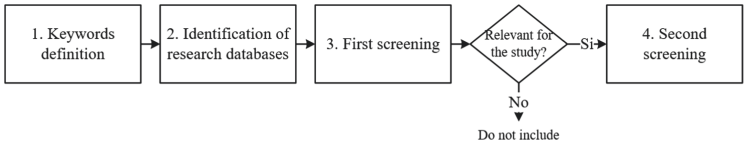

Fig. 1. Research stages

First of all, the keywords were defined as the basis of the search strategy, which was based on the inclusion and combination of terms classified into two groups. The first is related to the technological field (Additive Manufacturing and 3D printing), and the second is related to the fields of knowledge (operations management, supply chain, inventory management, production planning and scheduling), plus the term 'challenges'. In total there were twelve combinations that were then used to carry out paper search activities (Fig. 2).

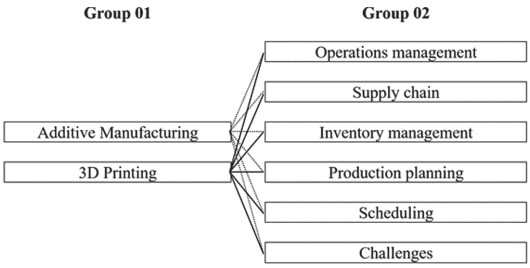

Fig. 2. Keywords used for paper search

Second, four scientific online databases were identified and used to retrieve research articles relevant to the study: Science Direct, Scopus, Core and IntechOpen. For the search process, Boolean operators such as AND and OR were used to find articles through these search engines. The publications considered in this study range from 1997 to the day of submission of this research paper. It is important to mention when some concepts were unclear independent search was done by consulting trusted books and reliable websites.

Thirdly, the selection of the most relevant papers was done by screening the titles and abstracts. At this stage, we verified and made sure that the content of each research paper was closely related to the combinations of the keywords defined in stage one.

Lastly, in stage four, an in-depth qualitative analysis of the selected papers was done by reading the full-content of every research material. Here, we looked in detail for weaknesses, problems, challenges, disadvantages, etc. for each field of knowledge (defined in stage two) applied to AM technology.

3 Additive Manufacturing Global Challenges

The total gross number of research papers that emerged from the search in Science Direct, Scopus, Core and IntechOpen databases was 9,889 for the twelve keyword combinations. However, after removing duplicates and conducting the first and second screening, only 64 documents met the study requirements defined in Sect. 2 and were selected as relevant for this research. Table 1 presents a summary of the pertinent papers according to the keyword (group 2) and publication time range. Additionally, 6 technical research reports and institutional publications were considered, 8 websites with related content were consulted as well as 5 books were referenced as of interest.

Table 1. Relevant papers for the study

Keyword (group 2)	Number of relevant papers	Publication time range
Operations management	19	From 1997 to 2020
Supply chain	14	From 2004 to 2021
Inventory management	2	From 2019 to 2021
Production planning	3	From 2018 to 2019
Scheduling	4	From 2019 to 2021
Challenges	22	From 2010 to 2020

To the extent that in-depth analysis of the literature was carried out, the findings and the deductions made by the authors were classified into 5 categories of challenges: technical limitations, supporting technologies, management of operations, supply chain configuration and legal innovation. See Fig. 3 below.

Fig. 3. AM challenge category

3.1 Technical Limitations

These are the limitations of AM technology itself from a technical point of view, and within this category, two subgroups were identified. The first one is the generic limitations which includes general drawbacks that apply to most of the seven AM techniques defined by the American Society for Testing and Materials (ASTM), Binder Jetting, Directed Energy Deposition, Powder Bed Fusion, Material Extrusion, Material Jetting, Sheet Lamination and Vat Photopolymerization [16]. And the second one is the specific limitations which precisely refer to the restrictions that apply to each of the seven AM techniques.

Based on the literature review, it was found that four generic limitations stand out and are widely discussed by researchers. First of all, the limited palette of build materials [17], although AM can be flexible in the use of a variety of plastics and metals, their availability on the market is very limited and quite expensive, which leads to the use of non-standard materials and generates extra cost, either through material properties or through price. The most commonly used polymer, metal and ceramic build materials are shown below in Table 2.

Table 2. Polymer, metal and ceramic build materials [18–21]

Material type	Commercial name	Material	Platform	Type
Polymer	Fortus ABS M30	ABS	Fortus 400mc	FDM
	ULTEM 9085	PEI	Fortus 400mc	FDM
	PA2200	Nylon 12	ESO P	LS
	Tangoblack FLX973	Acrylic	Object Connex	Jetting
	Veroclear RGD810	Acrylic	Object Connex	Jetting
	Polylactide	PLA	–	FDM
	Polycarbonate	PC	–	FDM
	Nylon 3200	Glass filled nylon	–	SLS
	XTC-3D	Epoxy resin	–	SLA / SLS
	–	Wax	–	FDM
Metal	Ti6Al4V alloy	Titanium	Renishaw SLM250	SLM
	Al 7075	Aluminium	Realizer SLM50	SLM
	Al 6061	Aluminium	Realizer SLM50	SLM
	AlSi10Mg	Aluminium	–	SLM
	Stainless 316L	Steel	Renishaw SLM250	SLM
	Maraging steel 1.2709	Steel	–	SLM
	15-5ph	Steel	–	SLM
	Inconel 625	Nickel alloy	Realizer SLM50	SLM
	Co28Cr6Mo	Cobalt chrome alloy	–	SLM
Ceramic	–	Silica/Glass	–	SLS
	Dental porcelain	Porcelain	ExOne	Jetting
	–	Silicon-Carbide	–	SLM

Second, the slow process speed [17] is the main limiting factor when we talk about the possibility to adopt AM for high volume production. For example, in a study conducted by using a Laser Sintering EOSINT P100 system, the total processing time ranged from 720 up to 1430 min to produce from 5 up to 55 volume package of spare parts [17, 22]. Third, the poor dimensional accuracy [17, 22], in comparison to some non-additive manufacturing processes. This property is important especially when we need precise parts to be compatible with other hardware, so under this situation high dimensional accuracy is a must. For example, it is said that in a Fusion Deposition Modelling process an accuracy greater than ±0.5 mm is bad, less than ±0.5 mm is average, less than ±0.2 mm is good and less than ±0.1 mm is excellent [23]. So if a good or excellent accuracy is not reached, it could lead to expensive post processing activities. And fourth, the roughness of the surface finish [17, 22, 24] which includes the removal of support structures activities, and depending on how much work it requires, it could also lead to costly processing requirements as well.

Table 3. Defined AM process and cons of technology class [25]

Technology category	Example vendor technology	Challenges for industrial parts production
Binder jetting	ExOne M-Flex, Voxeljet	Composite microstructure (usually), intensive post-processing may be required
Directed energy deposition	Optomec LENS, Lincoln Electric, Hybrid Laser-Arc, Sciaky EBDM	Difficult to manufacture direct parts
Powder bed fusion	EOS DMLS, 3D Systems SLS, Arcam EBM	Relatively slow, relatively expensive, limited build volume of parts
Material extrusion	Stratasys Fused, Deposition Modeling	Surface roughness due to raster, requires support material
Material jetting	Objet Connex, Optomec Aerosol Jet	Requires materials compatible with jetting (stricter for structural than functional)
Sheet lamination	Fabrisonic VHP-UAM, CAM-LEM	z-Axis strength penalty, maturing technology
Vat photopolymerization	3D Systems Stereolithography	Lack of engineering polymers

On the other hand, specific process-driven limitations were identified for each of the seven AM techniques [25]. These factors explicitly justify the non-adoption of AM techniques at an industrial level. For example, in Powder Bed Fusion technology, the platforms EOS DMLS, 3D Systems SLS and Arcam EBM the limitations are relatively slow process speed, relatively expensive process and limited volume capacity. See Table 3 above.

3.2 Supporting Technologies

Unlike the technical limitations (Sect. 3.1) that depend solely on AM processes capability, the limitations associated with supporting technologies (for AM) depend on other fields of study such as electronics, optics, etc. In this case, the focus is on metrology, the science of measurement [26]. This field plays a key role in any transformation process in the industry and has an intrinsic relationship with quality control because it is with the instruments and equipment that metrology carries out the data acquisition. However, to date, metrology in the field of AM has not made enough progress as to support the deployment of AM at an industrial level [27].

Among the many features being considered by metrology in AM processes are surface topography, surface texture [27–30], porosity [31, 32], cracking [33], thermal issues [31, 34, 35], material supply [35, 36]. To have the control over these characteristics, it is necessary to make the measurements in two moments of the process, during the process (monitoring), and at the end of the process (inspection) when the final product is out of the 3D printing machine.

Regarding monitoring techniques, one of the main objectives is to deal with porosity. It is defined as a measure of the void spaces in a material which could be located between layers or within a layer of a 3D printed product [32]. Porosity has a direct relationship with a number of input parameters such as energy density, transverse speed and hatch spacing so to a large extend voids depend on these factors that could affect the quality of final product. Among the technologies that can help to quantify this variable, we have, X-ray computed tomography [37] which was used to demonstrate that porosity in structures made of TI6A14V by electron beam-PBF directly depends on hatching and process parameters; infrared cameras, used to investigate porosity and other irregularities caused by insufficient heat dissipation during the laser-PBF [31]; photodiodes and in-line cameras, in order to stabilize a meltpool and keep the temperature within a pre-defined window by doing this the occurrence of over-melted and zones of porosity (gas voids) were prevented [34]. Another concern is temperature monitoring during the AM process of metals, and for this purpose pyrometers have been used to understand the solidification process of molten powder by studying the relationship between consolidation and surface temperature [35]. But in addition to porosity and temperature, there are other variables that need to be monitored in an AM metal process, in that sense several studies have been carried out. For example, a high speed camera (Photron FASTCAM SA5 model 1300K C2) was used to study the effect of changing the layer thickness in a laser-PBF [38], and an integrated visual control system (Phenix PM-100) was used to monitor the deposition of powder layers and to check the position of the laser beam [36]. In Table 4, a summary of the current available in-situ monitoring modules are shown.

Table 4. In-situ measurement techniques available [32, 39]

AM process	Machine manufacturer	Module name	Failure mode monitored	Parameter altered	Equipment
EB-PBF	Arcam	LayerQam™	Porosity	N/A	Camera
L-PBF	B6 Sigma, Inc. specialist	PrintRite3D® INSPECT™	Unknown	N/A	Thermocouple and high-speed camera
	Concept Laser	QM melt pool	Melt pool monitoring	Laser Power	High-speed CMOS-camera
	EOS	N/A	Unknown	N/A	Camera
	Edison Welding Institute	N/A	Layer area height profile	N/A	Digital single-lens reflex + digital light processing (DLP) projector
DED	DEMCON	LCC 100	Melt pool monitoring and build height	Laser Power	Camera
	DM3D Technology	DMD closed-loop feedback system	Depth measurement	Laser Power	Dual-colour pyrometer and three high-speed CCD cameras
	Laser Depth	LD-600	Depth measurement	Laser Power	Inline coherent imaging
	Promotec	PD 2000 PM 7000	Melt pool monitoring Melt pool monitoring	N/A N/A	CMOS-camera 1D photo detector
	Stratonics	ThermaViz system	Melt pool temperature	Laser Power	Two-wavelength imaging pyrometer

On the other hand, when it comes to 3D printed product inspection the main focus is on the surface texture, and to carry out this activity different types of inspection technologies are being explored and validated although most of them focus on AM of metals as in the previous one. For example, based on the type of information they can extract from the measured surface there are five groups of technologies [27, 29, 40] as shown in Table 5. The most commonly used is the stylus-based measurement (profile topography measurement), but it is required to be quite careful while doing the assessment since it could cause damage to the work piece. The reasons why it is being highly utilized are ubiquitousness, low cost, lower training requirements and high comfort for operators. However, it is important to highlight that areal technologies such as focus variation and confocal microscopy (both optical techniques) have advantages over

contact stylus because these offer the possibility of doing a three-dimensional (surface topography is three-dimensional) analysis while the latter just offers the chance of doing a two-dimensional analysis. A detailed study of the suitability of these techniques is presented in [29]. So it is highly probable that focus variation and confocal microscopy technologies would be the most common used as AM evolves overall.

Table 5. Surface texture measurement technologies [27, 29, 40]

Group	Available technologies
Profile stylus	Contact stylus
Areal topography measurement	Imaging confocal microscopy
	Focus variation microscopy
	Continuous confocal
	Coherence/vertical scanning interferometry
	Chromatic confocal microscopy
	Conoscopic holography
	Atomic force microscopy
	Elastomeric sensor
2D imaging	Optical microscopy
	SEM
Volumetric	X-ray computed tomography
Other	Raman spectrometry

Looking further, another study proposes an ideal smart production system [41] based on the integration of thermal cameras and smart sensors, which could perform real-time monitoring, collect data, implement corrective actions and continuously improve the system's performance. Although the authors acknowledge that to reach such a level requires the development in the same direction of other I4.0 technologies, such as cloud computing, big data management and artificial intelligence. In other words, this is about smart manufacturing systems [42, 43] which could lead us to another level of challenges such as cybersecurity [44, 45], aspects that are beyond the scope of this study.

The ASTM and the International Organization for Standardization (ISO) are also playing a key role in accelerating the development of AM metrology. So they issued the standard ISO/ASTM 52902 – 19 in order to normalise the measurement of process parameters such as geometric accuracy, surface finish and minimum feature sizes [46]. But not only this, these institutions have been also working together, since 2013, on a set of global standards applicable to AM materials and processes that definitely support the AM deployment as well as the management of Quality Assurance within which metrology is contained [47].

Despite the efforts made by academics and institutions such as ISO and ASTM until today, we have to recognize that AM metrology is at research state [27], in other words

literature evidence that all technologies being explored are being used to study and understand different variables related to process parameters and final products characteristics but not for data acquisition as part of an AM manufacturing system.

3.3 Management of Operations

Management of operations is concerned with creating, operating and controlling a transformation system that takes a variety of resources as inputs and produces outputs of goods and services needed by customers [48]. In a manufacturing environment several types of decisions are made including operations strategy, product design, process design, quality management, capacity management, facilities planning, production scheduling and planning and inventory control [49]. So following this line of concepts, the following weaknesses have been identified from an operations management perspective:

First, the design for manufacturing and assembly (DfMA), which means the design for ease of manufacture of the collection of parts that will form the product after assembly with an end goal of making a better product at a lower cost [50]. The process of DfMA in conventional manufacturing methods work under the design for manufacturing and assembly guidelines, however with AM designers need to change the paradigm, since the freedom of geometry to manufacture complex 3D products [8, 51] reduces the need to design for assembly. Thus, engineers and designers needs to rethink the Design for Additive Manufacturing (DfAM) process; otherwise, it may continue being advocated as a limiting factor for AM adoption by industry [52].

Secondly, production cost management, which could be defined as a set of mathematical methods and models used by companies who make products in order to ensure that a product meets its profit targets. This subject is in a very early stage of research since only two models have been developed according to the findings in the current published literature. The first cost approach evaluates two different AM systems used commercially for the manufacture of end-use metal parts, Electron Beam Melting (EBM) and Direct Metal Laser Sintering (MLS), and by taking into account the cost of each cm^3 of material used, it was demonstrated that EBM and MLS are not suitable yet for a high volume production since the productivity levels are still not the desired ones [22]. Even though the model reflects what happens in practice while using these EMB and MLS processes, it only evaluates the scenarios of two of the seven AM techniques. The second cost approach, unlike the previous one, proposes a model based on the stages of the process that an AM system may require such as preparing geometry, building job assembly, machine setup, building up, removing and cleaning up, then, the total production cost is just simply the addition of the costs that each step generates [53]. Therefore, there is a lot of work to be done in this direction, such as developing costing methods considering the particularities of each of the AM techniques.

A subsequent limitation in AM is production scheduling, which deals with the allocation of resources required to create products. Here, although the models focus on the scheduling problem, they pursue different objectives. A time-oriented build utilization model [54], in order to optimize the use of 3D machines' capacity, focuses on grouping the production orders and combining them according to the product parameters; then, by taking into account the available working time of the operators, the jobs are assigned to the machines according to their availability. However, there is a notorious

weakness in this model, it does not take into account demand and deadlines, aspects that are essential in scheduling. An energy-aware model [7] aims to reduce the cost of energy consumption in Fusion Deposition Modelling AM process, it argues that by changing the product parameters (layer thickness) and process parameters (temperature, speed, etc.) a production scheduling could be prepared and by doing this electricity costs would be potentially reduced. Although energy savings can be significant by applying the model, the quality of the final product could be greatly affected. A time-oriented model pursues to reduce the cycle time [55], since the author recognizes that this drawback is one of the main reasons why AM is not implemented in large-scale production, so the model proposes a Fused Filament Fabrication (FFF) AM system with two printheads that could work simultaneously and thus reduce cycle time. Nevertheless, the method just applies for FFF AM process and there is little formal evidence that it could be replicated at an industrial level. A profit model [56] attempts to maximize the return per unit by developing a maximization algorithm which applies to a Powder Bed Fusion (PBF) system, but it ignores the process and product parameters. A simulation model [57] assesses different scheduling policies, such as FIFO and Earliest Due Date, to assign jobs to AM chambers. The objective is to optimize the overall throughput of the system, but without considering the costs. Other studies [58–60] focus only on optimizing the orientation of the products to be printed within the AM cameras or 3D printing platforms, that is to say in a single stage of the process, and do not evaluate the (potential) AM production system as a whole.

How to manage capacity in a potential AM manufacturing system in order to run a process efficiently is another challenge that need to be addressed. It has been said that AM is a parallel technology because multiple parts can be printed in individual builds or in one batch as long as they require the same raw materials [17], but how to fully utilize a 3D printing platform? Considering that we may require just one or multiples parts but with different characteristics (different materials). In other words, operators face a build volume capacity utilization problem, because if capacity is not fully used, the process may be run inefficiently [17]. A good example, is the study which focused on exploring the effect of "parallelity" [61]. It demonstrated that printing just one part versus printing a fully used 3D platform, the specific energy consumption per Kg deposited is higher in all six AM evaluated platforms (SLM 250, M3 Linear, EOSINT M 270, A1, EOSINT P 390, FDM 400c). Thus, how to manage capacity in an AM environment remains unclear and has not been sufficiently explored.

Another important point in operations management that has been slightly studied so far is spare parts inventory management because very few approaches have been developed to address this issue. First, we have a Poisson-based demand inventory management approach, which based on a parametrical analysis of the mechanical properties, and economic and technological parameters, helps to make a decision between using AM and CM by applying decision trees models [62]. Another approach addresses the issue assuming that a producer has infinite capacity to make slow moving parts with either CM or AM, and who manages a policy (S-1, S) for inventory, then, by applying Markov Chain models gets the conclusion that AM is better than CM since the latter has long set-up times [63]. Looking at it in another way, AM could potential help the armed forces to manage inventory of weapons during war times. The proposed model

states that after fighting in the battlefield damaged spare parts can be printed and guns can be immediately repaired [64]; however, we will need to make sure that 3D printing machines are in a safe place; otherwise, machines may be destroyed by enemy's attacks. Researchers agree that the use of AM for spare parts inventory would provide benefits over CM [62] due to the short setup times of machines and the tool-less processes [65], the possibility of making the right part, in the right quantity and at the place of consumption [66], and the opportunity to tremendously reduce inventory holding costs [67]. Beyond all the potential advantages that AM can offer for inventory management, there is still a high price, at least until today, we have to pay that is, quality (see technical limitations in Subsect. 3.1 and supporting technologies in Subsect. 3.2).

3.4 Supply Chain Configuration

It may be said that AM could change the entire supply chain (SC) configuration in a potential scenario in which AM technologies govern industrial production. Many authors agree about the potential benefits that it brings to the table for environmental sustainability such as reducing carbon emissions [68], material consumption [69, 70], material waste [10], the number of suppliers [71] and reduction for logistic services of final parts [72]. Thus, it seems that the benefits that AM offers to the environment are not under discussion.

From another perspective, sustainability is also supported by the economic pillar. In other words, a potential adoption of AM has to generate economic value for the economic actors; otherwise, the gaze of industry practitioners will go in another direction. So what does AM bring to SC from an economic perspective? According to current literature, it basically offers the possibility of having a distributed SC [73] instead of a centralized or decentralized one (see Fig. 4), which means production facilities would be located closer to the customer or near the point of consumption. The benefits that could be derived from this potential change are: (a) virtual inventory [74] instead of physical, which means no need for regional warehouses or distribution centres (for final products), (b) reduction of the SC lead times [75] which means a better responsiveness to customer demand, and (c) reducing the need for factories with huge facilities. Although a SC with localized AM production assumes simplification and substitution for conventional manufacturing, the current state of AM does not yet satisfy these assumptions [72]. Therefore, the challenges for this aspect are the absence of frameworks and models to manage (1) the design of AM facilities, (2) the location of AM facilities, and (3) the logistics service to deliver build materials in a distributed supply chain. To the knowledge of the authors, there is no evidence in the current literature regarding these points.

Fig. 4. Supply Chain configurations: (a) Centralized, (b) Decentralized, and (c) Distributed [76]

There are points at which economic and environmental sustainability are interdependent such as, in AM technologies, energy consumption and production costs. AM is frequently prone to higher unit costs [73] than CM, and one of the reasons is the quite high demand for energy, especially if we project to use AM for large scale parts and mass production [77], electricity consumption would be extremely high which could have a direct impact on production costs and the environment as well. A number of researchers have addressed this issue and have developed a series of models [7, 78, 79]; nonetheless, others [80, 81] claim that to date there is no clear and strong evidence to argue that AM is better than CM environmentally speaking (from an energy consumption point of view). Therefore, this particular matter remains under research and is probably the biggest challenge in ensuring a healthy supply chain.

3.5 Legal Innovation

AM is guiding us towards a new era of manufacturing and beyond the technical aspects that this implies, along the way, new concerns are emerging such us the legal facet. The required work in this regard, rather than the participation of the researchers, it requires the action of the people responsible for making the law. The crucial concerns that need to be addressed from a legal perspective, include intellectual property (IP), liability, and security issues.

Intellectual property refers to creations of the mind, such as inventions; literary and artistic works; designs; and symbols, names and images used in commerce [82]. The main AM issue related to this is who actually owns the IP rights of 3D printed product since AM allows almost anyone to re-create an existing product and modify, print, use and distribute it without permission of the original creator [83]. One of the means that greatly facilitates the dissemination of 3D CAD designs in an illegal way is the Internet, so stealing a 3D design has probably never been easier than now [84]. According to current laws [e.g. U.S.] it is clear that 3D machines, 3D materials and process could be protected by patent laws, while 3D software design could be protected by copyright laws [85]; however, what is unclear is to define if the designer or the manufacturer or both own the IP rights. Additionally, there are some queries that remain opened for an answer. For example, whether modified files by a third-party could be considered as infringement of IP laws or not, if so how to track them all over the world.

With respect to liability, the issue under discussion, in current literature, is about who assumes responsibility in case a user gets a 3D printed product with defects [86] and may be injured by using this product [87], or even worse when a patient gets a 3D bio-printing organ or device and it fails afterwards. Many actors involved in the production process and in supply chain could be liable such as the owner of the 3D printer, the supplier of the 3D printer, the supplier of the materials, the designer, the person loading and sharing the files, and the person printing the 3D product [87]. It seems that the process of identifying who is responsible for this would be quite difficult and it has not been yet addressed by the law makers.

Regarding security matters, the objective is to make sure that AM is used properly and for good reasons, so the society can fully enjoy the benefits. Nevertheless, AM could be misused and potential risks may include designing and making weapons [88, 89] which can be easily distributed through internet, combining animal and human tissue

to improve organs of patients who can get competitive edge over others (e.g. sports and military), and producing biohazards or bioweapons [87]. Therefore, the way to prevent these situations from occurring in practice is a challenge that mainly governments have to address because it is an issue that could somehow endanger the security of civil society.

4 Summary of Findings

So far as we have analysed in detail the five categories of challenges that are slowing down the adoption of AM technology by industry. A total of 18 challenges were identified or deducted by the authors. See Table 6 below.

Table 6. AM global challenges

Category	Challenge	Subsection
Technical limitations	1. The limited palette of build materials 2. The slow process speed 3. The poor dimensional accuracy 4. The roughness of the surface finish	3.1
Supporting technologies	5. In-process monitoring techniques under development 6. 3D printed product inspection techniques under development	3.2
Management of operations	7. No standardized and approved methodology for the DfAM process 8. Lack of production cost management models 9. Lack of production scheduling models 10. Lack of capacity management approaches 11. Lack of spare parts inventory management models	3.3
Supply chain configuration	12. Lack of methods to manage AM facilities design 13. Lack of methods to manage AM facilities location 14. Lack of methods to manage logistics service to deliver build materials 15. High energy consumption	3.4
Legal innovation	16. Intellectual property issues 17. Liability issues 18. Security issues	3.5

Technical limitations are shortcomings of AM itself such as the limited palette of build materials, the slow process speed, the poor dimensional accuracy and the roughness of the surface finish. Supporting technologies is basically about AM metrology and the current limitations are related to in-process monitoring techniques and 3D printed

product inspection techniques which both are under development. Management of operations limitations include a no standardized and approved methodology for the DfAM process and the lack of methods or models for production cost management, production scheduling, capacity management and spare parts inventory management. Supply configuration drawbacks include lack of methods to manage AM facilities design and location, methods to manage the logistics service to deliver build materials and high energy consumption. And legal innovation challenges are related to intellectual property, liability and security issues. It is important to highlight that these challenges represent the main limiting factors of AM and the same time are the key points in which research should focus on in order to accelerate the adoption of AM technology by industry.

5 Conclusions

AM's challenges were identified and analysed from a broader perspective rather than just the technical angle. It may be said that now it is clearly stated that there are five categories in which AM's challenges lie, technical limitations of AM itself, supporting technologies such as metrology, management of operations, supply chain configuration, and legal innovations.

The technical line includes challenges of AM itself and it is associated with the availability of input materials and capability of AM techniques to 3D print products that meet technical requirements. Two groups were identified, the generic and specific limitations. The first one encompasses drawbacks than apply to most of the seven AM techniques defined by ASTM, these are limited pallet of build materials, slow process speed, poor dimensional accuracy, and roughness of the surface finish, while the second describes shortcomings that apply exactly to each of the AM techniques such for Directed Energy Deposition is difficult to manufacture direct parts, for Vat Photopolymerization there is lack of engineering polymers, and so on.

Metrology plays a vital role in any manufacturing process and in AM transition could not be the exception. It is crucial for AM deployment at an industrial level as a supporting technology. Two categories were identified here, technologies for monitoring AM processes, and technologies for inspections of 3D printed products. There is a variety of technologies being explored in each category; however, all of them are at research state at this point. In other words, none of the metrology methods presented in this research paper has been universally accepted by manufacturers or regulators, so there is quite a lot of work to do in this direction.

The management of operations in an industrial system is supported by different types of decision models, methods, techniques, and frameworks. Concerns regarding how to manage, DfAM, production costs, capacity, production planning and scheduling, and inventory have been explored and different preliminary models have been proposed; nonetheless, as AM technologies have not been fully adopted by industry, it is expected that more research would be needed to adjust the current models or to develop new ones.

The impact of AM on SC was clearly stated, AM supply chains configuration would potentially change from a centralized and/or decentralized shape (traditional) to a distributed one (current). As a consequence, environmental sustainability seems to be guaranteed, but economic sustainability is not yet. Specific challenges in a distributed supply

chain include, the high demand for energy consumption, the location of AM facilities, and distribution of building materials.

The emergence of any new technology implies innovation in legal matters in order to make sure that society may enjoy the benefits that it brings. AM is a digitalized technology so 3D CAD designs and products can be easily reproduced and distributed without authorization of the original creator. Additionally, in a distributed SC, AM losses control, now consumers can freely design, modify and printed 3D products, but who is liable when a 3D product causes damage to the user (e.g. injuries, poisoning by toxic materials) has not been addressed yet. Lastly, AM could be hypothetically misused such as to make 3D printed guns, biohazards, bioweapons, etc. thus, put the security of nations at risk. Therefore, holistic approaches to address IP rights, liability matters and potential security issues are required from academics, researchers, institutions and governments.

6 Directions for Future Research

This research has presented a conceptual summary of AM challenges, which can serve as an underlying basis for understanding issues that need attention from researchers, regulators, and governments. The findings presented are not free of a set of limitations inherent to the research question and method chose for this investigation. Consequently, this research discloses further research directions concerning to AM deployment or AM adoption by industry, which may help in fostering research on AM.

First of all, quality control in a prospective scenario in which AM is the main production technology requires further research. In CM manufacturing sampling is required in order to collect process' data, after that by applying statistical analysis control charts are drawn, and then judgment whether the process is under control or not is done. However, AM promises to be a completely automated technology which would capable of managing its own data collection and in real time (although it depends on advances in metrology), so how to perform AM quality control is a problem waiting for answers.

Secondly, safety and security issues, for the researchers' opinion, not only require further but also urgent and deeper research in order to put limits to all conceivable possible ways in which AM can be misused and endanger the public security. The initiative of governments is vital but the support of researchers and academia would be essential to address the issue in a preventive manner and clearly define what can and cannot be printed using AM technology.

Lastly but not least, organizational innovation in relation to how willing the industry is to adopt technologies in its processes, because to make a technological change, companies do not have to wait for AM to be fully developed, they can make partial migrations and obtain benefits along the way, in other words, AM can flourish as they begin to innovate by adopting it. But how willing are companies to adopt AM at this point is something that needs to be addressed and measured as well, then we have an idea about how far we are from the heyday of I4.0.

Acknowledgements. This research was funded by the Guangdong Pearl River Plan (2019QN01X890), National Natural Science Foundation of China (Grant No. 71971127), and the Hylink Digital Solutions Co., Ltd. (120500002).

References

1. Chiarelloa, F., Trivellib, L., Bonaccorsia, A., Fantonic, G.: Extracting and mapping industry 4.0 technologies using wikipedia. J. Comput. Ind. **100**, 244–257 (2018)
2. Kerin, M., Pham, D.T.: A review of emerging industry 4.0 technologies in remanufacturing. J. Clean. Prod. **237**, 117–805 (2019)
3. Kumar, R., Singh, R.K., Dwivedi, Y.K.: Application of industry 4.0 technologies in SMEs for ethical and sustainable operations: analysis of challenges. J. Clean. Prod. **275**, 124063 (2020)
4. Liao, Y., Deschamps, F., Loures, E., Ramos, L.: Past, present and future of Industry 4.0-a systematic literature review and research agenda proposal. Int. J. Prod. Res. **55**(12), 3609–3629 (2017)
5. Bai, C., Dallasega, P., Orzes, G., Sarkis, J.: Industry 4.0 technologies assessment: a sustainability perspective. Int. J. Prod. Econ. **229**, 107776 (2020)
6. ISO/ASTM 52900: Additive manufacturing – general principles – terminology. International Organization for Standardization, Geneva, Switzerland (2015)
7. Karimi, S., Kwon, S., Ning, F.: Energy-aware production scheduling for additive manufacturing. J. Clean. Prod. **278**, 123183 (2021)
8. Tuck, C., Hague, R., Ruffo, M., Ransley, M., Adams, P.: Rapid manufacturing facilitated customization. Int. J. Comput. Integr. Manuf. **21**(3), 245–258 (2008)
9. https://www.ptc.com/en/blogs/cad/10-additive-manufacturing-advantages
10. Mellor, S., Hao, L., Zhang, D.: Production economics additive manufacturing: a framework for Implementation. Int. J. Prod. Econ. **149**, 194–201 (2014)
11. Ford, S., Despeisse, M.: Additive manufacturing and sustainability: an exploratory study of the advantages and challenges. J. Clean. Prod. **137**, 1573–1587 (2016)
12. Sandström, C.: Adopting 3D printing for manufacturing - evidence from the hearing aid industry. Technol. Forecast. Soc. Change **102**, 160–168 (2015)
13. Fu, Y., Xia, W., Chen, X.: 3D printing of porous alginate/gelatin hydrogel scaffolds and their mechanical property characterization. Int. J. Polym. Mater. Polym. Biomater. **66**(6), 299–306 (2016)
14. Duan, B., Hockaday, L., Kang, K., Butcher, J.: 3D bioprinting of heterogeneous aortic valve conduits with alginate/gelatin hydrogels. J. Biomed. Mater. Res. Part A **2013**(101), 1255–1264 (2013)
15. Snyder, H.: Literature review as a research methodology: an overview and guidelines. J. Bus. Res. **104**, 333–339 (2019)
16. ASTM F2792-12a: Standard terminology for additive manufacturing technologies. ASTM (2015)
17. Ruffo, M., Hague, R.: Cost estimation for rapid manufacturing - simultaneous production of mixed components using laser sintering. Proc. Inst. Mech. Eng. Part B J. Eng. Manuf. **221**(11), 1585–1591 (2007)
18. Baumers, M.: Raw material pricing and additive manufacturing. University of Nottingham (2014)
19. Miyanaji, H., Zhang, S., Lassell, A., Zandinejad, A.A., Yang, L.: Optimal process parameters for 3D printing of porcelain structures. In: 44th Proceedings of the North American Manufacturing, vol. 5, pp. 870–887 (2016)
20. Bourell, D., et al.: Materials for additive manufacturing. CIRP Ann. Manuf. Technol. **66**, 659–681 (2017)
21. https://www.lboro.ac.uk/research/amrg/about/materials/
22. Baumers, M., Dickens, P., Tuck, C., Hague, R.: The cost of additive manufacturing: machine productivity, economies of scale and technology-push. Technol. Forecast. Soc. Chang. **102**, 193–201 (2016)

23. https://all3dp.com/2/dimensional-accuracy-3d-printing-tips-tricks/
24. https://3dprinterly.com/how-to-fix-a-poor-rough-surface-above-3d-print-supports/
25. Bandyopadhyay, A., Bose, S.: Additive Manufacturing. Taylor & Francis Group, Routledge (2016)
26. Vora, H.D., Sanyal, S.: A comprehensive review: metrology in additive manufacturing and 3D printing technology. Prog. Addit. Manuf. **5**(4), 319–353 (2020). https://doi.org/10.1007/s40964-020-00142-6
27. Townsend, A., Senin, N., Blunt, L., Leach, R.K., Taylord, J.S.: Surface texture metrology for metal additive manufacturing: a review. Precis. Eng. **46**, 34–47 (2016)
28. Morse, E.: Design for Metrology – a new idea? Procedia CIRP **84**, 165–168 (2019). 29th CIRP Design 2019 (CIRP Design 2019)
29. Tatoa, W., Bluntb, L., Llavoria, I., Aginagaldea, A., Townsend, A., Zabalaa, A.: Surface integrity of additive manufacturing parts: a comparison between optical topography measuring techniques. Procedia CIRP **87**, 403–408 (2020). 5th CIRP CSI 2020
30. Kaji, F., Barari, A.: Evaluation of the surface roughness of additive manufacturing parts based on the modelling of cusp geometry. IFAC-PapersOnLine **48–3**, 658–663 (2015)
31. Krauss, H., Eschey, C., Zaeh, M.F.: Thermography for monitoring the selective laser melting process. In: 23rd International Solid Freeform Fabrication Symposium, Austin, TX (2012)
32. Everton, S.K., Hirscha, M., Stravroulakis, P., Leach, R.K., Clare, A.T.: Review of in-situ process monitoring and in-situ metrology for metal additive manufacturing. Mater. Des. **95**, 431–445 (2016)
33. Wang, F., Mao, H., Zhang, D., Zhao, X., Shen, Y.: Online study of cracks during laser cladding process based on acoustic emission technique and finite element analysis. Appl. Surf. Sci. **255**(5, Part 2), 3267–3275 (2008)
34. Berumen, S., Bechmann, F., Lindner, S., Kruth, J.-P., Craeghs, T.: Quality control of laser and powder bed-based Additive Manufacturing (AM) technologies. Phys. Procedia **5**(Part B), 617–622 (2010)
35. Furumoto, T., Ueda, T., Alkahari, M.R., Hosokawa, A.: Investigation of laser consolidation process for metal powder by two-color pyrometer and high-speed video camera. CIRP Ann. Manuf. Technol. **62**(1), 223–226 (2013)
36. Doubenskaia, M., Pavlov, M., Chivel, Y.: Optical system for on-line monitoring and temperature control in selective laser melting technology. Key Eng. Mater. **437**(1), 458–461 (2010)
37. Tammas-Williams, S., Zhao, H., Léonard, F., Derguti, F., Todd, I., Prangnell, P.B.: XCT analysis of the influence of melt strategies on defect population in Ti–6Al–4V components manufactured by selective electron beam melting. Mater. Charact. **102**(4), 47–61 (2015)
38. Furumoto, T., Alkahari, M.R., Ueda, T., Aziz, M.S.A., Hosokawa, A.: Monitoring of laser consolidation process of metal powder with high speed video camera. Phys. Procedia **39**(1), 760–766 (2012)
39. Land, W.S., Zhang, B., Ziegert, J., Davies, A.: In-situ metrology system for laser powder bed fusion additive process. In: 43rd Proceedings of the North American Manufacturing Research, vol. 1, pp. 393–403 (2015)
40. Leach, R.: Advances in Optical Surface Texture Metrology. University of Nottingham, Nottingham (2020)
41. Moshiri, M., Charles, A., Elkaseer, A., Scholz, S., Mohanty, S., Tosello, G.: An Industry 4.0 framework for tooling production using metal additive manufacturing-based first-time-right smart manufacturing system. Procedia CIRP **93**, 32–37 (2020). 53rd CIRP Conference on Manufacturing Systems
42. Lu, Y., Ju, F.: Smart manufacturing systems based on Cyber-physical Manufacturing Services (CPMS). IFAC PapersOnLine **50–1**, 15883–15889 (2017)

43. Zenisek, J., Wild, N., Wolfartsberger, J.: Investigating the potential of smart manufacturing technologies. Procedia Comput. Sci. **180**, 507–516 (2021)
44. Zarreh, A., Saygin, C., Wan, H., Lee, Y., Bracho, A., Nie, L.: Cybersecurity analysis of smart manufacturing system using game theory approach and quantal response equilibrium. Procedia Manuf. **17**, 1001–1008 (2018)
45. Zarreh, A., Wan, H., Lee, Y., Saygin, C., Janahi, R.A.: Cybersecurity concerns for total productive maintenance in smart manufacturing systems. Procedia Manuf. **38**, 532–539 (2019)
46. ISO/ASTM52902-19: Additive manufacturing — test artifacts — geometric capability assessment of additive manufacturing systems. ASTM International, West Conshohocken, PA (2019)
47. ISO/TC 261 and ASTM F42: Joint plan for additive manufacturing standards development (2013)
48. Naylor, J.: Introduction to Operations Management, 2nd edn. Pearson Education, Harlow (2002)
49. Krajewski, L.J., Ritzman, L.P., Malhorta, M.J.: Operations Management: Processes and Supply Chains, 10th edn. Pearson, London (2013)
50. Marinescu, I., Boothroyd, G.: Product Design for Manufacture and Assembly, 2nd edn. Marcel Dekker Inc., New York (2002)
51. Thompson, M.K., et al.: Design for additive manufacturing: trends, opportunities, considerations and constraints. CIRP Ann. Manuf. Technol. **65**(2), 737–760 (2019)
52. Müller, J.R., Panarotto, M., Malmqvist, J., Isaksson, O.: Lifecycle design and management of additive manufacturing technologies. Procedia Manuf. **19**, 135–142 (2018)
53. Fera, M., Macchiaroli, R., Fruggiero, F., Lambiase, A.: Production Management Fundamentals for Additive Manufacturing. IntechOpen, London (2018)
54. Baumung, W., Fomin, V.: Optimization model to extend existing production planning and control systems for the use of additive manufacturing technologies in the industrial production. Procedia Manuf. **24**, 222–228 (2018). 4th International Conference System-Integrated Intelligence
55. Bui, H., Pierson, H.A., Nurre, S.G., Sullivan, K.M.: Tool path planning optimization for multi-tool additive manufacturing. Procedia Manuf. **39**, 457–464 (2019)
56. Li, Q., Zhang, D., Kucukkoc, I.: Order acceptance and scheduling in direct digital manufacturing with additive manufacturing. IFAC PapersOnLine **52–13**, 1016–1021 (2019)
57. Kapadia, M.S., Starly, B., Thomas, A., Uzsoy, R., Warsing, D.: Impact of scheduling policies on the performance of an additive manufacturing production system. Procedia Manuf. **39**, 447–456 (2019)
58. Szykman, S., Cagan, J.: Constrained three-dimensional component layout using simulated annealing. J. Mech. Des. **119**(1), 28–35 (1997)
59. Ransikarbum, K., Ha, S., Ma, J., Kim, N.: Multi-objective optimization analysis for part-to-printer assignment in a network of 3D fused deposition modeling. J. Manuf. Syst. **43**, 35–46 (2017)
60. Wu, S., Kay, M., King, R., Vita-Parrish, A., Warsing, D.: Multiobjective optimization of 3D packing problem in additive manufacturing. In: IIE Annual Conference and Expo 2014, pp. 1485–1494 (2014)
61. Baumers, M., Tuck, C., Wildman, R., Ashcroft, I., Hague, R.: Energy inputs to additive manufacturing: does capacity utilization matter? Additive Manufacturing Research Group, Wolfson School of Mechanical and Manufacturing Engineering, Loughborough University (2011)
62. Sgarbosa, F., Peron, M., Lolli, F., Balugni, E.: Conventional or additive manufacturing for spare parts management: an extensive comparison for Poisson demand. Int. J. Prod. Ergon. **233**, 107993 (2021)

63. Cestana, A., Pastore, E., Alfieri, A., Matta, A.: Reducing resupply time with additive manufacturing in spare part supply chain. IFAC-PapersOnLine **52**(13), 577–582 (2019)
64. Kim, S., Kim, M., Ahn, N.: 3D printer scheduling for shortest time production of weapons parts. Procedia Manuf. **39**, 439–446 (2019)
65. Walter, M., Holmström, J., Yrjölä, H.: Rapid manufacturing and its impact on supply chain management. In: Proceedings of the Logistics Research Network Annual Conference, no. November, p. 12 (2004)
66. Marchese, K., Crane, J., Haley, C.: 3D opportunity for the supply chain: additive manufacturing delivers. Technical report (2015)
67. Liu, P., Huang, S.H., Mokasdar, A., Zhou, H., Hou, L.: The impact of additive manufacturing in the aircrafts spare parts supply chain: supply chain operation reference (SCOR) model based analysis. Prod. Plann. Control **25**(13–14), 1169–1181 (2014)
68. Rinaldi, M., Caterino, M., Fera, M., Manco, P., Macchiaroli, R.: Technology selection in green supply chain – the effects of additive and traditional manufacturing. J. Clean. Prod. **282**, 124554 (2021)
69. Paris, H., Mokhtarian, H., Coatanea, E., Museau, M., Ituarte, I.F.: Comparative environmental impacts of additive and subtractive manufacturing technologies. CIRP Ann. **65**(1), 29–32 (2016)
70. Minetola, P., Eyers, D.R.: Additive manufacturing as a driver for the sustainability of short-lifecycle customized products: the case study of mobile case covers. In: Campana, G., Howlett, R.J., Setchi, R., Cimatti, B. (eds.) SDM 2017. SIST, vol. 68, pp. 766–775. Springer, Cham (2017). https://doi.org/10.1007/978-3-319-57078-5_72
71. Nyamekye, P., Leino, M., Piili, H., Salminen, A.: Overview of sustainability studies of CNC machining and LAM of stainless steel. Phys. Procedia **78**, 367–376 (2015)
72. Holmström, J., Gutowski, T.: Additive manufacturing in operations and supply chain management: no sustainability benefit or virtuous knock-on opportunities? J. Ind. Ecol. **21**, S21–S24 (2017)
73. Baumers, M.: 3D printing production planning: reactive manufacturing execution driving distributed manufacturing. University of Nottingham (2018)
74. https://www.supplychaindigital.com/supply-chain-2/additive-manufacturings-rise-enabler-supply-chain-efficiencies
75. Huang, R., et al.: Environmental and economic implications of distributed additive manufacturing: the case of injection mold tooling. J. Ind. Ecol. **21**(S1), S130–S143 (2017)
76. Baumers, M.: Management and operations of additive manufacturing. University of Nottingham (2018)
77. Yoon, H.-S., et al.: A comparison of energy consumption in bulk forming, subtractive, and additive processes: review and case study. Int. J. Precis. Eng. Manuf. Green Technol. **1**(3), 261–279 (2014)
78. Faludi, J., Bayley, C., Bhogal, S., Iribarne, M.: Comparing environmental impacts of additive manufacturing vs traditional machining via life-cycle assessment. Rapid Prototyp. J. **21**(1), 14–33 (2015)
79. Verma, A., Rai, R.: Sustainability-induced dual-level optimization of additive manufacturing process. Int. J. Adv. Manuf. Technol. **88**(5–8), 1945–1959 (2016). https://doi.org/10.1007/s00170-016-8905-9
80. Peng, T.: Analysis of energy utilization in 3D printing processes. Procedia CIRP **40**, 62–67 (2016)
81. Tang, Y., Mak, K., Zhao, Y.F.: A framework to reduce product environmental impact through design optimization for additive manufacturing. J. Clean. Prod. **137**, 1560–1572 (2016)
82. World Intellectual Property Organization (WIPO): What is Intellectual Property? WIPO (2020)

83. https://www.industryweek.com/innovation/intellectual-property/article/21972196/3d-printing-raises-new-legal-questions
84. Chan, H.K., Griffin, J., Lima, J.J., Zenga, F., Chiuc, S.F.: The impact of 3D printing technology on the supply chain: manufacturing and legal perspectives. Int. J. Prod. Econ. **205**(2018), 156–162 (2018)
85. Hornick, J.F., Rajan, K.: 3D Bioprinting and Nanotecnology in Tissue Engineering. Elsevier, Amsterdam (2015)
86. Kirillova, A., Bushev, S., Abubakirov, A., Sukikh, G.: Bioethical and legal issues in 3D bioprinting. Int. J. Bioprint **6**(3), 272 (2020)
87. Kritikos, M.: 3D bioprinting for medical and enhancement purposes: legal and ethical aspects. Scientific Foresight Unit (STOA), European Parliament, Brussels (2018)
88. https://www.bbc.com/news/technology-44871588
89. https://www.theguardian.com/technology/2013/may/13/3d-printed-guns

Patient Transfer Under Ambulance Offload Delays: An Approximate Dynamic Programming Approach

Cheng Hua[1] and Wenqian Xing[2(✉)]

[1] Antai College, Shanghai Jiao Tong University, Shanghai 200030, China
cheng.hua@sjtu.edu.cn
[2] IEOR Department, Columbia University, New York 10027, USA
wx2261@columbia.edu

Abstract. Ambulance offload delay (AOD) occurs when emergency medical services (EMS) transferring a patient to a busy hospital emergency department (ED). It is a crucial bottleneck for patient cares on both patient and ambulance sides that delays the transfer of a patient from an ambulance to the emergency department, which will negatively influence the care quality and efficiency. This paper formulates the AOD problem as a Markov decision process (MDP) and develops an approximate dynamic programming (ADP) approach to overcome the curse of dimensionality. We formulate the problem based on the post-decision states and derive two approximate dynamic programming solution algorithms using linear regression and neural network frameworks. The numerical result shows that the transfer policy obtained from our solution approach outperforms the myopic policy, which always transfers patients to the closest hospital. Our findings suggest that our approach can effectively alleviate the AOD problem, improve health care quality, and improve the overall system efficiency.

Keywords: Approximate dynamic programming · Markov decision process · Ambulance offload delay · Healthcare

1 Introduction

Ambulance offload delay (AOD) occurs when emergency medical services (EMS) transferring a patient to a busy hospital emergency department (ED). It is a crucial bottleneck for patient cares on both patient and ambulance sides. If the ambulance cannot hand over the patient to the hospital immediately due to the absence of empty beds, the paramedic has to continue serving the patient until a bed becomes available. This causes a delay for the patient to get timely care and keeps the ambulance from getting back to serve incoming new calls.

Most EMS systems transfer patients based on static rules that always transfer patients to the nearest hospital in current practice. This scheduling policy is

C. Hua and W. Xing—These authors contributed equally to this work.

R. Qiu et al. (Eds.): ICSS 2021, LNOR, pp. 337–350, 2021.
https://doi.org/10.1007/978-3-030-90275-9_27

myopic because it only considers the current call and ignores the current level of congestion at each hospital and the potential impact on future patients. Many systems use ambulance diversion to handle AOD, which does not accept new patients transferred by ambulances when the ED is too crowded, but this does not fundamentally solve the AOD problem.

In this paper, we model the ambulance offload delay problem as a Markov decision process (MDP) to determine which hospital to transfer each patient to in order to reduce ambulance offload delay. However, due to the curse of dimensionality, this MDP is intractable in practice when the state space is large. We use an approximate dynamic programming approach with several designed basis functions to deal with this problem. We formulate the problem based on the post-decision states and derive two approximate dynamic programming solution algorithms using ridge regression and neural network. We find that both solution algorithms converge quickly, and the corresponding policies obtained from our solutions outperform the myopic policies.

The rest of this paper is organized as follows. In Sect. 2, we review the relevant literature. In Sect. 3, we introduce the Markov decision process formulation. In Sect. 4, we present the approximate dynamic programming formulation and two ADP algorithms using ridge regression and neural network approaches, while in Sect. 5, we discuss the basis functions used in our solution. In Section 6, we show the performance of the algorithm in numerical experiments. We conclude this paper in Sect. 7.

2 Literature Review

2.1 Ambulance Offload Delay

The ambulance offload delay problem has become an active research topic in recent years. It was first derived from the EMS turnaround time interval concept, and many works have been conducted in developing, measuring, and studying possible solutions to the AOD problem.

[1] first defined the concept of EMS turnaround interval, which is the time from the arrival of an ambulance at a hospital to the return of the ambulance to service. [2] analyzed the key factors that facilitate EMS turnaround time in the presence of overcrowding in receiving facilities. [3] showed the validity of this turnaround time interval as an accurate measure of the AOD problem.

The importance of the AOD problem was first studied by [4], who showed the potential impact of AOD on the overall efficiency of EMS and ED systems. [5] developed algorithms to calculate performance metrics for systems facing the AOD problem using Markov chain models. In recent years, [6] developed a queuing network to model the interaction between EMS providers and regional EDs and investigated the impact of patient routing decisions on AOD. [7] gives a comprehensive overview of the ambulance offload delay problem.

The paper most relevant to us is [8]. This paper develops an MDP model for determining the optimal ambulance destination policy with urban and community hospitals. They assume that only urban EDs face the AOD and the

community hospital is always empty. The main idea is that when there is a potential offload delay in the urban hospital, it may be better to transfer the patient to a community hospital that is empty even if it the travel distance is longer. The state space for the model is huge when the number of ambulances in a city is large, and solving such a large system becomes intractable using MDP.

Although MDP models guarantee to find the optimal policy, their computational complexity limits their use to small systems due to the curse of dimensionality. For larger problems, they usually fail severely computationally. Therefore, many works have tried to handle this issue using approximate dynamic programming (ADP).

2.2 Approximate Dynamic Programming

A comprehensive introduction to the application of Approximate Dynamic Programming in the operations research field can be found in [9] and [10].

[11] used the same model as [9] to solve the ambulance dispatching problem. They use a clustering approach to approximate the state value function and then adopt approximate dynamic programming to solve the emergency vehicle relocation and dispatching problem to reduce the average response time. The seminal paper by [12] applies approximate dynamic programming to the emergency vehicle redeployment problem. They design several basis functions and use a one-step bootstrap method to estimate complex expectations in Monte Carlo simulations and apply a least-squares method based on linear function approximation to learn approximate state values. [13] studied the dispatching and redeployment of emergency vehicles and also used approximate dynamic programming to solve this problem to obtain a good policy. [14] uses approximate dynamic programming algorithms to study when patients in busy departments need to be transferred to other departments in the emergency room to reduce patient wait times. [15] applies the value approximation method in time difference learning to find the optimal emergency service scheduling policy. [16] studies the military medical evacuation dispatching problem using approximate dynamic programming and basis functions.

Our paper models the ambulance offload delay problem as a Markov decision process (MDP) and derive two approximate dynamic programming solution algorithms to solve the problem. The corresponding policy obtained from our solutions reduce the offload delay time and potentially improve the survivability of the patient due to a faster delivery to the emergency department.

3 Markov Decision Process Formulation

We study a system with a total of N ambulances in a geographical region $R \subset \mathbb{R}^2$. We assume that the ambulances operate according to a centralized system following a fixed policy in dispatch and relocation. Our decision is made only when a unit finishes its service at the scene, and the patient needs to be transported to a hospital. Therefore, we only consider time points when patient

transports are needed. We assume a total of H hospitals in the region and let $\mathscr{H} := \{1, \cdots, H\}$ be the set of hospitals. Transporting requests arrive in region R according to a non-homogeneous Poisson point process with intensity $\{\Lambda(t, x, y, n) : t \geq 0, (x, y) \in R, 0 \leq n \leq N\}$ at time t of the day and location with coordinate (x, y) when the number of busy units is n.

$$\Lambda(t, x, y, n) = \begin{cases} \Lambda(t, x, y), & \text{if } n < N, \\ 0, & \text{if } n = N. \end{cases} \tag{1}$$

We note that arrival intensity is independent of the number of busy units when there is at least one available unit.

We partition the region R into J sub-regions and associate a center of mass with each sub-region $R_j \subset R$, which is also referred to as demand *node* j. Note that J can be as large as needed to make a granular division. Denote the total transporting request arrival rate in node j at time t as

$$\lambda_j(t) = \int_{R_j} \Lambda(t, x, y) dx dy. \tag{2}$$

Let B be the total number of call priority levels and let the set of priority levels be $\mathscr{B} = \{1, 2, \cdots, B\}$ each with probability $p_b(t)$, which is also time-dependent. Denote $\tau(x_1, y_1, x_2, y_2)$ as the mean travel time from point (x_1, y_1) to (x_2, y_2), which is assumed to be deterministic and known beforehand. Ambulance turnaround time at a hospital depends on the total number of patients. Let l_{bh} be the queue length of level-b patients at hospital h. We assume that patients with higher priorities will be served before those with lower priorities. Thus, a patient's total waiting time consists of three parts: i) waiting time for the patients with higher or equal priorities arriving before the patient, denoted by ψ_w; ii) waiting time for the patients with higher priorities arriving after the patient and before the completion of his service, denoted by ψ_a; iii) his service time, denoted by ψ_s, that follows a general distribution with cumulative distribution function F. Thus, the total time from call location until a patient is offloaded is $t^{tot} = \tau + \psi_a + \psi_w + \psi_s$ (Fig. 1).

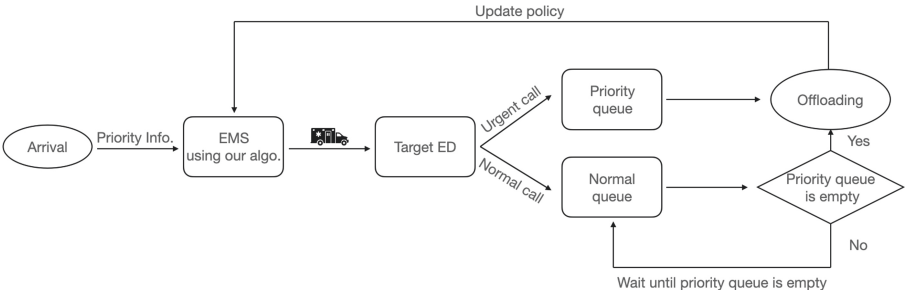

Fig. 1. M/M/1 priority queue workflow for the case $B = 2$

We let tuple $a_i = (u_i, t_i, x_i, y_i, d_i, b_i)$ be the state of ambulance i, where u_i is the status of the ambulance, t_i is the starting time of a new status, $d_i \in \mathscr{H}$ is the destination hospital if applicable or empty otherwise, $b_i \in \mathscr{B}$ is the priority level of its patient if applicable or empty otherwise, and (x_i, y_i) is the call location. There are three different statuses of an ambulance. In particular,

$$u_i = \begin{cases} 0, & \text{if unit } i \text{ is available,} \\ 1, & \text{if unit } i \text{ is ready for patient transportation,} \\ 2, & \text{if unit } i \text{ is transporting patients to hospital,} \\ 3, & \text{if unit } i \text{ is waiting for offload.} \end{cases} \tag{3}$$

We let $\mathbf{a} = (a_1, a_2, \cdots, a_N)$ be the state of all ambulances.

3.1 State Space

Let $\mathbf{l}$ be the set that contains the length of each queue at each hospital and the starting time of the current service at the beginning of the queue. We have

$$\mathbf{l} = \{(l_{bh}, t^*_{bh}) : b = 1, \cdots, B, h = 1, \cdots, H\}, \tag{4}$$

where t^*_{bh} is the starting time of the current service at hospital h for level-b patient. We let $t^*_{bh} = \emptyset$ if all patients in the queue are waiting for service. Define S as the state space and $s \in S$ is the state of the system. We have

$$s = (t, \mathbf{l}, \mathbf{a}), \tag{5}$$

which is a tuple of current time, all queue statuses, and all ambulance statuses. The times in the state variable allow a Markov formulation for the non-Markovian elements in the system.

3.2 Action Space

An action in this problem is the choice of the destination hospital for an ambulance that needs transporting to the hospital, so the action space is given as

$$A = \mathscr{H}. \tag{6}$$

We define $a \in A$ as an action from the action space. An action is needed when an ambulance is ready for patient transportation, i.e., if there exists an ambulance i such that $u_i = 1$.

3.3 Costs

We assume that the weight for each patient type is w_b, and the cost for each transport is the weighted total time $w_b t^{tot}$. However, we can not get the full information of t^{tot} during the state transition period. Instead, we use the expectation $\mathbb{E}[t^{tot}]$ to calculate the approximated cost.

Define $c^{\pi}(s)$ as the cost of being in state s following policy π. We have

$$c^{\pi}(s) = \begin{cases} w_b \mathbb{E}\left[t^{tot}\right], & \text{if } u_i = 1, \\ 0, & \text{otherwise.} \end{cases} \tag{7}$$

3.4 Policy Space

We define the policy space as Π, the set of all feasible policies. A policy $\pi \in \Pi$ is a mapping from the state space to the action space, $\pi : S \rightarrow A$. Specifically, $\pi(s) = a, a \in A_s$. The optimal policy $\pi^* \in \Pi$ is the policy that minimizes the average cost over all time steps. Our goal is to find a good policy that is close to the optimal policy.

We use a benchmark policy which transports the patient to the closest hospital, denoted by $\pi^m \in \Pi$. We have

$$\pi^m(s) = \arg\min \tau, \qquad \forall i \in A, \forall s \in S. \tag{8}$$

Transferring patients to the closest hospital is a policy widely used in emergency service systems. This policy is myopic as it does not consider ED congestion and other patients who are waiting at the hospital.

3.5 Bellman's Equation

Define $A^{\pi}(s_t)$ as the function that outputs an action a_t for a state $s_t \in S$ at time t based on a given policy π. Our MDP model aims to find the optimal policy π^* from the classes of policies $\pi \in \Pi$, which minimizes the expected total discounted cost. This objective can be expressed as

$$\min_{\pi \in \Pi} \mathbb{E}^{\pi} \left[\sum_{t=1}^{\infty} \gamma^{\tau_t} C\left(s_t, A^{\pi}\left(s_t\right)\right) \right], \tag{9}$$

where γ is the time discount factor and τ_t stands for the system time at state s_t. It can be solved using the Bellman's Equation

$$V\left(s_t\right) = \min_{a_t \in \mathscr{H}\left(s_t\right)} \left(C\left(s_t, a_t\right) + \gamma^{\left(\tau_{t+1} - \tau_t\right)} \mathbb{E}\left[V\left(s_{t+1}\right) \mid s_t, a_t\right] \right) \tag{10}$$

However, the exceptionally high dimensionality in this problem makes it intractable to solve. Thus, instead of solving Bellman's equation directly, we propose two solutions using approximate dynamic programming techniques to reduce the dimensionality of this problem.

4 Approximate Dynamic Programming Formulation

In this section, we present two approximate dynamic programming solutions to the ambulance optimal dispatch problem. They are based on the approximate

policy iteration but differ in the way of approximating the value function. Our solutions approximate the value function via a post-decision state, which refers to the state s_t^a right after a pre-decision state s_t and the corresponding action a is taken. The Bellman's Equation with post-decision state s_t can be written as:

$$V^a\left(s_t^a\right) = \mathbb{E}\left[\min_{a_{t+1}\in\mathscr{H}\left(s_{t+1}\right)}\left(C\left(s_{t+1}, a_{t+1}\right) + \gamma^{\left(\tau_{t+1}-\tau_t\right)}V^a\left(s_{t+1}^a\right)\right) \mid s_t^a\right] \tag{11}$$

Equation (11) is computationally intractable due to the curse of dimensionality. Thus, we construct five set of basis functions $\{\phi_n(\cdot) : n = 1, ..., N\}$ as the key representation of the state that are used to approximate the value function of each state. The basis functions are explained in detail in Sect. 5.

4.1 Policy Iteration with TD-Learning

The approach uses the policy iteration strategy with temporal difference learning for policy evaluation. Compared with the traditional least-squares temporal difference learning, we apply Ridge regression in the approximation algorithm to reduce variance. By updating the policy and the value function approximation iteratively through the policy evaluation phase and policy improvement phase, our solution converges within a short period. The value function approximation given the basis functions can be written as:

$$\bar{V}^a\left(s_t^a \mid \theta\right) = \sum_{n\in\mathscr{N}} \theta_n\phi_n\left(s_t^a\right) \equiv \theta^T\phi\left(s_t^a\right) \tag{12}$$

Moreover, for the Bellman's Equation with the post-decision state (11), we have

$$\theta^T\phi\left(s_t^a\right) = \mathbb{E}\left[C\left(s_t, A^\pi\left(s_t \mid \theta\right)\right) + \gamma^{\left(\tau_{t+1}-\tau_t\right)}\theta^T\phi\left(s_{t+1}^a\right) \mid s_t^a\right] \tag{13}$$

The TD-Learning algorithm (1) starts from initializing the basis function weights θ, and then enters into the phase of policy iteration. In each iteration, we first update the policy for each state based on the current approximation of the value function. We simulate T post-decision states given the current policy and record the corresponding cost and the temporal difference of the basis functions for each post-decision state in the simulation process. At the end of each iteration, we run Ridge regression for the temporal difference of the basis functions on the recorded costs to obtain the estimator for weights $\hat{\theta}_{\text{ridge}}$. Finally, we update the current weights by smoothing the old weights with the newly obtained ones. Then the algorithm enters into the next iteration.

Algorithm 1. Policy Iteration with TD-Learning

1: Specify T and K
2: Initialize the basis function weights with small, random value near zero: $\theta \leftarrow 0$
3: **while** $k \leq K$ **do**
4: Set $t = 0$
5: For each state $s_t \in S$, update the policy

$$A^{\pi_k}(s_t \mid \theta) = \underset{a_t \in \mathscr{H}(s_t)}{\operatorname{argmin}} \left\{ C(s_t, a_t) + \gamma^{(\tau_{t+1}-\tau_t)} \bar{V}^a(s^a_{t+1} \mid \theta) \right\}$$

6: Starting from a random state s_0, generate a post-decision state trajectory $\{s^a_t \mid t = 0, 1, \ldots T\}$ using the simulator based on the current policy π_k
7: Record the corresponding costs $\{c_t \in C \mid t = 0, 1, \ldots T\}$ from the output of the simulator
8: **for** $t = 0$ to T **do**
9: Record the basis functions for the current state: $\phi_i(s_t), i \in \{1, ..., N\}$
10: Rearrange Equation (13), we have all terms deterministic now:

$$\theta^T \left[\phi(s^a_t) - \gamma^{(\tau_{t+1}-\tau_t)} \phi(s^a_{t+1}) \right] = c_t$$

11: Calculate the temporal difference $\{d_t \in D \mid t = 0, 1, \ldots T\}$ by

$$d_t = \phi(s^a_t) - \gamma^{(\tau_{t+1}-\tau_t)} \phi(s^a_{t+1})$$

12: **end for**
13: Run Ridge regression for the recorded cost C on the recorded temporal difference D

$$\hat{\theta}_{\text{ridge}} = \left(D'D + \eta I\right)^{-1} D'C$$

14: Update the basis function weights

$$\theta = \alpha \hat{\theta}_{\text{ridge}} + (1 - \alpha)\theta$$

15: $k = k + 1$
16: **end while**
17: **Output:** Policy $\pi^* = \pi_K$

4.2 Policy Iteration with Multilayer Perceptron

In this solution, we use Multilayer Perceptron (MLP) as a representation of the neural network to approximate the value function. We construct a neural network with different layers of nodes and sigmoid activation function. Hence the value function approximation given basis functions can be written as:

$$\bar{V}^a(s^a_t \mid \Theta) = \mathbb{E}\left[C(s_t, A^\pi(s_t \mid \Theta)) + \gamma^{(\tau_{t+1}-\tau_t)} \bar{V}^a\left(s^a_{t+1} \mid \Theta\right) \mid s^a_t \right], \qquad (14)$$

where Θ is the set of all weights of the neural network. $\bar{V}^a\left(s_t^a \mid \Theta\right)$ are computed by forward propagation of the MLP, where the input is the set of basis functions of the current state.

The MLP algorithm (2) uses the neural network framework to approximate the value function, which is instantiated with MLP. The algorithm also starts by initializing the weights for each nodes in MLP and then enter into the policy iteration phase. In each iteration, we update the policy given the current MLP, and then simulate T state transitions with this policy. For each state, we calculate the approximated value by adding up the current cost and the prediction for the next state value using MLP forward propagation. Then we calculate the loss between the approximated value with result of MLP forward propagation for the current state, and then use back propagation to update the weights at the end of each iteration.

Algorithm 2. Policy Iteration with Multilayer Perceptron

1: Specify T and K
2: Initialize the node weights in MLP with small, random values near zero: $\Theta \leftarrow 0$
3: **while** $k \leq K$ **do**
4: Set $t = 0$
5: For each state $s_t \in S$, update the policy

$$A^{\pi_k}\left(s_t \mid \Theta\right) = \underset{a_t \in \mathscr{H}\left(s_t\right)}{\operatorname{argmin}} \left\{ C\left(s_t, a_t\right) + \gamma^{\left(\tau_{t+1} - \tau_t\right)} \bar{V}^a\left(s_{t+1}^a \mid \Theta\right) \right\}$$

6: Starting from a random state s_0, generate a post-decision state trajectory $\{s_t^a \mid t = 0, 1, \ldots T\}$ using the simulator based on the current policy π_k
7: Record the corresponding costs $\{c_t \in C \mid t = 0, 1, \ldots T\}$ from the output of the simulator
8: **for** $t = 0$ to T **do**
9: Calculate the realization of the value function approximation for current state s_t

$$v_t = c_t + \gamma^{\left(\tau_{t+1} - \tau_t\right)} \bar{V}^a\left(s_{t+1}^a \mid \Theta\right)$$

10: **end for**
11: Calculate the least square loss function

$$L(\Theta) = \sum_{t=0}^{T} \left[v_t - \bar{V}^a\left(s_t^a \mid \Theta\right) \right]^2$$

12: Use Back-propagation to update the neural weights Θ in MLP

$$\Theta = \alpha \widehat{\Theta} + (1 - \alpha)\, \Theta, \quad \widehat{\Theta} = \arg\min_{\Theta} L(\Theta)$$

13: $k = k + 1$
14: **end while**
15: **Output:** Policy $\pi^* = \pi_K$

5 Basis Functions

This section describes the basis functions $\{\phi_n(\cdot) : n = 1, ..., N\}$ that we used in our value function approximations. Our problem formulation has five basis functions that are designed to contain both the deterministic and stochastic information of a given state s.

5.1 Patient Priority Level

The first set of basis functions captures the patient priority level for each patient. The value of the priority level for the i_{th} patient in state s is denoted as $b_i(s) \in \{1, ..., B\}$. If the current ambulance is idle, this basis function will return the default value zero.

$$\phi_{1i}(s) = \begin{cases} b_i(s), & \text{if } u_i \in \{1, 2, 3\} \\ 0, & \text{otherwise.} \end{cases} \qquad i = 1, \cdots, N \tag{15}$$

5.2 Target Hospital of Patient on the Way

The second set of basis functions records the target hospital of each patient during the transportation process. For the i_{th} ambulance on the way of transportation in state s, its status $u_i = 2$ and the corresponding target hospital is $d_i(s)$.

$$\phi_{2i}(s) = \begin{cases} d_i(s), & \text{if } u_i = 2, \\ 0, & \text{otherwise.} \end{cases} \qquad i = 1, \cdots, N \tag{16}$$

5.3 Queue Length of Priority Level at Hospital

The third set of basis functions computes the queue length of each priority level at each hospital. For the b_{th} priority level at the h_{th} hospital in the current state s, the corresponding queue length is expressed as $l(s)_{bh}$.

$$\phi_{3bh}(s) = l(s)_{bh} \qquad b = 1, \cdots, B; \quad h = 1, \cdots, H \tag{17}$$

5.4 Expected Waiting Time of Patient

The previous basis functions have already captured the deterministic information in the current state s. However, the time for offloading the patient at the hospital and the arrival time for new calls are stochastic. The fourth set of basis functions attempts to capture the stochastic information for the total service time.

$$\phi_{4i}(s) = \begin{cases} \mathbb{E}\left[t_i^{tot}(s)\right] + t_i(s) - t(s), & \text{if } u_i = 1, \\ 0, & \text{otherwise.} \end{cases} \qquad i = 1, \cdots, N \tag{18}$$

where t^{tot} is the total service time mentioned in MDP formulation, which contains the travel time, waiting time within a queue, and the offload time. Since the waiting time within a queue and offloading time both are random variables, the t^{tot} is a random variable as well. To subtract the past time, we further add two adjustment term, where $t_i(s)$ is the starting time of current transportation and $t(s)$ is current system time.

5.5 Expected Number of Arrivals Within the Next T Unit of Time

The last set of basis functions considers another stochastic information in the current state s, the future expected number of call arrivals within a certain time T.

$$\phi_5(s) = \int_{t(s)}^{t(s)+T} \iint_V \Lambda(t, x, y) dx dy dt \tag{19}$$

The call arrival rate $\Lambda(t, x, y)$ is a function of the current time t and current location (x, y) in the region. We integrate it over a unit area V and a unit time T to obtain the expected number of call arrivals.

6 Numerical Results

This section shows the numerical results of our two ADP solutions compared with the myopic policy, which always sends the patient to the closest hospital in the system. We created an imaginary region that is partitioned into $J = 81$ demand nodes (9×9 grids). We chose the location of three hospitals to be uniformly distributed within the grids. The offload time for each ambulance at hospital were assumed to follow an exponential distribution. In the simulation, we placed 9 ambulance in the region. We also assumed two priority levels, urgent and non-urgent patients. The weight for the urgent type of patients was twice as the non-urgent type.

Our ADP solutions were applied to the post-decision states, which were obtained by running the simulation algorithm up to 25 iterations. Within each iteration, we simulated over 100,000 state transitions. Beyond the myopic policy, we also compared with the policy that transferring patients to the closest non-full hospital under the assumption that communication existed between the ambulance and the ED before transferring. The recorded weighted time in each iteration for both algorithms are shown in Figs. 2a, 2b respectively.

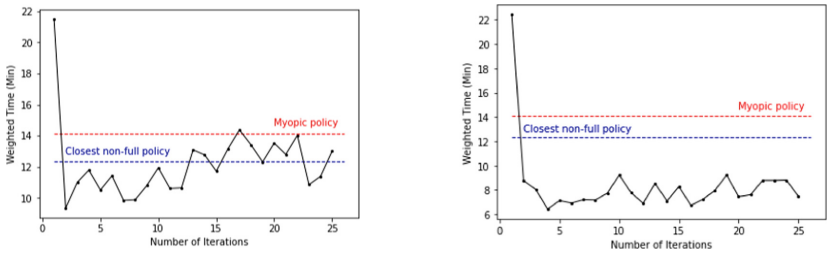

(a) Weighted time cost for TD-Learning Algorithm **(b)** Weighted time cost for MLP Algorithm

Fig. 2. Performance of TD-Learning and MLP solutions

We observed that the weighted time cost converged fast in the first several iterations, which showed that our approximation to the value function reached a reasonable accuracy. Compared with TD-Learning algorithm which uses Ridge regression to approximate the value function, the MLP approximation is more effective and accurate. This is due to the complexity of the system that cannot be approximated well with a linear structure.

Table 1. Numerical results for different parameter settings

Simulator settings					TD Settings	MLP settings		Weighted time (min)			Improvement	
$1/\lambda_1$	$1/\lambda_2$	α	γ	K	Penalty η	Layers	Nodes	TD	MLP	Myopic	TD(%)	MLP(%)
5	10	0.5	0.7	15	100	4	50	8.96	6.81	14.70	39.04%	53.67%
5	10	0.5	0.9	15	100	4	50	9.60	6.49	13.88	30.83%	53.24%
5	20	0.7	0.7	15	100	4	50	26.58	16.75	31.93	16.75%	47.54%
5	20	0.7	0.9	15	100	4	50	19.34	14.25	31.92	39.41%	55.35%
5	30	0.5	0.7	15	100	4	50	43.73	27.30	48.83	10.44%	44.09%
5	30	0.5	0.9	15	100	4	50	30.12	24.66	50.17	39.96%	50.84%
5	40	0.7	0.7	25	1000	6	100	53.93	35.23	66.07	18.37%	46.67%
5	40	0.7	0.9	25	1000	6	100	38.70	32.67	66.41	41.72%	50.80%
5	50	0.5	0.7	25	1000	6	100	62.94	40.83	81.80	23.05%	50.08%
5	50	0.5	0.9	25	1000	6	100	44.21	42.16	82.17	46.19%	48.69%
10	10	0.5	0.7	25	1000	6	100	8.96	5.87	9.09	1.43%	35.42%
10	20	0.5	0.9	25	1000	6	100	16.55	11.66	25.94	36.19%	55.05%
10	30	0.7	0.7	25	1000	6	100	31.49	22.37	46.92	32.88%	52.32%
10	40	0.7	0.9	25	1000	6	100	35.12	29.71	61.95	43.31%	52.04%
10	50	0.7	0.7	25	1000	6	100	41.41	40.63	79.44	47.87%	48.85%

Table 1 records our experiment results under different parameter settings. In the table, λ_1 and λ_2 are the average call arrival rate and the average service rate at the hospital, respectively. The numerical results show that the weighted time cost is positively correlated with the call arrival rate and negatively correlated

with the offloading rate at the hospital. Moreover, when the call arrival rate is low but offloading rate is high, the TD algorithm will have a similar performance with the myopic policy. This can be explained by the situation when the offloading patients at each hospital are very sparse, under which the myopic policy is good enough. Overall, both ADP solutions have a significant improvement compared with the myopic policy. The MLP algorithm is more stable and results in a 50% average improvement over the myopic policy.

7 Conclusion

In this paper, we model the patient transfer problem under ambulance offload delays as a Markov decision process. We aim to find a good patient transfer policy that reduces the total weighted waiting time at the hospital. To deal with the curse of dimensionality, we propose an approximate dynamic programming process based on the post-decision states with a few designed basis functions.

We present two solutions to this ADP problem using ridge regression and neural network techniques. In our numerical experiments, both of our solution algorithms converge quickly, and the corresponding policies obtained outperform the myopic policy, which always transfers the patient to the closest hospital. The performance of our solution algorithms are significant under different simulation environments, which have a 30% average improvement for the TD-Learning algorithm and a 50% average improvement for the MLP algorithm. The experiment results show that our approach can effectively alleviate the AOD problem and improve the overall system efficiency.

References

1. Cone, D.C., Davidson, S.J., Nquyen, Q.: A time-motion study of the emergency medical services turnaround interval. Ann. Emerg. Med. **31**(2), 241–246 (1998)
2. Eckstein, M., et al.: Facilitating ems turnaround intervals at hospitals in the face of receiving facility overcrowding. Prehosp. Emerg. Care **9**(3), 267–275 (2005)
3. Carter, A.J., Overton, J., Terashima, M., Cone, D.C.: Can emergency medical services use turnaround time as a proxy for measuring ambulance offload time? J. Emerg. Med. **47**(1), 30–35 (2014)
4. Cooney, D.R., et al.: Ambulance diversion and emergency department offload delay: resource document for the national association of EMS physicians position statement. Prehosp. Emerg. Care **15**(4), 555–561 (2011)
5. Almehdawe, E., Jewkes, B., He, Q.-M.: A Markovian queueing model for ambulance offload delays. Eur. J. Oper. Res. **226**(3), 602–614 (2013)
6. Almehdawe, E., Jewkes, B., He, Q.-M.: Analysis and optimization of an ambulance offload delay and allocation problem. Omega **65**, 148–158 (2016)
7. Li, M., Vanberkel, P., Carter, A.J.E.: A review on ambulance offload delay literature. Health Care Manage. Sci. **22**(4), 658–675 (2018). https://doi.org/10.1007/s10729-018-9450-x
8. Li, M., et al.: Determining ambulance destinations when facing offload delays using a Markov decision process. Omega **101**, 102251 (2020)

9. Powell, W.B.: Merging AI and OR to solve high-dimensional stochastic optimization problems using approximate dynamic programming. INFORMS J. Comput. **22**(1), 2–17 (2010)
10. Powell, W.B.: Approximate Dynamic Programming: Solving the Curses of Dimensionality, vol. 703. Wiley, New York (2007)
11. Schmid, V.: Solving the dynamic ambulance relocation and dispatching problem using approximate dynamic programming. Eur. J. Oper. Res. **219**(3), 611–621 (2012)
12. Maxwell, M.S., Restrepo, M., Henderson, S.G., Topaloglu, H.: Approximate dynamic programming for ambulance redeployment. INFORMS J. Comput. **22**(2), 266–281 (2010)
13. Nasrollahzadeh, A.A., Khademi, A., Mayorga, M.E.: Real-time ambulance dispatching and relocation. Manuf. Serv. Oper. Manage. **20**(3), 467–480 (2018)
14. Dai, J., Shi, P.: Inpatient overflow: an approximate dynamic programming approach. Manuf. Serv. Oper. Manage. **21**(4), 894–911 (2019)
15. Hua, C., Zaman, T.: Optimal dispatch in emergency service system via reinforcement learning. arXiv preprint arXiv:2010.07513 (2020)
16. Jenkins, P.R., Robbins, M.J., Lunday, B.J.: Approximate dynamic programming for military medical evacuation dispatching policies. INFORMS J. Comput. **33**(1), 2–26 (2021)

COVID-19 Epidemic Forecasting and Cost-Effectiveness Analysis: A Case Study of Hong Kong

Wanying Tao[1], Hainan Guo[1], Qinneng Xu[2], and Dandan Yu[3](✉)

[1] College of Management, Shenzhen University, Shenzhen 518000, Guangdong, China
[2] The Board of Directors, Shenzhen Liangyi Information Technology Co., Ltd., Shenzhen 518000, Guangdong, China
[3] Information Centre, The First Affiliated Hospital of Dalian Medical University, Dalian 116000, Liaoning, China
dayiyudandan@sina.com

Abstract. In December 2019, COVID-19 pneumonia was diagnosed and announced to the public for the first time in Wuhan, Hubei. The COVID-19 disease has spread worldwide. In the critical situation of lack of effective drug treatment in the early stage, Hong Kong, China has adopted various non-drug treatment measures to control the spread and spread of the epidemic, including isolating foreign tourists, closing public places, and compulsory wearing masks. This article divides the development of the Hong Kong epidemic into three stages, each of which has different scales, scope of influence and response measures. Therefore, this article establishes an individual-based stochastic simulation model of the spread of infectious diseases to fit and predict the future development trend of the Hong Kong epidemic. Based on the simulation results, it is predicted that the strict implementation of quarantine measures in the third stage can reduce the total number of patients with new coronary pneumonia in Hong Kong by 83.89%. Combined with the vaccination strategy, achieving 90% of the population's vaccination within a limited time can effectively control the epidemic in Hong Kong and have economic benefits, which will reduce the cost of 10.74% relative to non-vaccination.

Keywords: COVID-19 · Stochastic model · Quarantine measures · Infectious disease prediction · Vaccination

1 Introduction

In December 2019, unexplained pneumonia occurred in Wuhan City, Hubei Province, and then the epidemic spread to cities across the country. The World Health Organization (WHO) declared the epidemic caused by SARS-COV-2 to be COVID-19, which is a serious public health emergency [1]. By the end of 2020, cities in mainland China have basically returned to normal life and social order. As an important city in southern China, the epidemic in Hong Kong has not subsided. In order to cope with the sharp increase in

R. Qiu et al. (Eds.): ICSS 2021, LNOR, pp. 351–364, 2021.
https://doi.org/10.1007/978-3-030-90275-9_28

the number of confirmed diagnoses and the shortage of medical resources [2], the Hong Kong government has adopted a series of measures to deal with the epidemic, such as quarantine of entry personnel, isolation of patients and their close contacts, closure of public places and prohibition of gatherings. Promulgating the order that masks must be worn in public places and so on.

It is urgent to study the causes of COVID-19 disease transmission and predict its development trend. A definite COVID-19 cabin transmission model studied the social distance prescribed by the government to reduce the personal contact rate [3]. The establishment of the cabin model of covid-19 transmission, combined with the local epidemic situation, can greatly reduce the number of new patients [4]. In the absence of effective antiviral drugs, strategies to control and reduce the burden of this epidemic focus on non-drug interventions, such as maintaining social distancing, tracing contacts, quarantining, and wearing masks in public places [5]. By controlling social contact, non-drug intervention has effectively curbed the early outbreak of COVID-19 in China, won scientists time to explore the transmission route and determine effective public health interventions, and won time for the government to reserve resources [6]. Fangcang Hospital can effectively deal with the epidemic situation of COVID-19 and future public health emergencies [7]. The combination of social distance policy and other epidemic control measures can control the epidemic more significantly [8]. The traditional epidemic model is expressed as a system of differential equations, and the spread of epidemics is essentially a random dynamic process. Different types of infectious diseases, medical conditions in different regions, age, gender, and social distance are also the key factors affecting the spread of diseases. Elements [9]. Most Chinese adults have a good understanding of COVID-19, but there are still quite a large number of people in some areas who have misconceptions about prevention methods and medical advice [10]. Population migration plays an important role in the spread of the virus and cannot be ignored. Social distance and imported cases are considered in the mathematical model of infectious diseases [11]. In order to break through the limitations of the traditional cabin infectious disease transmission model and explore the specific effects of a series of non-pharmaceutical intervention measures adopted by Hong Kong, the simulation model in this paper combines different epidemic prevention measures, takes into account the influence of imported cases, dynamically fits the total number of patients at different stages and predicts the development trend of the epidemic in Hong Kong.

The cost of medical care and the socio-economic burden caused by COVID-19 are also concerns for policy makers. A Monte Carlo model simulates the spread of COVID-19 in the United States, indicating that reducing the burden of disease has potential economic benefits [12]. Currently in the vaccination period, the United Nations has emphasized the importance of the COVID-19 vaccine as a public product provided globally, and the vaccine is affordable [13]. Chinese COVID-19 vaccine development process reflects the cultural value of respecting life at all costs. In the near future, more high-quality and affordable vaccines will be provided as global public goods [14]. How to choose a vaccination strategy is also an important issue in this study. Based on the individual-based stochastic simulation model presented in this paper, decision analysis and cost-benefit models were developed to determine the costs and benefits associated with COVID-19 and to evaluate prevention strategies.

The main contributions of this article are as follows:

1. Propose an individual-based stochastic simulation model for the spread of COVID-19, compare the probability of susceptible people of different ages contacting the patient, and predict the future development trend of the epidemic based on the parameters.
2. Divide the development of the epidemic into three periods and analyse the development characteristics of the epidemic at different stages. According to the estimation of the parameters in the first and second periods, the total number of patients in the third outbreak in Hong Kong is predicted, and the impact of different epidemic prevention measures on reducing the number of infections is analysed and compared.
3. Based on the simulation model, consider the medical cost and social burden, and provide decision makers with the optimal vaccination combination strategy.

2 Methods

This section introduces the source of the data used in the study. First, it describes the characteristics of COVID-19 patients reported in Hong Kong, then describes the establishment of a random simulation model based on individuals, and finally gives the parameters of the economic efficiency model.

2.1 Data and Descriptive Statistics

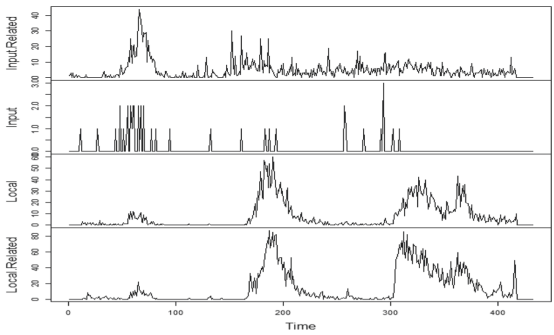

Fig. 1. Source of the infected

On January 23, 2020, Hong Kong notified the first COVID-19 patient who was not a local resident of Hong Kong and had a history of travel to Wuhan. The data collected in this study includes information about the onset time, age, gender, source of patients, and whether they are local residents of all patients officially reported in Hong Kong. The statistical data comes from the Hong Kong Department of Health [15]. Figure 1 shows the source of the infected. On February 8th, people arriving in Hong Kong from the Mainland must undergo compulsory quarantine at a designated place (quarantine center,

home or other residence) for 14 days. On March 17th, the same measures will apply to all people who have entered Hong Kong who have been to high-risk countries/regions. *The Prohibition of Group Gathering Regulations* were promulgated on 29th. After the first surge of the epidemic was effectively controlled, the Hong Kong government had to promulgate the *Wearing Masks Regulations* on July 15 to curb the second surge of increasingly serious outbreaks in Hong Kong [15]. And on November 15th, further strict control measures were taken to compulsory quarantining for people who are suspected of having contracted the specified disease based on clinical judgment.

According to the development of the epidemic in Hong Kong and the time taken by various non-pharmaceutical interventions, the development of the epidemic is divided into three periods. The composition of patients, the severity of the epidemic and the duration of each period are different. The first phase is from January 23 to April 23, 2020, and the start time happens to be the day when Wuhan, Hubei is closed. Most of the confirmed patients at this period were imported cases. Under strict quarantine measures, there were only 25 cases of infection related to overseas import. The second period is from April 24 to September 27, which lasts longer and affects more people. At the same time, the blockade of cities in mainland China has been lifted, and the Hong Kong epidemic at this time has attracted much attention. The third stage is from September 28 to present (March 14, 2021), and it is currently in the third period of the development of the epidemic in Hong Kong. Future development trends and response measures are also the focus of this research (Table 1).

Table 1. Characteristics of COVID-19 cases in Hong Kong by epidemic period

Age, years	Period 1(Jan 23 to Apr 23; n = 1036) 35 (22–52)	Period 2(Apr 24 to Sep 27; n = 4030) 46 (30–61)
Age group, years		
0–14	29/1036 (2.8%)	288/4030 (7.2%)
15–34	485/1036 (46.8%)	964/4030 (23.9%)
35–64	441/1036 (42.6%)	2027/4030 (50.3%)
≥65	81/1036 (7.8%)	751/4030 (18.6%)
Sex		
Female	478/1036 (46.1%)	2079/4030 (51.6%)
Male	558/1036 (53.9%)	1951/4030 (48.4%)
Classification		
Input	615/1036 (59.4%)	647/4030 (16.1%)
Input dependent	25/1036 (2.4%)	6/4030 (0.1%)
Local	169/1036 (16.3%)	1292/4030 (32.1%)
Local dependent	227/1036 (21.9%)	2085/4030 (51.7%)
Death	3/1036 (0.48%)	103/4030 (2.56%)

According to the statistics of the first and second periods of Hong Kong in the chart, the epidemic in the second period is more serious than the first, and the total number of patients is nearly four times the total number of patients in the first period. Analyzing the age group of patients, the median age in the first period is 35 years old, and the median age in the second period rises to 46 years among them, the prevalence of young people is declining, and the prevalence of middle-aged and elderly patients has increased greatly. In the second period, the proportion of female patients surpassed that of male patients, but relative to the sex ratio of the total population of Hong Kong, the incidence of male patients was always higher than that of female patients. The classification of the source of patients in Hong Kong is very characteristic: the first surge of epidemics is dominated by imported cases, and due to timely quarantine measures, the number of patients related to imported cases is small, while the second surge of epidemics is dominated by local and related cases, accounting for the ratio exceeds 80%, indicating that Hong Kong's internal prevention and control measures are not rigorous enough.

Related research [16] fitted the mathematical model of the age structure to the case data from China, Italy, Japan, Singapore, Canada and South Korea to assess the age difference of patients. The conclusion is close to this article: with age, the risk of disease increases. Cases in California and Washington state show that men are at higher risk of disease than women [17]. The situation is similar in Hong Kong.

2.2 Disease Transmission Model

We developed an age-stratified stochastic model of disease transmission considering overseas input cases to simulate the spread of COVID-19 in Hong Kong, China. We divided the susceptible people into four groups according to their age. Because of the different range and ways of daily activities, the probability of contacting the infected people in different age groups is also different. Based on the SIR model, we use the data of the first and second periods as the training set, and use the exponential smoothing method to predict the contact rate of each age group in the third period. The contact rate of this period is added to the random dynamic model as a parameter to predict the development trend of the final epidemic situation. And the data of the third period (September 28, 2020 to March 14, 2021) as a testing set to evaluate the effectiveness of the model (Fig. 2).

Zhang J et al. analysed the contact investigation data in Wuhan, Shanghai and Hunan Province before and during the outbreak, during the social distancing period of COVID-19, daily contact has been reduced by 7 to 8 times [18], and the dynamic change of the provincial net reproduction number (Rt) is estimated [19]. The model assumes that the incubation period of the exposed person obeys the gamma distribution of $\mu = 5.1$ and $\sigma = 0.86$; the recovery period of the infected person obeys the gamma distribution of $\mu = 18.8$ and $\sigma = 0.0.54$ [20].

It is assumed that every susceptible individual of the same age group has an equal opportunity to contact the infected person. The exposure rate P_{coni} is defined as the probability that a susceptible person of age group i will come into contact with an infected person. Since infected persons can infect susceptible persons, we use the transmission rate P_{infi} to represent the probability that a susceptible person in the age group i will be infected after contact with an infected person. On this basis, this study assumes that $N(t)$

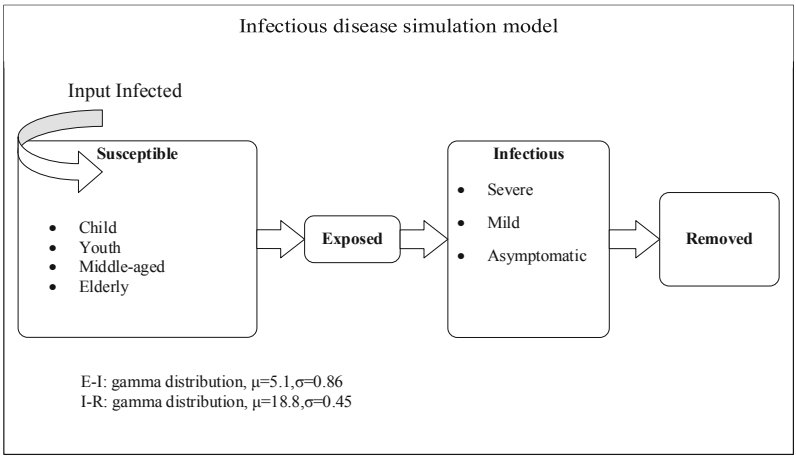

Fig. 2. Model structure of COVID-19 transmission

is the number of infected persons that susceptible persons of different ages can reach on day t. The value of i is 1–4, corresponding to different age groups. When the susceptible person is Child, $i = 1$, and when the susceptible person is Youth, Middle-aged, or Elderly, the corresponding values of i are 2, 3, and 4 respectively. Therefore, in this model, the probability of a susceptible person suffering from the disease is formula (1):

$$Pi = 1 - (1 - Pconi \times Pinfi)^{N}(t) \tag{1}$$

Since the patient has carried the infectious disease virus before being diagnosed and is exposed to the susceptible population. Suppose that a patient's contact time is 4 days, that is, from $(t - k)$ to $(t - 1)$ days are infectious. Then in formula (1), the value of the number of patients with transmissibility $N(t)$ on day t is given by formula (2):

$$N(t) = \sum_{i=1}^{k} \Delta I(t - i) \tag{2}$$

$\Delta I(t)$ is the patients diagnosed on day t, so the total number of infectious patients who can be contacted on day t is the total number of newly diagnosed patients in the past k days.

Assuming that any susceptible person has been in contact with patients, the probability of getting infected is $P_{infi} = 0.0275$ [18]. this research model estimates the probability that a susceptible person of age i will contact a patient based on the actual number of new patients every day P_{coni}, then use exponential smoothing method to fit the parameters and predict the contact rate of susceptible persons of different age groups in the future. It is assumed that the infected person is infectious at the time of symptoms and lasts until he is isolated for treatment and reported. Then according to the records of a total of 5066 cases in the first and second periods, the median time from the onset of symptoms to the isolation treatment of the patient is 4 days, so the model parameter k value is 4 (Table 2).

Table 2. Cost analysis model parameters (HKD). Cost estimates are from [19–27], as appropriate

Outcome category item	Child (0–14)	Youth (15–34)	Middle-aged (35–64)	Elderly (65+)
Outpatient visits				
Average no. visits per case [21, 23, 27]	1.54	1.54	1.54	1.54
Net payment per visit [22, 24, 26]	1554	1205	1205	1585
Average co-payment per visit [20, 23]	180	180	180	180
Net payment per prescription [22, 26]	12.1	17.3	17.3	17.3
Average co-payment per prescription [26]	15	15	15	15
Average prescriptions per visit [26]	0.9	1.8	1.8	1.4
Days lost [21, 26]	3	2	2	5
Value of one day lost [21, 22, 26]	156.9	784.5	836.8	104.6
Subtotal	**3,069.75**	**3,650.84**	**3,755.44**	**3,183.12**
Hospitalization				
Hospital costs [23–26]	10961	22361	23852	36140
Net payment per outpatient visit [23, 26]	2346	2982	3181	3234
Average co-payment for outpatient visit [20, 23]	180	180	180	180
Most likely no. of days lost [23, 27]	23	26	26	28
Value of one day lost [21, 22, 26]	156.9	784.5	836.8	104.6
Subtotal	**17,095.7**	**45,920.0**	**48,969.8**	**42,482.8**
Deaths				
Average age [21]	7	26	50	75
Present value of earnings lost [21]	17,222,400	13,027,200	5,520,000	2,208,000
Most likely hospital costs [26]	12824	28267	30151	43800
Subtotal	**17,235,224**	**13,055,467**	**5,550,151**	**2,251,800**
I'll but no medical care sought				
Days lost [21, 26]	3	2	2	5
Over-the-counter drugs [26]	80.3	80.3	80.3	80.3
Value of one day lost [21, 25, 26]	156.9	784.5	836.8	104.6
Subtotal	**551.0**	**1649.3**	**1753.9**	**603.3**
Staying at home				
Value of one day lost [21, 25, 26]	**156.9**	**784.5**	**836.8**	**104.6**

2.3 Economic Model

We evaluated the economic impact of multiple scenarios. In the baseline scenario, we used actual data from the Hong Kong epidemic to estimate the total cost associated with the pandemic. And we used the forecast results of the same period to calculate medical expenses to evaluate the economic cost of intervention measures such as isolation and quarantine and vaccination. The total cost of each intervention program is set as the sum of the medical expenses related to the disease and the indirect economic burden brought to the society by staying at home. Medical expenses related to illness, including outpatient visits, prescription and over-the-counter medications, and hospitalization. The indirect economic burden brought to society is related to the loss of absenteeism due to treatment and the value lost due to death. The calculation formula is: per capita gross national product × DALYs (disability adjusted life years) × productivity weight [25].

The cost calculation parameters in the economic model are different for different age groups [28]. Therefore, we divide the population into four age groups in the economic model: under 15 years old, 15–34 years old, 35–64 years old, and over 65 years old.

According to the *Gazette*, patients suffering from or suspected of suffering from diseases listed in the current *International Health Regulations* do not need to pay for hospitalization in accident and emergency departments or public wards, the cost of treatment of covid-19 virus pneumonia is borne by the Hong Kong government [25]. The Hong Kong COVID-19 vaccination plan was officially launched on February 26, 2021, and the Kelly ford vaccination was launched on February 26, 2021, the effective rate of the vaccine is 91.25% [20]. So far, no reports of serious side effects of the vaccine have been received. Therefore, this article does not consider the casualties and losses caused by the side effects of the vaccine. From the middle of 2019 to the middle of 2020, the government's health expenditure is HK $73.127 billion, accounting for 12% of the annual government expenditure [25]. These data will also be used as a reference for the economic model of this paper.

3 Results

3.1 Infectious Disease Model Prediction

The imported cases were separated from the data set of the second stage during model calibration, because in the first stage, the spread of the virus needs to be initiated by imported cases from abroad, and then strict quarantine and isolation measures were implemented for the immigrants in a timely manner. In addition, in the second stage of the 4030 cases, only 6 cases were related to importation, indicating that the probability of generally susceptible persons being exposed to overseas cases is extremely small. Therefore, this study assumes that susceptible people do not come into contact with imported patients from abroad. The number of imported patients from abroad was analysed using a time series model.

The picture shows the results of the parameter P_{coni} fitted by exponential smoothing. The left side of the baseline is the probability of the susceptible persons corresponding to each age group in the first period of contacting the patient, and correspondingly, the right side is the second period. The contact rate of children in the first period is extremely small,

but there is a substantial increase in the second period, and its changing trend is consistent with the total number of children in the two periods. On the contrary, the contact rate of the Elderly in the second period has decreased, but the proportion of the number of confirmed cases in the overall population has increased by 10.8%. The reason may be that their contact rate has been maintained at a high level for a long time in the second stage. The trends of youth and middle-aged people are similar to the fluctuations of the overall exposure rate. The effect of various epidemic prevention measures is analysed from the change trend of contact rate. *The Prohibition of Group Gathering Regulations* promulgated on March 29 have the greatest impact on the elderly. This result is similar to that in cities such as Wuhan and Shanghai [18]. There is almost no impact on children, it may be that the time of the epidemic occurs just before the children's holiday, and children have a fixed range of activities and are less likely to contact patients. From the results of the first and second periods and the epidemic prevention measures taken respectively, maintaining social distancing reduces the overall contact rate by about 30%, while wearing a mask has a better effect, which can be reduced by about 50%.

Figure 4 shows the results of the third period prediction. When no quarantine measures are taken, the total number of patients will still increase exponentially. The MAPE of the fitted data and the real data at this stage is 1.84%. In order to alleviate this growth trend, the Hong Kong government had to take further strict control measures on November 15 and compulsory testing for people suspected of having contracted the specified disease based on clinical judgment [20]. According to the experimental results, this measure reduces the total number of patients by 83.89% (MAPE is 2.03%). However, about 200 days after the start of the third phase, the epidemic will continue to develop rapidly again, which shows that the duration of the effect of non-drug intervention is limited. Studies have shown that looking for drugs or vaccines that can shorten the SARS-CoV-2 virus infection period can not only benefit the people receiving the drugs or vaccines, but may also reduce the spread among the wider population [28]. Based on the actual situation of the current Hong Kong epidemic situation and the analysis of the availability of medicines, the vaccination plan is urgent to permanently curb the further spread of the epidemic (Fig. 3).

3.2 Cost-Effectiveness of Vaccination

The world currently relies on social distancing and hygiene measures and re-used drugs, and the world is working hard to develop an effective vaccine against COVID-19 [16]. At present, there are many vaccines produced in different regions on the market, and the US Food and Drug Administration (FDA) requires 50%. Among them, the BNT162b2 vaccine jointly developed by Fosun Pharma, Pfizer and BioNTech provides 95% protection for people over the age of 16 [29], which is different from the comprehensive effective rate of 90% in news reports. The Hong Kong COVID-19 vaccination plan was officially launched on February 26, 2021, and the Kelly ford vaccine began on the same day [20]. In order to simplify the process of vaccine effectiveness simulation and to be more in line with the trend of popular choice, the effective probability of the vaccine in this research model is calculated based on the effectiveness of the Kelly ford vaccine at 91.25%, and the two-dose vaccine is priced at 37$ [13]. In the data experiment, we set an early or delayed vaccination start time based on the actual vaccination time on February

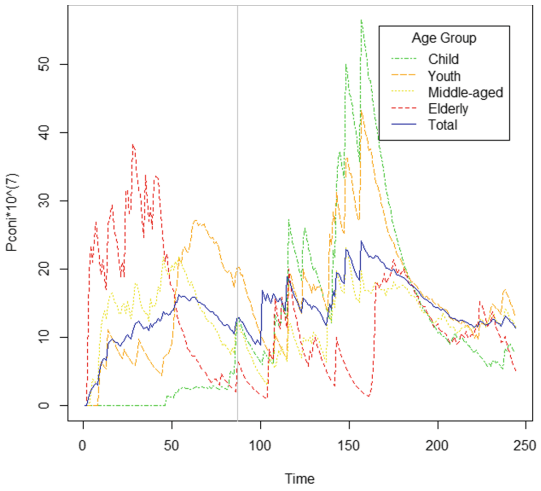

Fig. 3. P_{coni} of susceptible in different age group

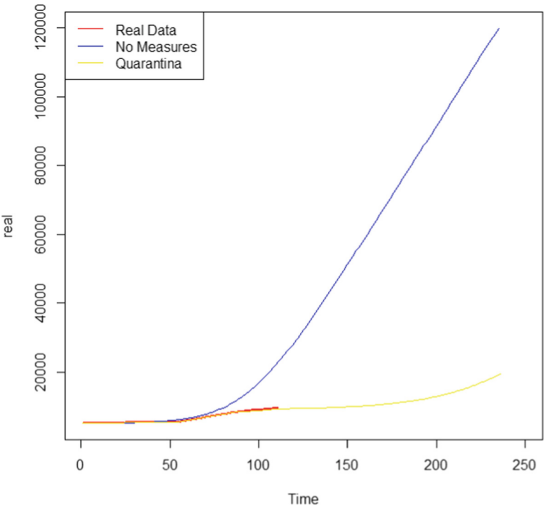

Fig. 4. Model prediction result

26, and simulated the difference in coverage of different vaccination. The study was simulated for a total of 125 days, and the prediction results were as of May 19, 2021, and the average value was taken after each experiment was performed 20 times.

From the experimental results of the data in Fig. 5, it can be seen that vaccination with maximum coverage in a limited time can greatly reduce the number of people infected with COVID-19. Compared with no vaccination, the best effect can be reduced by 50.64% by May 19, 2021. Cases. Similar to the effect of influenza vaccination, including influenza vaccination for children, the elderly and high-risk groups into the

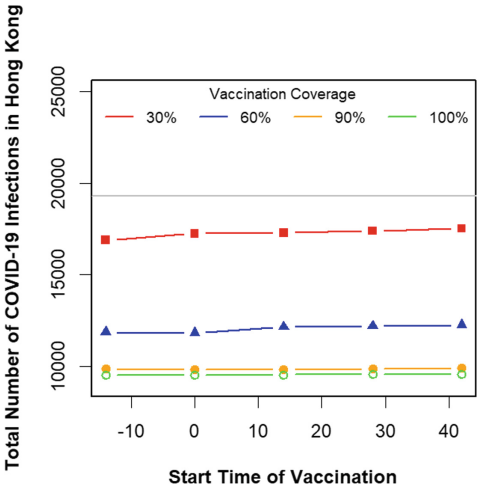

Fig. 5. Vaccination strategy

national vaccination plan can greatly reduce the morbidity and mortality of influenza at the population level [30]. However, the actual situation may be difficult to achieve the vaccination target of full population coverage in a short period of time. Analyzing vaccine coverage and vaccination time, a 90% vaccination rate can greatly reduce the total number of patients, and the analysis of the vaccination time span of this article is two months, the vaccination time is not obvious to the overall immune effect, so sufficient vaccine inventory is required. In addition, managers need to fully mobilize the enthusiasm of the masses to vaccinate, and achieve a greater coverage of vaccination in a shorter period of time as possible.

The Table 3 shows the economic costs of treating patients in each age group. Based on the random model, combined with vaccination strategies, this section analyzes the economic benefits of vaccination. According to the real data released by the Hong Kong Department of Health, 29.1% of the confirmed patients are mild patients who do not need to be hospitalized. From the results of the cost-benefit analysis of vaccines, it can be concluded that a 90% vaccination coverage rate can be achieved within a limited period of time.

4 Conclusion

This study divides the development of the Hong Kong epidemic into three periods. Based on the characteristics of the three periods, an individual-based random simulation model of the spread of infectious diseases is established. The exponential smoothing method is used to estimate the parameters of the contact rate of individuals in each age group with COVID-19 patients, and the simulation model is combined with the estimated results of this parameter to predict the development trend of the epidemic after different intervention methods are adopted in the third stage. Finally, it analyses the effect of quarantine measures adopted in Hong Kong on the reduction of the number of patients,

Table 3. Cost-effectiveness of vaccination

Measures	The Number of infected	Medical cost	Social cost	Total cost	Reduced cost
Baseline	119854	563.206	7216.325	7779.531	
0% coverage	19309	90.735	1162.581	1253.316	
30% coverage	17247	148.612	1038.430	1187.042	5.29%
60% coverage	11822	329.648	811.794	1141.442	8.93%
90% coverage	9830	526.816	591.857	**1118.673**	**10.74%**
100% coverage	9531	594.254	573.855	1168.109	6.80%

Cost unit: 10 million (HKD)

and the economic benefits of different vaccination strategies. The experimental results show that the series of quarantine measures adopted by Hong Kong can effectively control the epidemic and buy precious time for the development and vaccination of the COVID-19 vaccine. If these measures can be taken in time and strictly implemented, the total number of infected persons will be reduced by 83.89% in the third stage. Achieving a vaccination coverage rate of 90% of the population within a limited period of time can effectively control the epidemic and is cost-effective, while a low coverage vaccination strategy has no obvious effect.

It is demonstrated that non drug intervention and vaccine strategy are the most important measures to control the epidemic, which can reduce the number of patients and have economic efficiency at the same time. If the non-interventionist group immunization method is adopted, the country will bear a considerable burden [31]. There are still some limitations. First of all, the random model of disease transmission proposed in this study is only used to predict Hong Kong, which may be affected by the climate, and the model has not been used to predict other countries/regions. COVID-19 is less prevalent in countries close to the equator, where temperatures and humidity tend to be higher [32]. Secondly, the stochastic model does not subdivide contact scenarios, such as blocking small areas, and setting thresholds to turn on or off interventions may be a more effective and acceptable control strategy [16]. The transmission ability of patients before and after symptoms was not considered [4]. The economic burden of COVID-19 is enormous, with broader social and economic implications - for example, pain and suffering, loss of human capital (loss of labor) and loss of physical capital (transfer of savings) [31]. Therefore, in the future research, we will improve the model and deeply study the impact of the epidemic on the overall social economy.

References

1. Ge, H., Wang, X., Yuan, X.: The epidemiology and clinical information about COVID-19. Eur. J. Clin. Microbiol. **15**(6), 1011–1019 (2020)
2. Rodriguez-Morales, A.J., Cardona-Ospina, J.A., Gutiérrez-Ocampo, E., et al.: Clinical, laboratory and imaging features of COVID-19: A systematic review and meta-analysis. Travel Med. Infect. Dis. **34**(Mar-Apr), 101623 (2020)

3. Teslya, A., Pham, T.M., Godijk, N.G., et al.: Impact of self-imposed prevention measures and short-term government-imposed social distancing on mitigating and delaying a COVID-19 epidemic: a modelling study. PLoS Med. **17**(7), e1003166 (2020)
4. Chen, S., Chen, Q., Yang, J., et al.: Curbing the COVID-19 pandemic with facility-based isolation of mild cases: a mathematical modeling study. J. Travel Med. **28**(2), taaa226 (2020)
5. Ngonghala, C.N., Iboi, E., Eikenberry, S., et al.: Mathematical assessment of the impact of non-pharmaceutical interventions on curtailing the 2019 novel Coronavirus. Math. Biosci. **325**, 108364 (2020)
6. Chen, S., Chen, Q., Yang, W., et al.: Buying time for an effective epidemic response: the impact of a public holiday for outbreak control on COVID-19 epidemic spread. Engineering **6**(10), 1108–1114 (2020)
7. Simiao, C., Zongjiu, Z., Juntao, Y., et al.: Fangcang shelter hospitals: a novel concept for responding to public health emergencies. Lancet (London, England) **395**(10232), 1305–1304 (2020)
8. Chen, S., Yang, J., Yang, W., et al.: COVID-19 control in China during mass population movements at New Year. The Lancet **395**(10232), 764–766 (2020)
9. Kuzdeuov, A., Baimukashev, D., Karabay, A., et al.: A network-based stochastic epidemic simulator: controlling COVID-19 with region-specific policies. IEEE J. Biomed. Health Inform. **24**, 2743–2754 (2020)
10. Yu, F., Geldsetzer, P., Meierkord, A., et al.: Knowledge about coronavirus disease 2019 among adults in China: cross-sectional online survey (Preprint). Journal of Medical Internet Research (2021)
11. Davies, N.G., Klepac, P., Liu, Y., et al.: Age-dependent effects in the transmission and control of COVID-19 epidemics. Nat. Med. **26**(8), S13 (2020)
12. Bartsch, S.M., Ferguson, M.C., et al.: The potential health care costs and resource use associated with COVID-19 in the United States. Health Aff. **39**(6), 927–935 (2020)
13. Martonosi, S.E., Behzad, B., Cummings, K.: Pricing the COVID-19 vaccine: a mathematical approach. Omega **103**, 102451 (2021)
14. Hu, Y., Chen, S.: What can we learn from COVID-19 vaccine R&D in China? A discussion from a public policy perspective. J. Travel Med. **28**(4), taab026 (2021)
15. https://www.covidvaccine.gov.hk/zh-CN/dashboard/referenceData/
16. Sharma, O., Sultan, A.A., Ding, H., et al.: A review of the progress and challenges of developing a vaccine for COVID-19. Front. Immunol. **11**, 585354 (2020)
17. Lewnard, J.A., Liu, V.X., Jackson, M.L., et al.: Incidence, clinical outcomes, and transmission dynamics of severe coronavirus disease 2019 in California and Washington: prospective cohort study. BMJ, **369**, m1923 (2020)
18. Zhang, J., Litvinova, M., Liang, Y., et al.: Changes in contact patterns shape the dynamics of the COVID-19 outbreak in China. Science **368**(6498), eabb8001 (2020)
19. Zhang, J., Litvinova, M., Wang, W., et al.: Evolving epidemiology and transmission dynamics of coronavirus disease 2019 outside Hubei province, China: a descriptive and modelling study. Lancet Infect. Dis. **20**, 793–802 (2020)
20. Flaxman, S., Mishra, S., Gandy, A., et al.: Report 13: estimating the number of infections and the impact of non-pharmaceutical interventions on COVID-19 in 11 European countries (2020)
21. Andradóttir, S., Chiu, W., Goldsman, D., et al.: Reactive strategies for containing developing outbreaks of pandemic influenza. BMC Public Health **11**(Suppl 1), S1 (2011)
22. https://www.ha.org.hk/visitor/ha_visitor_index.asp?Content_ID=10045&Lang=CHIB5&Dimension=100/
23. https://www3.ha.org.hk/Data/DCL/ProjectDataCatalogue/
24. https://www.censtatd.gov.hk/sc/EIndexbySubject.html?scode=460&pcode=B1010003/

25. http://www.stats.gov.cn/tjsj/ndsj/2020/indexch.htm/
26. Wong, S.Y., Goldsman, D., Tsui, K.L.: Economic evaluation of individual school closure strategies: The Hong Kong 2009 H1N1 pandemic. PLoS One, **11**, e0147052 (2015)
27. Yu, B., Xu, Q., Liu, Z., et al.: Methodological research on the economic burden of emerging infectious diseases. Health Econ. Res. **7**, 25–29 (2017)
28. Boer, P., Mmath, L.N., Dolk, F., et al.: Cost-effectiveness of pediatric influenza vaccination in The Netherlands. Value Health **24**(1), 19–31 (2021)
29. Polack, F.P., Thomas, S.J., Kitchin, N., et al.: Safety and efficacy of the BNT162b2 mRNA Covid-19 vaccine. N. Engl. J. Med. **383**(27), 2603–2615 (2020)
30. Tuite, A.R., Fisman, D.N., Greer, A.L.: Mathematical modeling of COVID-19 transmission and mitigation strategies in the population of Ontario, Canada (2020)
31. Chen, S., Prettner, K., Kuhn, M., et al.: The economic burden of COVID-19 in the United States: Estimates and projections under an infection-based herd immunity approach. J. Econ. Ageing **20**(10), 100328 (2021)
32. Chen, S., Prettner, K., Kuhn, M., et al.: Climate and the spread of COVID-19. Sci. Rep. **11**(1), 9042 (2021)

Crowdsourcing Electrified Mobility for Omni-Sharing Distributed Energy Resources

Wenqing Ai[1], Tianhu Deng[1(✉)], and Wei Qi[2]

[1] Department of Industrial Engineering, Tsinghua University, Beijing, Beijing 100084, China
deng13@mail.tsinghua.edu.cn
[2] Desautels Faculty of Management, McGill University, Montreal, QC 31G5, Canada

Abstract. Ever-increasing coupling of energy and mobility sectors is underway in our cities, but whether and how to utilize such coupling to optimize the portfolio of urban energy assets has rarely been studied. A large amount of energy storage, an important energy asset of distributed energy resources (DERs), is not only costly but harmful to the environment. Improving efficiency and reducing redundancy of storage is imperative to the development of smart energy. We fill this gap by studying an omni energy sharing paradigm, which is a novel business model of crowdsourcing energy from the ride-sharing market into a local DER community. We formulate the omni energy sharing problem as a two-stage model including external and internal sharing. The external sharing model proposes the optimal energy payment scheme to obtain energy supply from crowdsourcing shared electric vehicles (CSEVs). Then, the internal sharing model designs the cost allocation rules to ensure the stability of the grand coalition between prosumers holding storage in the same DER community. As the existing analytical allocation rules are not suitable for the omni sharing problem and other methods are computationally intensive for a large-scale problem, we build scalable allocation rules and identify conditions to enable energy demand distributions within a community. Our major finding is that the omni-sharing strategy dominates the peer-to-peer energy sharing model by reducing both daily energy operating cost and total storage. We also uncover that omni energy sharing generates more synergy effects than competition effects for the ride-sharing market. From a wider perspective, this paper deepens our knowledge about the mobility-energy orchestration in future smart cities.

Keywords: Omni energy sharing · Crowdsourcing · Electrified mobility · Distributed energy resources · Cost allocation

1 Introduction

Urban energy around the world is shifting from a traditional model to a lower-carbon, cost-effective and localized system. Distributed energy resources (DERs) are one of the most rapidly growing parts of this transformation. The DER refers to any generator of renewable energy or any electric energy-storage resource that resides on the end user's side of the electric meter, such as solar photovoltaic (PV), small wind turbines, electric vehicles (EVs), etc. An electricity end user which installs at least one of DERs is a local

R. Qiu et al. (Eds.): ICSS 2021, LNOR, pp. 365–382, 2021.
https://doi.org/10.1007/978-3-030-90275-9_29

clean energy "prosumer." Multiple local prosumers compose a DER community, such as business, residual, and industrial districts. The annual growth of the DER market is double digits over the last few years. Until now, the electricity generated by solar PV satisfies up to 48% of the country's demand at midday in Australia in [1]. To withstand the inherent intermittency of renewable energy that might trigger a massive rotating blackout, prosumers have to install energy storage assets on a large scale and share storage within the DER community such as peer-to-peer energy storage sharing (P2P energy sharing). As an "uberization" of energy, the P2P energy sharing model establishes a local trading within the DER community, where each prosumer with an energy deficit is able to directly buy stored energy from her neighbors at a price which is not greater than the external price.

However, the heavy storage asset has become a stumbling block to the expansion of DERs. Specifically, the DER community with P2P energy sharing still has to install a large amount of storage that meets random energy demand in peak price periods but is redundant during off-peak price periods. Breaking out one day into peak and off-peak price periods is one of the most common pricing policies of grids, namely the time-of-use (TOU) pricing. In 2021, over 20 million residential customers default TOU pricing in California in [2]. Consequently, there are two non-negligible challenges. (1) Such heavy investment in the DER community brings serious financial risks for both companies and governments in the short term. Yeloha, a P2P solar power sharing company, went bankrupt due to a lack of financing in 2016. California sets a $200 million budget for DER projects, but it does not go far enough in [3]. (2) The extensive discharge of toxic metals from degraded storage into the environment causes serious and irreversible pollution in the long term. In 2020, the toxic lead pollution from a battery recycling plant in Senegal contaminated the nearby soil and caused the deaths of 18 children in [4].

From the perspective of optimizing the asset structure of the DER community, we design and analyze omni energy sharing. The omni energy sharing mode includes the internal energy sharing mode, like P2P energy sharing, and the external energy sharing mode, which crowdsources energy from ride-sharing electric vehicles to the DER community. Crowdsourcing shared electric vehicles (CSEVs) as mobile storage assets have the potential for substituting stationary storage. Following the trend of the rapid expansion of electric vehicles, both Uber and Lyft plan to transition 100% of their shared fleet to EVs by 2030 in [5]. In particular, more than 80% Uber drivers are part-time and prefer self-scheduling in [6]. According to the U.S. Energy Information Administration [7], the average household consumption is about 30 kWh per day, which is only one-half of the battery capacity of Nissan LEAF. Doing so is a lucrative business mode for the DER community. Crowdsourcing can transform an asset-heavy company to be asset-light through effectively exploring external potential resources. In practice, urban delivery services, such as Amazon Flex and Uber Eats, engage crowdsourcing ride-sharing mobility to meet their delivery demand.

The goal of this paper is to evaluate whether and how to utilize electric ride-sharing mobility to reduce the dependence of prosumers on stationary storage in peak periods. We assume that each prosumer aims to minimize her/his own daily operating costs in the presence of uncertain energy demand. We formulate the omni energy sharing process as a two-stage model including the model of internal sharing within a DER community and

the model of external sharing between a DER community and surrounding CSEVs, as shown in Fig. 1. The internal sharing model aims to create a cost allocation rule to ensure that all prosumers stably participate in omni energy sharing without any collusion. If prosumers' total storage cannot meet their total energy demand, then the DER community will buy external energy from nearby CSEVs and grids. Meanwhile, CSEV drivers will serve either the ride-sharing market or the energy sharing market, whichever is more profitable. The external sharing model designs the optimal payment scheme consisting of the amount of energy committed by CSEVs and the associated price. If prosumers' total energy demand still cannot be satisfied, the community will purchase grid energy at a peak price. Finally, all prosumers bear their own allocated daily operating cost according to the short-term or long-term agreements.

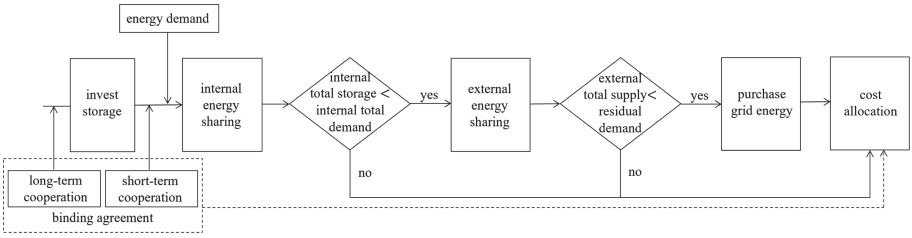

Fig. 1. Omni energy sharing process

The contributions of this paper are composed of four aspects: (1) This work is an initial attempt to design the analytical energy sharing model that features the energy supply from the ride-sharing market to a local DER community. Previous literature considers the modes of crowdsourcing delivery from the ride-sharing market and sharing energy from a fleet of electric vehicles. By comparison, this paper focuses on crowdsourcing electricity from the ride-sharing market, which was largely overlooked by the literature on mobility-energy orchestration. (2) Our major finding is that the omni energy sharing model always outperforms the P2P energy sharing model. For a whole DER community, omni energy sharing saves more daily energy operating costs while reducing storage requirements, even if gradually declining storage costs weaken the advantages of omni energy sharing in storage structures and operating costs. (3) Another major finding is that omni energy sharing creates a win-win situation for ride-sharing and energy markets. For ride-sharing markets, there are four major participants, such as passengers, ride-sharing platforms, drivers, and governments. Omni energy sharing have synergy effects on drivers and governments, which dominates the competition effects on passengers and ride-sharing markets. Especially, such domination is obvious in the low-income ride-sharing markets. For energy markets, the residual demand of the DER community in area with few drivers can still be met since omni energy sharing promotes the total number of CSEVs drivers. As the driver's income increases, omni energy sharing's implications for such two markets gradually disappear due to the reduction of energy shared by CSEVs that the DER community is willing to buy. (4) The theoretical contribution of this paper is that we develop a cost allocation rule which is applicable to cooperation among any number of prosumers in omni energy sharing. Common methods, such as

linear programming with several constraints, for obtaining cost allocation rules are too computationally intensive to solve large-scale problems. The existing scalable cost allocation rules in [8] are suitable to P2P energy sharing rather than omni energy sharing. Our rule ensures the stable grand coalition among all prosumers in the DER community when the ratio of maximum to minimum expected energy demand of a single prosumer is not greater than the ratio of mean square root of covariance of a prosumer's energy demand in any subcoalitions to the grand coalition.

2 Literature Review

As a classical mobility-energy synergy, Vehicle-to-Grid (V2G) enables electric vehicles to discharge back to the grid through bidirectional charging stations. The V2G literature considering electric vehicle operations can be divided into two parts. One group of literature studies operations of the V2G system from the perspective of maximizing social welfare. Qi et al. [9] address the dispatch problem of a shared autonomous electric fleet to satisfy mobility demands and support for the local microgrid. Zhang et al. [10] formulate a two-stage stochastic integer program to optimize the service regions planning and fleet operations of electric vehicle sharing at the same time. They consider these electric vehicles as a unified fleet instead of self-interested human beings. Another stream of literature is from the perspective of an agent. Broneske and Wozabal [11] evaluate the influence of parameters in the electric vehicle discharging contraction the revenue of an aggregator. The existing V2G research ignores the application of CSEVs in assisting urban energy. In contrast, we complement these papers by quantifying the potential of the omni energy sharing business model, where an agent can gain energy from ride-sharing drivers.

The CSEVs considered in our paper relates to the operations management literature on crowdsourcing business model. Within the crowdsourcing management research stream a small but growing body of work on crowdsourcing ride-sharing mobility into the parcel delivery problem has emerged. Several studies provide the analytical solutions that are more relevant to our study. For example, Qi et al. [12] develop the analytical framework to design and analyze the large-scale adoption of crowdsourcing shared vehicles. The authors build the wage response model to additionally compensate drivers for delivery service. We extend such wage response model and provide the optimal payment scheme for electric ride-sharing drivers to maximize the agent's profit. Both Wu et al. [13] and Lin et al. [14] also design the optimal pricing scheme to each driver but they focus on charging rather than discharging. Fatehi and Wagner [15] additionally consider an on-time delivery based on a robust crowdsourcing optimization model. Different from crowdsourced deliveries, we develop an analytical model to explore how to crowdsource energy from ride-sharing electric vehicle drivers.

Our paper is also related to the literature on renewable energy storage operations under sharing economy, such as P2P energy storage sharing. Kalathilet al. [16] formulate the energy storage sharing as a classical Newsvendor model and find an equilibrium solution in a non-cooperative game. Chakraborty et al. [8] also use the classical Newsvendor model but describe the P2P energy storage sharing system as a cooperative game. The authors design the scalable cost allocation rules to maintain the stable grand coalition.

Kiedanski et al. [17] explore the stylized cooperative model by considering the realistic factors that affect the utility of the system such as ramp constraints of storage. Collectively, existing papers only focus on the energy sharing among stationary DERs, namely internal energy sharing which has a limited impact on optimizing storage asset structure. In contrast, omni energy sharing diversifies the source of energy by crowdsourcing external mobile energy to improve the DER community becoming asset-light.

3 External Energy Sharing

3.1 Individual Rational Payment

A rational CSEV driver is willing to share residual energy to the DER community only if the profit from payment for residual energy is at least no lower than ride-sharing. We assume that all CSEVs are homogeneous. In other words, the individually rational payment is based on a CSEV driver's expected wage from ride-sharing.

Expected Profit from Ride-Sharing. A CSEV driver's expected profit from ride-sharing is the difference between the income from carrying passengers and the cost during ride-sharing. When carrying a passenger, the driver receives payments from the ride-sharing platform whose commission rate is η^p. We assume that the ride fare of most ride-sharing platforms, such as Uber and Lyft, are composed of base fare w^b, per-mile fare, and per-minute fare. Set w^m as the fare per minute which includes both a per-mile fare and a per-minute fare since we assume that the driving time is proportional to the travel distance and the average speed is s. For a t'-minute ride, the driver's income is $(1-\eta^p)\cdot(w^b+w^m t')$.

Whether a driver is carrying or waiting for passengers, the driver has to shoulder the operating cost consisting of electricity and labor costs. We set the electricity loads per minute of carrying and waiting for passengers as l^r and l^w ($l^r \geq l^w$), respectively. The driver's labor costs per minute of carrying and waiting are c^r and c^w ($c^r \geq c^w$), respectively. We assume that drivers fully charge their batteries only once a day in an off-peak period (e.g. midnight) at λ^L dollars per kWh, since per charge range of electric vehicles has exceeded the trip length of the ride-sharing driver per day in [18]. Thus, the carrying cost per minute is $\lambda^L l^r + c^r$, and the waiting cost per minute is $\lambda^L l^w + c^w$.

We assume both carrying and waiting time are exponentially distributed with means $1/v$ and $1/\mu$, respectively. For any riding time t, the expected profit that a CSEV driver earns from ride-sharing is expressed as

$$\prod^R(t) = (\phi-\varphi)\cdot[\mu v\cdot t+\mu^2(1-\exp(-(\mu+v)t))/(\mu+v)]/(\mu+v), \quad (1)$$

where we define the profit in a carrying process as $\phi = (1-\eta^p)(w^b+w^m/v)-(\lambda^L l^r + c^r)/v$ and the cost in a waiting process as $\varphi = (\lambda^L l^w + c^w)/\mu$. In Eq. (1), $\prod^R(t)$ is the product of a driver's expected profit in a cycle of carrying and waiting for a passenger, $\phi-\varphi$, and the expected number of complete cycles up to time t, $[\mu v\cdot t+\mu^2(1-\exp(-(\mu+v)t))/(\mu+v)]/(\mu+v)$. The proof of Eq. (1) is available in the online appendix. Similarly, the expected electricity loads of the CSEV from ride-sharing during time t can be expressed as $L(t) = (\phi^\tau+\varphi^\tau)\cdot\mu[vt+\mu(1-\exp(-(\mu+v)t))]/(\mu+v)$,

where $\phi^{\tau} = l^{r}/v$ denotes the expected loads per order, and $\varphi^{\tau} = l^{w}/\mu$ means the expected loads while waiting for a passenger.

Expected Profit from Energy Sharing

The individually rational payment (denoted by $\Lambda^{E}(t, r)$) to a driver should ensure that the driver's expected profit from sharing energy is no smaller than the expected profit (denoted by $\prod^{R}(t)$) from sharing rides. The driver's expected profit from sharing energy is the difference between the energy payment by the DER community and the operating costs consisting of electricity and labor costs. We assume all prosumers to be located at the same point due to their spatial adjacency so that the distances r from a CSEV driver to all prosumers are the same. Thus, the individually rational payment to a driver with residual energy $L(t)$ kWh and the distance r miles is

$$\Lambda^{E}(t, r) = \lambda^{L} L(t) + c^{w} r/s + \eta^{d} \prod^{R}(t), \tag{2}$$

In Eq. (2), the individually rational payment covers the driver's operating costs, $\lambda^{L} L(t) + c^{w} r/s$, and the driver's minimum expected profit from sharing energy, $\eta^{d} \prod^{R}(t)$. In the former, $\lambda^{L} L(t)$ is the cost of discharging all the residual electricity and $c^{w} r/s$ is the labor cost of moving to the DER community from the current location. In the latter, we assume that the driver's profit of energy sharing should be no less than $\eta^{d} \prod^{R}(t)$. The discount factor $\eta^{d} > 1$ captures the additional disutility shouldered by the driver because of faster battery degradation when engaged in energy sharing services.

3.2 Uniform Payment

The individually rational payment $\Lambda^{E}(t, r)$ varies by a driver's residual riding time t and distance r. However, such a payment scheme creates price discrimination among drivers, and may thus cause a bad press or even be prohibited under competition law. Hence, a uniform energy payment scheme which is independent from t and r is more implementable than $\Lambda^{E}(t, r)$ in omni energy sharing.

The DER community proposes the uniform unit payment price based on its remaining energy demand that cannot be satisfied by internal energy sharing. Therefore, the key problem of designing the uniform payment scheme is to find how the expected total amount of energy that drivers are willing to share, denoted by $G(\lambda)$, depends on the offer by the DER community, denoted by λ dollars per kWh (we then will optimize λ in Sect. 3.3). We assume each driver's residual time of ride-sharing t and distance to the DER community r are independent and identically distributed (i.i.d) continuous random variables with known probability density functions, $f_t(t)$ and $f_r(r)$, respectively. Then $G(\lambda)$ is given by the following equation:

$$G(\lambda) = \int_{0}^{T} \int_{0}^{R(t,\lambda)} (L(t) - l^{w} r/s) f_t(t) f_r(r) dt dr. \tag{3}$$

In Eq. (3), $G(\lambda)$ is a double integral of an amount of energy shared by a CSEV over $[0, T] \times [0, R(t, \lambda)]$. For a driver with residual energy $L(t)$ and distances r, an amount of

energy shared to the DER community is $L(t)-l^w r/s$, where $l^w r/s$ is energy consumed by driving from the CSEV driver's current location to the DER community. Define \$T\$ as the length of ride-sharing time when a CSEV battery is full. The residual ride-sharing time t ranges from 0 to T. Define $R(t, \lambda)$ as the largest distance that a CSEV driver with residual energy $L(t)$ is willing to share energy for a given uniform energy payment λ. The distance from a DER community r ranges from 0 to $R(t, \lambda)$. We derive $R(t, \lambda)$ in Proposition 1 based on the individually rational condition, i.e. $\lambda \cdot (L(t) - l^w r/s) \geq \Lambda^E(t, r)$.

Proposition 1 *(Largest distance function). The largest distance that a CSEV driver is willing to overcome to share energy to the DER community is*

$$R(t, \lambda) = \prod^R(t) \cdot [(\lambda - \lambda^L)(\phi^\tau + \varphi^\tau)/(\phi - \varphi) - \eta^d]/[(\lambda l^w + c^w)/s] \quad (4)$$

which is a monotonically increasing concave function of a uniform energy payment λ.

In Eq. (4), the largest distance $R(t, \lambda)$ is determined by three factors: (1) the numerator, $(\lambda - \lambda^L)(\phi^\tau + \varphi^\tau)/(\phi - \varphi) - \eta^d$, represents the additional yield from sharing energy relative to ride-sharing. (2) The denominator, $(\lambda l^w + c^w)/s$, represents the compensation cost per mile. (3) The product of the numerator and the driver's expected profit from ride-sharing $\prod^R(t)$ denotes the total additional return of the driver with residual energy $L(t)$ under a given uniform energy payment λ. Given the above construction of $G(\lambda)$, we next provide the optimal payment scheme based on the uniform payment scheme in the next subsection.

3.3 Optimal Payment

The optimal payment scheme aims to minimize the cost of making up for the DER community's residual energy demand $\overline{h}$ that cannot be met by internal energy sharing. The key to designing the optimal payment scheme is to decide the amount of energy h that the DER community is willing to buy from CSEVs. Set $G^{-1}(h)$ as the uniform payment scheme which is the inverse function defined by Eq. (3). The DER community's total cost of purchasing external energy includes the total uniform energy payment for CSEVs, i.e. $h \cdot G^{-1}(h)$, and the total cost of purchasing peak electricity from the external grid, i.e. $\lambda^H \cdot (\overline{h} - h)$.

The optimal amount of energy h depends on the shape of the uniform payment scheme $G^{-1}(h)$ in Proposition 2.

Proposition 2. *The inverse function $G^{-1}(h)$ is monotonically increasing with the amount of energy that the DER community is willing to buy h.*

In Proposition 2, the monotonically increasing function $G^{-1}(h)$ indicates that the DER community's marginal cost of total energy payment to CSEVs, $d(h \cdot G^{-1}(h))/dh$, increases with h. In other words, the DER community prefers to buy energy from CSEVs to meet all its residual demand $\overline{h}$ when $\overline{h}$ does not exceed $\hat{h}$, which is the solution to

$$d(h \cdot G^{-1}(h))/dh = \lambda^H, \quad (5)$$

Equation (5) implies $\hat{h}$ is the maximum amount of energy h so that the marginal cost of total energy payment to CSEVs equals the marginal cost of purchasing peak electricity

from the external grid. Hence, we let h^* be the optimal amount of energy h, which is shown as $h^* = \min\{\hat{h}, \bar{h}\}$.

We build the optimal payment scheme $\Lambda^*(\bar{h})$ as a piecewise nonlinear function of the DER community's total residual energy demand h, which is shown as

$$\Lambda^*(h) = G^{-1}(h^*). \tag{6}$$

Equation (6) shows that the optimal payment scheme $\Lambda^*(\bar{h})$ is composed of two pieces. If $\bar{h} \leq \hat{h}$, the DER community purchase external energy only from CSEVs with the optimal energy payment $G^{-1}(\bar{h})$. If $\bar{h} > \hat{h}$, the DER community purchases the maximum amount of energy $\hat{h}$ from CSEVs with the constant maximum uniform energy payment $G^{-1}(\hat{h})$ and purchases an amount of energy $\bar{h} - \hat{h}$ from the grid with the peak price λ^H.

3.4 Interplay with the Ride-Share Market

Both the external energy sharing system and the ride-sharing system are dynamically self-regulating and interacting with each other. For external energy sharing, according to Eqs. (1)–(6), the DER community's optimal payment scheme is dependent on the ride-sharing market's parameters. For ride-sharing, whether a CSEV driver chooses energy sharing instead of ride-sharing is affected by the optimal energy payment scheme. Thus, CSEV drivers' behaviors influence the ride-sharing market's parameters. For instance, if more CSEV drivers choose sharing energy over sharing rides, then the mean driver idling time in the ride-sharing market will become smaller. To distinguish between the ride-sharing market's states with and without omni energy sharing, hereafter we define them as the initial state and the new state, respectively.

To identify the new state for the DER community, we endogenize $f_r(r)$ and μ in this subsection. Specifically, $f_r(r)$ is the number of CSEV drivers whose distance to the DER community is r. The value of $f_r(r)$ positively depends on a CSEV driver's expected profit of ride-sharing $\pi^R = \mathrm{E}[\prod^R(t)]$, where $\prod^R(t)$ is defined by Eq. (1). We let $f_r(r)$ be the endogenous function of π^R as follows:

$$f_r(r; \pi^R) = f_r(r) \cdot F_r^{\pi}(\pi^R), \tag{7}$$

where $f_r(r)$ is the potential pool size of CSEVs whose distance to the DER community is r and $F_r^{\pi}(\pi^R)$ is a non-decreasing continuous function, which satisfies $\lim_{\pi^R \to 0^+} F_r^{\pi}(\pi^R) = 0$ and $\lim_{\pi^R \to +\infty} F_r^{\pi}(\pi^R) = 1$. We assume that both $f_r(r)$ and a function $F_r^{\pi}(\pi^R)$ are given.

Parameter μ is the ride-share service request rate that each CSEV driver faces. The value of μ is determined by the number of available drivers n_a, i.e. the CSEV drivers who continue to share rides rather than share energy. We assume that the expected passenger ride requirements per hour n_p is an exogenous parameter and estimated by real data. Therefore, μ is the endogenous function of n_a as follows:

$$\mu(n_a) = n_p / n_a, \tag{8}$$

where $n_a = n_d - n_h$, i.e. n_a equals the difference between the number of total CSEV drivers n_d and the number of energy sharing CSEV drivers n_h in a certain area.

The new state is represented by the equilibrium solution of two endogenous functions (7) and (8). In Eq. (7), the density of CSEV drivers $f_r(r; \pi^R)$ depends on $\mu(n_a)$ since a ride-sharing driver's expected profit π^R increases with $\mu(n_a)$ according to Eq. (1). In Eq. (8), the ride-share service request rate $\mu(n_a)$ in turn depends on $f_r(r; \pi^R)$ since the number of available CSEVs $n_a = n_d - n_h$ is a function of $f_r(r; \pi^R)$. We will solve two endogenous functions (7) and (8) to obtain the new state in Sect. 5. Based on the known optimal energy payment scheme, we introduce internal energy sharing within the DER community in the next section.

3.5 Centralized Power Grid Profits

The centralized power grid, as the main external energy, has to stably transmit energy to the distant DER communities when the DER communities' residual energy demand cannot be met locally in peak periods. An amount of energy $\tilde{h}$ that the centralized power grid needs to transmit to the DER communities is a random variable which affects the expected profits of the centralized power grid. The power system reliability level ρ is one of the most important decision variables for the centralized power grid, which determines its expected total cost. Therefore, the centralized power grid profits are the function of the amount of energy $\tilde{h}$ and the reliability level ρ as follows:

$$\prod{}^{G}(\tilde{h}, \rho) = \lambda^H (1 - \eta^L) \cdot \tilde{h} - J_T^G(\tilde{h}, \rho), \tag{9}$$

where $\lambda^H (1-\eta^L) \cdot \tilde{h}$ is the expected electricity sales income and $J_T^G(\tilde{h}, \rho)$ is the expected total costs. Set the income as the product of peak price λ^H and an amount of energy $(1 - \eta^L) \cdot \tilde{h}$ that the DER communities purchase from the centralized power grid, where $\eta^L \in (0, 1)$ is a constant energy transmission loss rate. The marginal expected electricity sales income of the centralized power grid is a constant, i.e. $\lambda^H (1 - \eta^L)$.

For a given $\tilde{h}$, the centralized power grid has a minimum expected total cost $J_T^G(\tilde{h}, \rho^*(\tilde{h}))$ under the optimal reliability level $\rho^*(\tilde{h})$. According to the energy probabilistic reliability management, the expected total cost $J_T^G(\tilde{h}, \rho)$ is regarded as a convex function of the reliability level ρ, which is shown as

$$J_T^G(\tilde{h}, \rho) = F_\rho(\rho) \cdot h \cdot c^G + J_O^G(\tilde{h}, \rho). \tag{10}$$

In Eq. (10), the expected interruption cost $F_\rho(\rho) \cdot h \cdot c^G$ is a decreasing convex function of ρ and the sum of all other expected energy costs $J_O^G(\tilde{h}, \rho)$ is a increasing convex function of ρ. The expected interruption cost is the product of the probability of a certain interruption $F_\rho(\rho) \in (0, 1)$, the amount of energy $\tilde{h}$ kW and the constant cost of interruptions c^G dollars per kWh. The relationship between the minimum expected total cost $J_T^G(\tilde{h}, \rho^*(\tilde{h}))$ and the variable $\tilde{h}$ is illustrated in Proposition 3.

Proposition 3. *The centralized power grid's minimum expected total cost $J_T^G(\tilde{h}, \rho^*(\tilde{h}))$ is an increasing convex function of the amount of energy $\tilde{h}$ that the centralized power grid needs to transmit to the distant DER communities.*

Proposition 3 implies that the marginal expected cost of the centralized power grid per kWh is increasing with $\tilde{h}$. In other words, the centralized power grid profits $\prod{}^{G}(\tilde{h}, \rho^*(\tilde{h}))$

under the optimal reliability level is a concave function of $\tilde{h}$ has a unique maximum value $\prod^G(\tilde{h}^*, \rho^*(\tilde{h}^*))$ under the optimal amount of energy $\tilde{h}^*$.

The effect of omni energy sharing on the centralized power grid profits depends on the optimal amount of energy $\tilde{h}^*$ that the centralized power grid transmits to the distant DER communities, which is the solution to $d\prod^G(\tilde{h}, \rho^*(\tilde{h}))/d\tilde{h} = 0$. We set $\tilde{h}_O$ and $\tilde{h}_P$ are the known amounts of expected energy generated by the centralized power grid in omni energy sharing and P2P energy sharing, respectively. Due to crowdsourcing energy from ride-sharing electric vehicles, $\tilde{h}_O$ is smaller than $\tilde{h}_P$. We provide the conditions for determining whether omni energy sharing has a positive or negative impact on the centralized power grid profits in Proposition 4.

Proposition 4. *Compared to P2P energy sharing, the impact of omni energy sharing on the centralized power grids profits is (1) positive if* $\tilde{h}^* \leq \tilde{h}_O < \tilde{h}_P$, *(2) negative if* $\tilde{h}_O < \tilde{h}_P \leq \tilde{h}^*$, *(3) not determined if* $\tilde{h}_O \leq \tilde{h}^* \leq \tilde{h}_P$.

In Proposition 4, we can directly identify positive or negative effects based on the relationships among $\tilde{h}_O$, $\tilde{h}_P$ and $\tilde{h}^*$ in conditions (1) and (2). In condition (3), we have to calculate and compare the centralized power grids profits in omni and P2P energy sharing.

4 Internal Energy Sharing

4.1 Preliminaries on Cooperative Game

Constructing a cost allocation rule in the *core* is a key of the cooperative game (N, J), where N represents a finite set of prosumers in the same DER community and $J : 2^N \rightarrow \mathbb{R}$ means a characteristic daily operating cost function. A set of all cost allocation vectors $\overrightarrow{\beta} = (\beta_1, \beta_2, ..., \beta_N)$ that are both *efficient* and *rational* can be called a core such as $C(N, J) := \{\overrightarrow{\beta} \in \mathbb{R}^N : J(S) \geq \sum_{i\in S} \beta_i, \forall S \subseteq N, J(N) = \sum_{i\in N} \beta_i\}$, where $J(S)$ is the total daily operating cost incurred by the collaboration that involves only the prosumers in set S ($\forall S \subseteq N$). An efficient cost allocation rule $\overrightarrow{\beta}$ indicates the sum of the cost allocated to each prosumer i ($\forall i \in N$) equals to the total cost of the *grand coalition*, i.e. $\sum_{i\in N} \beta_i = J(N)$. A rational cost allocation rule $\overrightarrow{\beta}$ implies no subset of prosumers has an incentive to depart from the grand coalition N, i.e. $\sum_{i\in S} \beta_i \leq J(S)$. However, the core of a cooperative game might be empty, namely no efficient and rational cost allocation vector. The Bondareva-Shapley theorem, that a cooperative game has a nonempty core if and only if there is no mapping $\kappa : 2^{|N|} \rightarrow \mathbb{R}_+^{|N|}$ such that $\sum_{S\subseteq N: i\in S} \kappa(S) = 1$ for all $i \in N$ and $\sum_{S\subseteq N} \kappa(S)J(S) < J(N)$, can be used to determine whether the core of a specific game is empty. We use the Bondareva-Shapley theorem to prove that both our short-term and long-term cooperative games have a nonempty core in the following.

4.2 Daily Operation Cost Function

The goal of any prosumers coalition $S \subseteq N = \{1, 2, ..., n\}$ is to minimize its daily energy operating cost by optimizing installed storage capacity c^S. For any coalition $S \subseteq N$, the daily energy operating cost function is

$$J_S(S) = (\lambda^C + \lambda^L) \cdot c^S - \lambda^L \cdot (c^S - q^S)^+ + [\Lambda^*(\overline{h}_S) \cdot h_S^* + \lambda^H \cdot (\overline{h}_S - \hat{h})^+]/\overline{h}_S \cdot (q^S - c^S)^+. \quad (11)$$

Equation (11) shows an extended form of the classical Newsvendor model consisting of the purchase, overage, and underage costs. Specifically, the daily energy operating cost function $J_S(S)$ includes three parts: (1) the cost of storing and purchasing electricity during off-peak periods, i.e. $(\lambda^C+\lambda^L)\cdot c^S$, where λ^C is the daily amortized cost of storage per kWh, λ^L is the external grid's off-peak price per kWh, and $c^S = \sum_{i\in S} c_i$ represents the sum of storage capacity of all prosumers in coalition S; (2) the value of redundant energy $(c^S - q^S)^+$ that is reserved in storage, i.e. $\lambda^L \cdot (c^S - q^S)^+$, where $q^S = \sum_{i\in S} q_i$ is the amount of random energy demand in coalition S; (3) the cost of making up for the residual energy demand $(q^S - c^S)^+$, i.e. $[\Lambda^*(\overline{h}_S) \cdot h_S^* + \lambda^H \cdot (\overline{h}_S - \hat{h})^+]/\overline{h}_S \cdot (q^S - c^S)^+$, where $[\Lambda^*(\overline{h}_S) \cdot h_S^* + \lambda^H \cdot (\overline{h}_S - \hat{h})^+]/\overline{h}_S$ indicates the average price per kWh of external energy purchased from CSEVs and the grid. We define $\overline{h}_S$ as the DER community's total residual energy demand that cannot be met by internal energy sharing when prosumers in the subset S deviate from the grand coalition and cooperate among each other in coalition S. According to Sect. 3.3, $\Lambda^*(\overline{h}_S) \cdot h_S^*$ is the optimal total uniform energy payment for CSEVs and $\lambda^H \cdot (\overline{h}_S - \hat{h})^+$ is the total cost of purchasing peak electricity from the external grid.

One of the biggest differences between the daily energy operating cost function $J_S(S)$ and the classical Newsvendor model is the underage cost, i.e. the third item in Eq. (11). In the classical Newsvendor model, the underage cost of energy would be generally expressed as $\lambda^H \cdot (q^S - c^S)^+$, where the price of purchasing external energy λ^H is a constant parameter. By contrast, in Eq. (11), the underage cost of energy has the variable price of purchasing the external energy, i.e. $[\Lambda^*(\overline{h}_S) \cdot h_S^* + \lambda^H \cdot (\overline{h}_S - \hat{h})^+]/\overline{h}_S$. The DER community's total residual energy demand $\overline{h}_S$ is the sum of the residual energy demand of coalition S, $(q^S - c^S)^+$, and the residual energy demand of other coalitions in a subset N/S. Thus, $\overline{h}_S$ is determined by the decision variables c_i for all $i \in N$. However, the variable price results in the invalidity of existing analytical solutions for the optimal storage decision and cost allocation rules. To show that the omni energy sharing business mode can be applied to the DER community with and without installed storage, we create the analytical solutions for short-term and long-term energy sharing in Sects. 4.3 and 4.4, respectively.

4.3 Short-Term Energy Sharing

The goal of the short-term internal energy sharing is to identify whether there are cost allocation rules and how to build such rules that allow prosumers to get excess profit even if they have already installed electricity storage. The decision variable c_i and random variable q_i for any $i \in N$ are realized values in the short-term cooperation and are denoted by c_{Ri} and q_{Ri}, respectively. The value of the short-term characteristic function is no longer a random variable, which can be expressed as $J_{SR}(S) = (\lambda^C + \lambda^L)c_R^S - \lambda^L(c_R^S - q_R^S)^+ + [\Lambda^*(\overline{h}_{SR}) \cdot h_{SR}^* + \lambda^H \cdot (\overline{h}_{SR} - \hat{h}_R)^+]/\overline{h}_{SR} \cdot (q_R^S - c_R^S)^+$, where the subscript R indicates the short-term sharing. According to the Bondareva-Shapley theorem, we

prove the short-term cooperative game (N, J_R) has at least one efficient and rational cost allocation rule in Theorem 1.

Theorem 1. *The cooperative game* (N, J_R) *in the short-term energy sharing has the nonempty core.*

Theorem 1 implies the short-term cooperative game has at least a cost allocation rule to ensure no sub coalition has the motivation to leave from the grand coalition. The daily operating cost function of the grand coalition in stable short-term cooperation is

$$J_R(N) = (\lambda^C + \lambda^L)c_R^N - \lambda^L(c_R^N - q_R^N)^+ + [\Lambda^*(h_R) \cdot h_R^* + \lambda^H \cdot (h_R - h_R)^+]. \quad (12)$$

Generally, a nonempty core game has multiple allocation rules and several approaches to find these rules. The remarkable thing of finding a cost allocation rule in the core of (N, J_R) is to avoid the computationally intensive methods and construct an extensible allocation mechanism. We create the cost allocation vectors for the game (N, J_R), which can be directly and quickly calculated, to substitute for solving linear programs with a number of constraints that grow exponentially with the cardinality of the grand coalition in Proposition 5 and prove our cost allocation vectors are in the core in Theorem 2.

Proposition 5 (Short-term cost allocation rule). *Define* $\beta_R = (\beta_{1R}, \beta_{2R}, ..., \beta_{NR})$ *as the cost allocation vector of the short-term cooperative game* (N, J_R)*, where* β_{iR} *for any* $i \in N$ *is shown as*

$$\beta_{iR} = (\lambda^C + \lambda^L)c_{Ri} + (q_{Ri} - c_{Ri}) \cdot \begin{cases} \lambda^L, & \text{if } c_R^N \geq q_R^N, \\ G^{-1}(\overline{h}_R), & \text{if } c_R^N < q_R^N < c_R^N + \hat{h}_R, \\ [\lambda^H - \hat{h}_R(\lambda^H - \lambda^E)/\overline{h}_R], & \text{if } c_R^N + \hat{h}_R \leq q_R^N. \end{cases} \quad (13)$$

Theorem 2. *The cost allocation vector* $\overrightarrow{\beta}_R = (\beta_{1R}, \beta_{2R}, ..., \beta_{NR})$ *defined in Proposition 3 is in the core of the short-term cooperative game* (N, J_R).

In Eq. (13), the cost allocated to prosumer $i(\forall i \in N)$ has three values owing to the different relationships between the realized total energy demand q_R^N and a given total storage capacity c_R^N. The same item, $(\lambda^C + \lambda^L)c_{Ri}$, is the off-peak storing cost that each prosumer must bear. The three types of second item of β_{iR} result from the different market structures. If $c_R^N \geq q_R^N$, we regard the internal energy sharing market as a buyer's market, where prosumers with an energy deficit become price makers and have the right to trade with other prosumers at the marginal variable storing cost λ^L; otherwise, it is a seller's market, where prosumers with an energy redundancy become price makers and can trade with counterparties at the highest market price. The highest market price is $G^{-1}(\overline{h}_R)$ when the energy shared by CSEVs could cover the total energy demand. In turn, the highest market price is $\lambda^H - \hat{h}_R(\lambda^H - \lambda^E)/\overline{h}_R$. Since both $G^{-1}(\overline{h}_R)$ and $\lambda^H - \hat{h}_R(\lambda^H - \lambda^E)/\overline{h}_R$ are less than the unit peak price λ^H, which is the highest market price with the seller's market in P2P energy sharing, the omni energy sharing is not conductive to prosumers with redundant storage. In other words, omni energy sharing can restrain the growth of redundant storage by reducing the excess income of arbitrageurs from trading energy, thereby alleviating environmental pollution caused

by storage equipment degradation. The short-term omni energy sharing is more cost-effective and environmentally friendly than the short-term P2P energy sharing, however, such sharing is not optimal. Next, we consider the long-term omni energy sharing that has the potential to minimize the daily energy operating cost and optimize the storage asset structure.

4.4 Long-Term Energy Sharing

The long-term omni energy sharing addresses two main problems: how much the capacity for prosumers to jointly invest in the installation of storage, thereby minimizing the daily total operating cost; and how to design a scalable cost allocation policy to ensure the stable grand coalition in the long-term cooperation with random energy demand.

Quantifying the optimal total storage capacity c^{N*} is based on the premise that the long-term grand coalition is stable. The cooperative game of long-term omni energy sharing is (N, J_E^*), where $J_{SE}^*(S) = \min\{\mathrm{E}[J_S(S)]\}$ with the optimal storage investment decision $c^{S*} = \arg\min_{c^S \geq 0} J_{SE}(S)$ for any $S \subseteq N$. Similar to the short term, we use the Bondareva-Shapley theorem to verify the long-term game (N, J_E^*) has at least one cost allocation rule in the core in Theorem 3, which implies the existence of a stable grand coalition.

Theorem 3. *The cooperative game (N, J_E^*) in the long-term energy sharing has the nonempty core.*

The expected daily operating cost function of the grand coalition in the long-term cooperation is

$$J_E(N) = (\lambda^c + \lambda^L) \cdot c^N - \lambda^L \cdot \mathrm{E}\left[\left(c^N - q^N\right)^+\right] + \mathrm{E}\left[\Lambda^*\left(\overline{h}\right) \cdot h^* + \lambda^H \cdot \left(\overline{h} - \hat{h}\right)^+\right], \tag{14}$$

where $\overline{h} = (q^N - c^N)^+$ and $q^N = \sum_{i \in N} q_i$ is the random total energy demand. The format of Eq. (14) is similar to the long-term P2P energy sharing such as $(\lambda^C + \lambda^L)c^N - \lambda^L \mathrm{E}[(c^N - q^N)^+] + \lambda^H \mathrm{E}[\overline{h}]$, a type of classical Newsvendor model. A unique optimal decision of the classical Newsvendor is $F_N^{-1}(\gamma)$, where $\gamma = 1 - \lambda^C/(\lambda^H - \lambda^L)$ is called the "critical ratio". However, a piecewise non-linear variable trading price in the third item of Eq. (14) makes the problem too complex to use the conclusion of the classical Newsvendor. To overcome this challenge, we propose the analytical solution of the optimal total storage capacity c^{N*} and the minimum expected total daily operating cost $J_E^*(N)$ in Theorem 4.

Theorem 4. *For the long-term energy sharing, the unique and optimal total storage capacity of the grand coalition is*

$$c^{N*} = \Omega^{-1}(\gamma), \tag{15}$$

where $\Omega(c^N) = F_N(c^N) + [F_N(c^N + \hat{h}) - F_N(c^N)] \cdot (\lambda^H - \lambda^M)/(\lambda^H - \lambda^L)$, and $\lambda^M = \mathrm{E}[d(\overline{h} \cdot G^{-1}(\overline{h}))/d\overline{h}|0 < \overline{h} < \hat{h}]$ means the average marginal subsidy cost for

CSEVs. The optimal expected total daily operating cost is

$$J_E^*(N) = \lambda^L \mathrm{E}[q^N] + (\lambda^H - \lambda^L)\mathrm{E}[q^N | q^N \geq c^{N*}] \cdot [1 - F_N(c^{N*})] \tag{16}$$

$$-(\lambda^H - \lambda^M)E[q^N | c^{N*} < q^N < c^{N*} + h][F_N(c^{N*} + h) - F_N(c^{N*})] - (\lambda^H - \lambda^E)h[1 - F_N(c^{N*} + h)].$$

Equation (15) shows that c^{N*} is also determined by the critical ratio γ and can be easily calculated, although the form of $\Omega^{-1}(\cdot)$ is different from the classical Newsvendor model. Moreover, comparing the form of $\Omega(\cdot)$ with $F_N(\cdot)$, it is easy to see that the optimal total storage capacity in the omni sharing is less than in the P2P sharing. Equation (16) in Theorem 4 implies that the optimal expected total daily operating cost in the long-term omni energy sharing is composed by three-part conditional expectations. The first part, $\lambda^L \mathrm{E}[q^N] + (\lambda^H - \lambda^L)\mathrm{E}[q^N | q^N \geq c^{N*}] \cdot [1 - F_N(c^{N*})]$, reflects the potential highest expected total operating cost when internal storage cannot cover the energy demand. The second part, $(\lambda^H - \lambda^M)E[q^N | c^{N*} < q^N < c^{N*} + \hat{h}][F_N(c^{N*} + \hat{h}) - F_N(c^{N*})]$, implies the expected saving cost from energy shared by CSEVs that can satisfy the residual energy demand. The third part, $(\lambda^H - \lambda^E)\hat{h}[1 - F_N(c^{N*} + \hat{h})]$, indicates the expected saving cost from accepting CSEVs energy if the energy shared by CSEVs is not enough.

Following the principle of scalability, we allocate the optimal expected total daily operating cost $J_E^*(N)$ according to the weight of individual expected energy demand in the total expected energy demand in Proposition 6.

Proposition 6 (Long-term cost allocation rule). *Define $\beta_E = (\beta_{1E}, \beta_{2E}, ..., \beta_{NE})$ as the cost allocation vector of the long-term cooperative game (N, J_E), where β_{iE} for any $i \in N$ is shown as*

$$\beta_{iE} = \lambda^L \mathrm{E}[q_i] + (\lambda^H - \lambda^L)\mathrm{E}[q_i | q^N \geq c^{N*}] \cdot [1 - F_N(c^{N*})] - (\lambda^H - \lambda^E)h\mathrm{E}[q_i / q^N | q^N > c^{N*} + h] \cdot [1 - F_N(c^{N*} + h)] \tag{17}$$

$$-(\lambda^H - \lambda^M)E[q_i | c^{N*} < q^N < c^{N*} + h][F_N(c^{N*} + h) - F_N(c^{N*})].$$

The allocation mechanism in Proposition 6 suggests that both the operating cost and the fluctuation of random total energy demand allocated to each prosumer are proportional to their expected energy demand. Different from the short term, the long-term cost allocation not only allocates operating cost but also distributes uncertain. Theorem 5 proposes the requirements for the energy demand distributions of the long-term omni energy sharing participants.

Theorem 5. *The cost allocation vector $\overline{\beta}_E$ defined in Proposition 4 is in the core of the long-term cooperative game (N, J_E^*) if the energy demand distributions of any coalition $S \subseteq N$ satisfy*

$$q_{\max}/q_{\min} \leq \sigma_S/\sigma_N, \tag{18}$$

where $q_{\max} = \max\{\mathrm{E}[q_i], \forall i \in N\}$ and $q_{\min} = \min\{\mathrm{E}[q_i], \forall i \in N\}$ indicate the maximum and minimum expected energy demand of a single prosumer, and $\sigma^S = (\sum_{i,j \in S} \mathrm{cov}(q_i, q_j))^{1/2}/|S|$ is the square root of average covariance of energy demand of a single prosumer in subset $S(\forall S \subseteq N)$.

Theorem 5 provides a sufficient condition of all energy demand distributions that $\overline{\beta}_E$ defined in Proposition 4 ensures a stable long-term cooperation. Inequality (18) requires the smallest volatility of random energy demand in the grand coalition than in any coalition. Furthermore, compared with any sub coalition S, the internal demand volatility of the grand coalition is smaller, the greater the range of expected energy demand within the stable long-term cooperation.

5 Case Study

This section presents a numerical analysis of the omni energy sharing model from perspectives of the ride-sharing market and energy market, respectively. Our goal is to demonstrate the model's validities about optimizing the fixed storage structure in a DER community and to evaluate the model's implication to the ride-sharing market. We calibrate our model using real baseline data from the energy industry, ride-sharing industry, census bureau, and other academic studies. Details of parameter estimates and sources are shown in the online appendix.

5.1 Implications for the Ride-Sharing Market

Changes in utilities of the ride-sharing stakeholders can measure the implications of omni energy sharing on the ride-sharing market. If the stakeholder's interests with omni sharing are better than without omni sharing, then we consider omni sharing has a synergy effect on the ride-sharing market; otherwise, we claim omni sharing has a competition effect on the ride-sharing market. There are three types of stakeholders and their respective indicators: (1) CSEVs drivers, who want the higher expected income from ride-sharing; (2) governments, which have to accelerate the popularization of electric vehicles and care about the total number of CSEVs in a city; (3) ride-sharing passengers and platforms, which utilities increases in the number of available CSEVs for ride-sharing.

Define three ratios as indicators, which are a driver's expected income from ride-sharing, the number of total CSEVs, and the number of available CSEVs for ride-sharing, with and without omni energy sharing as k_1, k_2, and k_3, respectively. Figure 2 shows the changes of such three ratios for varying levels of a driver's expected daily income for ride-sharing. Because $k_1 > 1$ and $k_2 > 1$ for any levels of income, we conclude that omni energy sharing has synergy effects on CSEVs drivers by increasing their income and on governments by expanding the popularity of electric vehicles. Conversely, due to $k_3 < 1$, omni energy sharing has competitive effects on ride-sharing passengers and platforms by attracting more CSEVs drivers to serve for the energy market. Tendencies of the three ratios in Fig. 2 provide two insights. (1) Omni energy sharing is beneficial to the ride-sharing market since the synergy effects always dominate the competition effects. (2) The influence of omni energy sharing becomes smaller as the driver's expected income rises.

To explain the principle of the above two insights, we analyze the impact of the interaction between ride-sharing and energy markets, which is caused by the omni energy sharing paradigm. Figure 3 illustrates the influences of the interaction on energy sharing

with different driver income. The dotted and solid line represent the values of energy sharing from CSEVs to a DER community that is calculated based on the initial and new equilibrium state, respectively. The energy demand of a DER community is about 12,306 kWh in a peak period. When the driver's expected daily income is lower than \$80, the sharp increase of energy sharing from CSEVs to the community results from the jump of total number of CSEVs. Hence, a surge of total number of CSEVs weakens the competition effect on the ride-sharing market. When the driver's expected daily income is higher than \$100, the individual rational subsidy that tends to exceed the peak energy price triggers a sharp decline in the energy accepted by the community. Moreover, the high income from ride-sharing also attracts a large number of drivers. Therefore, the more drivers in the ride-sharing market and the fewer drivers required by the energy market together diminish synergy and competition effects. Furthermore, Fig. 3 also describes that omni energy sharing is valid in most cities, but it is unsuitable for cities where driver's wage is extremely high, such as New York and San Francisco.

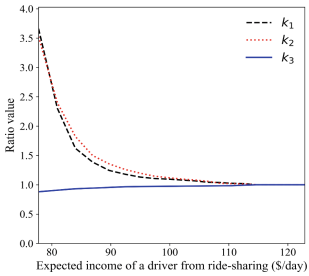

Fig. 2. Values of k_1, k_2, and k_3

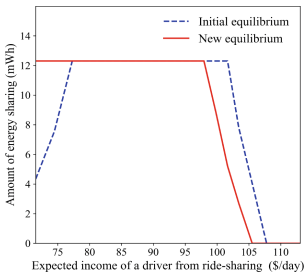

Fig. 3. Amount of energy sharing

5.2 Implications for the Energy Market

We test and quantify the improvement brought by the omni energy sharing strategy in terms of saving storage and reducing operating costs based on real data. For short-term sharing, we compare the community's expected total operating cost of omni sharing with P2P sharing for different levels of storage capacity. As shown in Fig. 4, we first verify that the minimum expected operating cost and optimal storage capacity of omni sharing is reduced by 9.8% and 17.7% compared with those of P2P sharing, respectively. The cost saving rate from omni energy sharing relative to P2P energy sharing reaches its maximum when the DER community has no storage.

For long-term sharing, we are interested in understanding how the optimal total storage capacities and expected daily operating cost of omni energy sharing change in the future. The development of storage technology might decrease the amortized cost of storage from \$0.14 per kWh to \$0.07 per kWh in the next thirty years. Figures 5 and 6 exhibit the trends of the omni and P2P energy sharing models in terms of optimal total storage capacity and optimal expected daily total operating cost as the amortized cost of storage drops, respectively. Although the advantages of omni sharing are weakened by the drop in storage cost, omni sharing still save 7.4% operating cost and 10.7% storage relative to P2P energy sharing when the amortized cost of storage is \$0.07 per kWh.

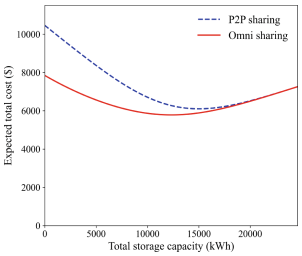

Fig. 4. Expected cost in short-term

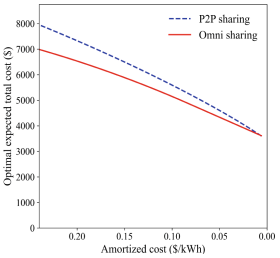

Fig. 5. Optimal total storage in long-term

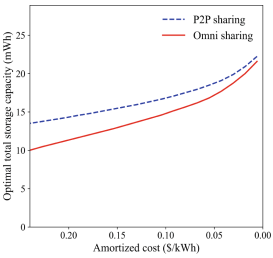

Fig. 6. Optimal total cost in long-term

6 Summary

In this paper, we investigate whether and how to utilize crowdsourcing electric ride-sharing mobility to reduce DERs' dependence on fixed storage. The paper proposes the omni energy sharing model combined with external and internal sharing. The external sharing model creates the optimal subsidy policy to attract CSEVs to share energy. The internal sharing model provides new cost allocation rules to ensure the grand coalition since the existing methods are not suitable for omni sharing. In the case study, we find that the omni-sharing strategy dominates the peer-to-peer energy sharing model by reducing both daily energy operating costs and total storage. This paper is the first attempt to discuss the operations of omni energy sharing. Future research could consider the potential effects of multiple DER communities, such as the competition for CSEVs among the multiple communities.

References

1. Zenneck, J., Bader, M., Baker, T., Rubel, H.: The M&A Way Into Distributed Energy. BCG (2019)
2. Trabish, H.K.: California Utilities Prep Nation's Biggest Time-of use Rate Rollout. Utility Dive (2018)
3. John, J.: "California Sets $200m Budget for 'Complex, Multi-Property Microgrid' Projects. Greentech Media (2021)
4. Pearce, F.: Getting the Lead Out: Why Battery Recycling is a Global Health Hazard. Yale Environment 360 (2020)
5. Hawkins, A.J.: Uber Pledges to Shift to '100 Percent' Electric Vehicles by 2030. The Verge (2020)
6. Takahashi, I.: How Much Do Uber Drivers Work? How Many Hours Do They Drive? RideGuru (2018)
7. EIA: How Much Electricity Does an American Home Use? U.S. Energy Information Administration (2020)
8. Chakraborty, P., Baeyens, E., Poolla, K., Khargonekar, P.P., Varaiya, P.: Sharing storage in a smart grid: a coalitional game approach. IEEE Trans. Smart Grid **10**(4), 4379–4390 (2017)
9. Qi, W., Shan, M., Li, S.: When Shared Autonomous Electric Vehicles Meet Microgrids: Citywide Energy-Mobility Orchestration. Preprint, submitted June 10, 2019
10. Zhang, Y., Lu, M., Shen, S.: On the values of vehicle-to-grid electricity selling in electric vehicle sharing. Manuf. Serv. Oper. Manag. **23**(2), 488–507 (2021)

11. Broneske, G., Wozabal, D.: How do contract parameters influence the economics of vehicle-to-grid? Manuf. Serv. Oper. Manag. **19**(1), 150–164 (2017)
12. Qi, W., Li, L., Liu, S., Shen, Z.J.M.: Shared mobility for last-mile delivery: design, operational prescriprions, and environmental impact. Manuf. Serv. Oper. Manag. **20**(4), 737–751 (2018)
13. Wu, O., Yücel, S., Zhou, Y.: Smart Charging of Electric Vehicles. Preprint, submitted November 12, 2021
14. Lin, C.A., Shang, K., Sun, P.: Wait Time Based Pricing for Queues with Customer-Chosen Service Times. Preprint, Submitted November 25, 2020
15. Fatehi, S., Wagner, M.R.: Crowdsourcing Last-Mile Deliveries. Manufacturing & Service Operations Management (2021)
16. Kalathil, D., Wu, C., Poolla, K., Varaiya, P.: The sharing economy for the electricity storage. IEEE Trans. Smart Grid **10**(1), 556–567 (2019)
17. Kiedanski, D., Orda, A., Kofman, D.: The effect of ramp constraints on coalitional storage games. In: e-Energy 2019: Proceedings of the Tenth ACM International Conference on Future Energy Systems, pp.226–238 (2019)
18. Shahan, Z.: New US Electric Vehicles Now Have 250-Mile Median Driving Range. Clean Technica (2021)

Covid-19 Intervention Policy Optimization Using a Multi-population Evolutionary Algorithm

Luning Bi, Mohammad Fili, and Guiping Hu(✉)

Industrial and Manufacturing Systems Engineering, Iowa State University, Ames, IA 50011, USA
gphu@iastate.edu

Abstract. The rapid spread of COVID-19, caused by the SARS-CoV-2 virus, has resulted in and continues to pose a significant threat to global health. We proposed a predictive model based on the gated recurrent unit (GRU) that investigates the influence of non-pharmaceutical interventions (NPIs) on the progression of COVID-19. The proposed model is validated by applying in different states in the United States, although it can be generalized to any region of interest in the world. The results show that the predictive model can achieve accurate forecasts across the entire US. The forecast is then utilized to identify the optimal mitigation policies. The goal is to find the best stringency level for each policy that can minimize the total number of new Covid-19 cases while minimizing the mitigation costs. A meta-heuristics method, named multi-population evolutionary algorithm with differential evolution (MPEA-DE), has been developed. The goal is to identify optimal mitigation strategies that minimize COVID-19 infection cases while controlling the costs and other negative impacts. We compared the optimal mitigation strategies identified by the MPEA-DE model with the random search and the blind greedy search strategies. The results show that MPEA-DE performs better than other baseline models based on prescription dominance.

Keywords: COVID-19 prediction · Differential evolution (DE) · Gated recurrent unit (GRU) · Multi-population evolutionary algorithm · Policy prescription

1 Introduction

Since March 2020, COVID-19 has been rapidly spreading worldwide. Today there are over 173 million documented COVID-19 cases and over 3 million deaths, constituting major health, economic, and social harms to many countries and regions [1]. To mitigate the burden on the healthcare institutions and provide a good understanding of policy decisions, the accurate prediction of COVID-19 cases is essential.

Many of the models designed to predict COVID-19 cases are based on traditional epidemiological methods, such as susceptible-infected-recovered (SIR) [2]. These models consider susceptible individuals, the number of people infected, and the number of people recovered and incorporate parameters, such as the basic reproduction number R_0, to predict the outbreak of the COVID-19 [3]. However, the susceptibility to infection has been manipulated dramatically because authorities have implemented different

R. Qiu et al. (Eds.): ICSS 2021, LNOR, pp. 383–396, 2021.
https://doi.org/10.1007/978-3-030-90275-9_30

non-pharmaceutical interventions (NPIs), such as face coverings and social distancing, to reduce the spread of the virus [4]. The non-linear complexity of these NPIs will reduce the generalization and robustness of the models. Another issue of epidemiological methods is the non-stationarity of the factors [5]. Since these NPIs and their influence change over time, static models cannot achieve high prediction accuracy for long-term prediction.

To overcome the shortcomings of epidemiological methods, machine learning-based methods have been developed for outbreak prediction. Yin *et al.* proposed a stacking model for the prediction of antigenic variants of the H1N1 influenza virus, which achieved 80–95% prediction accuracy [6]. Agarwal *et al.* discovered the correlation between weather parameters and dengue outbreak using the regression model and the k-means clustering algorithm [7]. Liang *et al.* presented a random forest based algorithm for the prediction of global African swine fever outbreaks and achieved a higher test accuracy [8]. For the prediction of the COVID-19 spread, time-series prediction using the infection data (e.g., daily new cases, total cases, daily deaths, daily recoveries) has been widely adopted since the infection cases are the result of unknown epidemiological, cultural, and economic factors [9]. However, a significant amount of information on transmission rates has been included in the NPIs [2]. Thus, it is necessary to consider the time-series infection data and NPIs simultaneously. Due to non-linear interactions among NPIs, linear models are inappropriate and ineffective. Instead, deep learning models can strengthen the generalization ability and flexibility. Zandavi *et al.* proposed an LSTM-based hybrid model for forecasting the spread of COVID-19 in the most affected countries, and the results show that the model achieved high prediction accuracy [10]. Chandra *et al.* developed long short-term memomry (LSTM) models for COVID-19 infection forecasting in India. Their results show that long-term forecast using LSTM is promising [11]. One disadvantage of LSTM is that the training speed is much slower due to the increased number of parameters. To improve training speed, the gated recurrent unit (GRU) simplified the model structure by using only two gates, namely, reset gate and update gate [12]. In this paper, GRU has been implemented for the prediction of the COVID-19 spread.

After obtaining the predicted daily cases, the policymakers need to make appropriate intervention plans that optimize COVID-19 mitigation strategies while reducing the economic and social impacts. The two goals are often conflicting. For example, when people are required to quarantine in their homes, the number of new cases can be significantly reduced. However, the economy will also be negatively impacted. Therefore, this problem can be formulated as a bi-objective optimization problem that searches for the Pareto frontier between the two competing objectives.

The major challenge is that the time-series prediction model of COVID-19 is a non-linear model which cannot be solved by traditional operation research methods such as linear programming. Under this context, evolutionary algorithms which search for improved solutions iteratively become an option. An evolutionary algorithm (EA) is an optimization algorithm that mimics biological mechanisms such as mutation, recombination, and natural selection to find an optimal design within specific constraints [4]. Since evolutionary algorithms do not make any assumption about the objective function, they perform well in searching for approximate optimal solutions to all types of problems

[13]. In this paper, the evolutionary algorithm generates groups of prescriptions (NPIs) for each region. Then these prescriptions are evaluated from two perspectives. One is to evaluate the new cases using the prediction model. This poses great challenges to the prediction model since there are large numbers of possible combinations of time-series NPIs that need to be evaluated. The other is to evaluate the social and economic impacts. We assume that for each region, the impact of different levels of a specific NPI can be represented by a fixed value defined by a cost matrix. Then the evolutionary strategy will decide the evolution direction based on the objective values of each prescription. After a specific number of iterations, the algorithm will terminate and output Pareto solutions. Evolutionary algorithms are usually effective since they can automatically determine the searching direction. Although evolutionary algorithms have been successfully used in many studies, there are trade-off considerations in the algorithm design. If the algorithms only use a single strategy for evolution, they can easily get trapped in the local optimum [14]. To ensure the generalization ability and stability of the algorithm, different evolutionary strategies are necessary. Thus, a multi-population evolutionary algorithm with differential evolution (MPEA-DE) is proposed in this paper.

The main contributions of this research can be summarized as follows:

- An approach that connects the predictive model with the prescriptive model has been proposed to provide optimal NPI prescriptions for policymakers based on the historical NPIs and other context information.
- For prediction, a GRU-based ensemble model has been implemented to predict the spread of COVID-19 in the 50 regions of the United States. The time-series infection data and NPIs are considered simultaneously.
- For prescription, based on the prediction of the GRU-based model, a multi-population evolutionary algorithm using blind greedy has been proposed to search for optimal intervention plans that can minimize the newly infected cases as well as the social and economic cost. Different initialization strategies are used to generate the population. To improve the exploration ability and exploitation ability of the algorithm, multiple evolutionary algorithms are utilized to evolve the sub-populations together in a cooperative way by using the DE strategy.
- Both the proposed predictive model and the prescriptive model have been compared with other baseline models using different test time windows in multiple geographical areas. The comparison results have proved the effectiveness of the proposed approach.

The rest of this paper is organized as follows: Sect. 2 describes the datasets used in this study as well as the data preprocessing steps. Prediction and optimization models are also detailed in this section. In Sect. 3, the results for the predictive and prescriptive models are presented and discussed. Finally, we summarize the findings and discuss the future research directions in Sect. 4.

2 Materials and Method

In this section, we describe the datasets used for the predictive and the prescriptive models. We also explain the newly introduced variables as a part of the data preprocessing

procedure. We then discuss the predictive model, including the mechanism to predict the daily new Covid-19 cases. Finally, we describe the decision-making framework and the procedure to identify the best policies.

2.1 Datasets

In this study, we used the Covid-19 dataset prepared by Oxford Covid-19 Government Response Tracker (OxCGRT). This dataset includes systematic information on the policies implemented in different countries regarding the Covid-19 pandemic [15]. This dataset also contains information regarding different categories of policies: closure policies, economic policies, and healthcare-related policies. In the case study, we focus on the United States and used the policies corresponding to the closure and healthcare-related categories.

Closure policies include guidelines that restrict gatherings. Policies in this group are school closure, workplace closure, public events cancellation, gathering restrictions, public transport closure, stay-at-home requirement, internal movement restriction (between cities and regions), and international travel control for foreign travelers.

Healthcare policies are about guidelines related to the healthcare system. Vaccination policies, protection of elderly people, facial coverings guidelines, emergency investment, vaccination investments, testing availability, contact tracing, and public information campaigns are the policies in this group. Emergency and vaccination investments are two continuous variables recorded in dollars. The rest of the policies are categorical variables. Figure 1 shows the number of levels for each policy in each of the categories.

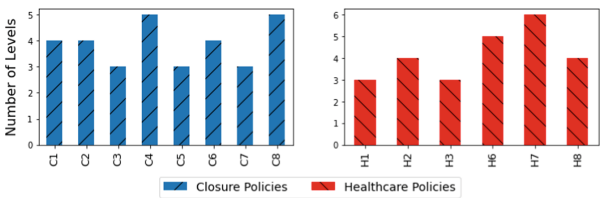

Fig. 1. The number of levels for each policy in closure and healthcare categories.

The values for policies start from 0, indicating no measure taken, all the way up to a maximum level for each policy. For instance, school closure has four levels, with 0 as the lowest stringency level and 3 as the highest value requiring the closure of schools at all levels. The definition of each level is explained in [16]. The codes for each policy are described in Table 1.

To find the optimal policy for a region, we evaluate the cost-benefit trade-off. In fact, there is a cost associated with the implementation of any policy for each government. Setting all policies at the maximum level is expected to decrease the number of new cases significantly; however, this decision can be too costly, and it can affect a country economically, both in the short and long term. Besides, many countries may have limitations in the amount of money they can spend for such emergency circumstances.

Table 1. The code and description of categorical policies.

Category	Policy	Description
Closure	C1	School closure
	C2	Workplace closure
	C3	Public events cancellation
	C4	Gathering restriction
	C5	Public transport closure
	C6	Stay at home requirements
	C7	Internal movement restrictions
	C8	International travel controls
Healthcare	H1	Public information campaigns
	H2	Testing policy
	H3	Contact tracing
	H6	Facial coverings
	H7	Vaccination policy
	H8	Protection of elderly people

Therefore, mitigation strategy needs to consider the cost and benefit simultaneously. For this purpose, we used a cost matrix to illustrate the cost of implementing each policy.

For the purpose of this study, we used a cost matrix generated from a uniform distribution with values between 0 and 5 for different policies. Figure 2 shows how much it costs on average for each state to implement closure and healthcare-related policies based on the generated cost matrix. We used this basic cost matrix for the model performance evaluation without loss of generality. Other cost structure can be adopted without significant impact on the decision-making framework.

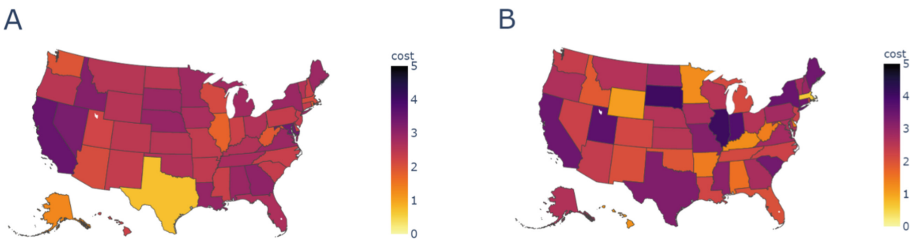

Fig. 2. A) Average cost for applying closure policies, B) Average cost for implementing healthcare policies for different states

In this study, we used the US states population dataset [17] to calculate the ratio of confirmed cases to the overall population, as the proportion of people infected. This new variable is added to the dataset as a new feature.

2.2 Preprocessing

In this study, feature engineering has been employed to introduce relevant new variables. It should be noted that the primary attribute corresponding to the number of Covid-19 cases is the number of confirmed cases which is a cumulative variable. We denote this variable by y_t^a which shows the total number of new cases until time point t for state a.

We created a new variable Z_t^a as the new cases at time point t for state a which can be calculated as Eq. 1.

$$Z_t^a = y_t^a - y_{t-1}^a \tag{1}$$

For the missing values of confirmed cases, we assumed the same value as the previous day, which means there were no new cases at that time point. We smoothed the daily new cases using rolling mean with weekly windows as shown in Eq. 2.

$$\tilde{Z}_t^a = \frac{\sum_{i=t-6}^{t} Z_i^a}{7}, i \geq 7 \tag{2}$$

where, $\tilde{Z}_t^a$ is the smoothed new cases for time point t and state a. Another newly introduced variable is the percent change in the smoothed new cases denoted by R_t^a. This feature can be calculated as in Eq. 3.

$$R_t^a = \frac{\tilde{Z}_t^a - \tilde{Z}_{t-1}^a}{\tilde{Z}_{t-1}^a} \tag{3}$$

We used the population information to define a new attribute as the proportion of infected people in state a and time point t. This variable is denoted by p_t^a and defined as in Eq. 4.

$$p_t^a = \frac{y_t^a}{N_a} \tag{4}$$

where, N_a represents the population of state a.

The target variable, here, is defined as the ratio of the percent of change in the number of smoothed new cases to the proportion of people not being infected at time t and state a (φ_a^t). This new dependent variable is represented in Eq. 5.

$$\varphi_a^t = \frac{R_t^a}{1 - p_t^a} \tag{5}$$

2.3 Predictive Model

GRU is a variant of LSTM since both use the gating mechanism in recurrent neural networks [18]. The performance of GRU on tasks such as speech recognition was found to be comparable to that of LSTM [12]. GRU also converges faster than LSTM because it has fewer parameters.

A GRU cell consists of two gates: reset gate r and update gate z. A reset gate is used to determine which part of information should be reset. The value of reset gate at time t, i.e., r_t, is calculated based on the previous output h_{t-1}, and the current input x_t as presented in Eq. 6.

$$r_{\mathrm{t}} = \sigma\left(W_r \bullet \left[h_{t-1}, x_t\right]\right) \tag{6}$$

where, σ is a sigmoid function, W_r is the parameter matrix of the reset gate. The update gate is used to update the output of the GRU, h_t. The value of update gate at time t, i.e., z_t, is computed using previous output h_{t-1} and the current input x_t as presented in Eq. 7.

$$z_t = \sigma\left(W_z \bullet \left[h_{t-1}, x_t\right]\right) \tag{7}$$

where, W_z is the parameter matrix of the update gate. Then the candidate hidden layer is calculated according to Eq. 8.

$$\tilde{h}_t = \tanh\left(W \bullet \left[r_t * h_{t-1}, x_t\right]\right) \tag{8}$$

where, W is the parameter matrix of the candidate hidden layer. Finally, the current output can be obtained according to Eq. 9. The gates, namely, z_t and r_t, and parameters, namely, W_z, W_r, and W will be updated in the training process.

$$h_t = (1 - z_t) * h_{t-1} + z_t * \tilde{h}_t \tag{9}$$

In this study, a stacked model consisting of two parts has been designed. For the first part, the input is the time-series policy values, and the output is computed with a GRU layer of 32 units. For the second part, the input is the time-series prediction ratio, and the output is obtained with another GRU layer of 32 units. Then the two parts are combined and connected to a dense layer to get the final output. The length of the time series is set to 21, meaning only the policies and cases of the past 21 days are considered to make the prediction. It is assumed that the increase of NPI levels can suppress the spread of the COVID-19. Thus, all parameters of the GRU layer are set to be non-negative to ensure the monotonic influence of NPI levels. The batch size is set to 1000. The optimizer is Adam [19].

2.4 Prescriptive Model

The prediction model can provide more guidance and information for policymakers by evaluating the outcome of policies. However, since the search space of NPIs is huge, setting the NPIs manually by experts is still limited. Thus, an automated algorithm that can identify the optimal mitigation strategies with minimum costs is needed. Due to the non-linear complexity of the optimization problem, evolutionary algorithms which can evolve prescriptions through population-based search are good candidates. On the basis of the traditional population-based algorithm, this paper uses MPEA, in which multiple algorithms are added to the framework to ensure the adaptability of the algorithm. Aimed to improve the exploitation ability of MPEA, the mechanism of differential evolution (DE) is introduced to strengthen the communication between different populations in this paper. It is assumed that there are m algorithms available for the proposed model. The components of MPEA-DE are as follows.

1. *Initialization*: Generate m populations. Then each sub-population is assigned with an algorithm.
2. *Encoding and Evaluation*: The individuals, i.e., NPIs prescriptions, are encoded using the real integer value encoding method. To improve the consistency of the policy, we assumed that NPIs can only change every 10 days. Since the number of NPIs considered is 12, the total number of decision variables can be calculated by dividing the number of days to prescribe by 10 and then multiplying by 12. For example, if the number of days to prescribe is 60, the number of decision variables is 72. In each iteration, the two objectives of each individual, i.e., new cases and cost, will be evaluated. The individual is used as the input of the predictor to get the predicted new cases. The social and economic cost is calculated according to the cost matrix.
3. *Evolution*: Based on the objective values of individuals, the corresponding algorithm of each population will determine the evolution direction. The old individuals will be replaced by the newly generated individuals that have dominated objective values.
4. *Migration*: After several iterations, the diversity of individuals in each population will be reduced dramatically. To improve the evolution efficiency of each population, a migration mechanism is introduced. When the number of iteration reaches, the worst individuals in the current population are evolved towards the best ones in the other populations, using the DE scheme as expressed in Eq. 10.

$$I_{worst}^{new} = I_{worst}^{old} + F * \left(I_{best} - I_{worst}^{old}\right) \tag{10}$$

where, I_{worst}^{old} is the worst individual in the current population, I_{best} is the best individual in other populations, F is the scaling factor in DE.

The pseudo-code for the MPEA-DE is shown in Fig. 3. In Fig. 4, we summarized the whole procedure applied in this study to find the best policies.

```
Algorithm: MPEA-DE
Initialization: generate m populations, pop 1, pop 2,…,pop m
While stopping conditions are not satisfied do
   Evaluate the new cases and cost of all individuals;
   For i =1:m
      Evolve pop i using algorithm A^i
   End for
   If a migration interval is reached, then do
      For i=1:m
         Using DE to update the worst individuals;
      End for
   End if
End
```

Fig. 3. The pseudo-code for MPEA-DE used to create policy prescriptions

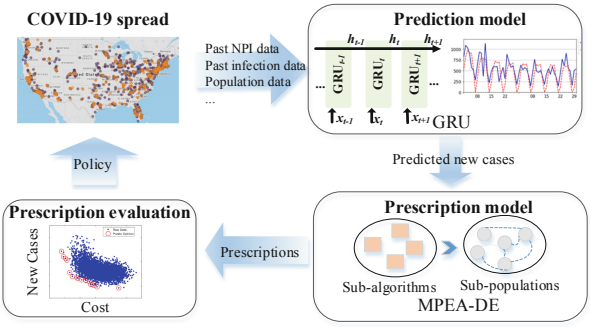

Fig. 4. The policy prescription framework

3 Results and Analyses

In this section, the results regarding both the predictive and the prescriptive models are discussed. In the first subsection, we show the predictive model's results using the GRU. Then the results for the prescriptive model is described.

3.1 Predictive Model

In this study, we defined two test windows, each of length of two months. The first period starts on August 1, 2020, and ends on September 30, 2020. The second window starts from February 1, 2021 up to April 1, 2021.

The training set for each of the test windows starts from April 1, 2020, up to the starting point of the corresponding test window. Prediction results for the GRU method are plotted in Fig. 5 for the two test windows for the United States. As we can see, for both test windows, the predictive model is following the true daily new cases closely and has captured the pattern.

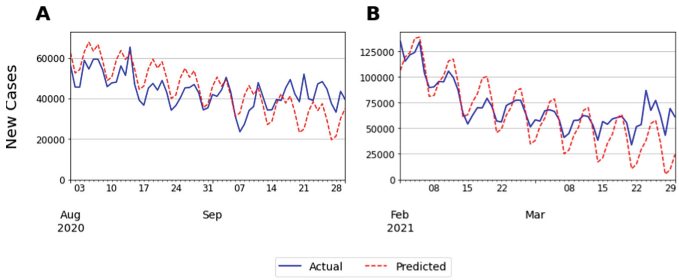

Fig. 5. A) The predicted and actual daily new cases for the United States using GRU for the first test window (August 2020 to the end of September 2020), B) The predicted and actual daily new cases for the United States using GRU for the second test window (February 2021 to the end of March 2021)

We also explored the performance of the predictive model at the state's level rather than the entire United States. For this purpose, the predicted values for daily new Covid-19 cases are plotted for three states, Iowa, Georgia, and Texas, for both test windows, in Fig. 6.

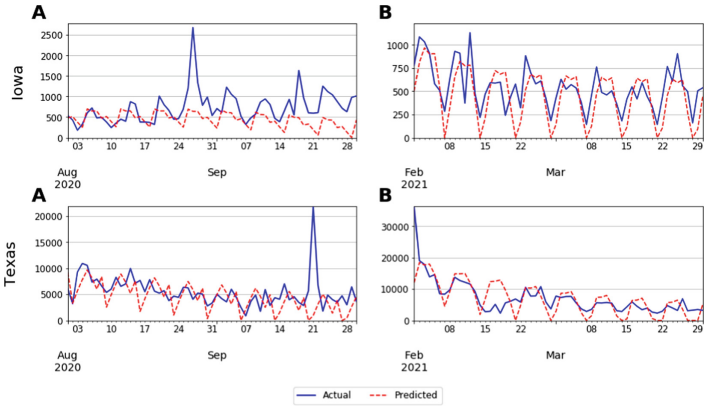

Fig. 6. The predicted and actual daily new cases for Iowa, Georgia, and Texas using GRU. For each state, plot A shows the first test window (August 2020 to the end of September 2020), and plot B shows the second test window (February 2021 to the end of March 2021).

As it is shown, we can predict the future new cases based on the previous policies applied, the number of new cases, and the population. We showed that the model is performing well both at the country level as well as the region level (state). Besides, three methods, i.e., least absolute shrinkage and selection operator (LASSO), fully connected neural network (FCNN) and convolutional neural network (CNN), were adopted as baseline models. LASSO was used as a non-time series prediction model which use the NPIs and prediction ratio of the previous day as the input. FCNN and CNN used time-series NPIs and prediction ratio for prediction. Mean absolute error per million people (MAE_1M) and mean absolute percentage error (MAPE) were used as measurements to compare the proposed model and other baseline models. To verify the robustness of the proposed model, all models were tested using eight time windows, *i.e. August, September, October, November and December in 2020, and January, February and March in 2021.* As shown in Table 2, the average MAE_1M of GRU was 13–22% less than the baseline models. The average MAPE of GRU was 7–11% lower than the other three models, which proved the advantage of the proposed method.

Table 2. Comparisons among GRU and baseline models.

Methods	MAE_1M	MAPE (%)
GRU	143.34	32.72
LASSO	183.40	43.32
FCNN	176.07	39.95
CNN	176.65	41.97

3.2 Prescriptive Model

After predicting the new cases for the future, we use the outputs to feed into the prescriptive model so the optimal set of policies for a state can be identified. In this study, we used random search and blind greedy search strategies as two baseline/benchmark models.

In the random search strategy, a population consisting of 40 individuals has been generated randomly. In each iteration, new individuals are generated by perturbating the old ones and replacing the individuals of bad objective values. The number of iterations is set to 20. The blind greedy search strategy starts with all NPIs as zeros and then iteratively sets the NPI that has the least cost to the maximal level.

For MPEA-DE, two populations have been generated. Each population consists of 20 individuals. The first 60% of the individuals in each population is generated by the blind greedy search strategy. To increase the diversity of the population, the remaining 40% of the individuals are generated by the random search strategy. The two populations are evolved using the standard genetic algorithm (GA) [20] and DE [21], respectively. The total number of iterations is 20. Every 5 iterations, the DE scheme will be performed to strengthen the communication between two populations.

Each model generated 10 prescriptions/mitigation strategies for each region. The quality of a prescription is calculated as the number of prescriptions it dominates (i.e., have better new cases and stringency level). For example, if a prescription of model A dominates 5 prescriptions of model B and 2 prescriptions of model C, the score of this prescription is 7. Thus, the performance of a prescriptive model can be calculated as the sum of the scores of its prescriptions.

In the prescription phase, we defined three test periods, each of length of one month. The first test window starts from July 2020 to the end of the month, the second test window is October 2020, and the last window is January 2021. The new cases and stringency level averaged a day were used as the two objectives. For each region, the prescriptive model that has the highest score is selected as the winner of the region. In other words, the region is claimed by the best model. To measure the performance of prescriptive models across all regions, the percentage of regions claimed by each model is calculated. In Table 3, the percentage of regions claimed by the prescriptive model (MPEA-DE) is shown. As we can see, the proposed method is completely superior to the other two baseline models.

Table 3. Claim percentage of the three prescriptive models

Window	MPEA-DE	Baseline models
1	84.0	16.0
2	84.0	16.0
3	88.0	12.0

In Fig. 7, the Pareto frontier generated by each algorithm has been plotted for three states. On the x-axis, we have the average cost across the whole test window, and on the y-axis, we have the average of new Covid-19 cases. Each point represents a policy suggested by one of the algorithms. We are interested in policies with both small cost and small number of new cases. As we can see, the proposed method is outperforming the baseline models since, on average, for the majority of the policies, MPEA-DE dominated the other two models in both objectives.

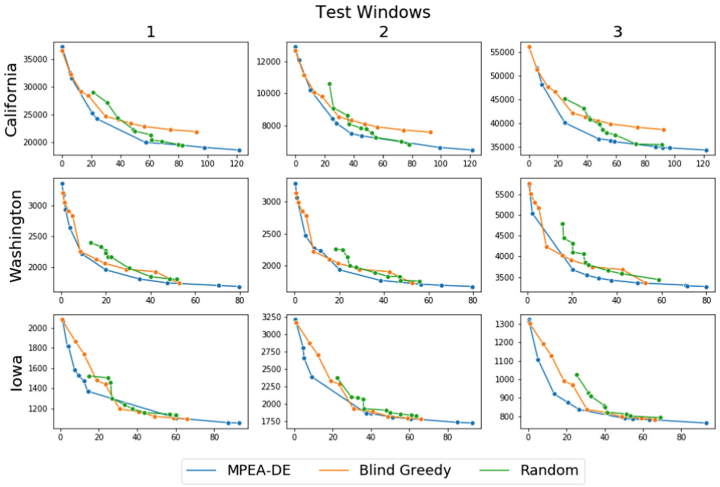

Fig. 7. Pareto frontier of prescriptive models for California, Washington, and Iowa, for three test windows. (x-axis represents the average cost, and the y-axis shows the average number of new cases)

4 Conclusion

Accurate forecasting of infected cases and the right mitigation strategies are key to reducing the spread of COVID-19. In this study, we proposed a framework to identify sets of superior policies from which a decision-maker can choose according to the goals and budgets. In this paper, a GRU-based model is proposed to predict the spread of COVID-19 using time-series infection data and NPIs. The results have shown that the

predictive model can predict the spread of COVID-19 accurately. The prediction results are then employed to identify which policies can be applied to reduce the number of new cases while minimizing the overall costs. To search for the optimal intervention policy, a multi-population evolutionary algorithm named MPEA-DE is proposed. We compared the prescriptive model to two baseline models: random selection strategy and blind greedy search method. The performance of the proposed prescriptive models is evaluated based on the dominancy of the generated prescriptions over the other two models. The experiments have shown that in terms of prescription quality, MPEA-DE performs better than random and blind greedy search methods. Based on our approach, the authorities can have a better recognition of the outcome of their policies and make policy shifts in time.

This study is subject to a few limitations, which suggest a few research directions. First, in the forecasting model, the vaccination rate is not considered. Since the vaccination period is relatively short at the time of this study, it is better to consider the vaccination factor after collecting sufficient data. Second, in the prescription phase, we used random costs for the policies generated from a uniform distribution. However, the social and economic impacts of intervention plans in the real world are more complicated than what has been assumed in this study. For this purpose, we consider testing a variety of more complicated cost matrices as a part of the robustness check and use models based on real data to predict the social and economic impacts of NPIs for future research studies.

Acknowledgments. In the context of the pandemic response challenge, codes and data were provided by XPRIZE to build predictors and prescriptions to achieve better intervention support to mitigate between people safety and opening back the economy. We thank XPRIZE for sharing the ideas and codes.

References

1. https://www.worldometers.info/coronavirus/
2. Miikkulainen, R., et al.: From prediction to prescription: evolutionary optimization of non-pharmaceutical interventions in the COVID-19 pandemic. IEEE Trans. Evol. Comput. **25**(2), 386–401 (2021)
3. Kermack, W.O., McKendrick, A.G.: A contribution to the mathematical theory of epidemics. In: Proceedings of the Royal Society of London. Series A, Containing Papers of a Mathematical and Physical Character, vol. 115, no. 772, pp. 700–721 (1927)
4. Whitley, D.: A genetic algorithm tutorial. Stat. Comput. **4**(2), 65–85 (1994)
5. Ardabili, S.F., et al.: Covid-19 outbreak prediction with machine learning. Algorithms **13**(10), 249 (2020)
6. Yin, R., Tran, V.H., Zhou, X., Zheng, J., Kwoh, C.K.: Predicting antigenic variants of H1N1 influenza virus based on epidemics and pandemics using a stacking model. PloS One **13**(12), e0207777 (2018)
7. Agarwal, N., Koti, S.R., Saran, S., Senthil Kumar, A.: Data mining techniques for predicting dengue outbreak in geospatial domain using weather parameters for New Delhi. India. Curr. Sci. **114**(11), 2281–2291 (2018)

8. Liang, R., et al.: Prediction for global African swine fever outbreaks based on a combination of random forest algorithms and meteorological data. Transbound. Emerg. Dis. **67**(2), 935–946 (2020)
9. Hu, Z., Ge, Q., Li, S., Boerwinkle, E., Jin, L., Xiong, M.: Forecasting and evaluating multiple interventions for COVID-19 worldwide. Front. Artif. Intell. **3**, 41 (2020)
10. Zandavi, S.M., Rashidi, T.H., Vafaee, F.: Forecasting the spread of covid-19 under control scenarios using LSTM and dynamic behavioral models (2020). https://arxiv.org/abs/2005.12270
11. Chandra, R., Jain, A., Chauhan, D.S.: Deep learning via LSTM models for COVID-19 infection forecasting in India (2021). https://arxiv.org/abs/2101.11881
12. Chung, J., Gulcehre, C., Cho, K., Bengio, Y.: Empirical evaluation of gated recurrent neural networks on sequence modeling (2014). https://arxiv.org/abs/1412.3555
13. Peng, X., Liu, K., Jin, Y.: A dynamic optimization approach to the design of cooperative co-evolutionary algorithms. Knowl.-Based Syst. **109**, 174–186 (2016)
14. Gutierrez, A., Dieulle, L., Labadie, N., Velasco, N.: A multi-population algorithm to solve the VRP with stochastic service and travel times. Comput. Ind. Eng. **125**, 144–156 (2018)
15. Hale, T., Petherick, A., Phillips, T., Webster, S.: Variation in government responses to COVID-19. Blavatnik School of Government Working Paper, vol. 31, 11p (2020)
16. https://github.com/OxCGRT/covid-policy-tracker/blob/master/documentation/codebook.md
17. http://www2.census.gov/programs-surveys/popest/datasets/2010-2019/national/totals/nst-est2019-alldata.csv
18. Cho, K., Van Merriënboer, B., Bahdanau, D., Bengio, Y.: On the properties of neural machine translation: encoder-decoder approaches. https://arxiv.org/abs/1409.1259 (2014)
19. Kingma, D.P., Ba, J.: Adam: a method for stochastic optimization (2014). https://arxiv.org/abs/1412.6980
20. Murata, T., Ishibuchi, H.: MOGA: multi-objective genetic algorithms. IEEE Int. Conf. Evolut. Comput. **1**, 289–294 (1995)
21. Xue, F., Sanderson, A.C., Graves, R.J.: Pareto-based multi-objective differential evolution. In: 2003 Congress on Evolutionary Computation, vol. 2, pp. 862–869 (2003)

Data-Driven Joint Pricing and Inventory Management Newsvendor Problem

Pengxiang Zhou and Wai Kin (Victor) Chan(✉)

Intelligent Transportation and Logistics Systems Laboratory, Tsinghua University, Shenzhen 518055, Guangdong, China
chanw@sz.tsinghua.edu.cn

Abstract. Data-driven methods are proposed to optimize both pricing and inventory management strategies in price and quantity setting newsvendor problem. Simulation experiments show that prescriptive method and casual sample average approximation outperform Predict-then-Optimize method. Sample average approximation might be even worse when ignoring pricing effect on demand uncertainty.

Keywords: Data-driven · Pricing · Inventory management · Causality

1 Introduction

The newsvendor problem [1] optimizes the order quantity q of perishable good, and makes penalty on the cost of unmet demand, backorder cost and the cost of unsold good, holding cost. The objective is to minimize the backorder cost and holding cost,

$$\min_{q} C(q) = E_D\Big[b\big[D-q\big]^+ + h\big[q-D\big]^+\Big] \tag{1}$$

where D is demand and b, h represent backorder cost and holding cost per unit respectively.

Assumption on exogenous price works in perfect competition market, but in monopolistic competition market, firms make decisions on both pricing and inventory management strategies simultaneously. Moreover, incorporating pricing strategy into newsvendor problem effects uncertainty in demand. Single-period price and quantity-setting newsvendor [2] considers additive demand uncertainty and multiplicative demand uncertainty, and mainly focuses on optimality conditions and unimodality, but there are great limitations on assumptions about demand distribution. Gregory D DeYong [3] review price-setting newsvendor and offer detailed extensions on demand, supply scenario and objective function, and even behaviour newsvendor.

Data driven methods show prevailing advantages in supply chain management and have no restriction on demand distribution. Predict-then-Optimize method first generates deterministic demand prediction using supervised learning, and then derives order quantity by solving the optimization model while resulting in estimation error and information loss. Sample average approximation method optimizes on order quantity and

R. Qiu et al. (Eds.): ICSS 2021, LNOR, pp. 397–403, 2021.
https://doi.org/10.1007/978-3-030-90275-9_31

price to maximize average empirical profit using finite samples of demand. Gah-Yi Ban and Cynthia Rudin [4] apply empirical risk minimization with regularization using linear hypothesis class, develop kernel optimization method to solve big data newsvendor problem and provides theoretical guarantees, but do not consider pricing-setting newsvendor problem. Dimitris Bertsimas and Nathan Kallus [5] propose prescriptive method and use non-parametric method to construct weights, conditional distribution to some extent, and then optimize decision variables over the demand distribution conditional on auxiliary data, and deal with problem when decision effects uncertainty.

In this paper, we apply data-driven methods to solve joint pricing and inventory management newsvendor problem using finite samples and mainly focus on pricing effect on demand uncertainty.

2 Problem Formulation

Both pricing and inventory management strategies are important for newsvendor problem especially in monopolistic competition markets where manufacturers have pricing power. Price and quantity setting newsvendor problem optimizes on order quantity and price to maximize the expectation of profit.

$$\pi(p, q) = pD(p, \varepsilon) - cq - h\big[q - D(p, \varepsilon)\big]^{+} - b\big[D(p, \varepsilon) - q\big]^{+} \tag{2}$$

where $D(p, \varepsilon) = a - bp + \varepsilon (a > 0, b > 0)$ in additive demand case and $D(p, \varepsilon) = ap^{-b} + \varepsilon (a > 0, b > 1)$ in multiplicative demand case.

In decision making problem without auxiliary data, we maximize $E\big[\pi\big[p, q; D\big]\big]$ only use demand distribution. As for decision making problem with auxiliary data, we decide optimal price and order quantity p, q over P, Q to maximize profit $E\big[\pi(p, q; D(p))|X = x\big]$ conditional on observation $X = x$ and distribution of demand. However, we would get biased solution because of pricing effect on demand uncertainty as shown in formula (3) and (4)

$$\pi^{*}(x) = \max_{(p,q)\in(P,Q)} E\big[\pi(p, q; D(p))X = x\big] \tag{3}$$

$$\big(p^{*}(x), q^{*}(x)\big) = \arg\max_{(p,q)\in(P,Q)} E\big[\pi(p, q; D(p))X = x\big] \tag{4}$$

Hence, we make assumptions on price and quantity setting newsvendor problem:

Assumption 1: Only P effects demand uncertainty.

Assumption 2: Conditional independence, for every $q \in \mathrm{Q}$, $D \perp q|p, x$

We discretize price into multiple cases and solve the optimization problem with fixed price, which is the newsvendor problem with exogenous price, finally we sort out the scenario with largest profit.

3 Method

3.1 Optimization with Full Information

First, we optimize price and order quantity using full information as benchmark, where we get real demand given price and auxiliary features. Given testing set S_{te} with auxiliary

data X, we generate full information set with demand and price according to data generating process. Using true demand d and price p_i in full information set, we optimize order quantity $q^*(d, p_i)$ given p_i and auxiliary data and obtain profit $\pi^*(d, p_i)$. Sort profit $\pi^*(d, p_i)$ and get optimal strategies $(p_{i^*}, q^*(d, p_{i^*}))$ with largest profit $\pi^*(d, p_{i^*})$. For each sample with demand non-parametric method, in testing set S_{te},

$$q^*(d, p_i) = \max_{q \in Q} \pi(q; d, p_i) \tag{5}$$

$$\pi^*(d, p_i) = \operatorname*{argmax}_{q \in Q} \pi(q; d, p_i) \tag{6}$$

$$i^* = arg\ max_i \pi^*(d, p_i), \pi^*(d, p_{i^*}) = max_i \pi^*(d, p_i) \tag{7}$$

3.2 Casual Sample Average Approximation

Data-driven method does not assume exact demand distribution, for example, sample average approximation [6] method solves the stochastic problem with objective function as sample average using finite samples for approximation. We suppose that $\{d_1, d_2, \ldots, d_N\}$ are samples of demand D and use general profit formulation $\pi = p\ min(d_i, q) - cq - b\left[d_i - q\right]^+ - h\left[q - d_i\right]^+$, where p, price of good per unit and q, order quantity are decision variables, $p\ min(d_i, q)$ represents sales profit given demand d_i and cq measures purchase cost. Therefore, the mean sample profit is as follows:

$$\max_{(p,q) \in (P,Q)} \frac{1}{N} \sum_{i=1}^{N} \left(p\ \min(d_i, q) - cq - b\left[d_i - q\right]^+ - h\left[q - d_i\right]^+ \right) \tag{8}$$

where $\boldsymbol{p}, \boldsymbol{q} \geq 0$ and $\boldsymbol{p}$ is integer variable and $\boldsymbol{q}$ is continuous variable.

We introduce dummy variable $\boldsymbol{o_i}, \boldsymbol{u_i}$ to represent holding cost and backorder cost. Because of formula $\boldsymbol{min(d, q)} = \boldsymbol{d} - \left[\boldsymbol{d} - \boldsymbol{q}\right]^+$, we have equivalent formulation of profit function $\boldsymbol{\pi} = \boldsymbol{dp} - \boldsymbol{pu} - \boldsymbol{cq} - \boldsymbol{bu} - \boldsymbol{ho}$ where $\boldsymbol{u_i} \geq \boldsymbol{d_i} - \boldsymbol{q}, \boldsymbol{o_i} \geq \boldsymbol{q} - \boldsymbol{d_i}, \boldsymbol{u_i}, \boldsymbol{o_i} \geq 0, \boldsymbol{i} = 1, \ldots, \boldsymbol{N}$.

Given training set S_{tr} with demand $\{d_1, d_2, \ldots, d_N\}$, we optimize price and order quantity and get solution of sample average approximation method as $\left(q^{SAA}, p^{SAA}\right)$

$$\left(q^{SAA}, p^{SAA}\right) = \operatorname*{arg\ max}_{(p,q) \in (P,Q)} \frac{1}{|S_{tr}|} \sum_{i \in S_{tr}} \pi(p, q; d_i) \tag{9}$$

$$\pi\left(q^{SAA}, p^{SAA}\right) = \max_{(p,q) \in (P,Q)} \frac{1}{|S_{tr}|} \sum_{i \in S_{tr}} \pi(p, q; d_i) \tag{10}$$

Considering pricing effect on demand uncertainty, we optimize order quantity over Q using samples in training set with given each price p_i. Sort the profit $\pi^*(p_i)$ and select the pricing strategy with index i^{SAA} which has largest profit π^{SAA}.

$$q^*(p_i) = \operatorname*{arg\ max}_{q \in Q} \frac{1}{|\{i \in S_{tr} : P = p_i\}|} \sum\nolimits_{i \in s_{tr}: P = p_i} \pi(q; p, d_i) \tag{11}$$

$$\pi^*(p_i) = \max_{q \in Q} \frac{1}{|\{i \in S_{tr} : P = p_i\}|} \sum\nolimits_{i \in s_{tr}: P = p_i} \pi(q; p, d_i) \tag{12}$$

$$i^{SAA} = arg\ max_i \pi^*(p_i), \pi^{SAA} = max_i \pi^*(p_i) \tag{13}$$

3.3 Prescriptive Method

Dimitris Bertsimas and Nathan Kallus [5] put forward prescriptive method and the main idea is to match each testing sample with amounts of samples from training set which share similar characteristics. Given past data in training set $S_{tr} = \{(d_1, x_1, p_1), (d_2, x_2, p_2), ..., (d_N, x_N, p_N)\}$, we use decision tree to fit demand D with auxiliary data X and price P in training set and apply the estimated tree to predict demand in testing set.

Step 1. Given CART [7] map rule $R : X \times P \to D$, we calculate weights using tree model in Eq. (14). $R(x, p)$ is the leaf index which the sample with input (x, p) belongs to, $|\{j : R(xj, pj) = R(x, p)\}|$ measures total number of samples in training set with same estimated value and $\mathbb{I}\big[R(x, p) = R(xi, pi)\big]$ is the indicator function to justify whether the sample (xi, pi) shares the same leaf index with (x, p).

$$w_{N,i}^{CART}(x, p) = \frac{\mathbb{I}\big[\mathcal{R}(x, p) = \mathcal{R}(x_i, p_i)\big]}{\big|\big\{j : R\big(x_j, p_j\big) = R(x, p)\big\}\big|}. \tag{14}$$

Step 2. Solve the optimization problem

$$q_N^{CART}(x, \overline{p}) = arg\ \max_{q \in Q} \frac{1}{|\{i : R(x_i, p_i) = R(x, \overline{p})\}|} \sum_{i:R(x_i,p_i)=R(x,\overline{p})} \pi(q; d_i), \tag{15}$$

$$\pi^*(x, \overline{p}) = \max_{q \in Q} \frac{1}{|\{i : R(x_i, p_i) = R(x, \overline{p})\}|} \sum_{i:R(x_i,p_i)=R(x,\overline{p})} \pi(q; d_i). \tag{16}$$

Step 3. For each $\overline{p} \in P$ given x, we get

$$\pi_N^{CART}(x) = \max_{\overline{p} \in P} \pi^*(x, \overline{p}), \tag{17}$$

$$p_N^{CART}(x) = arg\ \max_{\overline{p} \in P} \pi^*(x, \overline{p}), \tag{18}$$

$$q_N^{CART}(x) = arg\ \max_{q \in Q} \frac{1}{\big|\big\{i : R(x_i, p_i) = R\big(x, p_N^{CART}(x)\big)\big\}\big|} \sum_{i:R(x_i,p_i)=R\left(x,p_N^{CART}(x)\right)} \pi(q; d_i) \tag{19}$$

3.4 Predict-then-Optimize Method

Predict-then-Optimize method always predicts the variable we are interested in first and then applies the estimated value to the optimization problem in second stage. As for Predict-then-Optimize framework, we consider pricing effect on demand uncertainty and use both auxiliary data X and P to fit demand, then select optimal strategies using estimated demand $\hat{d}$.

$$q^{PTO}(d, p_i) = arg \max_{q \in Q} \pi\left(q; \hat{d}, p_i\right) \tag{20}$$

$$\pi^{PTO}(d, p_i) = \max_{q \in Q} \pi\left(q; \hat{d}, p_i\right) \tag{21}$$

$$i^{PTO} = arg\ max_i \pi^{PTO}(d, p_i), \pi^{PTO} = max_i\, \pi^{PTO}(d, p_i) \tag{22}$$

4 Simulation Experiment

In this section, we compare the method performance with full information benchmark using two simulation datasets. We experiment on the simulated data set which takes additive demand uncertainty into consideration, A, B in Eq. (23) measure mean-dependence and heteroscedasticity of demand on auxiliary data, and k describes demand reduction for per unit increase in price. Equation (24) guarantees price higher than cost. 1^{st} dataset contains 1000 training samples respectively and both use 100 testing samples.

$$D = max\left\{0, A^T X + \left(B^T X\right) * \varepsilon\right\} + (P_{max} - P) * b \tag{23}$$

$$P = max\left\{D^T X + \varepsilon\right], c\right\}, P_{max} = maxP \tag{24}$$

where $X \sim N(\mu, \Sigma), \mu = [50, 40, 20],\ \Sigma = \begin{pmatrix} 1 & 0.5 & 0 \\ 0.5 & 1 & 0.5 \\ 0 & 0.5 & 1 \end{pmatrix}, \varepsilon \sim N(0, 1), b = 50, A^T = [0.8, 0.1, 0.1], B^T = [0, 0.1, 0.1], D^T = [-1, 1, 1.25]$ (Table 1).

We use the above methods to get optimal strategy in training set then apply it to testing test and find out whether it works or not. Results show that prescriptive method and casual sample average approximation method show prevailing advantages relative to Predict-then-Optimize method and sample average approximation. Both of the methods decide optimal price the same as the case with full information and the optimal order quantity is close to what we find in full information. On the other hand, all the methods show tendency to over-purchase and thus occurs holding cost, but the result is even worse in the case using sample average approximation due to biased pricing strategy. Method performance comparison is described in Fig. 1(a). It's worth noting that total profit using sample average approximation or Predict-then-Optimize method is always lower than that of casual sample average approximation and prescriptive method and does not converge to profit in full information case when sample size reaches 800 or even higher.

Table 1. Optimal strategies of newsvendor problem

Method	1^{st} Experiment				2^{nd} Experiment			
	Price	Quantity	Demand	Profit	Price	Quantity	Demand	Profit
Full information	16.0	532.2	532.2	5854.4	14.0	481.5	481.5	4333.2
Prescriptive method	16.0	540.2	531.2	5797.1	14.1	472.1	474.5	4291.7
Sample average approximation	22.0	688.6	232.2	1209.5	19.0	526.6	231.5	1469.9
Causal sample average approximation	16.0	542.4	532.2	5790.5	14.0	480.6	481.5	4299.3
Predict-then-Optimize method	22.0	395.0	232.2	2970.9	19.0	329.2	231.5	2653.9

Real data complies with log-normal distribution instead of normal distribution, we suppose that $ln(x_1) \sim N(3.91, 0.02)$, $ln(x_2) \sim N(3.68, 0.025)$, $ln(x_3) \sim N(3.00, 0.05)$, which has same expectation and variance as 1^{st} dataset but mutually independent. 2^{nd} dataset contains 260 training samples respectively and both use 100 testing samples. Comparing with data simulated from normal distribution, both optimal solution and objective value varies, results show in Fig. 1(b). Causal sample average approximation and prescriptive method converge to profit in full information with smaller sample size.

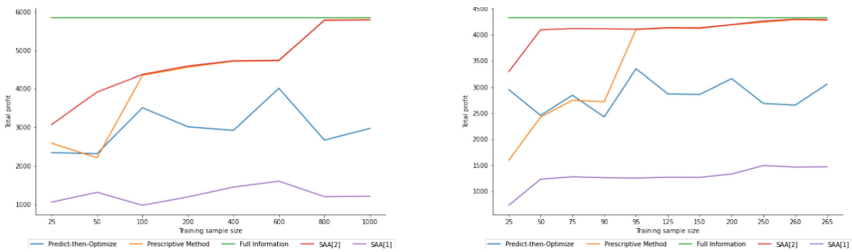

(a) Result in 1^{st} dataset (b) Result in 2^{nd} dataset

Fig. 1. Method performance comparison

As for computation time comparison, both casual sample average approximation and prescriptive method shows linear computational complexity and casual sample average approximation method's performance is significantly better than other methods. Sample average approximation method uses quadratic objective function without fixed price technique and computation time increases exponentially accompanying with increasing sample size (Fig. 2).

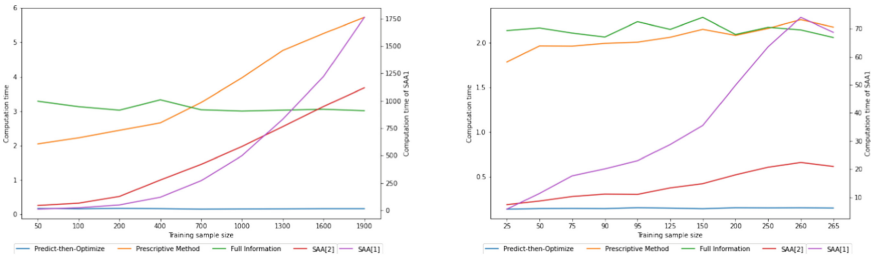

(a) Result in 1^{st} dataset (b) Result in 2^{nd} dataset

Fig. 2. Computation time comparison

5 Summary

Causal sample average approximation and prescriptive method outperform predict-then-Optimize method and sample average approximation and converge to full information profit when sample size approaches to 800, 260 in the simulation experiments. Intersection of machine learning and optimization methods provides a more powerful technical approach in supply chain management using auxiliary data. Huge amounts of data enhance decision making ability, and machine learning methods can improve prediction accuracy or approach to the demand distribution that most closely matches the characteristics of the sample. On the other hand, decision effects uncertainty should be taken into consideration, such as pricing strategy' effect on demand uncertainty in price and quantity setting newsvendor problem. In future work, directions to be considered include multi-period joint pricing and inventory management problem setting [8], censored demand.

Acknowledgements. This research was funded by the Guangdong Pearl River Plan (2019QN01X890), National Natural Science Foundation of China (Grant No. 71971127), and the Hylink Digital Solutions Co., Ltd. (120500002).

References

1. Snyder, L.V., Shen, Z.-J.M.: Fundamentals of Supply Chain Theory. Wiley, New York (2019)
2. Petruzzi, N.C., Dada, M.: Pricing and the newsvendor problem: A review with extensions. Oper. Res. **47**(2), 183–194 (1999)
3. DeYong, G.D.: The price-setting newsvendor: review and extensions. Int. J. Prod. Res. **58**(6), 1776–1804 (2020)
4. Ban, G.-Y., Rudin, C.: The big data newsvendor: practical insights from machine learning. Oper. Res. **67**(1), 90–108 (2019)
5. Bertsimas, D., Kallus, N.: From predictive to prescriptive analytics. Manage. Sci. **66**(3), 1025–1044 (2020)
6. Kleywegt, A.J., Shapiro, A., Homem-de Mello, T.: The sample average approximation method for stochastic discrete optimization. SIAM J. Optimiz. **12**(2), 479–502 (2002)
7. Breiman, L., Friedman, J., Stone, C.J., Olshen, R.A.: Classification and Regression Trees. CRC Press, Boca Rotan (1984)
8. Chen, B., Chao, X., Ahn, H.-S.: Coordinating pricing and inventory replenishment with nonparametric demand learning. Oper. Res. **67**(4), 1035–1052 (2019)

Author Index

R. Qiu et al. (Eds.): ICSS 2021, LNOR, pp. 405–406, 2021.
https://doi.org/10.1007/978-3-030-90275-9